
Fundamentals of Natural Gas Behavior, Reservoir Engineering and Field Production

Lecture Notes and Project Exercises

Jann-Rune Ursin

STAVANGER
2016, VERSION 1

Preface

The purpose of this book is to introduce natural gas reservoir engineering and production to an audience with scarcely, if any prior knowledge in the field. It is however assumed, that the reader is familiar with general petroleum technology terms and has a basic knowledge in subjects related to reservoir engineering and petroleum geology. It is also undoubtedly an advantage if the reader has background in basic mathematics and physics, since much of the content in this book and in the exercises, are presented in form of physical and mathematical models. Natural gas reservoir engineering and production is in this book presented through physical and mathematical models, through a process of deduction of equations and models, reflecting the current understanding of the field.

This book includes subjects covered in courses taught at the University of Stavanger.

The basic idea behind this book, is to present the theory of natural gas reservoir engineering and production through basic models describing the physical processes. The models are then presented through equations which are then numerically represented. The practical calculations using these equations are introduced as elements in various computer programs. These programs allows the student to perform calculations related to various subjects in natural gas engineering and production. The different programs are subsequently and systematically brought together, to form a "complete" package or simulation model. The model is then used to simulate gas field production and associated processes.

The simulation program is initiated by a set of input data, read from a data file. This file contains all necessary information, i.e. reservoir information, production rates, PVT-data and information related to the simulation process and more.

This book could therefore be said to be *a mathematical laboratory*, where various aspects of natural gas reservoir engineering and production are learned by "doing it"

The process of learning adopted in this book is based on the following items;

1. based on a physical presentation of various processes, followed by
2. a theoretical description and deduction of mathematical equations, which leads to the formation of a model suitable for
3. discretization and numerical representation in the form of a numerical simulation program.

The mathematical laboratory permits the student to focus on a single parameter in an equation, change it and view the impacts on the overall simulation process.

This book contains two parts; *Lecture Notes*, representing the fundamentals of the course and *Project Exercises*, which addresses the fundamentals through practical exercises and numerical simulations.

The simulation model is built up step by step, by including new elements, in part constituting a model for performing the process of gas reservoir and production simulation. After a short introduction to general aspects of gas reservoirs; like rocks, migration and reserves (Chapter 1), an introduction to gas characteristics and phase behavior is given (Chapter 2), followed by a presentation of various important parameters describing gas properties (Chapter 3).

Fundamental equations describing material balance (Chapter 4) under volumetric and non-volumetric reservoir conditions are presented. This model is subsequently used in a project exercise, demonstrating the nature of material balance in gas condensate reservoirs by parameter variation.

Equations describing single-phase gas flow (Chapter 5) is further included in the model. This modification allows the user to calculate the bottom hole pressure relative to the mean block pressure. Using the extended model, various simulations are supposedly performed with the purpose of testing the implication on the bottom hole pressure caused by variation of well bore skin, non-Darcy flow and various shape factors. At the end of this chapter, a model describing two-phase flow is introduced. This model allows for modeling a revised GOR and oil and gas production of semi steady-state reservoir flow.

The well bore flow (Chapter 6) is described as single-phase gas flow in a cylindrical well bore of constant cross-section. The deduced equations, are allowing for both homogeneous liquid condensate and water to be present in the well stream. Various tests, including dip angle, well bore cross-section, well length and other, are then performed and the effect on the well-head pressure observed. The model is further developed by introducing heat losses in the well-bore. Based on thermodynamical considerations a non-linear temperature profile is developed where steady state radial heat transfer in the well-bore can be studied.

Finally, all program segments are properly unified, forming a natural gas reservoir depletion simulation program (Chapter 7). The program can simulate the production of gas and condensate from numerous individual (non-communicating) blocks where the different blocks might be produced by one or several wells. In this last section of the program, field rates and cumulative production is included in the model as well as the ability to choose the well sequence and start-up time for individual wells.

In the last chapter (Chapter 8), gas field modeling and production is presented. A statistical model is used in ranking the different reservoir and cross-flow between reservoirs or blocks are calculated based on various strategies for well sequence and production. An example from a Norwegian gas-condensate field is presented and worked out using this statistical technique.

The Project Exercise part of this book contains various exercises, related to fundamentals presented in the Lecture Notes. Most exercises are performed by running a computer program (.exe file), describing a development of the full size simulation program. The initial version of the program contains only the material balance part, while the full size program contains additional options for single flow, well flow and multi well

and block simulations.

References throughout the text are given at the end of each chapter. Some general references are presented below:

- B.C. Craft and M.F. Hawkins, *Applied Petroleum Reservoir Engineering*, Prentice-Hall, INC.
- Jacques Hagoort, *Fundamentals of Gas Reservoir Engineering*, Elsevier, 1988.
- Donald L. Katz and Robert L. Lee, *Natural Gas Engineering, Production and Storage*, McGraw-Hill International Editions, 1990.
- Sanjay Kumar, *Gas Production Engineering*, Gulf Publishing Company, 1960
- L.P. Dake, *The Practice of Reservoir Engineering*, Elsevier, 1994.
- James W. Amyx, Daniel M. Bass, Jr. and Robert L. Whiting, *Petroleum Reservoir Engineering*, MaCraw-Hill Book Company, 1960.

Units and Conversion Factors

A basic knowledge of units and conversion factors are absolutely necessary in reservoir engineering, although the preferred choice of industrial units depend on company, country and tradition. Since the choice of units has been largely a question of preference, the knowledge of conversion factors is mostly needed in the petroleum field.

English and American units are most commonly used in the petroleum industry, but there is now a trend to use SI-units or practical SI-units, especially as part of the practices in Norwegian and other European oil companies.

In this book we will use mainly SI-units and industrial units are rarely represented. Since both SI-units and industrial units are used in the oil industry, it is important to be confident of both systems.

A selection of some of the most frequently used parameters are listed in the table below. The *Metric unit* is seen as a practical SI-unit, often used in displaying data or calculations.

$$\mathbf{Metric\ unit = Conversion\ factor \times Industry\ unit,}$$

i.e. the metric unit is found by multiplying a given industry unit with an appropriate conversion factor.

The letter symbols for physical quantities used in mathematical expressions in the text are primarily in accordance with a standard for symbols in reservoir engineering, adopted by the Society of Petroleum Engineers. For example, V stands for the volume. With subscript, V_p stands for the pore volume; etc.

| Parameter (SI unit) | Industry unit | Conversion factor | Metric unit |
|-----------------------------------|----------------------------|----------------------|--------------------------------|
| Area, m ² | sq mile | 2.589988 | km ² |
| | acre | 4046.856 | m ² |
| | sq ft | 0.09290304 | m ² |
| | sq in. | 6.4516 | cm ² |
| Compressibility, Pa ⁻¹ | psi ⁻¹ | 0.1450377 | kPa ⁻¹ |
| Density, kg/m ³ | g/cm ³ | 1000.0 | kg/m ³ |
| | lbm/ft ³ | 16.01846 | kg/m ³ |
| | °API | 141.5/(131.5 + °API) | (γ_{sg}) [*] |
| Flow rate, m ³ /s | bbl/d | 0.1589873 | m ³ /d |
| | ft ³ /d | 0.02831685 | m ³ /d |
| Force, N | lbf | 4.448222 | N |
| | pdl | 138.2550 | mN |
| | dyne | 0.01 | mN |
| Length, m | mile | 1.609344 | km |
| | ft | 30.48 | cm |
| | in. | 2.54 | cm |
| Pressure, Pa | atm | 101.325 | kPa |
| | bar | 100.0 | kPa |
| | lbf/in. ² (psi) | 6.894757 | kPa |
| | mm Hg (0°C) | 1.333224 | kPa |
| | dyne/cm ² | 0.1 | Pa |
| Mass, kg | ton | 1000 | kg |
| | lbm | 0.4535924 | kg |
| Temperature, K | °C | + 273.15 | K |
| | °F | (°F-32)/1.8 | °C |
| | R | 5/9 | K |
| Surface tension, N/m | dyne/cm | 1.0 | mN/m |
| Viscosity, Pa·s | cp (poise) | 0.001 | Pa·s |
| Volume, m ³ | acre-ft | 1233.489 | m ³ |
| | cu ft | 0.02831685 | m ³ |
| | bbl | 0.1589873 | m ³ |
| | U.S. gal | 3.785412 | dm ³ |
| | liter | 1.0 | dm ³ |

* Specific gravity of oil.

Project Exercises

The purpose of these exercises is primarily to expand on topics presented in the textbook or topics otherwise related to natural gas engineering. Through the study of the text in combination with a detailed examination of the exercises, the student may find the learning process more easy and inspiring in addition to gain important knowledge about the various topics within the field of natural gas engineering. Bridging the space between theory, represented by the lectures, and the experience of working through practical examples dealing with closely related topics, - a general understanding of the field natural gas engineering should be gained.

Inspecting and modification of the simulation input-data can be performed simply by opening the chosen data-file, using any editor, ie. Microsoft Notice Book. Plotting data results are easily done with e.g. Microsoft Excel. (A demonstration on how to run the program, open and modify the data files, import and plot data using Excel and finally how to prepare a report using Word, will be given as part of a practical introductory project exercise.)

The computer program and the associated data input file are both updated for each new project exercise. The two files are being distributed, through "it's: learning" (the local stud-web service program), and found under the course name.

In the process of reporting the work done in relation to the exercises, Microsoft Word or any other suitable text editor can be used. Plots from Excel can easily be imported into a Word document, being an important part of the complete report. It is important to notice that all plots should be accompanied with figure text, explaining the data plotted. In these exercises; "one half" the work should be invested in the comments on how and why the presented results are looking the way it does.

When the report is completed, it'learning should be used in submitting the report for approval and comments. In the process of completing the reports, no paper version or - copy is ever needed. The final report and all relevant files (program - and data files) should be stored in a file on your private disk. If preferred, these exercises may be copied to your home computer, laptop, etc. and worked on form there. As long as you are capable of filing a copy of your report for approval, you may choose any work arrangement that suits you best.

Lastly, - a piece of friendly advise: *Save copies of what you are doing, - all the time!!! When ever a work process is ended, a copy of the latest changes should be stored* . Follow this advise and you will be saved from many regrets!

Keep on the good work and remember that all exercises has to be approved as part of the prerequisite for completing this course.

Contents

| | | |
|----------|--|-----------|
| I | Lecture Notes | 1 |
| 1 | Gas Reservoirs | 3 |
| 1.1 | Natural Gas - The Fuel of Tomorrow | 3 |
| 1.2 | Reservoir Rocks | 4 |
| 1.2.1 | Source Rock and Generation of Petroleum [11] | 4 |
| 1.2.2 | Petroleum Migration and Accumulation | 6 |
| 1.2.3 | The Golden Zone | 9 |
| 1.3 | Gas and Oil Reservoirs | 10 |
| 1.4 | Recoverable Reserves | 11 |
| | References | 13 |
| 2 | Gas Characteristics and PVT-relations | 15 |
| 2.1 | Gas Characterization | 15 |
| 2.1.1 | Groups of Hydrocarbons | 16 |
| 2.1.2 | Components of Reservoir Gases | 17 |
| 2.2 | Phases | 20 |
| 2.2.1 | Gibbs Phase Rule | 20 |
| 2.2.2 | Single Component Systems | 21 |
| 2.2.3 | Multi Component Systems | 23 |
| 2.3 | Practical Aspect Of Gas Production | 28 |
| 2.4 | Molar Composition | 29 |
| 2.5 | Reservoir Fluids | 32 |
| 2.6 | Phase Equilibrium | 33 |
| 2.6.1 | The K-value Method | 34 |
| 2.6.2 | The Equation Of State Method | 36 |
| 2.6.3 | The Experimental Method | 38 |
| | References | 41 |
| 3 | Thermodynamics, Phase Behavior and Gas Properties | 43 |
| 3.1 | Determination of Phase Equilibrium | 43 |
| 3.1.1 | Definition of Equilibrium Ratio | 45 |
| 3.2 | Basic Thermodynamics | 47 |
| 3.2.1 | Laws of Thermodynamics | 47 |
| 3.2.2 | Thermodynamic Equilibrium | 51 |
| 3.2.3 | Fugacity and Equilibrium Ratio | 53 |

| | | |
|----------|---|------------|
| 3.3 | Equation of State (EoS) | 55 |
| 3.3.1 | The van der Waals Equation | 56 |
| 3.3.2 | Cubic Equations | 58 |
| 3.3.3 | The Peng-Robinson Equation | 59 |
| 3.3.4 | The Equilibrium Coefficients | 61 |
| 3.4 | Simulation of Phase Behavior | 64 |
| 3.4.1 | General Cubic EoS | 64 |
| 3.4.2 | Calculation and Simulation | 65 |
| 3.4.3 | Simulation Results | 67 |
| 3.5 | Gas Properties | 71 |
| 3.5.1 | Gas Density | 73 |
| 3.5.2 | Gas Compressibility | 75 |
| 3.5.3 | Condensate-Gas Ratio | 77 |
| 3.5.4 | Gas Formation Volume Factor | 80 |
| 3.5.5 | Gas Viscosity | 82 |
| 3.6 | PVT parameters | 85 |
| | References | 87 |
| 4 | The Material Balance Equation | 89 |
| 4.1 | The Material Balance Equation, MBE | 90 |
| 4.2 | Wet-Gas Reservoirs | 90 |
| 4.3 | Gas-Condensate Reservoirs | 94 |
| 4.3.1 | Derivation of a Gas Recovery Equation | 96 |
| 4.3.2 | Numerical representation of MBE | 98 |
| 4.3.3 | Simulation of Volumetric Depletion | 101 |
| 4.4 | Non-Volumetric Depletion | 103 |
| 4.4.1 | Significance of Reservoir Rock -, Initial Water and Gas Compressibility | 105 |
| 4.5 | Aquifer Influx | 107 |
| 4.5.1 | Natural Water Influx | 110 |
| 4.5.2 | Application of Aquifer Water Influx | 112 |
| 4.5.3 | Aquifer Models | 114 |
| 4.6 | Simulation of Non-Volumetric Depletion | 118 |
| 4.7 | History Matching and Predictive Performance | 123 |
| 4.7.1 | p/z Interpretation Method | 123 |
| 4.7.2 | The Havlena - Odeh Interpretation Method | 125 |
| 4.7.3 | The Direct Interpretation Method | 127 |
| | References | 130 |
| 5 | Reservoir Gas Flow | 133 |
| 5.1 | Single-Phase Gas Flow | 135 |
| 5.1.1 | Steady-State Darcy Flow | 136 |
| 5.1.2 | Steady-State Radial Flow | 140 |
| 5.2 | Semi Steady-State Radial Flow | 142 |
| 5.2.1 | Well skin factor | 144 |
| 5.2.2 | Non-Darcy Flow | 146 |

| | | |
|--------|---|-----|
| 5.2.3 | Correction for Turbulent Radial Flow | 147 |
| 5.3 | The General Non-Steady-State Flow Solution | 150 |
| 5.3.1 | Radial Flow at Constant Terminal Rate | 153 |
| 5.3.2 | Infinite-Acting Period | 154 |
| 5.4 | The Late Transition Period | 156 |
| 5.4.1 | Time Dependent Semi Steady-State Solution | 156 |
| 5.4.2 | Infinite-Acting - to Semi Steady-State Period | 158 |
| 5.5 | Radial Flow Equations | 161 |
| 5.5.1 | Non-Radial Reservoir Flow | 161 |
| 5.5.2 | Flow Equations | 164 |
| 5.6 | Simulation Examples | 165 |
| 5.6.1 | Pressure development as function of time | 165 |
| 5.6.2 | Relative bottom-hole pressure development | 167 |
| 5.7 | Near Well Flow Characteristics in Gas Condensate Reservoirs | 167 |
| 5.7.1 | Gas Condensate Well Deliverability | 167 |
| 5.7.2 | Single phase semi steady-state reservoir gas flow | 169 |
| 5.7.3 | Simulation of one-phase reservoir gas production | 170 |
| 5.8 | Two phase semi steady-state oil and gas flow | 171 |
| 5.8.1 | Volume factors | 172 |
| 5.8.2 | Density | 172 |
| 5.8.3 | Viscosity | 174 |
| 5.8.4 | Relative permeability | 174 |
| 5.9 | Modeling production GOR | 175 |
| 5.9.1 | A two-phase reservoir production model | 176 |
| 5.9.2 | Reservoir oil saturation profile | 177 |
| 5.9.3 | Surface production | 181 |
| 5.9.4 | Additional surface oil production | 182 |
| 5.9.5 | The production GOR factor; R_p | 183 |
| 5.10 | Simulation of two phase semi steady-state flow | 184 |
| 5.10.1 | Pressure and production developments | 184 |
| 5.10.2 | Effect of critical oil saturation; S_{co} | 187 |
| 5.10.3 | Effect of saturation profile | 189 |
| 5.10.4 | Effect of gas composition | 192 |
| 5.11 | Final Comments | 196 |
| | References | 198 |

| | | |
|----------|---|------------|
| 6 | Gas Well-Bore Flow | 201 |
| 6.1 | Basic Equation for Well-Bore Flow of Real Gas | 202 |
| 6.1.1 | Mass Conservation | 203 |
| 6.1.2 | Momentum Balance | 203 |
| 6.1.3 | Real Gas Law | 207 |
| 6.2 | Pressure Distribution in Shut-In Wells | 208 |
| 6.2.1 | Thermal Effects in The Well-Bore | 209 |
| 6.2.2 | Effect of a Temperature Gradient | 211 |
| 6.3 | Rate Dependent Pressure Losses | 214 |
| 6.3.1 | Uniform Temperature and No Gravity Effect | 214 |

| | | |
|----------|---|------------|
| 6.3.2 | Linear Temperature Variation and No Gravity Effect | 216 |
| 6.4 | Pressure Distribution in a Producing Well | 218 |
| 6.5 | Multi-Phase Flow | 221 |
| 6.5.1 | Gas-Condensate Mixtures | 222 |
| 6.5.2 | Gas-Condensate-Water Mixtures | 223 |
| 6.6 | Liquid Accumulation in Gas Wells | 225 |
| 6.7 | Simulation Examples | 228 |
| 6.7.1 | Well-Head Pressure as Function of Dip Angle | 229 |
| 6.7.2 | Well-Head Pressure as Function of Time for Two Different Well Flow Rates | 230 |
| 6.7.3 | Well-Head Pressure as Function of Time for Two Different Well- Bore Diameters. | 230 |
| 6.7.4 | Well-Head Pressure as Function of Time for Associated Water Production | 231 |
| 6.8 | Heat Losses in Producing Well | 231 |
| 6.8.1 | Basic Thermodynamics | 232 |
| 6.8.2 | Temperature in Well-Bore Flow | 234 |
| 6.9 | No-Heat Exchange | 236 |
| 6.10 | Radial Heat Flow | 239 |
| 6.11 | Steady-State Radial Heat Flow | 241 |
| 6.12 | Steady-State Radial Heat Transfer | 245 |
| | References | 251 |
| 7 | Natural Gas Reservoir Depletion | 253 |
| 7.1 | Development of Natural Gas Fields | 253 |
| 7.2 | Reservoir Performance | 255 |
| 7.3 | Constraints on Gas Production | 257 |
| 7.3.1 | Well-Inflow Performance | 257 |
| 7.3.2 | Tubing-Flow Performance | 259 |
| 7.3.3 | Well Deliverability | 262 |
| 7.4 | Simulation Examples | 263 |
| 7.4.1 | Production Flow Rates | 264 |
| 7.4.2 | Cumulative Gas Production | 265 |
| 7.4.3 | Pressure Development | 265 |
| | References | 266 |
| 8 | Gas Field Modeling and Production | 267 |
| 8.1 | Introduction | 268 |
| 8.2 | Reservoir Modeling and - Simulation | 270 |
| 8.3 | Alternative Reservoir Modeling | 270 |
| 8.3.1 | Characteristics of Natural Gas Production | 270 |
| 8.3.2 | Drainage Compartments | 271 |
| 8.4 | Fault Block Modeling (FBM) | 272 |
| 8.4.1 | Principles of FBM | 272 |
| 8.4.2 | The FBM - A Bit of Theory | 273 |
| 8.4.3 | A Simplified Model Example | 275 |

| | | |
|---------------------------------|---|------------|
| 8.4.4 | Cross-through communication | 277 |
| 8.4.5 | Handling Uncertainty | 279 |
| 8.5 | FBM Characteristics | 280 |
| 8.6 | Application of The Fault Block Model | 282 |
| 8.6.1 | The Gas Field | 284 |
| 8.6.2 | Well Location Sequence | 285 |
| 8.6.3 | Well Rate Adjustments | 287 |
| 8.6.4 | Uncertainty in Field Production | 289 |
| 8.6.5 | Balanced Field Production | 291 |
| 8.6.6 | Reduced Uncertainty in Field Production | 293 |
| 8.7 | Final Comments | 294 |
| | References | 296 |
| II Project Exercises | | 299 |
| 1 | Molar Phase Split | 301 |
| 1.1 | Parameters | 301 |
| 1.2 | Calculation of Vapor - Liquid Equilibrium | 303 |
| 1.3 | Phase Composition | 305 |
| | References | 307 |
| 2 | PVT-Simulation | 309 |
| 2.1 | Running the Program | 309 |
| 2.1.1 | The Data Input File | 309 |
| 2.2 | Data File Manipulation | 311 |
| 2.2.1 | Simulation Data | 312 |
| 2.2.2 | Program Data | 312 |
| 2.2.3 | Fluid Data | 312 |
| 2.3 | PVT Simulations | 312 |
| 3 | Introduction to the Simulation Model and Material Balance Calculations | 315 |
| 3.1 | Simulation of Material Balance | 316 |
| 3.1.1 | Organization of The Simulation Program | 316 |
| 3.1.2 | The Data Input-File | 318 |
| 3.2 | Data-File Manipulation | 321 |
| 3.3 | Plotting of Production Data | 323 |
| 3.4 | Plotting of Pressure Data | 323 |
| 3.5 | Water Influx and Water Production | 323 |
| 3.6 | Aquifer Type, Form and Size | 324 |
| 4 | Project Exercise: Material Balance and Interpretation Methods | 327 |
| 4.1 | History Matching and Predictive Performance | 327 |
| 4.2 | The Base Case Model | 328 |
| 4.3 | p/z Interpretation Method | 328 |
| 4.4 | The Havlena - Odeh Interpretation Method | 329 |

| | | |
|----------|--|------------|
| 5 | Project Exercise: Radial Gas Flow | 333 |
| 5.1 | Simulation of Radial Gas Flow | 333 |
| 5.1.1 | Organization of The Simulation Program | 333 |
| 5.1.2 | Data Input File | 335 |
| 5.2 | Simulation of Semi Steady-State Period | 338 |
| 5.3 | Simulation of Single Phase Gas Flow | 339 |
| 5.4 | The Effect of Reservoir Permeability on Bottom Hole Pressure | 340 |
| 5.5 | Well Skin and Bottom Hole Pressure | 341 |
| 5.6 | The Effect of Shape-Factor and Non-Darcy Flow | 341 |
| 6 | Project Exercise: Well Bore Flow | 343 |
| 6.1 | Simulation of Well-Bore Flow | 344 |
| 6.1.1 | Organization of The Simulation Program | 344 |
| 6.1.2 | The Data Input-File | 344 |
| 6.2 | General pressure solution and pressure uncertainty | 349 |
| 6.3 | Pressure Developments | 351 |
| 6.4 | Well Bore Flow Conditions | 352 |
| 7 | Project Exercise: Natural Depletion | 353 |
| 7.1 | Simulation of Natural Gas Reservoirs | 353 |
| 7.1.1 | Organization of The Simulation Program | 353 |
| 7.1.2 | The Data Input-File | 356 |
| 7.2 | Tubing Flow Performance and Bottom-Hole Pressure | 360 |
| 7.3 | Multi Well and Multi Block Simulation | 361 |
| 7.4 | Well Deliverability | 361 |
| 7.5 | Gas Production From 3 Independent Reservoir Blocks | 363 |
| 8 | Project Exercise: Field Simulation | 367 |
| 8.1 | General Reservoir Description | 367 |
| 8.2 | Description of Parameters | 368 |
| 8.3 | Drainage Strategies | 370 |

Part I
Lecture Notes

Chapter 1

Gas Reservoirs

Reservoir engineers should have a good understanding and appreciation for the nature of the main object in natural gas reservoir engineering, i.e. *the reservoir*. This is primarily the domain of production geology, or more rightfully, the branch of petroleum geology that deals with the geological aspects of hydrocarbon reservoirs.

After a short introduction about the importance of natural gases as the fuel of tomorrow, we shall in this chapter briefly review basic properties and dynamic behavior of reservoir rocks of direct relevance for gas reservoir engineering. For further reading on the geology of gas and oil reservoirs, see various textbooks like e.g. "Elements of Geology" [5]. In addition we would like to introduce the reader to some basic considerations and definitions, which forms a basis for further reading of subsequent chapters [11].

1.1 Natural Gas - The Fuel of Tomorrow

Natural gas is viewed as the compelling next fuel of choice and as a necessary stepping-stone in to the future, towards the hydrogen society [3]. The transition to natural gas as the fuel of tomorrow, superior to coal, oil and nuclear in economic attractiveness and environmental concerns, is already an ongoing process. This awareness is rising in the world of today where the expected world energy demand growth for the next 20 years, is at an annual rate of more than 3% for natural gas in particular [10].

We believe now that we are entering the "Age of Energy Gases" [7] and that in a not to distant future, the consumption of energy gases will surpass both coal and oil and possibly have captured more than 70% of the global energy market. This will be possible since natural gas is likely, by far, the Earth's most abundant hydrocarbon, exceeding in quantity both coal and oil. Conventional wisdom tells us that natural gas resources rank third behind coal and oil. Studies of the origins of natural gas, the abundance of methane in the solar system, the known and yet unknown resources of natural gas in the Earth's crust, and the vast quantities of methane trapped in hydrates, challenges the old thinking about the hierarchy of energy resources.

Natural gas production and trade will be greatly enhanced in the next decades in the form of liquid natural gas (LNG), compressed natural gas (CNG), other conversions such as gas to power (GTP) and gas to liquid (GTL) and even chemical transformations to such as methanol and others. In the past, natural gas trade has been quite limited

relative to oil because many of the potential producers have not pursued identification of their reserves through exploration and drilling. There has therefore always been a significant disparity between proven reserves and potential reserves in the domain of natural gas. Said more directly; search for hydrocarbon has always been synonymous with search for oil, where gas has been part of the bargain.

1.2 Reservoir Rocks

Virtually all reservoir rocks are of sedimentary origin. All sedimentary rocks have been formed by either mechanical deposition of erosion fragments of older rock or by chemical or organic precipitation. Sedimentary rocks may be broadly classified as *sandstones*, *carbonates* and *shales*. Shale is the most abundant of the sedimentary rocks and it makes up roughly 50% of the world's sedimentary rocks. Sandstone and carbonate rocks constitute about 25% and 20%, respectively [6].

Sandstones are fragmentary rocks consisting of sand grains. The main mineral constituent of sandstones is quartz. In addition, sandstones may contain varying amounts of clay minerals, feldspar, calcite and other rock fragments.

Carbonates are predominantly composed of calcite and dolomite, with clay and quartz as common secondary minerals. Carbonates can be both fragmentary and precipitated rock. If the main mineral is calcite, carbonate rock is referred to as *limestone*. Dolomite rock is almost always a secondary rock, formed from limestone by replacement in part of the calcium in limestone by magnesium, a process called *dolomitization*.

Shale consists of compacted beds of clay and other fine grained minerals. Shales are generally tight and impervious rocks that do not classify as reservoir rocks. Yet shales are very important in connection with hydrocarbon reservoirs. Shales often provide the sealing *cap-rock* for sandstone or carbonate reservoirs. Secondly, shale streaks and intercalations are very common in hydrocarbon reservoirs and may have profound effect on the flow characteristic of reservoirs. But perhaps most importantly, shales may contain considerable amount of hydrocarbon source rock material, which given the right maturation time and temperature could generate hydrocarbons.

1.2.1 Source Rock and Generation of Petroleum [11]

Local large concentrations of organic matter in sedimentary rocks, in the form of coal, oil or natural gas are called *fossil fuels*.

Many hypotheses concerning the origin of petroleum have been proposed over the years. One the most favored ones, is that oil and gas are formed from marine *phytoplankton* (microscopic floating plants) and to a lesser degree from algae and foraminifera [9]. In the ocean, phytoplankton and bacteria are the principal components of organic matter buried in sediment. Most of organic matter is trapped in clay mud that is slowly converted into shale under burial. During this conversion, the organic compounds are transformed (mainly by geothermal heat) into *petroleum*, defined as gaseous, liquid or semisolid natural substances that consist mainly of hydrocarbons.

In terrestrial sedimentary basins, it is plants such as trees, bushes, and grasses that contribute to most of the buried organic matter in mud rocks and shales. These large

plants are rich in *resins*, *waxes*, and *lignins*, which tend to remain solid and form coal, rather than petroleum.

Many organic carbon-rich marine and lake shales never reach the burial temperature level at which the original organic molecules are converted into hydrocarbons, forming oil and natural gas. Instead, an alteration process is causing certain wax-like substances with large molecules. This material, which remains solid, is called *kerogen*, and is the organic substance of so-called *oil shales*. Kerogen can be converted into oil and gas by further burial, when subjected to heat and time.

Petroleum is therefore generated when kerogen is subjected to a sufficient high temperature in the process of sediment burial. The alteration of kerogen to petroleum is similar to other thermal-cracking reactions, which usually require temperatures greater than 60°C , preferably between 150 to 170°C . At lower temperatures, during the early diagenesis, a natural biogenic methane called *marsh gas*, is generated through the action of microorganisms that live near the ground surface.

A temperature range between 60°C to 175°C is most favorable for the generation of hydrocarbons, and is commonly called the *oil window*. See Figure 1.1.

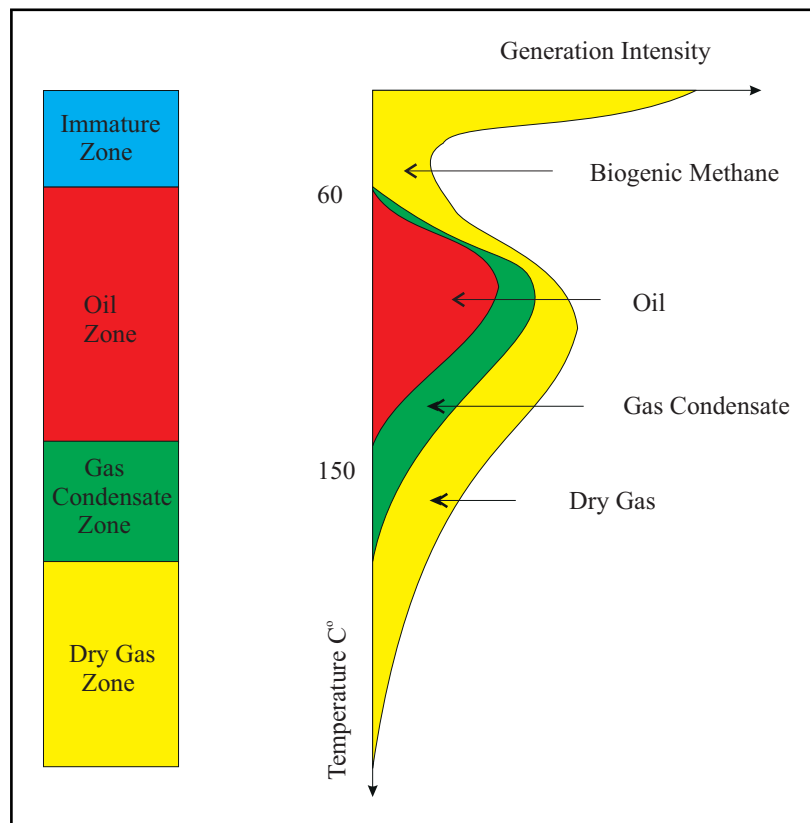


Figure 1.1: Generation of petroleum vs. burial temperature, commonly called the *oil window*.

At temperatures above about 150°C , the generation of liquid petroleum ceases and the formation of gas becomes dominant. When the formation rock temperature exceeds about 225°C , most of the kerogen will have lost its petroleum-generating capacity, as

illustrated by Figure 1.1.

The long and complex chain of chemical reactions involved in the conversion of raw organic matter into crude petroleum is called *maturation*. Additional chemical changes may occur in the oil and gas, even after these have been generated and accumulated. This explains, for example, why the petroleum taken from different reservoirs has different properties (compositions), despite a common source rock. Likewise, primary differences in the source composition may be reflected in the chemistry of the petroleum.

Two types of evidence support the hypothesis that petroleum is a product of the decomposition of natural organic matter [9],

- oil has the optical properties of hydrocarbons that are known only to derive from organic matter and
- oil contains nitrogen and certain other compounds that are known to originate from living organic matter only.

Oil source rocks are chiefly marine shales and mud rocks. Sampling of mud from the continental shelves and along the bases of continental slopes have shown that the shallowly buried mud contains up to 8% organic matter. Similar or even higher total organic-carbon content characterizes many ancient marine shales. Geologists conclude therefore that oil and gas have originated primarily from the organic matter deposited in marine sediments.

It is a fact that most of the world's largest hydrocarbon fields are found in marine sedimentary rock successions representing ancient continental shelves. However, some lake sediments may be just as oil-prone as marine source rocks. Many oil fields in various parts of the world are in ancient lacustrine deposits (formed at the bottom or along the shore of lakes, as geological strata). For further reading on geological aspects of gas reservoirs, see "Om Olje" (in Norwegian) [4].

1.2.2 Petroleum Migration and Accumulation

The accumulation of petroleum occur in only those areas, where geological conditions have provided the unique combination of both hydrocarbon prone source rocks and hydrocarbon traps.

Hydrocarbons are less dense than water. Once released from the source rock, they thus tend to migrate upwards in the direction of minimum pressure, until they either escape at the ground surface, or hit an impervious barrier i.e. a *cap rock*, called a *trap*.

In a trap, the oil and gas accumulate by displacing pore water from the porous rock. The cap rock may be imperfectly sealed, which means that gas and possibly also some oil may "leak" to yet higher lying traps or up to the ground surface. The part of the trap that contains hydrocarbons is called a *petroleum reservoir*.

Water generally underlaying the hydrocarbons in a trap. The water bearing part of the trap is called an *aquifer*, and is normally hydrologically connected to the reservoir. This means that any pressure change in the aquifer will also affect the reservoir as a whole. Depletion of the reservoir will therefore often make the aquifer expand into the space previously occupied by oil and/or gas.

Both oil and gas are generated together, in varying proportions, from a source rock. This may result in a primary gas cap above the oil in the reservoir. If a tight cap rock is overlaying the reservoir, further migration is halted and the hydrocarbons are trapped and a petroleum reservoir is formed.

At temperatures above 60 to 70 °C further generation of oil and gas from the source rock may take place, but also other chemical processes becomes active. Further temperature increase due to e.g. basin burial, chemical diagenesis will lead to precipitation of quartz grains and formation of mica/illite within the pore space [1]. These processes are common for all parts of the reservoir, not only the petroleum reservoir but also the aquifer underlying the reservoir, - in general the whole basin. The quartz cementation will in turn reduce pore space and lead to increased pore pressure. Even though the loss of porosity is very low locally, the fact that it takes place throughout the whole basin, leads to a significant increase in pore pressure.

Since the gas will have a lower density than the oil and the oil a lower density than the aquifer water, gas pressures are higher than oil pressures, which again are higher than water pressures (at equal elevation), where pressures generally will decrease upwards towards the cap rock. See Figure 1.2.

The overpressure in the reservoir, created by the cementation process, will gradually reduce the pressure difference between the gas - and oil phase, below the cap rock and the lithostatic overburden pressure present in the cap rock. If the general pore pressure in the reservoir increases such that the gas pressure exceeds the overburden pressure, gas will hydraulically fracture the cap rock and penetrate upwards and into layers above [8]. The gas will lead on, followed by the oil and this process will continue as long as porosity is reduced by cementation. As the volume of gas and oil is increased due to formation, migration and accumulation processes in the reservoir, the gas (and oil) pressure at the cap rock will also increase, as depicted in Figure 1.2.

When gas and oil migrate upward through cap rocks by hydraulic fracturing, permeability are created in previously non-permeable rocks, as a result of increasing overpressure in the reservoir. These processes will continue as long as porosity is reduced due to cementation and may eventually lead to migration patterns leading the oil and gas far away from the source rock.

Under accumulation and formation of a petroleum reservoir, the hydrocarbon fluids are in either a single-phase or a two-phase state. The single phase may be a liquid phase in which all the gas present is dissolved in the oil. There are therefore dissolved gas reserves as well as oil reserves to be estimated. On the other hand, the single phase may be a gas phase. If there are hydrocarbons vaporized in this gas phase which are recoverable as liquids on the surface, the reservoir is called a gas-condensate. In this case there are associated liquid (condensate or distillate) reserves as well as the gas reserves to be estimated. Since the liquid part compressed into the gas phase in gas-condensate reservoirs, these reservoirs are normally found where overpressure is high.

When the accumulation is in a two-phase state, the vapor phase is called the gas cap and the underlying liquid phase, the oil zone. In this case there will be four types of reserves to be estimated: the free gas cap gas, the dissolved gas, the oil in the oil zone and the recoverable liquid from the gas cap.

In summary, several factors are required for the formation of a petroleum reservoir.

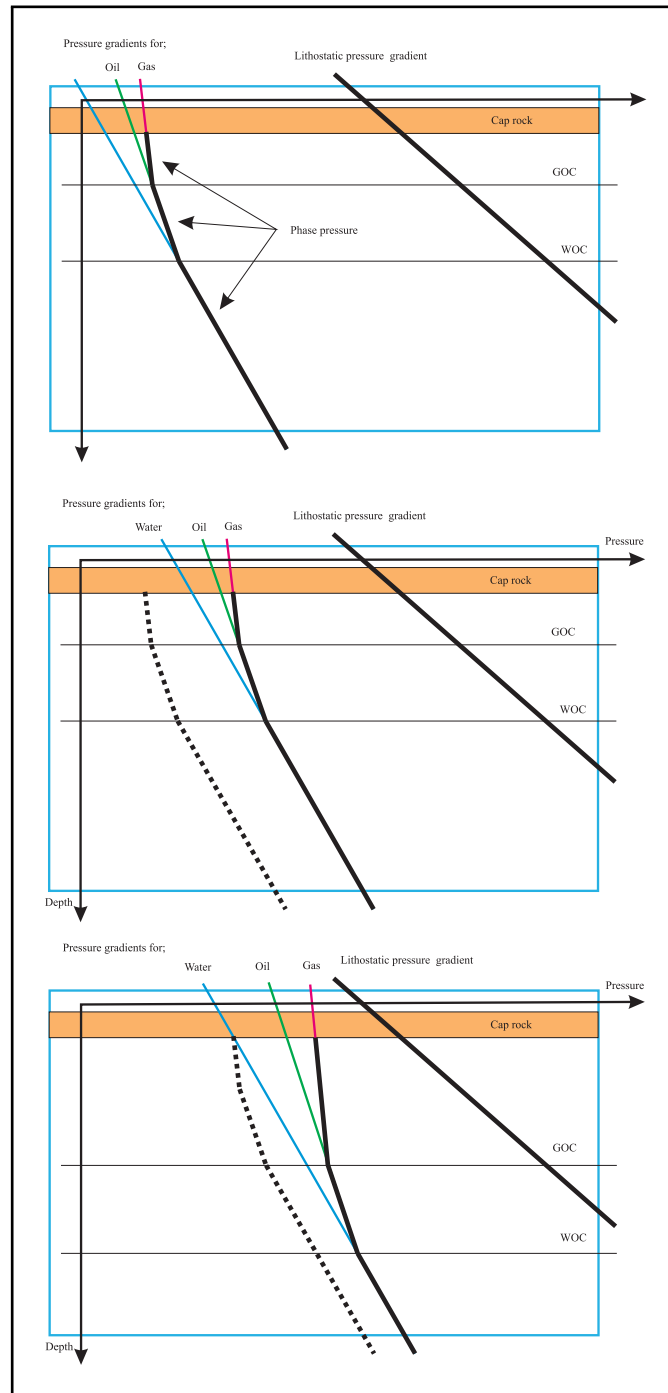


Figure 1.2: Static pressure distribution in the reservoir; Upper: initially (after formation of oil and gas), Middle: after a period with increasing pore pressure due to cementation and Lower: after both pore pressure increase and formation of additional oil and gas. The dotted line refers to the above gas pressure curve.

1. There must be a *source rock*, preferably rich in primary organic matter (carbon-rich marine or lacustrine shale). This source rock must be deeply buried to reach efficient temperatures to cause the organic matter to mature and turn into petroleum.
2. There has to be a *migration* pathway that enables the shale-released petroleum to migrate in a preferential direction.
3. There must be a *reservoir rock* that is sufficiently porous and permeable to accumulate the petroleum in large quantities.
4. There must be a *trap* closed by a *cap rock* that is sealed sufficiently to withhold the petroleum. Otherwise, the majority of petroleum will bypass the porous rock towards layers above, be dispersed or escape to the ground surface.
5. An impermeable *seal* or cap rock, is critical in preventing the petroleum from leaking out from the reservoir or escaping to the surface.

If any of these key factors are missing or inadequate, a petroleum reservoir field cannot be formed.

Finally, a large isolated reservoir or group of closely adjacent reservoirs is referred to as an oil or gas field.

1.2.3 The Golden Zone

When the pore pressure in sedimentary basins is measured against the depth of burial one observes an increasing pressure gradient that is larger than the normal hydrostatic pressure gradient. This observation is made for all sedimentary basin and is considered a characteristic feature of individual basins, related to sedimentary processes, history of sedimentation, age and size (volume) of the basins. Figure 1.3 Left, shows the pressure profile as function of depth for three different sedimentary basins. The depth where the overpressure is observed differs from basin to basin and can normally not be predicted.

If the pressure is compared to the temperature in the reservoir, as seen in Figure 1.3 Middle, all curves seems to overlap. Temperature is therefore a more interesting parameter in comparing different reservoirs, than the depth of burial. From the figure, it is clear that the temperature relates to the pore pressure in the same way for all sedimentary basins. If we would know the temperature we would also know the pressure, irrespective of the type and size of basin.

The above observation has led the geoscientists to believe that when source rocks are buried deep enough for the temperature to raise above $150C^{\circ}$ generation of oil and gas have already taken place. At such low depths the pore pressure would become similar to the formation hydraulic fracturing pressure and oil and gas may escape to lower depths through fractures generated in the cap rocks. The migration paths may lead the hydrocarbons to formation traps which are at a lower depths and temperatures.

Some hydrocarbons will migrate quite high up in the structure, but normally not higher than the temperature to be less than $60C^{\circ}$, as the porosity reduction due to cementation is less effective at lower temperatures and will eventually come to a halt. At temperatures lower than $60C^{\circ}$ it normally is assumed that micro-organisms will have

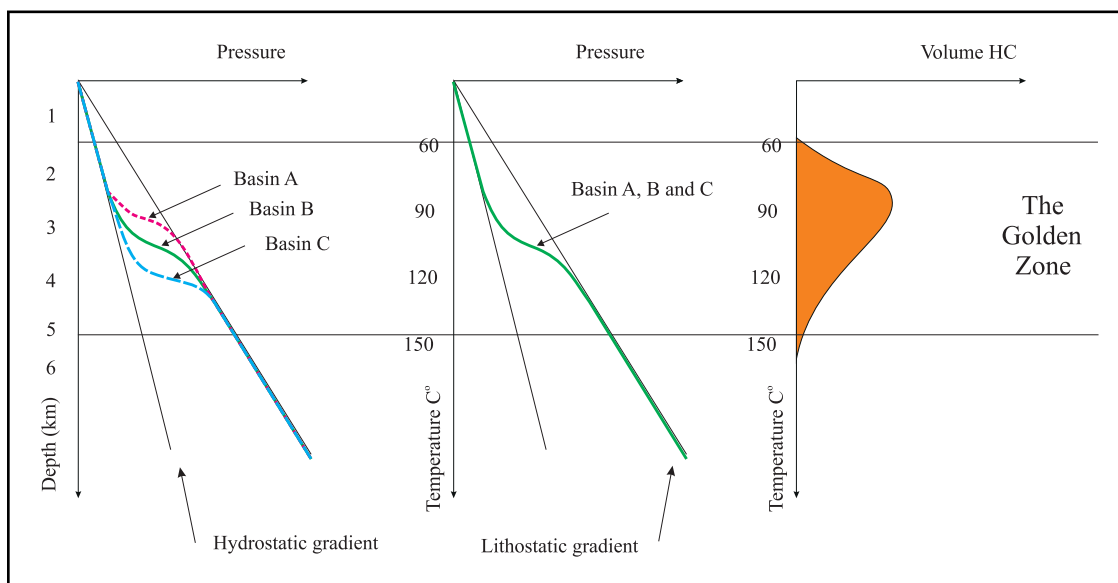


Figure 1.3: Left: Basin pressure profile as function of burial depth. Middle: Basin pressure profile as function of temperature. Right: Hydrocarbon reservoir volume as function of temperature.

consumed most of the hydrocarbons at these shallow depths. For layers deeply buried and later uplifted this may not be true, as oil or gas in these layers may still exist since all micro-organisms would generally be killed at lower depths and higher temperatures.

From geochemical experiments it is proven that gas is generated at higher temperatures than oil. The gas migration routes are therefore longer than for oil and the probability for entrapment at higher depths is higher for gas compared to oil. This is exactly what is observed in nature, where gas reservoirs are found at somewhat higher depths than oil reservoirs.

From these considerations, it is clear that hydrocarbons are generally found at temperatures higher $60C^{\circ}$ and lower than about $150C^{\circ}$. This temperature zone is called *The Golden Zone* and is the accumulation zone for hydrocarbons in all types of basins, irrespective of actual burial depths.

1.3 Gas and Oil Reservoirs

A reservoir is that portion of a trap which contains oil and/or gas as a single hydraulically connected system. Many hydrocarbon reservoirs are hydraulically connected to various volumes of water bearing rock, called aquifers. Many reservoirs are located in large sedimentary basins and share a common aquifer. In this case the production of fluid from one reservoir will cause the pressure to decline in other reservoirs by fluid communication through the aquifer. In some cases an entire trap is filled with oil or gas, and in this case the trap and the reservoir are the same.

Oil and gas are displaced through wells by mainly four processes [2];

- fluid expansion,

- fluid displacement, natural or artificial,
- gravitational drainage, and /or
- capillary expulsion.

Where there is no aquifer and no fluid is injected into the reservoir, the hydrocarbon recovery is brought about mainly by fluid expansion. However, in the case of oil this may be materially aided by gravitational drainage. When there is water influx from the aquifer or water is injected into selected wells, recovery is accomplished by the displacement mechanism, which again may be aided by gravitational drainage or capillary expulsion.

Gas is also injected as a displacing fluid to help in the recovery of oil, and is also used in gas cycling to recover gas condensate fluids. In many reservoirs all four recovery mechanisms may be operated simultaneously, but generally one or two predominate. During the producing life of a reservoir the predominance may shift from one mechanism to another, either naturally or because of operations planned by engineers. For example, a volumetric reservoir (no aquifer) may produce initially by fluid expansion. When its pressure is largely depleted, it may produce to wells mainly by gravitational drainage, the fluid being lifted to the surface by pumps. Still later, water may be injected in some wells to drive additional oil to other wells. Such a process is commonly called water flooding or secondary recovery. In this case the cycle of the mechanisms is expansion gravitational drainage displacement. There are, of course, many alternatives in these cycles, and it is the object of reservoir engineering to plan these cycles for maximum recovery, usually in minimum time and at minimum cost.

1.4 Recoverable Reserves

One of the main responsibilities in reservoir engineering is the estimation of the recoverable reserves of natural gas reservoirs, i.e. the recovery of dry gas and liquid condensate, that can be recovered from that reservoir by means of a specified recovery method. Recoverable dry gas reserves are commonly expressed in volume at standard conditions, in cubic meters. Recoverable condensate reserves are expressed in volume at *stock tank conditions* in cubic meters.

The recoverable reserves of a gas reservoir are a measure of its economical value. The magnitude of the recoverable reserves determines whether a gas accumulation can be economically exploited. Recoverable reserves data are required by government and regulatory agencies, banks and investment firms involved in the financing of natural gas development projects, and finally also by the gas purchasing and distribution company with which a gas sale contract is to be concluded.

The recoverable reserves are the product of the amount of gas and liquid initially present in the reservoir, commonly referred to as the *gas initially in place*, GIIP and the *liquid condensate initially in place* LIIP. Secondly, the recoverable reserves is the recovery efficiency defined as the fraction of the GIIP and LIIP that is recoverable

$$G_{pa} = \epsilon_{pa} G_{GIIP}, \quad (1.1)$$

where the subscript pa is the *pressure at abandonment*. ϵ_{pa} is then the recovery efficiency of gas at the abandonment pressure.

Similarly the liquid recovery is defined

$$G_{L,pa} = \epsilon_{L,pa} G_{LIIP}. \quad (1.2)$$

Determination of the recoverable reserves partly also rely on the recovery process, by which we will mainly consider the *volumetric method*. In this method the GIIP and LIIP are based on the estimation of the pore volume of the reservoir rock occupied by the hydrocarbon. The volumetric GIIP is then given by

$$G_{GIIP} = V_b \bar{\phi} (1 - \bar{S}_w) / B_{gi}, \quad (1.3)$$

where V_b is the bulk volume of the reservoir. $\bar{\phi}$ and \bar{S}_w is the average porosity and initial water saturation, respectively and B_{gi} is the gas formation volume factor at initial pressure.

The associated LIIP follows from the GIIP

$$G_{LIIP} = R_{VLG,i} G_{GIIP}, \quad (1.4)$$

where $R_{VLG,i}$ is the volumetric condensate-gas ratio at initial reservoir pressure.

The volumetric method is used in the appraisal and early development stages. In the later stages of reservoir development, the GIIP and LIIP may also be estimated by the material balance method, in which use is made of observed reservoir performance.

As we infer from Eqs. 1.1 to 1.4, the estimation of the recoverable reserves by the volumetric method amounts to the successive calculation of the following quantities. In the order as indicated, we get

$$\begin{aligned} \text{Bulk volume of gas reservoir} &\Rightarrow V_b \\ \text{Pore volume} &\Rightarrow V_p = V_b \bar{\phi} \\ \text{Hydrocarbon pore volume} &\Rightarrow V_{HC} = V_p (1 - \bar{S}_w) \\ \text{Gas initially in place} &\Rightarrow G_{GIIP} = V_{HC} / B_{gi} \\ \text{Condensate initially in place} &\Rightarrow G_{LIIP} = R_{VLG,i} G_{GIIP} \\ \text{Recoverable reserves} &\Rightarrow G_{gas,pa} = \epsilon_{gas,pa} G_{GIIP} \text{ and} \\ &G_{oil,pa} = \epsilon_{oil,pa} G_{LIIP} \end{aligned}$$

References

- [1] Per Arne Bjørkum and Paul H. Nadeau. Temperature controlled porosity/permeability reduction, fluid migration, and petroleum exploration in sedimentary basins. *APPEA*, 38(Part 1):453–464, 1998.
- [2] B.C. Craft and M.F. Hawkins. *Applied Petroleum Reservoir Engineering*. Prentice-Hall, INC, 1991. ISBN: 0130398845.
- [3] M.J. Economides, A.S. Demarchos, and L. Saputelli. Energy Sources and Energy Intensity for the Twnty-Firs Century. (SPE75504). Prepared for presentation at the SPE Gas Technology Symposium held in Calgary, Alberta, Canada, 30 April - 2 May, 2002.
- [4] E. Egeland, K. Kirkemo, R. Kirkhus, O. Minsaas, R. Seland, and E Sjulsen. Om Olje. Technical report, Elf Petroleum Norge AS, 1994.
- [5] Jacques Guillemot. *Elements of Geology*. Editions Technip, Institut Francais du Petrole, 1991. ISBN 2-7108-0699-1.
- [6] Jacques Hagoort. *Fundamentals of gas reservoir engineering*, volume 23 of *Developments in Petroleum Science*. Elsevier, 1988.
- [7] Robert A. Hefner. The Age of Energy Gases in the New Millennium. Technical report, The GHK Company, Oklahoma City, Oklahoma USA, 2002.
- [8] P.H. Nadeau, P.A. Bjørkum, and Walderhaug O. Petroleum systems analysis: impact of shale diagenesis on reservoir fluid pressure, hydrocarbon migration, and biodegradation risks. *Petroleum Geology*, pages 1267–1274, 2005. North-West Europe and Global Perspectives - Proceedings of the 6th Petroleum Geology Conference.
- [9] B.J. Skinner and S.C. Porter. *The Dynamic Earth (An introduction to physical geology)*, volume 4. edition. John Wiley and Sons (WIE), 2000. ISBN: 0471161187.
- [10] Arlie M. Skov. World Energy Beyond 2050. *Journal of Petroleum Technology*, Januar 2003.
- [11] A.B. Zolothukhin and J.R. Ursin. *Introduction to Petroleum Reservoir Engineering*. Høyskoleforlaget, Norwegian Academic Press, 2000. ISBN 82-7634-065-2.

Chapter 2

Gas Characteristics and PVT-relations

Knowledge about natural gas characteristics and PVT-relations are important when considering optimum depletion processes. The phase behavior of gas condensates are much more complex than that of conventional dry gases. Dry gases contain primarily methane and thus remain as a single phase fluid, all the way from reservoir to surface (standard) conditions. Methane is the main constituent of natural gases, while rich gas condensates will contain significant amounts of more heavy hydrocarbon compounds. The presence of higher hydrocarbon compounds in gas condensates may lead to liquid condensation in the reservoir and consequently to loss of hydrocarbon production.

Water is always present in off-shore gas production. Water vapor, connate water and aquifer water, are all natural compounds of gas production. Water is separated from the gas and normally not reported as part of the natural gas composition.

The changing (declining) pressure and temperature encountered in the production of natural gases may lead to liquid precipitation in the reservoir and to complex phase behavior phenomena in natural gas systems. The PVT behavior of natural gases is therefore of particular interest when gas production is estimated. For further reading on this subject consult classical textbooks on gas engineering [4, 5, 6, 1].

This chapter gives a qualitatively presentation of PVT-relations and phase behavior related to natural gas depletion. We will address the more quantitative aspects of the same processes in the next chapter.

2.1 Gas Characterization

The main constituents of natural gases are volatile *paraffins* dominated by methane. Other compounds are *naphthenes* and *aromatics* and non-hydrocarbon compounds, such as carbon dioxide, nitrogen and hydrogen sulfide and others. Rare gases such as helium, argon and neon may also be present in minor quantities. Since water is always present in hydrocarbon formations, natural gas is normally saturated with water vapor.

Table 2.1: Some constituents of natural gases.

| Name | HC Component | Formula | MW <i>kg/k mol</i> | T_b K |
|------------------|--------------|-----------------|-----------------------|------------|
| Water | - | H_2O | 18.015 | 373.15 |
| Nitrogen | - | N_2 | 28.014 | 77.35 |
| Carbon Dioxide | - | CO_2 | 44.010 | 194.67 |
| Hydrogen Sulfide | - | H_2S | 34.082 | 212.80 |
| Methane | C_1 | CH_4 | 16.043 | 111.66 |
| Ethane | C_2 | C_2H_6 | 30.070 | 184.55 |
| Propane | C_3 | C_3H_8 | 44.096 | 231.11 |
| Iso-Butane | iC_4 | $i - C_4H_{10}$ | 58.123 | 261.43 |
| Normal-Butane | nC_4 | $n - C_4H_{10}$ | 58.123 | 272.65 |
| Iso-Pentanes | iC_5 | $i - C_5H_{12}$ | 72.150 | 300.99 |
| Normal-Pentanes | nC_5 | $n - C_5H_{12}$ | 72.150 | 309.22 |
| Hexanes | C_6 | C_6H_{14} | 86.177 | 341.88 |
| Heptanes | C_7 | C_7H_{16} | 100.204 | 371.58 |
| Octanes | C_8 | C_8H_{18} | 114.231 | 398.83 |
| Nonanes | C_9 | C_9H_{20} | 128.258 | 423.97 |
| Decanes | C_{10} | $C_{10}H_{22}$ | 142.285 | 447.30 |

2.1.1 Groups of Hydrocarbons

Hydrocarbon is a common name for chemical components that include hydrogen and carbon in the same molecule. Hydrocarbons are classified in different groups, depending on their chemical structure and properties. Hydrocarbon components are miscible and can move between gas and liquid states, all depending on pressure and temperature, and to some extent also on the molar composition. Liquid hydrocarbons can contain gas as natural gases can contain liquids.

Paraffins

Paraffins are also called *Alkanes* and contain only carbon and hydrogen bonds (single covalent bonds). The general formula for paraffins is C_nH_{2n+2} , see Table 2.1, where the carbon number is naming the hydrocarbon groups. Generally the boiling point and melting point are low for paraffins compare to other hydrocarbons (see table).

Paraffins are chemical stable and has therefore low tendency to react with other substances except oxygen. They are therefore used mostly as fuel, lubricants and solvents.

Alkenes

Alkenes have similar properties to those of Alkanes (Paraffins) except for a double bonded in the molecule. They contain two hydrogen atoms less than the Alkanes and are therefore referred to as "undersaturated". The general formula is C_nH_{2n} .

Alkenes are considerably more reactive than Alkanes and are therefore often used as feed for polymer production. Components with two or more double bounds are called Alkadienes, Alkatrienes, etc., depending on the number of double bonds.

Another important group of components are the Cyclic Aliphatic hydrocarbons, or the Naphtenes as they are also called. Their boiling- and melting points are somewhat higher than for Alkanes with the same carbon number. Their chemical reactivity is also higher than for Alkanes and they are often used as fuel or feed for petrochemical industry.

Aromatic

Aromatic components normally contain benzene, C_6H_6 , as building blocks. Benzene is a flat, hexagonal shaped ring structure with a lot of derivatives, such as toluene with a CH_3 -group attached to the ring structure. Aromatic components are normally poisonous. They form a lot of various components, some of which are used in the petrochemical industry.

The paraffinic, naphtenic and aromatic components are often called PNA groups. These groups may exist in various forms with the same molecular weight and number of atoms, so called isomers. Isomers differ by their molecular structure and they have slightly different properties, such as boiling points.

2.1.2 Components of Reservoir Gases

Table 2.1 shows the most frequent existing constituents of natural gases. Reservoir fluids may contain 100 to 1000 different components of which the tabulated components are the most common. Different hydrocarbon and non-hydrocarbon components are characterized by molecular weight and normal boiling temperature. Other parameters like critical temperature and -pressure are needed when phase behavior and equilibrium calculations are performed.

The weight of pure compounds are given in $kg/kmol$, i.e. *mol weight*. Mole is a basic SI-unit, describing the amount of substance. One mole of a gas is given as the number of gas molecules (elementary units) identical to the number of atoms contained in 12 grams of Carbon-12. The number of carbon atoms C_{12} in 12 grams is given by *Avogadros number*,

$$N_A = 6.022045 \cdot 10^{23} \frac{1}{mol}. \quad (2.1)$$

The lighter compounds in Table 2.1, i.e. methane, ethane, propane and butane have all boiling points below the standard temperature ($15^{\circ}C \simeq 288K$). These gases will therefore remain in the gaseous phase at surface conditions. Natural gases composed of such light components are normally called *Dry gases*. *Gas condensates* will contain larger fractions of heavier compounds and frequently heavier components than listed in the Table 2.1. The amount of heavier compounds will decide the degree of liquid condensation in the reservoir under natural depletion processes. *Wet gases* are Dry gases with additional fractions of heavier compounds. The characteristic of Wet gases are similar to Dry gases in the reservoir during production, in the sense that they all remain in a gas phase. At surface condition, wet gases will split into dry gas and liquid. Seen from a reservoir engineering point of view there is no real difference in the production of Dry - and Wet gases, as they both remain in single phase in the reservoir during natural depletion processes.

The heavier compounds such as Hexanes (C_6), Heptanes (C_7), \dots do all compose of different groups of hydrocarbons. Paraffins, Naphthenes and Aromatics are normally present in each of the compounds. Labeling Hexanes as a pure compound is therefore more convenient than correct. These heavier compounds are in reality *pseudo-compounds*, having similar characteristics such as molecular weight and bubble point temperature. The listing of heavier compounds are commonly shortened by grouping all heavier compounds into a *plus-fraction*. Natural gases are often presented by 7 or 10 hydrocarbon compounds. The heaviest compound, i.e. the plus-fraction (C_7^+ or C_{10}^+) is therefore a pseudo compound, representing all heavier compounds. A third class of pseudo-components is used in flash calculations in reservoir flow simulations, where the need of high speed calculation is a priority. In these situations, often no more than three components are used to describe the reservoir fluid, i.e. C_1 , C_2^* a combination of C_2 to C_6 and C_7^+ . In cases where non-hydrocarbon compounds are of importance for the phase behavior, pseudo-components are formed combining the characteristics of both classes.

A relatively high concentration of non-hydrocarbons in natural gases may cause additional problems in both producing and handling the gas. If the concentration of CO_2 is high, i.e. 10% or higher, the burning value of the gas is reduced. Such natural gases are called *low-calorific* gases. *Sour* natural gases contain significant amounts of H_2S . These gases cause even greater worries, due to corrosion and increased wear on physical equipment. The presence of N_2 in natural gases poses minor problems during production, other than reducing the commercial value of the gas.

The water compound is normally not specified as part of the composition of normal gas systems. The inherent water fraction of gas produced is quite small and of minor importance. On the other hand, if water is produced from reservoir water or aquifer, water production cuts can be quite high and in some cases fatal for continued gas production. Water as water vapor will always be in equilibrium with the gas in the reservoir. The amount of water contained in the gas is given by Dalton's Law, which states that the sum of partial pressures of water vapor and gas in the reservoir is equal to the reservoir pressure. Since the partial pressure of water in the reservoir is equal to the vapor pressure at reservoir temperature, the mol fraction of water vapor in the gas is therefore given by,

$$y_w = \frac{p_w(\text{vapor})}{p(\text{reservoir})}. \quad (2.2)$$

All gases behave ideally when the pressure approaches zero (becomes small enough). The pressure - volume relation for ideal gases, i.e. the Ideal Gas Law is,

$$pV_m = RT, \quad (2.3)$$

where V_m is the molar volume, p the absolute pressure and T is the absolute temperature. R is the universal gas constant, $R = 8341.41 \text{ Pa} \cdot \text{m}^3 / \text{k mol} \cdot \text{K}$.

In engineering applications most gases are considered to behave ideally at standard conditions. Hence, one mole of any (ideal) gas will occupy the same volume, namely V_m . The molar volume at standard conditions may vary according to the definition of standard conditions and units commonly used, is shown in Table 2.2.

Table 2.2: Molar volume of ideal gas at various standard conditions.

| Unit | Temperature | Pressure | Molar volume |
|--------|------------------|-----------|-----------------------|
| SI | 288 K | 1 atm | 23.664 $m^3/k\ mol$ |
| SI | 288 K | 100 kPa | 23.950 $m^3/k\ mol$ |
| Metric | 273.15 K | 1 atm | 22.414 $m^3/k\ mol$ |
| Field | 60.0 $^{\circ}F$ | 14.69 psi | 380 $ft^3/lb\ mol$ |
| Mixed | 60.0 $^{\circ}F$ | 1 atm | 379.51 $ft^3/lb\ mol$ |

Example: Associated water in gas production

Let us consider a gas well that is producing at a rate of 1 MSm^3/day at standard conditions, i.e. 15 $^{\circ}C$ and 1 atm. (1.01325 bar). The reservoir pressure is 300 bar and the reservoir temperature is 100 $^{\circ}C$.

The vapor pressure (boiling pressure) of water at a temperature of 100 $^{\circ}C$ is, as we all know, 1 atm. (water boils at 100 $^{\circ}C$ at natural or standard surface pressure). Following Dalton's Law, the mol fraction of water vapor in the gas mixture (gas and water vapor) is then; $y_w = 1/300$ or 1/3%.

From the principle of Corresponding States (see below) we know that 1 $kmol$ of gas at standard conditions occupies a volume of 23.664 m^3 . The molar volume of ideal gas is

$$V_m = 23.664\ m^3/k\ mol = 23664\ cm^3/g\ mol$$

A gas well rate of 1 MSm^3/day at standard conditions is equal to a molar rate,

$$q_{m,g} = (1\ MSm^3/day)/(23.664\ m^3/k\ mol) = 42258.28\ k\ mol/day.$$

The molar gas rate, $q_{m,g}$, is proportional to the mass rate and consequently invariant, from reservoir to standard conditions. The water molar rate $q_{m,w}$, is the relative molar fraction of water vapor to gas,

$$q_{m,w} = \frac{y_w}{1 - y_w} q_{m,g},$$

where we have used the fact that: $q_{m,w} = y_w q_m$ and $q_{m,g} = (1 - y_w) q_m$, and q_m is the total molar flow rate.

The water molar rate becomes, $q_{m,w} = 141.332\ k\ mol/day$. When the molecular mass of water is 18.015 $kg/k\ mol$, (see Table 2.1) and the density of water is 1000 kg/m^3 , then the water rate at standard conditions is therefore only; $q_w = 2.546\ m^3/day$.

2.2 Phases

Reservoir hydrocarbons exist as vapor, liquid and solid phases. Hydrocarbons in solid state are e.g. found in the northern parts of Canada, where huge shallow reservoirs of tar-sands are produced primarily through viscosity reducing techniques, like steam injection. Production of heavy hydrocarbons like tar (or asphalts) is facilitated during phase transition from solid to liquid using heat.

Similarly, phase transitions take place in the production of gas condensates as well as under production of saturated oils. Condensate gas is produced by liquid condensation when the reservoir pressure is reduced. Saturated oils will form a gaseous phase in the reservoir due to pressure decline. Two phases, i.e. gas and oil may co-exist under the same PT -conditions. A certain change in pressure and/or temperature can cause formation or disappearance of phases. The co-existence of gas and oil in the reservoir does not only occur as a result of declining reservoir pressure, it might also be a natural and stable phenomenon, as in the case of an oil reservoir with a gas cap.

Gas and oil do actually co-exist in the absence of changing pressure and temperature. Phase equilibrium between oil and gas is characterizing a state where no change will occur with time. The subdivision and composition of phases is the subject of phase behavior. When gas and oil co-exist under stable conditions, the phases are always saturated, i.e. the gas phase is "filled" with oil and the oil phase is "filled" with gas. The assumption of equilibrium between oil and gas in contact in a reservoir, is the prevailing situation in most engineering applications.

2.2.1 Gibbs Phase Rule

The state of equilibrium between gas and oil is completely defined when composition, temperature and pressure are specified. (We assume no influence by gravity, electrical- or magnetic forces, surface forces, etc.) Under these conditions, all intensive properties are fixed and identifiable. (The intensive properties are those which does not depend on the amount of substance, i.e. pressure, temperature, density, viscosity, compressibility, etc.)

At equilibrium a system may form several co-existing phases. Generally, a number of liquid, gaseous and solid phases in equilibrium can be formed. The number of independent variables needed to define such a system is determined by the *Gibbs Phase Rule* [2],

$$C + 2 - P = F, \quad (2.4)$$

where C is the number of components, P is the number of phases and F is the number of degrees of freedom.

For a single component system $C = 1$, the degrees of freedom are 3 minus the number of phases. A single phase system $P = 1$, has 2 degrees of freedom and can therefore exist at all possible temperatures and pressures. A two phase system $P = 2$, has only one degree of freedom. If either temperature or pressure is defined, the system equilibrium is determined. In a PT -diagram the state of equilibrium will fall on a line. See Figure 2.1. If three phases are defined, then the system has no freedom and equilibrium can only exist at the *Triple point* in the PT -diagram.

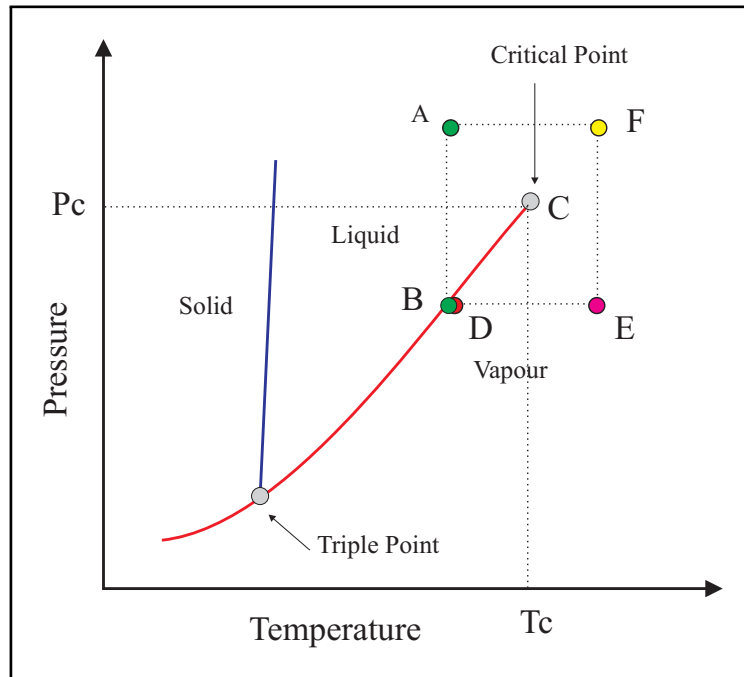


Figure 2.1: Pressure - temperature diagram of pure substance.

Let us characterize a multi component systems where $C > 1$, by looking at a binary system $C = 2$, involving vapor and liquid, i.e. gas and oil. The binary system has two pseudo components C_1^* and C_2^* , containing various hydrocarbon components forming a multi phase system. The system may exist in equilibrium either as pure gas, pure oil or as co-existing gas and oil (two-phase region). See Figure 2.2 and also 2.5. In the case of a binary system, where only one phase is present $P = 1$, the Gibbs Phase Rule tells us that there are 3 degrees of freedom. If temperature and pressure are determined, the system has only 1 degree of freedom left. If the last degree of freedom is defined by the composition in the two phases, i.e. the relative amount of gas to liquid, we may conclude that in a binary system, gas and oil can co-exist in equilibrium at different compositions. In the two-phase region $P = 2$, only 2 degrees of freedom exist. If we fix both temperature and pressure then the system becomes invariant. At a given temperature and pressure in the two-phase region, the composition is fully determined and the amount of C_1^* to C_2^* is fixed.

2.2.2 Single Component Systems

Single component systems have well defined boiling temperatures at a given pressure, e.g. water is boiling at 100°C at atmospheric pressure. If the pressure is increased, so will the boiling temperature. If the pressure is increased above a certain pressure, no boiling temperature can be found. There exist a phase boundary between water vapor and water liquid up to a certain pressure and temperature, called the *critical* pressure P_c and -temperature T_c . Above this critical point, two phases may no longer co-exist. The substance is in a super-state and the phase is called a fluid. The term fluid is often

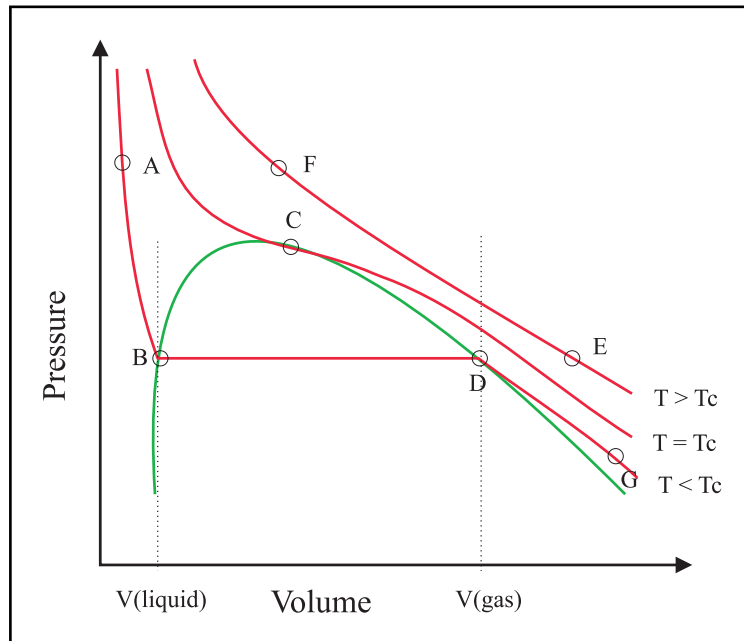


Figure 2.2: Pressure - volume diagram of pure substance.

used as a general term, meaning both gas and/or liquid.

Figure 2.1 shows the PT -diagram for a single component substance. C is the critical point of the system and may be defined as the highest pressure and temperature where the two phases, vapor and liquid, can co-exist. The transition from liquid to vapor in a pure component system is illustrated by the rectangular BAFED in Figure 2.1. The equilibrium between liquid and vapor is defined as a sharp line ending at the critical point. The phase transition from liquid to vapor can happen by increasing the temperature of the system, thus crossing the phase boundary from B to D . Alternatively, if the pressure and temperature is changed along the path of BAFED, the same transition from liquid to vapor is obtained. This last transition is done without crossing the phase boundary. Moving from a liquid phase to a vapor phase without crossing the phase boundary, above the critical point, demonstrates a need for an alternative definition of the system when it is not in a liquid or a vapor phase or alternatively, both in a liquid and a vapor phase at the same time. The one-phase region above the critical point is therefore often called the *fluid*-phase region.

Crossing the phase boundary from B to D , transform liquid to gas. The transition takes place at constant pressure and temperature but under a certain expansion of volume. Since a pure component can not exist in equilibrium in a two-phase region (when temperature and pressure are specified), as shown by the Gibbs Phase Rule, the expansion from liquid to gas is instantaneous. Figure 2.2 shows the PV -diagram of a pure substance. The phase transition from B to D is defined at a specified pressure and temperature, where the system can only exist in either point B or in point D .

Comparing the two figures shows that the line segment BD in Figure 2.2 is represented as a point in Figure 2.1. In a multi component system, this line segment will represent the two phase region, where vapor and liquid are in equilibrium. Above the

iso-term T_c in Figure 2.2, the system is defined as a one phase fluid. In the regions illustrated by the line segment AB and DG, the system is in pure liquid and gaseous state, respectively.

The critical point C , in Figure 2.1 and 2.2 is playing a key role in the characteristics of hydrocarbon systems. If we move along the constant critical pressure line ($P_c = \text{const.}$) or along the constant critical temperature line ($T_c = \text{const.}$) in Figure 2.1, we will finally end up at the critical point C . If the $P = P_c$ and the temperature is increasing, we would observe certain changes of the liquid. Equally we would observe the gas changing as pressure is increasing and $T = T_c$. At the critical point we would observe the same end state, regardless of the path chosen. The critical point is therefore a *conversion* point where physical properties of the system meet. The variation of saturated fluid density with temperature for a pure compound is shown in Figure 2.3. The density of vapor and liquid phases approach each other as the temperature increases and they become equal at the critical point. All differences between the phases are reduced as the system approaches this point. Indeed, all phases become the same and indistinguishable at the critical point.

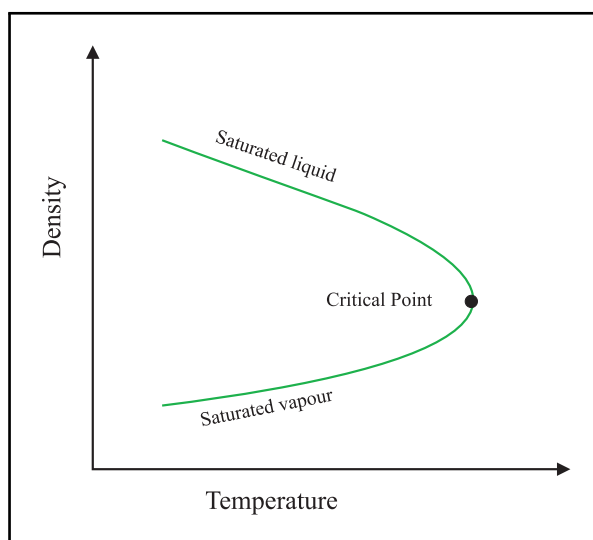


Figure 2.3: Variation of saturated fluid density with temperature.

All compounds show similar trend as depicted in Figure 2.3, i.e. vapor and liquid densities become equal at the critical point. Another definition of the critical point would be; - "the point where all intensive properties are equal". By intensive properties we mean all properties characterized by a system that are independent of the amount of material that is under consideration.

The critical pressure P_c and - temperature T_c for some frequent compounds in natural gases are given in Table 2.3.

2.2.3 Multi Component Systems

The phase behaviour of multi component systems are definitely more complex than that of pure compounds, but not necessarily particularly more complicated. Reservoir fluid

Table 2.3: Critical pressure and critical temperature for some typical natural gas compounds.

| Name | HC Component | Formula | P_c MPa | T_c K |
|------------------|--------------|-----------------|--------------|------------|
| Water | - | H_2O | 22.055 | 647.13 |
| Nitrogen | - | N_2 | 3.394 | 126.1 |
| Carbon Dioxide | - | CO_2 | 7.382 | 304.19 |
| Hydrogen Sulfide | - | H_2S | 8.963 | 373.53 |
| Methane | C_1 | CH_4 | 4.599 | 190.56 |
| Ethane | C_2 | C_2H_6 | 4.872 | 305.32 |
| Propane | C_3 | C_3H_8 | 4.248 | 369.83 |
| Iso-Butane | iC_4 | $i - C_4H_{10}$ | 3.648 | 408.14 |
| Normal-Butane | nC_4 | $n - C_4H_{10}$ | 3.796 | 425.12 |
| Iso-Pentanes | iC_5 | $i - C_5H_{12}$ | 3.381 | 460.43 |
| Normal-Pentanes | nC_5 | $n - C_5H_{12}$ | 3.370 | 469.7 |
| Hexanes | C_6 | C_6H_{14} | 3.025 | 507.6 |
| Heptanes | C_7 | C_7H_{16} | 2.740 | 540.2 |
| Octanes | C_8 | C_8H_{18} | 2.49 | 568.7 |
| Nonanes | C_9 | C_9H_{20} | 2.290 | 594.6 |
| Decanes | C_{10} | $C_{10}H_{22}$ | 2.110 | 617.7 |

systems are generally composed of hydrocarbons with similar structures and therefore maintain similar characteristic behaviour when mixed.

In multi component systems, the state of equilibrium between two phases can no longer be represented by a single line in a PT -diagram. Two lines are needed to form the phase boundary between the one-phase regions, i.e. liquid and vapor, and the two-phase region where co-existing phases are in equilibrium.

A binary mixture of ethane (C_2) and normal-heptane (C_7), as shown in Figure 2.4, can be used to demonstrate phase behaviour of hydrocarbons.

In the case of pure components, i.e. 100% ethane or heptane, we observe the characteristic single line, PT -behaviour of one component systems. When ethane is mixed with heptane in different mol-fraction, two-phase regions or envelopes are formed. Inside these envelopes, gas and oil co-exist in equilibrium. The shape of the envelope corresponds to the mol-fraction of the compounds. The mixture has a well defined critical point, which seems to move to higher temperatures as the fraction of the heavy component is increasing. The dotted line in Figure 2.4 indicates the path of the critical point as more and more heptane is added to the mixture. This is a general trend, valid for all mixtures of hydrocarbons, as well as for mixtures where typical non-hydrocarbons are present.

The shape of the two-phase envelope is dependent on the composition of the mixture; the number of components and the mol fraction and properties of each component. Inside the two-phase region, gas and oil co-exist at different iso-volumes, i.e. constant gas-to-liquid fractions. As given by Gibbs Phase Rule, Eq. 2.2, the quality of oil and gas is determined when P and T are fixed. The phase diagram of a multi component

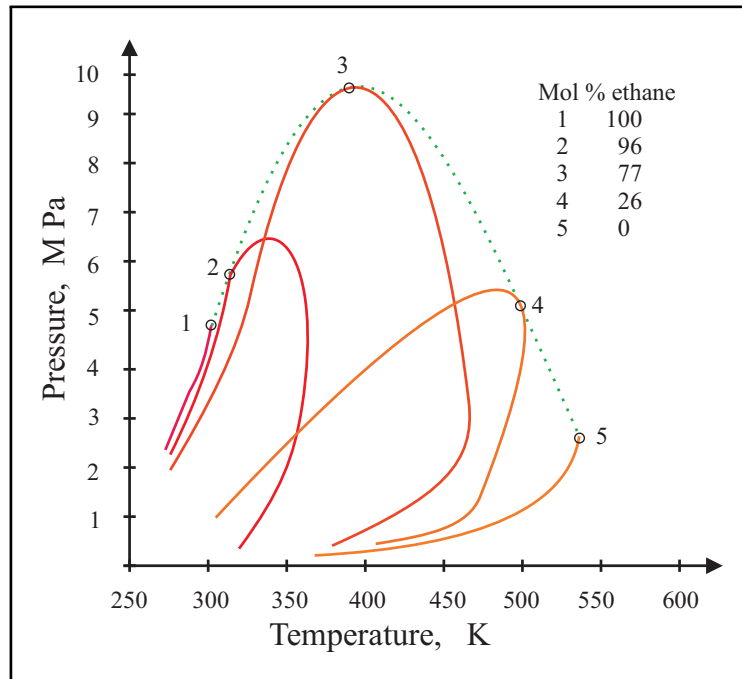


Figure 2.4: Phase diagrams of ethane - normal heptane mixtures.

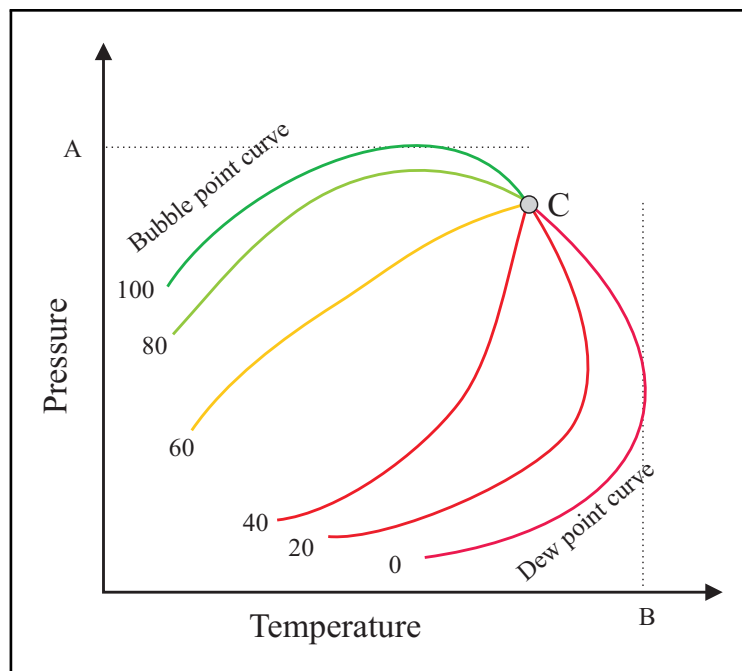


Figure 2.5: Phase diagram of a multi component mixture.

mixture is given in Figure 2.5. The iso-volumes or quality lines are given in percentage of pure liquid (oil). The 100% quality line is called the *bubble point curve* and the 0% curve is the *dew point curve*. In between these two quality lines, gas and oil are

in equilibrium. All quality lines meet at the critical point, where liquid and gaseous characteristics of the mixture converge.

The highest pressure at which gas and oil can co-exist is given by the *Cricondenbar* A and equally, the highest temperature is called the *Cricodentherm* B, in Figure 2.5.

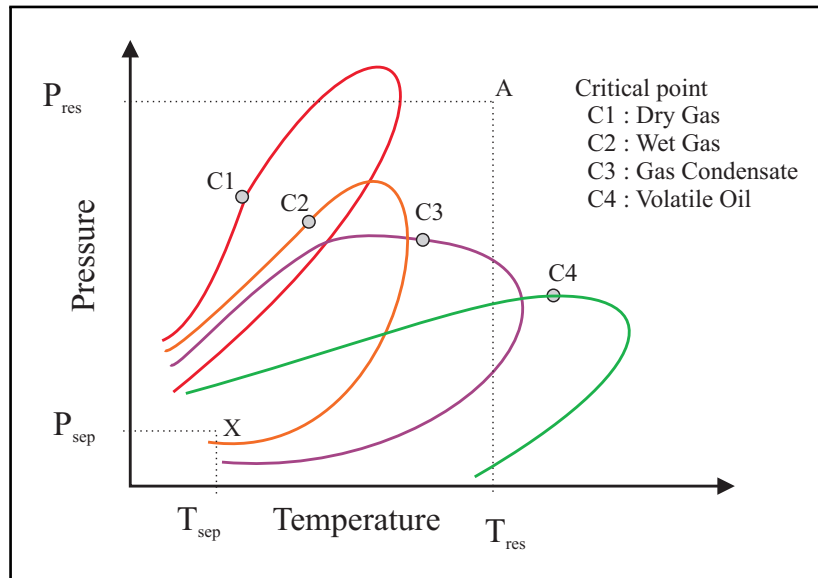


Figure 2.6: Phase behavior of dry gas -, wet gas - and gas condensate reservoirs.

Natural gases are defined according to reservoir temperature and pressure as well as to separator temperature and pressure, as shown in Figure 2.6. The subdivision of Dry gas -, Wet gas - and Gas condensate reservoirs are defined following the line of production from the reservoir to the (first) separator. If the gas remains gaseous (one phase) in the reservoir and the well, i.e. point A and X in Figure 2.6, are located outside the two-phase envelope, then we have a Dry gas reservoir.

Wet gas reservoirs behave similarly, in the sense that iso-thermal production (at reservoir temperature) never enters the two-phase region. Oil will finally condensate out, either somewhere in the well or connecting tube lines.

In gas condensate reservoirs, oil will drop out and lead to reduced hydrocarbon production under normal depletion condition. Liquidation will start when the pressure drops below the dew point pressure at reservoir temperature, i.e. entering the two-phase envelope in Figure 2.6. This will first happen in the close vicinity to the well, where the pressure is lowest. Liquid oil, occupying part of the pore volume will be a hinderance to gas flow. Progressively, when the saturation of oil has reached it's critical saturation for flow, oil will start to flow and two-phase flow in the reservoir will occur. Hydrocarbon gas production will be leaner as more oil drops out (condensate) in the reservoir. Seen from the well, more heavy components will drop out of the gas as the pressure decreases and this process will slowly evolve radially throughout the reservoir.

The difference between gas - and oil systems is demonstrated, by comparing the two-phase envelopes for gas condensates and volatile oils in Figure 2.6. Isothermal pressure reduction in the case of gas condensates will enter the two-phase region to the right of the critical point. In the case of oil systems, the two-phase envelope is entered to the

left of the critical point. In gas systems, the dew point curve is crossed while the bubble point curve is crosses, in case of oil systems, both as part of natural depletion processes.

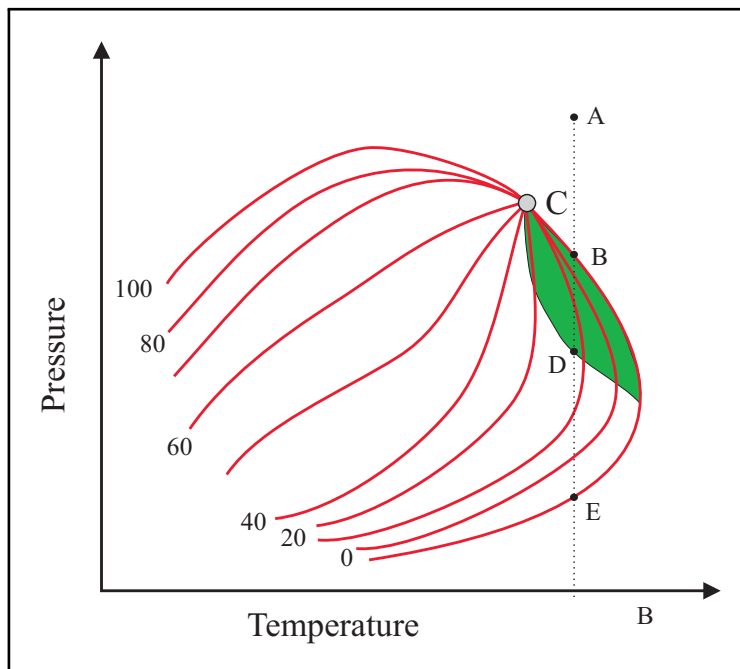


Figure 2.7: Retrograde condensation of gas condensate system.

A typical phase diagram of a gas condensate system is shown in Figure 2.7. The iso-volume lines are shown as function of liquid fraction, measured in percent. At the initial state, reservoir gas is in one phase. An isothermal reduction of pressure, starting at reservoir pressure A, forms the first drop of liquid in the reservoir at the dew point curve, at point B. Further reduction of pressure will result in continued condensation. At one point the 10% quality line is crossed and finally a maximum condensation of near to 23% liquid saturation is reached at point D. If pressure depletion is continued below this point re-vaporization will start. Along the pressure decline from D to E, liquefied gas will start to vaporize and finally at point E, no more liquid will remain in the reservoir. In most practical situations however, effective re-vaporization is complicated by secondary processes like i.e. wetting and smearing-out of the oil on the pore surfaces. It is therefore quite common to considered all liquids dropping out of the gas as lost production.

The shaded area of the two-phase envelope, where liquid condensation is taking place, is known as the *retrograde* region. The importance of this region is related to the loss of hydrocarbons due to liquid condensation; reduced gas well productivity, reduced hydrocarbon content in well flow and smearing out of liquid hydrocarbons in the reservoir due to capillary effects. Heavy hydrocarbons initially liquefied through condensation are in most cases permanently lost. Some fractions of the liquid volume may be recovered as part of normal gas production, but the greater part will remain in the reservoir.

The relative position of the critical point, related to the isothermal depletion line AE,

is of significant importance related to retrograde phenomena. The population (density) of iso-volume lines near to the critical point is rapidly increasing. If the composition of the gas fluid, presented by the critical point and the initial reservoir condition is close, i.e. the critical temperature of the gas fluid and the reservoir temperature are close, - then heavy condensation of the gas will take place during the normal depletion process. It is therefore quite critical to operate gas systems with critical temperatures close to the reservoir temperature, as these reservoirs often need special measures in form of e.g. pressure support in order to postpone the time when pressure is dropping below dew-point pressure and production of gas enters into the two-phase region.

2.3 Practical Aspect Of Gas Production

Dry gases contain primarily lighter hydrocarbons like C_1 and C_2 , where non-hydrocarbons can be N_2 , CO_2 or H_2S . Gas condensates contain in addition heavier compounds such as C_3 , C_4 , C_5 and C_6 . In some rich gas condensate, a significant fraction of heavier components are present. These compounds are often presented as a pseudo-component C_7^+ or C_{10}^+ .

It is the heavier components that constitute the liquid phase of the hydrocarbon production at standard condition. The fraction of heavy compounds is therefore directly related to the *gas-oil ratio*, GOR. Gas-to-oil ratios range between 570 to 30000 Sm^3/Sm^3 . For practical purposes; a gas reservoir that produces with a GOR above 10000 is considered to contain wet or dry gas. See also Table 2.6.

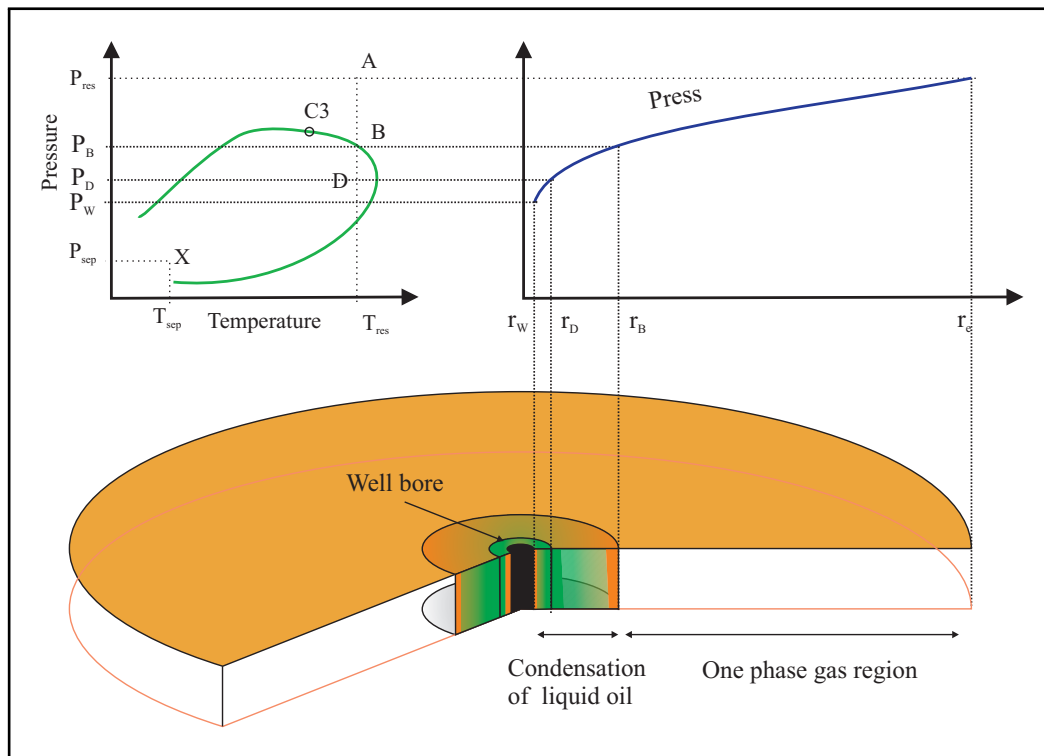


Figure 2.8: Liquid condensation close to the well-bore.

The liquid condensation process is depicted in Figure 2.8. At isothermal gas depletion, the reservoir pressure will eventually drop below the dew-point curve (see isothermal depletion curve A to D in Figure 2.8). The lowest reservoir pressure is always observed in the well. Thus, the reservoir liquid condensation does always commence in the closes vicinity of the well-bore. As the reservoir pressure continues to decline, more and more liquid is dropping out of the gas, further and further away from the well-bore.

Liquid production from gas condensate reservoirs is restricted at one end by the composition of hydrocarbons, where the fraction of heavier compounds C_7^+ or C_{10}^+ , often is directly proportional to the GOR. On the other end, liquid condensation will remove the heavier components from the gas, and make the gas leaner and thereby reduce liquid production. The optimum production of rich gas condensate reservoirs may therefore involve some additional pressure maintaining processes like gas - or water injection. The existence of aquifer can also be of great help. On the other hand, depletion of wet - and dry gas reservoirs is more a question of gas allocation, as pressure *blow down* is the recommended production strategy.

2.4 Molar Composition

The molar composition of a reservoir fluid plays an essential role in the development and definition of the various parameters needed in describing fluid transformation from reservoir to stock tank conditions.

We will here give four examples of fluids, taken from gas reservoirs in the North Sea, one dry-gas and three gas-condensate reservoirs. The molar composition from Frigg, see Table 2.4 and Figure 2.9, is an example of a dry-gas reservoir, while the molar composition of Sleipner Vest, Kvitebjørn and Gullfaks, are all examples of gas condensate reservoirs, even though both Gullfaks and Kvitebjørn, for all practical terms, can be considered as a wet-gas reservoir. Sleipner Vest should, in this context, be considered a light gas condensate reservoir.

Considering the molar compositions in Table 2.4, we observe that the Methane content in all four reservoir gases are considerable. Methane is, as seen, the principal component in all gases. A "typical" reservoir gas is said to contain about 80% Methane ($C_1 \sim 80$) and about one tenth of Ethane ($C_2 \sim C_1/10$) and half of that amount is Propane ($C_3 \sim C_2/2$). In the case of gas condensate, more heavy components are present and the Heptane plus fraction may be as high as 5% ($C_7^+ \sim 5$).

The content of non-hydrocarbon compounds can be considerable, as seen in the case of the Sleipner Vest fluid, where the molar composition of Carbon Dioxide is close to 9%. The CO_2 has to be stripped from the well flow as early as possible in the production line, a process that introduces difficulties both technically and economically.

The dry gas from the Frigg field contains practically only Methane and Ethane (99%), while the gas condensates also contain significant amounts of heavier compounds. See also Figure 2.9. These heavier compounds will finally condensate and form a liquid phase. Preferable, most of the gas is already produced to the surface, when this happens.

The molar composition of gas condensates may vary, as seen in Figure 2.9, by the amount of medium (C_4 to C_9) and heavier (C_{10}^+) components. The composition of a *wet gas* will in this context be a "heavy dry gas" where the molar composition show up

Table 2.4: Molar composition (in %) of fluids from Sleipner Vest, Kvitebjørn, Gullfaks and Frigg [7].

| Compounds | Sleipner Vest | Kvitebjørn | Gullfaks | Frigg |
|--------------------------|---------------|------------|----------|---------|
| N_2 , Nitrogen | 0.78 | 0.20 | 0.25 | 0.3599 |
| CO_2 , Carbon Dioxide | 8.72 | 3.51 | 3.27 | 0.2902 |
| C_1 , Methane | 71.00 | 77.83 | 83.27 | 95.5225 |
| C_2 , Ethane | 8.56 | 6.88 | 5.87 | 3.6887 |
| C_3 , Propane | 4.67 | 2.97 | 2.31 | 0.0379 |
| iC_4 , Iso-Butane | 0.71 | 0.49 | 0.34 | 0.0085 |
| nC_4 , Normal-Butane | 1.23 | 1.04 | 0.70 | 0.0047 |
| iC_5 , Iso-Pentanes | 0.41 | 0.39 | 0.24 | 0.0041 |
| nC_5 , Normal-Pentanes | 0.41 | 0.45 | 0.28 | 0.0004 |
| C_6 , Hexanes | 0.45 | 0.60 | 0.36 | 0.0049 |
| C_7 , Heptanes | 0.66 | 1.01 | 0.63 | 0.0030 |
| C_8 , Octanes | 0.70 | 1.03 | 0.69 | 0.0055 |
| C_9 , Nonanes | 0.41 | 0.65 | 0.37 | 0.0050 |
| C_{10}^+ , Decane plus | 1.29 | 2.95 | 1.43 | 0.0643 |

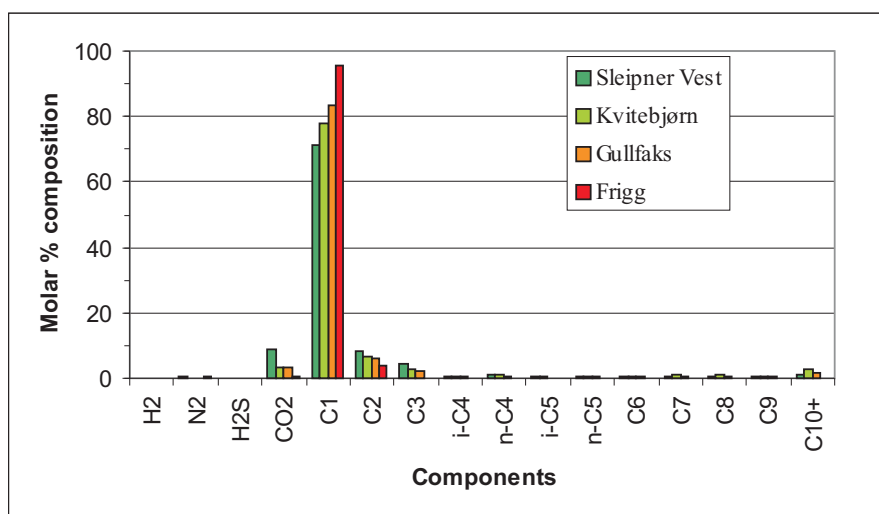


Figure 2.9: Molar composition of Selipner Vest, Kvitebjørn, Gullfaks and Frigg.

for the medium components in Figure 2.9. Judging from the composition of the three gas condensate fluids, it seems natural to expect more liquid condensate in the case of Sleipner Vest and Kvitebjørn than in the case of Gullfaks, since less lighter compounds would mean more heavier compounds and in the cases of Kvitebjørn, a rather high composition of C_{10}^+ components.

The molar compositions, as presented in Table 2.4 and Figure 2.9, represents the reservoir fluid located at a certain pressure and temperature. The pressure and temperature are again a result of the burial depth and the geological history of burial and

depth. Table 2.5 presents the reservoir pressure and temperature, the burial depth and the dew point pressure for the four reservoir gases.

Table 2.5: Reservoir characteristic for Sleipner Vest, Kvitebjørn, Gullfaks and Frigg.

| Reservoir | P_{res} [bar] | T_{res} $^{\circ}C$ | Depth [m MSL] | P_{dew} [bar] |
|---------------|-----------------|-----------------------|---------------|-----------------|
| Sleipner Vest | 434.0 | 120 | 3535 | 374.0 |
| Gullfaks | 757.0 | 142 | 3930 | 470.0 |
| Kvitebjørn | 774.9 | 152 | 4140 | 487.8 |
| Frigg | 197.9 | 61 | 1900 | - |

The general tendency is that gas reservoirs are found at greater depths than oil reservoirs. This observation is related to the temperature range most favorable for the generation of hydrocarbons, where gases normally are generated at temperatures somewhat higher than for oils. However, Table 2.5 shows that this is not always the case, since we then would expect to find the lightest gas at the deepest depths. In the table we see that the Frigg gas is buried more shallowly than the gas condensate fluids. The location of the Frigg gas reservoir may on the other hand, be a consequence of gas migration after the gas formation process had come to an end.

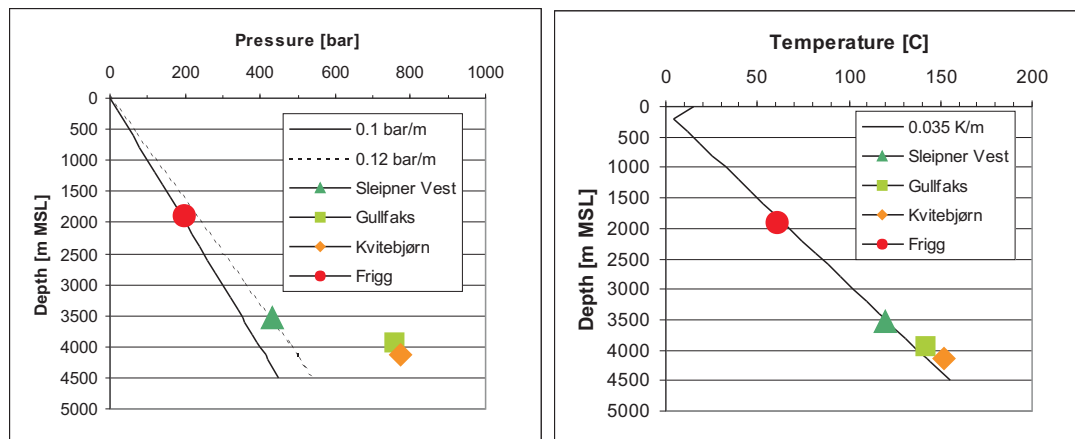


Figure 2.10: Reservoir pressure and temperature as function of depth.

In Figure 2.10 both the reservoir pressure and temperature are plotted as function of depth (TVD MSL: true vertical depth at mean sea level). The hydrostatic pressure, see example below, is given by the weight of the water column at reservoir level. The hydrostatic pressure in the reservoir may vary somewhat depending on the average water density and the density is again a function of water salinity.

Both Sleipner Vest and Frigg fall on the hydrostatic line in Figure 2.10, while Kvitebjørn and Gullfaks have a reservoir pressure significantly higher than the corresponding hydrostatic pressure. The consequence related to production from an over-pressurized reservoir has actually nothing to do with the fluid itself, more so, that the reservoir volume must be considered isolated from the surrounding aquifer. The effect of over-pressure when it comes to gas production, will therefore be related to a more rapid

pressure decline under depletion, due to lack of or very little water influx (pressure support).

When it comes to reservoir temperature, we observe from Figure 2.10 that all reservoirs practically fall on the same line, namely $35^\circ\text{C}/\text{km}$. The temperature gradient line is measured from a sea depth of 200 m and 4.5°C . Applying the same sea depths to all fields will of course increase scattering around the gradient line, as observed in the figure. In many observations of reservoir temperature and depth of North Sea reservoirs, temperature gradients in the range of $20 - 40^\circ\text{C}/\text{km}$ have been found.

Example: Hydrostatic pressure gradient.

Water found at the GWC (Gas Water Contact) is considered to be in continuous contact with all water sub surface and finally all of water in the seas. The hydrostatic water pressure is therefore equal to the weight of a water column per area, from the GWC and up to the sea surface. The hydrostatic pressure at any depth D is given by

$$p_w(D) = \int_{D_0}^D \left(\frac{dp}{dz} \right)_w dz + p(D_0), \quad (2.5)$$

where $(dp/dz)_w$ is the pressure gradient of water and D_0 is the datum plane or sea surface.

The salinity of water does change with temperature and thus the density of water will change as we move from the sea surface down to the reservoir. Density of sea water at 15°C is found to be $1025 \text{ kg}/\text{m}^3$ and at 100°C it has increased to $1160 \text{ kg}/\text{m}^3$.

If the hydrostatic pressure gradient is considered to be constant and the column pressure is written, $p_w = g\rho_w z$, then we may write

$$p_w(D) = g\rho_w D + 1\text{bar}, \quad (2.6)$$

where the datum plane $D_0 = 0$ is the sea surface.

Based on variation of salinity, as seen above, we may have typical pressure gradients as,

$$100.5 \text{ bar}/\text{km} < g\rho_w < 113.7 \text{ bar}/\text{km}.$$

2.5 Reservoir Fluids

Various thermodynamical properties of reservoir fluids are required in order to evaluate potential reserves, e.g. determine flow in porous media, design of separation and metering gas flow quantities. The risk of developing hydrocarbon resources is in part related to uncertainty in phase behavior at reservoir condition, but also related to determination of fluid properties, such as viscosity and density. (It is quite common to

Table 2.6: Thermodynamic properties of reservoir fluids. (Standard conditions/Stock Tank conditions are defined at a temperature of 288 K and a pressure of 0.1 MPa)

| Phase | Fluid | $V_{gas,ST}/V_{liquid,ST}$ | $\rho_{ST} [kg/m^3]$ |
|--------|------------|----------------------------|----------------------|
| gas | dry | - | - |
| gas | wet | > 9000 | < 700 |
| gas | condensate | 600 - 9000 | 700 - 800 |
| liquid | volatile | 350 - 600 | 800 - 875 |
| liquid | black oil | < 350 | 875 - 930 |
| liquid | heavy oil | - | > 930 |

consider the recorded measurement of density and viscosity, within an uncertainty of ± 1 and ± 10 percent, respectively.)

Reservoir fluids that only exhibit vapor-liquid phase behavior may be categorized as: dry gas; wet gas; gas condensate; volatile oil; black oil or heavy oil. Table 2.6 provides a summary of some characteristic properties that define and differentiate the various fluids [3].

A retrograde gas condensate is characterized by reservoir temperature above the critical temperature T_c , but below the temperature of the cricondentherm. During pressure depletion at reservoir temperature, liquids form within the formation by retrograde condensation. The relative volume of liquid in the formation and its impact on production is strongly related to how close the system temperature is to the critical temperature and secondly, but also related to the reservoir rock properties. For retrograde gas systems, liquid will also condensate in production tubing and in surface facilities as the production (p,T)-pathway enters the two-phase region.

Volatile oils behave similar to that of retrograde gas condensate, in the sense that one phase is leaving the other, i.e. gas is boiling out of the oil. Similarly to the increasing amount oil dropping out of the gas, as the temperature difference between reservoir temperature and critical temperature decreases, - the amount of gas boiling out of the oil is also increasing. The difference between the two fluids is that in the case of volatile oils, the gas is moving much faster through the reservoir and is therefore produced earlier than the associated oil, while the condensate liquid in most cases will not move at all. In both cases the separation of phases is seen as an disadvantage and the remedy is often the same. Production engineers often consider volatile oils and retrograde condensates the same, for the purpose of production design and pressure support.

2.6 Phase Equilibrium

In production of dry gas, as from the Frigg field, gas will remain in one phase during the entire production line and time period. The dry gas will expand according to the reduction in pressure, from reservoir to surface and thus occupy a considerable larger volume at the surface than initially in the reservoir. The gas expansion is described by the real gas law, where the z -factor (gas deviation factor) is characterizing the dry gas.

Production of gas condensate is considerable more complicated to describe, primar-

ily due to the fact that gas split in two phases; gas and liquid. The behaviour of gas condensates are therefore represented by two compositions, one describing the gas phase and the other describing the liquid phase. The initial molar composition of the condensate gas convey "key" information enabling us to derive all other gas properties needed to model both phases.

There are three essential methods available to determine gas composition and gas parameters in general. The K-value method and the Equation-Of-State (EOS) method use both historical data and correlations as the basis for predicting phase behaviour. The third method however, is based on experimental verification of phase behaviour.

- The K-value method is a purely empirical method which has been widely used in the past and is presently only used under particular circumstances.
- The EOS method is the modern way to calculate phase behaviour by using analytical computations in from of computer programs to solve the equation of state.
- The experimental method is based on experimental techniques by which gas equilibrium are reach in the laboratory by two depletion experiments; a constant composition depletion (CCD) experiment and by a constant volume depletion (CVD) experiment.

2.6.1 The K-value Method

A fluid may generally be considered to contains a gas fraction and a liquid fraction. The two phases are in equilibrium and the ratio between gas and liquid is called the equilibrium constant K .

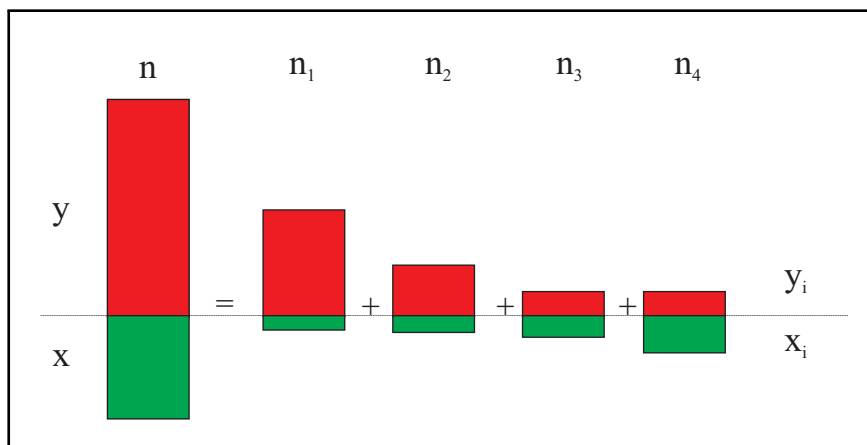


Figure 2.11: Gas - liquid mole fraction of mixture of four compounds.

The ratio between gas and liquid is illustrated in Figure 2.11, where the fluid contain n moles of hydrocarbon molecules. The *mixture* composition (mole fraction of component i) is given by $z_i = n_i/n$, where n_i is the number of moles of component i and n is the mole sum of all components. In the two phase region there will be two mixtures, vapor and liquid, in equilibrium. The composition of the two phases are y_i and x_i , respectively vapor and liquid. The equilibrium values are defined by

$$K_i = \frac{y_i}{x_i}, \quad (2.7)$$

where y_i and x_i are the mole fraction of component i in the gas - and liquid phase, respectively. The equilibrium values varies with pressure and temperature and to some degree also with the overall composition of the mixture. The variation due to composition is small at low pressures and increases as the pressure gets closer to the *convergence* pressure, which is defined as the pressure where all $K_i = 1$. (The convergence pressure will always be greater than the saturation pressure, except at the critical point where they coincide.)

The convergence pressure has to be obtained by graphical or mathematical extrapolation of equilibrium constants. Equilibrium constants for the most common hydrocarbons (methane, ethane, ...) and low shrinkage oils are available in the literature.

Let us assume that for a mixture, at a certain pressure and temperature and with a given overall composition, the K-values are known! (Generally the equilibrium values are not known.) Then, the phase split and the phase composition can be calculated as presented below;

The component material balance for the components in the mixture is given by

$$z_i = (1 - V)x_i + Vy_i, \quad (2.8)$$

where V is the vapor fraction of the gas-liquid mixture ($V + L = 1$).

Using Eq. 2.7 and 2.8 and eliminating the molar liquid fraction x_i , we get

$$y_i = \frac{z_i K_i}{1 + (K_i - 1)V}. \quad (2.9)$$

Similarly, elimination of y_i gives,

$$x_i = \frac{z_i}{1 + (K_i - 1)V}. \quad (2.10)$$

By definition, the molar fraction must sum to unity and

$$\sum_1^N y_i = \sum_1^N x_i = 1, \quad (2.11)$$

where N is the total number of components in the mixture.

Substitution of Eq. 2.9 and Eq. 2.10 into Eq. 2.11 yields the following sums,

$$\sum_1^N \frac{z_i K_i}{1 + (K_i - 1)V} = 1 \quad (2.12)$$

and

$$\sum_1^N \frac{z_i}{1 + (K_i - 1)V} = 1. \quad (2.13)$$

Eqs. 2.12 and 2.13 are polynomial equations of the n-th degree in the unknown V and each equation yields N roots for the unknown V . The correct solution is the

root that both equations have in common. Once the root has been found, the phase compositions follow directly from Eqs. 2.9 and 2.10.

The common root of Eqs. 2.12 and 2.13 will also be the root of the difference between Eqs. 2.12 and 2.13 and we may find V by solving the following equation,

$$\sum_1^N \frac{z_i(K_i - 1)}{1 + (K_i - 1)V} = 0. \quad (2.14)$$

Eq. 2.14 is particularly well suited for solution by the *Newton-Raphson* iteration method. According to this method the vapor fraction V is estimated by iteration. The iterative solution takes normally quite few iterations to converge. The result V (the molar phase split) is substituted in to Eqs. 2.9 and 2.10, giving the phase compositions of the liquid phase x_i and the gas phase y_i .

To apply the K-value method to a natural gas we need the composition of the gas z_i and appropriate K-values, K_i , for the individual components, where numerous empirical K-values correlations and charts are available.

2.6.2 The Equation Of State Method

An equation of state (EOS) is an analytical relation between pressure, temperature and volume of a gas or liquid. It also depends on the composition of the mixture and the fraction of gas and liquid. All EOS equations may be thought of as expansions of the ideal gas law. Through application of EOS equations, rigorous thermodynamic calculation of the phase behaviour of multi component systems can be performed.

The accuracy (success) of EOS programs depends to a large extent on the ability of correctly describing the PVT behaviour of a gas mixture. Over the years, numerous EOS have been proposed. Those, most frequently used in the petroleum industry are all variations of the well known Van der Waals two parameter EOS for single component substances,

$$\left(p + \frac{a}{V_M^2}\right)(V_M - b) = RT \quad (2.15)$$

valid both for gas and liquids. V_M is the molar volume and the constants a and b accounts for the attraction forces between molecules of the substance and for the gas volume occupied by molecules, respectively. Eq. 2.15 can be rewritten in the form of a cubic equation in the molar volume.

A cubic equation is well suited for describing the observed transformation from pure vapor (oil) state to the vapor (gas) state, as shown in Fig. 2.12.

The local maximum and minimum of the EOS curve, displayed in Fig. 2.12 is limited to the two-phase region. The behaviour of the curve between B and D is of limited practical significance and could in this connection be considered irrelevant.

Almost all cubic EOS can be generalized as a four constants equation.

$$p = \frac{RT}{V_M - b} - \frac{a}{(V_M - b + c)(V_M - b + d)}, \quad (2.16)$$

where a , b , c and d are constants defined by thermodynamic criteria or by fitting experimental data.

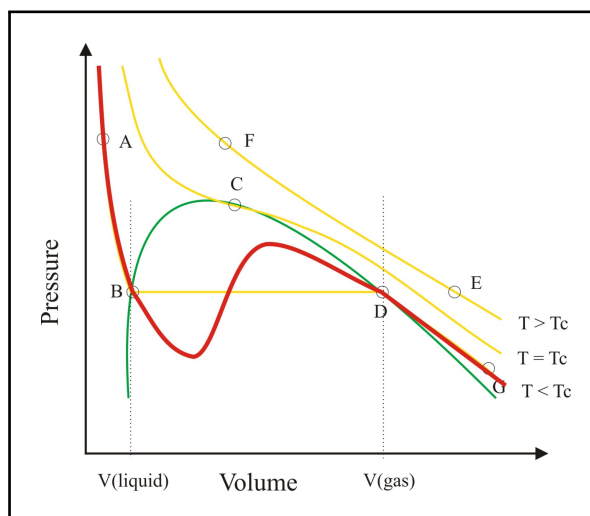


Figure 2.12: EOS curve describing the pressure - volume relation for a pure substance.

Eq. 2.16 is written in terms of pressure which is somewhat inconvenient since volume usually is the unknown parameter, while p and T are known.

Calculations of phase equilibrium of natural gases, using EOS methods and Eq. 2.16, requires certain input data as listed below:

1. A component breakdown of the fluids.
2. The critical pressure and temperature of each component in the mixture.
3. An acentric factor of the individual components (to be discussed in the following chapter).
4. The interaction coefficients for each component pair (to be mentioned in the next chapter).

These data are required for the calculation of the molar phase split and for calculation the composition of the liquid and gas phase. The calculation of phase densities also requires information of the molar masses of the individual components.

Liquid density predictions based on EOS calculations are generally of poorer quality than is the case for many other parameters. Because of the large number of components in natural gas systems, a compositional representation of pure components is only practical up to typically Hexane or Decane. All heavier components have to be lumped into one pseudo group. Properties of pseudo components are per definition not determined and are therefore subject to optimization and tuning. Whatever the process may be, it is always a question of matching calculations to measured data. If the measured data can be satisfactorily matched, then the EOS program can be used with some confidence for the prediction of phase behavior and PVT data beyond the ranges covered by these measured data.

2.6.3 The Experimental Method

The phase behaviour of natural gases during pressure depletion can be measured in the laboratory, by experiments. The depletion experiments normally start with a *constant composition depletion* experiment (CCD). Then follows a *constant volume depletion* experiment (CVD). Both experiments are started by first injecting reservoir gas into a cell at initial reservoir pressure and - temperature.

A constant volume depletion experiment is conducted at reservoir temperature and begins at the saturation pressure, i.e. the dew point pressure. The reservoir gas is contained at this pressure in a *celle* and the volume of gas $V = V_{celle}$ is noted and used as the reference volume [8].

Constant Composition Depletion

In a CCD experiment a known quantity (number of moles) of the reservoir gas is charged into a windowed, high pressure cell and raised to a pressure slightly higher than the initial reservoir pressure. The temperature is kept constant at the reservoir temperature during the experiment. The pressure in the cell is lowered stepwise by increasing the cell volume such that the gas will expand while the overall composition remains constant. The process of constant composition depletion is depicted in Figure 2.13.

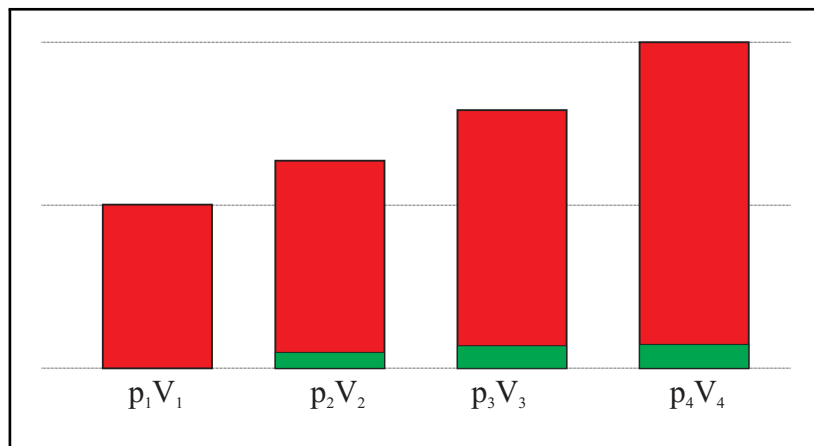


Figure 2.13: Constant composition depletion experiment.

At each pressure step, during a CCD experiment, the volume and pressure in the cell are measured. The initial one phase condition is verified and the dew-point is determined by visually observing the formation of the first liquid drop that appears in the cell. From the measured volume and pressure above the dew-point pressure, the z -factor of the gas can be readily determined by using the real gas law,

$$Z = \frac{pV}{nRT} = \frac{1}{nRT}(pV), \quad (2.17)$$

where nRT is kept constant during the experiment.

Below the dew-point pressure the condensation of oil is measured and the yield of oil represents the maximum liquid dropout during pressure depletion. The process of

stepwise pressure reduction is normally continued until a doubling of the initial cell volume is reached.

Constant Volume Depletion

If the CCD experiment indicates a significant retrograde condensation, the pressure in the cell is then increased up to the dew-point pressure and a constant volume depletion experiment is started.

The pressure is again reduced stepwise but now by first expanding the cell volume and then removing the excess gas volume at constant pressure. The extraction of excess gas is done by reducing the cell volume to its initial value. See Figure 2.14 for a schematic illustration of the CVD experiment.

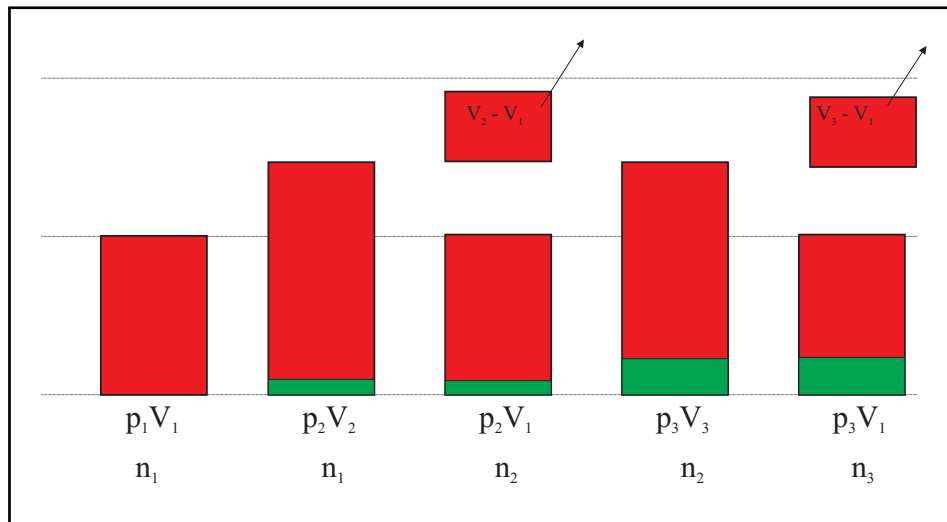


Figure 2.14: Constant volume depletion experiment.

Removing some of the gas will reduce the number of moles initially injected in the cell, while on the other hand, the cell volume is kept constant. For each step, the pressure, the excess gas volume and the amount of liquid deposited in the cell are measured. The withdrawn gas is analyzed for its composition. The stepwise depletion process is continued until a reduced pressure of 30-40 bar is reached. The total number of steps may then vary from 5 to 10 steps.

The CVD experiment resembles the process of normal pressure depletion that takes place under production from natural gas reservoirs. The data obtained from the CVD experiment are therefore useful in simulating natural gas depletion.

From the experimental pressure and volume data we can derive the z -factor for the produced gas as well as the two-phase z -factor of the hydrocarbon mixture in the cell. The two-phase z -factor (z_2 -factor) is the preferred parameter to use in natural gas depletion production since it also accounts for the volume occupied by condensate oil in the reservoir. The two-phase z -factor is given

$$Z_2 = \frac{pV}{nRT} = \frac{V}{RT} \left(\frac{p}{n} \right), \quad (2.18)$$

where V/RT is kept constant under the experiment.

The z_2 -factor is found to be useful in reservoir material balance calculation and will yield a correct results as long as condensate oil is not produced together with the gas. This would be true as long as the oil saturation remains below the critical oil saturation in the reservoir. Above this saturation value, the oil will start to flow and the accumulation of oil in the reservoir will not continue to increase as predicted by the CVD experiment. The error is, however, small and the z_2 -factor is used in estimating the true z -factor.

A CVD experiment does not provide data directly applicable to the liquid yield of a well stream, because the CVD experiment only simulates reservoir conditions and not what happens in the well, where cooling and expansion of the produced gas in the well-bore and at the surface, will lead to significant alteration of the gas-oil ratio and fluid composition in general. The CVD data does, however, provide the composition of the well stream as function of the declining reservoir pressure, to a high degree of accuracy.

References

- [1] J.W. Amyx, D.M. Bass, and R.L. Whiting. *Petroleum Reservoir Engineering*. McGraw-Hill Book Company, 1960. ISBN 07-001600-3.
- [2] Ali Danesh. *PVT and Phase Behavior of Petroleum Reservoir Fluids*. Elsevier, 1998. ISBN 0-44-82196-1.
- [3] Goodwin, A.R.H., Marsh, K.N. and Wakeham, W.A. *Measurement of the Thermodynamic Properties of Single Phases*. Elsevier, 2003. ISBN 0-444-50931-3.
- [4] D.L. Katz and R.L. Lee. *Natural Gas Engineering, Production and Storage*. McGraw-Hill Publishing Company, 1990. ISBN 0-07-100777-6.
- [5] S. Kumar. *Gas Production Engineering*, volume Huston, TX. Gulf Publishing Company, 1987. ISBN 0-87201-577-7.
- [6] J. Lee and R.A. Wattenbarger. *Gas Reservoir Engineering*. Henry L. Doherty Memorial Fund of AIME, SPE, 1996. ISBN 1-55563-073-1.
- [7] S.B. Steinnes. Gass Viskositet. Student project, Høgskolen i Stavanger, 1999.
- [8] C.H. Whitson and S.B. Torp. Evaluating Constant Volume Depletion Data. *SPE 10067*, 1981.

Chapter 3

Thermodynamics, Phase Behavior and Gas Properties

In the previous chapter, a more qualitative description of fluid phase behavior was presented. In this chapter we aim to be a bit more quantitative.

During the process of natural gas depletion, pressure will decrease gradually in all parts of the reservoir and in the well-bore system. However, the rate of pressure change in major parts of the reservoir is quite low. In particular is the time and spatial pressure gradients very low compared to the overall pressure levels in most parts of the reservoir. This fact allow us to apply basic principles related to phase equilibrium and thermodynamics, in describing the phase properties in reservoir and well-bore fluid flow. The area of thermodynamical models describing fundamental aspects of PVT relations and -simulation is a particular rich field of research [6, 7].

In this chapter however, we address the more quantitative aspects of the same processes as described previously. In particular, we wish to focus on the basic considerations needed, to deduce parameters suitable for numerical calculation of isothermal depletion, reservoir and well-bore condensation and surface gas production. Though, an extensive description of PVT and phase behavior of natural gases is not attempted here.

Based on molar composition of a natural gas, reservoir pressure and - temperature, it is quite possible to estimate all parameters that are directly or indirectly necessary to describe most fluid characteristics [8].

3.1 Determination of Phase Equilibrium

Different pressure potentials are supposed to be established in the reservoir, before fluids can start flowing. Then, the pressure potentials will differ at each spatial point and the potential at each spatial point will decrease as a result of normal depletion. Even though the reservoir temperature remains constant, a varying reservoir pressure challenges the image of what is normally understood as a static reservoir equilibrium. In most situations, however, the magnitude of the spatial pressure gradients are small compared to the general pressure level in the reservoir.

Under the assumption of a slow and stable pressure situation, - it is reasonable to assume that the condition for chemical equilibrium is present in the reservoir. Figure 3.1

depicts the situation of slow and stable flow in the reservoir, where the phase split between gas and liquid is slowly changing as we move from initial reservoir condition to standard condition at the surface. At initial condition, the unit cell contains one phase gas. As pressure and temperature decreases, liquid drops out of the gas. It is our assumption that the phase split and thus the phase equilibrium evaluated at different pressures and temperatures will describe the phase behavior observed locally along the flow path. This statement is more true for reservoir flow than for well-bore flow.

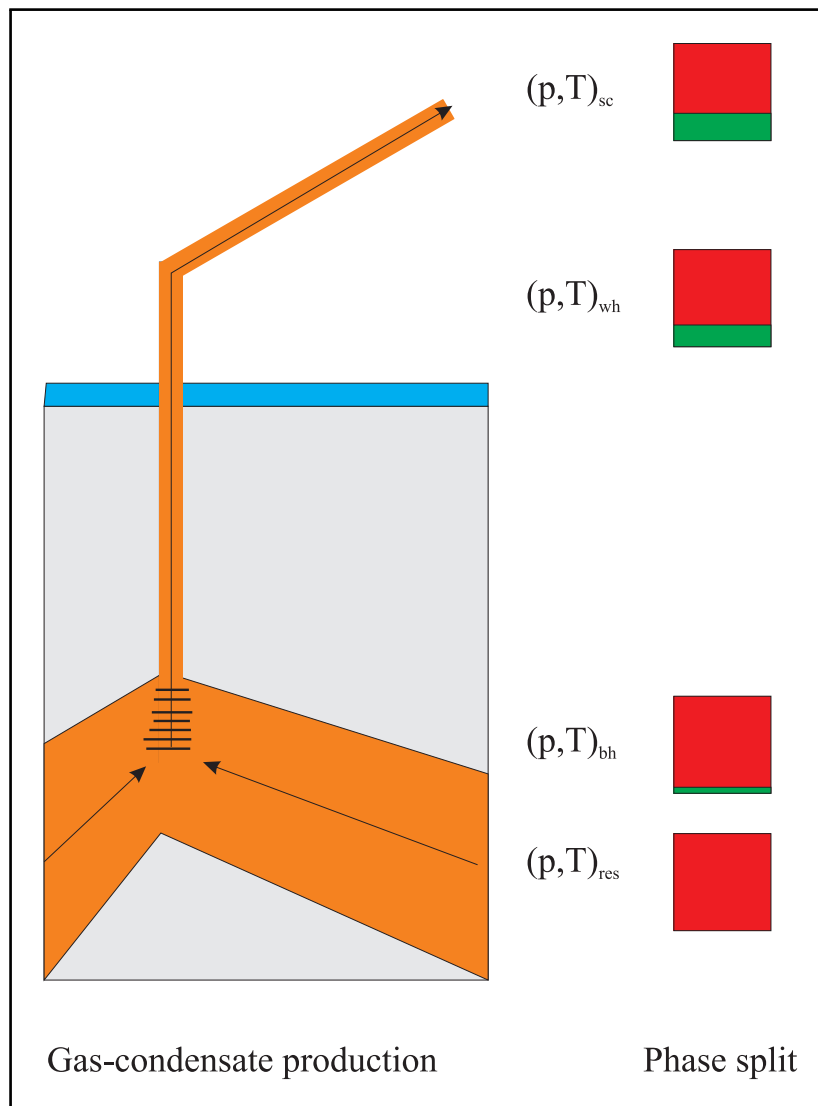


Figure 3.1: The figure shows the phase split as function of declining pressure and temperature, at initial reservoir pressure, at the bottom hole and well head pressure and finally at surface condition.

In the previous chapter we have already identified the equilibrium ratio $K_i = y_i/x_i$, as the key factor in determining the phase split ($V + L = 1$), where y_i and x_i are the molar ratio of component i contained in the vapor and liquid phase, respectively. When

K_i is determined, then the phase split is indirectly defined. The question is therefore how to determine the equilibrium ratio for a general hydrocarbon fluid!

3.1.1 Definition of Equilibrium Ratio

When vapor and liquid (gas and oil) are confined (defined volume) at constant temperature, the two phases will find its equilibrium. In this state of dynamical equilibrium, some oil molecules will move into the vapor and some gas molecules will move into the liquid (condensate), leading to a zero nett flux of molecules between phases.

If we fill some pure (one type of molecules) liquid into a vacuumed container, i.e. water could be a excellent example, - water molecules will vaporize and eventually form a vapor phase in equilibrium with the water phase. The pressure in the container defined by this process is the vapor pressure P^0 , where the vapor pressure is temperature dependent and as we already know; the vapor pressure of water at 100 C^0 is 1 atm. The vapor pressure of many (most) liquids are experimentally known; $P_i^0(T)$.

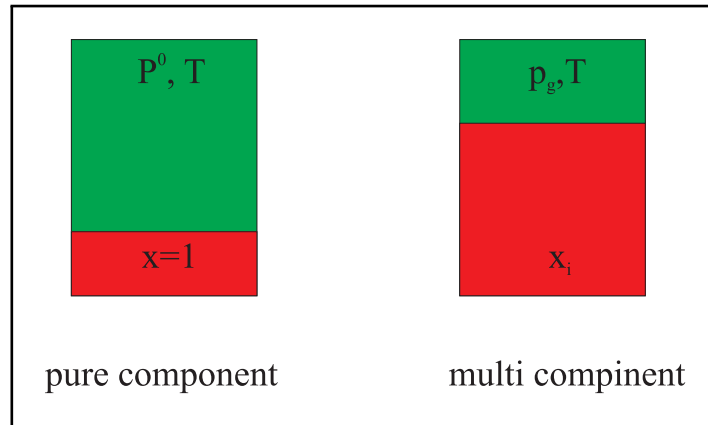


Figure 3.2: Left: Equilibrium in container filled with single component. Right: Container filled with multi component liquid.

Lets look at a situation where we fill a container with pure hydrocarbon, i.e. ethane, following the same procedure as above. See Fig 3.2, left. The gas or vapor pressure is then $p_g = P_{C_2}^0$. If we add another liquid phase which does not vaporize (or having a very high vapor pressure), the gas pressure is observed to decrease proportionally to the reduced mole fraction of ethane; x_{C_2} . This observation is known as Raoult's law,

$$p_g = x_{C_2} P_{C_2}^0. \quad (3.1)$$

If more hydrocarbon components are added, as described above and as shown in Fig 3.2, right, - the gas pressure will be the sum of all partial (vapor) pressures as defined by Raoult's law. Generally we get,

$$p_g = \sum_{i=1}^N p_i, \quad \text{where } p_i = x_i P_i^0, \quad (3.2)$$

where p_i is the partial vapor pressure of the i 'th component. x_i is the liquid molar ratio of each component and P_i^0 is the component vapor pressure. The linear relationship between gas pressure p_g , and composition x_{C2} is depicted in Fig. 3.3.

Since the vapor molar ratio is defined $y_i = p_i/p_g$, according to Dalton's Law (see Eq. 2.2), we get the following simple expression for the equilibrium ratio,

$$K_i = \frac{y_i}{x_i} = \frac{p_i/p_g}{p_i/P_i^0} = \frac{P_i^0}{p_g}. \quad (3.3)$$

Since Raoult's law is known as an asymptotic or limiting law, much the way the ideal gas law is known as a limiting law of real gas behavior (for low pressures), - Raoult's law fail to describe mixtures where different components are mixed at comparable molar ratios. Eq. 3.3 is therefore an asymptotic equilibrium ratio valid for the somewhat particular situation where the liquid and gas phases contained consist primarily of one principal component. Therefore, the above expression is not well suited for describing hydrocarbon mixtures.

The relationship between gas pressure and composition for real gases may certainly deviate from Raoult's law in so many ways. Fig. 3.3 depicts how the function $p_g(x_{C2})$ could vary (three different alternatives) when more components are added to the mixture.

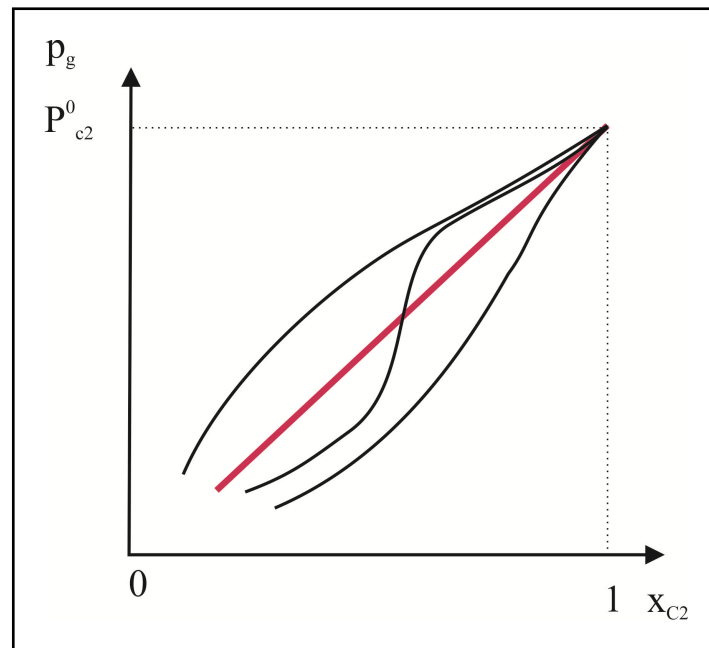


Figure 3.3: Raoult's linear relationship compared to three different alternatives for real gases, where the initial gas pressure is the vapor pressure of one component ethane.

There exist many K-value correlations considered to be extensions of Eq. 3.3. Common for many of these correlations are the fact that they neglect the effect of mixture composition, which again restrict the range and applicability for these correlations to low or moderate pressures. One of the most popular correlations in this category is the Wilson equation [8];

$$K_i = \frac{p_{ci}}{p} \exp \left\{ 5.373(1 + \omega_i) \left(1 - \frac{T_{ci}}{T} \right) \right\}, \quad (3.4)$$

where T_{ci} , p_{ci} and ω_i are critical temperature, critical pressure and acentric factor for component i , respectively. The Wilson equation generally provides reliable estimation of K-values for sub-critical components and is less reliable for supercritical components. The Wilson equation gives usually adequate equilibrium ratios for hydrocarbon mixtures below 3.5 MPa and is therefore often used as an initial estimate in more elaborate calculations, involving equation of state and fugacity calculations, which is an up-coming topic.

For real gases of higher or high pressure, Eq 3.4 gives erroneous results. In order to calculate the equilibrium ratio at these pressures, we therefore need a theory describing the state of thermodynamic equilibrium where also the molar mixing ratios are included.

3.2 Basic Thermodynamics

Thermodynamics is a particular rich field of science, theoretical of cause, but also to a surprisingly high degree of practical interest. In practical applications, equilibrium thermodynamics form a basic platform from which many physical parameters can be derived.

Thermodynamics consist essentially of the first, second and the third laws of thermodynamics. Derivations based on these laws, combined with an equation of state (EoS), can provide deep insights and knowledge of fluid systems, fluid properties and how they can be measured and calculated.

In this text we will focus on the task of defining an expression for the equilibrium ratio $K_i = y_i/x_i$. Other aspects of equilibrium thermodynamics which would be of more general nature and thus natural to elaborate on, are to a large degree omitted. The development we will follow, is therefore to the point and perhaps unnaturally brief. However, equilibrium thermodynamics are widely described and explained in nearly all text book on thermodynamics, chemical engineering or physical chemistry.

3.2.1 Laws of Thermodynamics

The first law of thermodynamics states that the change of internal energy in a closed system is equal to the heat absorbed by the system plus the work done on the system and is written,

$$dU = \delta Q + \delta W. \quad (3.5)$$

Notice that δQ and δW are not exact differentials (like e.g. the internal energy: dU), meaning that Q and W will depend on the interaction between the system and its surroundings. In Figure 3.4, this situation is depicted, i.e. where the heat, δQ , delivered to the system is used to increase the temperature in the system, while the work, δW on the boundary of system is used to compress the system.

The work done on the system, as shown in Figure 3.4, can be symbolized by a force F acting on a cylindrical cross section surface A , such that,

$$\delta W = F dx = p A dx = p dV, \quad (3.6)$$

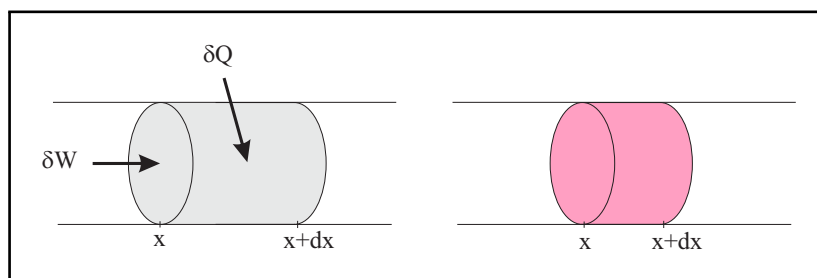


Figure 3.4: The figure shows how work and heat delivered to a system, is leading to a displacement of the system and to a temperature increase in the system.

where at constant area and pressure, $p = F/A$ and where $dV = Adx$ is the volume of the system shown in the figure. If the work δW delivered to the system under the influence of an external pressure p is leading to a negative change in the system volume, we may write the exact differential of volume change as

$$dV = -\frac{\delta W}{p}. \quad (3.7)$$

Following the exact same logic, we may state that the heat δQ delivered to a system at a certain temperature T , is leading to an increase in the *entropy* S , of the system and that the exact differential of change in entropy is written,

$$dS = \frac{\delta Q}{T}. \quad (3.8)$$

Eq. 3.8 is known as the 2. law of thermodynamics.

Combining the 1. and 2. law of thermodynamics gives,

$$dU = TdS - pdV, \quad (3.9)$$

where U , V and S are all external variables, depending on the quantitative aspects of the system, while T and p are internal variables, independent of the amount or number of molecules (or moles) in the system.

If a gas consists of various components (types of molecules) and amounts, - the total number of moles is written $n = n_1 + n_2 + n_3 + \dots + n_N$. Since the external variables are additive,

$$\begin{aligned} U &= U_1 + U_2 + \dots + U_N, \\ V &= V_1 + V_2 + \dots + V_N, \\ S &= S_1 + S_2 + \dots + S_N. \end{aligned} \quad (3.10)$$

The internal energy for the gas is therefore written,

$$U = U(S, V, n), \quad (3.11)$$

where the function $n = n(n_1, n_2, \dots, n_i, \dots, n_N)$ is used above.

Eq. 3.11 can be differentiated and we get,

$$dU = \left(\frac{\partial U}{\partial S}\right)_{V,n} dS + \left(\frac{\partial U}{\partial V}\right)_{S,n} dV + \sum_{i=1}^N \left(\frac{\partial U}{\partial n_i}\right)_{V,S,n_i} dn_i, \quad (3.12)$$

where we have used the convention $n_i = [n_1, n_2, \dots, n_{i-1}, n_{i+1}, \dots, n_N]$. Notice that under the derivation of dn_i all other variables $n_{\neq i}$ are treated as constants.

Combining Eq. 3.9 and Eq. 3.12 gives

$$T = \left(\frac{\partial U}{\partial S}\right)_{V,n}, \quad -p = \left(\frac{\partial U}{\partial V}\right)_{S,n} \quad \text{and} \quad \mu_i = \left(\frac{\partial U}{\partial n_i}\right)_{V,S,n_i}$$

where μ_i is known as the *chemical potential*. Eq. 3.12 is then written,

$$dU = TdS - pdV + \sum_{i=1}^N \mu_i dn_i, \quad (3.13)$$

The additive properties, shown in Eq. 3.10, demand that the internal energy (as well as S and V) are first-order homogenous functions of the other extensive properties, such that

$$U(\lambda S, \lambda V, \lambda n_1, \lambda n_2, \dots, \lambda n_N) = \lambda U(S, V, n_1, n_2, \dots, n_N), \quad (3.14)$$

where λ is a positive constant.

Differentiating Eq. 3.14 with respect to λ and later using $\lambda = 1$, gives the following expression of the internal energy U [3],

$$U = TS - pV + \sum_{i=1}^N \mu_i n_i. \quad (3.15)$$

The intensive properties; T , p and μ_i , in the above equation, are not all independent. This is shown by calculating the differential of Eq. 3.15,

$$dU = TdS + SdT - pdV - Vdp + \sum_{i=1}^N \mu_i dn_i + \sum_{i=1}^N n_i d\mu_i. \quad (3.16)$$

Combining Eq. 3.16 with Eq. 3.13, gives the well known *Gibbs-Duhem equation*,

$$SdT - Vdp + \sum_{i=1}^N n_i d\mu_i = 0, \quad (3.17)$$

which demonstrate that temperature (T), pressure (p) and chemical potential (μ_i) of a phase are not independent.

In Eq. 3.15 we observe that while some properties; T , p , V and n_i , are well defined in the sense that an absolute value can be found, the properties S and μ_i are not readily calculated. Both the entropy and the chemical potential are relative quantities, where the reference values (datum plan values) are not easily defined. (This point is to be discussed shortly.)

Eq. 3.15 could be regarded as the basic or fundamental equation from which quite a number of thermodynamic quantities can be calculated. When it comes to practical situations, different boundary conditions is tackled simply by using slightly different fundamental equations. We are here talking about; the enthalpy H , the Helmholtz free energy A , and the Gibbs free energy G , which are defined:

$$H = U + pV, \quad (3.18)$$

$$A = U - TS, \quad (3.19)$$

$$G = U - TS + pV. \quad (3.20)$$

Combining Eq. 3.15 with the above equations gives;

$$H = TS + \sum_{i=1}^N n_i \mu_i, \quad (3.21)$$

$$A = -pV + \sum_{i=1}^N n_i \mu_i, \quad (3.22)$$

$$G = \sum_{i=1}^N n_i \mu_i. \quad (3.23)$$

We may now differentiate the above equations, similarly to the differentiation of the internal energy and substituting by Eqs. 3.16 and 3.17, we get;

$$dH = TdS + Vdp + \sum_{i=1}^N \mu_i dn_i, \quad (3.24)$$

$$dA = -SdT - pdV + \sum_{i=1}^N \mu_i dn_i, \quad (3.25)$$

$$dG = -SdT + Vdp + \sum_{i=1}^N \mu_i dn_i. \quad (3.26)$$

From the above differential equations we may infer that,

$$H = H(S, p, n), \quad (3.27)$$

$$A = A(T, V, n), \quad (3.28)$$

$$G = G(T, p, n), \quad (3.29)$$

where by writing out the above equation in differential form as seen in Eq. 3.16 and Eq. 3.17, we may conclude that;

$$\mu_i = \left(\frac{\partial U}{\partial n_i} \right)_{S,V,n_i} = \left(\frac{\partial A}{\partial n_i} \right)_{T,V,n_i} = \left(\frac{\partial G}{\partial n_i} \right)_{T,p,n_i}, \quad (3.30)$$

$$\left(\frac{\partial A}{\partial V} \right)_{T,n} = -p, \quad (3.31)$$

$$\left(\frac{\partial G}{\partial p} \right)_{T,n} = V. \quad (3.32)$$

In the list of derivatives above, only those of immediate use in this text have been listed. From the equations above it is evident the both the Helmholtz free energy and the Gibbs free energy are particular well suited for processes at constant temperature and volume, and at constant temperature and pressure, respectively. The Gibbs free energy is particularly well suited for describing the state of fluids, since the independent variables p and T are both easily measurable and controllable.

3.2.2 Thermodynamic Equilibrium

The principle of minimum energy, states that for a closed system, with constant external parameters, such as pressure and temperature, the internal energy will decrease and approach a minimum value at equilibrium.

As a comparison, the second law of thermodynamics, see Eq. 3.8, states that for a isolated systems, (and fixed external parameters) the entropy will increase to a maximum value at equilibrium.

In thermodynamics, the Gibbs free energy is a potential that measures the capacity of a system to do non-mechanical work. The Gibbs free energy, as we have seen in Eq. 3.23, is a chemical potential that is minimized when the system reaches equilibrium, at constant pressure and temperature, i.e. at chemical equilibrium the change in Gibbs free energy is zero, $dG = 0$.

At equilibrium, and constant pressure ($dp = 0$) and temperature ($dT = 0$),

$$dG = \sum_{i=1}^N \mu_i dn_i = 0. \quad (3.33)$$

In a closed system, containing n^V moles of gas and n^L moles of liquid in equilibrium and at constant pressure and temperature, as depicted in Figure 3.5, Eq. 3.33 is written,

$$\sum_{i=1}^N (\mu_i^L dn_i^L + \mu_i^V dn_i^V) = 0, \quad (3.34)$$

where μ_i^L and μ_i^V are the chemical potential of component i in the gas and liquid phase, respectively.

Since the number of moles of each component contained in both phases are constant at equilibrium, i.e. the number of liquid moles leaving the liquid phase must be equal to the number of vapor moles leaving the vapor phase, or said differently, that the sum of the two must be zero, i.e. $dn_i^L + dn_i^V = 0$, - the above equation is written,

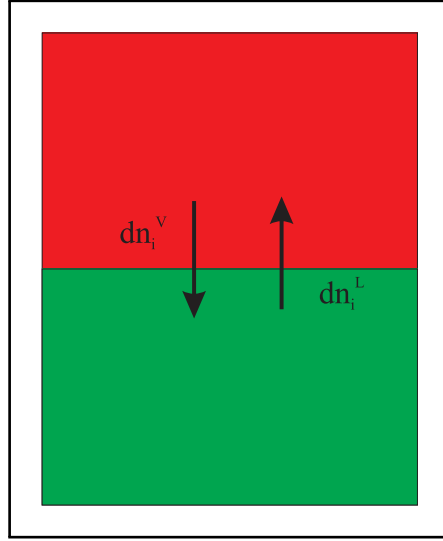


Figure 3.5: Gas and liquid at equilibrium showing the transport between phases.

$$\sum_{i=1}^N (\mu_i^L - \mu_i^V) dn_i = 0. \quad (3.35)$$

The number of vaporizing and condensing moles will vary between the different components and will thus be different from zero. This means that for the sum in Eq. 3.35 to become zero; $\mu_i^L = \mu_i^V$.

We have therefore reached the important result that at equilibrium; the chemical potentials for each component, in each phase, must be equal.

The chemical potential obviously plays an important role in defining the thermodynamic equilibrium. If we were able to calculate the μ_i in the two phases as function of pressure (and temperature), we might use the above criteria of equal chemical potential in both phases; $\mu_i^L = \mu_i^V$, as a measure for defining the equilibrium pressure (and temperature).

From the definition of the chemical potential, Eq. 3.30, and its derivative with respect to pressure, it follows that,

$$\begin{aligned} \left(\frac{\partial \mu_i}{\partial p} \right)_{T,n} &= \left(\frac{\partial}{\partial p} \left(\frac{\partial G}{\partial n_i} \right)_{T,p,n_i} \right)_{T,n} \\ &= \left(\frac{\partial}{\partial n_i} \left(\frac{\partial G}{\partial p} \right)_{T,n} \right)_{T,p,n_i} \\ &= \left(\frac{\partial(V)}{\partial n_i} \right)_{T,p,n_i}, \end{aligned} \quad (3.36)$$

where firstly the order of derivation has been interchanged and secondly the result of Eq. 3.32 is applied. Eq. 3.36 is an important result, relating the chemical potential of

component i in a mixture to other measurable properties such as pressure, temperature and composition.

Combining the real gas law and the differential $\partial V/\partial n_i = ZRT/p$, with the result of the above derivation, we find,

$$\begin{aligned} d\mu_i &= \frac{ZRT}{p} dp \\ &= RT Z d(\ln p). \end{aligned} \quad (3.37)$$

Eq. 3.37 tell us that the chemical potential can be found as an integral with respect to pressure and in the case of an ideal gas, integration gives,

$$\mu = \mu^0(T) + RT \ln \frac{p}{p^0}, \quad (3.38)$$

where μ^0 is defined in relation to a certain reference pressure p^0 .

Eqs. 3.37 and 3.38 points in the direction of defining a new concept related to pressure, namely the *fugacity*.

3.2.3 Fugacity and Equilibrium Ratio

It has been proven advantageous to define a new parameter, called *the fugacity*, f , such that the differential representing of the real gas equation in Eq. 3.37, can be presented similarly to the ideal gas equation 3.38.

The fugacity has thus the same unit as pressure and can be considered as an generalization of pressure or a correction to the real pressure. Another way of describing fugacity is characterized as: *its resemblance to the partial pressure in relation to equilibrium between phases and the escaping tendency of molecules in one phase to escape to the adjacent phase.*

Substituting the fugacity function in Eq.3.37, we get,

$$(d\mu_i = RT d \ln f_i)_{T,n}, \quad (3.39)$$

where f_i is the fugacity of each component; $1 \leq i \leq N$.

The above mentioned escaping tendency completes the definition of fugacity,

$$\lim_{p \rightarrow 0} \left(\frac{f_i}{x_i p} \right) = 1, \quad (3.40)$$

where the partial pressure is $p_i = x_i p$. x_i is the molar fraction of component i .

The ratio between fugacity and partial pressure in Eq. 3.40, is often called the *fugacity coefficient*, φ_i ,

$$\varphi_i = \frac{f_i}{x_i p}. \quad (3.41)$$

The fugacity coefficient is also an important parameter, as it is directly related to the equilibrium ratio, K_i , where we in the case of equilibrium between the liquid and vapor phase have,

$$K_i = \frac{y_i}{x_i} = \frac{f_i^V \varphi_i^L}{f_i^L \varphi_i^V} = \frac{\varphi_i^L}{\varphi_i^V}. \quad (3.42)$$

In the above equation we have used the result from Eq. 3.35, that at chemical equilibrium $\mu_i^L = \mu_i^V$. By using the definition of fugacity as in Eq. 3.39, it is clear that at equilibrium the fugacities must be equal, $f_i^L = f_i^V$. Hence, the two phases will be in equilibrium with no net transfer of molecules from one phase to another.

The important next step is therefore to develop the fugacity coefficient into a comprehensive variable suitable for further calculation.

Let's start with the definition of fugacity, as in Eq. 3.39, and subtract the term $d(RT \ln x_i p)$.

$$(d\mu_i - d(RT \ln x_i p)) = RT d \ln f_i - d(RT \ln x_i p)_{T,n}. \quad (3.43)$$

Using the definition of the fugacity coefficient, Eq. 3.41 and the fact that $d(\ln x_i) = 0$, since the composition is not varying, the above equation can be written,

$$\begin{aligned} RT d \ln \varphi_i &= d\mu_i - RT d \ln p \\ &= d\mu_i - RT \frac{dp}{p}. \end{aligned} \quad (3.44)$$

Differentiating the real gas law gives (when $T \sim \text{contant}$),

$$\frac{dp}{p} = \frac{dZ}{Z} - \frac{dV}{V}. \quad (3.45)$$

Differentiating the chemical potential with respect to volume V and recalling the result from Eq. 3.31, where $(\partial A / \partial V)_{T,n} = -p$, we may write,

$$\begin{aligned} \left(\frac{\partial \mu_i}{\partial V} \right)_{T,n} &= \left(\frac{\partial}{\partial V} \left(\frac{\partial A}{\partial n_i} \right)_{T,p,n_i} \right)_{T,n} \\ &= \left(\frac{\partial}{\partial n_i} \left(\frac{\partial A}{\partial V} \right)_{T,n} \right)_{T,p,n_i} \\ &= - \left(\frac{\partial(p)}{\partial n_i} \right)_{T,p,n_i}, \end{aligned} \quad (3.46)$$

where the result of the above development is,

$$d\mu_i = \left(\frac{\partial \mu_i}{\partial V} \right) dV = - \left(\frac{\partial p}{\partial n_i} \right) dV. \quad (3.47)$$

Inserting Eqs. 3.45 and 3.47 into Eq. 3.44, yield the result,

$$\begin{aligned} RT d \ln \varphi_i &= - \frac{\partial p}{\partial n_i} dV - RT \left(\frac{dZ}{Z} - \frac{dV}{V} \right), \\ &= \left(- \frac{\partial p}{\partial n_i} + \frac{RT}{V} \right) dV - RT d \ln Z \end{aligned} \quad (3.48)$$

Integration of the above equation extends all possible volumes down to a well defined volume, i.e. from ∞ to V . Switching the integration limits and rearranging, gives,

$$\ln \varphi_i = \int_V^\infty \left(\frac{1}{RT} \frac{\partial p}{\partial n_i} - \frac{1}{V} \right) dV - \ln Z. \quad (3.49)$$

The above equation is the final result of this development. From Eq. 3.49, we may calculate the fugacity coefficient under the circumstances that we have a representation of the volumetric behavior of gas and liquids. Such volumetric properties are normally represented by the equation of states (EoS). There exist a great variety of different EoS to choose from, some more accurate than others depending on the fluids at hand, the range of parameter variation and the complexity of representation.

The important lesson at this point is that; given an EoS, the fugacity coefficients φ_i can be calculated using Eq. 3.49. At equilibrium, we therefore have the following results,

$$\begin{aligned} \mu_i^L &= \mu_i^V \\ f_i^L &= f_i^V \\ x_i^L \varphi_i^L &= x_i^V \varphi_i^V \end{aligned} \quad (3.50)$$

From the above we may use Eq. 3.50 in order to define the equilibrium and when equilibrium has been reached, use Eq. 3.42 to calculate the equilibrium ratio K_i .

3.3 Equation of State (EoS)

Cubic equations of state are relatively simple equations relating pressure, volume and temperature. Given as input are also a few other experimental parameters such as critical properties, (P_{ci} and T_{ci}) and specific factors describing the interaction between different molecules.

The EoS describe the volumetric and phase behavior of pure components and mixture of components to a surprisingly high degree of accuracy. The robustness of the EoS is somewhat unexpected, since the nature of reservoir fluids are complex, consisting of hydrocarbon components of more than 100 carbon atoms and additionally of non-hydrocarbons such as; N_2 , CO_2 , H_2S , H_2O , He , Ar and others, - often to rather high concentrations.

The chemistry of natural reservoir fluids are complex, where reservoir temperature may vary between $30 - 170^\circ C$ and reservoir pressure between $5 - 1300 \text{ bar}$. The good performance of EoS in describing phase behavior is particular evident in vapor - liquid calculations, but also solid states can be described by equation of states. In general vapor phase behavior is slightly better described than the liquid phase, where in particular the liquid density is often poorly determined.

Non-cubic equations is a class of EoS with usually many parameters and are thus a bit more difficult to handle both mathematically and through simulations. The advantage of these equations is that they can be *tuned* to simulate phase behavior of well defined fluids and in particular for pure fluids and substances. These equations does not, on the other hand, show superior behavior in describing complex hydrocarbons,

like those we find in normal reservoirs. In fact, in the case of natural reservoir fluids, cubic equations of state show superior predictability of phase behavior.

3.3.1 The van der Waals Equation

The simplest known cubic equation of state, is the *van der Waals* equation, introduced already in 1873,

$$\left(p + \frac{a}{v^2}\right)(v - b) = RT, \quad (3.51)$$

where $v = V/n$ is the molar volume and a and b are experimental constants.

The van der Waals (vdW) equation is an improvement of the ideal gas law, where some physical characteristics are introduced through the parameters a and b . The vdW equation introduces a whole new class of equation of states, highly appreciated and with great success. Though, the success of the vdW equation was not immediately recognized as the procedure of handling the calculations involved in applying the equation, does to a high degree depend on modern numerical calculations, - as we will see later in this section.

The parameters a and b in Eq. 3.51 are considered as corrections to the pressure and volume (molar volume) in the ideal gas law, where:

b is the hard-core or co-volume parameter. The parameter is said to be the packing limit, by which the fluid can not become any denser or differently, the limiting volume occupied by the fluid molecules themselves. Therefore, $v > b$.

a has a more composed (difficult) meaning, related to potential and affinity of the different molecules. a is known as *the attractive term*, to depend on temperature and on dimension aspects of molecules,

$$a(T) = a(T_c)\alpha(T_r, \omega), \quad (3.52)$$

where α is a dimensionless function of the pseudo reduced temperature and the acentric factor, respectively. (The acentric factor is a measure of the difference in molecular structure between various components in the gas. For a gas with spherical symmetry, i.e. like the argon molecule, $\omega = 0$.)

For the time being, we will assume a to be a constant.

If we multiply Eq. 3.51 by v^2 and carry out the multiplication, we get,

$$v^3 - \frac{bp + RT}{p}v^2 + \frac{a}{p}v - \frac{ab}{p} = 0. \quad (3.53)$$

The above equation is a cubic equation where the pressure - volume solution can indirectly be depicted as in Figure 3.6. Please notice that the figure depicts the pressure - explicit equation, $p(V)$ of Eq. 3.53.

Figure 3.6 illustrates that Eq. 3.53 generally has three different roots; A, B and D for temperatures $T < T_c$. For temperatures higher than the critical temperature ($T \geq T_c$), only one root exist. Of the three roots, $v_A < v_D < v_B$, the lowest root, $v_A = v_L$ is the

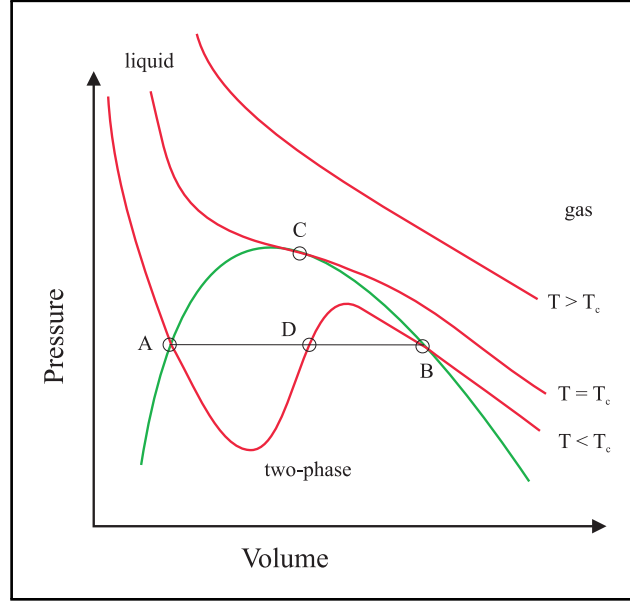


Figure 3.6: Pressure - volume relation for a cubic equation, illustrating the PV-plot for a pure substance.

liquid solution, while the largest root, $v_B = v_V$ is the vapor solution. The root v_D in the two-phase region has no significant meaning, as the system in equilibrium will be either in its vapor or liquid state (or differently; some of the original fluid will be in its liquid phase while other parts of the fluid will behave as a vapor).

At the critical point $T = T_c$, all roots in Eq. 3.53 will coincide and $v_A = v_B = v_D = v_c$, where the cubic equation Eq. 3.53 will reduce to,

$$(v - v_c)^3 = v^3 - 3v_c v^2 + 3v_c^2 v - v_c^3 = 0 \quad (3.54)$$

Using the above cubic equations, Eqs. 3.53 and 3.54, yields the value of the constants a , b and R ,

$$\left. \begin{aligned} 3v_c &= \frac{bp_c + RT_c}{p_c} \\ 3v_c^2 &= \frac{a}{p_c} \\ v_c^3 &= \frac{ab}{p_c} \end{aligned} \right\} \begin{aligned} a &= 3p_c v_c^2 \\ b &= \frac{v_c}{3} \\ R &= \frac{8p_c v_c}{3T_c} \end{aligned} \quad (3.55)$$

Inserting for the constants a , b and R in the vdW equation, Eq. 3.51, gives

$$\left(\frac{p}{p_c} + \frac{3v_c^2}{v^2} \right) \left(\frac{v}{v_c} - \frac{1}{3} \right) = \frac{8T}{3T_c}. \quad (3.56)$$

Introducing pseudo reduced quantities; $p_r = p/p_c$, $v_r = v/v_c$ and $T_r = T/T_c$, the vdW equation can be written on dimensionless form,

$$\left(p_r + \frac{3}{v_r^2}\right) \left(v_r - \frac{1}{3}\right) = \frac{8}{3}T_r. \quad (3.57)$$

The above equation demonstrates the principle of *the corresponding states*, which states that at the pseudo reduced state, (p_r, v_r, T_r) is the same for all fluids, i.e. when the normal pressure, volume and temperature is reduced to pseudo reduced variables, all fluids behave similarly. Pseudo reduced quantities, generally reduce the complexity of mathematical handling as all cases are handled simultaneously, where the solution is given on a general form, applicable for all fluids.

The critical compressibility factor Z_c , for gases described by the vdW equation can be written,

$$Z_c = \frac{p_c v_c}{RT_c} = \frac{3}{8}, \quad (3.58)$$

where we have used the result found for R , from Eq. 3.55.

For gases behaving ideally, we have $Z = Z_c = 1$ while for gases obeying the vdW equation $Z_c = 0.375$. The critical compressibility factor is an observable quantity and can be measured. Experimentally there are very few (if any) compounds that have a Z_c factor greater than 0.3, which again indicate that, seen from a practical point of view, the van der Waal EoS may not be the preferred equation of state.

3.3.2 Cubic Equations

A simple equation such as the vdW equation cannot accurately model the phase behavior of complex fluid mixtures. On the other hand, the vdW equation introduces a family of cubic equations from which many of the most popular EoS originate. Numerous attempts have been made to modify the two parameter vdW equation. In most cases, it is the attractive term a , that has been subject for modification while the b-term has remained unchanged.

One of the more successful modification of the vdW EoS was introduced by Redlich and Kwong in 1949 and later modified by Soave in 1972, by introducing an temperature dependence in the attractive term $a = a(T)$, as already discusses above. The Soave-Redlich-Kwong (SRK) equation of state is usually written,

$$p = \frac{RT}{v-b} - \frac{a(T)}{v(v+b)}. \quad (3.59)$$

Another, yet popular EOS, belonging to the family of two parameter cubic equations was introduced in 1976 by Peng and Robinson,

$$p = \frac{RT}{v-b} - \frac{a(T)}{v(v+b) + b(v-b)}. \quad (3.60)$$

Cubic equations with more than two constants exists in many variations, but seem to fail to improve the volumetric phase behavior prediction of complex reservoir fluids. In fact, of all cubic EoS belonging the the vdW-family, the two parameter equations often do better.

It therefore seems just, to concentrate further efforts on the Peng-Robinson (PR) equation, as the best choice of EoS, both with respect to simplicity and reliability.

3.3.3 The Peng-Robinson Equation

The modifications made by Peng and Robinson in Eq. 3.60, relative to the SRK EoS, had the purpose of primarily improving the prediction of liquid density. The term $b(v - b)$ in the PR-equation is therefore intended to reduce the attractive term such that liquid densities are better represented.

Multiplying by the denominators in Eq 3.60 and dividing by $p^2/(RT)^3$, gives

$$\left(\frac{p}{RT}\right)^3 (v^3 + bv^2 - 3b^2v + b^2) = \left(\frac{p}{RT}\right)^2 (v^2 + 2bv - b^2) - \left(\frac{p}{RT}\right)^2 \frac{a}{RT}(v - b). \quad (3.61)$$

Inserting the compressibility factor defined by the real gas law; $Z = pv/(RT)$, in the above equation, and introducing two new parameters A and B , Eq. 3.61 is written,

$$Z^3 - (1 - B)Z^2 + (A - 2B - 3B^2)Z - (AB - B^2 - B^3) = 0, \quad (3.62)$$

where $A = \frac{ap}{(RT)^2}$ and $B = \frac{bp}{RT}$

The solution of the cubic equation, Eq. 3.62 is illustrated in Figure 3.7. From the discussion related to the van der Waals equation, it is clear that the molar volume must be larger than the hard-core value, $v > b$. This means that the realistic solutions of the cubic equation must be positive (since p and T are both positive) and satisfy, $Z > pb/(RT)$.

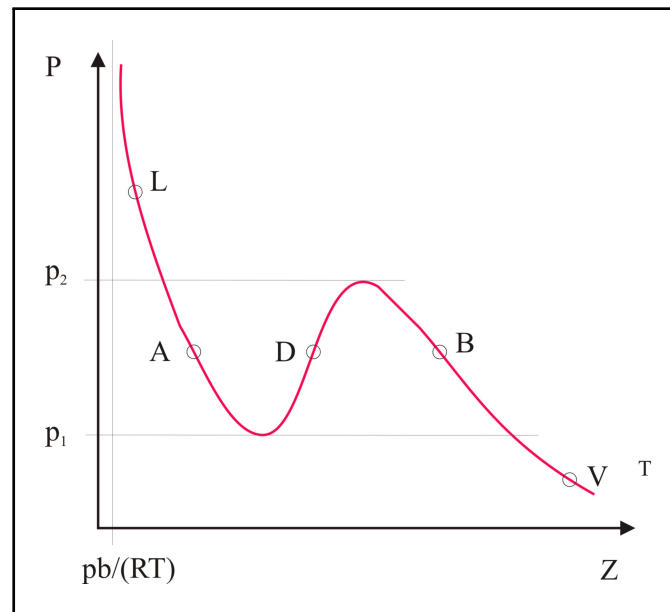


Figure 3.7: Possible solution of the pressure-explicit cubic equation for a chosen fixed pressure and temperature.

For pressures larger than p_1 and lower than p_2 , and given a certain temperature T , only one solution will exist, i.e. the liquid solution, Z_L or the vapor solution, Z_V , respectively. For pressure $p_1 < p < p_2$, three real solution may exist $Z_A < Z_D < Z_B$,

where the lowest value is the liquid solution, $Z_L = Z_A$ and the highest value is the vapor solution, $Z_V = Z_B$. The intermediate solution Z_D has no physical meaning, as the fluid is either a liquid or a vapor.

At the critical point $Z_C = p_c v_c / (RT_c)$, all three solutions fall on the same point in the PV-diagram (see Figure 3.6) and we may write the cubic equation similarly as in Eq. 3.54,

$$Z^3 - 3Z_c Z^2 + 3Z_c^2 Z - Z_c^3 = 0. \quad (3.63)$$

Combining Eqs. 3.63 and 3.62, and solving the three equations gives,

$$\left. \begin{aligned} 3Z_c &= 1 - B \\ 3Z_c^2 &= A - 2B - 3B^2 \\ Z_c^3 &= AB - B^2 - B^3 \end{aligned} \right\} \begin{aligned} A &= 0.45723 \\ B &= 0.77796 \\ Z_c &= 0.30740 \end{aligned} \quad (3.64)$$

From the above calculations, the compressibility factor related to the PR-EoS is found to be $Z_c = 0.307404$, which is closer to the experimental values obtained for pure hydrocarbons. Figure 3.8, gives an overview of the various compressibility factor. In the figure, the value obtained from the SRK-EoS is also included, for comparison.

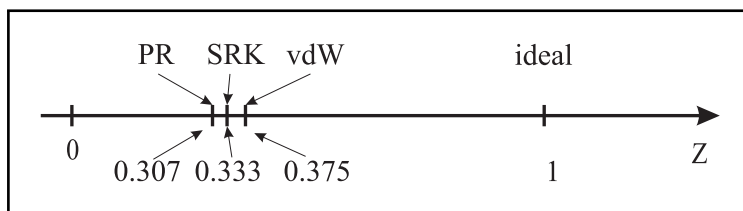


Figure 3.8: Graphic representation of compressibility factors for different EoS.

From the definition of the parameters A and B in Eq. 3.62 and the above results, we can define the physical parameters introduced in the PR-EoS, a and b , such as

$$\begin{aligned} a &= 0.45723 \frac{(RT_c)^2}{p_c}, \\ b &= 0.77796 \frac{RT_c}{p_c}. \end{aligned} \quad (3.65)$$

Up to this point in the development of the PR-EoS, all deductions has been purely academic and the only ties to the experimental world have been through the critical values p_c and T_c . As already mentioned, experimental data has been most successfully introduced into the PR-EoS through the attractive constant $a = a(T_c)$. From Eq. 3.52 we have learned that a is temperature dependent through the $\alpha(T_r, \omega)$ function.

The adjustment done to fit experimental data from various components and fluids to obtain satisfactory correspondence between observed and predicted fluid phase behavior is a lengthy and tedious elaboration of measurements and calculations. In this text, we only sum up the results [1];

$$a(T) = a(T_c) \alpha(T_r, \omega),$$

$$\alpha = (1 + m(1 - \sqrt{T_r}))^2, \quad (3.66)$$

$$m = 0.37464 + 1.54226 \omega - 0.26992 \omega^2, \quad (3.67)$$

$$\omega = \frac{3}{7} \left(\frac{\log(p_c/p_{atm})}{T_c/T_b - 1} \right) - 1, \quad (3.68)$$

where ω is known as the *acentric factor*. T_b is the normal boiling point temperature. Pressure and temperature is measured in *atm.* and *K*, respectively.

3.3.4 The Equilibrium Coefficients

Based on the PR-EoS, Eq. 3.60, we may now calculate the fugacity coefficients φ_i , presented in Eq. 3.49. For pure components the calculation seems to be straight forward, where the constants a and b are taken directly for Eqs. 3.65 and 3.52. In the case of a mixture of components, these calculations become a bit more elaborately.

For a fluid containing a mixture of components, the value of the constants a and b used in the PR-EoS, should represent an average over all components in the mixture. The averaging process should also secure a collective representation of the fluid.

One of the most favored averaging rules for hydrocarbon mixtures used, combine both geometric and arithmetic averaging processes, where the following mixing rules are used,

$$a = \sum_{i=1}^N \sum_{j=1}^N x_i x_j a_{ij}, \quad \text{where } a_{ij} = (1 - \delta_{ij}) \sqrt{a_i a_j} \quad (3.69)$$

$$b = \sum_{i=1}^N x_i b_i, \quad (3.70)$$

where δ_{ij} is an interaction parameter, $\delta_{ij} = \delta_{ji}$, generally independent of pressure, temperature and composition. $x_i = n_i/n$ is the mole fraction of component i . a_i and b_i represent the parameters of pure substance i , defined by Eqs. 3.65.

From the above mixing rules, we have that the parameters a and b are both functions of the molar content n_i , while the pure substance parameters a_i and b_i are constants (experimental values characteristic for that particular pure substance). Thus $a = a(n_i)$ and $b = b(n_i)$.

The PR-EoS can be written,

$$p = \frac{RT}{v - b} - \frac{a}{(\delta_1 - \delta_2)b} \left(\frac{1}{(v + \delta_2b)} - \frac{1}{(v + \delta_1b)} \right), \quad (3.71)$$

where

$$\delta_1 = 1 + \sqrt{2} \quad \text{and} \quad \delta_2 = 1 - \sqrt{2},$$

$$\delta_1 - \delta_2 = 2\sqrt{2} \quad \text{and} \quad \delta_1 \delta_2 = -1 \quad \text{and} \quad \delta_1 + \delta_2 = 2.$$

(Note that we in this text are here using two different delta functions $\delta_{i,j}$ and δ_1, δ_2 , where $\delta_{i,j} = 0$ if $i \neq j$ and δ_1, δ_2 are defined above.)

Reintroducing the volume $V = nv$ in the PR-EoS, gives

$$p = \frac{nRT}{V - nb} - \frac{n^2a}{(\delta_1 - \delta_2)nb} \left(\frac{1}{(V + \delta_2nb)} - \frac{1}{(V + \delta_1nb)} \right). \quad (3.72)$$

The PR-EoS, on the form as presented above is well suited for the derivation $\partial p / \partial n_i$, as prescribed by Eq. 3.49. Derivation gives,

$$\begin{aligned} \frac{\partial p}{\partial n_i} &= \frac{RT}{V - nb} \frac{\partial n}{\partial n_i} - nRT \frac{1}{(V - nb)^2} \left(-\frac{\partial nb}{\partial n_i} \right) \\ &- \left[\frac{1}{(\delta_1 - \delta_2)nb} \frac{\partial(n^2a)}{\partial n_i} - \frac{n^2a}{(\delta_1 - \delta_2)(nb)^2} \frac{1}{\partial n_i} \frac{\partial nb}{\partial n_i} \right] \left(\frac{1}{V + \delta_2nb} - \frac{1}{V + \delta_1nb} \right) \\ &- \left[\frac{n^2a}{(\delta_1 - \delta_2)nb} \right] \left(\frac{-\delta_2}{(V + \delta_2nb)^2} \frac{\partial nb}{\partial n_i} - \frac{-\delta_1}{(V + \delta_1nb)^2} \frac{\partial nb}{\partial n_i} \right), \end{aligned} \quad (3.73)$$

where the derivatives with respect for n_i are,

$$\begin{aligned} \frac{\partial n}{\partial n_i} &= 1 \\ \frac{\partial nb}{\partial n_i} &= b_i \\ \frac{\partial n^2a}{\partial n_i} &= 2 \sum_{j=1}^N n_j a_{ij} = 2n \sum_{j=1}^N y_j a_{ij} \end{aligned}$$

Substituting for the above derivatives in Eq. 3.73 and rearranging, gives,

$$\begin{aligned} \frac{\partial p}{\partial n_i} &= \frac{RT}{V - nb} + \frac{nRT}{(V - nb)^2} b_i \\ &- \frac{a}{(\delta_1 - \delta_2)b} \left[\frac{2 \sum_{j=1}^N y_j a_{ij}}{a} - \frac{b_i}{b} \right] \left(\frac{1}{V + \delta_2nb} - \frac{1}{V + \delta_1nb} \right) \\ &+ \frac{b_i}{(\delta_1 - \delta_2)} \frac{n^2a}{nb} \left(\frac{\delta_2}{(V + \delta_2nb)^2} - \frac{\delta_1}{(V + \delta_1nb)^2} \right), \end{aligned} \quad (3.74)$$

Substituting the differential pressure, Eq. 3.74 into Eq. 3.49, and regrouping, gives,

$$\ln \varphi_i = \int_V^\infty \frac{1}{RT} \left[\underbrace{\left(\frac{RT}{V-nb} - \frac{RT}{V} \right)}_{I_1} - \underbrace{\frac{a}{(\delta_1 - \delta_2)b} \left(\frac{2 \sum_{j=1}^N y_j a_{ij}}{a} - \frac{b_i}{b} \right) \left(\frac{1}{V + \delta_2 nb} - \frac{1}{V + \delta_1 nb} \right)}_{I_2} + \underbrace{\frac{nRT}{(V-nb)^2} b_i + \frac{b_i}{(\delta_1 - \delta_2) nb} \left(\frac{\delta_2}{(V + \delta_2 nb)^2} - \frac{\delta_1}{(V + \delta_1 nb)^2} \right)}_{I_3} \right] dV - \ln Z. \quad (3.75)$$

Subdividing the integral in Eq 3.75 into three parts and integrating, we get,

$$\begin{aligned} \int_V^\infty \frac{I_1}{RT} dV - \ln Z &= \frac{-1}{RT} [RT \ln(V-nb) - RT \ln V] - \ln Z \\ &= -\ln \left(Z - \frac{Znb}{V} \right) = -\ln(Z-B), \end{aligned} \quad (3.76)$$

$$\begin{aligned} \int_V^\infty \frac{I_2}{RT} dV &= \frac{-1}{RT} \left[\frac{1}{(\delta_1 - \delta_2)b} \frac{a}{b} \left(\frac{2 \sum_{j=1}^N y_j a_{ij}}{a} - \frac{b_i}{b} \right) \ln \frac{V + \delta_2 nb}{V + \delta_1 nb} \right] \\ &= \frac{1}{(\delta_1 - \delta_2)B} \frac{A}{b} \left(\frac{2 \sum_{j=1}^N y_j a_{ij}}{a} - \frac{b_i}{b} \right) \ln \frac{Z + \delta_2 B}{Z + \delta_1 B}, \end{aligned} \quad (3.77)$$

$$\begin{aligned} \int_V^\infty \frac{I_3}{RT} dV &= \frac{1}{RT} \left[\frac{-nRT}{V-nb} b_i - \frac{b_i}{b} \frac{1}{(\delta_1 - \delta_2) n} \frac{V}{(V + \delta_2 nb)(V + \delta_1 nb)} \left(\frac{-(\delta_1 - \delta_2)n^2 a}{(V + \delta_2 nb)(V + \delta_1 nb)} \right) \right] \\ &= \frac{b_i}{b} \left(\frac{1}{RT} \frac{-nbRT}{V-nb} + \frac{V}{n} \frac{1}{RT} \left(\frac{nRT}{V-nb} - p \right) \right) \\ &= \frac{b_i}{b} (1-Z). \end{aligned} \quad (3.78)$$

In the integration above, we have used the real gas law $pV = ZnRT$, the parameters $B = bp/(RT)$ and $A = ap/(RT)^2$ and the definition of the PR-EoS presented in Eq. 3.71.

The final expression defining the equilibrium coefficient for the PR-EoS is written,

$$\ln \varphi_i = (1-Z) \frac{b_i}{b} - \ln(Z-B) + \frac{1}{2\sqrt{2}} \frac{A}{B} \left(\frac{2 \sum_{j=1}^N y_j a_{ij}}{a} - \frac{b_i}{b} \right) \ln \frac{Z + (1 - \sqrt{2})B}{Z + (1 + \sqrt{2})B}, \quad (3.79)$$

where the above equation gives the equilibrium coefficient for the i th component in a multi component mixture. Eq. 3.79 should be calculated for all components, given a certain predefined pressure and temperature. From the definition of the equilibrium coefficient φ , given by Eq. 3.41, - first the fugacities f_i , should be calculated. When the equilibrium is found, the equilibrium ratio K_i , defined in Eq. 3.42, is calculated.

3.4 Simulation of Phase Behavior

Using the PR-EoS equilibrium coefficient in Eq. 3.79, we could start designing an automatic calculation procedure leading up to the complete characterization of the fluid phase behavior for all pressures and temperatures of interest.

However, with a minimum amount of extra effort we may expand the calculation done in the above section, to include a broad class of cubic EoS.

3.4.1 General Cubic EoS

Almost all known cubic EoS can be represented by the general equation,

$$p = \frac{RT}{v-b} - \frac{a}{(v-b+c)(v-b+d)}, \quad (3.80)$$

where c and d are two new constants. The parameter $a = a(T)$ is defined as above.

Depending on the chosen values for c and d , the three EoS mentioned so far can be represented by Eq. 3.80 if,

$$\begin{aligned} \text{vdW: } & c = d = b \\ \text{SRK: } & c = b \text{ and } d = 2b \\ \text{PR: } & c = (2 - \sqrt{2})b \text{ and } d = (2 + \sqrt{2})b \end{aligned}$$

Introducing the compressibility factor Z in Eq. 3.80 similarly as in Eq. 3.62, we get,

$$\begin{aligned} Z^3 + Z^2[-3B + (C + D - 1)] + Z[3B^2 - 2B(C + D - 1) + (A + CD - C - D)] \\ + [B^3 + B^2(C + D - 1) - B(A + CD - C - D) - CD] = 0, \end{aligned}$$

where $A = \frac{ap}{(RT)^2}$, $B = \frac{bp}{RT}$, $C = \frac{cp}{RT}$ and $D = \frac{dp}{RT}$

(3.81)

The above equation can be solved at the critical point and $Z = Z_c \Rightarrow (Z - Z_c)^3 = 0$ gives the following three equations,

$$\begin{aligned} -3Z_c &= -3B_c + (C_c + D_c - 1) \\ 3Z_c^2 &= 3B_c^2 - 2B_c(C_c + D_c - 1) + (A_c + C_c D_c - C_c - D_c) \\ -Z_c^3 &= B_c^3 + B_c^2(C_c + D_c - 1) - B_c(A_c + C_c D_c - C_c - D_c) - C_c D_c \end{aligned}$$

where the constants $A_c = A_c(p_c, T_c)$, $B_c = B_c(p_c, T_c)$, $C_c = C_c(p_c, T_c)$ and $D_c = D_c(p_c, T_c)$. If a fourth equation is introduced,

$$C_c = \lambda B_c,$$

stating a linear relationship between C and B , we may find the constants A_c , B_c , C_c and D_c solving the following four equations, where Z_c and λ are predefined,

$$B_c^3 + (-3Z_c + 3\lambda - \lambda^2)B_c^2 + (-3\lambda Z_c + 3Z_c^2 + \lambda)B_c - Z_c^3 = 0 \quad (3.82)$$

$$C_c = \lambda B_c \quad (3.83)$$

$$D_c = (3 - \lambda)B_c - 3Z_c + 1 \quad (3.84)$$

$$A_c = (\lambda^2 - 3\lambda + 3)B_c^2 + (3\lambda Z_c - \lambda - 6Z_c + 3)B_c + (3Z_c^2 - 3Z_c + 1) \quad (3.85)$$

The solution of the above equations are done for the following choice of Z_c and λ ;

$$\text{vdW: } Z_c = 0.375 \text{ and } \lambda = 1 \quad (3.86)$$

$$\text{SRK: } Z_c = 0.333, \lambda = 1 \text{ and } m = 0.480 + 1.574\omega - 0.176\omega^2 \quad (3.87)$$

$$\text{PR: } Z_c = 0.307, \lambda = 2 - \sqrt{2} \text{ and } m = 0.3746 + 1.542\omega - 0.270\omega^2 \quad (3.88)$$

Integration of Eq. 3.80, using Eq. 3.49 and following the same procedure as in the Peng-Robinson case, gives the equilibrium coefficient,

$$\begin{aligned} \ln \varphi_i &= \frac{b_i}{Z - B} - \ln(Z - B) \\ &+ \frac{A}{D - C} \left(\frac{b_i - d_i}{Z - B + D} - \frac{b_i - c_i}{Z - B + C} \right) \\ &- \left(\frac{2 \sum_{j=1}^N y_{ij} a_{ij}}{D - C} - \frac{A(d_i - c_i)}{(D - C)^2} \right) \ln \frac{Z - B + D}{Z - B + C} \end{aligned} \quad (3.89)$$

In the above equation the parameters $A(p, T)$, $B(p, T)$, $C(p, T)$ and $D(p, T)$ are defined according to Eq. 3.81, while the constants A_c , B_c , C_c and D_c , in Eqs. 3.82 to 3.85 are calculated, such that the mixing parameters a_i , b_i , c_i and d_i are defined;

$$a_i = A_{ci} \frac{(RT)^2}{p} \quad (3.90)$$

$$b_i = B_{ci} \frac{RT}{p} \quad (3.91)$$

$$c_i = C_{ci} \frac{RT}{p} \quad (3.92)$$

$$d_i = D_{ci} \frac{RT}{p} \quad (3.93)$$

where again a , b , c and d are defined according to the mixing rules, such as in Eqs. 3.69 and 3.70.

3.4.2 Calculation and Simulation

All major elements needed to calculate the two phase behavior at equilibrium for a mixture of components are now present. When the fugacities for the liquid and vapor

state are equal, chemical equilibrium is found and the phase split and then compositions are readily available.

The complete calculation procedure can now be described as a stepwise process, where reference is made to equations already developed. Based on the items presented below, a data simulation program is constructed by which all calculations are done automatically.

The calculations involved in the PVT simulations are the following:

1. The choice of EoS; vdW, SRK or PR is done by choosing the correct set of parameters; Z_c , λ and m , defined in Eqs. 3.86 to 3.88. The acentric factor ω_i , defined for each component is normally part of the input data.
2. Critical pressure and temperature, $(p_c, T_c)_i$, together with fluid composition z_i and molar weight of composition m_i and as already mentioned, the acentric factor, constitute the input data needed to perform these calculations.
3. The constants A_c , B_c , C_c and D_c are calculated for all components $i = 1, \dots, N$, using Eqs. 3.82 to 3.85.
4. The mixing parameters a_i , b_i , c_i and d_i are calculated for a given pressure and temperature, using Eqs. 3.90 to 3.93. The parameters a , b , c and d are calculated using mixing rules such as in Eqs. 3.82 to 3.85.
5. The the parameters A , B , C and D are calculated and the compressibility factor $Z(p, T)$ is calculated using Eq. 3.81. From the (in principle) three solution of Eq. 3.81; $Z_1 < Z_2 < Z_3$, the lowest is defined as the liquid solution, $Z_L = Z_1$ and the highest as the vapor solution, $Z_V = Z_3$.
6. The equilibrium coefficients φ_L and φ_V , are calculated using Eq. 3.89 and the fugacities f_L and f_V are calculated using Eq. 3.41. Both the equilibrium coefficients and the fugacities are calculated for all components.
7. If $f_{Li} = f_{Vi}$, $i = 1, \dots, N$, then the two phases are in equilibrium and the phase split can be calculated.
8. The equilibrium ratio K_i is defined by Eq. 3.42 and the vapor molar split V is calculated using the Newton-Raphson iteration, described in the previous chapter. When the molar phase split is found, the compositions x_i and y_i are readily available. At this point we are ready to start calculating the vapor-liquid equilibrium for new pT point.
9. If, on the other hand, the fugacities are not identical, a new iteration is initiated, where a *successive substitution* method is used, where

$$K_i^{M+1} = \left(\frac{\varphi_{Li}}{\varphi_{Vi}} \right)^M = K_i^M \left(\frac{f_{Li}}{f_{Vi}} \right)^M,$$

where M is the iteration variable.

A solution is reached when the following tolerance criteria is met,

$$\sum_{i=1}^N \left(\frac{f_{Li}}{f_{Vi}} - 1 \right)^2 < \epsilon,$$

where $\epsilon \ll 1$ is used.

3.4.3 Simulation Results

Based on the above development, a PVT-simulation program has been developed where the main results derived in the previous sections, have been used. The PVT program is based on many of the equations developed above and is designed to demonstrate the applicability of the theory presented. The PVT program, as it appear here in this text, is not a fully developed PVT-simulation program, compared to the many commercial available PVT packages.

In the program presented here, the only fluid specific input parameter is the composition. No options for *tuning* the calculations to e.g. an experimental measured dew- or bubble point value or densities, are allowed for in this program. The use of the present program is therefor limited to demonstration purposes only. In the continuation of this text, in the coming chapters, a commercial PVT-simulation package (PVTsim from Calsep) is therefore used in calculations involving PVT phase behavior.

The PVT-simulation program has the capability to do the following calculations;

1. Two phase envelope calculations and
2. depletion pressure calculations.

An input file is defining the simulation process as well as the form and type of output data.

In order to demonstrate the capability of the PVT-simulation program, the composition of a dry gas (Lean Gas) and a gas-condensate (Rich Gas) have been chosen. The composition of the two gases are presented in Fig. 3.9 and in Table 3.1.

The two gases are characterized by 14 compounds, which are reasonably well defined with respect to molar weight, critical temperature and pressure and other parameters such as the accentric factors (see Eq. 3.68). The 14'th compound however is a C^+ component, where all heavier components are lumped into. The C^+ components are supposed to characterize all heavier components and can therefore not be defined accurately. The C^+ component can be characterized experimentally, but more commonly these pseudo-components are treated as tuning parameters. In a PVT-simulator, these pseudo-components are defined according to overall important and general parameters such as liquid yields, condensate gas ratios and other parameters determining the extent of mass transfer from liquid to gas and vice versa [2].

The two phase envelope for the two gases are shown in Figure 3.10, where the pressure and temperature limits are 10 to 250 bars and 250 to 450 Kelvin, respectively. The critical point for the gas condensate is located at (232.8 bars, 322.2 K), while the critical point for the dry gas would be located outside the plot, where the simulation program was not been able to locate this point, due to convergence errors. This is not

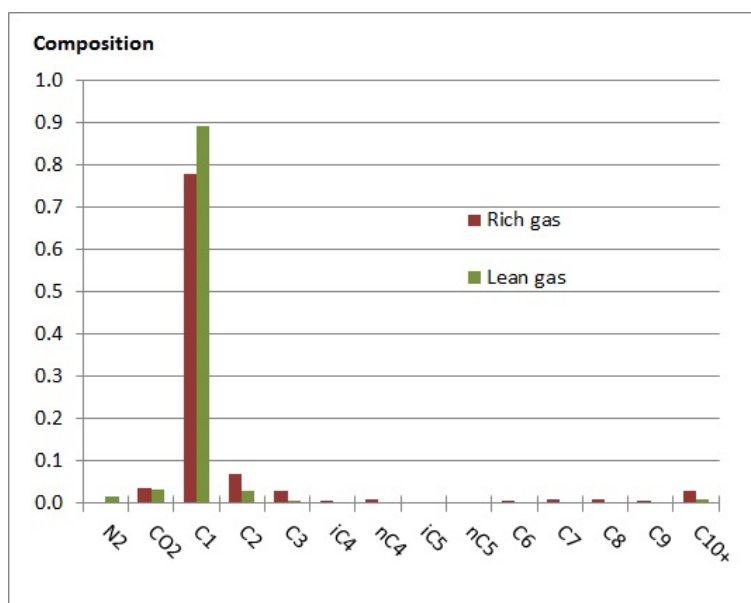


Figure 3.9: Composition of rich and lean gas.

Table 3.1: Composition of rich and lean gas.

| Component | Lean Gas | Rich Gas |
|--------------------------------|----------|----------|
| N ₂ , | 0.0170 | 0.0020 |
| CO ₂ , | 0.0328 | 0.0351 |
| C ₁ , | 0.8924 | 0.7783 |
| C ₂ , | 0.0308 | 0.0688 |
| C ₃ , | 0.0068 | 0.0297 |
| iC ₄ , | 0.0012 | 0.0049 |
| nC ₄ , | 0.0013 | 0.0104 |
| iC ₅ , | 0.0006 | 0.0039 |
| nC ₅ , | 0.0004 | 0.0045 |
| C ₆ , | 0.0006 | 0.0060 |
| C ₇ , | 0.0024 | 0.0101 |
| C ₈ , | 0.0024 | 0.0103 |
| C ₉ , | 0.0013 | 0.0065 |
| C ₁₀ ⁺ , | 0.0100 | 0.0295 |

unusual for light gases as their critical points often are found at quite low pressure and temperature values.

In calculating the two phase envelopes, a fugacity tolerance of $\epsilon < 1.0 \cdot 10^{-12}$ has been used. (The same Decane Plus molar weight: $MW_{C_{10+}} = 231.787$ is used for both gases!)

In the depletion pressure calculations, the vapor molar fractions are calculated for certain pre-selected temperatures. The left part of Figure 3.11 shows the depletion lines for temperatures 350 K and 370 K.

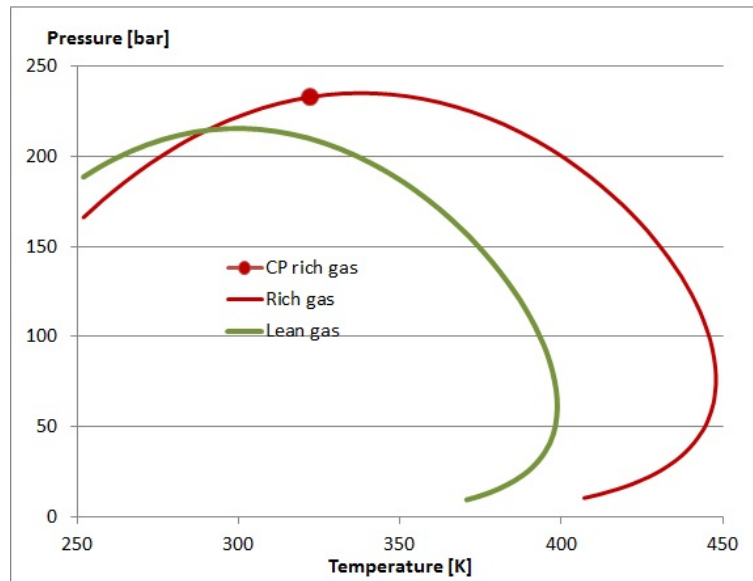


Figure 3.10: Two phase envelope for a rich and lean gas

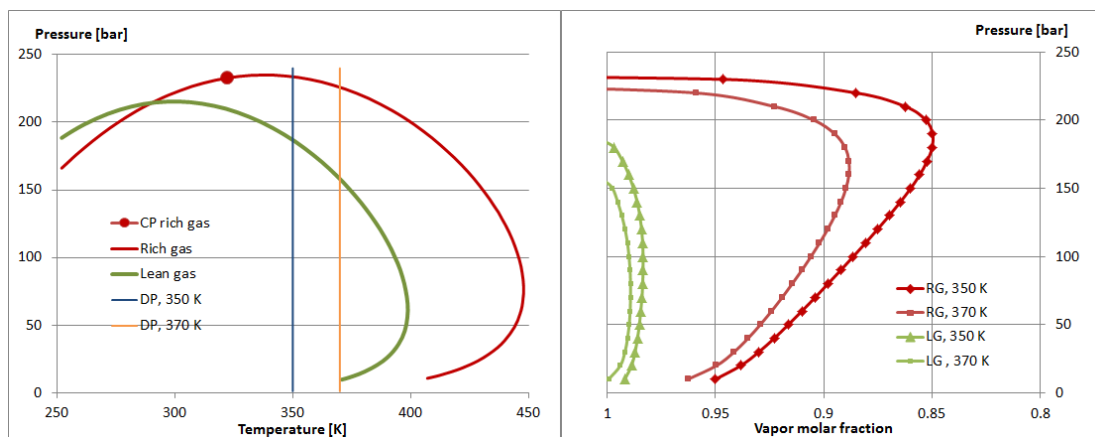


Figure 3.11: Depletion pressure calculations and vapor molar fractions.

The right hand side of the figure shows the vapor molar fraction as function of pressure. Inside the two-phase envelope, the molar fraction defines the equilibrium phase split of vapor and liquid in the mixture. On the dew point curve this vapor molar fraction would therefore be equal to 1. Figure 3.11 shows that the lean gas contains very little oil compared to the rich gas, as the vapor fraction is high. The maximum dropout of liquid for the lean gas is less than 1.5 % (370 K), compared to about 15 % in the rich gas case. We also observe; as the depletion temperature moves toward the critical point (to the left in on the two-phase envelope), ie. from 370 K to 350 K, - more liquid drops out of the gas.

The depletion pressure option, in the program, renders the opportunity to perform various calculations based on equilibrium as function of pressure and temperature. Fig-

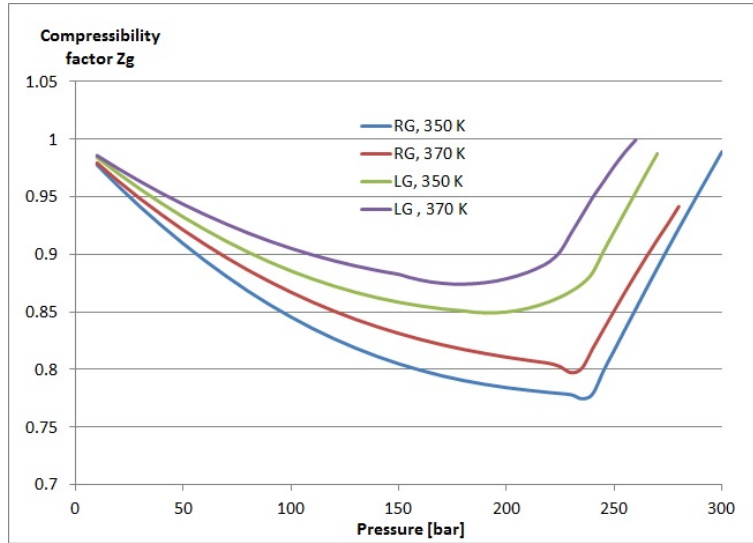
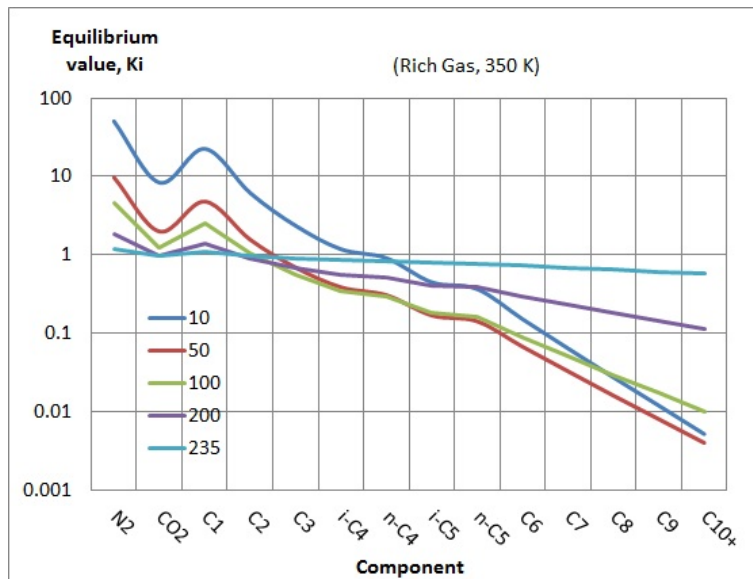
Figure 3.12: Gas compressibility factor, Z_g

Figure 3.12 shows the gas compressibility factor, Z_g for the two temperatures; 350 K and 370 K, as function of pressure. The compressibility factor is particularly important as coefficient in the real gas law. As seen from the figure, the behavior of lean gases are more "ideal" than rich gases, as Z_g is closer to unity and that gases behave more "ideally" for lower temperatures than for higher temperatures.

Figure 3.13: Equilibrium values, K_i

The depletion pressure calculations also renders the composition data for the Z -, X - and Y - phases, related to pressure and temperature. The equilibrium coefficients K_i , as defined in Eq. 3.42 are depicted in Figure 3.13 for pressures from 10 to 235 bars.

For increasing pressures and finally ending up at the dew-point pressure, all K_i 's are approaching unity. For a given pressure and temperature, $K_i = 1$ defines the *conversion point*.

As observed earlier, the position or point in the two phase envelope where the depletion line crosses the dew-point line, - the saturation of liquid in the gas is infinitesimal small (for a gas condensate mixture). This point is therefore called the *saturation point*. The two-phase envelope can therefore be defined as those pressure and temperature points where the conversion point is equal to the saturation point.

3.5 Gas Properties

Four different natural gas fields from the North Sea are here presented as typical examples of natural gases. Figure 3.14 presents the two-phase envelope from the different fields; Frigg, Gullfaks, Kvitebjørn and Sleipner Vest.

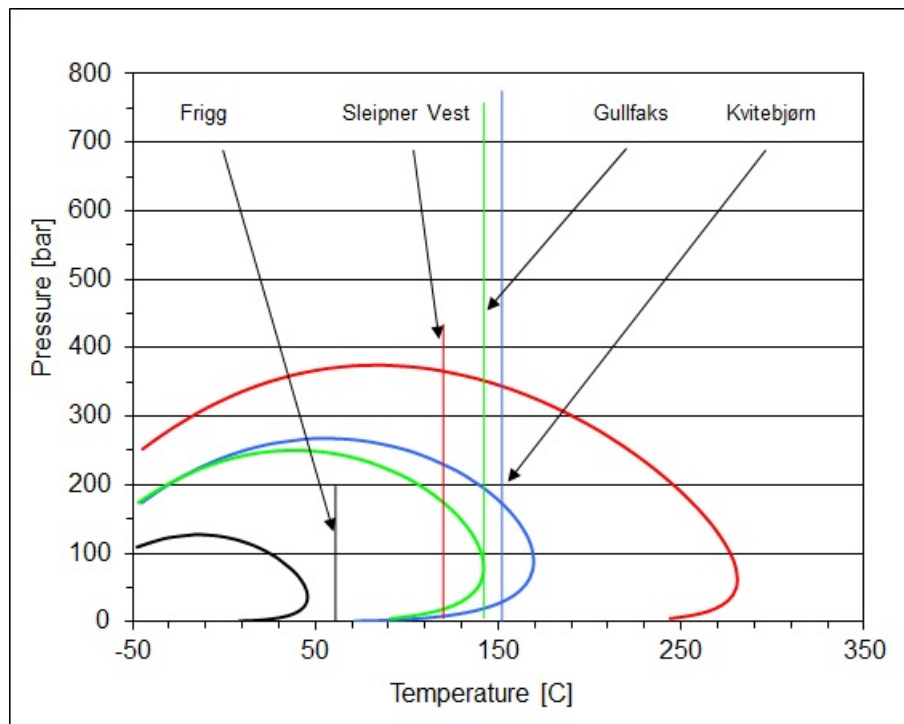


Figure 3.14: Two-phase envelope from Frigg, Gullfaks, Kvitebjørn and Sleipner Vest and pressure depletion line.

Common for all four two-phase envelopes, as presented in Figure 3.14, is that the critical points are all located outside the temperature range defined in the figure. Thus, the part of the two-phase envelope shown in Figure 3.14, is primarily the dew-point curve. The vertical lines in Figure 3.14 are the isothermal depletion line, starting at initial reservoir pressure.

In the case of the gas from Frigg, we clearly see that at reservoir condition, the two-phase region is never entered, which is why Frigg is a dry gas fields. In the case of

Gullfaks, the two-phase envelope is close and barely touching the isothermal pressure depletion line. Two phases (gas and liquid) does not occur in the reservoir, but can be expected to occur in the well-bore or associated tubings. The combination of no liquid condensation in the reservoir and two-phase production at standard condition is typical for wet gas reservoirs. Gas production from Kvitebjørn will eventually pass into the two-phase region with some but small retrograde condensation of liquid in the reservoir, - which again is typical for gas condensate reservoirs. The fact that both Gullfaks and Kvitebjørn are over-pressurized leads to significant gas production before the two-phase region is entered and in the case of Kvitebjørn only a minor part of the gas will condensate. In the case of Sleipner Vest, retrograde condensation will start quite early and the amount of liquid condensation will be considerable (compared to Kvitebjørn).

Of the four fields described above, Sleipner Vest is the most interesting, seen from a reservoir production point of view. Liquid condensation in the reservoir under natural depletion does represent a greater challenge, than one-phase gas production. Secondly, from a purely modeling point of view, all models describing gas production from gas condensate reservoirs are automatically also models of dry - and wet gas reservoirs.

Figure 3.15 shows the dew-point curve ($V = 1$) for Sleipner Vest gas, the same curve as shown in Figure 3.14. The dotted line, however, is the iso-fraction line $V = 0.974$, i.e. the line inside the two-phase envelope where the gas-liquid fraction is 0.974. The isothermal pressure line is merely touching the iso-fraction line at a reservoir pressure of about 140 bars. At this pressure the retrograde condensation has reached its maximum in the reservoir and further pressure reduction will in principle cause liquid to evaporate.

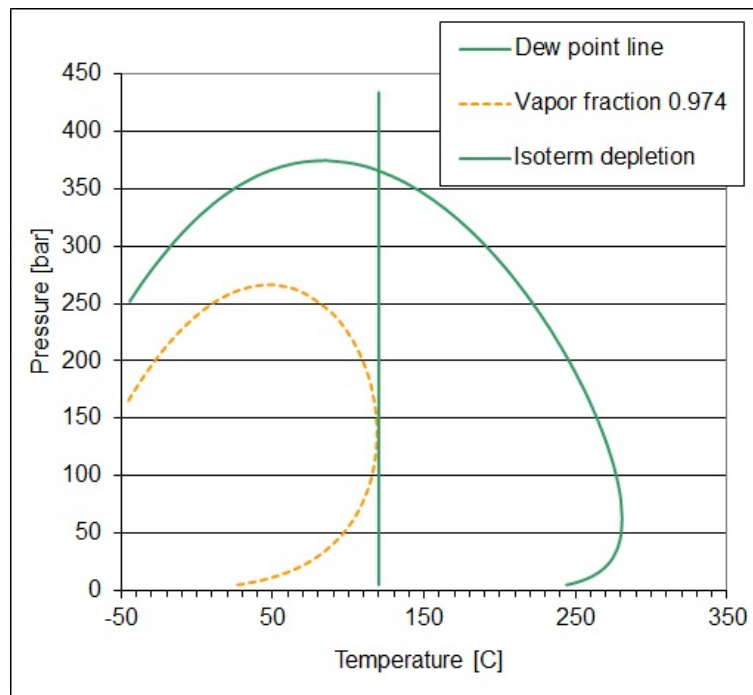


Figure 3.15: Dew-point curves $V = 1.0$ and $V = 0.974$ for Sleipner Vest gas.

A consequence of liquid condensation, as shown in Figure 3.15, is a lighter reservoir gas. Since the more heavier components of the gas is "falling out" and are forming a liquid, the remaining gas must be lighter and thus, the composition of the gas must become leaner. Examples of produced gas compositions are given as function of pressure in Table 3.2.

Table 3.2: Composition in mole % of produced well stream at 120°C (Sleipner Vest gas).

| Pressure [bar] | 434 | 359 | 138 | 30 |
|----------------|-------|-------|-------|-------|
| N_2 , | 0.78 | 0.78 | 0.80 | 0.78 |
| CO_2 , | 8.72 | 8.72 | 8.85 | 8.88 |
| C_1 , | 71.00 | 71.02 | 72.53 | 71.57 |
| C_2 , | 8.56 | 8.56 | 8.63 | 8.81 |
| C_3 , | 4.67 | 4.67 | 4.62 | 4.91 |
| iC_4 , | 0.71 | 0.71 | 0.69 | 0.76 |
| nC_4 , | 1.23 | 1.23 | 1.18 | 1.32 |
| iC_5 , | 0.41 | 0.41 | 0.38 | 0.45 |
| nC_5 , | 0.41 | 0.41 | 0.38 | 0.45 |
| C_6 , | 0.45 | 0.45 | 0.39 | 0.48 |
| C_7 , | 0.66 | 0.66 | 0.50 | 0.61 |
| C_8 , | 0.70 | 0.70 | 0.47 | 0.52 |
| C_9 , | 0.41 | 0.41 | 0.24 | 0.23 |
| C_{10}^+ , | 1.29 | 1.28 | 0.35 | 0.24 |

The four pressures chosen in Tabel 3.2 are the initial pressure, a pressure close to the dew-point but inside the two-phase envelope, a pressure close to maximum liquid condensation in the reservoir and lastly the end point pressure where gas production is halted, respectively.

From the gas composition (y_i) as presented in Table 3.2, and the composition of the condensate liquid (x_i) we may calculate all other parameters needed to carry out material balance and other fundamental relationships.

3.5.1 Gas Density

The PVT behavior of ideal gases (no interaction between the gas molecules) is described by the Ideal-Gas Law. Real gases behave as ideal gases at low pressure. At higher pressure the deviation from the ideal gas behavior is characterized by a correction factor, a z-factor, and the Real Gas Law is written,

$$pV = ZnRT, \quad (3.94)$$

where n is the number of moles in the gas and R is the gas constant $R = 8314.413 \text{ Pa} \cdot \text{m}^3 / (\text{k mol} \cdot \text{K})$. p , V and T is the pressure, volume and temperature, respectively.

The correction factor is also known as the *gas deviation factor*, the *compressibility factor* or simply as the z-factor. For ideal gases the z-factor is equal to unity. For

real gases it may be greater or less than unity, depending on the pressure, temperature and the composition of the gas. The z-factor may vary considerably, but is commonly found in the interval $0.63 < Z < 1.58$. z-factors can be determined by experiments or calculated from PVT simulations.

If the mean molecular mass of a gas is M (average mass of one mole gas). Then, using the real gas law Eq. 3.94, the gas density is written,

$$\rho = \frac{nM}{V} = \frac{Mp}{ZRT} \quad (3.95)$$

The z-factor can be derived by the K-value method or alternatively by using the EoS method. Figure 3.16 show the z-factors for the Sleipner Vest gas, where the the z-factor for the produced gas and the two-phase z-factor for the reservoir gas, are plotted. Both lines are calculated at reservoir temperature of 120°C . Figure 3.16 illustrates quite clearly the dependence of pressure and composition as mentioned above.

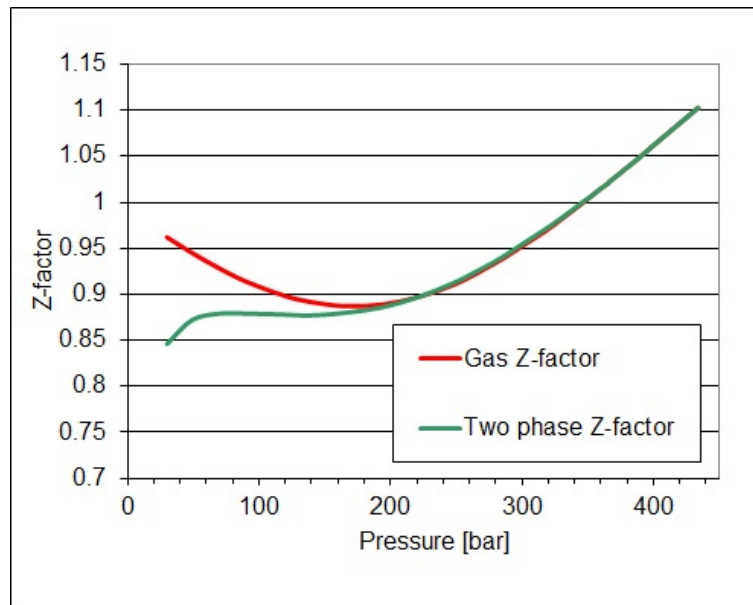


Figure 3.16: z-factors for Sleipner Vest gas.

An alternative to expressing the density in kg/m^3 , is to use dimensionless unit as the *gas gravity*. The gas gravity is the gas density divided by the density of air at standard conditions. At standard conditions the z-factor is close to unity and we get,

$$\gamma = \frac{\rho_{sc}}{\rho_{air,sc}} = \frac{M}{M_{air}} = 0.0345M, \quad (3.96)$$

where ρ_{sc} and $\rho_{air,sc}$ are the density at standard condition for the gas and air, respectively. M_{air} is the average molar mass of air, $M_{air} = 28.97$ (unit: kg/kmol).

Example: Average molar mass of air

The components of atmospheric air, exclusive water vapor, consist mainly of nitrogen, oxygen, carbon dioxide and argon as shown in Table 3.3.

Table 3.3: Composition and atomic weight of air.

| Component | Content [%] | Atomic weight |
|-----------|-------------|----------------------------|
| N_2 | 78.084 | $2 \cdot 14.0067$ |
| O_2 | 20.946 | $2 \cdot 15.9994$ |
| CO_2 | 0.033 | $12.011 + 2 \cdot 15.9994$ |
| Ar | 0.934 | 39.948 |

The average molar mass is the written

$$M_{air} = \frac{78.084}{100} 2 \cdot 14.0067 + \frac{20.946}{100} 2 \cdot 15.9994 + \frac{0.033}{100} (12.011 + 2 \cdot 15.9994) + \frac{0.934}{100} 39.948 = 28.964$$

The average molar mass is given in units of *atomic mass* u , defined as

$$u = \frac{1}{N_A} \frac{kg}{kmol} = 1.660566 \cdot 10^{-27} kg,$$

where $N_A = 6.022045 \cdot 10^{23} mol^{-1}$ is Avogadro's constant.

The average molar mass is therefore given as

$$M_{air} = 28.964 (1.660566 \cdot 10^{-27}) (6.022045 \cdot 10^{23}) kg/k mol = 28.964 kg/k mol.$$

Example: Gas density of the Sleipner Vest gas

The gas density is calculated by using Eq. 3.95. The average molecular mass M is found by considering the gas composition and molecular mass of each component as given in Table 3.4.

The average molecular mass is $M = 26.78 g/mol$ and thus using Eq. 3.96, the gas gravity is $\gamma = 0.924$.

Form Figure 3.16 it can be verified that the z-factor at initial reservoir conditions is $Z = 1.103$. The gas density is then given

$$\rho = \frac{26.78 \cdot 434 \cdot 10^5}{1.103 \cdot 8314.413(120 + 273)} = 322.5 kg/m^3.$$

3.5.2 Gas Compressibility

The gas compressibility is defined as the relative volume increase per unit pressure drop at constant temperature

Table 3.4: Calculation of average molecular mass.

| Component | y_i | M_i | $y_i M_i / 100$ |
|--------------|--------|---------|-----------------|
| N_2 , | 0.78 | 28.014 | 0.21850 |
| CO_2 , | 8.72 | 44.010 | 3.83767 |
| C_1 , | 71.00 | 16.043 | 11.39053 |
| C_2 , | 8.56 | 30.070 | 2.57399 |
| C_3 , | 4.67 | 44.096 | 2.05928 |
| iC_4 , | 0.71 | 58.123 | 0.41267 |
| nC_4 , | 1.23 | 58.123 | 0.71491 |
| iC_5 , | 0.41 | 72.150 | 0.29581 |
| nC_5 , | 0.41 | 72.150 | 0.29581 |
| C_6 , | 0.45 | 86.177 | 0.38779 |
| C_7 , | 0.66 | 100.204 | 0.66134 |
| C_8 , | 0.70 | 114.231 | 0.79961 |
| C_9 , | 0.41 | 128.258 | 0.52585 |
| C_{10}^+ , | 1.29 | 202.000 | 2.60580 |
| Sum | 100.00 | | 26.77962 |

$$c = -\frac{1}{V} \left(\frac{\partial V}{\partial p} \right)_T. \quad (3.97)$$

In the case of ideal gas ($pV = nRT$), the compressibility becomes

$$c = \frac{1}{p}. \quad (3.98)$$

For real gases ($pV = ZnRT$), Eq. 3.97 is written

$$c = \frac{1}{p} - \frac{1}{Z} \left(\frac{\partial Z}{\partial p} \right)_T. \quad (3.99)$$

The general trend is that the compressibility is declining as the reciprocal of the pressure. A correction for real gases is proportional to the tangent (the slope) of the $Z = Z(p)$ curve in Figure 3.16 and the reciprocal of the z-factor in each pressure point. The compressibility are therefore calculated directly from Figure 3.16.

Example: Compressibility of reservoir gas

The derivative of Eq. 3.99 may be approximated with the well known central difference formula. Let three successive pressures be given by; p_{i-1} , p_i and p_{i+1} . The derivative at pressure p_i , then follows from the formula

$$\left(\frac{\partial Z}{\partial p} \right)_{p=p_i} = \frac{Z(p_{i+1}) - Z(p_{i-1})}{p_{i+1} - p_{i-1}}.$$

Using the formula above we may calculate the gas compressibility at a pressure of 400 bars of the Sleipner Vest reservoir (temperature is $120^\circ C$).

The following data is available from Figure 3.16:

| Pressure [bar] | z-factor |
|----------------|----------|
| 434 | 1.103 |
| 400 | 1.062 |
| 387 | 1.046 |

According to Eq. 3.99, the compressibility at 400 bars is given by

$$c = \frac{1}{400} - \frac{1}{1.062} \frac{1.103 - 1.046}{434 - 387} = 0.001358$$

The compressibility at 400 bars is $0.001358 \text{ bar}^{-1}$. The ideal compressibility is 0.0025 bar^{-1} . The relative deviation between the two values is

$$\frac{\Delta c}{c} = \frac{0.001358 - 0.0025}{0.001358} = -0.8409,$$

i.e. the deviation is close to 84 %, which is a significant error.

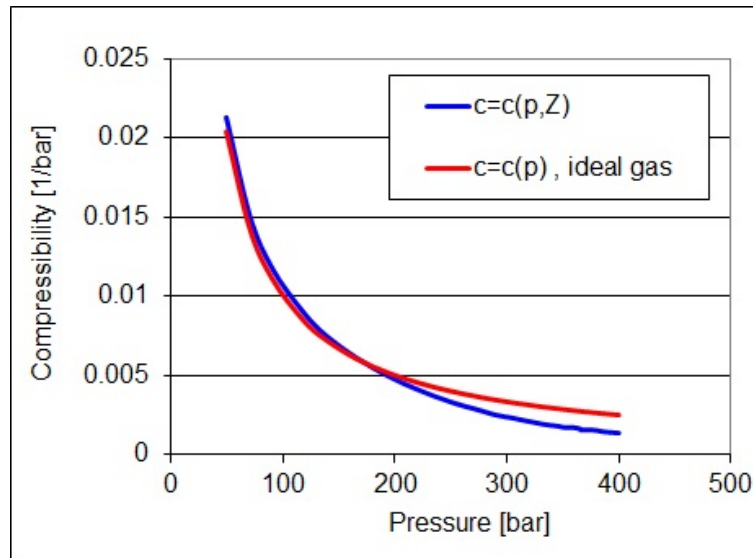


Figure 3.17: Gas compressibility for Sleipner Vest reservoir gas.

Applying the central difference formula to all data point in Figure 3.16 we may derive the gas compressibility curve as shown in Figure 3.17. The figure displays the real gas compressibility and the corresponding ideal gas compressibility, for comparison. The deviation from ideal behaviour is more pronounced at higher pressure, as can be expected.

3.5.3 Condensate-Gas Ratio

The condensate-gas ratio of natural gas expresses the content of condensate relative to gas. This ratio may be expressed on a molar or on a volumetric basis. Let assume we

have n moles of a natural gas which split into n_G moles of gas and n_L moles of liquid when brought to the surface. The molar condensate-gas ratio (or the Ratio of Molar Liquid to Gas) is then defined by

$$R_{MLG} = \frac{n_L}{n_G}. \quad (3.100)$$

Similarly, the volumetric condensate-gas ratio is defined as the ratio of volume condensate at stock-tank conditions, V_{Lst} and the volume of gas at standard conditions, V_{Gsc} . The Ratio of Volume Liquid to Gas is defined by

$$R_{VLG} = \frac{V_{Lst}}{V_{Gsc}}. \quad (3.101)$$

The volume of gas at standard conditions is related to the number of moles of gas by the Ideal Gas Law and given by

$$V_{Gsc} = n_G \frac{RT_{sc}}{p_{sc}}. \quad (3.102)$$

The volume of liquid condensate is related to the number of moles of condensate by

$$V_{Lst} = n_L \frac{M_L}{\rho_{Lst}}, \quad (3.103)$$

where M_L is the molecular mass of liquid condensate and ρ_{Lst} is the density of condensate at stock-tank conditions.

Combining Eqs. 3.99 to 3.103, we obtain the relation between the volumetric - and the molar condensate-gas ratios

$$R_{VLG} = R_{MLG} \frac{M_L p_{sc}}{\rho_{Lst} RT_{sc}} = R_{MLG} \frac{M_L \rho_{Gsc}}{\rho_{Lst} M_{sc}}, \quad (3.104)$$

where ρ_{Gsc} and M_{sc} are the density and molar mass of gas at standard conditions.

We have earlier, in Eq. 2.8, defined the molar fraction of gas in a gas-liquid mixture as V . The number of gas moles in a mixture is then given by

$$n_G = Vn = V(n_G + n_L), \quad (3.105)$$

where V is the molar fraction of vapor (gas) at surface conditions.

Eq. 3.105 can be rewritten as

$$\frac{1 - V}{V} = \frac{n_L}{n_G} = R_{MLG}. \quad (3.106)$$

giving the molar condensate-gas ratio as function of the molar fraction of gas. The importance of Eq. 3.106 is its relation to Eq. 2.8 and the molar composition of the feed gas z_i , the liquid x_i and the gas y_i . With the basis in these three compositions, we are able to calculate the molar fraction of gas in the mixture V and thus also the molar condensate-gas ratio R_{MLG} .

The liquid density ρ_{Lst} , in Eq 3.104 is often related to the average molecular mass of the liquid M_L through Standing's empirical formula [4]

$$\gamma = \frac{\rho_{Lst}}{\rho_w} = \frac{1.03M_L}{44.29 + M_L}, \quad (3.107)$$

where γ is the condensate specific gravity and ρ_w is the water density.

Combining Eqs. 3.104, 3.106 and 3.107, we may calculate the volumetric condensate-gas ratio with the basis of molar composition of the reservoir feed, the stock-tank liquid composition and the standard condition gas composition.

Example: Volumetric condensate-gas ratio

The volumetric condensate-gas ratio of the Sleipner Vest gas is found by considering the molar composition of the feed gas z_i at reservoir conditions and the liquid x_i and the gas y_i at surface conditions, as presented in Table 3.5.

Table 3.5: Composition in molar % at 1 bar and 15.6°C.

| Component | M_i [kg/kmol] | Feed, z_i [%] | Vapor, y_i [%] | Liquid, x_i [%] | V | M_L [kg/kmol] |
|--------------------|--------------------|--------------------|---------------------|----------------------|-------|--------------------|
| N_2 , | 28.014 | 0.78 | 0.803 | 0.001 | 0.971 | 0.000 |
| CO_2 , | 44.010 | 8.72 | 8.969 | 0.143 | 0.972 | 0.063 |
| C_1 , | 16.043 | 71.00 | 73.053 | 0.360 | 0.972 | 0.058 |
| C_2 , | 30.070 | 8.56 | 8.800 | 0.302 | 0.972 | 0.091 |
| C_3 , | 44.096 | 4.67 | 4.787 | 0.656 | 0.972 | 0.289 |
| iC_4 , | 58.123 | 0.71 | 0.723 | 0.253 | 0.972 | 0.147 |
| nC_4 , | 58.123 | 1.23 | 1.246 | 0.665 | 0.972 | 0.387 |
| iC_5 , | 72.150 | 0.41 | 0.405 | 0.588 | 0.973 | 0.424 |
| nC_5 , | 72.150 | 0.41 | 0.399 | 0.801 | 0.973 | 0.578 |
| C_6 , | 86.177 | 0.45 | 0.384 | 2.707 | 0.972 | 2.333 |
| C_7 , | 100.204 | 0.66 | 0.268 | 14.151 | 0.972 | 14.180 |
| C_8 , | 114.231 | 0.70 | 0.122 | 20.568 | 0.972 | 23.495 |
| C_9 , | 128.258 | 0.41 | 0.027 | 13.584 | 0.972 | 17.423 |
| C_{10}^+ , | | 1.29 | 0.013 | 45.221 | 0.972 | 91.620 |
| C_{10}^+ , molwt | - | 201.99 | 140.092 | 202.604 | - | - |
| | - | - | - | - | 0.972 | 151.087 |

The molar vapor fraction $V = 0.972$ in the table above is calculated as an average based on Eq. 2.8

$$V = \frac{1}{14} \sum_1^{14} \frac{z_i - x_i}{y_i - x_i},$$

where the molar liquid fraction $L = 0.028$, since $L + V = 1$. If the average molecular mass of liquid condensate is $M_L = 151.085 \text{ kg/kmol}$, given by

$$M_L = \sum_1^{14} x_i M_i,$$

then the condensate liquid density is calculated by Standing's formula (Eq. 3.107) and we find $\rho_{Lst} = 796.51 \text{ kg/m}^3$, where the water density $\rho_w = 1000 \text{ kg/m}^3$.

The molar condensate-gas ratio is given by Eq. 3.106 and $R_{MLG} = 0.0288$.

Using Eq. 3.104, we may calculate the liquid density of condensate at stock-tank conditions.

$$R_{VLG} = 0.0288 \frac{151.087 \cdot 1}{786.51 \cdot 8314.41 \cdot (273.2 + 15.6)} = 0.0002275 \frac{\text{m}^3}{\text{m}^3},$$

where both the gas and liquid is brought up to standard conditions defined by 1 bar and 15.6 °C.

The volumetric condensate-gas ration can be written as

$$R_{VLG} = \frac{227.5 \text{ m}^3}{1000000 \text{ m}^3} = 227.5 \frac{\text{m}^3}{\text{Mm}^3},$$

which states that if all gas initially in place in the reservoir is brought up to the surface at standard conditions, then for each million standard cubic meter of gas produced there will be 227.5 m³ condensate liquid produced.

Comment: In Table 3.5 the cell indicating the molar weight of the C_{10}^+ fraction is left open. This is done on purpose since the C_{10}^+ fraction will change as a result of changing conditions. The correct C_{10}^+ fraction is therefore tabulated under the corresponding composition. When calculation the average molecular mass M_L , the C_{10}^+ fraction used has a numerical value 202.604 .

The condensate-gas ratio is not a property of natural gas composition alone. It depends also on the conditions under which separation at the surface is carried out. The phase equilibrium computations has therefore an effect resulting from separator conditions and the yield of condensate is related to operating pressure and temperature and the number of separator stages involved. This effect has to be accounted for in any situation where gas wells are producing through a surface separator system. Such a system will consist of a simple separator unit or of separator units in series, all operating at different pressure and temperature (multistage separation).

3.5.4 Gas Formation Volume Factor

The gas formation volume factor B_G is defined as the ratio of a volume of gas at reservoir condition to the volume of surface gas at standard conditions. The term *standard conditions* seems not to be so standard as it sounds, as it may vary geographically as well as socially. A frequently appearing definition of standard conditions is referenced to atmospheric pressure (1 atm.) and a temperature of 15 °C.

Let us consider n moles of reservoir gas. The volume occupied by the gas at initial reservoir conditions (p, T) is defined by the Real Gas Law

$$V_{Gres} = n \frac{ZRT}{p}. \quad (3.108)$$

In the case of dry-gas reservoirs, all gas is converted to surface gas. According to the Ideal Gas Law, n moles of surface gas at standard conditions occupy a volume

$$V_{Gsc} = n \frac{RT_{sc}}{p_{sc}}. \quad (3.109)$$

The dry-gas volume factor, B_{Gd} , is defined as the ratio V_{Gres}/V_{Gsc} , a combination of Eqs. 3.108 and 3.109 yields,

$$B_{Gd} = \frac{V_{Gres}}{V_{Gsc}} = \frac{ZTp_{sc}}{T_{sc}p}. \quad (3.110)$$

In the case of wet gas production and production from gas-condensate reservoirs above the dew-point pressure, the well stream splits into a gas and a liquid phase. The deduction of the gas formation volume factor becomes somewhat more involved, since the liquid volume is not contributing to the surface gas volume.

If the well stream consist of n_G moles of gas and n_L moles of liquid, then the Real Gas Law is written

$$V_{Gres} = (n_G + n_L) \frac{ZRT}{p}. \quad (3.111)$$

Similarly it follows that the surface gas volume is given by

$$V_{Gsc} = n_G \frac{RT_{sc}}{p_{sc}}. \quad (3.112)$$

Combining Eqs. 3.111 and 3.112 and using the definition of the molar condensate-gas ratio Eq.3.100, we may write the gas formation volume factor as

$$B_{Gw} = \frac{V_{Gres}}{V_{Gsc}} = \frac{ZTp_{sc}}{T_{sc}p} (1 + R_{MLG}) = B_{Gd}(1 + R_{MLG}), \quad (3.113)$$

when all gas moles are brought to the surface. The B_{Gw} is sometimes called the "wet"-gas volume factor and is a hypothetical ratio where the "dry"-gas volume and the condensate volume is converted to an equivalent surface-gas volume. Refereing to the gas formation volume factor, we will write B_G , always meaning B_{Gw} as defined in Eq. 3.113.

The gas formation volume factor is used to convert a volume of gas at reservoir conditions to a volume at standard conditions. If the hydrocarbon pore volume is V_{HC} , then the corresponding gas volume initial in place V_{GIIP} at standard conditions is expressed

$$V_{GIIP} = V_{HC}/B_G. \quad (3.114)$$

Like the volumetric condensate-gas ratio, the gas formation volume factor is not a true gas property. It depends not only on the type of gas, but also on the definition of standard conditions as well as on separator condition.

Example: Characteristics of Gas Formation Volume Factor

The gas formation volume factor is defined by Eq. 3.113, where the varying parameters are the z-factor, the molar condensate-gas ratio and the pressure. In order to derive the two first parameters, Z and R_{MLG} , we have to carry out a flash calculation making a step by step calculation of the gas and liquid compositions. Table 3.6 presents the results of these flash calculations and the calculation of the gas formation volume factor.

Table 3.6: Gas formation volume factor calculation based on data for flash calculations.

| p [bar] | Z | Z_2 | V | R_{MLG} | B_G [Rm^3/Sm^3] |
|---------|--------|--------|--------|-----------|-----------------------|
| 445 | 1.1142 | 1.1143 | 0.9517 | 0.0508 | 0.0036 |
| 350 | 1.0035 | 1.0045 | 0.9524 | 0.0500 | 0.0041 |
| 300 | 0.9530 | 0.9556 | 0.9544 | 0.0478 | 0.0046 |
| 260 | 0.9206 | 0.9233 | 0.9571 | 0.0449 | 0.0051 |
| 200 | 0.8920 | 0.8994 | 0.9626 | 0.0389 | 0.0064 |
| 160 | 0.8885 | 0.8851 | 0.9662 | 0.0349 | 0.0078 |
| 100 | 0.9073 | 0.8837 | 0.9701 | 0.0308 | 0.0124 |
| 60 | 0.9348 | 0.8864 | 0.9708 | 0.0301 | 0.0208 |
| 40 | 0.9524 | 0.8778 | 0.9709 | 0.0300 | 0.0308 |

The flash calculation gives the z-factor (Z), the two-phase z-factor (Z_2) and the molar vapor fraction (V). The molar condensate-gas fraction is calculated using Eq. 3.106. The the gas formation volume factor, as shown in Figure 3.18, is calculated using Eq. 3.113, where standard condition is defined by 1 bar and 15 °C. The reservoir temperature is 120 °C (393 °K).

Comment: It was stated above that gas formation volume fraction defined in Eq. 3.113 is valued under the condition that all gas moles are brought to the surface, i.e. no liquid condensation in the reservoir. In the case of gas production from Sleipner Vest we know that the pressure in the reservoir eventually will cross the dew-point line and consequently liquid condensate will form in the reservoir. The number of moles of gas in the reservoir is not conserved under production and the number of liquid moles produced is less than n_L . Similarly will the volume available to the gas in the reservoir be slightly reduced due to liquid condensation. However, this effect is accounted for when the two-phase z-factor (Z_2) is used instead of the gas z-factor (Z).

3.5.5 Gas Viscosity

Viscosity is reflecting the internal resistance in fluids against flow. The viscosity of natural gases can be expressed by Newton's flow model, according to which viscosity is a proportionality coefficient linking the tangential shear stress component with the

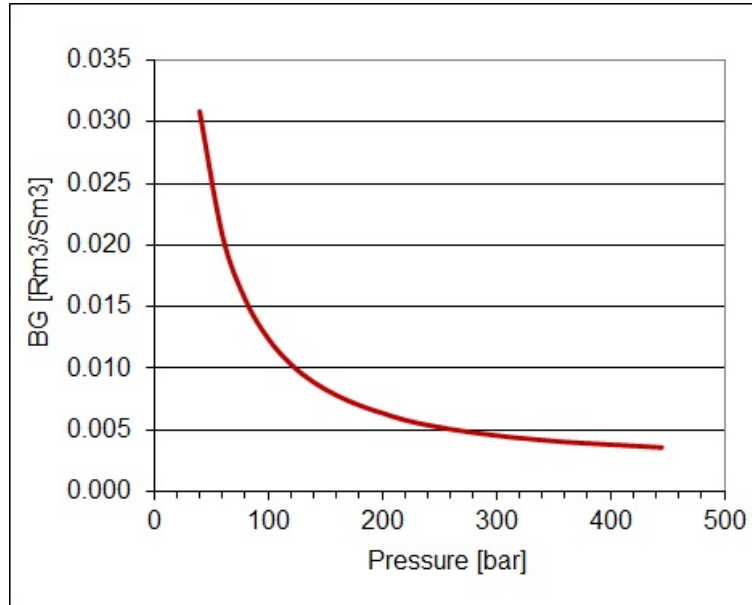


Figure 3.18: Gas formation volume factor for Sleipner Vest gas.

tangential velocity gradient. By definition the proportionality constant is called the viscosity of fluids.

Classical kinetic theory has been applied to describe idealized gas viscosity. The restriction set by the use of idealized classic theory, prevents any practical application of its results but it is found that gas viscosity is a function of temperature, average molecular mass and a factor describing molecular size (molecular diameter). Gas viscosity is therefore only indirectly dependent on an important parameter such like pressure.

A great variety of different methods exist by which gas viscosity can be estimated.

- Empirical and semi-empirical prediction methods are available where various correlation diagrams can be used. These methods apply both to low (atmospheric) - and higher pressure.
- Empirical models on functional form are also available, where various parameters and characteristic constants are included.

One of the most popular methods for prediction of viscosity of natural gases was proposed by Lee et al. and is given by the following relation [5]

$$\mu = Ke^{(X\rho^Y)}, \quad (3.115)$$

where

$$\begin{aligned} K &= \frac{(9.4 + 0.02M_G)T^{1.5}}{209 + 19M_G + T}, \\ X &= 3.5 + 986/T + 0.01M_G, \\ Y &= 2.4 - 0.2X. \end{aligned}$$

The viscosity is measured in micro Poise ($\mu P = 10^{-6} P$). The temperature is given in absolute Rankine ($^{\circ}R = 1.8 \cdot ^{\circ}K$). M_G is the average molecular mass and ρ is the gas density ($\rho = (M_G p)/ZRT$), measures in g/cm^3 .

The pressure dependence of viscosity is related to the average molecular mass and the density, indirectly through M_G and Z and directly through p . All these parameters can be obtained from PVT simulations with the basis of molar compositions.

Gas viscosity obtained by Lee's correlation is found to be accurate within $\pm 3\%$ and with a maximum deviation of approximately 10% . For most reservoir engineering purposes this is sufficiently accurate.

Example: Viscosity of The Sleipner Vest gas

The gas viscosity will decrease as pressure decreases. The basic parameters involved in Eq. 3.115 are pressure p , average molecular mass M_G , z-factor Z and temperature T . These parameters are tabulated in Table 3.7.

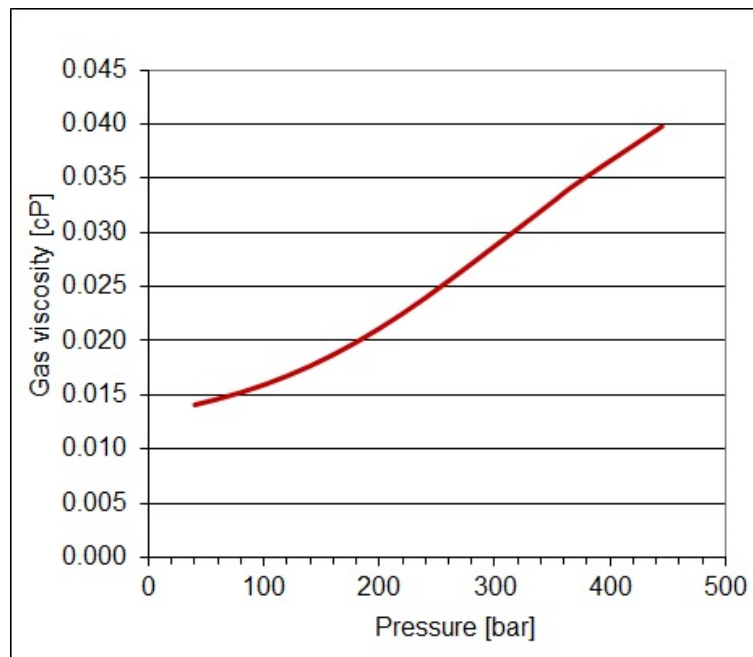


Figure 3.19: Gas viscosity from Selipner Vest.

Reservoir gas viscosity is a monotonous increasing function of pressure. The viscosity is measured in centi Poise (cP), where water at $20^{\circ}C$ has an approximate viscosity of $1 cP$. The viscosity-pressure relation is plotted in Figure 3.19.

Table 3.7: Calculation of viscosity for Selipner Vest gas.

| p [bar] | M_G [kg/kmol] | Z | ρ [g/cm^3] | K | X | Y | μ [cP] |
|-----------|-----------------|-------|---------------------|---------|-------|-------|------------|
| 445 | 26.56 | 1.114 | 0.325 | 131.490 | 5.159 | 1.368 | 0.0398 |
| 350 | 26.42 | 1.004 | 0.282 | 131.700 | 5.158 | 1.368 | 0.0328 |
| 300 | 26.03 | 0.953 | 0.251 | 132.287 | 5.154 | 1.369 | 0.0287 |
| 260 | 25.61 | 0.921 | 0.221 | 132.927 | 5.150 | 1.370 | 0.0255 |
| 200 | 24.88 | 0.892 | 0.171 | 134.056 | 5.143 | 1.371 | 0.0211 |
| 140 | 24.30 | 0.892 | 0.117 | 134.970 | 5.137 | 1.373 | 0.0177 |
| 100 | 24.10 | 0.907 | 0.081 | 135.289 | 5.135 | 1.373 | 0.0159 |
| 60 | 24.16 | 0.935 | 0.047 | 135.193 | 5.135 | 1.373 | 0.0146 |
| 40 | 24.41 | 0.952 | 0.031 | 134.796 | 5.138 | 1.372 | 0.0141 |

3.6 PVT parameters

It has been shown in the previous sections that the basis for continued calculation of various gas parameters such as; z-factor, density, compressibility, viscosity and formation volume factor, are all related to the gas phase behavior. The molar composition is the key element in these calculations can be estimated on the basis of PVT-simulations. In practical situations, not only molar compositions are calculated by PVT-simulations, also parameters as mentioned above and several other thermodynamic parameters are based on calculations coming from the molar composition.

Table 3.8: Average parameters for phase behaviour of reservoir gas.

| p [bar] | T [$^{\circ}K$] | MWT | $MWTG$ | $MWTL$ | V | Z | Z_2 |
|-----------|---------------------|-------|--------|--------|--------|--------|--------|
| 445 | 392 | 26.56 | 26.56 | 26.56 | 0.9517 | 1.1142 | 1.1143 |
| 370 | 392 | 26.56 | 26.56 | 26.56 | 0.9517 | 1.0258 | 1.0258 |
| 350 | 392 | 26.57 | 26.42 | 90.14 | 0.9524 | 1.0035 | 1.0045 |
| 320 | 392 | 26.57 | 26.19 | 89.32 | 0.9535 | 0.9721 | 0.9743 |
| 300 | 392 | 26.59 | 26.03 | 88.19 | 0.9544 | 0.9530 | 0.9556 |
| 280 | 392 | 26.61 | 25.83 | 87.18 | 0.9556 | 0.9356 | 0.9385 |
| 260 | 392 | 26.65 | 25.61 | 86.86 | 0.9571 | 0.9206 | 0.9233 |
| 240 | 392 | 26.72 | 25.36 | 87.52 | 0.9588 | 0.9082 | 0.9102 |
| 220 | 392 | 26.81 | 25.11 | 89.16 | 0.9606 | 0.8986 | 0.8994 |
| 200 | 392 | 26.94 | 24.88 | 91.68 | 0.9626 | 0.8920 | 0.8994 |
| 180 | 392 | 27.13 | 24.66 | 95.05 | 0.9645 | 0.8886 | 0.8910 |
| 160 | 392 | 27.38 | 24.47 | 99.27 | 0.9662 | 0.8885 | 0.8851 |
| 140 | 392 | 27.95 | 24.30 | 104.49 | 0.9678 | 0.8916 | 0.8808 |
| 120 | 392 | 28.52 | 24.18 | 110.81 | 0.9692 | 0.8979 | 0.8807 |
| 100 | 392 | 29.33 | 24.10 | 118.48 | 0.9701 | 0.9073 | 0.8837 |
| 80 | 392 | 30.51 | 24.08 | 127.84 | 0.9705 | 0.9197 | 0.8862 |
| 60 | 392 | 32.36 | 24.16 | 139.47 | 0.9708 | 0.9348 | 0.8864 |
| 40 | 392 | 35.59 | 24.41 | 154.40 | 0.9709 | 0.9524 | 0.8778 |
| 20 | 392 | 38.91 | 25.13 | 169.85 | 0.9858 | 0.9720 | 0.8220 |
| 1.01 | 288 | 26.57 | 23.28 | 151.57 | 0.9739 | 1.0000 | 1.0000 |

Instead of handling the molar composition for, say 10 vapor and liquid components per pressure point, it is more practical to deduce the average molar weight for the total

gas-liquid mixture (MWT), the average gas weight ($MWTG$) and the average liquid weight ($MWTL$). Together with these average weights, the only necessary parameters we will use in many of the calculations to be discussed in the next chapter, are the vapor fraction (V) and the Z-factors (Z and Z_2). See Table 3.8.

Table 3.8 gives a set of average parameters describing the phase behavior of the gas-condensate. From these parameters material balance and other important calculations are easily deductible.

References

- [1] Ali Danesh. *PVT and Phase Behavior of Petroleum Reservoir Fluids*. Elsevier, 1998. ISBN 0-44-82196-1.
- [2] D. Imer F.B. Thomas, E.Shtepani and D.B.Bennion. How many pseudo-components are needed to model phase behaviour? *JCPT*, 41(1):48–54, 2002.
- [3] Abbas Firoozabadi. *Thermodynamics of Hydrogen Reservoirs*. McGraw-Hill, 1999.
- [4] Jacques Hagoort. *Fundamentals of gas reservoir engineering*, volume 23 of *Developments in Petroleum Science*. Elsevier, 1988.
- [5] A.L. Lee, M.H. Gonzales, and B.E. Eakin. The viscosity of natural gases. *Gas Technology, SPE Preprint Series*, 1(13), 1977.
- [6] Michael L. Michelsen and Jørgen M: Mollerup. *Thermodynamic Models: Fundamentals & computational Aspects*. Tie-Line Publications, 207.
- [7] M.A. Saad. *Thermodynamics, Principles and Practice*. Prentice-Hall, Inc., 1997.
- [8] C.H. Whitson and M.R. Brule. *Phase Behavior*. Henry L.Doherty Memorial Fund of AIME, SPE, 2000. ISBN 1-55563-087-1.

Chapter 4

The Material Balance Equation

The material balance estimation method is a fundamental tool applicable to reservoir engineering and evaluation of past and future global reservoir performance. The method is based on the principle of *Mass Conservation*, applied to the reservoir at large, by considering it as a large tank of uniform pressure.

Applied to production data, a material balance analysis provides insights in the prevailing production mechanism and allows for estimation of hydrocarbon initially in place. In its predictive mode the material balance method can be used in estimating future reservoir performance and the potential recovery of hydrocarbons initially in place.

In practical situations, adequate use of the material balance method rests on the fulfillment of some necessary conditions of which the two below are among the most important.

- A successful use of the material balance method is based on the collection and use of adequate data with respect to production, pressure, temperature and fluid characteristics. The MBE method is therefore not directly subjected to geological or petro-physical interpretations, since the reservoir parameters of interest are solely related to volumetric dimensions.
- The assumption that the reservoir is characterized by an average pressure is a necessary condition for a "tank like" pressure decline. This includes;
 - Reference to a common pressure datum plane, which is the basis for a concept of average or mean reservoir pressure.
 - Fast and monotonous process towards pressure equilibrium in the reservoir. In practical terms this translates to high hydraulic diffusivity, i.e. that $k/(\phi\mu c)$ is large.
 - Well pressure behavior does plot similarly, i.e. all pressure decline curves are showing the same characteristic form.

In this chapter we shall apply the material balance equation to the process of natural depletion performance, to both wet gas and gas-condensate reservoirs. We will first derive a general material balance equation and discuss the basic example of volumetric

depletion (no rock compaction nor influx of aquifer water). In the case of non-volumetric depletion, the material balance equation becomes more involved and iterative solution techniques have to be applied. A simple numerical solution method is outlined, involving the calculation of water influx from either radial or linear aquifers. Finally, we shall present some plotting techniques, applicable to gas reservoirs, widely used in the industry.

4.1 The Material Balance Equation, MBE

The material balance equation applied to gas reservoirs states that at any time, the number of moles of hydrocarbons in place in the reservoir n_{HC} is equal to the number of moles of hydrocarbons initially in place in the reservoir n_{HCi} minus the number of moles of hydrocarbons produced n_{HCp} ,

$$n_{HC} = n_{HCi} - n_{HCp}. \quad (4.1)$$

For material balance analysis of gas reservoirs, the in-situ reservoir fluid is generally considered to be composed of two pseudo components at standard conditions, i.e. a dry gas fraction and a liquid condensate fraction. The dry gas comprises all gas produced at stock-tank condition and the gas that is liberated during the storage of condensate. The condensate is the liquid produced at the surface and stored at stock-tank conditions. In addition, in the case of gas condensate reservoirs, some liquid produced in the reservoir is normally considered as lost production and will thus remain unproduced.

4.2 Wet-Gas Reservoirs

Dry gas reservoirs are a special sub-class of wet gas reservoirs. Dry gas reservoir production resembles wet gas reservoir production when no liquid is produced. The two cases are therefore treated simultaneously by considering wet gas reservoir production.

During depletion of wet gas reservoirs, the compositions of the reservoir gas, i.e. dry gas and condensate remain constant and so does the condensate/gas ratio. Constant condensate/gas ratio is, however, subject to surface treatment and is here considered to be constant.

The material balance equation Eq. 4.1 is rewritten as follows

$$\frac{n_{HC}}{n_{HCi}} = \left(1 - \frac{n_{HCp}}{n_{HCi}}\right). \quad (4.2)$$

Using the Real Gas Law, the number of moles hydrocarbon in place at pressure p is

$$n_{HC} = \frac{p}{ZRT} V_{HC}, \quad (4.3)$$

where V_{HC} is the hydrocarbon pore volume. Z is the z-factor at pressure p .

Similarly, we write the number of moles hydrocarbon initially in place

$$n_{HCi} = \frac{p_i}{Z_i RT} V_{HCi}, \quad (4.4)$$

where V_{HCi} is the initial hydrocarbon pore volume and Z_i is the initial z-factor.

Since the hydrocarbons produced generally consist of dry gas and condensate, we can write for n_{HCp}

$$n_{HCp} = n_{Gp} + n_{Lp} = n_{Gp}(1 + R_{MLG}), \quad (4.5)$$

where n_{Gp} and n_{Lp} are the number of moles produced as dry gas and condensate, respectively. R_{MLG} is the surface molar condensate/gas ratio.

The molar dry gas production is related to the cumulative volumetric dry gas production at standard conditions. Using the Real Gas Law, we get

$$n_{Gp} = \frac{p_{sc}}{RT_{sc}} G_p, \quad (4.6)$$

where G_p is the cumulative dry gas production at standard conditions. The z-factor at standard condition is assumed equal to unity.

The number of hydrocarbon moles initially in place n_{HCi} , is equal to the sum of the number of moles of dry gas and liquid condensate and

$$n_{HCi} = n_{Gi} + n_{Li} = n_{Gi}(1 + R_{MLGi}), \quad (4.7)$$

where n_{Gi} and n_{Li} are the number of moles of dry gas and condensate initially in place.

Applying the Real Gas Law again, gives the number of moles of dry gas initially in place and we write

$$n_{Gi} = \frac{p_{sc}}{RT_{sc}} G_i, \quad (4.8)$$

where G_i is the dry gas initially in place (GIIP) at standard conditions.

Combining Eqs. 4.5 to 4.8, for the ratio n_{HCp}/n_{HCi} in Eq. 4.2 we get

$$\frac{n_{HCp}}{n_{HCi}} = \frac{n_{Gp}(1 + R_{MLG})}{n_{Gi}(1 + R_{MLGi})} = \frac{G_p T_{sc} p_{sc}}{G_i T_{sc} p_{sc}} = \frac{G_p}{G_i}, \quad (4.9)$$

where $R_{MLG} = R_{MLGi}$ indicates that all condensate is produced to the surface.

Substituting Eqs. 4.3, 4.4 and 4.9 into Eq. 4.2, we obtain

$$\frac{p}{Z} = \frac{p_i V_{HCi}}{Z_i V_{HC}} \left(1 - \frac{G_p}{G_i} \right). \quad (4.10)$$

Eq. 4.10 is the general material balance equation for wet gas reservoirs. The equation relates the reservoir pressure to the cumulative dry gas production G_p . It contains the parameters characterizing the gas; Z and Z_i as well as the initial pressure p_i and the amount of dry gas initially in place G_i . The hydrocarbon pore volume initially in place is V_{HCi} while the volume at pressure p is V_{HC} . Eq. 4.10 therefore reflects the fact that the hydrocarbon volume may change during the depletion process.

The general material balance equation Eq. 4.10, is often represented by a plot where the reduced pressure p/z is plotted as function of gas production G_p , as seen in Figure 4.1.

In the case of volumetric depletion (curve A), production is continued until the abandonment reservoir pressure, p_a , is reached. The abandonment pressure condition

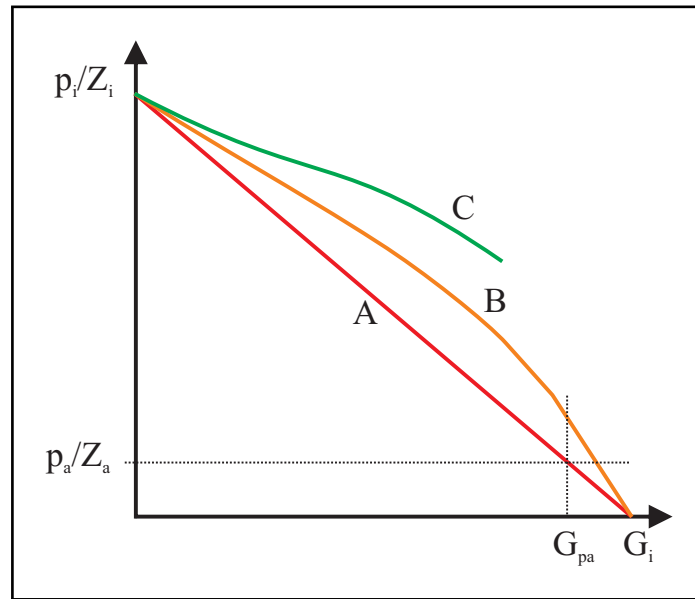


Figure 4.1: p/z plot of wet gas reservoir production.

is reached when the minimum *bottom-hole pressure* is surpassed during normal reservoir production. The volume of gas produced at this pressure is G_{pa} . Under strict volumetric depletion, i.e. the hydrocarbon pore volume remains constant during the production period, - the general material balance equation Eq. 4.10 reduces to a simple linear relation

$$\frac{p}{Z} = \frac{p_i}{Z_i} \left(1 - \frac{G_p}{G_i} \right). \quad (4.11)$$

Curve B and C in Figure 4.1 illustrate the cases of non-volumetric depletion. In the case of moderate aquifer water influx and/or reservoir (rock) compaction, the non-volumetric depletion (curve B) indicates a somewhat higher abandonment gas production, relative to the linear volumetric depletion. In most practical cases, however, the abandonment pressures are generally higher than in the volumetric case. In the case of aquifer water influx, some part of the reservoir gas can be surpassed and isolated, leading to reduced recoverable gas volume and thus abandonment at higher pressure. If the reservoir is experiencing massive aquifer influx, as indicated by curve C , the reservoir pressure is maintained at a higher level, though the accumulated production is very often seen to be reduced. Gas production is generally quite often reduced in non-volumetric depletions cases due to gas entrapment, leaving pockets of gas behind the flowing aquifer water.

In some rare cases when volumetric depletion turns out to be the correct model, production data can be plotted as a straight line, as in curve A in Figure 4.1. The plot can then be used to determine the GIIP based on the observed data of declining reservoir pressure and measured gas production. The material balance equation Eq. 4.11 is thus used in a history matching mode. In most cases, however, a non-volumetric depletion model is a more correct model to use, as in Eq. 4.10.

History matching using Eq. 4.11 is normally not applied unless sufficient production history data is available. As a rule of thumb, it is assumed that cumulative dry gas production from a reservoir should yield at least 25% of the initial gas volume, before its proper use [9].

In applying linear history matching, caution is recommended. The errors normally encountered in applying the volumetric depletion model are listed below. Before applying a volumetric depletion model to a set of general production data, one should answer the following questions. See also the book of L.P. Dake [6].

1. What would be the effect of applying a linear trend through non-linear data points?
2. What would be the effect of erroneous extrapolation of data through the points which is believed to lay on a straight line?
3. How could this linearization mask both the effect of the drive mechanism and the volume of GIIP?

For volumetric depletion, the recovery efficiency of dry gas (and condensate) production is defined at the abandonment pressure. The gas recovery efficiency is defined by rewriting Eq. 4.11 and we get

$$E_R = \frac{G_{pa}}{G_i} = \left(1 - \frac{p_a Z_i}{p_i Z_a}\right), \quad (4.12)$$

where E_R is the recovery efficiency for dry gas production as well as for wet gas production since the condensate/gas ratio is constant.

Example: Estimation of GIIP using a volumetric depletion model

Cumulative volumetric gas production data and average reservoir pressure from a gas field are presented in Table 4.1. The z-factors used is taken for the Sleipner Vest fluid data, presented in earlier chapters.

Table 4.1: Pressure and cumulative gas production data.

| p [bar] | G_p [Sm ³] | Z | p/Z [bar] |
|--------------|-----------------------------|--------|----------------|
| 445 | 2.4988E+06 | 1.1142 | 399.3897 |
| 370 | 7.7463E+07 | 1.0258 | 360.6941 |
| 320 | 1.5243E+08 | 0.9721 | 329.1842 |
| 280 | 2.1490E+08 | 0.9356 | 299.2732 |
| 240 | 3.0236E+08 | 0.9082 | 264.2590 |

The data plotted in Figure 4.2 shows a linear trend with a *regression coefficient* $R^2 = 0.998$, where the linear trend is parameterized as $y = -4.49 \cdot 10^{-7}x + 397.95$. The point where the linear trend is crossing the x-axis in Figure 4.2, is the point where $y = 0$, i.e. the gas initial in place is

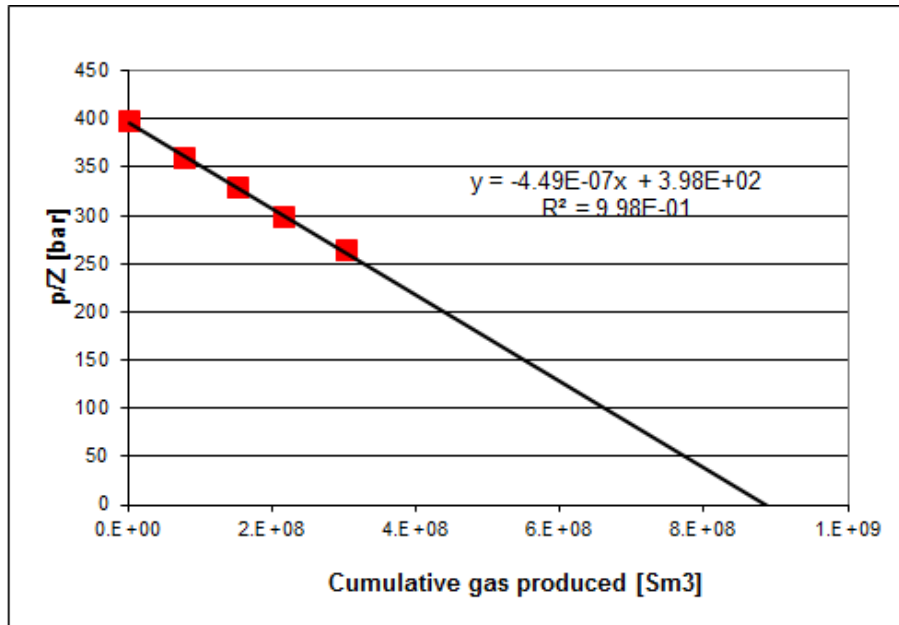


Figure 4.2: p/Z plot of data presented in Table 4.1

$$G_i = \frac{387.95}{4.48 \cdot 10^{-7}} = 886302895 \text{ Sm}^3,$$

and the gas initially in place is $G_i = 886 \text{ MSm}^3$.

4.3 Gas-Condensate Reservoirs

Derivation of the material balance equation for gas-condensate reservoirs are more complex compared to the wet gas case, due to liquid drop-out in the reservoir. During natural depletion of such reservoirs, parts of the gas will condensate in the reservoir when pressure drops below the dew-point pressure. As a consequence, both the gas composition and the production gas-condensate ratio will change. This makes the derivation of the material balance equation more involved.

If we assume that the liquid condensate is immobile and thus cannot be produced, we can derive a material balance equation similarly to the one derived for wet gas reservoirs. Under this assumption, the depletion process in the reservoir can be accurately simulated and compared to the laboratory constant-volume-depletion (CVD) experiment. The immobile liquid concentration being formed as part of the condensation process, implies that the liquid saturations in the reservoir is relatively low and always below the critical liquid saturation. This condition of sub-critical liquid saturation is usually satisfied in most parts of the reservoir. The result from the CVD experiments can therefore be directly applied as model in the derivation of the material balance equation.

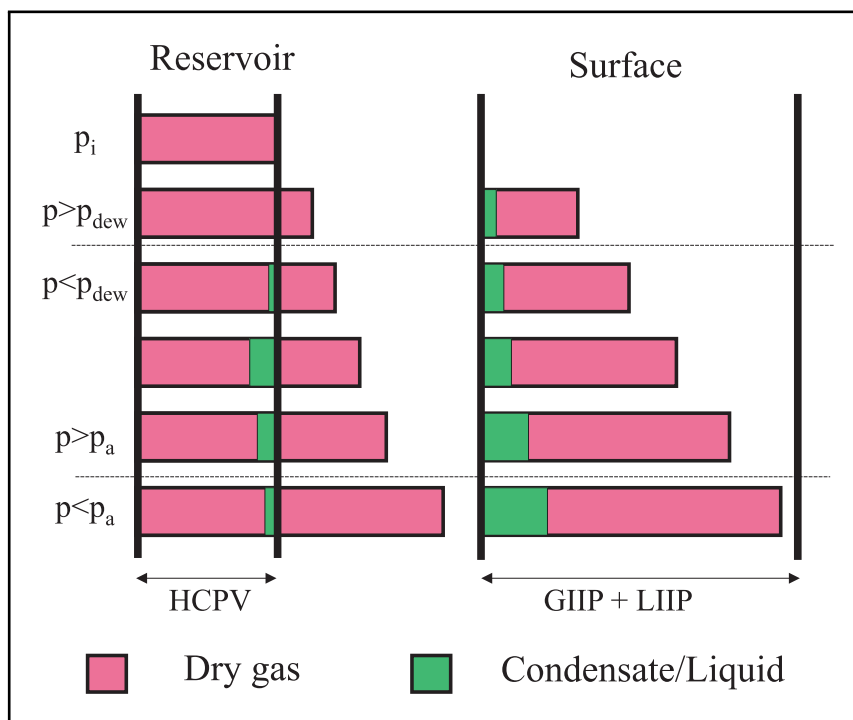


Figure 4.3: Constant-volume-depletion process applied to reservoir and surface condition.

The constant-volume-depletion process from reservoir to surface condition is depicted in Figure 4.3. At initial pressure p_i , all gas is contained in the reservoir. Gas production down to the dew-point pressure p_{dew} , is happening as previously described in the wet gas case, where liquid and gas are produced to the surface at a constant molar ratio. At all pressures $p > p_{dew}$, as shown in Figure 4.3, a certain amount of gas has been produced to the surface. The reservoir gas expands the whole reservoir (the HCPV) and as seen to the left in the figure, the additional produced gas would occupy an additional volume if it would remain at reservoir conditions. On the left hand side in the figure, the gas is seen to split in a liquid and a dry gas part at surface conditions.

Below the dew-point pressure, liquid condensate is formed in the reservoir. The saturation of liquid condensation will increase with decreasing pressure. This process is known as *retrograde condensation*. If the pressure continues to decrease, as part of normal gas production, liquid condensate should in principle start to evaporate. Due to wetting preferences in the reservoir and other liquid-rock interactions, liquid condensate will in reality remain in the liquid phase in the reservoir even though the CVD-experiment tells a different story.

At abandonment pressure p_a , a certain amount of liquid will remain in the reservoir, while gas produced to the surface will split into dry gas and condensate. The initially in place volumes of gas and liquid, GIIP and LIIP, are not shown in Figure 4.3, as the volume of GIIP and LIIP at standard conditions represent the split of all gas brought to the surface. Producing a gas-condensate reservoir down to atmospheric pressure would thus yield a production volume less than the initially in place volumes.

4.3.1 Derivation of a Gas Recovery Equation

The derivation of the material balance equation for gas-condensate reservoirs runs parallel to that of wet gas reservoirs. The starting point is again Eq. 4.2, whose terms are to be converted to volumes

$$\frac{n_{HC}}{n_{HCi}} = \left(1 - \frac{n_{HCp}}{n_{HCi}}\right). \quad (4.13)$$

The number of moles of hydrocarbon in-place (reservoir gas and liquid condensate) are related to the hydrocarbon pore volume by the Real Gas Law, provided the two-phase z-factor Z_2 , is used instead of the single phase z-factor. The two-phase z-factor is derived from a CVD experiment and does therefore describe gas compressibility where the liquid condensate volume is included. The condensation of liquid in the reservoir will occupy some part of the pore volume and therefore reduce the volume available for the gas phase. The number of moles of hydrocarbon in-place at any reservoir pressure is

$$n_{HC} = \frac{p}{Z_2 RT} V_{HC} \quad (4.14)$$

and for the number of moles of hydrocarbon initially in place

$$n_{HCi} = \frac{p_i}{Z_{2i} RT} V_{HCi}, \quad (4.15)$$

where Z_2 and Z_{2i} are the two-phase z-factor at pressure p and p_i , respectively. (For pressures above the dew-point pressure, the two z-factors are equal, i.e. if $p > p_{dew}$ then $Z_2 = Z$.)

The number of moles of hydrocarbon produced is therefore,

$$n_{HCp} = n_{Gp} \left(1 + \frac{n_{Lp}}{n_{Gp}}\right) = n_{Gp}(1 + R_{MLGp}), \quad (4.16)$$

where R_{MLGp} is a function of pressure p , since the surface molar liquid gas ratio is reduced with pressure.

For gas-condensate reservoirs, the condensate-gas ratio R_{MLG} is not constant, due to liquid drop-out in the reservoir. The pressure dependence is written

$$R_{MLG}(p) = \frac{dn_{Lp}}{dn_{Gp}}, \quad (4.17)$$

where n_{Lp} is pressure dependent.

The condensate-gas ratio is constant at pressures $p > p_{dew}$, as shown in Figure 4.4, while at lower pressures it is a monotonous decreasing function.

The re-definition of the condensate-gas ratio R_{MLG} , as the differential dn_{Lp}/dn_{Gp} follows the same logic as for the definition of speed, where the average speed is $v = s/t$, while the general definition is $v = ds/dt$. The general condensate-gas ratio is therefore defined as in Eq. 4.17.

The cumulative production of hydrocarbon moles is the sum of dry gas and liquid condensate. As the condensate-gas ratio depends on the reservoir pressure, the cumulative molar hydrocarbon production is given

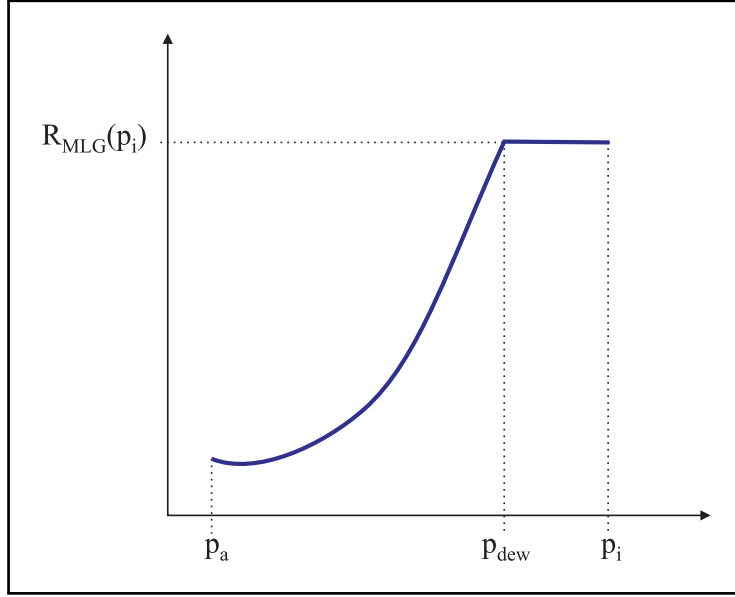


Figure 4.4: Condensate-gas ratio as function of reservoir pressure.

$$n_{HCp} = n_{Gp} + n_{Lp} = n_{Gp} + \int_{p_i}^p R_{MLG}(p^*) \frac{dn_{Gp}}{dp^*} dp^* = n_{Gp}(1 + R_{MLGp}), \quad (4.18)$$

where $R_{MLG}(p)$ is the producing molar condensate-gas ratio at pressure p and R_{MLGp} is the cumulative molar condensate-gas ratio at the same pressure. p^* is an integration variable. R_{MLGp} is defined as

$$R_{MLGp} = \frac{1}{n_{Gp}} \int_{p_i}^p R_{MLG}(p^*) \frac{dn_{Gp}}{dp^*} dp^* = \frac{1}{Gp} \int_{p_i}^p R_{MLG}(p^*) \frac{dGp}{dp^*} dp^*. \quad (4.19)$$

The number of hydrocarbon moles initially in place is given by

$$n_{HCi} = n_{Gi} + n_{Li} = n_{Gi}(1 + R_{MLGi}), \quad (4.20)$$

where R_{MLGi} is the initial condensate-gas ratio.

Substituting Eqs. 4.14, 4.15, 4.18 and 4.20 in Eq. 4.13, we will obtain

$$\frac{\frac{pV_{HC}}{Z_2RT}}{\frac{p_iV_{HCi}}{Z_{2i}RT}} = 1 - \frac{n_{Gp}(1 + R_{MLGp})}{n_{Gi}(1 + R_{MLGi})}, \quad (4.21)$$

and

$$\frac{pZ_{2i}V_{HC}}{p_iZ_2V_{HCi}} = 1 - \frac{Gp(1 + R_{MLGp})}{G_i(1 + R_{MLGi})}. \quad (4.22)$$

The relative fraction of cumulative gas produced (gas recovery) is then given by

$$\frac{G_p}{G_i} = \left(1 - \frac{Z_{2i} p V_{HC}}{Z_2 p_i V_{HCi}}\right) \frac{1 + R_{MLGi}}{1 + R_{MLGp}}. \quad (4.23)$$

For gas-condensate reservoirs, the correction relative to wet gas reservoirs as stated in Eq. 4.23, is the term $(1 + R_{MLGi})/(1 + R_{MLGp})$. Since $R_{MLG}(p)$ is a decreasing function with pressure, so is the integrated function R_{MLGp} and the term $(1 + R_{MLGi})/(1 + R_{MLGp})$ becomes larger than unity. The relative production (recovery) of dry gas from a gas-condensate reservoir, is therefore slightly larger than the corresponding recovery from a similar dry- or wet gas reservoir, at the same abandonment pressure, - all due to the formation of a liquid saturation in the reservoir. Another modification relative wet gas reservoirs, as shown in Eq. 4.23, is the substitution of the z-factor by the two-phase z-factor; Z_2 .

The general material balance equation for gas-condensate reservoirs can be deduced from Eq. 4.23 and we get

$$\frac{p}{Z_2} = \frac{p_i V_{HCi}}{Z_{2i} V_{HC}} \left(1 - \frac{G_p (1 + R_{MLGp})}{G_i (1 + R_{MLGi})}\right). \quad (4.24)$$

Eq. 4.24 is an implicit equation in pressure, since R_{MLGp} is pressure dependent and in the non-volumetric case, V_{HC} will also vary with pressure. Eq. 4.24 and consequently also Eq. 4.23 have no analytical solution and are therefore solved by iteration.

Because of condensate drop-out, the fractional recovery of condensate is no longer equal to the dry-gas fractional recovery. It follows from the dry gas recovery and the cumulative condensate-gas ratio that

$$\frac{G_{Lp}}{G_{Li}} = \frac{n_{Lp}}{n_{Li}} = \frac{n_{Gp} R_{MLGp}}{n_{Gi} R_{MLGi}} = \frac{G_p R_{MLGp}}{G_i R_{MLGi}}. \quad (4.25)$$

See also the article by Wang [17], where further classification of the MBE is given.

4.3.2 Numerical representation of MBE

Let us assume that a gas-condensate reservoir is being produced at constant surface rate q_{sc} . During a time-step period of Δt a gas volume $\Delta V = q_{sc} \cdot \Delta t$ is produced. The relative cumulative production (recovery) after j time-steps is

$$\left(\frac{G_p}{G_i}\right)_j = \frac{1}{G_i} \sum_1^j (\Delta V)_j. \quad (4.26)$$

Suppose we wish to solve Eq. 4.23 at N discrete pressure levels p_j where $j = 1, 2, 3, \dots, N$ and where $p_1 = p_i$ and $p_j > p_{j+1}$. The iteration strategy is based on the assumption that we already know the fractional dry gas production and the condensate-gas ratio at steps up to the j 'th simulation step, i.e.

$$j : \quad \begin{array}{cccccc} 1 & 2 & \cdots & j-1 & j, \\ p_1 & p_2 & \cdots & p_{j-1} & p_j, \\ \left(\frac{G_p}{G_i}\right)_1 & \left(\frac{G_p}{G_i}\right)_2 & \cdots & \left(\frac{G_p}{G_i}\right)_{j-1} & \left(\frac{G_p}{G_i}\right)_j, \\ (R_{MLGp})_1 & (R_{MLGp})_2 & \cdots & (R_{MLGp})_{j-1} & (R_{MLGp})_j, \end{array}$$

where all parameters are known up to the time step j

The calculations at the next simulation step $j + 1$ follows an iteration procedure where one step is followed by the next.

Step 1 Definition of $(Gp/G_i)_{j+1}$ (as indicated above).

Step 2 Calculation of $(R_{MLGp})_{j+1}$, by applying Eq. 4.19 which translates in numerical terms to the following equation

$$(R_{MLGp})_{j+1} = \frac{1}{(Gp/G_i)_{j+1}} \sum_1^j \left(\frac{(R_{MLG})_{j+1} + (R_{MLG})_j}{2} \right) \left(\left(\frac{Gp}{G_i} \right)_{j+1} - \left(\frac{Gp}{G_i} \right)_j \right), \quad (4.27)$$

where $(R_{MLG})_{j+1}$ is the condensate-gas ratio at the new pressure step p_{j+1} . At the very first pass through the iteration list, this ratio is not known and therefore set to the old value at step j . As soon as a pressure at step $j + 1$ is estimated, $(R_{MLG})_{j+1}$ is calculated.

Step 3 Using Eq. 4.24, we may now calculate the pressure p_{j+1} and we write

$$p_{j+1} = p_i \frac{(Z_2)_{j+1} V_{HCi}}{Z_{2i} (V_{HC})_{j+1}} \left(1 - \left(\frac{Gp}{G_i} \right)_{j+1} \frac{1 + (R_{MLGp})_{j+1}}{1 + R_{MLGi}} \right). \quad (4.28)$$

Step 4 Based on the the pressure at step $j + 1$, the fractional dry gas production is recalculated using Eq. 4.23 and we get

$$\left(\frac{Gp}{G_i} \right)_{j+1}^{New} = \left(1 - \frac{Z_{2i} (pV_{HC})_{j+1}}{(Z_2)_{j+1} p_i V_{HCi}} \right) \left(\frac{1 + R_{MLGi}}{1 + (R_{MLGp})_{j+1}} \right). \quad (4.29)$$

Step 5 The last step in the iteration process is a convergence test. For the $(j + 1)$ 'th time step we started out by defining the fractional dry gas production (since a constant gas rate is chosen) equal to $(Gp/G)_{j+1}$. The convergence test is therefore a test on the newly calculated fractional gas production $(Gp/G)_{j+1}^{New}$ found in Step 4. If

$$\left| \left(\frac{Gp}{G_i} \right)_{j+1}^{New} - \left(\frac{Gp}{G_i} \right)_{j+1} \right| < \text{GPGERR}, \quad (4.30)$$

then the fractional dry gas production is defined by $(Gp/G_i)_{j+1}$ and the pressure is equal to p_{j+1} as given by Eq. 4.28.

If however,

$$\left| \left(\frac{Gp}{G_i} \right)_{j+1}^{New} - \left(\frac{Gp}{G_i} \right)_{j+1} \right| > \text{GPGERR}, \quad (4.31)$$

then the iteration process has to be repeated by starting at Step 2 redefining R_{MLGp} by the updated pressure p_{j+1} in Eq. 4.28.

The iteration tolerance $GPGERR$ in Eqs. 4.30 and 4.31 is defined by the user. $GPGERR$ is normally a small number, typically 10^{-7} . A tight conversion restriction will make the iteration more accurate but at the same time, less time efficient.

Example: Molar condensate-gas ratio

The iteration process above has been applied in an attempt to estimate the molar condensate-gas ratio R_{MLGp} as given by Eq. 4.27. The data used is taken for the Sleipner Vest case. Table 4.2 presents the input - and calculated data.

Table 4.2: Depletion data from the Sleipner Vest reservoir.

| p [bar] | Z_2 | V | G_p [Sm ³] | G_p/G_i | R_{MLG} (1 - V)/V | R_{MLGp} Eq. 4.27 |
|--------------|--------|--------|-----------------------------|-----------|------------------------|------------------------|
| 445 | 1.1142 | 0.9517 | 0.0000E+00 | 0.00000 | 0.05075 | 0.05075 |
| 370 | 1.0258 | 0.9517 | 2.4988E+06 | 0.00282 | 0.05075 | 0.05075 |
| 320 | 0.9743 | 0.9535 | 7.7463E+07 | 0.08742 | 0.04877 | 0.04979 |
| 280 | 0.9385 | 0.9556 | 1.5243E+08 | 0.17202 | 0.04646 | 0.04872 |
| 240 | 0.9102 | 0.9588 | 2.1490E+08 | 0.24252 | 0.04297 | 0.04756 |
| 200 | 0.8994 | 0.9626 | 3.0236E+08 | 0.34122 | 0.03885 | 0.04563 |
| 160 | 0.8851 | 0.9662 | 3.8981E+08 | 0.43991 | 0.03498 | 0.04368 |
| 120 | 0.8807 | 0.9692 | 4.7727E+08 | 0.53861 | 0.03178 | 0.04179 |
| 80 | 0.8862 | 0.9705 | 5.7722E+08 | 0.65141 | 0.03040 | 0.03994 |
| 40 | 0.8779 | 0.9709 | 6.8967E+08 | 0.77831 | 0.02997 | 0.03835 |
| 1 | 0.8580 | 0.9710 | 7.6214E+08 | 0.86010 | 0.02987 | 0.03755 |
| GIP | | | 8.8611E+08 | | | |

The molar condensate-gas ratios R_{MLG} and R_{MLGp} are plotted in Figure 4.5, where we observe that R_{MLGp} is a monotonous decreasing function.

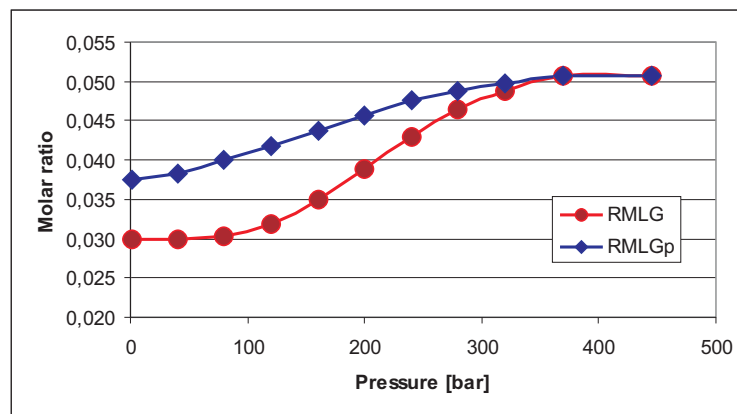


Figure 4.5: Molar condensate-gas ratio for Sleipner Vest gas.

As seen from Figure 4.6, the p/Z_2 data points fall on the straight line fit with a regression coefficient very close to unity. We may therefore conclude

that in this example, a plot of p/Z yields a straight line, provided the two-phase z-factor is being used instead of the single phase z-factor.

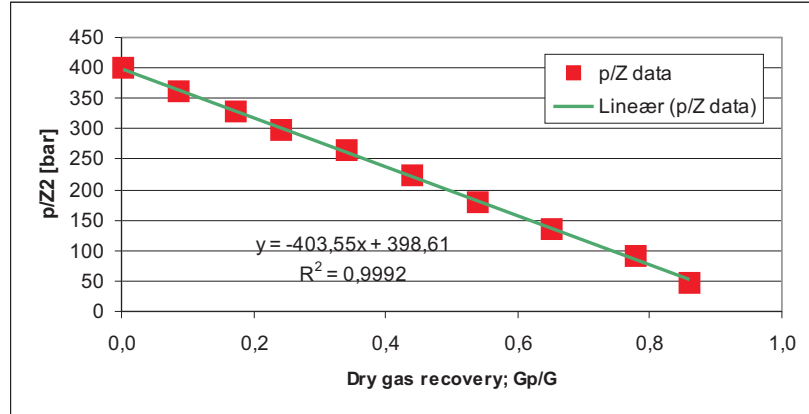


Figure 4.6: p/Z_2 plot for volumetric depletion process.

In the Figure 4.6 we have used the material balance calculations in the predicting mode where the reservoir performance is obtained by solving the material balance equation. The dry gas production G_p is based on parameters solely included in Eq. 4.29.

4.3.3 Simulation of Volumetric Depletion

Production from a gas-condensate reservoir is simulated, using the numerical representation presented above. The reservoir fluid is identical to the Sleipner Vest gas and have the characteristics presented in earlier chapters. The surface dry gas rate is constant and equal to $5 \cdot 10^5 \text{ Sm}^3/\text{day}$. The reservoir pore volume is $4 \cdot 10^6 \text{ Rm}^3$ and the initial water saturation and porosity is set to 20%. The production is continued until the reservoir pressure reaches a minimum pressure of 50 bar, at which time the production is halted.

The simulated gas production, at constant rate, takes 1524 days to finish, at which time $0.762 \cdot 10^9 \text{ Sm}^3$ dry gas and $0.285 \cdot 10^5 \text{ Sm}^3$ condensate are produced. The initial and rest reservoir volumes are given in Table 4.3.

Table 4.3: Cumulative volumes.

| | | |
|-------|---|---------------------------------|
| GIIP | = | $0.876 \cdot 10^9 \text{ Sm}^3$ |
| LIIP | = | $0.417 \cdot 10^6 \text{ Sm}^3$ |
| GREST | = | $0.114 \cdot 10^9 \text{ Sm}^3$ |
| LREST | = | $0.132 \cdot 10^6 \text{ Sm}^3$ |

The simulation of gas and condensate production is performed by adding up the produced gas G_p through consecutive time steps

$$G_p = \sum_{j=1}^n q_g \cdot \Delta t_j, \quad (4.32)$$

where q_g is the constant gas rate measured in Sm^3/day and Δt_j is the time step increment in number of days. n is the total number of time steps. The reservoir pressure is calculated using Eq. 4.24 and the condensate production is given by Eq. 4.25.

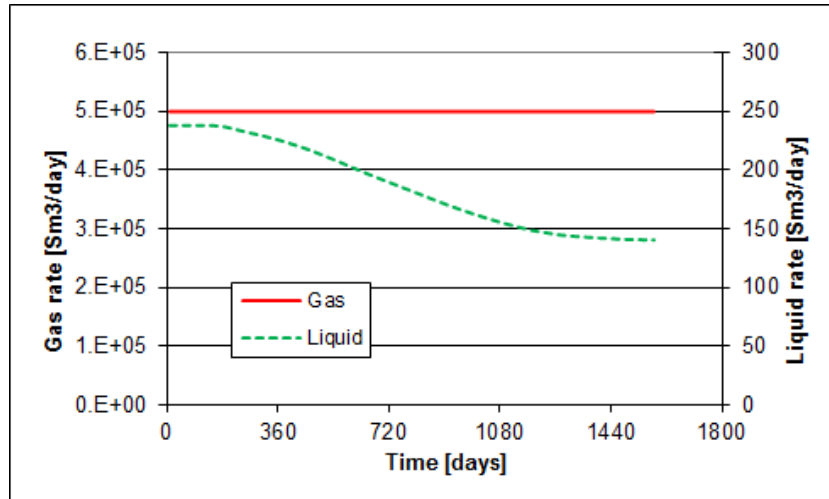


Figure 4.7: Gas and condensate production rates.

Figure 4.7 shows the production rates, where the dry gas rate is kept constant for the whole production period. The liquid rate is initially also constant as long as the reservoir pressure is higher than the dew point pressure. After this point in time, liquid condensate starts to drop out in the reservoir and less amount of condensate is produced to the surface. The decline in the liquid rate is continued almost throughout the whole production period.

The cumulative production of dry gas and liquid condensate is shown in Figure 4.8. Constant gas rate yields a linear (straight line) gas production while the cumulative liquid production follows a declining trend. The non-linear cumulative liquid production becomes quite apparent when the production data is plotted relative to initial in place volumes, as seen in Figure 4.9. The relative dry gas production reaches all together 89.8%, while the similar condensate production only reaches 70.1% of initial in place volumes. The production numbers presented above represent the most optimistic view of what can be produced from a gas condensate reservoir. There are many reasons to believe in reduced recoveries when actual natural gas reservoirs are considered. Among the most important factors that will reduce these numbers is entrapment of reservoir gas due to aquifer influx.

The gas and liquid recovery is also presented in Figure 4.10. This plot is similar to Figure 4.9 in the sense that it displays the difference between gas and liquid condensate production. The recovery plot however, displays the relative production as function of reservoir pressure. Figure 4.10 is therefore quite useful in assessing how much the reservoir can deliver of gas and liquid before production eventually has to be shut-

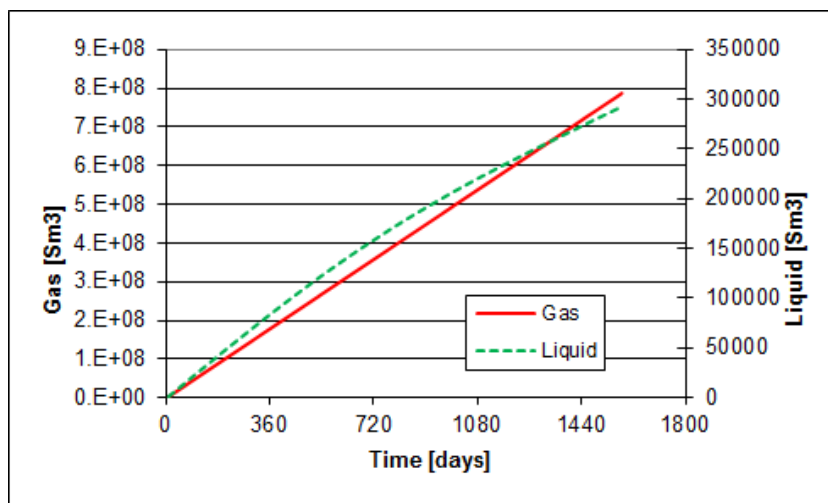


Figure 4.8: Cumulative gas production

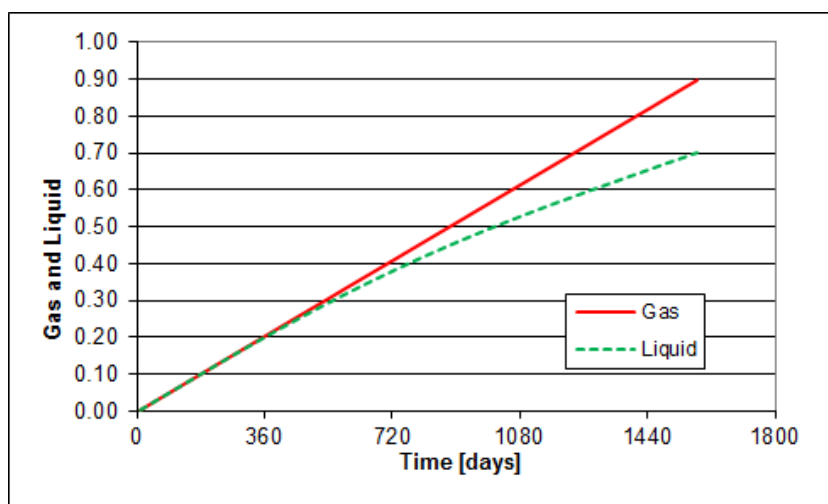


Figure 4.9: Relative cumulative production.

down. Since the recovery curves is gradually curving upwards and relatively more gas is produced per bar, it could be advantageous to lower the minimum pressure as much as possible.

In gas reservoir production, it could therefore be economical attractive to install some sort of pressure support to extend the production by e.g. lowering the abandonment pressure.

4.4 Non-Volumetric Depletion

Natural depletion of real gas reservoirs does very rarely appear to be pure volumetric. In most cases declining reservoir pressure will eventually lead to aquifer water influx, to a lesser or higher degree. Aquifer water influx may significantly reduce the hydrocarbon

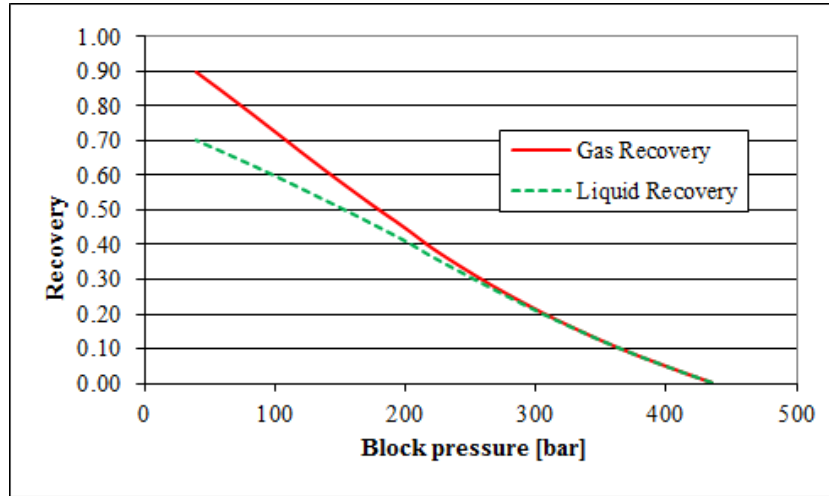


Figure 4.10: Gas and liquid recovery.

pore volume in the cause of the depletion period.

The hydrocarbon pore volume is frequently also reduced in *geo-pressured* reservoirs, where reservoir rock - and initial water compressibility both contribute to reduction in hydrocarbon pore volume. Reservoir rock - and initial water compressibility are normally small, typically $5 \cdot 10^{-5} \text{ bar}^{-1}$, but integrated over the whole reservoir volume, the resultant volume expansion can be significant.

In order to account for the effects of non-volumetric depletion, these contributions have to be explicitly incorporated into the material balance equation. Since the effect of all contributions are to reduce the effective hydrocarbon pore volume, the correction can be introduced as follows.

1. The hydrocarbon pore volume V_{HC} is equal to the initial pore volume V_{pi} minus the volume of initial water $V_{pi}S_{wi}$,

$$V_{HC} = V_{pi} - V_{pi}S_{wi}. \quad (4.33)$$

2. As a result of reservoir pressure decline, the initial pore volume is reduced due to reservoir rock expansion and the following substitution is valid

$$V_{pi} \rightarrow V_{pi}(1 - c_r\Delta p), \quad (4.34)$$

where c_r is the rock compressibility and $\Delta p = p_i - p$ is the pressure drop in the reservoir. (Notice that Δp is positive since $p_i > p$.)

3. Similarly, there is a reduction in the hydrocarbon pore volume caused by an expansion of initial water

$$V_{pi}S_{wi} \rightarrow V_{pi}S_{wi}(1 - c_w\Delta p), \quad (4.35)$$

where c_w is the water compressibility and $V_{pi}S_{wi}$ is the average initial water volume in the reservoir.

4. Finally the hydrocarbon pore volume is influenced by the influx of aquifer water or/and the production of initial water

$$V_{HC} \rightarrow V_{HC} - W_e + W_p B_w, \quad (4.36)$$

where W_e and W_p are the cumulative aquifer water influx and the cumulative water produced from reservoir volume, respectively. Since both volumes are reservoir volumes, W_e is measured in Rm^3 , while W_p is measured in Sm^3 and where the volume factor unit is Rm^3/Sm^3 .

Combining all effects introduced in Eqs. 4.33 to 4.36, the hydrocarbon pore volume is defined

$$V_{HC} = V_{pi}[1 - S_{wi} - (c_r + c_w S_{wi})\Delta p] - W_e + W_p B_w. \quad (4.37)$$

The expansion of reservoir rock and aquifer water is pressure dependent and can be evaluated at any pressure. The cumulative aquifer water influx is dependent on the pressure development and is as such both dependent on pressure and time. The cumulative water production is also time and pressure dependent since a rising water cut is dependent on both production history and pressure draw-down. The hydrocarbon pore volume is therefore a function both dependent on pressure and time, i.e. $V_{HC} = V_{HC}(p, t)$.

The pressure equation Eq. 4.24 is therefore written

$$p(t) = p_i \frac{Z_2(p)V_{HCi}}{Z_{2i}V_{HC}(p, t)} \left(1 - \frac{G_p(t)(1 + R_{MLGp}(p, t))}{G(1 + R_{MLGi})} \right). \quad (4.38)$$

Eq. 4.38 is the general material balance equation for non-volumetric depletion. Eq. 4.38 is an implicit equation in pressure p and time t , where p is a dependent variable and t is an independent variable. To solve this equation we have to specify the cumulative dry gas production $G_p(t)$ as function of time. The two-phase z-factor is a tabulated function of pressure, while the hydrocarbon pore volume $V_{HC}(p, t)$ is given by eq. 4.37. The molar condensate-gas ratio $R_{MLGp}(p, t)$ is solved by iteration and is thus a function of both pressure and time.

4.4.1 Significance of Reservoir Rock -, Initial Water and Gas Compressibility

Hydrocarbon reservoir bulk volume comprises of both a pore volume and a rock volume: $V_b = V_p + V_r$. If the pore volume is proportional to the bulk volume and $V_p = \phi V_b$, then reservoir rock volume is written

$$V_r = V_b - V_p = \left(\frac{1}{\phi} - 1 \right) V_p, \quad (4.39)$$

where ϕ is the porosity

If the reservoir pressure drop is positive, $\Delta p > 0$, then the volume expansion, due to the compressibility, can be approximated by

$$c = -\frac{1}{V} \frac{dV}{dp} \implies \Delta V = -cV\Delta p, \quad (4.40)$$

where c is the compressibility and V the initial volume.

"What is the condition under which the rock and water compressibility is negligible compared to the gas compressibility?" In comparing the effect of the reservoir rock - and initial water compressibility on one hand with the gas compressibility on the other we may evaluate the inequality,

$$\Delta V_w + \Delta V_r \ll \Delta V_g, \quad (4.41)$$

where the water and rock expansion is supposed to be less than 5% of the gas expansion

$$\Delta V_w + \Delta V_r < 0.05\Delta V_g. \quad (4.42)$$

Substituting the relations derived above into Eq. 4.42, yields

$$-c_w S_w - c_r \left(\frac{1}{\phi} - 1 \right) < -0.05 c_g (1 - S_w). \quad (4.43)$$

Since the real gas compressibility is given by

$$c_g = \frac{1}{p} - \frac{1}{Z} \frac{dZ}{dp},$$

we write the inequality in Eq. 4.43,

$$p > \frac{0.05(1 - S_w)}{c_w S_w + c_r (1/\phi - 1) + 0.05(1/Z)(dZ/dp)(1 - S_w)} \quad (4.44)$$

Eq. 4.44 tells us that there exists a pressure, above which the gas compressibility is the dominating source of volume expansion under non-volumetric depletion.

Example: Threshold pressure for gas compressibility to be dominant

A typical sandstone gas condensate reservoir has an average water saturation of $S_w = 0.2$. The porosity is $\phi = 0.3$ and the water- and rock compressibility are, $3 \cdot 10^{-5} \text{ bar}^{-1}$ and $5 \cdot 10^{-5} \text{ bar}^{-1}$, respectively.

The threshold pressure is estimated by applying the ideal gas version of Eq. 4.44. i.e. $dZ/dp = 0$ and we get

$$p > \frac{0.05(1 - 0.2)}{3 \cdot 10^{-5} \cdot 0.2 + 5 \cdot 10^{-5}(1/0.3 - 1)} = 326 \text{ bar.}$$

At reservoir pressures higher than 326 bars, we may safely neglect the effect of rock and water compressibility compared to the compressibility of the gas itself.

The contribution of the real gas correction term, relative ideal gas behaviour, is to reduce the pressure limit at which gas compressibility is the

dominating effect.

4.5 Aquifer Influx

A continuous production of gas and condensate will lead to a declining reservoir pressure. In a flat cylindrical reservoir, the reservoir pressure will have its lowest value in the well. The pressure will gradually increase towards the outer boundary. At the outer radius, r_e , see Figure 4.11, the pressure will eventually decrease below the initial pressure and a pressure drop, $\Delta p = p_i - p(r_e)$ will cause expansion of aquifer water and create a flow of water into the reservoir.

The aquifer could be considered as a continuous water volume surrounding the gas reservoir, where the aquifer inner radius is coinciding with the reservoir outer radius. (We will later consider other aquifer shapes.) The approach of water encroachment calculations and the interference of reservoirs, sharing a common aquifer is readily presented by Fetkovich, in his classic article [7].

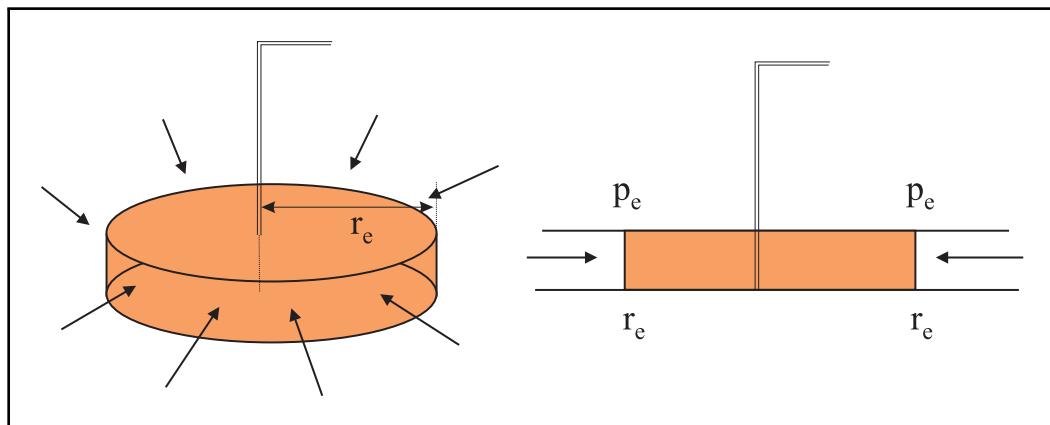


Figure 4.11: Cylindrical gas reservoir with surrounding aquifer.

The aquifer influx, W_e is in its simplest form defined as the expansion of the aquifer water volume W_i , controlled by the aquifer compressibility, c_w and the aquifer formation compressibility, c_f . The aquifer influx is therefore defined by the law of isothermal expansion and we can write

$$W_e = (c_w + c_f)W_i \cdot \Delta p, \quad (4.45)$$

where Δp is the average pressure drop in the aquifer.

If the aquifer volume is small, i.e. comparable to the reservoir pore volume, most of the water volume would be in close contact with the reservoir and any pressure drop in the gas reservoir would immediately result in an influx of additionally water. In the case of large to infinite size aquifers, similar encroachment processes will take longer time to activate and there will be a time lag between the pressure drop at the reservoir

boundary and the corresponding influx of water, through the same boundary surface. This time difference between pressure drop and water influx is due to the nature of water flow in the aquifer. Since the flow potential (pressure difference) at distant locations in the aquifer are relatively reduced, relative to the pressure drop experienced near to the reservoir, the corresponding water flow is lower further away from the gas reservoir than close to it. The response from small aquifers are therefore more or less time independent, while the water influx from larger aquifers are dependent of the pressure drop, Δp and the aquifer time lag response, i.e. water permeability, shape of aquifer and contact flow area, and in addition the aquifer and formation compressibility; c_w and c_f .

The gas production rate is important when considering the effect of aquifers. If the well rates are high and thus the reservoir gas is produced very fast, the resulting response from the aquifer could be small and therefore its importance as pressure support is reduced. The aquifer influx depends on aquifer type and aquifer strength, and on the pressure history of the reservoir. Since aquifer responses are generally slow compared to the pressure development in the reservoir, aquifer water influx will never "catch up" with a too hasty hydrocarbon production. In these cases, the pressure support inherently related to aquifers, will be lower than normal.

The maximum water influx from a cylindrical aquifer of limited radial dimension, r_a , as depicted in Figure 4.11, is given by the formula

$$W_e = (c_w + c_f)(r_a^2 - r_e^2)\pi h\phi\Delta p, \quad (4.46)$$

where h is the height of the aquifer and ϕ is the aquifer porosity.

The uncertainty related to aquifer estimation and water influx is illustrated by the formula above, where the only term known with any degree of certainty is the porosity, ϕ ! See also the presentation of natural water influx in the book from L.P.Dake [5].

Forecasting normal gas production is related to large uncertainties primarily due to imperfect reservoir description. Calculation of aquifer water influx, inherently involves the greatest uncertainty in the whole subject of reservoir engineering. The information basis related to aquifers are in most, if not all, cases resting on qualified guess work and is often likely not supported by reliable reservoir information, since wells are generally not drilled in the unproductive water zones. Prudence is therefore advised when dealing with aquifer modeling.

The process of aquifer influx into a gas reservoir is physically the same process, and to a high degree, similar to the known process of gas production through the well-bore in the reservoir. Therefore the aquifer influx could be considered as a steady-state aquifer inflow, where the water rate is being modeled by Darcy's law,

$$q_w = \frac{dW_e}{dt} = \frac{kh}{\mu} \frac{\Delta p}{\ln(r_a/r_e)}, \quad (4.47)$$

where all parameters are associated to the aquifer.

Introducing an aquifer influx constant C and integrating with time, we may write,

$$W_e = C \int_0^t (p_i - p) dt, \quad (4.48)$$

where integration can be approximated by summation. Using the trapezoidal rule, we get,

$$W_e = C \sum_0^t \Delta p \Delta t = C \left[\frac{p_i - p_1}{2} (t_1 - 0) + \frac{(p_i - p_1) + (p_i - p_2)}{2} (t_2 - t_1) + \frac{(p_i - p_2) + (p_i - p_3)}{2} (t_2 - t_1) + \dots \right]. \quad (4.49)$$

The integration shown in Eq. 4.48 is performed by using the trapezoidal rule as in Eq. 4.49, or can be performed by any other numerical integration method. Figure 4.12 depicts the integration technique of calculating the area under the pressure curve as sums of rectangles.

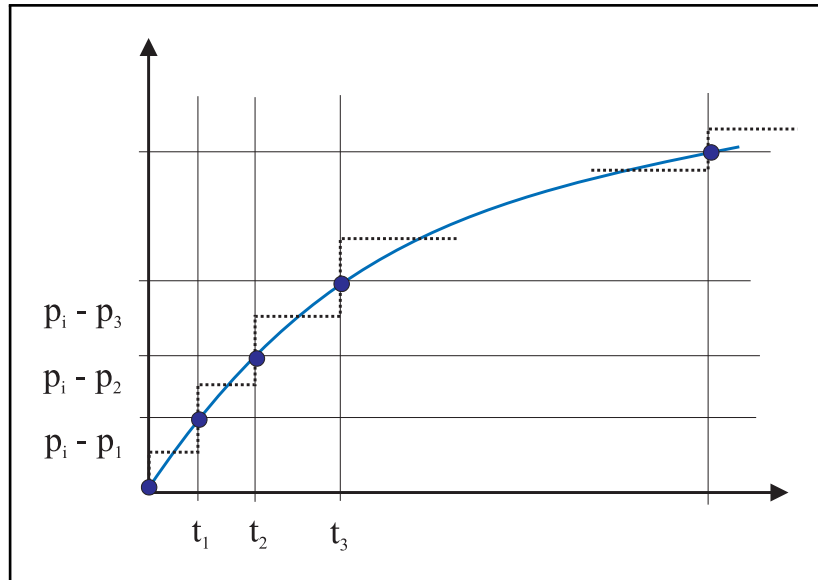


Figure 4.12: Applying the trapezoidal rule to calculate the area under the pressure curve.

The above model of aquifer influx, called Schilthuis' steady-state model, can be verified by assuming values of C as an integrated part of material balance calculations.

An extension of Schilthuis' model is to allow for gradual increasing aquifers, simply by treating the aquifer outer boundary as radially increasing with time, i.e. $r_a = a \cdot t$, in Eq. 4.47.

Then Eq. 4.48 becomes,

$$W_e = C' \int_0^t \frac{(p_i - p)}{\ln(at)} dt, \quad (4.50)$$

where the new unknowns C' and a can be found, simply by plotting the linear data $\Delta p / (dW_e/dt)$ against $\ln(t)$.

4.5.1 Natural Water Influx

Single phase reservoir fluid flow is described by the diffusivity equation. (The reservoir fluid flow behavior will be discussed in more details in the next chapter.) The flow of aquifer water into a reservoir is in principle the same physical process as the flow of gas or oil into a well. See Figure 4.13. This fact has been recognized by van Everdingen and Hurst in their classical article [16], where they presented a solution to the radial diffusivity equation at an outer boundary reservoir radius r_e . The dimensionless diffusivity equation given below is solved at a dimensionless radius $r_D = 1$, where $r_D = r/r_b$. r_b is the inner boundary radius of the aquifer. In the case where the reservoir outer radius coincide with the inner aquifer radius, then $r_b = r_e$ and

$$\frac{1}{r_D} \frac{\partial}{\partial r_D} \left(r_D \frac{\partial p_D}{\partial r_D} \right) = \frac{\partial p_D}{\partial t_D}, \quad (4.51)$$

where the dimensionless time is defined

$$t_D = \frac{kt}{\phi\mu cr_b^2}, \quad (4.52)$$

and where all parameters are average aquifer quantities. k is the aquifer permeability, ϕ is the porosity, μ is the water viscosity, c is the total compressibility, r_b is the inner aquifer boundary radius, i.e. $r_b = r_e$, and r_a is the aquifer outer radius, as depicted in Figure 4.13.

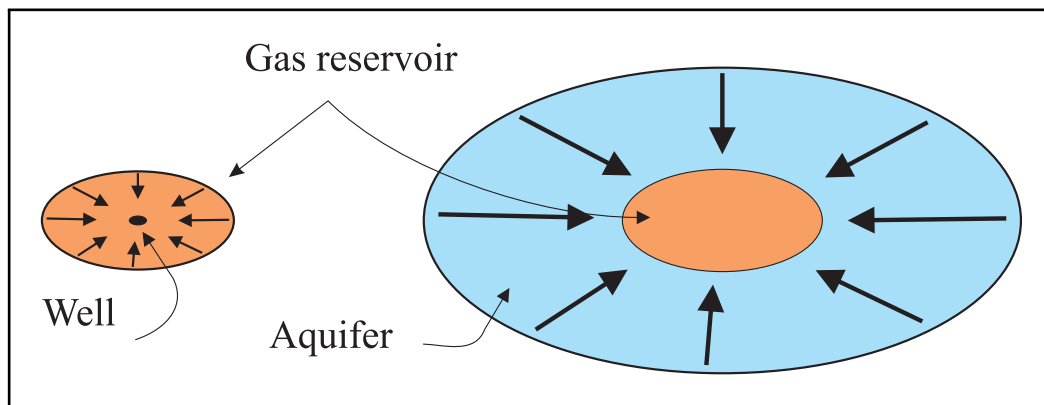


Figure 4.13: Similar flowing patterns in cylindrical gas reservoir (left) and cylindrical aquifer (right) .

There are in principle two sets of solutions to Eq. 4.51. One is *the constant terminal rate case* and the other is *the constant terminal pressure case*. In the constant terminal rate case, the rate is increased to a constant level and the well pressure is calculated as function of time. (This case is similar to the situation of constant terminal rate production, to be discussed further in the next chapter.)

In the constant terminal pressure case, a predefined pressure drop is kept constant and the water flow rate is calculated as function of time. This is the method that was adopted, in calculating the aquifer water influx, by van Everdingen and Hurst. In their

article, they solved Eq. 4.51 for an aquifer - reservoir system by applying the Laplace transformation.

The constant terminal pressure solution of Eq. 4.51, gives the dimensionless rate of aquifer water into the reservoir as function of dimensionless time at constant pressure drop Δp

$$q_D(t_D) = \frac{q\mu}{2\pi kh\Delta p}, \quad (4.53)$$

where $\Delta p = p_i - p$ is applied at the border between the reservoir and the aquifer. (Notice that the pressure drop Δp in Eq. 4.53 is constant.)

The cumulative aquifer water influx W_e is the volume water initially located inside the aquifer, that flows into the reservoir within the time t caused by a constant pressure drop Δp ,

$$W_e = \int_0^t q_w dt, \quad (4.54)$$

where q_w is the flow rate of aquifer water into the reservoir.

Transforming to dimensionless variables, we get

$$\begin{aligned} W_e \frac{\mu}{2\pi kh\Delta p} &= \frac{\mu}{2\pi kh\Delta p} \int_0^t q_w dt \\ &= \int_0^t q_D(t_D) dt \\ &= \int_0^{t_D} q_D(t_D) \frac{dt}{dt_D} dt_D \\ &= \frac{\phi\mu cr_b^2}{k} \int_0^{t_D} q_D(t_D) dt_D \\ &= \frac{\phi\mu cr_b^2}{k} W_{eD}(t_D). \end{aligned} \quad (4.55)$$

From Eq. 4.55 we may write the aquifer water influx W_e as function of the dimensionless aquifer influx W_{eD}

$$W_e = U\Delta p W_{eD}(t_D), \quad (4.56)$$

where the aquifer constant U is defined $U = 2\pi\phi hcr_b^2$, for a cylindrical aquifer. W_{eD} is a dimensionless function of dimensionless time t_D , dependent only on the volumetric dimensions of the aquifer.

The dimensionless aquifer influx $W_{eD}(t_D)$, has been calculated for both radial and linear aquifers of final and infinite dimensions. Knowing this function allows us to calculate the actual water influx, simply by applying Eq. 4.56.

In their article van Everdingen and Hurst presented tabled data representing the dimensionless influx for various cylindrical aquifers. However, for the solution of the constant terminal pressure case, reference is made to the book of Carlslaw and Jeager [3].

Polynomial representations of the data presented by van Everdingen and Hurst have been made available by several authors. Figure 4.14 shows W_{eD} plotted as function of t_D for the cases of cylindrical and linear aquifers of finite and infinite dimensions.

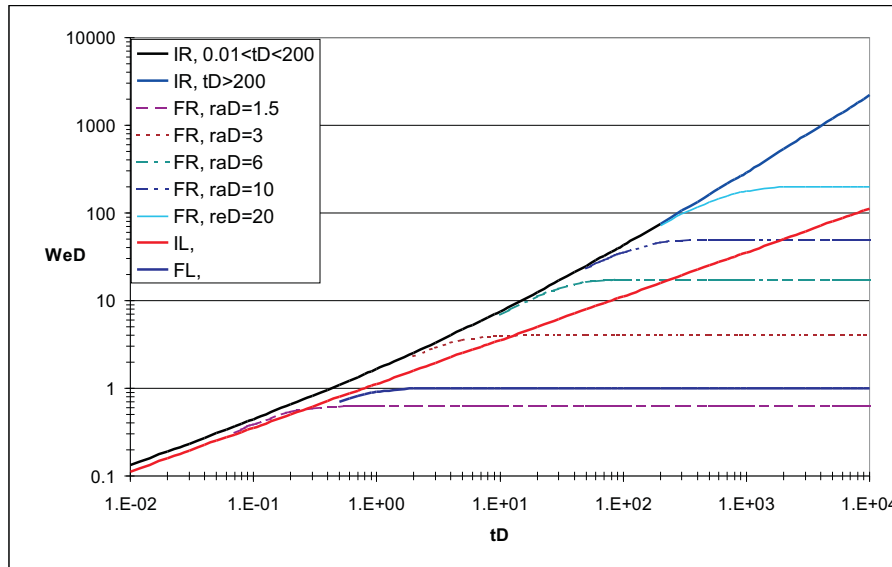


Figure 4.14: Dimensionless water influx for radial and linear aquifers of finite and infinite dimensions.

The curves plotted in Figure 4.14 represents polynomial fits to the data presented by van Everdingen and Hurst, where (IR) refers to infinite radial data and where (FR) refers to finite radial data. The finite radial data are presented for five choices of dimensionless radius $r_{aD} = r_a/r_b$; 1.5, 3, 10 and 20. Infinite and finite polynomial fits for linear data (IL and FL) are also presented in the same plot.

Typical for both radial and linear aquifers of finite dimension are that they all follow the infinite trend until a certain dimensionless time, after which they more or less becomes constant. This has to do with the fact that any finite aquifer, initially will behave as if it was of infinite size. As time develops, the aquifer volume is reduced and further water influx is reduced towards zero. The transition between these two stages is controlled by the cross section area available for flow, which again is in part controlled by the definition of dimensionless time t_D defined in Eq. 4.52.

4.5.2 Application of Aquifer Water Influx

The aquifer influx for an arbitrary pressure history can be calculated by using the dimensionless function $W_{eD}(t_D)$ at various time interval. The function is pressure independent and describe the water influx as a function of dimensionless time for a constant pressure drop in the reservoir imposed at initial time.

Since Eq. 4.56 is a linear equation of independent variables, it is possible to calculate the contribution of sequential pressure drops by using the *superposition principle*.

The average reservoir pressure can be observed to decrease step-wise as function of time, where the time $T = t_n$ is representing the present time i.e. the latest time step.

Pressure at aquifer boundary: $p_0 = p_i, p_1, p_2, p_3, \dots p_n$
 Changin time steps : $0, t_1, t_2, t_3, \dots t_n$

Figure 4.15 shows the decreasing average reservoir pressure. The full line represents the dynamical pressure decline, while the dotted line represents a step-wise approximation to the average reservoir pressure. Each step represents an instantaneous change in the pressure and the corresponding influx at each step is shown in the lower diagram. The water influx at each step follows form the dimensionless function evaluated at the appropriate dimension-less time. The total water influx is obtained by the summation of the influxes for the individual steps.

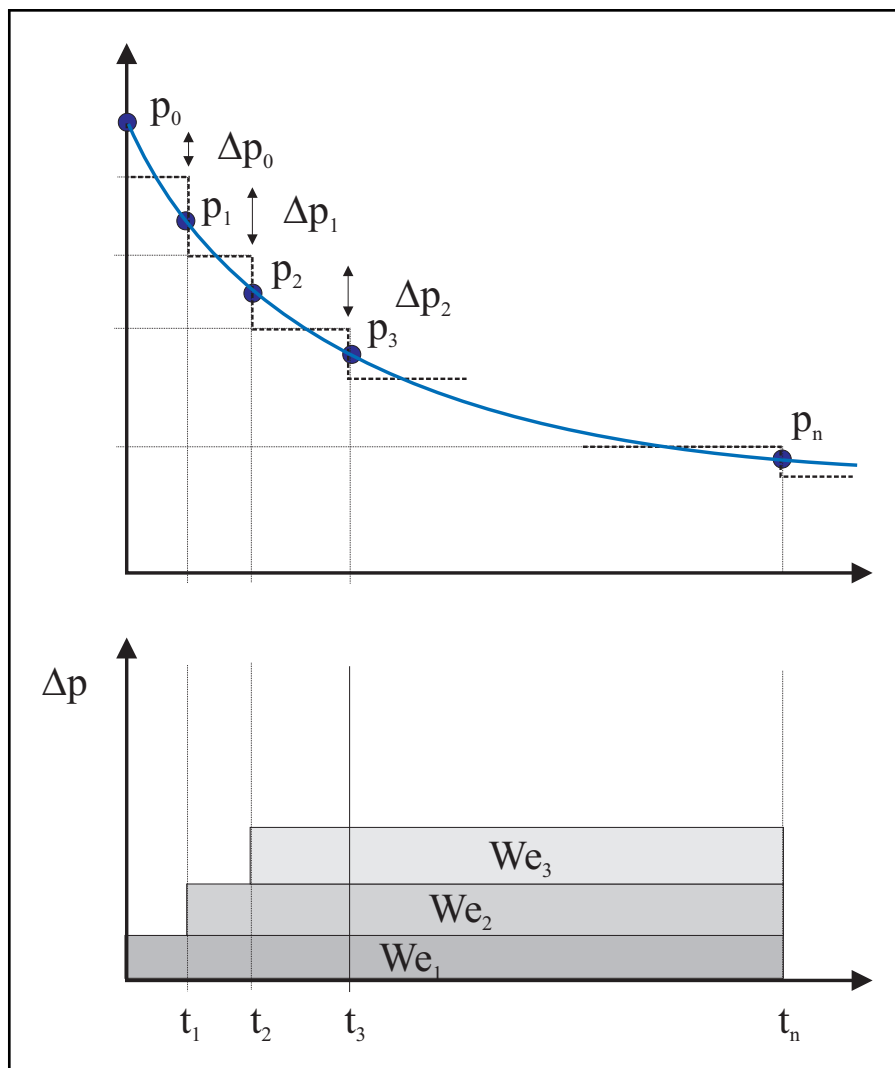


Figure 4.15: Average reservoir pressure decline creates a superposition of water influxes.

The average pressure levels at the aquifer boundary during the time intervals between each time step, as indicated in Figure 4.15, are given

$$\begin{aligned}
\langle p_1 \rangle &= (p_0 + p_1)/2, \\
\langle p_2 \rangle &= (p_1 + p_2)/2, \\
&\vdots \\
\langle p_j \rangle &= (p_{j-1} + p_j)/2,
\end{aligned} \tag{4.57}$$

where j is the j 'th time step.

The corresponding pressure drop at different time steps: $0, t_1, t_2, \dots$ can be written

$$\begin{aligned}
\Delta p_0 &= (p_0 - \langle p_1 \rangle) = \dots = (p_0 - p_1)/2 \\
\Delta p_1 &= (\langle p_1 \rangle - \langle p_2 \rangle) = (p_0 + p_1)/2 - (p_1 + p_2)/2 = (p_0 - p_2)/2 \\
&\vdots \\
\Delta p_j &= (\langle p_j \rangle - \langle p_{j+1} \rangle) = (p_{j-1} + p_j)/2 - (p_j + p_{j+1})/2 = (p_{j-1} - p_{j+1})/2
\end{aligned} \tag{4.58}$$

The aquifer water influx W_e , in Eq. 4.56, is the cumulative influx under the assumption that the reservoir experiences a pressure drop equal to Δp . As seen from Figure 4.15, a dynamical pressure decline can be represented by a step wise pressure decline Δp_j , where each pressure drop is associated with a specific water influx W_{ej} . The total water influx is therefore the sum of all influxes from time t_0 to the time t_n . Since the present time $T = t_n$, the cumulative aquifer influx is

$$\begin{aligned}
W_e(T) &= W_{e1} + W_{e2} + W_{e3} + \dots + W_{en} \\
&= U[\Delta p_0 W_{eD}(T_D) + \Delta p_1 W_{eD}(T_D - t_{D1}) \\
&\quad + \Delta p_2 W_{eD}(T_D - t_{D2}) + \dots + \Delta p_{n-1} W_{eD}(T_D - t_{D(n-1)})]
\end{aligned} \tag{4.59}$$

The principle of superposition applied in Eq. 4.59 is based on the assumption that the cumulative water influx W_e can be represented by a sum of individual influxes W_{ej} , where the j 'th influx is caused by the j 'th pressure drop Δp_j . The time period over which the j 'th influx is active is then represented by the time difference $(T - t_j)$. In dimensionless parameters, this time difference becomes $(T_D - t_{Dj})$.

The cumulative aquifer water influx at time $T = t_n$ is therefore written

$$W_e(T) = U \sum_{j=0}^{n-1} \Delta p_j W_{eD}(T_D - t_{Dj}), \tag{4.60}$$

where n is the number of time steps being calculated.

4.5.3 Aquifer Models

The aquifer dimensionless function W_{eD} has been derived for certain geometrical aquifer shapes. The polynomial representation, already presented in Figure 4.14, are found in the books of J. Hagoort [9] and T. Ahmed [1]. They give polynomial fits to the dimensionless aquifer influx W_{eD} for infinite radial aquifers, finite radial aquifers, infinite linear aquifers, finite linear aquifers in addition to bottom water influx.

Infinite Radial Aquifers

An infinite radial aquifer can be limited by e.g. faults such that it covers only a limited fraction of the whole circumference. The sector where the aquifer is active might be defined by an angle α , as shown in Figure 4.16.

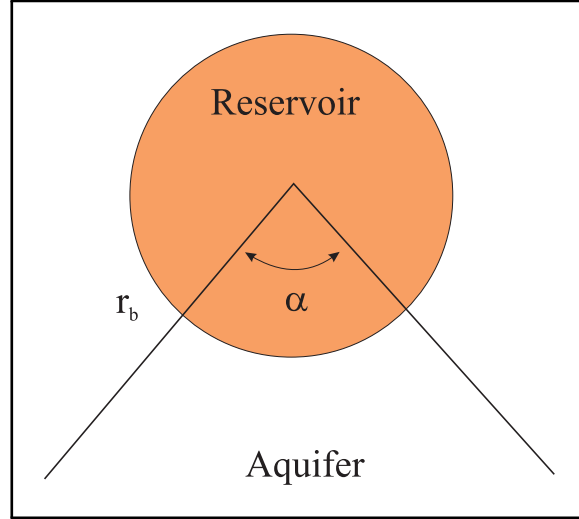


Figure 4.16: Infinite radial sector aquifer.

The polynomial fit of $W_{eD}(t_D)$ for a radial infinite aquifer is, - as in the book of T. Ahmed, subdivided into three time regions,

$$t_D < 0.01 : W_{eD} = 2 \left(\frac{t_D}{\pi} \right)^{0.5}, \quad (4.61)$$

$$0.01 \leq t_D < 200 : W_{eD} = \frac{1.2838\sqrt{t_D} + 1.19328t_D + 0.269872t_D^{3/2} + 0.00855294t_D^2}{1 + 0.616599\sqrt{t_D} + 0.0413008t_D} \quad (4.62)$$

$$t_D \geq 200 : W_{eD} = \frac{-4.29881 + 2.02566t_D}{\ln(t_D)}, \quad (4.63)$$

where the dimension-less time is given by Eq. 4.52

The aquifer constant U in Eq. 4.56, is in the radial case defined by

$$U = 2\pi \frac{\alpha}{360} \phi h c r_b^2, \quad (4.64)$$

where α is called the encroachment angle, defined in degrees. Aquifer porosity ϕ , aquifer thickness h , aquifer total compressibility c , comprising both rock and water and aquifer inner radius r_b , are all defined as previously.

Finite Radial Aquifers

A finite radial aquifer has a finite outer boundary r_a . The dimensionless function now depends on the aquifer radial extent and in dimensionless form is characterized by $r_{aD} = r_a/r_b$.

The response from a finite radial aquifer will at early times be similar to the response from an infinite aquifer. Not until the outer boundary is reached, will the finite aquifer

start to behave differently compared to the infinite aquifer. Seen from Figure 4.14, a transition time indicating the shift from infinite to finite acting aquifers, can be approximated based on the dimensionless radius r_{aD} ,

$$t_{aD} = 0.3(r_{aD} - 1)^{2.25}. \quad (4.65)$$

After t_{aD} , an analytical representation, given by J. Hagoort, is representing the dimensionless function W_{eD} for a finite aquifer,

$$W_{eD} = 0.5(r_{aD}^2 - 1) \left(1 - \exp\left(\frac{-2t_D}{J^*}\right) \right), \quad (4.66)$$

where the function J^* is defined as

$$J^* = r_{aD}^4 \frac{\ln r_{aD}}{r_{aD}^2 - 1} + 0.25(1 - 3r_{aD}^2). \quad (4.67)$$

Notice that the dimensionless time t_D and aquifer constant U for finite - and infinite radial aquifers are defined similarly.

Infinite Linear Aquifers

The dimensionless function W_{eD} for infinite linear aquifers is given by

$$W_{eD} = 2\sqrt{\frac{t_D}{\pi}}, \quad (4.68)$$

where the dimension-less time t_D is defined

$$t_D = \frac{k}{\phi\mu cw^2}t, \quad (4.69)$$

and where w is the aquifer width, as depicted in Figure 4.17.

The aquifer thickness h is represented in the aquifer constant U , which is defined,

$$U = \phi h c w^2. \quad (4.70)$$

Finite Linear Aquifers

The finite linear aquifer is defined by a finite width w , height h and length L , as shown in Figure 4.17.

The dimensionless time is defined by

$$t_D = \frac{k}{\phi\mu c L^2}t, \quad (4.71)$$

and the aquifer constant is written

$$U = \phi c h w L. \quad (4.72)$$

The dimensionless water influx for a linear aquifer is, following J.Hagoort, given as

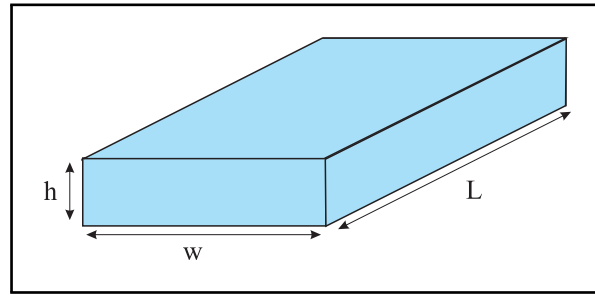


Figure 4.17: Finite linear aquifer.

$$W_{eD} = 1 - \sum_{n=0}^{\infty} \frac{\exp(-(2n+1)^2 \pi^2 t_D / 4)}{(2n+1)^2}. \quad (4.73)$$

The summation index n is supposed to run from zero to infinity but in practical terms $n \leq 10$ is proven to be quite sufficient, as can be seen from Figure 4.18.

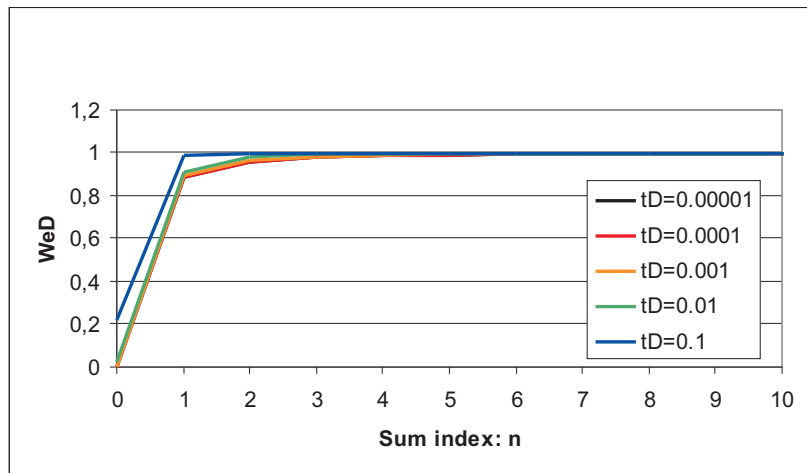


Figure 4.18: Finite linear aquifer function.

The transition time, between infinite and finite acting linear aquifer, is found to be about $t_D = 0.5$ from Figure 4.14.

Finite linear aquifers is in Figure 4.14 represented by a single curve (FL), even though finite aquifers may come in different shapes and volumes. Information of the particular aquifer is entirely contained in t_D and U . All finite aquifers will therefore act similarly and the only difference between one aquifer to the other is the definition of actual transition time.

Bottom Aquifer Influx

In many cases gas reservoirs are located on top of an underlying aquifer, where a horizontal gas-water-contact (GWC) is separating the two phases. The height of the water column, being part of the gas reservoir, might be considerable. Connate water may

stand all the way from the GWC and up to the crust or cap of the reservoir. In cases with high vertical water permeability, considerable water support from bottom aquifers could be expected, as depicted in Figure 4.19.

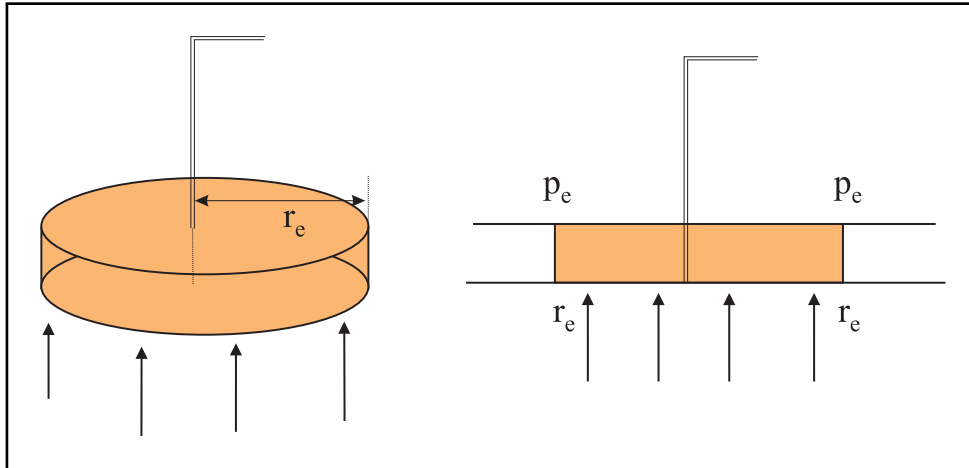


Figure 4.19: Cylindrical gas reservoir with bottom aquifer influx.

The aquifer flow model used by van Everdingen and Hurst describes horizontal water encroachment and does not generally account for the kind of vertical flow generated by an underlying aquifer. To be applicable in these situations, the diffusivity equation Eq. 4.51 can be modified with an additional term, describing vertical flow. The introduction of a vertical flow term would necessarily also introduce a vertical permeability k_v and a ratio between vertical and radial permeability can be defined, $F_v = k_v/k_r$.

Solutions of such an extended diffusivity equation has been presented by Coats [4]. In his calculations, the aquifer influx is estimated using the same form as van Everdingen and Hurst in Eq. 4.56, where the aquifer constant now is defined $U = 2\pi\phi cr_e^2 h$. h is here the aquifer height or thickness below the gas reservoir, where r_e is the reservoir radial dimension.

Even though the dimensional aquifer influx W_{eD} is different for the function derived by van Everdingen and Hurst, the solution procedure is identical in the two cases. Bottom aquifer influx may therefore approximately be represented by vertical inflow models, i.e. solutions derived by van Everdingen and Hurst. In comparing the two solutions, the bottom aquifer models gave somewhat 20% less water influx, compared to the infinite radial model.

4.6 Simulation of Non-Volumetric Depletion

In non-volumetric depletion, the aquifer water will flow into the reservoir and occupy part of the pore volume. The effects on the overall gas recovery due to aquifer influx are both positive and negative. On the positive side, it seems evident that the aquifer water helps to maintain the pressure in the reservoir by reducing the rate of normal pressure decline, which again will improve the recovery to pressure ratio. On the negative side, however, the impact of aquifer influx will immobilize part of the reservoir gas by confining large amounts of gas in closed pockets. Laboratory experiments,

logging data and reservoir material balance calculations have demonstrated that the trapped gas saturation in water-invaded regions could be as high as 50% of the total pore space [8]. A second effect is the danger of possibly water break-through and consequently increased water-cut production, which again could lead to "killing the well" and early well abandonment.

In the simulations presented here, the gas reservoir is similar to what was presented in section 4.3.3. The simulation of trapped gas, as mentioned above, and other related reservoir characteristics are not part of these simulations. Thus, only the positive effect of aquifer influx is considered here, i.e. only the effect directly related to the material balance calculations due to aquifer influx is considered.

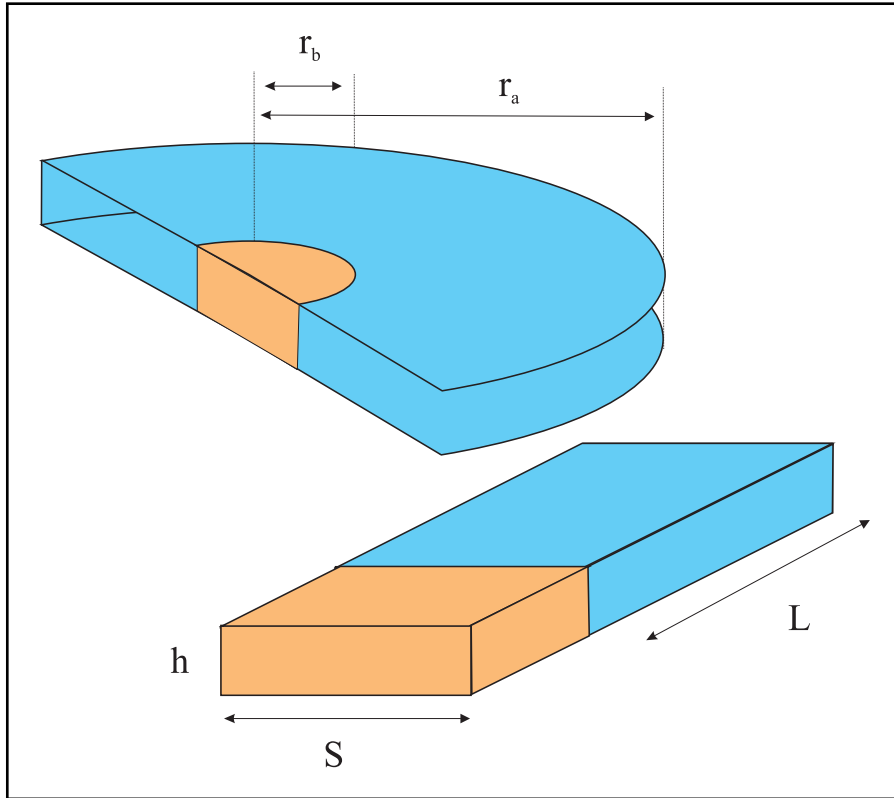


Figure 4.20: Radial and linear aquifer dimensions.

Simulation of non-volumetric depletion is demonstrated using a radial and a linear (rectangular) shaped aquifer, as depicted in Figure 4.20. The reservoir and aquifer thickness is equal to 50 m. The effect of water encroachment is compared to the case of a semi cylindrical aquifer ($\alpha = 180^\circ$) and a rectangular shaped aquifer, where

1. the initial water volume (pore volume) in the finite cases are equal, i.e. $0.5\phi\pi(r_a^2 - r_b^2)h = \phi SLh$ and
2. the flux surface joining the the reservoir and aquifer is the same, i.e. $0.5 \cdot 2\pi r_b \cdot h = S \cdot h$.

The length of the rectangular aquifer is therefore determined by the radial dimension

of the cylindrical aquifer, and $L = (r_a^2 - r_b^2)/2r_b$. Thus, parameters characterizing the aquifers and their dimensions are given in Table 4.4.

Table 4.4: Average aquifer parameters and dimensions.

| k [mD] | c_w [1/bar] | ϕ | μ [mPa · s] | α | $r_b = r_e$ [m] | r_a [m] | S [m] | L [m] |
|----------|-------------------|--------|-----------------|----------|-----------------|-----------|-------|-------|
| 5 | $5 \cdot 10^{-5}$ | 0.2 | 1.0 | 180 | 360 | 2000 | 1131 | 5375 |

Figure 4.21 shows the cumulative water influx as function of time, for the four aquifers. It is interesting to notice that for a certain time period, the infinite and finite radial aquifers plot similarly. During approximately a year, the two radial aquifers are indistinguishable and it is seemingly impossible to distinguish which type of aquifer is active; infinite or finite dimension.

In the case of linear aquifers, the influx of cumulative water is considerably lower than for the radial aquifers, even though the flux area connecting the aquifers and the gas reservoir is exactly the same. This points to the fact that the aquifer water is generally located further away from the reservoir in the linear cases than in radial cases. This assumption is further underlined by the fact that the finite radial and linear (rectangular) aquifer have the same initial water volume.

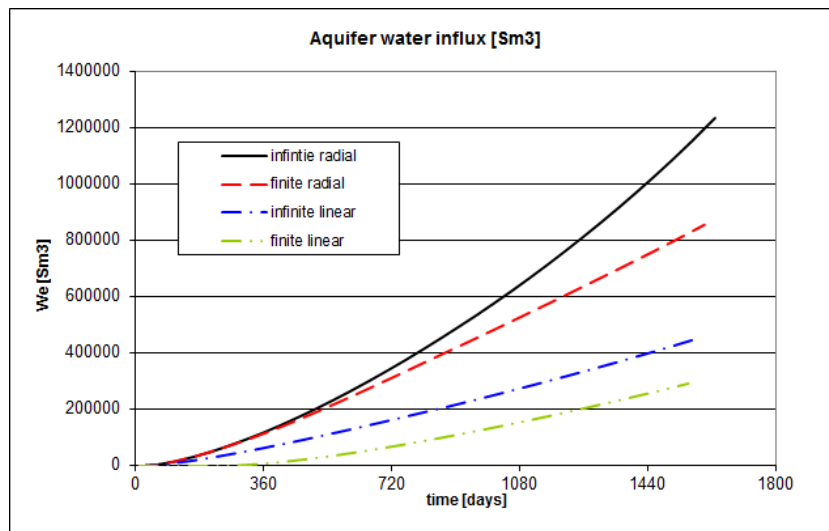


Figure 4.21: Water influx for radial and linear aquifers of infinite and finite dimensions.

The average reservoir pressure as function of time is plotted in Figure 4.22. Of the five simulations presented in the plot, four involves aquifer influx from radial and linear aquifers of infinite and finite dimensions. All parameters and spacial dimensions are as presented above. The pressure profiles representing the radial aquifers shows evidence of pressure support, to a higher degree than is the case for linear aquifers. The contribution from the rectangular aquifers are quite limited and of minor importance for the pressure development and appears to be quite similar to the non-aquifer case. The effect of prolonged production period in the cases of aquifer encroachment is anyhow quit clear.

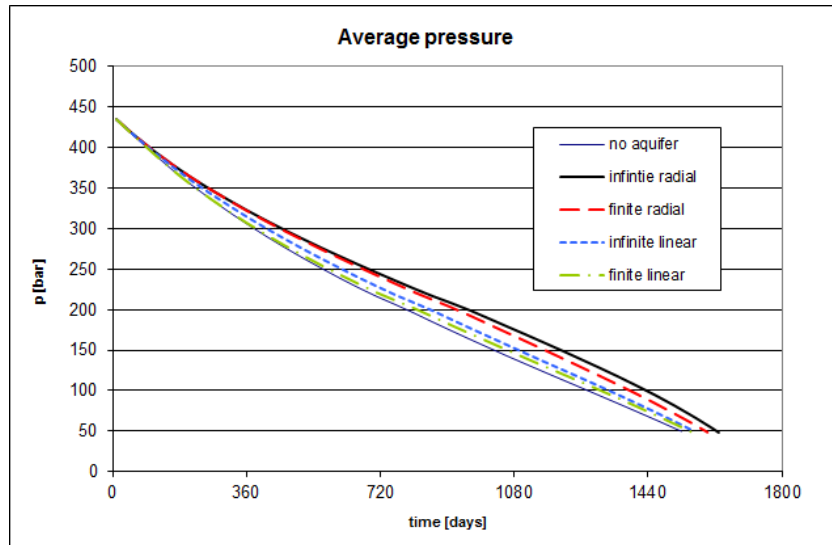


Figure 4.22: Average reservoir pressure decline for four cases of aquifer water support.

The relative production of gas and liquid condensate are plotted in Figure 4.23, as function of reservoir pressure. The most striking effect, observed in the recovery plots, is the observation that liquid production benefits more from pressure support than the gas production. In the case of the infinite radial aquifer there is a significant increase in the recovery for all pressures, say lower than 350 bar. At lower pressure than 150 bar the recovery seems to flatten out somewhat. This observation is related to the reduced pressure decline in the reservoir at late times, caused by the fact that most of the gas has already been produced.

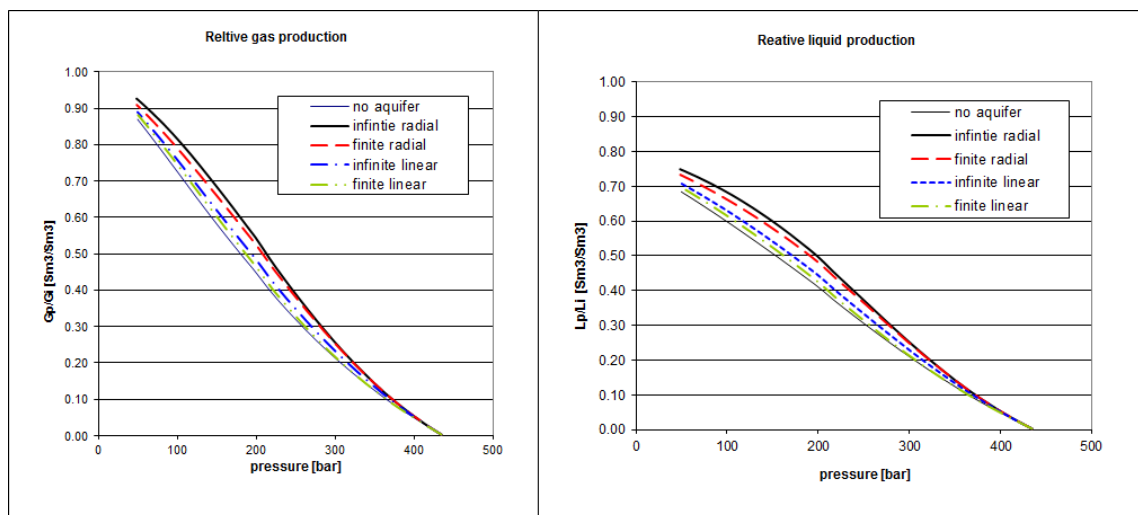


Figure 4.23: Recovery plots for gas and liquid condensate production.

The effect of aquifer support is particularly interesting in the case of liquid condensate production. Relative to the case of no aquifer support, there is a noticeable increase in

liquid recovery of more than 5% in the infinite radial case, as seen from Figure 4.23.

Figure 4.24 shows the water influx W_e as function of time for three cases of increasing aquifer permeability, i.e. 1, 5 and 10 mD. The aquifer is infinite radial and otherwise characterized, as presented in Table 4.4. The water influx is, as can be expected, a strong function of aquifer permeability, where a 10 fold increase in permeability gives somewhat less than 3 times increase in cumulative water influx. The average aquifer permeability is therefore an important parameter when aquifer support is being evaluated.

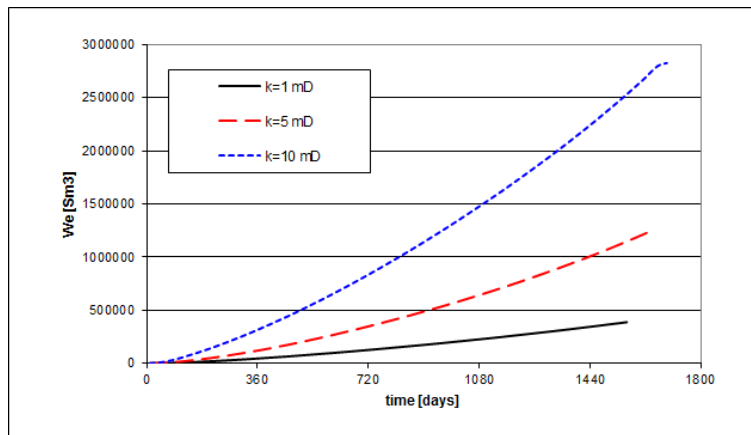


Figure 4.24: Infinite radial aquifers of different permeability.

In Figure 4.25, two different dry gas production rates are simulated, $q_g = 0.25 \text{ MSm}^3$ and $q_g = 0.5 \text{ MSm}^3$. The aquifer is in these simulations of infinite radial dimension and otherwise as presented in the Table 4.4, above. The effect of a reduced gas rate, 0.25 MSm^3 , is of course an extended production period. More interesting, however, is the increased cumulative aquifer influx in the low gas rate case. The total water influx W_e is, in the low rate case, considerable higher than in the high rate case. Consequently, slightly more gas is produced in the low rate case. The additional increased cumulative gas production in the low rate case, is marginal and would in this case not support a decision of reduced gas rate.

Generally speaking, the importance of the aquifer is reduced when the gas out-take is high compared to low gas production rates. At high gas rates the aquifer does not have the time to properly respond to the pressure drop in the reservoir and consequently the water influx is less than it otherwise would have been. In the case of dry and wet gas reservoirs, the aquifer support is in reality not particular significant. It is primarily in the case of gas condensate reservoirs, that the aquifer size and strength becomes important. In these reservoirs the cumulative liquid production is critically dependent on the general pressure decline in the reservoir. If the pressure drops too quickly below the dew point pressure, valuable liquid is condensed in the reservoir and thus considered lost production. In these cases could pressure support generated by aquifer influx prove to be of great importance for the whole economy of the project.

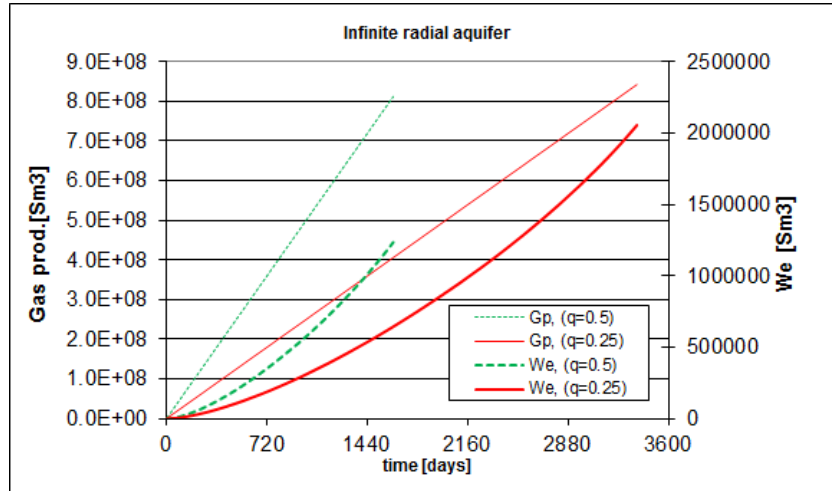


Figure 4.25: Cumulative dry gas production and aquifer influx.

4.7 History Matching and Predictive Performance

Even though material balance is supposed to be one of the simplest subjects in the whole of reservoir engineering, there are great misunderstandings related to the application of material balance calculations as a predictive tool. The lack of proper knowledge and understanding of the prerequisites in dealing with MBE, can lead to serious error in assessing the reservoir drive mechanism (interpretation of the depletion process) and in estimating GIIP. Generally, some methods are easier to use than other and some methods are more trustworthy than others.

Using the traditional p/z versus cumulative production plots, can lead to a complete misinterpretation of the drive mechanism and a serious overestimation of the GIIP. In an attempt to avoid doing these mistakes, other methods should be preferred. One of these methods is the Havlena - Odeh Interpretation Method [10, 11], where the production data is plotted as a straight line. The interception between the straight line and the y-axis defines the GIIP, in such a way that linearity can be checked. Another method is the Direct Method, proposed by F. Hsieh [12, 13]. In this model, the water influx is calculated without any prior knowledge of the aquifer and GIIP is estimated based on a horizontal line fit.

4.7.1 p/z Interpretation Method

A general pressure equation, as presented in Eq. 4.24, has been deduced under the assumption of molar balance in gas condensate reservoir production.

$$p = p_i \frac{Z_2 V_{HCi}}{Z_2 V_{HC}} \left(1 - \frac{G_p (1 + R_{MLGp})}{G_i (1 + R_{MLGi})} \right) \quad (4.74)$$

In the equation above, the aquifer influx is introduced in the V_{HC} term and liquid dropout is given by the term R_{MLG} . The p/z interpretation method can be displayed by using the more simplified pressure - production equation Eq. 4.11, derived for dry and wet gas reservoirs,

$$p = p_i \frac{Z}{Z_i} \left(1 - \frac{G_p}{G_i} \right), \quad (4.75)$$

where aquifer influx is not accounted for and where liquid condensation in the reservoir is neglected.

The danger of uncritically using the p/z interpretation method, as in Eq. 4.75, can be illustrated by plotting nonlinear data as shown in Figure 4.26. In the plot, the volumetric depletion line is presented for comparison, as the straight line is ending at the cumulative production $G_p/G_i = 1$.

The data points describing the non-volumetric production are always located above the volumetric data line. When non-volumetric data for the first two years of gas production is linearized, as if they were volumetric depletion data, - the linear trend is seen to intercept the x-axis at values of G_p/G_i much greater than unity. The difficulties of distinguishing natural depletion cases where no aquifer water is entering the reservoir with those cases where we do have aquifer influx, are sometimes quite difficult. In these cases, the danger of extrapolating the straight line fit and determining a grossly overestimated GIIP, is particular pertinent, as has been clearly documented by Bruns et al. [14] as early as in 1965.

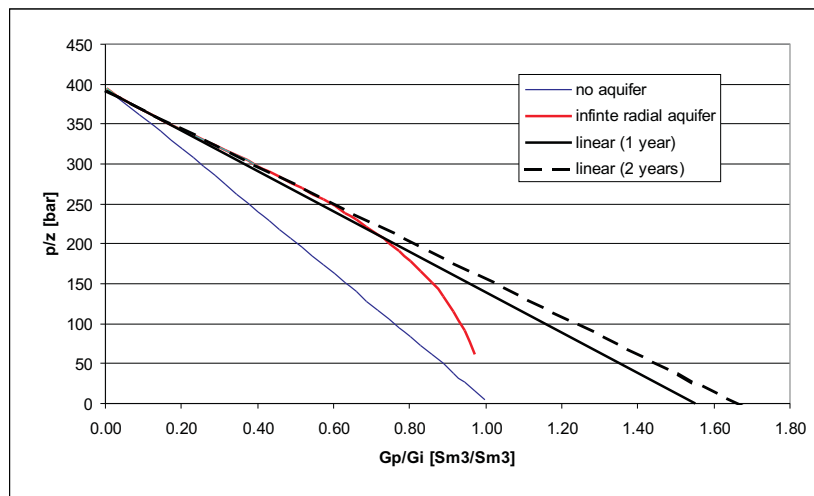


Figure 4.26: p/z plot for non-volumetric depletion.

The early data, up to 1 year, seems to be quite linear, while a linear trend through these data shows a considerable overestimation of the initial gas in place by nearly 160%. If a second year of production is added to the data basis, the estimation of GIIP seems to be even worse, as seen from Figure 4.26.

The error done in this analysis is related to the misinterpretation of non-volumetric data as volumetric data. The early data seems to be quite linear, but they are not! This point is further emphasized by the fact that the aquifer in this simulation example only represents a moderate water influx and thus only slightly modifies the non-volumetric data basis.

4.7.2 The Havlena - Odeh Interpretation Method

A general material balance equation for natural gas reservoirs can be derived from the molar balance equation, Eq. 4.23, presented above, where the molar balance equation can be written,

$$\frac{G_p}{G_i} = \left(1 - \frac{Z_{2i}pV_{HC}}{Z_2p_iV_{HCi}}\right) \left(\frac{1 + R_{MLGi}}{1 + R_{MLGp}}\right).$$

If we assume no water influx nor water production, use the definition of hydrocarbon pore volume (V_{HC}), given in Eq. 4.37, and use the gas volume factor (B_g) defined in Eq. 3.111, - then

$$\begin{aligned} V_{HC} &= V_{pi} \{(1 - S_w) + (c_r + S_w c_w)(p - p_i)\}, \\ B_g &= (1 + R_{MLG}) Z \frac{T}{p} \left(\frac{p}{T}\right)_{SC}, \end{aligned}$$

and then the material balance equation for natural gas reservoirs (dry- and wet gas reservoirs) is written,

$$G_p B_g = G_i (B_g - B_{gi}) + G_i B_{gi} \frac{(c_r + S_w c_w)}{(1 - S_w)} \Delta p. \quad (4.76)$$

The pressure difference $\Delta p = p_i - p$ is always positive. If the water influx W_e and the water production W_p are included into the above equation, the general material balance equation for gas reservoirs can be written,

$$\underbrace{G_p B_g + W_p B_w}_{\text{Underground-withdrawal}} = \underbrace{G_i (B_g - B_{gi})}_{\text{Gas-expansion}} + \underbrace{G_i B_{gi} \frac{(c_r + S_w c_w)}{(1 - S_w)} \Delta p}_{\text{Expansion and Compaction}} + \underbrace{W_e}_{\text{Influx}}, \quad (4.77)$$

where B_w is the volume factor for water, often assumed to be unity. All underground volumes in the above equation are reservoir volumes (Rm^3).

Adopting the nomenclature frequently used in linearization of the general material balance equation,

$$\begin{aligned} F &= G_p B_g + W_p, \\ E_g &= B_g - B_{gi}, \\ E_f &= B_{gi} \frac{(c_r + S_w c_w)}{(1 - S_w)} \Delta p, \end{aligned}$$

the reduced linear equation is written,

$$\frac{F}{E_g + E_f} = G_i + \frac{W_e}{E_g + E_f}. \quad (4.78)$$

Using production, pressure and PVT-data, the left-hand side of the above equation can be plotted as function of cumulative gas production, G_p . In the case of no water

influx ($W_e = 0$), i.e. volumetric depletion, the data should plot linearly as a horizontal straight line.

Any deviation from a straight horizontal line would therefore indicate non-volumetric depletion and possible aquifer influx. F , E_g and E_f can be calculated as function of G_p . The volume gas factor, as defined above, is dependent on the molar-condensate-gas ratio R_{MLG} , where $R_{MLG} = (1 - V)/V$, where V is tabulated in Table 3.8.

In the simulation examples above, gas and liquid condensate have been produced from a reservoir containing all together $8.763 \cdot 10^8 \text{ Sm}^3$ dry gas initial in place. Assuming a radial infinite aquifer as in the p/z - plot above, the impact of water influx during normal production is plotted in Figure 4.27, using the Havlena - Odeh interpretation method.

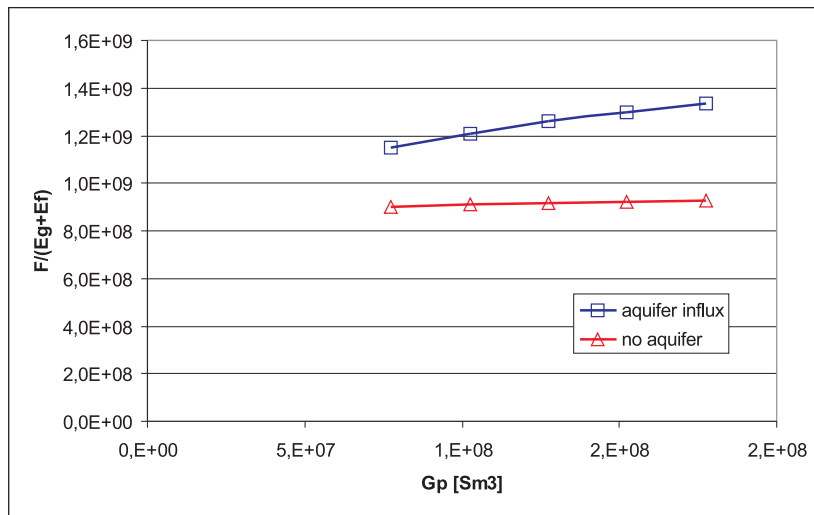


Figure 4.27: Aquifer influx using the Havlena - Odeh interpretation method.

In Figure 4.27, the aquifer influx case is compared with the no influx case. When there is no aquifer present, i.e. $W_e = 0$, Eq. 4.78 is a horizontal line intercepting the y-axis at G_i . From the figure above it is clear that this line intersects the y-axis at about $9 \cdot 10^8 \text{ Sm}^3$, in good agreement with what is mentioned above, referring to the GIIP. An extensive analysis of this data plotting technique as in Figure 4.27, is given by Pletcher [15].

In the case of aquifer influx, data is plotted as a seemingly straight line having a positive slope. The fact that the line is no longer horizontal shows that an aquifer is present. This information is of great significance in further analysis of the production data and prevents misinterpretation of the gas initial in place. A valuable estimation of the GIIP can be made, using Figure 4.27, by simply extrapolating the the straight line back to the point of zero gas production, i.e. $G_p = 0$, where the intercept with the y-axis gives the GIIP .

The advantage of the Havlena - Odeh interpretation method over the p/z- method is primarily the ability to verify the existence of aquifer influx. If the plotted line in Figure 4.27 has a slope relative the horizontal line, an aquifer is present. Secondly, a linear trend through the data points will intercept the y-axis at G_i , thus providing a

relatively correct estimate of the initial volume of gas in the reservoir.

4.7.3 The Direct Interpretation Method

In the direct interpretation method, aquifer water influx is calculated without any prior knowledge of the aquifer size or strength. The basic equation behind this model is obviously the general material balance equation, here represented by the linearized MBE, Eq. 4.78.

In the case of gas reservoirs, the expansion and compaction term E_f is normally much smaller than the gas expansion term E_g and can therefore be neglected. If additionally, the water production is set to zero, the linearized equation can be written

$$\frac{G_p B_g}{B_g - B_{gi}} = G_i + \frac{W_e}{B_g - B_{gi}}, \quad (4.79)$$

where the gas volume factors $B_g \geq B_{gi}$.

The cumulative water influx is calculated directly from the above equation,

$$W_e = G_p B_g - G_i (B_g - B_i), \quad (4.80)$$

where the water production $W_p = 0$. The gas production G_p is known, while the gas initial in place G_i is generally not known. If the size of the initial gas volume G_i is estimated too high, then the water influx is too low and vice versa.

The aquifer water influx W_e has previously been introduced as a function of a dimensionless function W_{eD} in Eq. 4.56. Substituting this equation in Eq. 4.80, the aquifer constant U can be expressed

$$U = \frac{W_e}{\Delta p W_{eD}(t_D)} = \frac{G_p B_g - G_i (B_g - B_i)}{\Delta p W_{eD}(t_D)}. \quad (4.81)$$

The aquifer constant U is uniquely defined by the size and form of the aquifer, where the constant is defined as $U_{r=\infty} = 2\pi\phi h c r_b^2$ for an infinite radial aquifer and $U_{L=\infty} = \phi h c \omega^2$ for an infinite linear aquifer. The aquifer constant has the dimension volume over pressure [m^3/bar], and is thus time independent. If the aquifer constant in Eq. 4.81 is plotted as function of time it would define a horizontal line.

In the direct interpretation method, Eq. 4.81 is redefined and an aquifer influx index C is defined, where the dimensionless function W_{eD} is substituted by the time difference Δt

$$C = \frac{W_e}{\Delta p \Delta t} = \frac{G_p B_g - G_i (B_g - B_i)}{\Delta p \Delta t}. \quad (4.82)$$

The aquifer influx index C has the dimensions volume over pressure and time [$m^3/\text{bar}/\text{days}$] and is thought to have the same characteristics as the aquifer constant U . If the water influx W_e is correctly estimated the aquifer influx index will plot as a horizontal line. If the gas initially in place is overestimated, C will become negative. If on the other hand, G_i is underestimated the aquifer influx index will be positive and not necessarily horizontal.

The basic idea behind the direct interpretation method is that there is only one particular G_i that consistently yields the same aquifer influx index C , which is a unique

property of a given reservoir - aquifer system. If the estimated G_i is too low or too high, then C becomes a non consistent function of time that deviate from a horizontal strait line.

The direct interpretation method can be evaluated through the following steps:

1. Estimate the gas initial in place G_i .
2. Calculate the water influx W_e by Eq. 4.80 for all time steps n ; $\Delta t = t_n - t_i$, where t_n and t_i is the actual and initial time, respectively. (Normally would $t_i = 0$.)
3. Calculate the aquifer influx index C using Eq. 4.82, where $\Delta p = p_i - p_n$. The pressures p_n should be a consistent choice of reservoir pressures, e.g. the average reservoir pressure $\bar{p}_n = p_n$.
4. Plot the value of C as function time t_n .
5. Reconsider the initial gas in place until $C(t)$ does plot as a strait horizontal line.

In order to illustrate the process presented above, typical production data such as gas produced G_p and pressure drop $\Delta p = p_i - p_n$ have to be recorded as function of time.

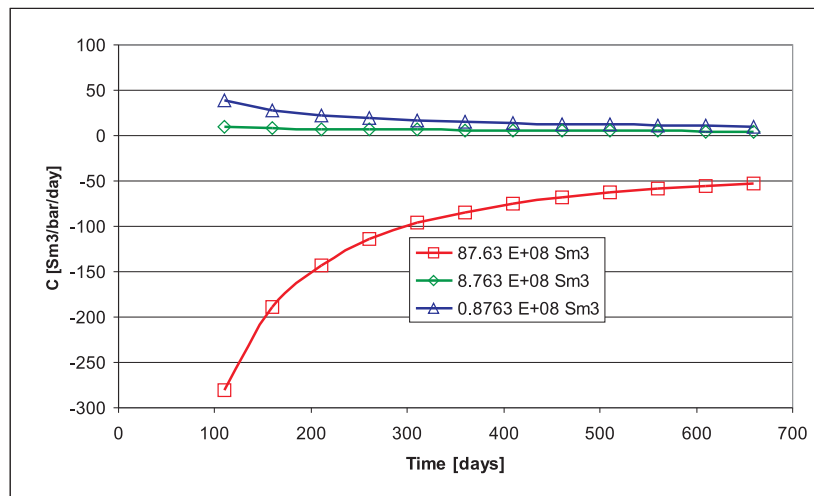


Figure 4.28: Aquifer influx index as function of time.

Figure 4.28 presents the aquifer influx index C as function of time, for three choices of initial gas in place, namely; $87.63 \cdot 10^8 \text{ Sm}^3$, $8.763 \cdot 10^8$ and $0.8763 \cdot 10^8 \text{ Sm}^3$. Figure 4.28 clearly demonstrates that the high volume alternative ($87.63 \cdot 10^8 \text{ Sm}^3$) is obviously not correct. The challenge in deciding between the two low alternatives is primarily related to deciding which line is more horizontal. The data plotted in Figure 4.28 is the same data as used in Figures 4.27 and 4.26, where the initial gas in place is $8.763 \cdot 10^8 \text{ Sm}^3$. An extended application of the Direct Method has been proposed by Bhuiyan et al. [2], where the "subjectivity" in the analyzes has been replaced by a optimization process finding the "best fit" horizontal line.

Example: Justification of the aquifer influx index C

The aquifer water influx is defined as the cumulative flow of water into the reservoir volume as shown in Eq. 4.54.

$$W_e = \int_0^{\Delta t} q_w dt,$$

For a cylindrical reservoir with a finite radial aquifer, with outer radial dimensions r_e and r_a , respectively, the steady state water flow from the aquifer in to the reservoir is defined by integrating Darcy's law over the full radial thickness of the aquifer.

$$q_w = \frac{k_w}{\mu_w} \frac{2\pi h_w}{\ln(r_a/r_e)} \Delta p.$$

Substituting q_w into the cumulative flow equation and integrating from time zero to t , the water influx is written

$$W_e = \frac{k_w}{\mu_w} \frac{2\pi h_w}{\ln(r_a/r_e)} \Delta p \cdot \Delta t.$$

A constant C can be defined, that characterizes the aquifer such that,

$$C = \frac{W_e}{\Delta p \cdot \Delta t}.$$

As seen from the above considerations, there are reasons to believe that the ratio $W_e/(\Delta p \cdot \Delta t)$ should be reasonable constant as function of time, and as such that an aquifer influx index C will exist.

References

- [1] Tarek Ahmed. *Reservoir Engineering Handbook, second edition*. Gulf Professional Publishing, 2000. ISDN: 0 88415 770 9.
- [2] M.H. Bhuiyan, A. Chamorro, and R. Sachdeva. Determination of ohip and aquifer constant without prior knowledge of aquifer models. (SPE 77489). Prepared for presentation at the SPE Annual Technical Conference and Exhibition held in San Antonio, Texax, 29 September - 2 October 2002.
- [3] H.S. Carslaw and J.C. Jeager. *Conduction of Heat in Solids*. Clarendon Press, Oxford, 1985. ISBN: 0198533683.
- [4] K. Coats. A Mathematical Model for Water Movement about Bottom-Water-Drive Reservoirs. *SPE Journal*, Trans. AIME:pp. 44–52, March 1962.
- [5] L.P. Dake. *Fundamentals of Reservoir Engineering*. Developments in Petroleum Science, 8. Elsevier Scientific Publishing Company, 1978.
- [6] L.P. Dake. *The Practice of Reservoir Engineering*. Developments in Petroleum Science, 36. Elsevier, 1994.
- [7] M.J. Fetkovich. A Simplified Approach to Water Influx Calculations - Finite Aquifer Systems. *Journal of Petroleum Technology*, pages 814–828, July 1971.
- [8] A. Firoozabadi, G. Olsen, and T. van Golf-Racht. Residual Gas Saturation in Water-Drive Gas Reservoir. (SPE16355). Prepared for presentation at the SPE California Regional Meeting held in Ventura, California, April 8-10, 1987.
- [9] Jacques Hagoort. *Fundamentals of gas reservoir engineering*, volume 23 of *Developments in Petroleum Science*. Elsevier, 1988.
- [10] D. Havelna and A.S. Odeh. The Material Balance as an Equation of a Strait Line. *Journal of Petroleum Technology*, Part 1:896–900, August 1963.
- [11] D. Havelna and A.S. Odeh. The Material Balance as an Equation of a Strait Line - Part 2, Field Cases. *Journal of Petroleum Technology*, Part 2:815–822, July 1964.
- [12] F.S. Hsieh, P.S. Kandel, and Vega C. Material-Balance Method for Production Rejuvenation With Horizontal Wells. (SPE/Petroleum Society of CIM 65484). Presented at the 2000 SPE/Petroleum Society of CIM International Conference on Horizontal Well Technology held i Calgary, Alberta, Canada, 6-8, November 2000.
- [13] F.S. Hsieh, C. Vega, and Vega L. Material Balance as a Horizontal Line for Gas-Condensate Reservoirs. (SPE 75516). Prepared for presentation at the SPE Gas Technology Symposium held in Calgary, Alberta, Canada, 30 April - 2 May 2002.
- [14] M.J. Fetkovich J.R. Burns and V.C. Meitzen. The Effect of Water Influx on p/z-Cumulative Gas Production Curves. *Journal of Petroleum Technology*, pages 287–291, March 1965.

-
- [15] J.L. Pletcher. Improvements to Reservoir Material-Balance Methods. *SPEREE*, (SPE 75354), February 2002.
- [16] A.F. van Everdingen and W. Hurst. The Application of the Laplace Transformation to Flow Problems in Reservoirs. *Petroleum Transactions, AIME*, 186(305-324), December 1949.
- [17] B. Wang and T.S. Teasdale. GASWAT-PC: A Microcomputer Program for Gas Material Balance With Water Influx. (SPE 16484), June,23-26 1987. Presented at the Petroleum Industry Applications of Microcomputers Conference, Montgomery, Texas.

Chapter 5

Reservoir Gas Flow

Production of gas from underground rock formations is directly related to the flow of gas in reservoirs towards strategically located wells. The flow of gas in porous media is therefore an essential element in depletion processes in gas reservoirs. In its own right, gas flow behavior in reservoirs is a huge area of great interest in reservoir engineering. Reservoir flow behavior are in most cases quite complex to model and therefore subjected to studies involving the latest and most advanced computers.

In this presentation, however, we will restrict ourselves to gas flow behavior in cylindrical, homogeneous and isotropic reservoirs of finite dimension. Under such restrictions, single gas flow is considered isothermal in the bulk part of the reservoir, while the near well region is treated separately. The practical interests in single or multi phase gas flow in this chapter, are primarily related to the determination of well inflow characteristics and well-bore pressures, and in particular the *bottom-hole* pressure.

In the case of constant terminal gas flow rate, the mean pressure in the reservoir will decrease in accordance to the cumulative volume of gas produced. This process is modeled through the use of material balance calculations, as described in the previous chapter. The process of radial gas flow and its representation as in this text, is therefore somewhat more complicated and complex, compared to the material balance calculations. The reason for this is primarily that gas is compressible and secondly that radial gas flow in the reservoir passes through different phases, i.e. the general pressure solution consists of different equations acting in different periods of time. Another complicating factor is the condensation of gas in the near well area and the formation of liquid oil as a separate phase, which again involves multi phase flow in the near well-bore volume.

In general reservoir flow, the pressure dependence of gas compressibility and viscosity leads to non-linear flow equations, and consequently flow equations where no analytical solutions can be found. This problem is, however, elegantly handled by using Kichhoff's transformation, which linearize the flow equation to the same form, known to us as the non-compressible liquid flow equation. Instead of handling pressure as the primary parameter, a *pseudo pressure function*; m is introduced. The method adopted in this text involves a four step process which results in a set of overlapping flow equations. A more general and consistent solution technique is available, but involves quite complicated and advanced mathematical formulation and is therefore not included in

this text.

The alternative method for solving the reservoir gas flow problem, and the one we will follow, is presented as follows:

In a cylindrical reservoir with the well in the center, the well production is initially characterized as if the reservoir was of infinite dimension, i.e. the pressure information wave or pressure information front has not yet reached far enough out into the reservoir to explore its limits. This period, in the life time of the reservoir, is known as the *infinite acting period*.

After a short transition period, a *semi steady-state period* starts. In this period, we assume the pressure profile in the reservoir to remain radially constant while the pressure value at each radial position in the reservoir is steadily decreasing proportionally to the decline in the mean reservoir pressure.

The pressure solutions in the two periods are separate equations describing an overlapping general pressure solution in the reservoir.

There are five steps involved in the development of the bottom-hole pressure and these are organized as separate sections:

Steady-state Darcy flow solution is the derivation of the radial rate - pressure solution. This part includes the introduction of the mean pseudo pressure; \bar{m} and the bottom-hole pressure p_{bh} .

Semi steady-state radial flow describes a closed reservoir where the average pressure decline is assumed to be uniformly distributed while the radial pressure profile is constant in form but otherwise declining with decreasing pressure.

In this section the well-bore skin S is introduced. Inertial forces like turbulence are also included in the derivation. The effect of inertial forces are introduced in the pressure equation as a non-Darcy skin S_{nD} .

General non-steady-state flow solution describes the infinite acting period, where the rate-pressure solution is derived by using *the line-source solution* technique. The radial flow at constant terminal rate is the derivation of a general pressure solution.

Late transition period is a sum-up and final presentation of the general solutions on a form adapted for further simulation.

Radial flow equations is a sum up of the flow solutions and a presentation of the flow equations as they are used in the flow simulations.

In the last sections in this chapter, gas condensation in the near well volume is studied. The formation of liquid condensate around the well-bore, often called "condensate banking" or "condensate drop-out" is of great interest in gas reservoir engineering.

The two phase gas flow equations are introduced, as well as other parameters involved in the calculation process.

Modeling of production gas oil ratio is one of the key element in the calculation of liquid drop out and well-bore pressure development.

Simulation of two phase flow sums up and depicts the effect of flow behavior due to condensate drop-out in the reservoir.

When the bottom-hole pressure is reduced, such that the dew point pressure is reached in the reservoir (first in the vicinity of the well-bore), liquid condensate (oil) drops out of the gas. The liquids will partly occupy the porous volume in the vicinity of the well, and thereby impair gas flow. Later, when the pressure has further decreased, some of this oil may become mobile and start to flow towards the well-bore, in which case we get two-phase flow in the reservoir. Well deliverability is further impaired. Maintaining a constant surface production rate, there will be an increased pressure drop in the well-bore, due to two phase flow in the parts of the reservoir nearest to the well-bore. The properties of the fluids and their interaction with the porous media are complex phenomena that pose problems at various levels of complication. A simple model is therefore introduced, which allow us to assess the problem of liquid drop out in a descriptive and hopefully enlightening manner.

5.1 Single-Phase Gas Flow

Let us first consider the simple case of steady-state flow in the absence of inertial effects. Under these conditions the flow of gas is governed by Darcy's Law and the law of Mass Conservation associated to steady-state flow. (A more comprehensive overview of the field of reservoir flow modeling is given by Heimsund [12])

The Darcy Law without gravitational effects is written on general and on linear form (flow along the x-axis)

$$\vec{u} = -\frac{k}{\mu}\nabla p \Rightarrow u_x = -\frac{k_x}{\mu}\frac{\partial p}{\partial x}, \quad (5.1)$$

where u is the volumetric flow velocity ($u = q/A$, where q and A are the flow rate and flow cross section area, respectively), μ is the gas viscosity, k is the permeability and p is the pressure.

The mass conservation law on general and on linear form are given

$$\nabla \cdot (\rho\vec{u}) = 0 \Rightarrow \frac{\partial}{\partial x}(\rho u_x) = 0, \quad (5.2)$$

where ρ is the gas density.

The steady-state gas flow equation on general form, without inertial forces is a combination of Eqs. 5.1 and 5.2

$$\nabla \cdot \left(\frac{\rho}{\mu} \nabla p \right) = 0, \quad (5.3)$$

where both the density and the viscosity are pressure dependent, i.e. $\rho = \rho(p)$ and $\mu = \mu(p)$, while permeability is considered to be constant.

Equation Eq. 5.3 is a non-linear differential equation of which there is no direct general and analytical solution.

5.1.1 Steady-State Darcy Flow

Equation Eq. 5.3 can however, be linearized using *Kirchhoff's transformation*. This transformation converts the pressure into a *pseudo-pressure* function $m(p)$, that eliminates the non-linearity in the steady-state equation. Kirchhoff's transformation [11] is defined as

$$m(p) = \frac{1}{(\rho/\mu)_r} \int_{p_r}^p \frac{\rho}{\mu} dp, \quad (5.4)$$

where p_r is an arbitrary reference pressure and $(\rho/\mu)_r$ is a constant defined by the density-viscosity ratio at pressure p_r .

Eq. 5.4 defines a one-to-one relationship between the pseudo-pressure m and the pressure p . Differentiating Eq. 5.4, it follows that

$$\nabla m = \frac{dm}{dp} \nabla p = \frac{\rho/\mu}{(\rho/\mu)_r} \nabla p. \quad (5.5)$$

Substitution of Eq. 5.5 into Eq. 5.3, yields the linear equation

$$\nabla \cdot \nabla m = 0. \quad (5.6)$$

Eq. 5.6 is the well known Laplace equation, which describes incompressible steady-state flow of liquids in porous media. A great number of analytical solutions exist for the liquid equation and consequently also for the gas equation when Kirchhoff's transformation is applied.

The procedure to solve the steady-state gas flow problem is thus, first to formulate and solve the problem in terms of pseudo-pressure and then to convert the results back to real pressures, using Kirchhoff's transformation.

Example: Pseudo-Pressure for Ideal Gases

The Ideal Gas Law at isothermal conditions is written

$$pV = nRT = (pV)_r,$$

where $(pV)_r$ is constant at a reference pressure p_r . The density is defined

$$\rho = \frac{m_g}{nRT} p,$$

where m_g is the mass of the gas.

The pseudo-pressure can then be calculated as follows

$$\begin{aligned} m(p) &= \frac{1}{(\rho/\mu)_r} \int_{p_r}^p \frac{\rho}{\mu} dp \\ &= \frac{nRT}{m_g} \left(\frac{\mu}{p} \right)_r \int_{p_r}^p \frac{m_g}{nRT} \frac{p}{\mu} dp. \end{aligned}$$

If the viscosity is considered to be a slow varying function or constant in the pressure range in question, i.e. $\mu \sim \text{constant}$, then the pseudo-pressure is given

$$m(p) = \frac{1}{p_r} \int_{p_r}^p p dp = \frac{1}{2} \left(\frac{p^2}{p_r} - p_r \right). \quad (5.7)$$

The pseudo-pressure function for ideal gas is thus, monotonously increasing as p^2 , starting at zero for a pressure equal to the reference pressure.

It is often more convenient to formulate the Kirchhoff's transformation in terms of the gas formation-volume factor B_g instead of density ρ . This can be done using the following relation between density and formation-volume factor

$$B_g = \frac{\rho_{sc}}{M_G} \frac{M}{\rho} (1 + R_{MLG}), \quad (5.8)$$

where ρ_{sc} is the gas density at standard conditions, M and M_G are the average molecular mass of the gas in the reservoir and at the surface, respectively. R_{MLG} is the molar condensate-gas ratio.

Eq. 5.8 is derived from Eq. 3.113 by using the substitution

$$\frac{M}{\rho} = Z \frac{RT}{p}$$

where the equation above is a combination of the Real Gas Law and the definition of number of moles $n = m_g/M$, where m_g is mass of gas.

Restricting ourselves to dry - and wet gas reservoirs where $R_{MLG} = R_{MLGi}$, we obtain for Kirchhoff's transformation

$$m(p) = (\mu B_g)_r \int_{p_r}^p \frac{1}{\mu B_g} dp, \quad (5.9)$$

where the differential of the pseudo-pressure is written

$$\nabla m = \frac{(\mu B_g)_r}{\mu B_g} \nabla p. \quad (5.10)$$

A necessary condition for derivation of Eq. 5.9, is the assumption that $M_G = M(1 + R_{MLG})$ in Eq. 5.8.

Example: Pseudo-Pressure Versus Pressure

The pseudo-pressure, defined by Eq. 5.9, can be calculated when we know the viscosity μ and the gas volume factor B_g as function of pressure p , as presented in Table 5.1. The pseudo-pressure $m^*(p)$ in the table below is the ideal gas pseudo-pressure derived in Eq. 5.7.

The integral in Eq. 5.9 is approximated by

Table 5.1: Gas properties as function of pressure for Sleipner Vest gas and for an ideal gas.

| p [bar] | μ [mPas] | B_g [Rm^3/Sm^3] | $m(p)$ [bar] | $m^*(p)$ [bar] |
|-----------|--------------|-----------------------|--------------|----------------|
| 20 | 1.20E-02 | 6.88E-02 | 24.58 | 0.00 |
| 50 | 1.34E-02 | 2.67E-02 | 114.08 | 52.50 |
| 100 | 1.59E-02 | 1.29E-02 | 431.59 | 240.00 |
| 150 | 1.86E-02 | 8.44E-03 | 896.00 | 552.50 |
| 200 | 2.19E-02 | 6.37E-03 | 1453.54 | 990.00 |
| 250 | 2.55E-02 | 5.25E-03 | 2054.56 | 1550.00 |
| 300 | 2.93E-02 | 4.58E-03 | 2665.74 | 2240.00 |
| 350 | 3.31E-02 | 4.14E-03 | 3269.78 | 3052.50 |
| 400 | 3.67E-02 | 3.83E-03 | 3859.58 | 3990.00 |
| 430 | 3.88E-02 | 3.68E-03 | 4205.73 | 4400.00 |

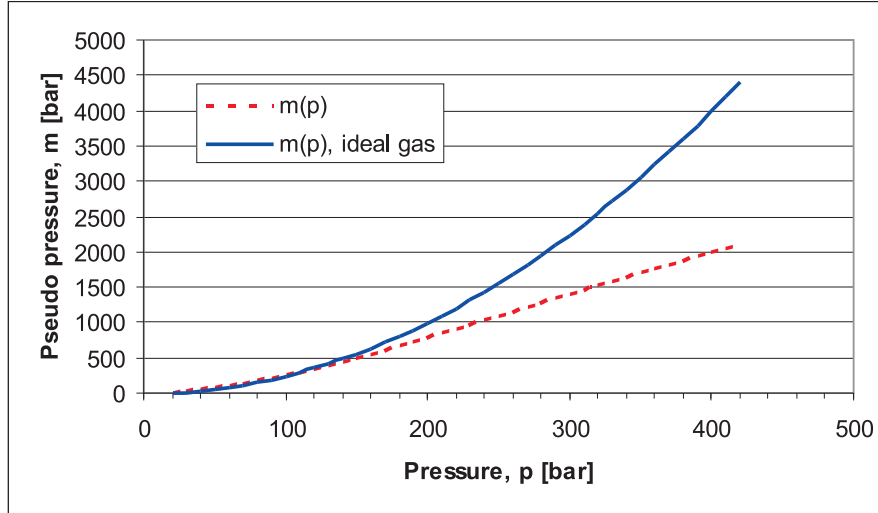


Figure 5.1: Pseudo-pressure as function of pressure.

$$m(p) \simeq (\mu B_g)_r \sum_{i=1}^{N-1} \frac{\Delta p_i}{\overline{\mu B}_i},$$

where $\overline{\mu B}_i$ is the harmonic mean at the pressures $i, i + 1$

$$\overline{\mu B}_i = \frac{2}{\frac{1}{(\mu B)_{i+1}} + \frac{1}{(\mu B)_i}},$$

giving the approximate pseudo-pressure

$$m(p) \simeq (\mu B_g)_r \sum_{i=1}^{N-1} \frac{(\mu B)_{i+1} + (\mu B)_i}{(\mu B)_i (\mu B)_{i+1}} \frac{(p_{i+1} - p_i)}{2}.$$

For data in the table above, the pseudo-pressure for real and ideal gases are presented in Figure 5.1.

The reference pressure p_r is normally defined as a minimum pressure and in the example above this is 20 bar.

Kirchhoff's transformation and the concept of pseudo pressure, Eqs 5.9 and 5.10 are equally well adapted for solving core flow problems, as for pressure draw-down calculations.

Due to varying gas compressibility, the gas flow through a core sample is not constant and thus Darcy's Law can not be applied directly, in solving the pressure - flow behavior.

The flow rate at standard conditions is written

$$q_{sc} = \frac{q}{B_g} = \frac{1}{B_g} A \frac{k}{\mu} \frac{dp}{dx} = kA \frac{1}{\mu B_g} \frac{dp}{dx}, \quad (5.11)$$

where the gas flow rate q , has been substituted by using the Darcy's Law. A is the flow cross-section and k and μ are the permeability and viscosity, respectively. dp/dx is the pressure gradient in the x-direction.

Applying Eq. 5.10 for the linear displacement dx , in Eq. 5.11, we get

$$q_{sc} = kA \frac{1}{(\mu B_g)_r} \frac{dm}{dx}, \quad (5.12)$$

Eq. 5.12 demonstrates the functionality of Kirchhoff's transformation. When the pseudo-pressure function $m(p)$ is defined as shown in Figure 5.1, we may thus calculate the pressure - rate relation directly by applying Eq. 5.12.

Example: Linear Gas Flow in a Core Sample

A regular cylindrical core sample has a diameter of 5 cm and a length of 10 cm. The permeability is estimated to 100 mD and the inlet pressure (p_1) and outlet pressures (p_2) are 50 and 10 bars, respectively.

The flow rate at standard conditions given by Eq. 5.12, can be approximated by the equation

$$q_{sc} = kA \frac{1}{(\mu B_g)_r} \frac{\Delta m}{L}, \quad (5.13)$$

where $L = 10$ cm is the length of the core sample.

We may now find $m(p = 10)$ and $m(p = 50)$ by using Figure 5.1, or alternatively we may assume the gas to be near ideal and use Eq. 5.7 instead. Combining Eqs. 5.7 and 5.13, we get

$$q_{sc} = \frac{kA}{(\mu B_g)_r L} \frac{1}{2} \left(\frac{p_2^2}{p_r} - \frac{p_1^2}{p_r} \right), \quad (5.14)$$

where $(\mu B_g)_r$ is evaluated at the reference pressure p_r .

Choosing the reference pressure equal to 20 bar, we find the following parameters from Table 5.1; $\mu = 1.2 \cdot 10^{-2} \text{ mPa} \cdot \text{s}$ and $B_g = 6.88 \cdot 10^{-2} \text{ Rm}^3/\text{Sm}^3$. Substituting in Eq. 5.14 and using SI-units we get

$$q_{sc} = \frac{(100 \cdot 0.987 \cdot 10^{-3} \cdot 10^{-12})\pi(0.05/2)^2 1}{(1.2 \cdot 10^{-2} \cdot 10^{-3})(6.88 \cdot 10^{-2})0.1} \frac{1}{2} \left(\frac{50^2}{20} - \frac{10^2}{20} \right) 10^5 = 0.01408$$

The core flow rate is therefore $q_{sc} = 1.41 \cdot 10^{-2} \text{ Sm}^3/\text{s}$.

5.1.2 Steady-State Radial Flow

We now return to the somewhat idealized problem of steady-state flow of gas towards a well in the centre of a cylindrical reservoir of uniform thickness, as depicted in Figure 5.2

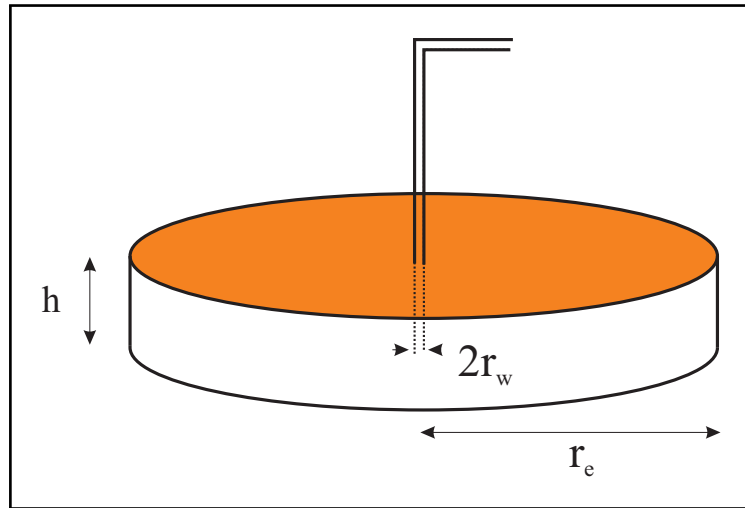


Figure 5.2: Cylindrical reservoir of constant thickness.

Darcy's Law and conservation of mass Eq. 5.2, give the general non-linear flow equation,

$$\nabla \cdot \left(\frac{\rho}{\mu} \nabla p \right) = 0, \quad (5.15)$$

where this flow equation is linearized using the Kichhoff's transformation and pseudo pressure m ,

$$m = \frac{1}{(\rho/\mu)_r} \int_{p_r}^p \frac{\rho}{\mu} dp, \quad (5.16)$$

where p_r is a reference pressure. Normally the reference pressure is chosen less than the lowest pressure reached in the reservoir.

Using Kirchhoff's transformation we get the following linear equation (Laplace's equation),

$$\nabla \cdot \nabla m = 0. \quad (5.17)$$

Laplace's equation for cylindrical symmetry is written

$$\frac{1}{r} \frac{\partial}{\partial r} \left(r \frac{\partial m}{\partial r} \right) = 0, \quad (5.18)$$

where the general solution in is known and given as,

$$m = a \ln(r) + b. \quad (5.19)$$

a and b are integration constants that follow from the boundary conditions.

Using the following boundary conditions, where we assume a well defined pressure in the well and at the outer boundary, we get

$$\begin{aligned} m(r_w) = m_w \\ m(r_e) = m_e \end{aligned} \Rightarrow a = \frac{m_e - m_w}{\ln(r_e/r_w)}. \quad (5.20)$$

From Eq. 5.19 we have

$$\frac{dm}{dr} = \frac{a}{r} = \frac{1}{r} \frac{m_e - m_w}{\ln(r_e/r_w)}. \quad (5.21)$$

Using Darcy's law for radial flow, we may write the steady-state flow rate at standard conditions (as written in Eq. 5.11 for the linear case)

$$q_{sc} = \frac{q}{B} = \frac{2\pi r h k}{\mu B} \frac{dp}{dr}, \quad (5.22)$$

where we have dropped the subscript g for the gas volume factor and where $A = 2\pi r h$.

In Eq. 5.22, we have used the fact that Darcy's Law in cylindrical coordinates are $q = A(k/\mu)(dp/dr)$. Eq. 5.22 is then further expanded using Kirchhoff's transformation $dp/dr = (\mu B)/(\mu B)_r (dm/dr)$ and we get

$$q_{sc} = \frac{2\pi h k}{(\mu B)_r} \frac{m_e - m_w}{\ln(r_e/r_w)} \quad (5.23)$$

The steady-state solution of Eq. 5.18 is thus written,

$$m_e - m_w = \frac{q_{sc}(\mu B)_r}{2\pi h k} \ln(r_e/r_w), \quad (5.24)$$

where $m_e - m_w$ is the pseudo-pressure drop in the reservoir due to production at constant surface rate q_{sc} .

In material balance calculations we have defined the reservoir pressure equal to the average reservoir pressure. In applying Eq. 5.24, it is therefore often more convenient to deal with the average reservoir pseudo-pressure \bar{m} than the outer boundary pressure m_e .

Average reservoir pseudo-pressure

The average pseudo-pressure is defined

$$\bar{m} = \frac{1}{V} \int_V m dV, \quad (5.25)$$

where $V = \pi\phi(r_e^2 - r_w^2)h$ is the pore volume of the reservoir, when the volume of the well is subtracted.

Using the general formula for a cylindrical volume and substituting Eq. 5.19 in Eq. 5.25, we get

$$\begin{aligned} \bar{m} &= \frac{2}{r_e^2 - r_w^2} \int_{r_w}^{r_e} (a \ln r + b) r dr, \\ &= \frac{2}{r_e^2 - r_w^2} \left[\frac{r_e^2}{2} (m_e - m_w) + \left(\frac{r_e^2}{2} - \frac{r_w^2}{2} \right) \left(m_w - \frac{a}{2} \right) \right]. \end{aligned} \quad (5.26)$$

When $r_e \gg r_w$, as often is the case, the average pseudo-pressure is

$$\begin{aligned} \bar{m} &\simeq (m_e - m_w) + (m_w - a/2), \\ &= a \left(\ln \frac{r_e}{r_w} - \frac{1}{2} \right) + m_w, \end{aligned} \quad (5.27)$$

In comparing Eq. 5.20 with the above equation, we see that when the average pseudo-pressure \bar{m} is substituted in the nominator in Eq. 5.20, the denominator is subtracted by $1/2$, and the constant a is written

$$a = \frac{\bar{m} - m_w}{\ln(r_e/r_w) - 1/2}, \quad (5.28)$$

From Eq. 5.23, we get the steady-state flow rate at standard conditions as,

$$q_{sc} = \frac{2\pi hk}{(\mu B)_r} \frac{\bar{m} - m_w}{\ln(r_e/r_w) - 1/2}. \quad (5.29)$$

Alternatively the average pseudo-pressure is given by

$$\bar{m} - m_w = \frac{q_{sc}(\mu B)_r}{2\pi hk} \left(\ln \frac{r_e}{r_w} - \frac{1}{2} \right). \quad (5.30)$$

5.2 Semi Steady-State Radial Flow

As stated in the introduction: - after a rather short period with production from an "infinite acting" reservoir, well production enters the *semi steady-state* period. In this period, well production is generally influenced by reservoir boundaries such as lateral extension, the presence of neighboring wells, faults or sands thinning out.

In this period, the mean pressure will decrease due to underground withdrawal of gas from a finite reservoir gas volume. The steady-state pressure profile is considered to

remain constant throughout this period, although the pressure at any location (radius position) in the reservoir is decreasing according to the declining average pressure.

At various advancing times, the pressure distribution in the reservoir could be represented by different pressure profiles, as depicted in Figure 5.3. The *draw-down* pressure profiles (at constant well production) are all assumed to have the same radial form. That is, - the rate of pressure change is constant at any point (radial positions) in the reservoir. If we convert to pseudo-pressure, we may translate this behavior into a mathematical form, by saying $\partial m(r)/\partial t = \text{constant}$. This is clearly seen in Figure 5.3, as the "copying" effect, where all pressure profiles are identical, only slightly displaced downwards along the pressure axis.

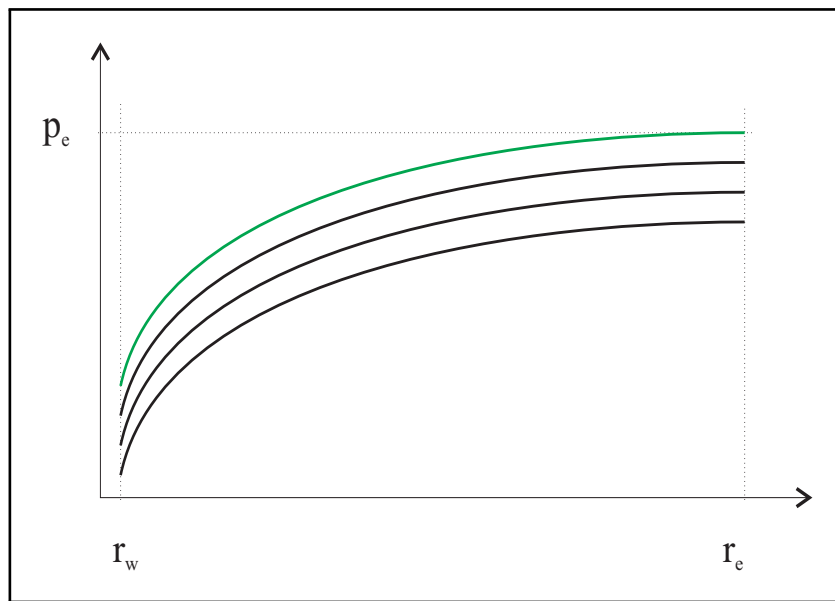


Figure 5.3: Semi steady-state pressure profiles.

As a result of a constant pressure profile, the diffusivity equation (see next section for a general treatment, i.e. the non-steady state) is time independent and equal to a constant (K_1), i.e.

$$\frac{1}{r} \frac{\partial}{\partial r} \left(r \frac{\partial m}{\partial r} \right) = K_1, \quad (5.31)$$

where the equation above is identical to Laplace's equation in Eq. 5.18, except for the constant K_1 .

Integration of Eq. 5.31 gives,

$$r \frac{\partial m}{\partial r} = \frac{1}{2} K_1 r^2 + K_2, \quad (5.32)$$

where K_2 is also a constant.

The boundary conditions in the semi steady-state period are given by the gas rate $q_{sc}(\mu B)_r$ in the well and the constant pressure profile at the outer limit of the reservoir.

Boundary condition in the well:

$$\left(r \frac{\partial m}{\partial r} \right)_{r=r_w} = \frac{q_{sc}(\mu B)_r}{2\pi h k}, \quad (5.33)$$

where the above equation states that the well rate is constant and independent of radial dimension.

Boundary condition at outer limit:

$$\left(r \frac{\partial m}{\partial r} \right)_{r=r_e} = 0, \quad (5.34)$$

where the pressure gradient is zero at the outer boundary.

Substitution of the boundary conditions, Eqs. 5.33 and 5.34 in Eq. 5.32, gives the two constants K_1 and K_2 . Further integration of Eq. 5.32 yields the pseudo pressure

$$m(r) = m(r_w) + \frac{q_{sc}(\mu B)_r}{2\pi h k} \left(\ln \frac{r}{r_w} - \frac{1}{2} \frac{r^2 - r_w^2}{r_e^2} \right). \quad (5.35)$$

The mean pseudo-pressure in the semi steady-state case is found, as previously done by applying the averaging as in Eq. 5.25. By integration and we find,

$$\bar{m} = m(r_w) + \frac{q_{sc}(\mu B)_r}{2\pi h k} \left(\ln \frac{r_e}{r_w} - \frac{3}{4} \right), \quad (5.36)$$

where the assumption $r_w/r_e \sim 0$ has been used.

Observe that the constant introduced by averaging of the semi steady-state equation, defined by Eq. 5.36 is $3/4$ and different from the constant of $1/2$ derived previously for the steady-state case.

5.2.1 Well skin factor

In order to prevent reservoir fluids from entering the well-bore while drilling, highly pressurized drilling fluids are used in stabilizing the drilling process. Particles suspended in these drilling fluids may normally penetrate the well-bore surface and partly plug the near-well region and thus reduce reservoir permeability in the vicinity of the well-bore. As a result of this process, a damaged zone near the well, a *skin zone*, is often created. The existence of such a skin zone will therefore lead to increased pressure drop compared to a non-damaged reservoir [16].

The effect of the mechanical well-bore skin, as depicted in Figure 5.4, is to reduce (when $S > 0$) the bottom-hole pressure, p_{bh} , relative to the ideal or non-skin pressure, $p(r_w)$.

In the case of negative skin (when $S < 0$), the well may have experienced a reduced pressure drop in the skin zone due to an increase in near-well permeability. Improved permeability could be caused by hydraulic fracturing or acidization of the near-well zone.

The fact that the near well volume is quite often impaired due to well operations or as part of the drilling process, will result in a skin zone with increased or reduced

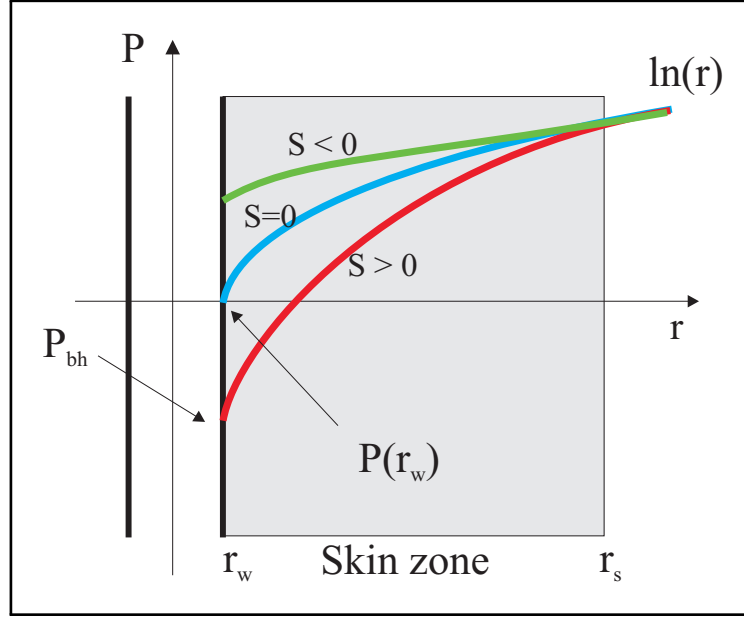


Figure 5.4: Well-bore skin pressure profiles.

permeability. This situation is formally handled by introducing a mechanical skin factor S which is generally defined as the skin resistance in the well-bore.

In terms of pseudo pressures, the well skin factor introduced by van Everdingen [20], is therefore a dimensionless number proportional to the difference between well-bore pressure and bottom-hole pressure: $m(r_w) - m_{bh}$.

$$m_w - m_{bh} = \frac{q_{sc}(\mu B)_r}{2\pi hk} S, \quad (5.37)$$

where $m_w = m(r_w)$ is the pseudo pressure in the case of no skin ($S = 0$), - considered to be an idealized pressure in the well as represented in Eq. 5.36. While on the other hand, the bottom-hole pseudo pressure, m_{bh} , is the actual well pressure including skin effects.

Introducing the well-bore pseudo pressure from Eq. 5.37 into equation Eq. 5.35, we get

$$\bar{m} = m_{bh} + \frac{q_{sc}(\mu B)_r}{2\pi hk} \left(\ln \frac{r_e}{r_w} - \frac{3}{4} + S \right). \quad (5.38)$$

or alternatively

$$q_{sc} = \frac{2\pi hk}{(\mu B)_r} \frac{\bar{m} - m_{bh}}{\ln(r_e/r_w) - 3/4 + S}, \quad (5.39)$$

Eqs. 5.38 and 5.39 are the semi steady-state pseudo-pressure equations defined for a cylindrical reservoir at constant thickness, when mechanical skin is included.

5.2.2 Non-Darcy Flow

Darcy's Law is valid for fluid flow in the reservoir at low to moderate flow rates, where the inertial effects can be considered negligible. Because of low viscosity and high mobility of gases, gas flow velocities can be quite high, in particular in the vicinity of the well, where the pressure gradient is highest, see Figure 5.5. Under these conditions, inertial forces can cause a departure from the linear trend between flow velocity and pressure drop, as described by Darcy's Law. This nonlinearity at high velocity gas flow is modeled by a Forchheimer-type equation [14],

$$-\nabla p = \frac{\mu}{k} \vec{u} + \underbrace{\beta \rho \vec{u} |\vec{u}|}_{\text{non linear term}}, \quad (5.40)$$

where β is the high velocity turbulent term, ρ is the gas density and k and μ are the permeability and viscosity, respectively. u is the gas flow velocity.

The non-linearity, as presented in the Forchheimer equation above, can be represented in the Darcy's law as we know it from before [11], where we write

$$\vec{u} = -\frac{k}{\mu} \delta \nabla p, \quad (5.41)$$

where the correction term for inertial forces (turbulence) is given by δ , defined by,

$$\delta = \frac{1}{1 + \beta \frac{\rho |\vec{u}| k}{\mu}}. \quad (5.42)$$

δ in Eq. 5.42 depends on the magnitude of the flow velocity. At low flow velocities, δ becomes unity and Forchheimer's Law becomes equal to Darcy's Law. For high velocities δ becomes less than 1, as depicted in Figure 5.5.

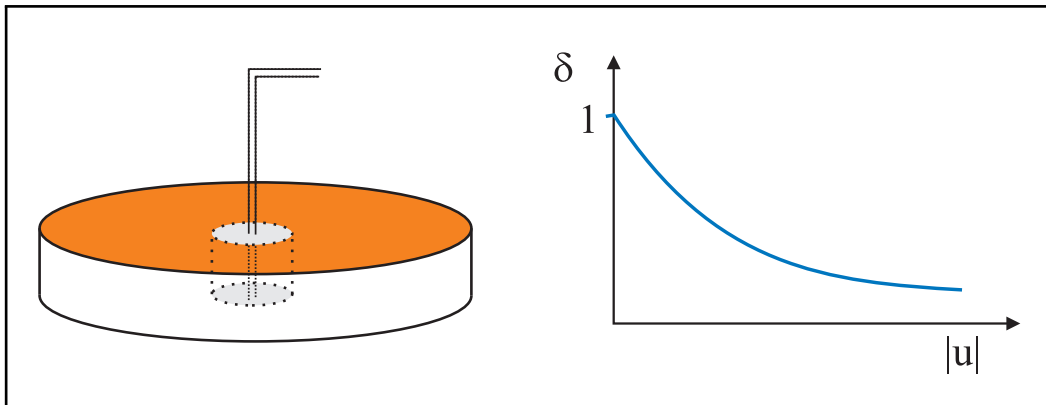


Figure 5.5: The Forchheimer's equation is applied in the vicinity of the well-bore and is valid for higher gas flow velocities.

Combining the Forchheimer equation Eq. 5.41 and the mass conservation Eq. 5.2, we get the equation

$$\nabla \cdot \left(\rho \frac{k}{\mu} \delta \nabla p \right) = 0. \quad (5.43)$$

Using Kirchhoff's transformation, Eq. 5.4, once more, we obtain a modified Laplace equation for non-linear and turbulent gas flow

$$\nabla \cdot (\delta \nabla m) = 0. \quad (5.44)$$

Since the non-Darcy correction factor depends on $|\vec{u}|$ and thus on an unknown pressure distribution, Eq. 5.44 is non-linear and can in general not be solved analytically.

5.2.3 Correction for Turbulent Radial Flow

Gas flow velocities increase drastically towards the wells. As a consequence, non-Darcy effect is primarily located in the vicinity of the well where gas flow patterns are radial. Fig. 5.6 shows the pore velocity field in the radius-pressure plane, for a cylindrical geometry [18]. In accordance with the figure, the lowest flow velocity $v_{g,pore} = 0.1$ m/day, is found at the reservoir outer boundary and at initial pressure. The highest pore velocity is approximately equal to 6500 m/day, and is observed in the close vicinity of the well at minimum bottom-hole pressure. As observed in the figure, the pore velocity is increasing as the gas moves close to the well-bore for all pressures, but the highest pore velocities are found at the lowest reservoir pressures. The pore velocity is thus increasing as pressure is decreasing.

Therefore a good approximation of the overall non-Darcy flow effect, as presented in Eq. 5.44, can be obtained by solving the special case of radial flow close to the well. Expressed in radial co-ordinates, using Kirchhoff's transformation and the Forchheimer equation, we get

$$\frac{dm}{dr} = \frac{(\mu B)_r}{\mu B} \frac{dp}{dr} = \frac{(\mu B)_r}{\mu B} \left(\frac{\mu}{k} u + \beta \rho u^2 \right) = (\mu B)_r \left(\frac{u}{kB} + \beta \frac{\rho u^2}{\mu B} \right), \quad (5.45)$$

where Eq. 5.40 has been used.

Under steady-state radial flow conditions the flow rate at standard conditions is constant and we write

$$q_{sc} = \frac{q}{B} = \frac{2\pi r h u}{B} \Rightarrow u = \frac{B}{2\pi r h} q_{sc}, \quad (5.46)$$

where u is the radial flow velocity in the reservoir close to the well at radial position r .

Combining Eqs. 5.45 and 5.46 we get

$$\frac{dm}{dr} = (\mu B)_r \left(\frac{q_{sc}}{2\pi r k h} + \beta \frac{\rho B}{\mu 4\pi^2 r^2 h^2} q_{sc}^2 \right). \quad (5.47)$$

Reorganizing Eq. 5.47 with the intention of integrating from the well and outwards in the reservoir, we write

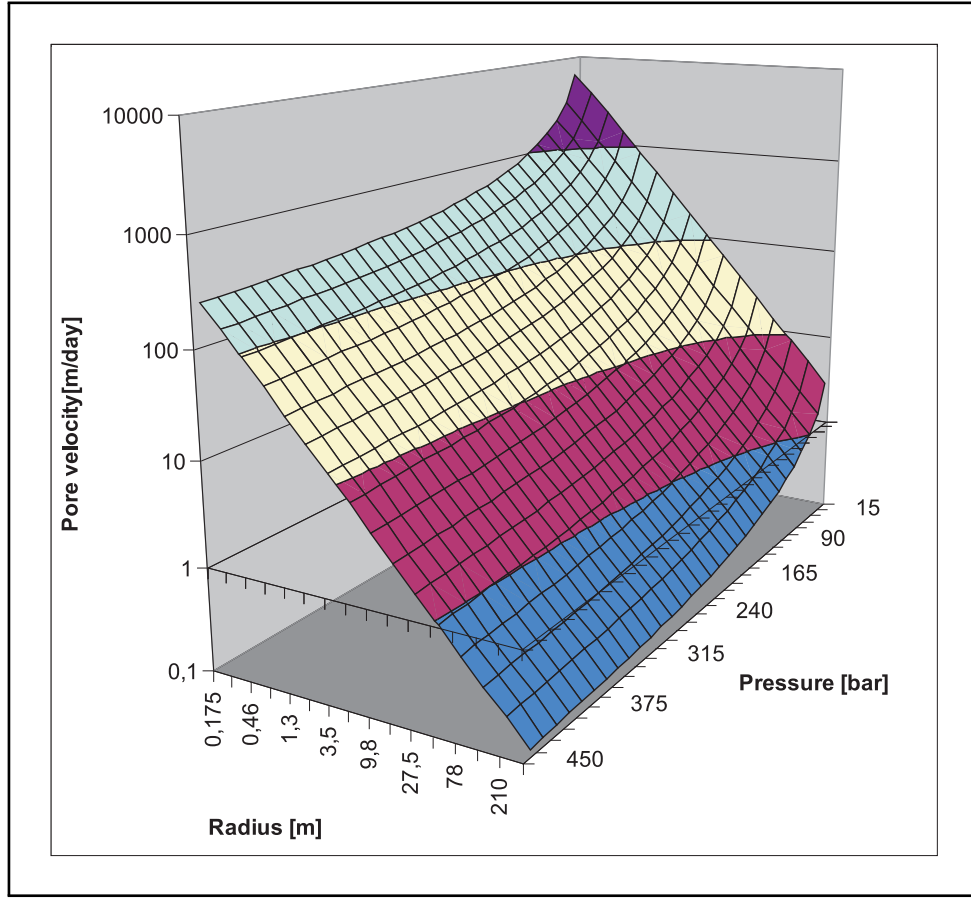


Figure 5.6: Gas flow pore velocity as function of reservoir radius and pressure.

$$\frac{dm}{dr} = (\mu B)_r \left(\underbrace{\frac{q_{sc}}{2\pi kh} \frac{1}{r}}_{\text{Darcy}} + \underbrace{\frac{\beta}{4\pi^2 h^2} \frac{\rho B}{\mu r^2} q_{sc}^2}_{\text{non-Darcy}} \right). \quad (5.48)$$

The ordinary Darcy term as we know it from before, represents the Darcy flow. The non-Darcy factor represents the effect of inertial forces. Integration of the Darcy term from the well to the outer boundary yields the pseudo-pressure drop as we know it from previous calculations, see Eq. 5.24. Integrating the non-Darcy term introduces an integral term and adding the two terms, we get

$$\Delta m = m_e - m_w = (\mu B)_r \left[\frac{q_{sc}}{2\pi kh} \ln \frac{r_e}{r_w} + \beta \left(\frac{q_{sc}}{2\pi h} \right)^2 \int_{r_w}^{r_e} \frac{\rho B}{\mu r^2} dr \right], \quad (5.49)$$

where $\rho B = \rho B(p(r))$ and $\mu = \mu(p(r))$ are both functions indirectly dependent of the integration parameter r . Here the pressure p , is increasing with radius distance from the well.

The integral in Eq. 5.49 is taken between the limits defined by the well radius r_w and the outer boundary radius r_e . The main contribution to this integral comes from the volume in immediate vicinity of the well-bore where the integrand ($1/r^2$) is large. For radial distances further away from the well-bore, the term above will become very small and consequently the contribution under the integrating equally small. We may therefore assume that all the contribution under the integration comes from the close vicinity of the well-bore. If we in addition assume the function $\rho B/\mu$ to be near constant in this range, we find

$$\Delta m = (\mu B)_r \left[\frac{q_{sc}}{2\pi kh} \ln \frac{r_e}{r_w} + \beta \left(\frac{q_{sc}}{2\pi h} \right)^2 \frac{\rho B}{\mu} \left(\frac{1}{r_w} - \frac{1}{r_e} \right) \right], \quad (5.50)$$

and when $r_w \ll r_e$ we may write

$$\Delta m = \frac{q_{sc}(\mu B)_r}{2\pi kh} \left[\ln \frac{r_e}{r_w} + q_{sc} \underbrace{\frac{\beta}{2\pi h} \frac{k\rho B}{\mu} \frac{1}{r_w}}_D \right], \quad (5.51)$$

where D is defined as the non-Darcy factor,

$$D = \beta \frac{1}{2\pi h} \frac{k\rho B}{\mu} \frac{1}{r_w}.$$

In analogy with the introduction of the average pressure and the case of well-bore skin, we can introduce a *non-Darcy skin factor* $S_{nD} = q_{sc}D$ and write the pseudo-pressure equation for non-Darcy flow on the form

$$m_e - m_w = \frac{q_{sc}(\mu B)_r}{2\pi hk} \left(\ln \frac{r_e}{r_w} + S_{nD} \right). \quad (5.52)$$

Eq. 5.52 is an implicit equation, where the inertial effects manifests it self as an additional flow resistance in close analogy to the well-bore skin as we know it from before.

The non-Darcy flow effect can therefore be added to the general steady-state flow equation, Eq. 5.38, simply by adding the non-Darcy skin factor. The general semi steady-state flow equation is therefore written

$$\bar{m} - m_{bh} = \frac{q_{sc}(\mu B)_r}{2\pi hk} \left(\ln \frac{r_e}{r_w} - \underbrace{\frac{3}{4}}_{\bar{p}} + \underbrace{S}_{\text{skin}} + \underbrace{S_{nD}}_{\text{non-Darcy}} \right), \quad (5.53)$$

where the $3/4$ -term is related to the average reservoir pressure, the S -term is the mechanical well-bore skin factor and the S_{nD} -term is a non-Darcy skin factor.

Example: Integration Parameters, $\rho B/\mu$

In deriving Eq. 5.50 we assumed that the contribution from the term $\rho B/\mu$ is small under integration from the well-bore to the outer boundary of the reservoir, i.e. that the change in $\rho B/\mu$ is small under integration.

All three parameters are pressure dependent, as shown in Table 5.2 and thus in-directly dependent on the radial distance from the well-bore. The $1/r^2$ term in Eq. 5.49 quenches the importance of the function $\rho B/\mu$, away from the well-bore and thus enhances the importance of this function close to the well.

From initial production to abandonment of the well, the absolute pressure will change in the vicinity of the well, from high to low. In order to verify the assumption made in Eq. 5.50, we need to check the pressure dependence of $\rho B/\mu$ in the whole pressure range.

Table 5.2: Parameters from Sleipner Vest gas.

| p [bar] | μ [mPas] | B_g [Rm^3/Sm^3] | ρ [g/cm^3] | $\rho B/\mu$ |
|-----------|--------------|-----------------------|---------------------|--------------|
| 40 | 0.0129 | 0.0337 | 0.0310 | 0.0808 |
| 60 | 0.0140 | 0.0221 | 0.0470 | 0.0743 |
| 100 | 0.0159 | 0.0129 | 0.0810 | 0.0655 |
| 140 | 0.0181 | 0.0090 | 0.1170 | 0.0586 |
| 200 | 0.0219 | 0.0064 | 0.1710 | 0.0498 |
| 260 | 0.0263 | 0.0051 | 0.2210 | 0.0428 |
| 300 | 0.0293 | 0.0046 | 0.2510 | 0.0392 |
| 350 | 0.0331 | 0.0041 | 0.2820 | 0.0353 |
| 430 | 0.0388 | 0.0037 | 0.3250 | 0.0308 |

Part of the data presented in Table 5.2, has previously been presented in Table 3.3 and Table 5.1.

Figure 5.7 shows the pressure dependence of the term $\rho B/\mu$ in Eq. 5.49. The change in absolute values as function of pressure is small and the overall change for the whole pressure range is not more than a factor of about two. The error introduced by assuming $\rho B/\mu$ being constant under integration of Eq. 5.49 is thus not negligible and should be corrected for. As part of the iteration procedure, the constant D in Eq. 5.52 should therefore be updated relative to varying pressure. The implementation of such corrections is easily done.

5.3 The General Non-Steady-State Flow Solution

We shall now address the more general case of non-steady-state, also known as transient flow. The general gas flow equation is derived using Darcy's law and the mass conservation law, as before, but in addition an accumulation term is included,

$$\underbrace{\frac{\partial}{\partial t}(\phi\rho)}_{\text{accumulation}} + \underbrace{\nabla \cdot (\rho\vec{u})}_{\text{flux}} = 0, \quad (5.54)$$

where ϕ is the average porosity, ρ is the gas density and \vec{u} is the gas flow velocity.

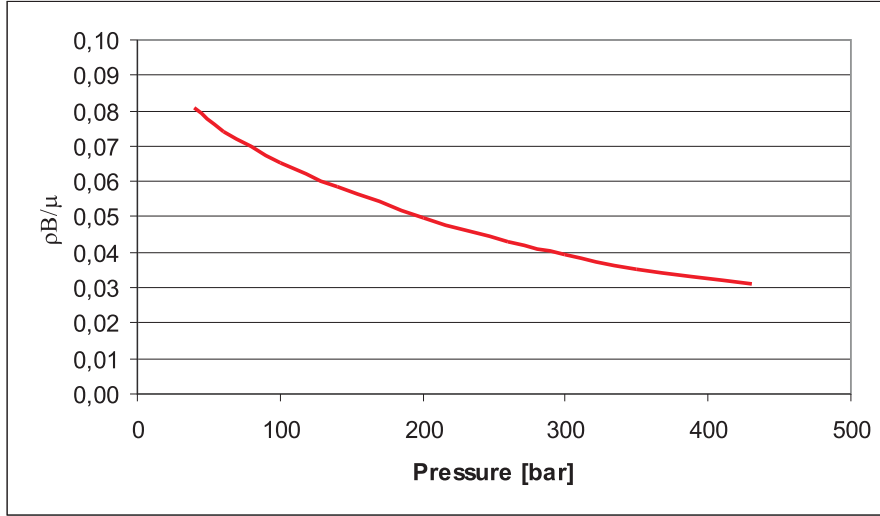


Figure 5.7: The term $\rho B/\mu$ as function of pressure.

Assuming constant porosity and using an alternative definition of gas compressibility Eq. 3.97, namely $c = (1/\rho)(\partial\rho/\partial p)$, we may write the accumulation term as follows

$$\frac{\partial}{\partial t}(\phi\rho) = \phi \frac{\partial\rho}{\partial p} \frac{\partial p}{\partial t} = \phi\rho c \frac{\partial p}{\partial t}, \quad (5.55)$$

where ϕ is kept constant.

Substituting for the Darcy's Law and including non-Darcy flow as in Eq. 5.41, we may substitute Eq. 5.55 into Eq. 5.54 and arrive at the following differential equation for the pressure p .

$$\phi\rho c \frac{\partial p}{\partial t} - \nabla \cdot \left(\rho \frac{k\delta}{\mu} \nabla p \right) = 0, \quad (5.56)$$

where the minus sign in the equation above comes from the definition of Darcy's Law.

Eq. 5.56 can be made more linear by means of the Kirchhoff's transformation and we may write

$$\begin{aligned} \frac{\partial p}{\partial t} = \frac{\partial p}{\partial m} \frac{\partial m}{\partial t} &= \frac{(\rho/\mu)_r}{\rho/\mu} \frac{\partial m}{\partial t} \quad \text{or} \\ \frac{\partial p}{\partial t} &= \frac{\mu B}{(\mu B)_r} \frac{\partial m}{\partial t}, \end{aligned} \quad (5.57)$$

which is then substituted in to Eq. 5.56, arriving at the equation

$$\frac{\partial m}{\partial t} - \underbrace{\frac{k}{\phi c \mu}}_{D_h} \nabla \cdot (\delta \nabla m) = 0, \quad (5.58)$$

where the permeability k is considered to be constant. The term $D_h = k/(\phi c \mu)$ is called the *hydraulic diffusivity* and we can write

$$\frac{\partial m}{\partial t} - D_h \nabla \cdot (\delta \nabla m) = 0. \quad (5.59)$$

Eq. 5.59 is the general flow equation for transient gas flow in porous media. Despite the transformation into pseudo-pressure, Eq. 5.59 is still non-linear, thus less non-linear than the flow equation in terms of real pressures, as compared to Eq. 5.56. The non-linearity of Eq. 5.59 is caused by the non-Darcy effect and the hydraulic diffusivity, where

δ : represents the non-Darcy effect and is a function of pressure; $\delta(p)$.

D_h : represents the hydraulic diffusivity, where D_h is indirectly pressure dependent through viscosity and compressibility; $D_h(\mu(p), c(p))$.

Eq. 5.59 is the basic equation for mathematical simulation of single gas flow, where the hydraulic diffusivity is assumed to be constant. In this case, Eq. 5.59 reduces to a linear diffusivity equation, having a solution which is also applicable for many other physical problems. The diffusivity equation, Eq. 5.59, describes the transient flow of gas in porous media.

Note that the non-Darcy correction factor δ in Eq. 5.59 can be handled similarly as in the case of steady-state flow, i.e. by simply adding a non-Darcy skin factor S_{nD} to the final solution of the following equation

$$\frac{\partial m}{\partial t} - D_h \nabla \cdot (\nabla m) = 0. \quad (5.60)$$

Eq. 5.60 is the diffusivity equation to be solved for radial flow and constant terminal rate.

Example: The hydraulic diffusivity factor

The hydraulic diffusivity factor

$$D_h = \frac{k}{\phi c \mu}$$

is defined as a function of viscosity and compressibility, both functions of pressure. Additionally, both permeability and porosity are considered as constants even though they may change throughout the reservoir.

The pressure dependence of D_h can be checked by investigating the pressure dependence of $(\mu c)^{-1}$, as shown in Table 5.3. The data shown in the table is partly taken from Table 5.2, in the case of viscosity and for the compressibility, where the reciprocal pressure is used $c \simeq p^{-1}$.

The relative hydraulic diffusivity parameter is then defined

$$\frac{D_h}{D_h(p = 40 \text{ bar})} = \frac{(\mu c)_{p=40 \text{ bar}}}{\mu c}$$

Figure 5.8 shows the relative hydraulic diffusivity as function of pressure. The plot shows that even though the hydraulic diffusivity is not constant, the relative change as function of pressure is quite small.

Table 5.3: Data describing the pressure dependence of D_h .

| p [bar] | μ [mPas] | $c \simeq 1/p$ [bar^{-1}] | $1/(\mu c)$ | $D_h/D_h(p = 40 \text{ bar})$ |
|-----------|--------------|--------------------------------------|-------------|-------------------------------|
| 40 | 0.0129 | 0.0250 | 3093 | 1.00 |
| 60 | 0.0140 | 0.0167 | 4301 | 1.39 |
| 100 | 0.0159 | 0.0100 | 6289 | 2.03 |
| 140 | 0.0181 | 0.0071 | 7751 | 2.50 |
| 200 | 0.0219 | 0.0050 | 9140 | 2.95 |
| 260 | 0.0263 | 0.0038 | 9893 | 3.19 |
| 300 | 0.0293 | 0.0033 | 10230 | 3.30 |
| 350 | 0.0331 | 0.0029 | 10580 | 3.42 |
| 430 | 0.0388 | 0.0023 | 11070 | 3.58 |

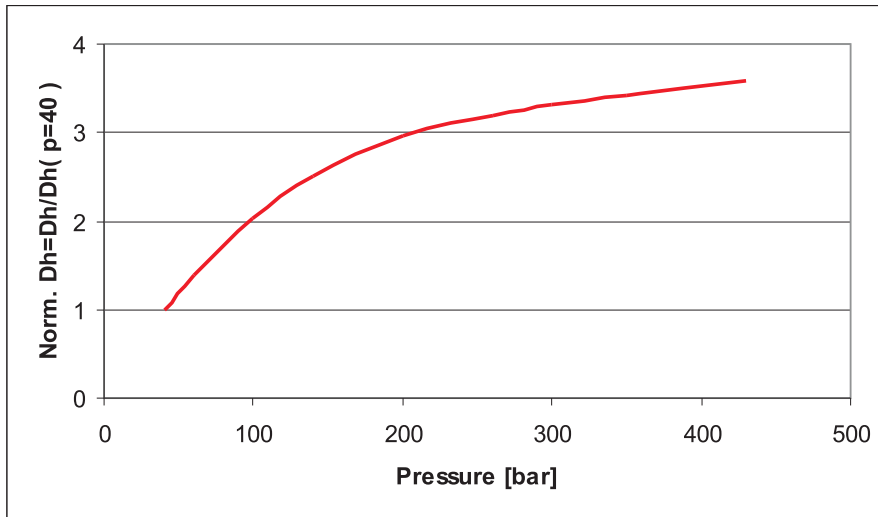


Figure 5.8: Relative hydraulic diffusivity as function of pressure.

As in the previous example, considering the term $\rho B/\mu$ under integration from the well-bore to the outer boundary of the reservoir, the hydraulic diffusivity D_h should be updated as part of the normal iteration procedure when numerically simulation of transient flow is performed.

5.3.1 Radial Flow at Constant Terminal Rate

The analytical solution for radial flow at constant terminal rate, describes the pressure distribution in a finite cylindrical reservoir. The reservoir is produced at constant surface flow rate, from a well placed in the center of a closed cylindrical reservoir. The reservoir has a constant thickness and a uniform distribution of porosity and permeability. The well is perforated along the full thickness of the reservoir, leading the fluid flow to be horizontal and radial.

Under these conditions the most important reservoir dimensions are the circular area A and the thickness h of the reservoir. Employing cylindrical co-ordinates, we may write Eq. 5.60 on the following form

$$\frac{1}{D_h} \frac{\partial m}{\partial t} - \frac{1}{r} \frac{\partial}{\partial r} \left(r \frac{\partial m}{\partial r} \right) = 0. \quad (5.61)$$

where the hydraulic diffusivity D_h is considered to be constant. Note also that the non-Darcy correction factor δ has simply been removed from Eq. 5.60, since we have shown that the non-Darcy effect can be represented by a non-Darcy skin factor S_{nD} in the final solution.

The general solution of the radial diffusivity equation Eq. 5.61, which was presented by Hurst and van Everdingen in 1949 [13], involves rather complex mathematical treatment and the solution involves a summation of an infinite series of Bessel functions. Its derivation is thus beyond the scope of this text.

One of the results from this analysis is the observation that the general solution is characterized by three different production periods; one infinite-acting period, one late transient period and one semi steady-state period, as depicted in Figure 5.9. The late transient period, i.e. the intermediate period, is normally considered to be rather short and can therefore be disregarded, in particular in the case of cylindrical symmetry. For a more complete description of these solutions and their interpretation, see the book of Dake [4].

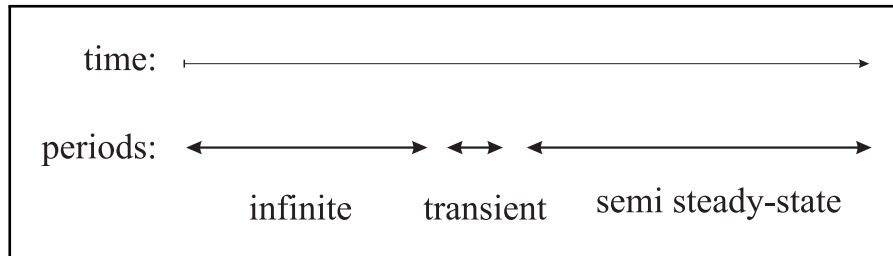


Figure 5.9: Production periods for radial flow at constant terminal rate.

The general equation contains both the time independent solution, i.e. the semi steady-state solution, which we already have derived in the previous sections of this chapter. In addition, a time dependent solution of Eq. 5.61 exist, valid in the infinite-acting period.

5.3.2 Infinite-Acting Period

The infinite-acting flow period can be approximately described by the so-called line-source solution. This solution satisfies Eq. 5.61 for the special case of a vanishing well-bore radius ($r_w \rightarrow 0$). The assumption of a vanishing well radius is justified when applying the solution of Eq. 5.61 to an apparently infinite reservoir.

At constant terminal rate, we have the following boundary solution in the vanishing well

$$\lim_{r \rightarrow 0} r \frac{\partial m}{\partial r} = \frac{q_{sc}(\mu B)_r}{2\pi kh}, \quad (5.62)$$

which is the boundary solution, Eq. 5.33, previously seen to be valid in the well.

The diffusivity equation, Eq. 5.61 is a differential equation in both time and radius. A simplification of this equation, reducing the number of variables from two to one, involves a version of the Boltzman substitution. The new variable $y = r^2/(4D_h t)$, reduces Eq. 5.61 to

$$y \frac{\partial m}{\partial y} + \frac{\partial}{\partial y} \left(y \frac{\partial m}{\partial y} \right) = 0. \quad (5.63)$$

Eq. 5.63 is solved by double integration and evaluated using the boundary condition, Eq. 5.62. The final solution is then written

$$m_i - m(r, t) = \frac{q_{sc}(\mu B)_r}{2\pi hk} \left(-\frac{1}{2} Ei \left(-\frac{r^2}{4D_h t} \right) \right), \quad (5.64)$$

where m_i is the initial reservoir pseudo-pressure and $m(r, t)$ is the pseudo-pressure at radial position r and time t . The function Ei is called the *Exponential integral function*. This function is quite often presented in the form of a table: $(Ei(x), x)$ and can be found in most tables of “mathematical data” [8].

In this context, we are primarily interested in the well-bore pressure, where $r = r_w$. For variables in Eq. 5.64, where $r^2/(4D_h t) < 0.01$, an approximation of the solution of Eq. 5.64 is given by

$$m_i - m(r_w, t) = \frac{q_{sc}(\mu B)_r}{2\pi hk} \frac{1}{2} \left(\ln \left(\frac{4D_h t}{r_w^2} \right) - \gamma \right), \quad (5.65)$$

where $\gamma = 0.577215$ is the Euler constant.

Including the well-bore skin S , the non-Darcy effect and using the non-Darcy skin factor S_{nD} , - the general approximate pressure solution for radial flow, valid in the infinite acting period is thus written

$$m_i - m_{bh}(t) = \frac{q_{sc}(\mu B)_r}{2\pi hk} \frac{1}{2} \left[\ln(t) + \ln \left(\frac{D_h}{r_w^2} \right) + 0.80907 + 2(S + S_{nD}) \right], \quad (5.66)$$

where the new numeric factor $0.80907 = \ln(4) - \gamma$.

Example: Approximation of The Exponential Integral Function

The exponential integral function is defined by

$$-Ei(-x) = \int_x^\infty \frac{e^{-s}}{s} ds.$$

For small values $x < 0.01$, an approximation $-Ei(-x) \simeq -\ln x - \gamma$ can be used. The question is therefore, - at which time interval, after start-up of well production, will the approximation be valid (?) .

In order for the approximation to be valid, the following in-equality has to be satisfied

$$\frac{r_w^2}{4D_h t} < 0.01,$$

where the hydraulic diffusivity is $D_h = k/(\phi\mu c)$.

If we choose the following set of "typical" reservoir - and fluid parameters

$$\begin{aligned} k &= 100 \text{ mD} & \phi &= 0.25 & r_w &= 15 \text{ cm} \\ \mu &= 0.04 \text{ mPa s} & c &= 0.02 \text{ bar}^{-1} \end{aligned}$$

we can write the in-equality

$$t > \frac{1}{0.01} \frac{r_w^2 \phi \mu c}{4k} = \frac{1}{0.01} \frac{(0.15)^2 \cdot 0.25 \cdot 0.04 \cdot 10^{-3} \cdot 0.02 \cdot 10^{-5}}{4 \cdot 100 \cdot 10^{-3} \cdot 0.987 \cdot 10^{-12}} = 11.4$$

The above pressure approximation in the well-bore is valid for times greater than 12 seconds, which in practical terms expand the whole infinite-acting period.

5.4 The Late Transition Period

As depicted in Figure 5.9, there exist an intermediate period between the infinite- and the semi steady-state period. This is the time in the history of the production from a gas reservoir where the pressure wave information from the well has just reached the nearest boundary of the reservoir. In the case of a cylindrical reservoir with the well at the center, this time would be the time when the pressure wave reaches the outer peripheral. In a rectangular shaped reservoir with the well at the center, the late transition period is defined by the different times encountered by the arrival of the pressure wave at the two boundary surfaces.

For a cylindrical reservoir with the well at the center, the late transition time is uniquely defined as the time when the infinite-acting period stops and the semi steady-state starts. Eq. 5.65 defines the infinite-acting pressure solution, while Eq. 5.53 represents the semi steady-state solution.

Since the time dependance in Eq. 5.53 is contained in the average pseudo-pressure function, \bar{m} , we have first to redefine the time dependence in the semi steady-state pressure solution.

5.4.1 Time Dependent Semi Steady-State Solution

The solution of semi steady-state flow is characterized by a closed and finite reservoir as presented in Eq. 5.53.

In the semi steady-state period the pressure wave has already reached the outer boundary and the pressure profile is well established. Further reservoir pressure decline

in the semi steady-state period is assumed to take place as illustrated in Figure 5.10, as shown for the pressure profiles 4 and 5.

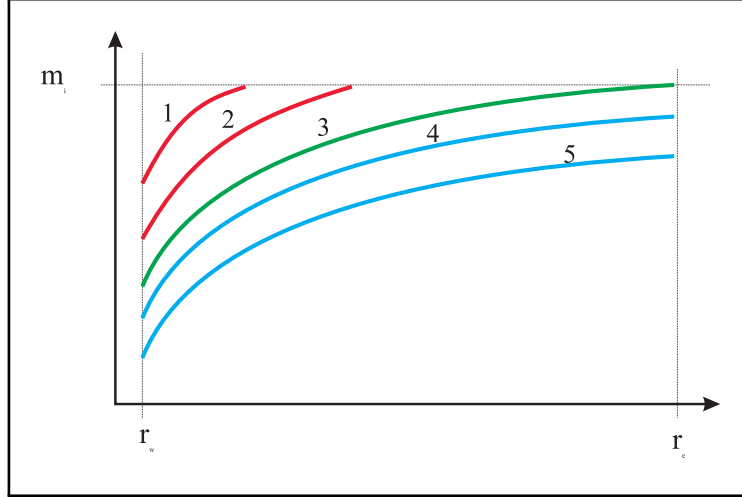


Figure 5.10: Reservoir pressure decline in the semi steady-state period.

Figure 5.10 shows an idealized picture of the pressure profiles in a reservoir after a certain time, at constant rate production. Curve 1 and 2 are two pressure profiles taken from the infinite-acting period. At this early time in the production history of the reservoir, the pressure wave has not yet reached the outer boundary of the reservoir. Pressure curve 3 shows the pressure profile at the transition time. At this time the pressure profile changes from the infinite-acting period to the semi steady-state period. From this point in time and onwards the pressure profile in the reservoir preserves a constant form while the absolute pressure is decreasing equally much for all radial positions. Pressure curve 4 and 5 have identical *form* or profile and have a constant pressure difference for all radial positions.

In the semi steady-state period the average pressure in the reservoir will decrease with time at constant terminal rate. The primary drive-mechanism is gas compressibility and the gas flow rate is therefore a function of the gas compressibility $c = -(1/V)(dV/dp)$. The average pressure decline in the reservoir can thus be expressed as function of the gas compressibility,

$$\frac{dp}{dt} = -\frac{1}{cV} \frac{dV}{dt} = -\frac{1}{cV} q = -\frac{q_{sc}B}{cV}, \quad (5.67)$$

where q is the reservoir flow rate, V is the reservoir volume of gas and B is the gas volume factor.

Integration of Eq. 5.67 yields

$$\int_{p_i}^{\bar{p}} dp = -\int_0^t \frac{q_{sc}B}{cV} dt \Rightarrow \bar{p} - p_i = -\frac{q_{sc}B}{cV} t, \quad (5.68)$$

where \bar{p} is the average reservoir pressure.

Substituting for the reservoir volume $V = \pi(r_e^2 - r_w^2)h\phi$ and using Kirchoff's transformation, Eq. 5.68 is written (where $r_w \ll r_e$)

$$m_i - \bar{m} = \frac{q_{sc}(\mu B)_r}{\mu c \pi r_e^2 h \phi} \cdot t = \frac{q_{sc}(\mu B)_r}{2\pi h k} \frac{2k}{\phi \mu c r_e^2} \cdot t = \frac{q_{sc}(\mu B)_r}{2\pi h k} \frac{2D_h}{r_e^2} \cdot t, \quad (5.69)$$

where D_h is the well known hydraulic diffusivity.

Combining the semi steady-state equation Eq. 5.69 and the steady-state flow equation Eq. 5.53, we arrive at the time dependent semi steady-state flow solution,

$$m_i - m_{bh} = \frac{q_{sc}(\mu B)_r}{2\pi h k} \left[\frac{2D_h}{r_e^2} t + \ln(r_e/r_w) - \frac{3}{4} + S + S_{nD} \right]. \quad (5.70)$$

5.4.2 Infinite-Acting - to Semi Steady-State Period

The duration of the infinite-acting period, illustrated by the pressure curves 1 and 2 in Figure 5.10, and the start-up of the semi steady-state period, curve 3, can be estimated from the radial flow equations Eqs. 5.66 and 5.70. The two pressure solutions are written,

Infinite-acting period:

$$(m_i - m_{bh})_{IA} = \frac{q_{sc}(\mu B)_r}{2\pi h k} \frac{1}{2} \left[\ln(t) + \ln\left(\frac{D_h}{r_w^2}\right) + 0.80907 + 2(S + S_{nD}) \right]. \quad (5.71)$$

Semi steady-state period:

$$(m_i - m_{bh})_{SSS} = \frac{q_{sc}(\mu B)_r}{2\pi h k} \left[\frac{2D_h}{r_e^2} t + \ln(r_e/r_w) - \frac{3}{4} + S + S_{nD} \right], \quad (5.72)$$

The infinite-acting pressure difference is proportional to the logarithm of the time, i.e. $(m_i - m_{bh})_{IA} \propto \ln(t)$, while in the case of the semi steady-state period the pseudo-pressure difference is directly proportional to time, i.e. $(m_i - m_{bh})_{SSS} \propto t$.

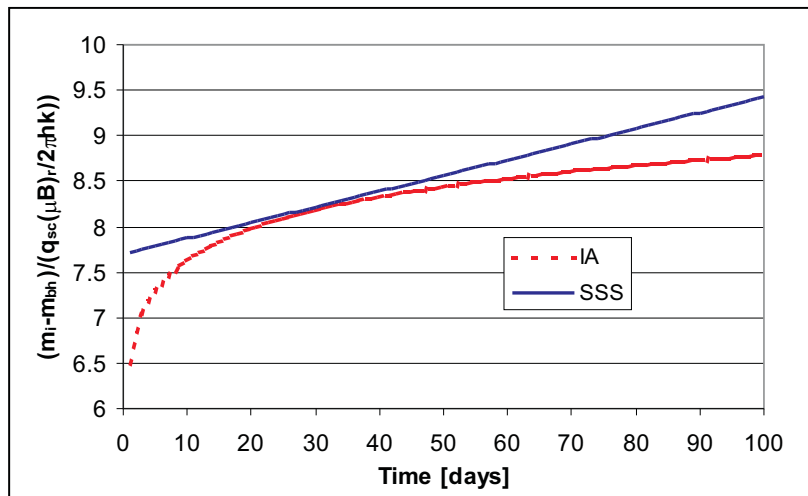


Figure 5.11: Transition time between infinite-acting - and semi steady-state periods.

Figure 5.11 shows the two pressure solutions as function time. The plotted data represent the reduced pseudo-pressure, i.e. the function: $(m_i - m_{bh})/(q_{sc}(\mu B)_r/2\pi hk)$ on the y-axis and time in days on the x-axis. The data used in the plot is identical with the data in the example below. The plot shows the characteristic pressure behavior in the two periods. At early times, in the infinite-acting period, the pseudo-pressure difference will increase as the logarithm of time compared to a linear increase with time as the reservoir progresses into the semi steady-state period. The transition time is therefore defined as the Start of the Semi steady-state period t_{SS} and can be defined as the time where the distance between the two pseudo-pressure curves in Figure 5.11 has its minimum. In mathematical terms, we write

$$\frac{d}{dt}|(m_i - m_{bh})_{SSS} - (m_i - m_{bh})_{IA}| = 0. \quad (5.73)$$

Substituting for Eqs. 5.71 and 5.72 in Eq. 5.73, we arrive at a transition time

$$t_{SS} = \frac{r_e^2}{4D_h}. \quad (5.74)$$

In practical terms we may use the transition time t_{SS} as the time-marker for switching from the infinite-acting solution to the semi steady-state pressure solution.

Example: Start Semi Steady-State Period

We have seen above that the infinite-acting period commences shortly after the start-up of well production. A natural question is therefore; for how long time will this period last and when could we expect the semi steady-state period to start?

If we choose the same reservoir and fluid data as in the example on page 155 and add a “typical” outer radius $r_e = 700 \text{ m}$, we may use the following data

$$\begin{array}{lll} k = 100 \text{ mD} & \phi = 0.25 & r_w = 15 \text{ cm} \\ \mu = 0.04 \text{ mPas} & c = 0.02 \text{ bar}^{-1} & r_e = 700 \text{ m} \end{array}$$

The transition time t_{SS} is calculated as follows

$$t_{SS} = \frac{r_e^2}{4D_h} = \frac{r_e^2 \phi \mu c}{4k}$$

and

$$t_{SS} = \frac{(700)^2 \text{ m}^2 \cdot 0.25 \cdot 0.04 \text{ mPas} \cdot 0.02 \text{ bar}^{-1}}{4 \cdot 100 \text{ mD}} = 2482269 \text{ s} \simeq 29 \text{ days}.$$

The time of start semi steady-state as found above is in total agreement with what is presented in the Figure 5.11, as the same data was used. From Eq. 5.74 we see that t_{SS} is increasing as reservoir permeability is decreasing and reservoir size (volume) is increasing.

The definition of a start semi steady-state, Eq. 5.74, is valid for a cylindrical reservoir with the well at the center. Since most reservoirs are neither cylindrical nor have their wells at the center, we realize there are limitations to the usefulness of Eq. 5.74.

A rectangular reservoir with the well at the center, as depicted in Figure 5.12, is defined by two sides, S_1 and S_2 , where $S_1 > S_2$. In this situation we would expect the the infinite acting period to end when the pressure wave has reached the nearest boundary (longest side S_1) and the semi steady-state period to start when the pressure wave has reached the outer boundary (shortest side S_2).

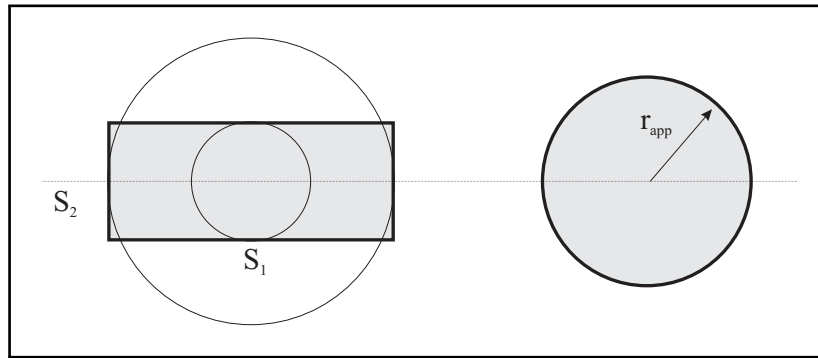


Figure 5.12: Rectangular shaped reservoir and corresponding appearing reservoir.

As seen from Figure 5.12, the start semi steady-state time does not coincide with the end of infinite acting period and Eq. 5.74 does not apply directly. However, we may introduce an appearing reservoir area of cylindrical shape, where the two areas are identical. Under these circumstances, an appearing radius can be defined,

$$r_{app} = \sqrt{\frac{A}{\pi}}, \quad (5.75)$$

where the drainage area $A = S_1 S_2$. Then, $t_{SS}(r = r_{app})$ will represent the time symbolizing the end of infinite acting period and the start of semi steady-state period.

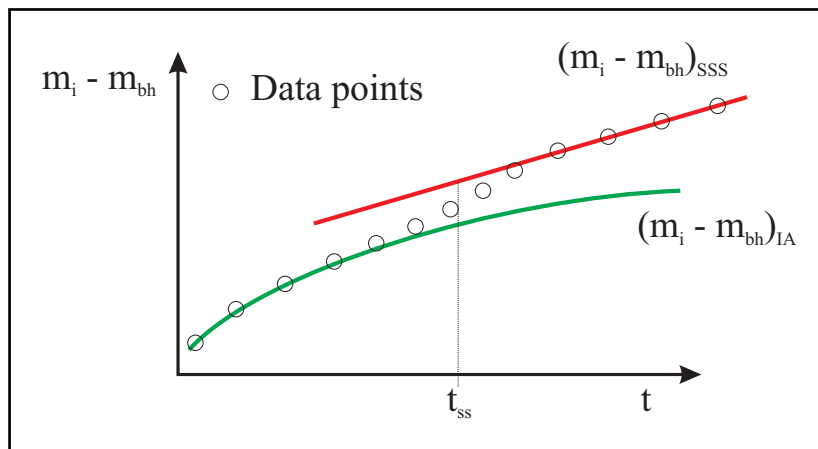


Figure 5.13: Late transition time between infinite acting period and semi steady-state period for a rectangular shaped reservoir with the well at the center.

Figure 5.13 depicts the late transition period as the time between the end of the infinite acting period and the start of the semi steady-state period. The start of semi steady-state time t_{SS} is here defined in correspondence to an appearing reservoir, as defined above.

5.5 Radial Flow Equations

As already stated above, - the general shape of reservoirs are neither cylindrical nor is the well centered. On the other hand is the assumption of cylindrical symmetry and centered well position, valid to a surprisingly high degree of accuracy in many real field examples.

The infinite acting pressure solution is, as can readily be expected, quite independent of the outer boundary conditions and the location of the well. In this rather short time period, the well response is totally dependent of the near well region.

The semi steady-state solution, on the other hand, is quite dependent on the outer boundaries such as reservoir extension, well locations and inter well interference. Under these conditions, non-radial flow behavior occur and a certain modification of the pseudo-pressure solution is necessary.

5.5.1 Non-Radial Reservoir Flow

The shape of the reservoir area and the location of the well are rarely symmetrical as in our radial flow model. Production from non-radial shaped reservoirs where the well is off-center will however in principle show the same characteristics with respect to pressure behavior, as is the case above. It is clear that a non-radial shaped reservoir or a cylindrical reservoir with the well off-centered will observe different transition periods compare to the radial flow model. Generally the transition period will be longer and the transition times defined by end of infinite-acting period and the start of semi steady-state period will be more dubious. The pressure development within the two periods are, on the other hand, expected to be unchanged and thus the pressure solutions derived are valid also for non-radial flow.

The significance of non-cylindrical reservoir geometry has been considered for various examples and a general shape factor is introduced to compensate the non-ideal reservoir shape. The substitution done is relative to a cylindrical reservoir with a centered well. The substitution done for non-radial flow is a modification which only concerns the semi steady-state flow solution, since the pressure development per definition will proceed unaffected by any outer boundary conditions in the infinite-acting period.

The modification proposed by Dietz is related to the $\ln(r_e/r_w)$ term in Eq. 5.72 and is written

$$\ln\left(\frac{r_e}{r_w}\right) - \frac{3}{4} \Rightarrow \frac{1}{2} \ln\left(\frac{4A}{e^\gamma C_A r_w^2}\right), \quad (5.76)$$

where A is the top - or surface area of the reservoir and C_A is the Dietz shape factor. γ is the Euler constant. Alternatively, as suggested by Fetkovitch and Vienot, the modification for non-radial flow could also be introduced as a skin factor S_{CA} , defined as

$$S_{CA} = \frac{1}{2} \ln \left(\frac{4\pi}{e^\gamma C_A} \right). \quad (5.77)$$

Various shape factors and skin shape factors are presented in Figure 5.14.

Example: Dietz Shape-factor and Shape-factor Skin

A shape-factor C_A and a shape-factor skin S_{CA} were introduced in the text above without revealing the true motivation for such an action. The Dietz shape factor or drainage shape factor has its origin in the field of pressure analysis, i.e. see the book of Dake (section 7.6) [4].

In what is known as MBH (Matthews, Brons and Hazebroek) pressure buildup theory, various charts are displaying the different geometries and different asymmetries of the producing well with respect to the no-flow boundary. The Dietz shape-factor or more correctly the logarithm of the shape-factor, $\ln(C_A)$, can be determined simply by letting a dimensionless time function $t_{DA} = 1$ in the dimensionless semi steady-state flow equation. The derivation of these shape-factors goes beyond the scope of this text, but interested readers are referred to the reference above.

The purpose of the Dietz shape-factor, as presented in this text, is to extend the semi steady-state pressure solution, Eq. 5.72, to cases of non-cylindrical reservoir shapes and asymmetric well locations. In doing so, we may put forward the following rather tenuous argumentation.

We start this generalization with the following terms from Eq. 5.72,

$$\begin{aligned} \ln \left(\frac{r_e}{r_w} \right) - \frac{3}{4} &= \frac{1}{2} \left(\ln \frac{r_e^2}{r_w^2} - \ln e^{3/2} \right) \\ &= \frac{1}{2} \ln \frac{\pi r_e^2}{\pi e^{3/2} r_w^2} \\ &= \frac{1}{2} \ln \frac{4A}{4\pi e^{3/2} r_w^2} \\ &= \frac{1}{2} \ln \frac{4A}{e^\gamma 31.62 r_w^2} \\ &= \frac{1}{2} \ln \frac{4A}{e^\gamma C_A r_w^2}, \end{aligned}$$

where A is the reservoir drainage area, γ the Euler constant and C_A the Dietz shape-factor. The above deduction is valid for a cylindrical reservoir $A = \pi r_e^2$ with the well at the center. Then the Dietz shape-factor is $C_A = 31.62$. What Dietz actually showed in his theory was that a generalization of the semi steady-state equation to different geometries and well locations is made possible by defining the drainage area and a new shape-factor characteristic for the reservoir at hand. This modifies the semi steady-state flow equation, Eq. 5.72, and we get


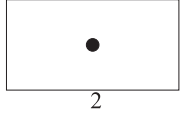
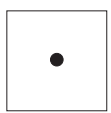
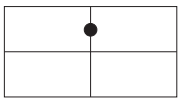
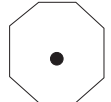
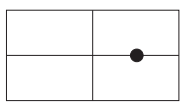
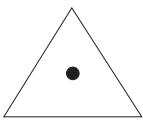
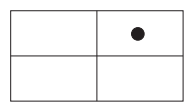
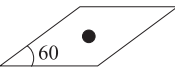
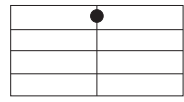
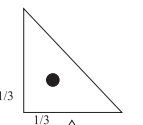
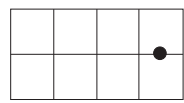
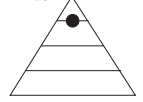
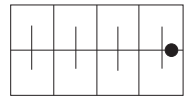
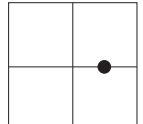

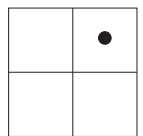
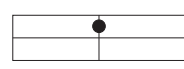
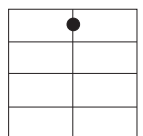
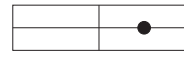
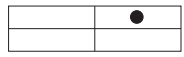
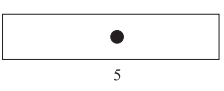
| Drainage shape | C_A | S_{CA} | Drainage shape | C_A | S_{CA} |
|---|-------|----------|--|--------|----------|
|  | 31.62 | -0.75 |  | 21.837 | -0.56 |
|  | 30.88 | -0.74 |  | 10.837 | -0.21 |
|  | 31.60 | -0.75 |  | 4.514 | 0.22 |
|  | 27.60 | -0.68 |  | 2.077 | 0.61 |
|  | 27.10 | -0.67 |  | 3.157 | 0.40 |
|  | 21.90 | -0.57 |  | 0.581 | 1.25 |
|  | 0.098 | 2.14 |  | 0.111 | 2.08 |
|  | 12.99 | -0.31 |  | 5.379 | 0.14 |
|  | 4.51 | 0.22 |  | 2.69 | 0.48 |
|  | 3.335 | 0.37 |  | 0.232 | 1.71 |
| | | |  | 0.1155 | 2.06 |
| | | |  | 2.3606 | 0.55 |

Figure 5.14: Dietz shape-factors and skin shape factors. (In part after J.Hagoort, *Fundamentals of gas reservoir engineering*.)

$$(m_i - m_{bh})_{SSS} = \frac{q_{sc}(\mu B)_r}{2\pi hk} \left(\frac{2Dh}{r_e^2} t + \frac{1}{2} \ln \frac{4A}{e^\gamma C_A r_w^2} + S + S_{nD} \right), \quad (5.78)$$

If we use the definition of the apparent reservoir radius in Eq. 5.75, we may substitute the drainage area A in the above equation with the this radius,

$$\frac{1}{2} \ln \frac{4A}{e^{\gamma} C_A r_w^2} = \ln \frac{r_{app}}{r_w} + \frac{1}{2} \ln \frac{4\pi}{e^{\gamma} C_A},$$

where the last term is called the Shape-factor skin,

$$S_{CA} = \frac{1}{2} \ln \frac{4\pi}{e^{\gamma} C_A}.$$

The semi steady-state flow equation can now be written,

$$(m_i - m_{bh})_{SSS} = \frac{q_{sc}(\mu B)_r}{2\pi h k} \left(\frac{2D_h}{r_e^2} t + \ln \frac{r_{app}}{r_w} + S_{CA} + S + S_{nD} \right). \quad (5.79)$$

5.5.2 Flow Equations

The radial flow solution include two equations, the infinite-acting solution Eq. 5.71 and the semi steady-state solution Eq. 5.72, modified by the non-radial flow correction, given by Eq. 5.76.

The two pressure solutions are the written,

Infinite acting period

$$m_i - m_{bh} = \frac{q_{sc}(\mu B)_r}{2\pi h k} \frac{1}{2} \left[\ln(t) + \ln \left(\frac{D_h}{r_w^2} \right) + 0.80907 + 2(S + S_{nD}) \right], \quad (5.80)$$

which can be written in a more compact form

$$m_i - m_{bh} = \frac{q_{sc}(\mu B)_r}{2\pi h k} \frac{1}{2} \left[\ln \left(\frac{4D_h}{e^{\gamma} r_w^2} t \right) + 2(S + S_{nD}) \right], \quad (5.81)$$

Semi steady state period

$$m_i - m_{bh} = \frac{q_{sc}(\mu B)_r}{2\pi h k} \left[\frac{2D_h}{r_e^2} t + \frac{1}{2} \ln \left(\frac{4A}{e^{\gamma} C_A r_w^2} \right) + S + S_{nD} \right], \quad (5.82)$$

or alternatively

$$m_i - m_{bh} = \frac{q_{sc}(\mu B)_r}{2\pi h k} \left[\frac{2D_h}{r_e^2} t + \ln \frac{r_{app}}{r_w} + S_{CA} + S + S_{nD} \right]. \quad (5.83)$$

Notice that the two time dependent terms in the equations above contains the outer boundary radius r_e , while we in the generalized case is using r_{app} . This discrepancy is simply omitted by using the mean pressure as the time dependent variable, - as we soon will see.

In the flow equations above, the initial pseudo-pressure m_i can be substituted with the mean pseudo-pressure \bar{m} . In the case for the Infinite acting period there will be no practical difference between the two pseudo-pressures and $m_i \approx \bar{m}$. This holds for Eqs. 5.80 and 5.81.

In the case of the Semi steady-state period, the substitution $m_i \approx \bar{m}$ is simply done by using Eq. 5.69 in reverse order.

Recalling the definition of the non-Darcy skin factor $S_{nD} = D \cdot q_{sc}$, where $D = (\beta k \rho B) / (2\pi h \mu r_w)$, it might be more practical to present the general radial solution, valid for both periods in one equation. This form is well adapted for further numerical simulation, and we might write

$$m_{bh} = \bar{m} - (A \cdot q_{sc} + B \cdot q_{sc}^2), \quad (5.84)$$

where A and B are constants, defined as

Infinite acting period:

$$A = \frac{(\mu B)_r}{2\pi h k} \frac{1}{2} \left[\ln \left(\frac{4D_h}{e\gamma r_w^2 t} \right) + 2S \right], \quad (5.85)$$

$$B = \frac{(\mu B)_r}{2\pi h k} D. \quad (5.86)$$

Semi steady state period:

$$A = \frac{(\mu B)_r}{2\pi h k} \left[\frac{1}{2} \ln \left(\frac{4A}{e\gamma C_A r_w^2} \right) + S \right], \text{ or alternatively} \quad (5.87)$$

$$A = \frac{(\mu B)_r}{2\pi h k} \left[\ln \frac{r_{app}}{r_w} + S_{CA} + S \right], \quad (5.88)$$

$$B = \frac{(\mu B)_r}{2\pi h k} D. \quad (5.89)$$

5.6 Simulation Examples

In these examples the terminal flow rate is $q_g = 5 \cdot 10^5 \text{ Sm}^3/\text{day}$ and the hydrocarbon pore volume is $V_p = 4 \cdot 10^6 \text{ Rm}^3$, similar to previous simulation examples. The data input-file, presents all necessary and relevant data for a successful simulation. Most data included in the input-file are kept unchanged. Only data related to reservoir flow are subject to change in these simulations.

5.6.1 Pressure development as function of time

Figure 5.15 shows the average pressure profile in the reservoir and the bottom-hole pressure, both relative to the left y-axis. The pressure draw-down is the pressure difference between the reservoir pressure and the pressure in the well (bottom-hole pressure), relative to the right hand y-axis. The figure shows a situation where the reservoir permeability is rather high, in case the pressure difference between well and reservoir is seemingly quite low.

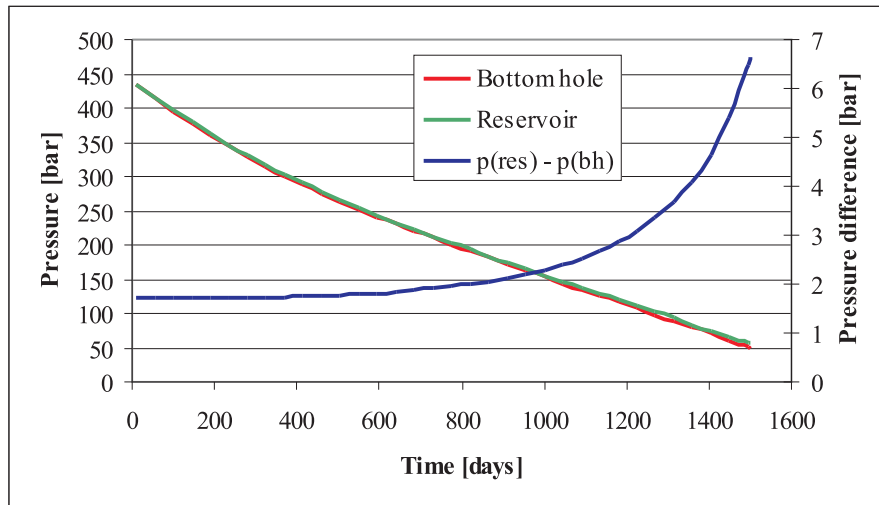


Figure 5.15: Pressure development as function of time.

Figure 5.16 shows the bottom-hole pressure where we have simulated two similar reservoirs where the only difference is related to the reservoir permeability. When the reservoir permeability is reduced, a higher pressure difference is required to bring the same amount of gas to the well-bore. Thus, more energy is used in producing the gas and consequently the bottom-hole pressure declines faster. Another observation, from Figure 5.16, is that the gas production is therefore halted at earlier time.

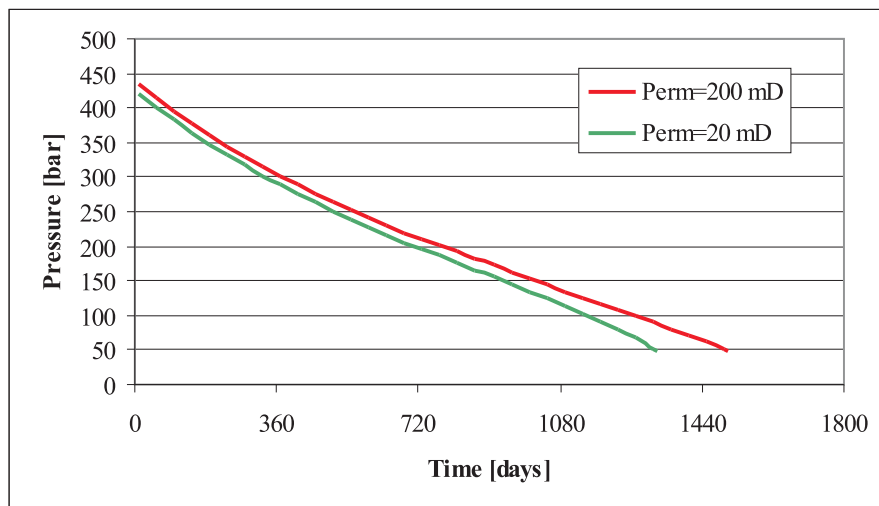


Figure 5.16: Bottom-hole pressure as function of time.

5.6.2 Relative bottom-hole pressure development

The bottom-hole well pressure is plotted in Figure 5.17, as function of average reservoir pressure. It is seen from the plot, that when the reservoir permeability is reduced to "very" low values, here 2 mD, a substantial draw-down pressure is reducing the gas production significantly and the well is abandoned at quit high pressure.

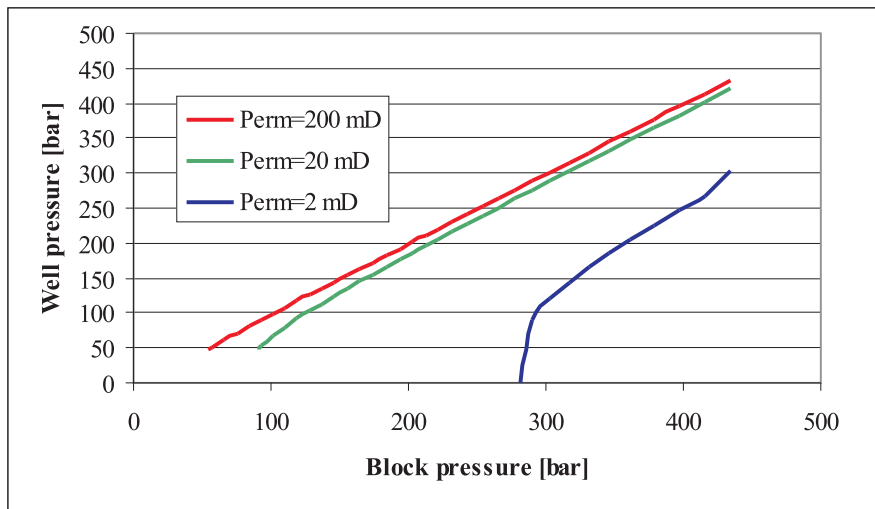


Figure 5.17: Bottom-hole pressure as function of block pressure.

5.7 Near Well Flow Characteristics in Gas Condensate Reservoirs

In the following sections we will take a closer look at the dynamics of fluid flow in gas condensate reservoirs. We will use the tools already developed in the previous sections and by way of analytical description study radial two phase flow caused by gas condensation in the vicinity of the well.

Based on the single phase semi steady-state solution, the application of Kirchhoff's transformation and a simple dynamic model of reservoir oil saturation, - revised calculations of the bottom hole pressures and additional production volumes from initially condensed oil, are performed.

Calculations are based on assumptions about shape and profile of the condensed oil saturation in the reservoir; $S_o(r, t)$, as presented by Ursin [19]. The model shows how pressure draw-down and oil/gas production can be revised given the information about this saturation profile. In the model, all condensed oil not contained within the saturation profile, is produced to the surface.

5.7.1 Gas Condensate Well Deliverability

Production from gas condensate reservoirs is characterized by the liquid condensation of gas in the reservoir during normal production [5, 6]. Liquid drop-out commences

as the reservoir pressure drops below the fluid dew-point pressure. Since the reservoir pressure is always lowest in the producing well, the first drops of oil are formed in the close vicinity of the well-bore, as previously discussed in Chapter 2.

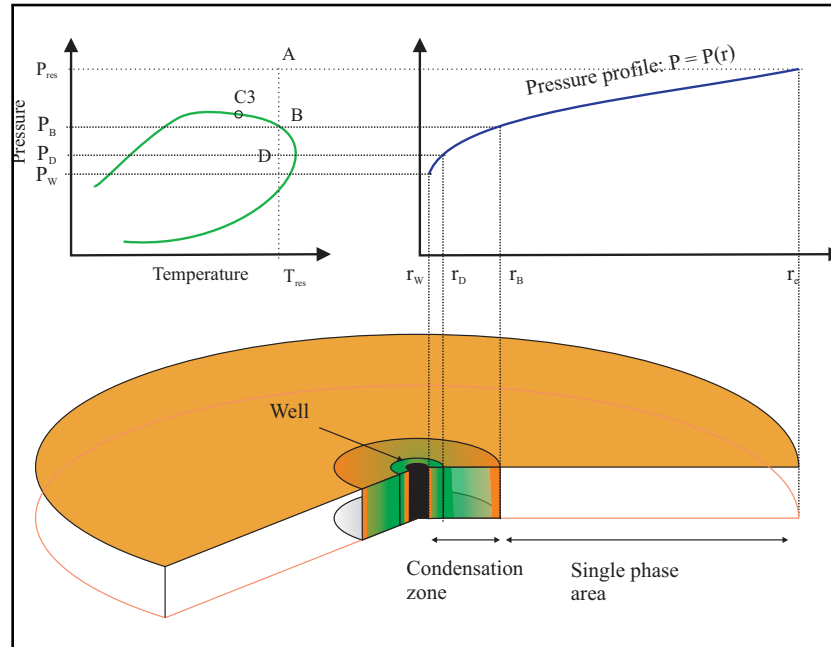


Figure 5.18: Formation of liquid condensate related to fluid phase and reservoir pressure draw-down. Upper left: Gas two-phase envelope, where C3 is the critical point, A indicates initial reservoir conditions and B is the dew-point. Upper right: Radial pressure profile as from a cylindrical, homogenous reservoir. Lower: Formation of oil zone in a cylindrical reservoir. Figure taken from [18].

Figure 5.18, also from Chapter 2, depicts this process for a cylindrical reservoir with the well at the centre.

As the pressure is further decreased and as a result of normal production, a saturation of liquid condensate expands radially with time. When the pressure is lowered below the dew-point pressure in all parts of the reservoir, (liquid) condensation is present throughout the whole reservoir volume. However, the saturation profile throughout the reservoir will vary considerably. The modeling of this saturation profile is a key point and main objective in the continuation of this chapter.

When the liquid condensate (oil) saturation S_o increases above the critical oil saturation S_{oc} , the oil becomes mobile and is subject to the pressure gradient in the reservoir. Oil formed as a result of the process of liquid condensation will flow alongside the produced gas and will cause a reduced gas permeability. This results in an increased well-bore pressure drop. On the positive side, there will be a marginal overall increase in surface oil production.

The model of gas condensation in the reservoir, which is introduced here is based on an dynamic oil saturation profile $S_o(r, t)$, as being the key parameter in the model from which we may calculate the above mentioned increase in well-bore pressure drop as well as the increased yield of produced gas condensate oil. This model may be of

interest in well pressure and production forecast simulations as well as for analysis of well-pressure-test data.

In this model, we take a rather simplistic view of the reservoir, having a flat cylindrical shape where the well is located at the centre. Parameters characterizing the reservoir are presented in Table 5.4. The reservoir fluid is initially one phase gas as presented in Table 5.5. The reservoir gas is split in two phase gas and liquid using single flash calculations.

Table 5.4: Reservoir related data.

| | | | | |
|----------------------|--------|----------------------------|----------------------------|-------|
| $V_p = 4 \cdot 10^6$ | Rm^3 | $S_w = 0.2$ | $p_i = 440$ | bar |
| $r_w = 0.175$ | m | $k = 10$ | $T_i = 392$ | K |
| $r_e = 360$ | m | $C_A = 31.62$ | $c_w = 4.35 \cdot 10^{-5}$ | 1/bar |
| $h = 50$ | m | $S = 0$ | $c_R = 4.5 \cdot 10^{-5}$ | 1/bar |
| $\phi = 0.15$ | | $S_{nD} = 5 \cdot 10^{-6}$ | | |

Table 5.5: Molar composition (in %) of gas condensate reservoir fluid.

| | | | | | | | |
|-------------|--------|--------|-------|-------|-------|--------|------------|
| Compounds | N_2 | CO_2 | C_1 | C_2 | C_3 | iC_4 | nC_4 |
| Composition | 0.78 | 8.72 | 71.00 | 8.56 | 4.67 | 0.71 | 1.23 |
| Compounds | iC_5 | nC_5 | C_6 | C_7 | C_8 | C_9 | C_{10}^+ |
| Composition | 0.41 | 0.41 | 0.45 | 0.66 | 0.70 | 0.41 | 1.29 |

The simulation model considers the reservoir gas to be contained as in a tank, and all simulations are performed using analytical descriptions of the reservoir, flow processes and well production.

5.7.2 Single phase semi steady-state reservoir gas flow

In section 5.5.2 we have summarized all what we had learned about single phase gas flow. We also concluded that for all practical purposes, semi steady-state gas flow is prevailing in the reservoir. Single phase horizontal flow in porous media is well documented in the literature [4, 2], and the general solution of the diffusivity equation under semi steady-state conditions is,

$$\bar{m} - m_{bh} = \frac{q_{sc}(\mu B_g)_r}{2\pi h k} \left(\ln \frac{r_e}{r_w} - \frac{3}{4} + S + S_{nD} \right). \quad (5.90)$$

The above equation should be compared with the even more general equation, Eq. 5.84, where also a general reservoir and well location is modeled.

The equation above represents the pressure solution at constant terminal flow rate of one-phase gas in a cylindrical reservoir, where the well is at the centre. Both the mechanical skin S and the non-Darcy skin $S_{nD} = q_{sc} \cdot D$ (turbulence), are "manually" added to the equation. D is the non-Darcy factor, containing various parameters describing both the gas and the reservoir. D is indirectly both pressure and temperature dependent and will thus vary as function of time. The derivation of non-Darcy skin,

as shown above, is given in Section 5.2.2. q_{sc} is the constant terminal gas rate, m_{bh} is the bottom hole pseudo-pressure and B_g is the gas volume factor. (We are reintroducing subscript on the gas volume factor because several more volume factors are to be introduced.)

5.7.3 Simulation of one-phase reservoir gas production

The bottom hole pressure can be found explicitly when \bar{m} is known, using Eq. 5.90. Calculation of the mean pressure is based on mass balance calculations involving the real gas law and the principle of mass conservation, as seen in Chapter 4.

In the case of volumetric depletion processes, where no water production or influx of aquifer water is present, the pressure development in the reservoir (see data in Table 5.4) can be calculated. The result can be depicted as in Figure 5.19.

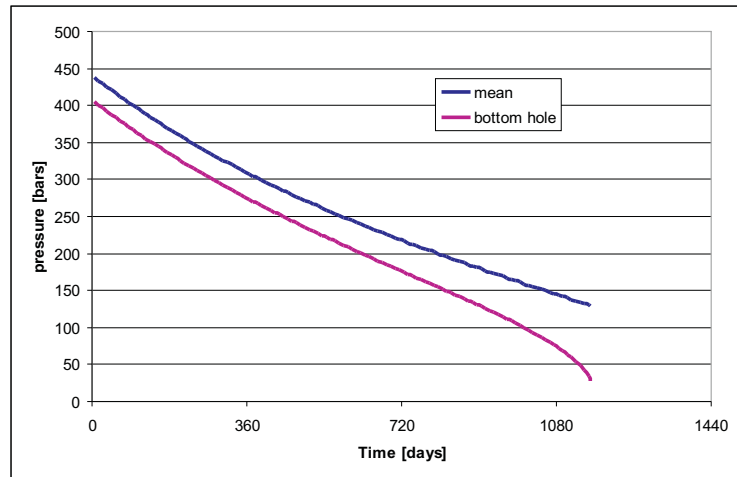


Figure 5.19: Pressure development as function of time.

The figure shows the pressure as function of time in the cases of a constant terminal rate $q_{sc} = 0.5 \cdot 10^6 \text{ Sm}^3$. The minimum bottom hole pressure is set to 10 bars.

The gas and liquid surface production are shown in Figure 5.20, where the normalized production profiles (gas/liquid produced over initial gas/liquid in-place) are shown as a function of mean reservoir pressure.

The relative production of gas and liquids are shown to be equal as long as the reservoir fluid remains in a single phase. As soon as the liquid starts to drop out of the gas, less liquid is produced to the surface and, as seen in the figure, the gas and liquid production profiles start to deviate.

In the simulation above, all liquid condensed in the reservoir is considered immobile and thus lost production. From Figure 5.19 it is seen that the effect of an increasing liquid phase is neglected and therefore does not act as a hindrance towards the flow of gas.

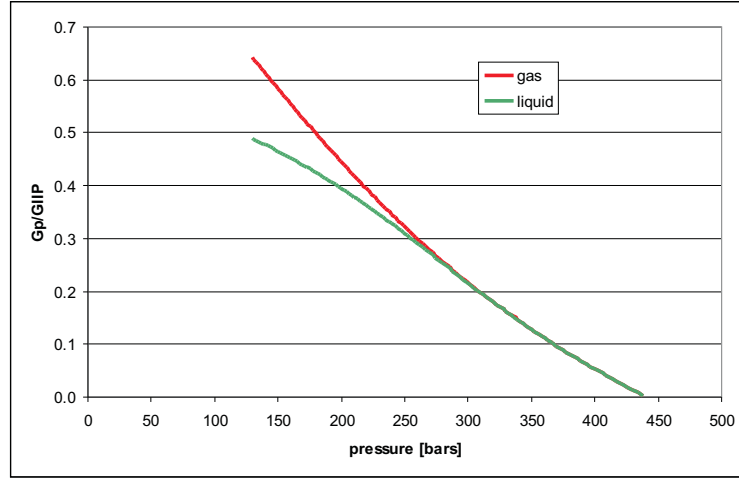


Figure 5.20: Relative gas and liquid production as a function of mean pressure.

5.8 Two phase semi steady-state oil and gas flow

A consequence of gas condensation in the reservoir is the formation of an increasing oil saturation. First in the close vicinity of the the well-bore, later radially distributed in the reservoir (see Figure 5.18). Eventually the whole reservoir will be subjected to liquid drop-out and a varying distribution of oil will occur.

The reservoir, which initially contains a single gas phase, is therefore gradually transformed to a system of two-phases: gas and oil. Oil will become mobile as the saturation increases above the critical saturation. In those parts of the reservoir where the oil saturation is greater than the critical oil saturation, ($S_o > S_{co}$), oil will start to flow and two-phase flow conditions will prevail. In two-phase flow, a competition between the phases will reduce the reservoir deliverability of gas to the surface and a decreasing bottom hole pressure will be observed (under constant terminal gas rate conditions).

In the case of two-phase gas and oil flow, Darcy's law of Eq. 5.1, is now written as,

$$\vec{u} = - \left(k_g \frac{\rho_g}{\mu_g} \nabla p_g + k_o \frac{\rho_o}{\mu_o} \nabla p_o \right), \quad (5.91)$$

where k_g and k_o are the effective permeability for gas and oil, respectively.

We now apply the following transformations

$$m = \frac{1}{\left(k_{rg} \frac{\rho_g}{\mu_g} + k_{ro} \frac{\rho_o}{\mu_o} \right)_r} \int_{p_r}^p \left(k_{rg} \frac{\rho_g}{\mu_g} + k_{ro} \frac{\rho_o}{\mu_o} \right) dp, \quad (5.92)$$

and the one to one transformation,

$$\nabla m = \frac{dm}{dp} \nabla p = \frac{k_{rg} \frac{\rho_g}{\mu_g} + k_{ro} \frac{\rho_o}{\mu_o}}{\left(k_{rg} \frac{\rho_g}{\mu_g} + k_{ro} \frac{\rho_o}{\mu_o} \right)_r} \nabla p. \quad (5.93)$$

This enables us to use Eq. 5.90, from the one-phase case, directly. The parameters k_{rg} and k_{ro} in Eqs. 5.92 and 5.93 are the relative permeability for gas and oil, respectively. From these deductions, it is to be observed that the capillary pressure P_{go} is assumed negligible.

The pressure solution, Eq. 5.90, developed for semi steady-state single gas flow case, is also valid in the two-phase case, when the substitution, Eq. 5.92, and the transformation Eq. 5.93, are applied as shown above.

If the sets of parameters; ρ_i , μ_i and k_{ri} , where $i = g, o$, were known as functions of pressure (and temperature), the bottom-hole pressure could be readily calculated using Eq. 5.90 in combination with Eq. 5.93, as already done in the single phase case.

The purpose is therefore to establish these parameters and use the equations above to calculate the bottom hole pressure drop.

5.8.1 Volume factors

A single flash separation of gas and oil to surface conditions is based on an extended "Black oil formulation" where the volume factors are defined in accordance with Figure 5.21,

$$B_g = \frac{V_g}{V_{ggn}}, \quad B_o = \frac{V_o}{V_{oon}}, \quad R_s = \frac{V_{ogn}}{V_{oon}} \quad \text{and} \quad r_s = \frac{V_{gon}}{V_{ggn}}, \quad (5.94)$$

where B_g and B_o are the volume factors for gas and oil respectively, R_s is the gas/oil solution ratio while r_s is the oil/gas solution ratio.

The volume factors defined in Eq. 5.94, are all calculated based on the gas composition in Table 5.5, using a commercial PVT-simulation program (PVTsim 11 [1]). From these calculations we find that the gas dew point pressure, $p_{dew}(gas) = 370$ bars, while the equilibrium reservoir oil bubble point, $p_{bob}(oil) = 240$ bars.

5.8.2 Density

Using the principle of material balance and the volumes as depicted in Figure 5.21, we may express the reservoir densities as functions of the surface densities,

$$\rho_g = \frac{1}{B_g} (\rho_{gn} + r_s \rho_{on}), \quad (5.95)$$

$$\rho_o = \frac{1}{B_o} (R_s \rho_{gn} + \rho_{on}), \quad (5.96)$$

where we have used the assumption that $\rho_{on}(\text{oil from gas}) = \rho_{on}(\text{oil from oil})$ and $\rho_{gn}(\text{gas from gas}) = \rho_{gn}(\text{gas from oil})$. Normal conditions, ($p_n = 1$ atm and $T_n = 288$ K) is given by the ideal gas law; $\rho_{gn} = (p_n \cdot M_g)/(R \cdot T_n)$. The oil density at normal

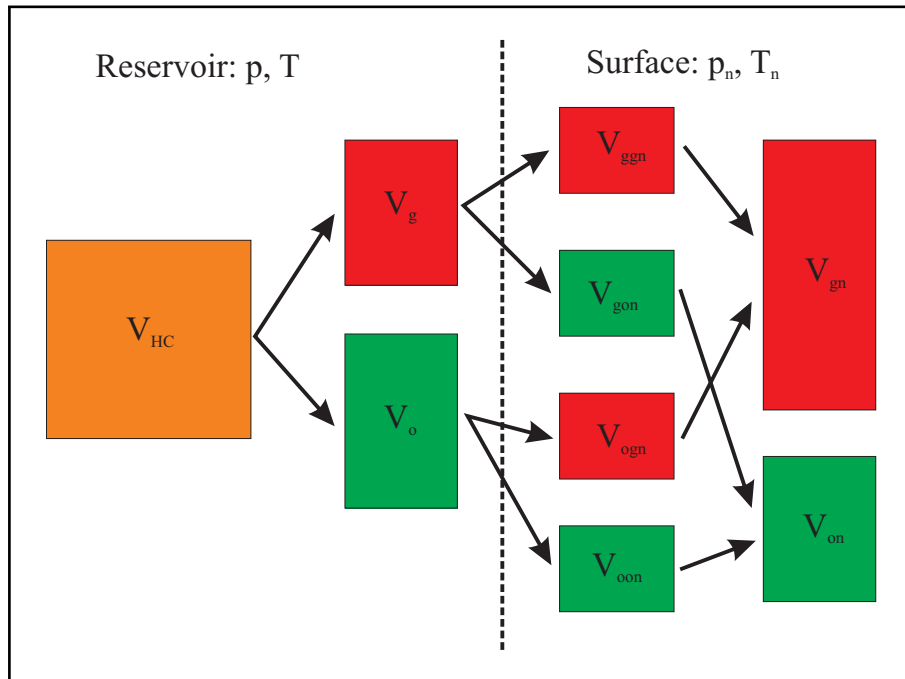


Figure 5.21: Extended black oil model: Single flash separation from reservoir to surface conditions.

condition is given by Standings formula [17]; $\rho_{on} = \rho_w(1.03 \cdot M_o)/(44.24 + M_o)$, where ρ_w is the water density and M_o is the molar weight of oil at normal conditions. (M_g is the molar weight of gas at normal conditions.)

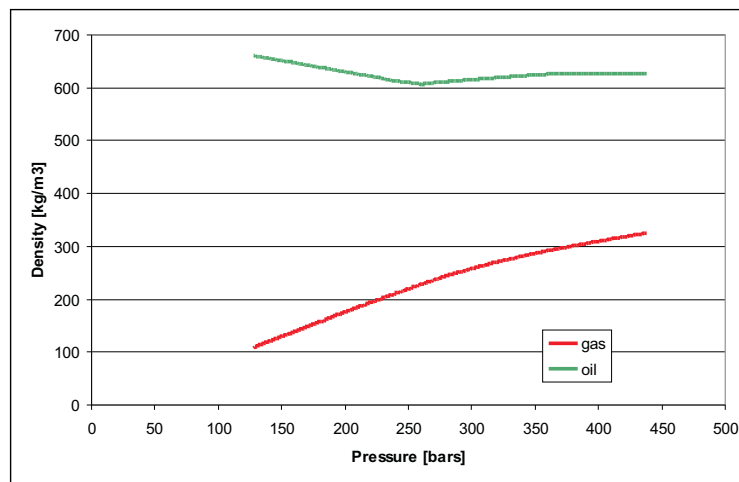


Figure 5.22: Gas and oil densities at reservoir conditions.

Figure 5.22 shows the densities as presented in Eqs. 5.95 and 5.96. The densities for gas and oil at natural conditions are 1.1 and 796.5 kg/m^3 , respectively. Notice that the oil density is defined in the whole pressure range, while the formation of reservoir

oil starts at the gas dew-point pressure ($p_{dew} = 370 \text{ bars}$) and that the bubble-point of the same oil is calculated to be at about 240 bars.

5.8.3 Viscosity

The gas and oil viscosities used in these calculations have been partially derived through PVT simulations and partially modeled as functions taken from the literature.

A formula for gas viscosity is proposed by Lee et al. [15], and previously presented in Chapter 3, Section 3.5.5.

$$\mu_g = K \cdot e^{X\rho_g^Y}, \quad (5.97)$$

where the parameters $K = (9.4 + 0.02 \cdot M_g)T^{1.5}/(209 + 19M_g + T)$, $X = 3.5 + 986/T + 0.01M_g$ and $Y = 2.4 - 0.2X$. M_g , T and ρ_g are average molecular mass, reservoir temperature and gas density, respectively. The gas viscosities are compared in Figure 5.23. In the figure is Eq. 5.97 compared with the PVT-simulations. A close overlap between the two curves is observed in the figure.

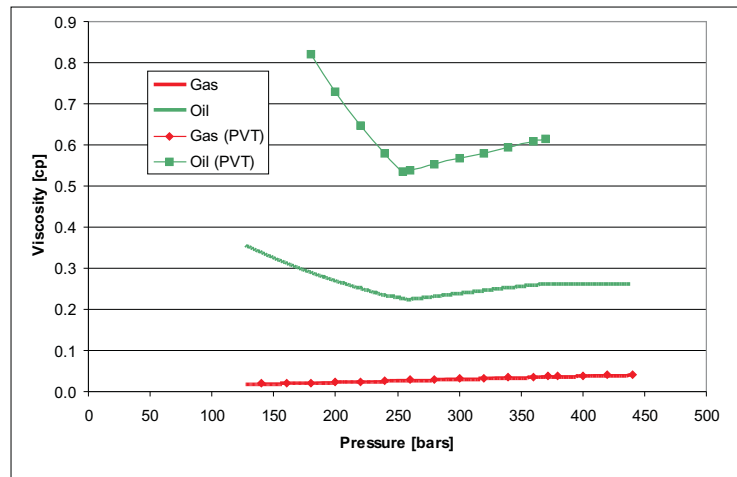


Figure 5.23: Gas and oil viscosities.

The reservoir oil viscosity, on the other hand, does not compare equally well to the PVT-simulation, as can be seen from Figure 5.23. The oil viscosity presented in the figure is proposed by Abu-Kanu and Al-Morhan [21] and written as follows,

$$\ln(\mu_o) = -2.65 + 8.48\rho_o^4 \quad (5.98)$$

The viscosity in Eq. 5.98, is said to correlate well with saturated oil densities and is therefore chosen as the preferred correlation over the simulated values, which seem to be slightly too "dramatic".

5.8.4 Relative permeability

The formal treatment of gas and oil relative permeability given here, follows the same lines as presented by Fevang and Whitson in their well received article [9] from 1996.

Based on the separation of volumes as defined in Figure 5.21, the definition of volume factors in Eq. 5.94 and a dynamical representation of reservoir flow by Darcy's law - a ratio of relative permeability can be written,

$$\frac{k_{rg}}{k_{ro}} = \frac{R_p - R_s \mu_g B_g}{1 - R_p r_s \mu_o B_o}, \quad (5.99)$$

where $R_p = V_{gn}/V_{on}$, is the GOR, i.e. the volume of gas produced over the volume of oil produced, at normal (surface) conditions.

Above the dew-point pressure ($p > p_{dew}$), all oil is produced from the reservoir gas, i.e. $R_p = 1/r_s$ and the relative gas permeability is defined as equal to unity ($k_{rg} = 1$ and $k_{ro} = 0$). When the pressure is lowered below the dew-point pressure, $R_p < 1/r_s$ and $k_{rg} < 1$ and the ratio in Eq. 5.99 is well defined and finite.

Based on empirical relations describing experimental relative permeability, Brooks and Cory (1964) proposed a set of equations defining the wetting and non-wetting relative permeability as functions of effective saturations. A parameter λ describes the pore size distribution. A comprehensive description of this model can be found in Dullien [7]. Based on these equations, it is straight forward to define a functional relationship between k_{rg} and the ratio of relative permeability, as defined in Eq. 5.99.

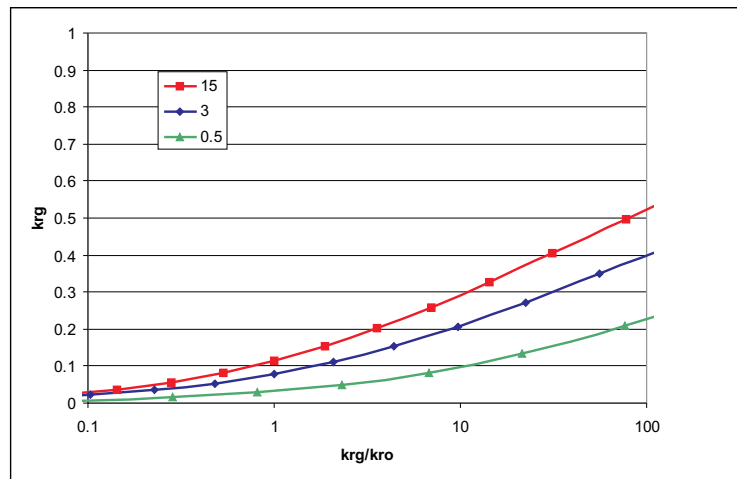


Figure 5.24: Functional relationship $k_{rg}(k_{rg}/k_{ro})$ based on empirical relations.

Figure 5.24 shows the function $k_{rg}(k_{rg}/k_{ro})$ for three choices of λ . In all calculations presented here, $\lambda = 15$ is used. The pore size distribution index is a number that relates the effective saturation to the capillary pressure between wetting and non-wetting fluids, as pointed out by Dullien.

5.9 Modeling production GOR

The relative gas and oil permeabilities can be calculated by using Eq. 5.99 in combination with the functional relationship, presented in Figure 5.24. All parameters in Eq. 5.99 are accounted for, except for the production GOR; R_p .

5.9.1 A two-phase reservoir production model

In a single phase reservoir production model, all liquid condensate drop-out is assumed to remain in the reservoir as an immobile liquid saturation of practically no hinderance to radial gas flow. The liquid saturation, $S_o(r, t)$ is everywhere and at all times considered to be less than the critical saturation S_{co} and thus, all oil in the reservoir is considered lost production.

However in reality the liquid saturation is radially increasing as the average reservoir pressure is declining and sooner or later the saturation of oil will reach the level of critical saturation where oil will start to flow. As a result of general pressure decline in the reservoir, a bank of oil will develop from the well-bore and radially expand into the reservoir. This is a continuous process.

The liquid condensate saturation is therefore a function of radial position. Since the pressure profile is increasing radially (seen from the well), it is safe to assume that the liquid saturation must decrease radially. On the other hand, since the average (mean) reservoir pressure is declining during normal depletion, the overall liquid saturation in the reservoir is generally increasing. A combination of these two effects points towards a liquid saturation which is decreasing radially as it expands radially in to the reservoir. All excessive oil, above the critical saturation S_{co} , is subjected to radial flow in parallel with the gas flow and therefore removed from the reservoir.

In addition, one may expect a decreasing critical saturation level in the region where the saturation already has reached its critical level, due to the fact that gas flow velocity, in particular in the vicinity of the well, will increase as the mean reservoir pressure is decreasing. The flow of gas and oil is generally parallel, even though the fluids are located in different parts of the pore system or pore channels. The flow velocity, however, is quite different as the gas is flowing much faster than the oil [18].

The formation of an oil region that develops into the reservoir will eventually result in:

1. Production of additional oil which otherwise would be considered lost from production.
2. A two phase flow situation in the reservoir, especially in the vicinity of the well-bore.
3. Observation of increased pressure drop in the well-bore.

The saturation profile $S_o(r, t)$ may vary considerably during the production lifetime of the reservoir. This saturation function will relate to many of the parameters in play, such as: gas flow rate, PVT-relationships, reservoir wetting characteristics and the type of prevailing flow regime.

The formation of oil, as liquid dropout, is controlled by pressure and temperature, as explained above. The residing oil saturation will be subjected to the various forces acting in the reservoir and as such also to the relative strength of these forces. The interaction between gas and oil in the reservoir and the reservoir itself can possibly be broken down into a study of the relative strength between basic forces such as; viscous, capillary, gravitational and inertial forces. In principle it should be possible to relate the saturation profile $S_o(r, t)$ to the competition between the various forces acting inside the

reservoir pore system, as indicated by Ursin [18]. This would certainly be an interesting project for further study. However, here we chose a more simplistic approach in defining the saturation profile, $S_o(r, t)$.

5.9.2 Reservoir oil saturation profile

The saturation profile to be presented below represents a crude simplification of the ideas related to the near well gas condensing process, as presented by Ursin [19]. A proper assessment of the distribution of condensed oil in the reservoir would need to involve petro-physical considerations, represented by all aspects of fluid flow, reservoir - and fluid characteristics.

The reasoning presented in the previous section, relates oil formation in the reservoir to the existence of a saturation profile. Accepting the existence of such a saturation model, it then turns out to be straight forward to construct it. The model may be split into three radially defined regions following the same approach as discussed by Fevang and Whitson [9]. The proposed model should therefore be considered as an attempt to quantify the physical observation described in the literature about the three zone model;

Region 1 is the region next to the well-bore, starting at a radial position (r_w). This region is characterized by a radially increasing oil saturation. The oil saturation will increase until its critical saturation is reached at a position r_{co} . All oil in excess of S_{co} is considered mobile and will be produced. Oil will flow in this region but not in the other regions. All oil condensed in this region will therefore either remain as part of the critical oil saturation or be transported to the well-bore. There is reason to believe that the oil saturation will decrease towards the well-bore since drag-forces are acting on the oil in the close vicinity of the well-bore. Another term describing this phenomena which is frequently used in the literature, [3, 10], is "viscous stripping".

Region 2 is an intermediate region where the oil saturation is building up radially. This region is limited by r_{co} (Region 1) and the radial position in the reservoir where the first drop of liquid condensate occurs (r_{dew}). This position in the reservoir is defined as the radial position where the pressure equals the dew-point pressure. There is no flow of oil in Region 2. The only effect on gas flow performance is the reduced space for gas flow due to the build up of an oil saturation.

Region 3 is the single gas phase flow region, where $S_o = 0$. This region is reaching out to the reservoir boundary, r_e .

The main characteristics of a saturation model, as described above, are the existence of an oil saturation that is reasonably constant out to a certain radial position and thereafter steadily decreasing. The following saturation model, meets these requirements.

$$S_o(r) = \begin{cases} S_{co} \left(\frac{r - r_w}{r_{co} - r_w} \right)^{L1} & r_w \leq r < r_{co}, \\ S_{co} \left(\frac{r_{dew} - r}{r_{dew} - r_{co}} \right)^{L2} & r_{co} \leq r < r_{dew}, \\ 0 & r_{dew} \leq r < r_e. \end{cases} \quad (5.100)$$

The saturation model defined by Eq. 5.100, is an attempt to model the many processes that are of importance in the formation of gas condensation in the reservoir. Many other models may exist. Depending on the degree of knowledge about the reservoir and fluids involved, quite sophisticated models could be designed.

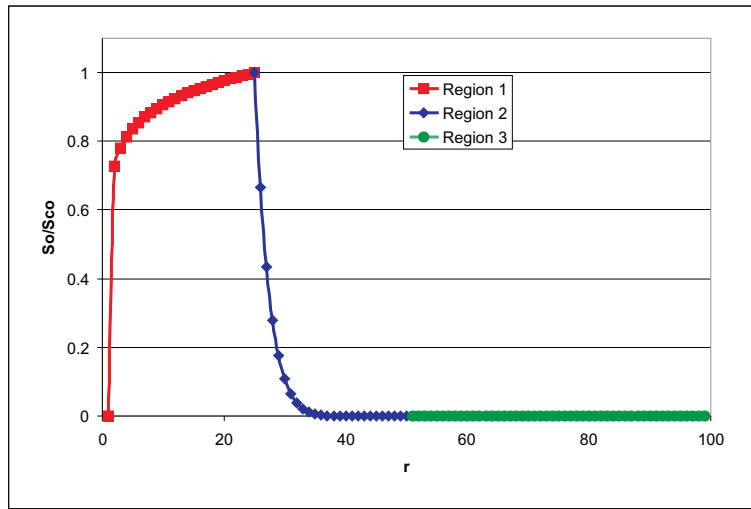


Figure 5.25: Saturation profile model; $S_o(r)/S_{co}$.

Figure 5.25 represents the saturation model as defined by Eq. 5.100. In this example the following parameters were selected: $r_w = 1$, $r_{co} = 25$, $r_{dew} = 50$ and $r_e = 100$. The set of exponents, $L1$ and $L2$ are 0.1 and 10, respectively. Figure 5.25 depicts the radial profile of oil saturation in the reservoir, as explained above. The volume of oil confined within this saturation profile is the volume of critical oil, contained in the reservoir. This volume is found simply by integration of Eq. 5.100 over the full radius range. In the case of cylindrical symmetry, we get;

$$V_{co} = 2\pi h\phi(1 - S_w) \left[\int_{r_w}^{r_{co}} r S_o(r) dr + \int_{r_{co}}^{r_{dew}} r S_o(r) dr \right], \quad (5.101)$$

which after integration gives,

$$V_{co} = 2\pi h\phi(1 - S_w) S_{co} \left[\frac{r_{co} - r_w}{L1 + 1} \left(r_{co} - \frac{r_{co} - r_w}{L1 + 2} \right) + \frac{r_{dew} - r_{co}}{L2 + 1} \left(r_{co} + \frac{r_{dew} - r_{co}}{L2 + 2} \right) \right] \quad (5.102)$$

V_{co} is the irreducible volume of oil that will remain in the reservoir, i.e. the volume of immobile oil. All additional oil condensed in the reservoir will be produced. Notice that in Eq. 5.102, r_w and r_e are constants, while r_{co} and r_{dew} are both pressure dependent.

The radial positions r_{co} and r_{dew} , do both initially start at the position r_w . The speed by which r_{co} and r_{dew} progress into the reservoir would be quite different. When semi-steady-state analysis is used, we may derived a functional relationship between a radial position in the reservoir and the corresponding (pseudo) pressure at that position.

Derivation: Radial pressure development

Following semi-steady-state analysis, i.e. as presented by Dake, the following formulas are solutions of the radial diffusivity equation for a cylindrical reservoir with the well at the centre.

$$m(r) = m(r_w) + \frac{q_{sc}(\mu_g B_g)_r}{2\pi h k} \left(\ln \frac{r}{r_w} - \frac{1}{2} \frac{r^2 - r_w^2}{r_e^2 - r_w^2} \right) \quad (5.103)$$

$$\bar{m} = m(r_w) + \frac{q_{sc}(\mu_g B_g)_r}{2\pi h k} \left(\ln \frac{r}{r_w} - \frac{3}{4} \right) \quad (5.104)$$

Substituting $m(r_w)$ with the pseudo bottom-hole pressure m_{bh} is readily done, simply by adding the skinfactor S to the ln-term in the equations above. Restricting to radial positions in the near and far vicinity of the wellbore, where r and r_w are very much less than r_e , we may get by combining Eqs. 5.103 and 5.104;

$$\frac{m(p) - m_{bh}}{\bar{m} - m_{bh}} \frac{\ln r_e/r_w - 3/4 + S}{\ln r_e/r_w} = \frac{\ln r/r_w + S}{\ln r_e/r_w}, \quad (5.105)$$

where $m(p)$ is the pseudopressure at positions $r(p)$ in the reservoir. p is here considered a fixed pressure value in time. The position $r(p)$ is then defined,

$$r(p) = r_w \cdot e^{-S} \left(\frac{r_e}{r_w} \right)^{\frac{m(p) - m_{bh}}{\bar{m} - m_{bh}} \frac{\ln r_e/r_w - 3/4 + S}{\ln r_e/r_w}}. \quad (5.106)$$

From Eq. 5.106, we may define the radial position in the reservoir where the oil saturation has its maximum value, by r_{oc} and the position where the first drops of oil are formed, as r_{dew} . Assuming zero skin, we get;

$$r_{oc} = r_w \left(\frac{r_e}{r_w} \right)^{\frac{m(p_{oc}) - m_{bh}}{\bar{m} - m_{bh}} \frac{\ln r_e/r_w - 3/4}{\ln r_e/r_w}} \quad \text{and} \quad (5.107)$$

$$r_{dew} = r_w \left(\frac{r_e}{r_w} \right)^{\frac{m(p_{dew}) - m_{bh}}{\bar{m} - m_{bh}} \frac{\ln r_e/r_w - 3/4}{\ln r_e/r_w}}, \quad (5.108)$$

where the pressures p_{oc} and p_{dew} represents the bubble point pressure of the formation-oil in the reservoir and the gas condensate dew point pressure, respectively.

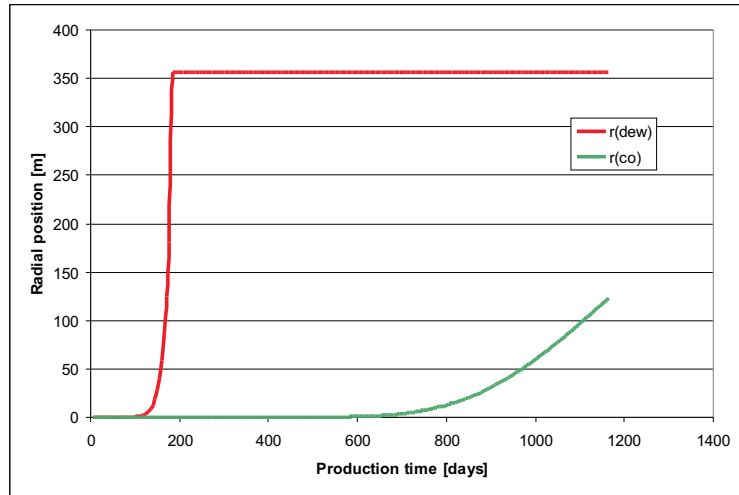


Figure 5.26: Radial position as a function of mean reservoir pressure.

Figure 5.26 shows the two radial positions as a function of production time. The outer boundary of Region 2, defined by r_{dew} , seems to travel quite fast towards the reservoir peripheral. This observation is similar to observing that the mean pseudo pressure \bar{m} in Eq. 5.108, quickly declines towards the pseudo dew point pressure $m(p_{dew})$, leaving the exponent in Eq. 5.108 close to unity.

The radial position r_{oc} , that defines the division between Region 1 and 2, is in these calculations defined by the bubble point pressure of the condensed oil. In the work by Fevang and Whitson [9], this pressure point was defined as the dewpoint of the producing wellstream, where the argument was related to the observation of a constant flowing composition (GOR) within Region 1. By associating the regional division to the bubble point pressure of condensed oil we are accepting an advance of Region 1 that would be somewhat slower than otherwise observed by using the dewpoint pressure of the producing wellstream as a reference. Another practical point is that the bubble point pressure is more readily accessible in our cases, than the dewpoint pressure of the producing wellstream. A third point is related to the viscosity change in the oil as the pressure is lowered below the bubble point pressure. This change in oil viscosity acts in the direction to immobilizes the oil and thereby stabilizes the saturation profile in Region 1.

Comparing Eq. 5.107 with Eq. 5.108 and r_{oc} with r_{dew} , it is obvious that r_{oc} advances much more slowly in the reservoir compared to r_{dew} , since the bubble point pressure is considerably lower than the dewpoint pressure.

The reservoir oil saturation profile is depicted in Figure 5.27. On the z-axis a normalized oil saturation is presented as a function of a normalized radial position r/r_e (x-axis). Various profiles are presented with increasing production time steps (y-axis). In the first 100 days, no oil is condensed. After that time period saturation of liquid drop-out is seen to increase above the zero level (when the mean pressure drops below the dew-point pressure). The region of reservoir oil (Region 2 in Figure 5.25) is gradually building up and then advancing into the reservoir. As the saturation reaches

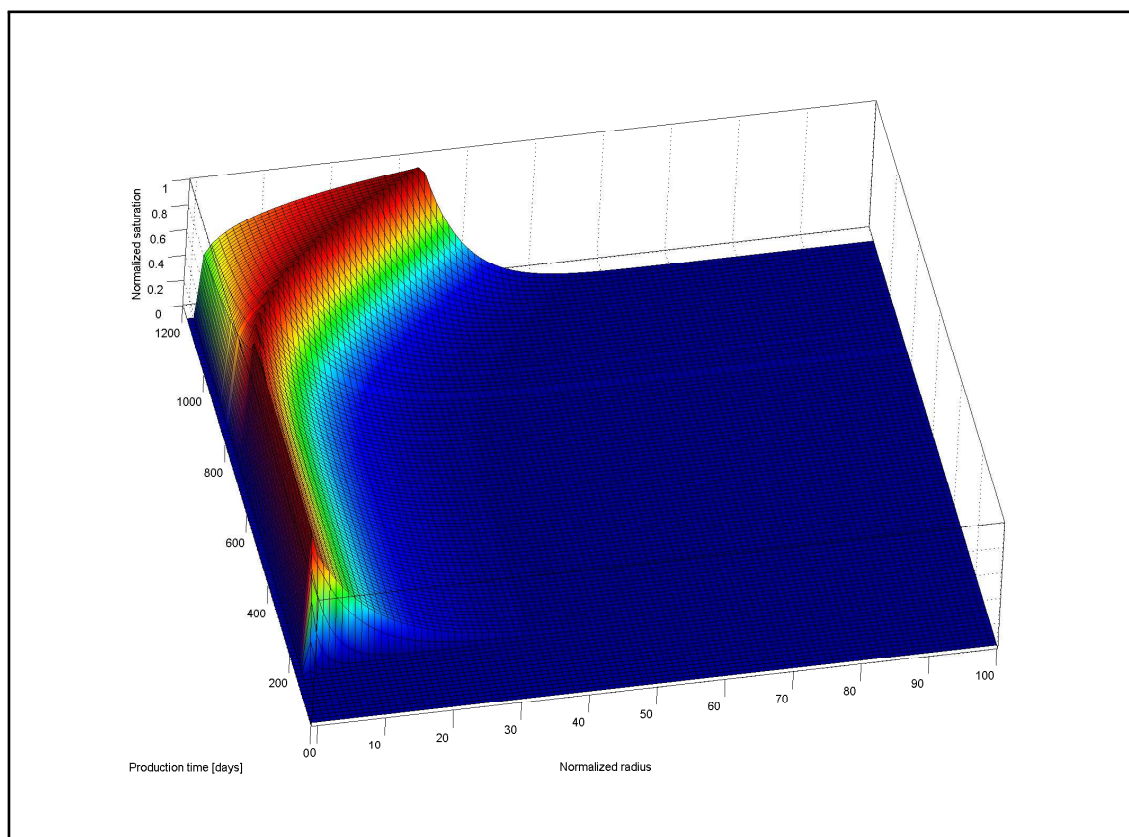


Figure 5.27: Oil saturation in the reservoir as a function of normalised radius position for different production time steps , where $L1 = 0.1$, $L2 = 10$ and $S_{co} = 0.6$.

the critical saturation (normalised saturation equals 1), all additional formation of oil in the reservoir is produced oil to the surface. This process continues until Region 1 is formed (at about 600 days) and quite a while thereafter.

The saturation profile in Figure 5.27 is primarily defined by the pressure development in the reservoir, as seen from Eqs. 5.107 and 5.108. The volume of oil contained in the reservoir is thus pressure dependent. The two phase flow is therefore related to the balance between the oil present in the reservoir, as shown in Figure 5.27 and the process of liquid condensation. Both processes are compared at each single time step. The two-phase flow time-period will therefore come to a halt when the increase in accessible volume under the saturation profile in Figure 5.27 becomes larger than the liquid drop-out during that same time period.

5.9.3 Surface production

Natural depletion of gas-condensate reservoirs can be described using a tank-model, where the hydrocarbon volume V_{HC} could be corrected for various non-volumetric effects; such as reservoir - and initial water expansion, water production and aquifer influx.

The described model is in principle identical to the well known dry (or wet) gas

model. In the gas condensate case, an additional term is added to include the effect of liquid drop-out in the reservoir. The material balance calculation of gas condensate is therefore performed by solving the following implicit equation, Eq. 4.23 in Chapter 4,

$$\frac{G_p}{G_i} = \left(1 - \frac{Z_{2i} p V_{HC}}{Z_2 p_i V_{HCi}}\right) \left(\frac{1 + R_{MLGi}}{1 + R_{MLGp}}\right). \quad (5.109)$$

In the case of constant terminal rate, the relative dry gas production G_p/G_i is pre-defined. The molar liquid-gas ratio R_{MLGp} is defined as the cumulative molar phase split and is an integral of the regular molar phase split R_{MLG} , which again is directly found from PVT-simulations. Eq. 5.109 is implicit since both the z-factor $Z_2(p)$ and the molar phase split $R_{MLG}(p)$, as well as the hydrocarbon volume $V_{HC}(p)$ are pressure dependent.

The liquid production G_{Lp} is then defined by,

$$\frac{G_{Lp}}{G_{Li}} = \frac{G_p R_{MLGp}}{G_i R_{MLGi}}, \quad (5.110)$$

where the relative production of liquid is proportional to the relative production of dry gas until liquid drop out starts, when $R_{MLGp} < R_{MLGi}$. The relative production of gas and liquid, shown in Figure 5.20, are the results of calculations using Eqs. 5.109 and 5.110.

5.9.4 Additional surface oil production

In the process of natural depletion as described above, some oil will remain in the reservoir (and is traditionally considered as lost production). The oil volume that remains in the reservoir V_o (in reservoir units), is derived as a function of dynamic flow parameters.

Derivation: Cumulative volume oil produced in the reservoir

The liquid drop out of oil is initially considered to remain in the reservoir during the process of natural gas production. In order to quantitatively define this volume, reference is made to Figure 5.21.

The following steps lead to the derivation of a formula for the volume of reservoir oil due to liquid condensation.

1. Oil produced to the surface is $V_{gon} = r_s V_{ggn}$, where V_{ggn} is the cumulative volume of gas produced.
2. Oil not produced to the surface is the difference between the initial phase split and and the phase split at a particular pressure, i.e.

$$\Delta V_{gon} = (r_{si} - r_s) V_{ggn}.$$

3. Mass of oil not produced to the surface is therefore

$$\Delta M_o = \rho_{on} \Delta V_{gon} = \rho_{on} (r_{si} - r_s) V_{ggn}.$$

4. Mass of oil not produced to the surface that remains in the reservoir,

$$\Delta M_o = \rho_o V_o,$$

where ρ_o and V_o are the density of oil and the volume of oil in the reservoir.

5. The volume of oil in the reservoir is therefore,

$$V_o = \rho_{on} / \rho_o (r_{si} - r_s) V_{ggn}.$$

Using the definition of r_s in Eq. 5.94 and the formula for relative liquid production, Eq. 5.110, we may derive an expression for V_o , containing the dynamic parameters of gas and liquid production. The volume of oil that remains in the reservoir as a result of gas condensation, is therefore written,

$$V_o = \frac{\rho_{on}}{\rho_o} \frac{R_{MLGi} - R_{MLGp}}{R_{MLGi}} \frac{G_p}{G_i} G_{Li}. \quad (5.111)$$

Some of this oil will be produced to the surface when the saturation in Region 1 exceeds the critical saturation S_{co} , and will therefore not be stored in the reservoir.

The produced reservoir oil ΔV_o , is associated with the volume of condensed oil in the reservoir (Eq. 5.111) and the volume of irreducible oil that will remain in the reservoir (Eq. 5.102),

$$\Delta V_o(t_i) = V_o(t_i) - V_{co}(t_i) - \sum_{j=1}^{i-1} \Delta V_o(t_j), \quad (5.112)$$

where t_i is a time step function.

The basic idea behind the formula presented in Eq. 5.112, is that all oil condensed in the reservoir as part of the normal depletion process and in excess of irreducible oil present, will be produced and that this process is continuous. Eq. 5.112 is indirectly defining the additional reservoir oil flow rate, as $q_o = \Delta V_o(t_i) / (t_i - t_{i-1})$.

5.9.5 The production GOR factor; R_p

The part of reservoir oil that is produced, ΔV_o , will at the surface split into an oil and a gas part. From Eq. 5.94 and Figure 5.21, the corresponding surface volumes are defined,

$$\Delta V_{ogn} = \frac{R_s}{B_o} \Delta V_o \quad \text{and} \quad \Delta V_{oon} = \frac{1}{B_o} \Delta V_o. \quad (5.113)$$

The production GOR, R_p which is defined as the ratio of total produced gas and oil, is therefore defined as,

$$R_p = \frac{G_p + \Delta V_{ogn}}{G_{Lp} + \Delta V_{oon}}, \quad (5.114)$$

where the cumulative productions G_p and G_{Lp} are defined by Eqs. 5.109 and 5.110, respectively.

Finding R_p , is the final step in the process of calculating the relative permeabilities k_{rg} and k_{ro} , defined by Eq. 5.99 and Figure 5.24.

5.10 Simulation of two phase semi steady-state flow

With the derivation of production GOR, in Eq. 5.114, all parameters needed are readily presented. The pressure calculation may follow the same procedure outlined in the case of single gas reservoir production and simulation results are presented similarly to Figures 5.19 and 5.20.

5.10.1 Pressure and production developments

In all simulations presented hereafter a pore size distribution index, $\lambda = 15$, has been chosen. This relates a "maximum" variation of the gas relative permeability k_{rg} to the corresponding change in the ratio k_{rg}/k_{ro} , of the three cases shown in Figure 5.24.

The saturation profile is characterized by the parameters $L1 = 0.1$, $L2 = 10$ and $S_{co} = 0.6$. All three parameters are related to the shape and form of the oil saturation profile and defined in Eq. 5.102.

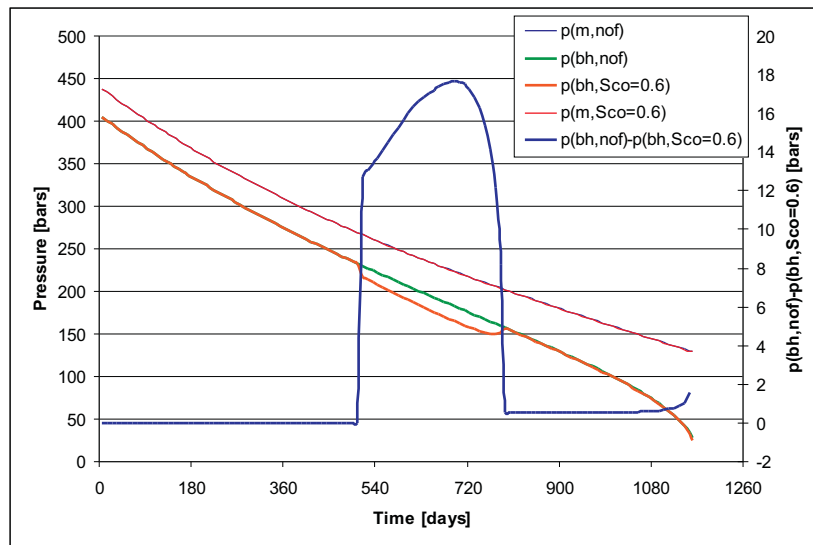


Figure 5.28: Pressure profiles; mean pressure and bottom hole pressure for single and two phase flow conditions.

Figure 5.28 shows the mean pressure ($p(m)$) and the bottom hole pressures ($p(bh)$). The result of two cases of "no oil flow" (nof), i.e. single gas flow is compared to a case of two phase flow. The figure shows that the bottom hole pressure experiences an additional pressure drop shortly after 500 days, which lasts until about 800 days. This pressure difference relates to the right y-axis. The maximum pressure difference is about 18 bars. When the average liquid saturation exceeds the level of 0.6, oil starts to

flow and a sudden drop in the bottom hole pressure is observed. The pressure difference $p_{bh}(nof) - p_{bh}(S_{co} = 0.6)$ passes through a maximum before the two-phase period ends. This happens when the volume of additional condensed oil becomes less than the increase in accessible pore space. The dynamics is controlled by the radial movement of the oil saturation that moves further and further into the reservoir. Notice that when the volume limited by Region 1 (in Figure 5.25) increases more than the additional liquid drop out, the flow of oil halts and single phase flow conditions prevail. The radial increase in Region 1 can also be recognized in Figure 5.27, where the restart of single phase flow is vaguely indicated by a stripe at about 800 days.

The effect of increased bottom hole pressure drop in the two phase flow period should in principle have resulted in an additional pressure decline in the mean reservoir pressure. In order to sustain the extra pressure drop due to two-phase gas flow, pressure energy should have been subtracted from the mean pressure energy in the reservoir. However, the functional relation between the bottom hole pressure and the mean reservoir pressure is weak in this model. Thus this energy loss is not properly reflected in the equation of material balance. As can be seen from Eq. 5.109 the mean pressure is merely a function of material balance calculations and therefore does not reflect an additional loss of reservoir energy related to the dynamics of reservoir flow behaviour.

The only functional relationship between the mean pressure and additional flow of oil in the reservoir is associated with the two-phase gas compressibility factor Z_2 . When parts of the condensed oil become mobile, and are transported to the surface, less oil will remain in the reservoir and consequently more volume is available to the residual gas. A correction to the gas compressibility factor can be introduced. The new gas compressibility factor follows the same line of thought as in the deduction of the two-phase gas compressibility factor, as presented in the SPE Monograph by Whitson and Brule [21].

Deduction: Modification of two-phase gas compressibility factor

In a CVD-experiment, the volume effect of liquid drop-out (in a gas-condensate reservoir gas) is incorporated in the material balance equation by introducing a Z_2 -factor. This allows the dry gas material balance equation, associating reservoir pressure and production, to be used in the gas condensate case;

$$\frac{p}{Z_2} = \frac{p_i}{Z_{2i}} \left(1 - \frac{n_p}{n_i} \right).$$

The principal purpose of the Z_2 -factor is to secure linearity in the equation above, as described in Monolog. Thus, several effects are incorporated in this factor; such as gas composition changes, phase transition characteristic and phase volume changes.

At a constant terminal gas rate, all additional oil produced due to reservoir two-phase flow in the reservoir, will result in an additional withdrawal ΔV_o , from the reservoir oil volume which is otherwise assumed lost production. This volume of oil produced, will inevitably increase the available volume accessible for reservoir gas.

If V_{gi} is the volume of gas that is used in the material balance equation, then $V_g = V_{gi} + \Delta V_o$ is the volume of gas now accessible in the reservoir.

Using the real gas law, we may state the situation at initial conditions, when the production $n_p = 0$,

$$p_i V_{gi} = Z_{2i} n_i RT,$$

where V_{gi} is the accessible gas volume, before any gas condensation has taken place.

After a production of n_p , we find,

$$p V_g = Z_2 (n_i - n_p) RT,$$

where V_g reflects the fact that more reservoir space is available to gas than the normal depletion process would infer.

Combining the two equations above gives,

$$\frac{p}{Z_2} \frac{V_g}{V_{gi}} = \frac{p_i}{Z_{2i}} \left(1 - \frac{n_p}{n_i} \right).$$

Since there are no changes in the composition of the gas due to the gas volume change in the reservoir, a redefinition of the two-phase compressibility factor Z_2^* is advised. We may define a correction to the two-phase compressibility factor by;

$$Z_2^* = Z_2 \frac{V_{gi}}{V_g} = Z_2 \left(1 + \frac{\Delta V_o}{V_{gi}} \right)^{-1}.$$

The new compressibility factor is therefore,

$$Z_2^* = Z_2 \left(1 + \frac{\Delta V_o}{V_{HCi}} \right)^{-1}, \quad (5.115)$$

where ΔV_o is the additional withdrawal of oil from the reservoir, due to two-phase flow.

Introducing Z_2^* into Eq. 5.109 gives a marginal change in the mean pressure, as shown in Figure 5.29. The effect of additional oil production from condensed oil is an increased pressure drop in the reservoir. This is seen in Figure 5.29 as an increased pressure difference $\bar{p}(nof) - \bar{p}(S_{co} = 0.6)$, over the period where two-phase flow is active. However, the pressure modification is marginal and of minor practical importance.

The production profiles are shown in Figure 5.30. Additional oil is produced in the two phase flow case (Region 1), and an increase in relative production of surface oil of about 1.7% is observed. The time period where extra oil is produced, corresponds to the period in Figure 5.28 where the bottom hole pressure experiences an extra down-dip. The legend is related to the definition of volume factors, as shown in Figure 5.21.

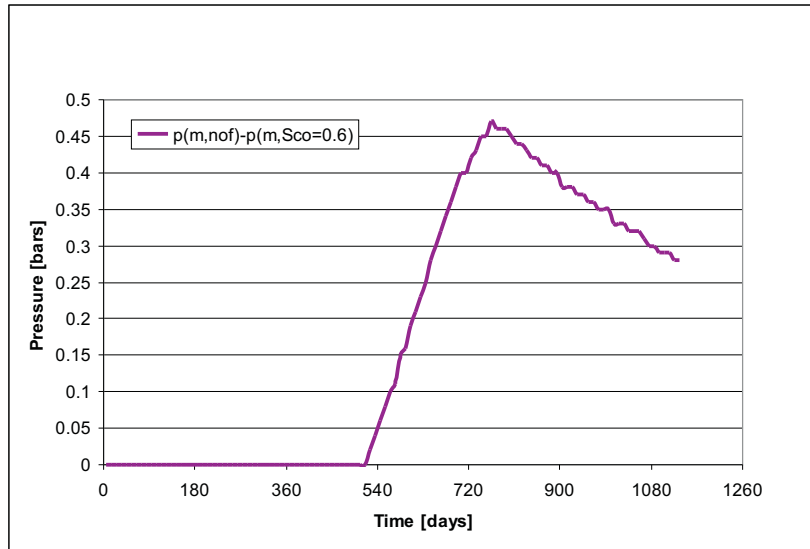
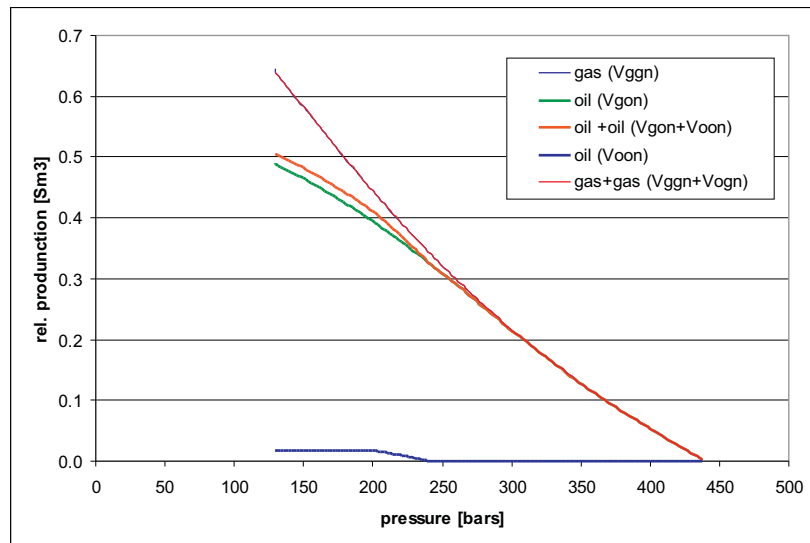
Figure 5.29: Pressure difference $\bar{p}(nof) - \bar{p}(S_{co} = 0.6)$ 

Figure 5.30: Relative production profiles in the two cases of "no oil flow" and in the case of two phase reservoir flow.

5.10.2 Effect of critical oil saturation; S_{co}

When the critical oil saturation is generally low in the reservoir, a minor fraction of the condensed liquid will remain in the reservoir and all excess liquid drop outs will flow towards the well. In the limiting case when $S_{co} \simeq 0$, all condensed liquid will be produced and the gas reservoir behaves as a wet-gas reservoir. S_{co} therefore defines the storing capacity of liquid condensate in Regions 1 and 2 in the reservoir.

The reservoir capacity for liquid drop outs is met at an early time in the production

period when S_{co} is low. In these cases an early start-up of the two-phase flow period is expected. During this period the reservoir two-phase flow (in Region 1) leads to an extra pressure drop in the bottom-hole pressure.

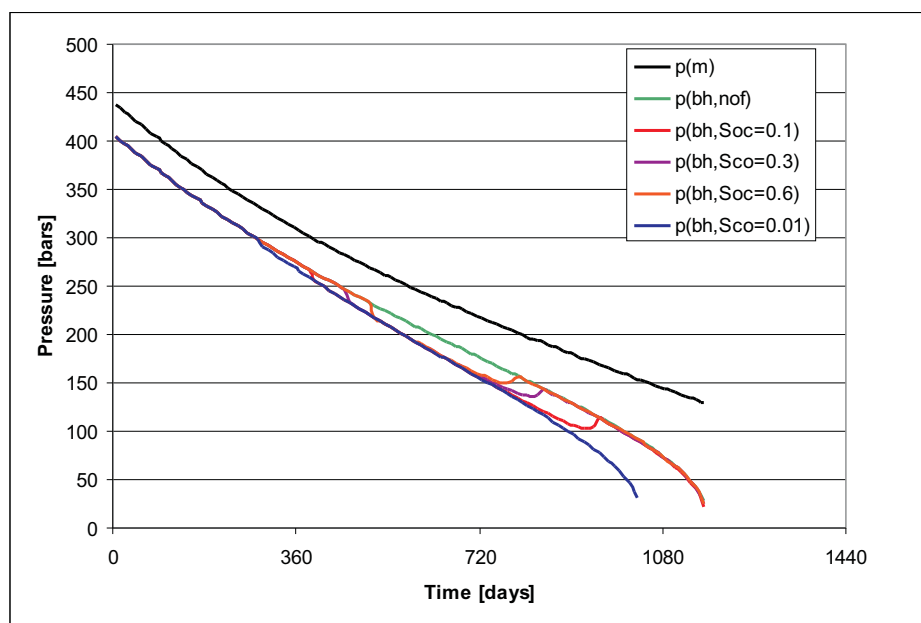


Figure 5.31: The figure shows the bottom-hole pressure for 4 cases of varying critical oil saturation.

Figure 5.31 shows the bottom-hole pressure for 4 cases of decreasing critical saturation, S_{co} ; 0.6, 0.3, 0.1 and 0.01. For comparison, the mean- ($p(m)$) and no oil flow ($p(bh,nof)$) pressure developments are also shown in the figure.

In the limiting case, when $S_{co} = 0.01$, the two-phase period is continuous from production onset to the time when the minimum bottom hole pressure is reached ($p_{MBHP} = 10 \text{ bars}$). This happens after only 1030 days. Due to the two-phase flow and the increased bottom-hole pressure drop, the production period is shortened by about 11% compared to the "no oil flow" case, which is a considerable shortening of the gas production period.

In the cases when S_{co} is 0.1, 0.3 and 0.6, the two-phase period is of decreasing duration. In all three cases the bottom-hole pressure is recovering to "nof" levels as soon as the two-phase period is ended (in Region 1). In reality however, one would expect the bottom-hole pressure in these cases not to completely recover from the additional pressure drop. The reason why this is not seen in the figure is related to the very weak coupling between the mean pressure and the bottom-hole, as mentioned above. In these cases one would have expected the abandonment pressure point to be placed at times somewhere between the limiting case where ($S_{co} = 0.01$) and the "nof" case.

Figure 5.32 shows the pressure difference $p_{bh}(nof) - p_{bh}$ for the four cases of $S_{co} = 0.1, 0.3, 0.6$ and 0.01. What is particularly evident in three of the cases is that after the end of the two-phase flow period, the bottom hole pressure is brought up to a level close to the "nof"-case. In the figure this is seen as a pressure drop, when pressure difference

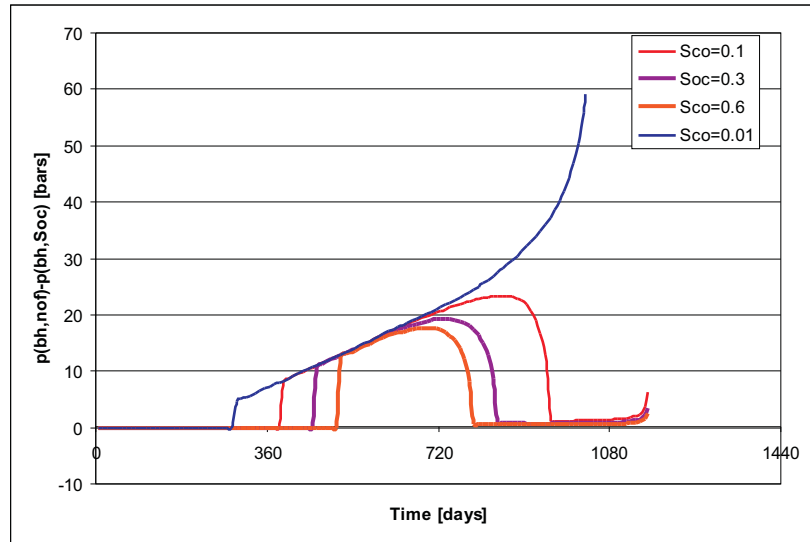


Figure 5.32: Pressure difference $p_{bh}(nof) - p_{bh}$ in four cases of varying critical oil saturation $S_{co} = 0.1, 0.3, 0.6$ and 0.01

drops to the baseline. The simulations as shown in Figure 5.32, therefore represent an underestimation of the pressure effect in the two-phase case. This under-estimation is particular evident in the case of defining times for well abandonment.

None the less, Figure 5.32 shows very clearly that the increased pressure drop due to two-phase flow in the reservoir is considerable and will undoubtedly lead to an early shut-down of that particular well.

The effect on liquid production is shown in Figure 5.33. The limiting case ($S_{co} = 0.01$) is shown as a straight line since practically no liquid is left in the reservoir, i.e. the liquid production is proportional to the gas production. The potential for liquid production in gas condensate reservoirs is therefore given by the two extreme cases; of "no oil flow" and limiting case mentioned above. As seen from Figure 5.33 there is about a 6% increase in the relative liquid production between the two extreme cases (in the case of a very dry condensate gas).

The relative production of dry gas and liquid condensate is shown in Figure 5.34. For two-phase flow cases the well will reach the abandonment pressure at an earlier time than shown in the figure (of reasons we have mentioned already). In the case of $S_{co} = 0.01$, the effect of premature shut-in time is clearly seen, which amounts to a shortening of the gas production period of about 10%, compared to the "nof"-case.

5.10.3 Effect of saturation profile

Fig. 5.27 depicts the reservoir saturation profile as a function of normalized radial position and as a function of production time in days. The figure example the irreducible volume of condensed oil in the reservoir. The model is based on the saturation profiles as defined by Eq. 5.100 and depicted in Fig. 5.25.

In Eq. 5.100, the three regions are basically defined by the parameters $L1$ and $L2$

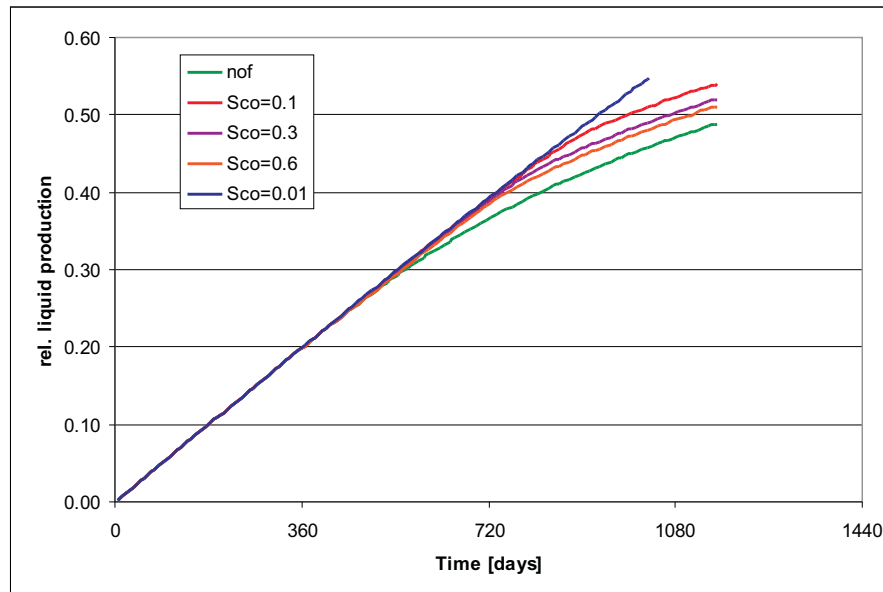


Figure 5.33: Relative liquid production as a function of time, spanning all cases of reservoir oil flow.

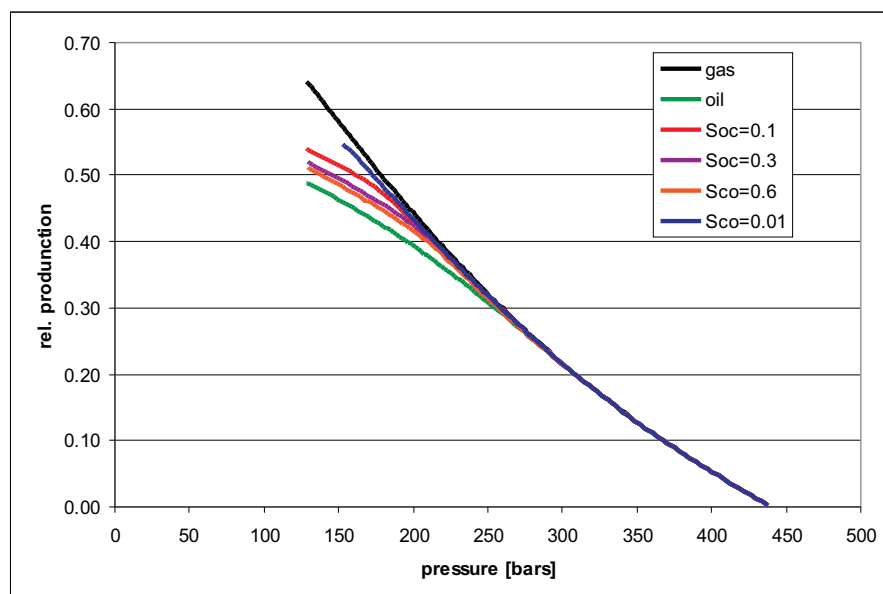


Figure 5.34: Relative production as a function of reservoir pressure.

(in addition to the critical oil saturation). The two parameters defines the "shape" or profile of the irreducible oil saturation in the reservoir.

Fig. 5.35 shows an example of the relative saturation profile S_o/S_{co} as function of relative radius. The figure shows various choices of $L1$ and $L2$. The parameter set $(L1, L2)=(0.2, 50)$ is the one used above and in all previous calculations and therefore

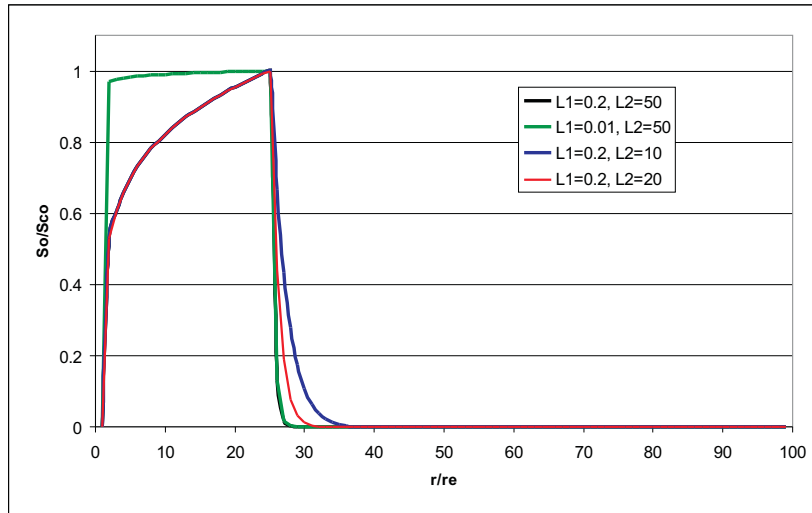


Figure 5.35: Saturation profiles as a function of relative radial position.

constitutes the base-case. It should be noted that the model depicted in Fig. 5.35 is a dynamic model where the expansion of region 1 and 2 moves radially as the pressure declines.

Region 1

When $L1=0.01$, the saturation profile is reshaped in Region 1 and as seen in Fig. 5.35, appears more or less flat throughout the whole region. This seemingly large change in the saturation profile does not really lead to any noticeable change in the bottom-hole pressure development nor in the relative liquid production, as can be seen in Fig. 5.36. The figure shows a continuous overlap between the $L1=0.01$ case and the base case. This is the case in both the pressure and production plots. The model is therefore quite insensitive to changes in the saturation profile in Region 1. This observation can be understood when comparing the quantitative aspects of the irreducible oil volume in the two cases. Since these volumes are quite similar in the two cases due to the small radial distances in question, they show similar simulation results.

Region 2

The saturation profile in Region 2 has been studied by changing the parameter $L2$ to 50, 20 and 10, while keeping $L1$ equal to 0.2. As can be seen from Fig. 5.35 and Fig. 5.36, relatively small changes in $L2$ cause relatively large changes in the pressure development. The same is seen for the liquid production. In all cases a critical oil saturation $S_{co} = 0.3$ is used.

In the case $(L1, L2)=(0.2, 20)$, the two-phase flow period is reduced to about one half of the length it had in the base case. Less oil is therefore produced to the surface. The changes are related to the volume in the reservoir accessible to liquid drop-outs and quite noticeable in the figure.

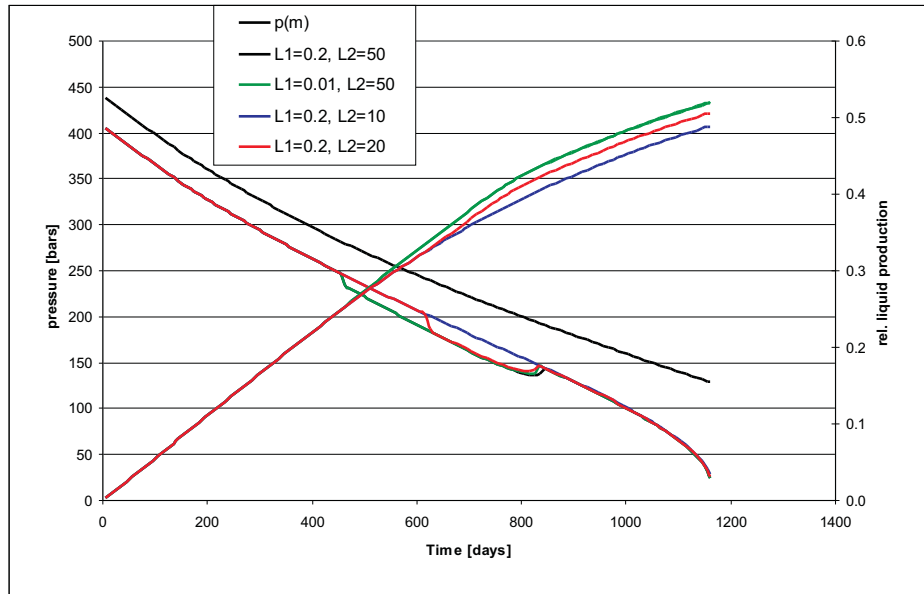


Figure 5.36: Bottom-hole pressure development and relative liquid production in the case of varying saturation profile.

In the case $(L1, L2)=(0.2, 10)$ this is further enhanced, as practically all condensed oil is stored in the reservoir and both the pressure development and the relative liquid production curves are similar to the "nof"-case. When $L2 = 10$, all liquid drop-out remains in the reservoir and the two-phase period never commences.

These observations show that the most important parameters in defining the saturation profile are the critical oil saturation and $L2$. It is quite interesting that the two-phase region at a distance from the well-bore is so important. Normally is the region in close vicinity of the well-bore considered the most important region. Similarly, the two-phase flow in the reservoir is more dependent on the saturation profile defined in Region 2, than in Region 1, i.e. the bulk of the reservoir is more important for the pressure- and production development than perhaps anticipated.

The above conclusion might be slightly surprising, since it is quite common to consider the close vicinity of the well to be of primary importance when adding up the overall pressure draw-down. This is still true, but the above considerations tells us that the dynamic development of this region (Region 1) is mostly significant in describing the total draw-down pressure.

5.10.4 Effect of gas composition

In all cases discussed up to this point, a lean condensate gas has been used. In order to investigate the effect of gas composition on the bottom-hole pressure development, a very rich gas with similar pressure and temperature characteristics has been chosen. The composition and reservoir data is taken from the book by Katz and Lee [14].

The gas characteristics are shown in Tables 5.6 and 5.7 and in Fig. 5.37. The data shown in the figure is the relative volume of a two-phase liquid condensed in a

Table 5.6: Molar composition (in %) of rich gas condensate reservoir fluid.

| | | | | | | | |
|-------------|--------|--------|-------|-------|-------|--------|------------|
| Compounds | N_2 | CO_2 | C_1 | C_2 | C_3 | iC_4 | nC_4 |
| Composition | 0.11 | 0.01 | 69.56 | 8.71 | 5.39 | 1.16 | 2.35 |
| Compounds | iC_5 | nC_5 | C_6 | C_7 | C_8 | C_9 | C_{10}^+ |
| Composition | 0.94 | 0.86 | 1.75 | 1.36 | 1.16 | 0.991 | 5.66 |

Table 5.7: Rich gas reservoir related characteristics.

| | |
|------------------------|-------------------|
| $p_{res} = 480$ bars | $T_{res} = 398$ K |
| $p_{dew} = 382.5$ bars | |
| $p_{co} = 315.6$ bars | |

CVD experiment, where the unit volume is the gas volume (cell volume) at dew-point pressure. While the lean gas has a maximum yield of liquid condensate of about 3.7%, the rich gas has a yield of about 32%.

Lean and rich gas comparison

Similar simulations, as for the lean gas case, have been made for the rich gas. A comparison of liquid rate, surface (sc.) and reservoir (res.) gas and liquid production are shown in Fig. 5.38.

A constant terminal gas rate is used. The associated liquid rate from the rich gas, shows in Fig. 5.38, to be nearly five times larger than of the lean gas. The ratio of cumulative surface liquid production in the two cases is about 2:1 at end production. This is associated with the fact that the lean gas production lasts for a longer time period than the rich gas production and as such, the degree of reservoir depletion is higher in the lean gas case. The consequence of liquid production, both to the surface and to the reservoir, is in the rich gas case due to a substantially faster gas depletion rate, as seen in Fig. 5.39. Thus it is interesting to notice that in the rich gas case, the condensation to the reservoir under "nof" conditions is about 4 times that of the lean gas case.

The pressure developments are presented in Fig. 5.39. Both the mean reservoir pressure and the bottom-hole pressure are observed to decline much faster in the rich gas case. This is associated with higher liquid production in the rich gas case. The pressure developments in the two cases are not completely comparable, but show similar trends. Due to the stronger liquid production in the rich gas case, the pressure drawdown is always larger and thus reaches the abandonment pressure at an earlier time.

The observation that production is halted at a higher bottom-hole pressure in the rich gas cases, as seen in Fig. 5.39, is simply due to the steeper decline of bottom-hole pressure. If smaller time steps or a declining flow rate had been used, then the abandonment pressure would appear to be quite similar in the two cases.

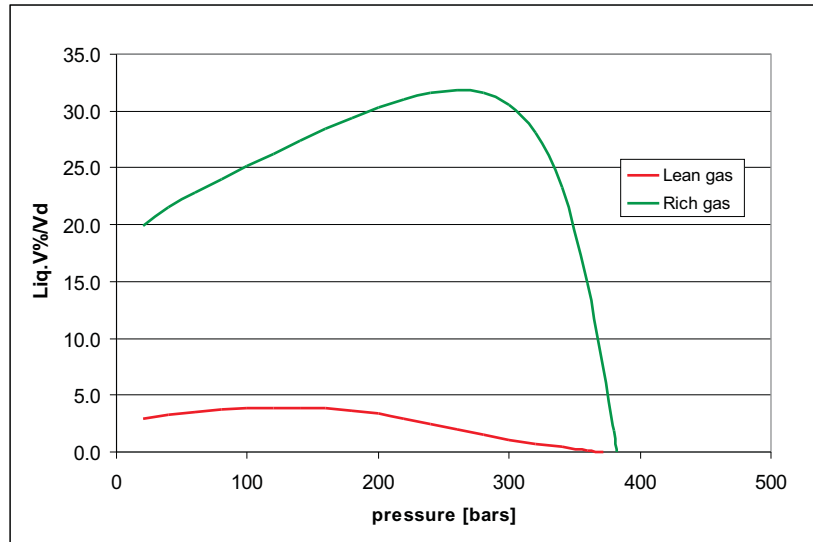


Figure 5.37: Ratio of liquid volume condensed to the initial cell volume at dew point pressure, in %.

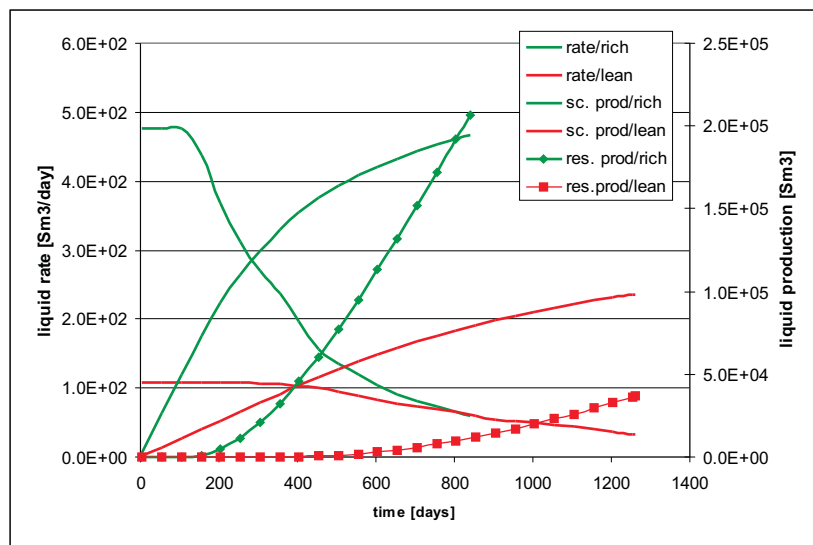


Figure 5.38: Lean and rich gas rate and production data is compared as a function of production time in the "nof" case.

Rich gas sensitivity

As pointed out in the discussion above, the principal parameters in this model turns out to be S_{co} and $L2$. Based on this background, several tests have been done to compare the effect of these parameters in the rich gas case. The pressure developments, as shown in Fig. 5.40, represent a systematic variation of $L2$ and S_{co} . In all cases discussed hereafter $L1 = 0.2$, as in the lean gas case.

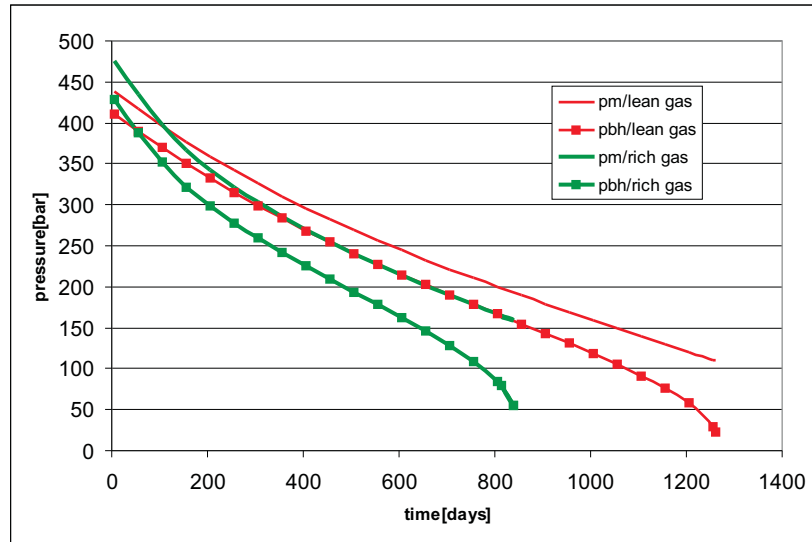


Figure 5.39: Lean- and rich gas pressure development as a function of time.

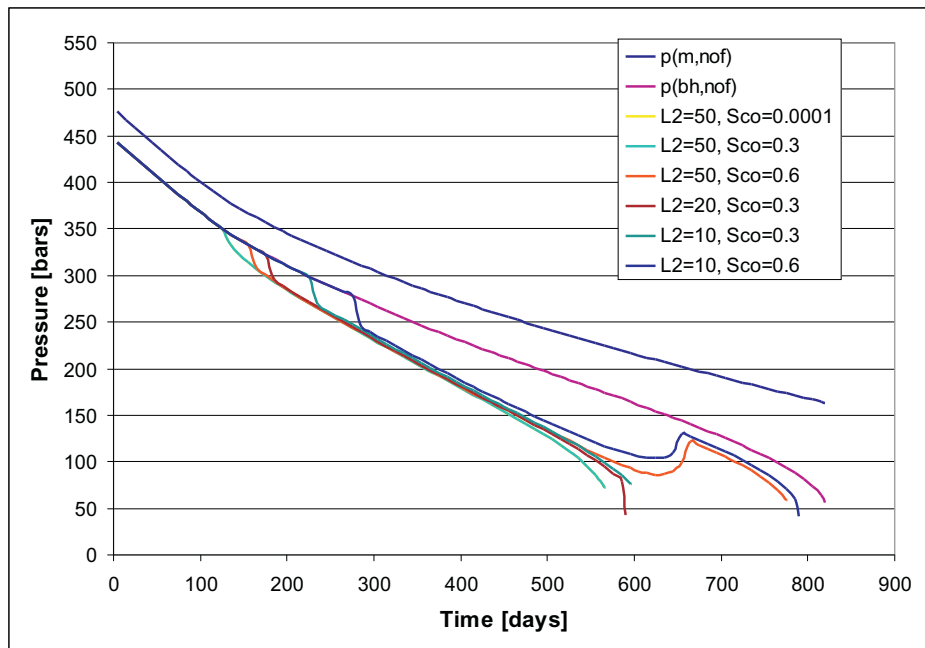


Figure 5.40: Pressure development in the rich gas cases for various choices of S_{co} and $L2$.

When $L2 = 50$, as used in the lean gas analysis, the critical gas saturation S_{co} is varied between 0.001 to 0.3, without observing any practical changes in the simulated results. In these two cases, seemingly all condensed oil is produced and the two-phase flow period starts shortly after the dew point pressure is reached in the reservoir. In the case when $S_{co} = 0.6$, a long (the longest) two-phase period is observed, where the

return to single gas flow starts as the gas production period comes to its end.

For choices of $L2 = 20$ and 10 , and $S_{co} = 0.3$, the two-phase period lasts through the entire production period, when first started. The results are early abandonment times (less than 800 days). In the case when $S_{co} = 0.6$ and $L2 = 10$, a well defined two-phase period is observed.

From these observations it seems likely that the parameter S_{co} is more important in controlling the two-phase flow than $L2$. This is somewhat surprising since $L2$ is controlling the integrated volume accessible for condensed liquid in Region 2 and thus decides whether condensed oil will remain in the reservoir or be produced. On the other hand S_{co} is defining the storing capacity of the reservoir and therefore defined both storage and two-phase oil production.

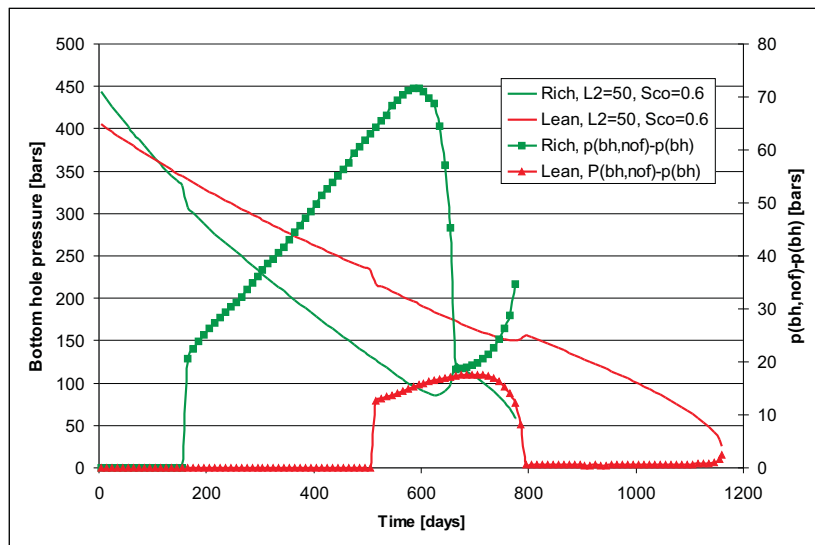


Figure 5.41: Bottom hole pressure development in the two cases of rich- and lean gas.

Fig. 5.41 shows a comparison between the two gases (light and rich gas) for the choice of $L2 = 50$ and $S_{co} = 0.6$. The plot shows the bottom hole pressure and the difference $p_{bh}(nof) - p_{bh}$ in the two cases. As seen from the figure, the bottom hole pressure draw-down can be considerable in the case of liquid condensation of rich condensates. A maximum of about 70 bars is observed in the rich gas case while the similar additional draw-down in the lean gas cases is about 18 bars.

5.11 Final Comments

The last part of this chapter describes the derivation of an analytic model for quantifying additional bottom hole pressure caused by two-phase flow in gas condensate reservoirs.

The model is important as it can be implemented in various tank models, where accurate assessments of bottom hole pressure is important.

The pressure calculations performed in this model represent an optimistic view of the bottom hole pressure development as the back coupling to the reservoir mean pressure is weak.

The mechanical model is defined by the following principle:

$$\text{Volume of condensed oil} = \text{Volume of immobile oil} + \text{Volume of produced oil},$$

where the separation between immobile and produced oil is performed by the use of a dynamic saturation profile. This saturation profile is controlled, in reality, only by two parameters; the critical oil saturation and a shape parameter.

The model has been demonstrated by various simulations and sensitivity studies, from which the following conclusions have been drawn;

1. A low critical oil saturation will lead to an early onset of two-phase flow in the reservoir.
2. The draw-down pressure development is strongly dependent on the radial development of the saturation profile in the close vicinity of the well, in what is called Region 1.
3. The saturation profile in Region 2 is of primary importance, whether two-phase flow will occur in the reservoir or not, and to the duration in time of such flow.
4. The existence of two-phase flow in the reservoir will in most cases lead to earlier fulfilment of abandonment conditions.
5. Increase in bottom hole pressure drop is substantial and depending on the gas type (composition) where a maximum pressure difference of 10 bars in the light gas cases and about 70 bars in the rich gas case, have been observed.
6. Comparing lean and rich gasses, the same characteristic flow behavior is observed, while in the rich gas case, relatively more liquid is produced to the reservoir as immobile oil, than in the case of lean gas.
7. The two-phase period is lengthened in the case of rich gas compared to the lean gas case.

This model may be included in analysis of well-pressure-test data as well as be of interest in well pressure and production forecast simulations.

A quantitative validation of this model would need experimental data input such as production -, reservoir - and fluid data in addition to a more realistic model of the condensed oil saturation profile. The most likely point to start would probably be to linearize the model and compare the result to long-core experiment. Initiative to such validation experiments are already taken.

References

- [1] CALSEP A/S. *PVTsim*. GI. Lundtoftsvei 1C, DK-2800 Kgs. Lyngby, Denmark, 13 edition, 2003.
- [2] K. Aziz and A. Settari. *Petroleum Reservoir Simulation*. Elsevier applied science publishers, 1985.
- [3] M. Briones, J.A. Zambrano, and C. Zerpa. Study og gas-condensate well productivity in santa barbara field, venezuela, by well test analysis. *Paper presented at the SPE Annual Technical Conference and Exhibition held in San Antonio, Texas, 29 September - 2 October, 2003*.
- [4] L.P. Dake. *Fundamentals of Reservoir Engineering*. Developments in Petroleum Science, 8. Elsevier Scientific Publishing Company, 1978.
- [5] L.P. Dake. *The Practice of Reservoir Engineering*. Developments in Petroleum Science, 36. Elsevier, 1994.
- [6] Ali Danesh. *PVT and Phase Behavior of Petroleum Reservoir Fluids*. Elsevier, 1998. ISBN 0-44-82196-1.
- [7] F.A.L. Dullien. *Porous Media, Fluid Transport and Pore Structure*. Academic Press Inc., 1979.
- [8] Herbert Bristol Dwight. *Tables and Integrals and Other Mathematical Data*. The Macmillian Company, 1961.
- [9] Ø. Fevang and C.H. Whitson. Modeling gas-condensate well deliverability. *SPE Reservoir Engineering*, November 1996.
- [10] A. C. Gringarten, A. AL-Lamki, S. Daungkaew, R. Mott, and T. M. Whittle. Well test analysis in gas-condensate reservoirs. *Paper presented at the 2000 SPE Annual Technical Conference and Exhibition held in Dallas, Texas, 1-4 October., 2000*.
- [11] Jacques Hagoort. *Fundamentals of gas reservoir engineering*, volume 23 of *Developments in Petroleum Science*. Elsevier, 1988.
- [12] Bjørn-Ove Heimsund. *Mathematical and Numerical Methods for reservoir Fluid Flow Simulation*. PhD thesis, University of Bergen, 2005.
- [13] W. Hurst and A.F. van Everdingen. The Application of the Laplace Transformation to Flow Problems in Reservoirs. *Trans. AIME*, 186:305–324, 1949.
- [14] D.L. Katz and R.L. Lee. *Natural Gas Engineering, Production and Storage*. McGraw-Hill Publishing Company, 1990. ISBN 0-07-100777-6.
- [15] A.L. Lee, M.H. Gonzales, and B.E. Eakin. The viscosity of natural gases. *Gas Technology, SPE Preprint Series*, 1(13), 1977.
- [16] J. Lee and R.A. Wattenbarger. *Gas Reservoir Engineering*. Henry L. Doherty Memorial Fund of AIME, SPE, 1996. ISBN 1-55563-073-1.

-
- [17] M.B. Standing. *Volumetric and Phase Behavior of Oil Field Hydrocarbon Systems.*, volume Ninth Printing, 1981. Society of Petroleum Engineers of AIME, 1977. Library of Congress Catalog Card No. 52-11180.
- [18] J.R. Ursin. Fluid flow in gas condensate reservoirs: the interplay of forces and their relative strengths. *Journal of Petroleum Science & Engineering*, 41:253–267, 2004.
- [19] J.R. Ursin. Linear dynamics of gas condensate well deliverability. *Transport in Porous Media*, pages 70:375–406, 2007.
- [20] A.F. van Everdingen. The Skin Effect and Its Impediment to Fluid Flow into a Wellbore . *Trans.AIME*, 198:171–176, 1953.
- [21] C.H. Whitson and M.R. Brule. *Phase Behavior*. SPE Monograph Series. Society of Petroleum Engineers Inc., 2000.

Chapter 6

Gas Well-Bore Flow

This chapter presents models describing flow of reservoir fluids in the well-bore. The main result of the development in this chapter is thus the well-head pressure, defined at a location above the mean sea level and before the first separation step.

The well is the link between surface and bottom-hole conditions represented by the reservoir and is as such an essential element of the gas-reservoir engineering. Typical reservoir engineering tasks such as estimating well deliverability and prediction of recovery efficiency cannot be performed properly without a thorough understanding of well-bore flow mechanics.

We will begin by deriving the basic flow equation for single-phase gas flow and then follow a step-wise approach leading to a final equation describing well-bore flow. These steps include:

Basic equation for well-bore flow of real gas is the derivation of an equation describing single gas flow in simple straight flow conduits of constant cross-section.

Pressure distribution in shut-in wells develops an analytical solution for the pressure distribution in a well-bore of a shut-in well and in a producing gas well.

Rate dependent pressure losses discusses the different terms in the general pressure equation and derives a pressure solution as function of well length.

The effect of temperature allows for a non-uniform temperature distribution in the well-bore.

Pressure distribution in a producing well adds up the different contributions to the the overall pressure drop in the well-bore and presents a general solution for single-phase gas well flow.

Multi phase flow introduces corrections relative to the single-phase solution, here represented by systems of gas and condensate, and gas, condensate and water systems.

Minimum unloading rate discusses the well-bore flow rate in relation to fluid density and buoyancy.

Heat losses in producing well constitutes the latter part of this chapter.

In practical situations, gas production frequently occur as single-phase, but quite often both condensate liquids and water may accompany the gas under normal production. The presence of condensate and water will have important bearings on the pressure distribution, depending of course on the content or fraction of these liquids in the well stream. Awareness of the restriction under which the basic equation is valid is therefore important for the successful application of this equation.

6.1 Basic Equation for Well-Bore Flow of Real Gas

Consider single-phase gas flow in a simple straight conduct section of constant cross-section A and diameter S , and at a deviation angle α , as depicted in Figure 6.1. The flow direction is up-ward, indicated by the flow velocity u . The well distance co-ordinate system, denoted by y is parallel to the well conduit direction. To simplify the problem we will consider steady-state flow conditions. In addition, since the well flow conduit is long compared to the width of the well-bore, we may consider the well flow to be one-dimensional, with the distance along the conduit as the dependent variable. Hence, pressure, velocity, gas density and other properties are considered to be constant on the cross-section perpendicular to the gas conduit.

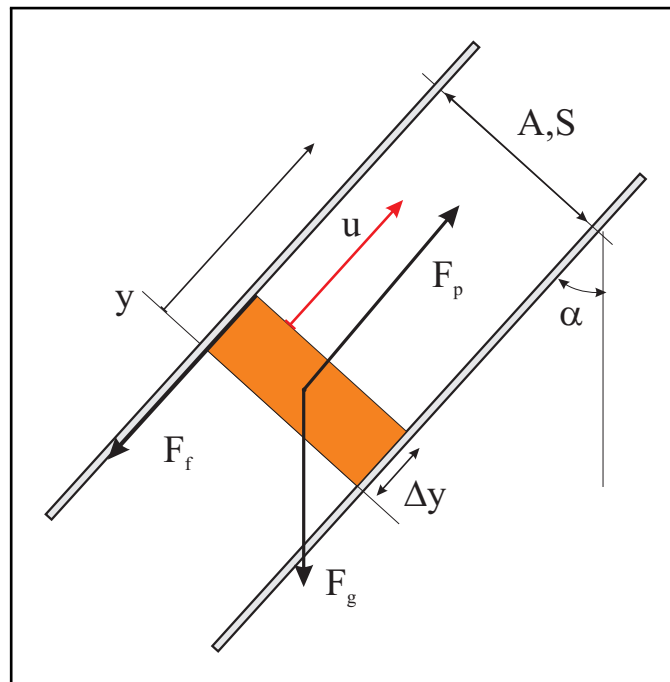


Figure 6.1: Straight section of well flow conduit.

The mathematical description of gas flow in a conduit as depicted in Figure 6.1 can be derived by applying;

1. the mass conservation equation,
2. the momentum balance equation and

3. the real gas law.

6.1.1 Mass Conservation

The mass flow conservation states that under steady-state flow conditions, the mass flow rate w must be constant along the flow conduit ($w=\text{constant}$). Constant mass flow means,

$$w = \rho u A = \rho q, \quad (6.1)$$

where ρ is the gas density, $u = dy/dt$ is the gas velocity, q is the gas rate and A is the well-bore cross-section.

For gas wells, flow rates are normally specified in terms of dry-gas w_G and gas condensate w_L mass rates, measured at surface conditions. The mass flow rate of hydrocarbon production is then

$$w_{HC} = w_G + w_L = \rho_{G,sc} q_{G,sc} + \rho_L q_L = \rho_{G,sc} q_{G,sc} \left(1 + R_{VLG} \frac{q_L}{q_{G,sc}} \right), \quad (6.2)$$

where ρ and q are density and rates, respectively. R_{VLG} is the volumetric liquid condensate-gas ratio, defined in Eq. 3.101.

The volumetric hydrocarbon velocity is defined as

$$u_{HC} = \frac{w_{HC}}{\rho_{HC} A}, \quad (6.3)$$

where ρ_{HC} is the density of the gas mixture in the well, i.e. the gas obtained by recombining surface dry-gas and condensate at well pressure and temperature.

Because well-bore pressure and temperature is continuously changing, the well-bore velocity will thus vary along the flow conduit.

6.1.2 Momentum Balance

The steady-state momentum balance, states that the sum of forces acting on a thin slice segment, $A\Delta y$, as depicted in Figure 6.1, must be balanced by the net momentum flux through the gas segment, given by the equation,

$$\vec{F}_p + \vec{F}_g + \vec{F}_f = \frac{\Delta(m \cdot u)}{\Delta t}, \quad (6.4)$$

where the momentum $m \cdot u = \rho A \Delta y \cdot u$.

The various elements, from left to right in the above equation are then described by:

\vec{F}_p : The pressure force is proportional to the pressure drop across the slice segment, i.e. $F_p = -A\Delta p$, where the minus sign originates from the definition of $\Delta p = p(y + \Delta y) - p(y)$ where $\Delta p < 0$.

\vec{F}_g : A component of the gravity force acts against the direction of flow and is written $F_g = -\rho g \cos(\alpha) A \Delta y$.

\vec{F}_f : The friction forces is anti-parallel to the direction of flow; $F_f = -F\Delta y\pi S$, where F is the shear-stress (force per length) exerted by the wall on the gas.

$\frac{\Delta(m \cdot u)}{\Delta t}$: The net momentum flux is thus written,

$$\frac{\Delta(m \cdot u)}{\Delta y/u} = \frac{((m \cdot u)_{y+\Delta y} - (m \cdot u)_y)u}{\Delta y} = \frac{(m \cdot u^2)_{y+\Delta y} - (m \cdot u^2)_y}{\Delta y} = \frac{\Delta(m \cdot u^2)}{\Delta y} = \frac{\Delta(A\rho u^2)}{\Delta y}$$

where the substitution of $\Delta t = \Delta y/u$ is done according to the definition of flow velocity; $u = dy/dt$. Thus, the net momentum flux $\Delta(A\rho u^2)$ is balancing the resultant force acting on the slice segment.

The friction force is acting on the slice surface facing the well-bore. The friction force is equal to the shear stress F , exerted on the area of the wall in interaction with the gas, i.e. "Friction force" = "Shear stress" · "Area of wall". From this, we may introduce the hydraulic diameter,

$$F \cdot \pi S \Delta y = A \frac{F}{A/(\pi S)} \Delta y = A \frac{F}{d_h} \Delta y, \quad (6.5)$$

where S is the diameter of the gas conduit ($A = \pi(S/2)^2$) and $d_h = S/4$ is the hydraulic diameter.

The concept of hydraulic diameter allows the generalization of the momentum balance to non-circular flow conduits, e.g. for annular flow between two concentric circular flow conduits.

The force equation, Eq. 6.4, can now be rewritten based on the above deductions. Dividing by the length of the gas slice (Δy), we find

$$-\frac{(A\Delta p)}{\Delta y} - \frac{g\rho \cos(\alpha)A\Delta y}{\Delta y} - \frac{AF/d_h\Delta y}{\Delta y} = \frac{\Delta(uA \cdot u\rho)}{\Delta y}. \quad (6.6)$$

The finite difference equation, Eq. 6.6, is converted into an ordinary differential equation by assuming an infinite decimal thin gas segment, i.e. $\Delta y \rightarrow 0$,

$$-\frac{dp}{dy} - \rho g \cos(\alpha) - \frac{F}{d_h} = \frac{d}{dy} \rho u^2. \quad (6.7)$$

The shear stress at the wall is normally related to the friction against fluid flow, defined by the Fanning friction factor f , and the shear stress is defined [9],

$$F = 2f\rho u^2. \quad (6.8)$$

The Fanning friction factor depends on the Reynolds number Re and on the roughness of the flow conduit, as shown in the graph Figure 6.2. The Reynolds number represents the ratio of inertial to viscous forces and is defined by

$$Re = \frac{\rho u d_h}{\mu} = \frac{w d_h}{A\mu}, \quad (6.9)$$

where μ is the gas viscosity. Note that the role of the hydraulic diameter in Eq. 6.9 is to scale the flow dimension, i.e. the distance between the flow boundaries.

The Reynolds number given as function of surface gas flow conditions is written

$$Re = \frac{w_{HC} d_h}{A \mu} = \frac{\rho_{sc} q_{sc} d_h}{A \mu} \left(1 + R_{VLG} \frac{q_L}{q_{sc}} \right). \quad (6.10)$$

The Fanning friction factor depends on the relative roughness of the well-bore wall and on the gas flow represented by the Reynolds number, through empirical relations as shown in Figure 6.2. The relative roughness is defined as the wall roughness ϵ divided by the diameter of the well, i.e. ϵ/S (ϵ/D in the figure). A typical well-bore roughness can be $\epsilon \sim 0.02 \text{ mm}$.

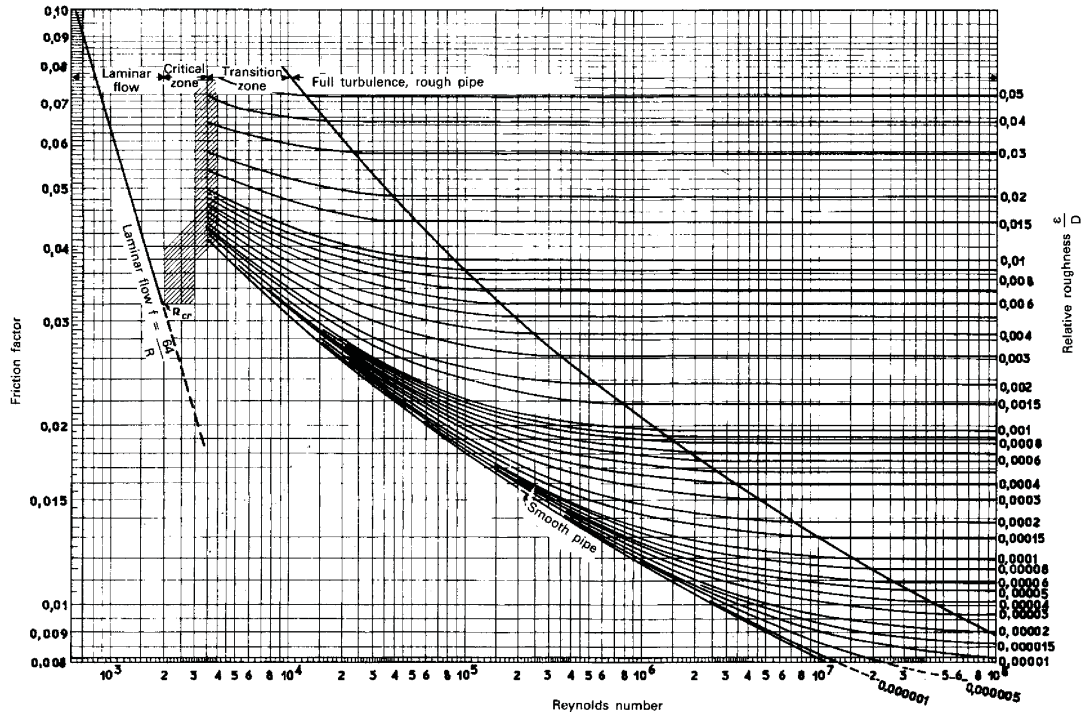


Figure 6.2: Moody friction factor as function of well-bore relative roughness and Reynolds number. (Copied from J.Vincent-Genod, *Fundamentals of pipeline engineering* [18].) Notice that the Fanning friction factor is one-fourth of the Moody friction factor.

Example: Typical Reynolds Number for Well-Bore Gas Flow

Eq. 6.10 can be used to determine the Fanning friction factor, where we assume the volumetric condensate-gas ratio to be small, and much less than unity.

The following set of data is considered to be typical for gas well flow.

$$\begin{aligned} q_{sc} &= 10^6 \text{ Sm}^3/\text{day} & \rho_{sc} &= 3 \text{ kg/m}^3 \\ d_h/A &= 1/\pi S \text{ and } S = 0.15 \text{ m} \\ \mu &= 0.02 \text{ mPa} \cdot \text{s} = 0.02 \cdot 10^{-3} \text{ Pa} \cdot \text{s} \end{aligned}$$

The Reynolds number is therefore

$$\begin{aligned} Re &= \frac{10^6 [Sm^3/day] 3 [kg/m^3] 1/(\pi 0.15) [m^{-1}]}{0.02 \cdot 10^{-3} [Pa \cdot s]} \\ &= \frac{10^6 1/(24 \cdot 60 \cdot 60) 3 \cdot 1/(\pi 0.15)}{0.02 \cdot 10^{-3}} \simeq 4 \cdot 10^6. \end{aligned}$$

A typical well-bore roughness of $\epsilon = 0.02 \text{ mm}$ and diameter $S = 0.15 \text{ m}$, gives a relative roughness equal to 0.00013. For Reynolds numbers in the order of $1.0 \cdot 10^7$, we can safely expect the Fanning friction factor to be constant for most well flow rates, as can be observed from Figure 6.2.

For non-laminar flow, which is the region of interest in producing gas wells, the friction factor can be obtained from empirical charts of correlations. In the case of partially-turbulent and fully-turbulent single phase flow, a number of correlations have been reported of which quite a few can be found in the book "Gas Production Engineering" by Sanjay Kumar [11].

Two well known and often used empirical relations are listed below:

Colebrook's equation

$$\frac{1}{\sqrt{f}} = 4.0 \log \left(\frac{d_h}{\epsilon} \right) + 2.28 - 4.0 \log \left(1 + \frac{4.67}{Re \sqrt{f}} \frac{d_h}{\epsilon} \right). \quad (6.11)$$

Wood's equation

$$\begin{aligned} f &= a + b Re^{-c}, \\ a &= 0.026 \left(\frac{\epsilon}{d_h} \right)^{0.225} + 0.133 \left(\frac{\epsilon}{d_h} \right), \\ b &= 22 \left(\frac{\epsilon}{d_h} \right)^{0.44} \text{ and} \\ c &= 1.62 \left(\frac{\epsilon}{d_h} \right)^{0.134}. \end{aligned} \quad (6.12)$$

The friction factors calculated in the Colebrook's - and in the Wood's equations above are both the Fanning friction factor. When these friction factors are compared with friction factors from the diagram in Figure 6.2, a factor of four is involved [15] such that:

$$f_{Fanning} = \frac{1}{4} \cdot f_{Moody}.$$

6.1.3 Real Gas Law

The gas density is defined by the real gas law and we write

$$\rho = \frac{m_g}{V} = \frac{M_g p}{ZRT}, \quad (6.13)$$

where m_g and M_g are the average mass of gas and the average molecular mass. p and T is the well pressure and temperature, respectively. Z is the gas z-factor and R is the molar gas constant.

Since the mass flow rate in Eq. 6.1 is assumed to be constant, i.e. $w = \rho u A = \text{constant}$, we may write the derivation term in Eq. 6.7 as

$$\frac{d}{dy} \rho u^2 = \rho u \frac{du}{dy}, \quad (6.14)$$

where both ρu and A are constants. (Notice that no partial differentiation has been done.)

Combining the equations from above; Eqs. 6.7 and 6.14, we obtain the well-bore flow equation

$$\underbrace{udu}_{\text{kinetic}} + \underbrace{\frac{dp}{\rho}}_{\text{pressure}} + \underbrace{g \cos(\alpha) dy}_{\text{gravitation}} + \underbrace{\frac{2fu^2}{d_h}}_{\text{friction}} dy = 0. \quad (6.15)$$

Eq. 6.15 is the differential form of the extended Bernoulli equation applied to flow of a single-phase fluid (liquid or gas). The terms in Eq. 6.15 have the dimension of energy per unit mass. The first three terms; kinetic, pressure and gravitation represent the change in mechanical energy. The last term is energy dissipation per unit mass due to friction forces. Hence, the extended Bernoulli equation can be interpreted as describing the degradation of mechanical energy in the flow direction as a result of friction forces. For this reason, it is sometimes referred to as the non-conservation equation of mechanical energy.

Following the assumption of constant mass flow rate, i.e. $w = \rho u A = \text{constant}$, we may write the derivative $du/d\rho = -u/\rho$. On the basis of the real gas law, the gas density given by Eq. 6.13, can be differentiated and we get $d\rho = (M_g/RT)d(p/Z)$. Using the above derivatives, we may write Eq. 6.15 as follows

$$\frac{w^2}{A^2} \frac{RT}{M_g} d\left(\frac{Z}{p}\right) + dp + \frac{M_g}{RT} g \cos(\alpha) \frac{p}{Z} dy + \frac{2f}{d_h} \frac{w^2}{A^2} \frac{RT}{M_g} \frac{Z}{p} dy = 0. \quad (6.16)$$

In Eq. 6.16 all parameters except from the pressure and the z-factor are considered constant relative to the well-bore elevation y . Eq. 6.16 is the basic equation for flow of real gases in straight flow conduits. The equation takes into account gravity, wall friction and kinetic energy. However, it does not include any thermal effects such as cooling due to gas expansion, frictional heating and heat exchange with the surroundings. Temperature gradients may thus be incorporated by solving the equation for a pre defined and fixed temperature profile. In this way we can handle the non-uniform well-bore temperatures that are commonly observed in well-bores.

6.2 Pressure Distribution in Shut-In Wells

Let us first consider the simple problem of a static pressure distribution in a well-bore filled with natural reservoir gas. This problem is of direct practical relevance since reservoir pressures are often determined by measuring the well-bore pressure in shut-in wells and subsequently calculating the static pressure drop between the well-head and the bottom of the well.

Under static conditions there is no gas flow, $w = 0$ and Eq. 6.16 reduces to

$$dp + \frac{M_g}{RT} g \cos(\alpha) \frac{p}{Z} dy = 0. \quad (6.17)$$

As a preliminary analysis of the pressure distribution in the well, we assume a uniform temperature distribution in the well bore. Further, we ignore the pressure dependence of the z-factor and replace the Z by some average and constant value \bar{Z} . Integration of Eq. 6.17 from the well bottom ($y = 0$) yields the pressure in the well at elevation y

$$p = p_{bh} e^{-N_{gp} y/L}, \quad (6.18)$$

where p_{bh} is the bottom-hole pressure at $y = 0$. N_{gp} is a dimensionless number defined as

$$N_{gp} = \frac{M_g g L \cos(\alpha)}{\bar{Z} R T}. \quad (6.19)$$

The dimension-less number N_{gp} is a measure of the ratio of gravitational to pressure forces. This fact is clearly stated by inspecting Eq. 6.15. L in Eqs. 6.18 and 6.19 is the total length of the well-bore.

From Eq. 6.18 it follows that the pressure relation between the bottom-hole pressure and the well-head pressure is given by

$$p_{wh} = p_{bh} e^{-N_{gp}}. \quad (6.20)$$

Eq. 6.20 describes the static pressure distribution in a gas filled well-bore of uniform temperature. The equation is essentially the well known *barometric height* formula.

Eq. 6.18 is based on an average z-factor for the entire length interval of the well-bore and should be considered a first approximation. For most practical purposes this approximation is sufficiently accurate. In the case where better accuracy is required, we can always subdivide the total well-bore length into a number of intervals and apply Eq. 6.18 successively to each individual interval. The total pressure drop is then obtained by summation of the pressure drops of the individual intervals. By taking sufficiently small intervals, any desired accuracy can be obtained.

Example: The Effect of Varying z-factor

To evaluate the number N_{gp} , we require an average z-factor \bar{Z} , which depends on the calculated pressure distribution.

In order to evaluate the approximation done by applying an average z-factor, we have to return to Eq. 6.18, which can be written.

$$p = ae^{b/\bar{Z}},$$

where here a and b are constants.

Recognizing that \bar{Z} is an average value, we may introduce an uncertainty $\Delta\bar{Z}$ which reflects the error done by substituting an average z-factor when integrating along the well. Applying the principle of error propagation, we are able to estimate the error in the pressure function by differentiating the equation above and we get

$$\frac{\Delta p}{p} = -\frac{b}{\bar{Z}} \frac{\Delta Z}{Z} = +N_{gp} \frac{\Delta Z}{Z}.$$

Applying the following numerical constants

$$\begin{array}{lll} M_g = 0.027 \text{ kg/mol} & & \\ L = 3000 \text{ m} & g = 9.8 \text{ m/s}^2 & \alpha = 0 \\ \bar{Z} = 1 & R = 8.314 \text{ J/(mol} \cdot \text{K)} & T = (100 + 273) \text{ K} \end{array}$$

we find the number $N_{gp} = 0.26$.

If the relative uncertainty in the z-factor is estimated to be approximately 2%, we find the relative uncertainty in pressure equal to

$$\frac{\Delta p}{p} = 0.26 \cdot 0.02 = 0.005.$$

The relative uncertainty in estimating the wellhead pressure is therefore reduced to about 0.5%.

Since the average z-factor occurs in the argument of the exponential function it is not a particular sensitive parameter and in most practical cases a single calculation, i.e. at the bottom-hole pressure, would be adequate.

6.2.1 Thermal Effects in The Well-Bore

When a gas is close to its liquefaction temperature, the molecules are necessary close enough to each other, so that their interaction energy will give a significant contribution to the total energy of the system. This contribution is negative. If we let the gas expand, as in a confined volume of a well, the interaction energy will decrease in absolute value, i.e. the gas total energy gets more positive, as work must be done against the attractive forces. If there are no other sources for this work, it will have to originate from the kinetic energy of the molecules of the gas and the gas will cool!

If all work is taken from the internal energy of the gas, i.e. an adiabatic process ($\delta Q = 0$), the energy balance is

$$dU = -pdV, \tag{6.21}$$

where U is the internal energy.

For expansion in a confined volume we have: $C_V \equiv (dU/dT)_V$, where C_V is the heat capacity at constant volume. For an ideal gas ($pV = nRT$), we may use the definition of the heat capacity C_V and Eq. 6.21, and we get

$$C_V dT = -pdV = -nR \left[dT - \frac{T}{p} dp \right], \quad (6.22)$$

which is rewritten

$$\frac{dT}{T} = \frac{nR}{C_V + nR} \frac{dp}{p}. \quad (6.23)$$

Using the fact that $C_p - C_V = nR$ for ideal gasses and that the ratio $C_p/C_V = \gamma$, integration of Eq. 6.23, yield

$$\frac{p^{(\gamma-1)/\gamma}}{T} = \text{constant}. \quad (6.24)$$

The above equation says that any two states of an ideal gas can be connected by a reversible adiabatic process, where the *expansion* process will produce the greatest drop in temperature, while a reversible adiabatic *compression* between the two specified volumes produces the least increase in temperature [5].

Example: Well-Head Temperature for somewhat Idealized Gas Flow

In the special case of reversible adiabatic flow (isentropic flow) of ideal gas (no heat dissipation and frictionless flow), i.e. free expansion of gas in the well, - the temperature and the pressure in the well-bore are related through the adiabatic law, given by Eq. 6.24, where γ is the ratio of the heat capacity at constant pressure to the heat capacity at constant volume (C_p/C_V). p and T are the pressure and temperature in the well stream. The adiabatic law in Eq. 6.24, is deduced on the assumption of zero entropy change. The formula can be found in most textbooks on thermodynamics [17, 5].

For a bottom-hole pressure $p_{bh} = 370$ bar and a well-head pressure of $p_{wh} = 100$ bar, we may use Eq. 6.24 to estimate the well-head temperature T_{wh} when the reservoir or bottom-hole temperature is $T_{bh} = 120^\circ C$. A typical value of the adiabatic ratio for a polyatomic gas: $\gamma = 1.3$ (e.g. Methane).

The adiabatic law Eq. 6.24 yields the following relation between the pressure and temperature at the bottom of the well and at the well-head

$$\frac{p_{bh}^{(\gamma-1)/\gamma}}{T_{bh}} = \frac{p_{wh}^{(\gamma-1)/\gamma}}{T_{wh}},$$

where some re-arrangement gives

$$T_{wh} = \left(\frac{p_{wh}}{p_{bh}} \right)^{(\gamma-1)/\gamma} T_{bh},$$

and substituting the numerical values

$$T_{wh} = \left(\frac{100}{370}\right)^{(1.3-1)/1.3} (120 + 273)^{\circ}K = 290.6^{\circ}K = 17.4^{\circ}C.$$

The expansion of reservoir gas in the well will cause the gas temperature to drop and in the case of ideal gas under isentropic conditions the temperature decreases from $120^{\circ}C$ to $17.4^{\circ}C$, which is then the limiting lowest temperature possible.

6.2.2 Effect of a Temperature Gradient

We may now proceed by including the effect of a temperature gradient and for simplicity we will use a linear profile given by

$$T = T_{bh} - \Delta T \frac{y}{L}, \quad (6.25)$$

where ΔT is the total temperature difference between bottom and top of the well and where T_{bh} is the bottom-hole temperature ($y = 0$).

The temperature gradient is then

$$\frac{dT}{dy} = -\frac{\Delta T}{L}, \quad (6.26)$$

where the gradient $\Delta T/L$ generally is the total temperature difference between bottom hole and well head locations. This definition must not be confused with the definition of the geothermal gradient, $(\Delta T/L)_G \sim 30 K/km$, referred to in Figure 2.10. If the well was treated as a cylindrical conduct, fully submerged in the subsurface and the well flow rate was low enough to minimize any temperature difference between well gas and surroundings, - then the geothermal gradient could be used in Eq. 6.26.

In most real cases the gas well-head temperature is substantially higher than the surrounding reservoir or rock temperature.

Inserting Eq. 6.26 in Eq. 6.17 we obtain

$$\frac{dp}{p} = \frac{M_g g L \cos(\alpha)}{\bar{Z} R \Delta T} \frac{dT}{T} = N_{gp} \frac{T_{bh}}{\Delta T} \frac{dT}{T}, \quad (6.27)$$

where the dimensionless number is redefined; $N_{gp} = (M_g g L \cos(\alpha)) / (\bar{Z} R T_{bh})$.

Integration of Eq. 6.27 from the bottom-hole yields

$$\frac{p}{p_{bh}} = \left(\frac{T}{T_{bh}}\right)^{N_{gp} T_{bh} / \Delta T} = \left(1 - \frac{\Delta T}{T_{bh}} \frac{y}{L}\right)^{N_{gp} T_{bh} / \Delta T}, \quad (6.28)$$

where we have used the definition Eq. 6.25 and where $\Delta T = T_{bh} - T_{wh}$ is assumed constant.

The well-head pressure is then given by

$$p_{wh} = p_{bh} \left(1 - \frac{\Delta T}{T_{bh}}\right)^{N_{gp} T_{bh} / \Delta T}. \quad (6.29)$$

The pressure solution in Eq. 6.28 can further be discussed by restricting the solution to three different intervals of temperature gradient.

$\Delta T \sim 0$

With basis in Eq. 6.29 we may turn back to the case of constant well-bore temperature, i.e. $\Delta T \rightarrow 0$ (no temperature effect). Eq. 6.29 is then written

$$p_{wh} = p_{bh} \lim_{\Delta T \rightarrow 0} \left(1 - \frac{\Delta T}{T_{bh}}\right)^{N_{gp} T_{bh} / \Delta T} = p_{bh} e^{-N_{gp}}, \quad (6.30)$$

where we have used the mathematical result; $\lim_{x \rightarrow \infty} (1 - 1/x)^{-x} = e$, found in most mathematical table books [8].

Eq. 6.30 is thus identical to Eq. 6.20, derived under the assumption of constant well-bore temperature.

$\Delta T > 0$ and $N_{gp} = \Delta T / T_{bh}$

In this limiting case, Eq. 6.28 reduces to

$$p(y) = p_{bh} \left(1 - \frac{\Delta T}{T_{bh}} \frac{y}{L}\right) = p_{bh} \left(1 - N_{gp} \frac{y}{L}\right). \quad (6.31)$$

With a linear temperature gradient, $\Delta T / T_{bh} = N_{gp}$, the gas pressure in the well-bore is linearly decreasing with increasing well height y . Figure 6.3 shows the limiting case in Eq. 6.31, where the dimensionless number N_{gp} is chosen equal to 0.2. The relative elevation (y/L) is plotted as function of relative pressure (p/p_{bh}). The pressure profile Eq. 6.18, describing a uniform temperature distribution, i.e. zero temperature difference ($\Delta T = 0$), is also shown in the plot. As can be seen from the plot, the pressure profile for uniform temperature distribution ($\Delta T = 0$) is slightly concave upwards. That is, relative pressure decrease is reduced as we move to the bottom of the well. This means that the pressure gradient decreases with increasing depth, reflecting an increase in gas density with increasing depth, which again is a stable configuration.

On the other hand and as shown in Figure 6.3, a temperature gradient ($\Delta T \neq 0$) causes a larger total pressure drop in the well bore. This linear pressure drop can be explained as a balance between a decrease in gas density due to gas expansion and a reduction in gas density due to a decrease in temperature, which exactly balances each other, i.e. the two effects of gas cooling and pressure release have the opposite effect and cancel each other exactly. Density is decreasing due to cooling of the gas and at the same time density of the gas is increasing due to the reduction in temperature in the well.

When the temperature gradient in the well-bore exactly balances the dimensionless number, $\Delta T / T_{bh} = N_{gp}$, the pressure profile becomes exactly linear. Under this special condition the gas density is constant in the well, where the effects of decreasing density due to pressure reduction is fully compensated by the increase in density due to temperature reduction.

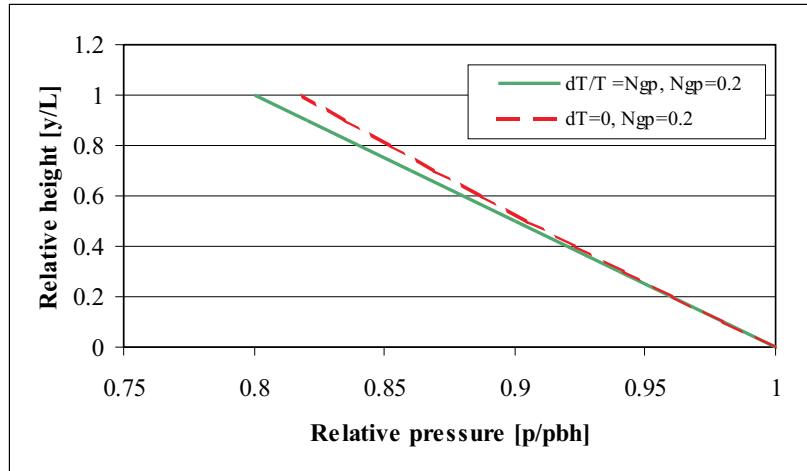


Figure 6.3: Pressure profile as function of well-bore depth.

$\Delta T/T_{bh} > N_{gp}$ and $\Delta T/T_{bh} < N_{gp}$

We have in Figure 6.4, plotted Eq. 6.28 for the two cases where the temperature gradient is greater and lower than the dimensionless number, where the number is chosen equal to $N_{gp} = 0.2$. The two curves seem to fall on either side of the linear temperature gradient $\Delta T/T_{bh} = N_{gp}$, with the $\Delta T/T_{bh} > N_{gp}$ curve below and the $\Delta T/T_{bh} < N_{gp}$ curve above the straight line.

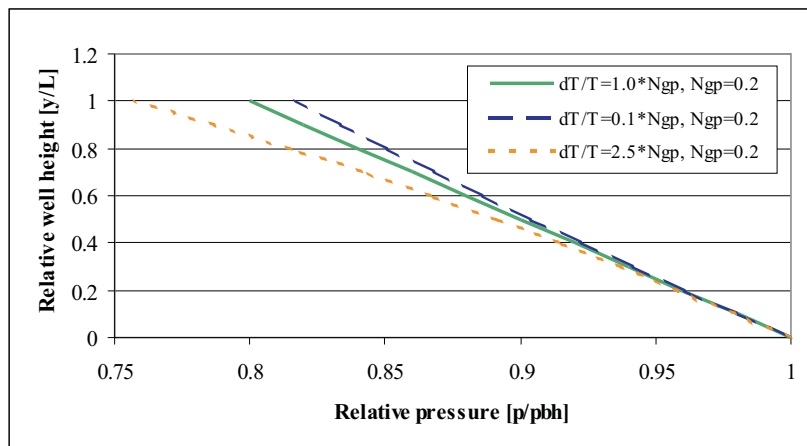


Figure 6.4: Relative pressure versus depth profiles.

Starting from the well-head position (at $y/L = 1$) in Figure 6.4, the $\Delta T/T_{bh} > N_{gp}$ pressure curve is concave, increasingly curving with decreasing depth. Compared to the straight line case, where the gas density is constant along the well length, a decreasing pressure drop with decreasing well depth is observed, i.e. an increasing pressure gradient. An increasing pressure gradient moving downwards in the well, would mean a decreasing pressure gradient moving upwards in the well, which again would lead to the

assumption of increase in gas density moving from bottom to the top of the well.

This condition where more dense gas rests on top of less dense gas, will in turn lead to gravitational convection and is considered physically unstable. The situation described with the curve $\Delta T/T_{bh} > N_{gp}$, is therefore non-physical and does not represent a stable well-bore situation. Consequently, N_{gp} must always be greater than $\Delta T/T_{bh}$.

In practice; adoption of a simple linear temperature profile is usually adequate for incorporating temperature effects in the calculations of vertical pressure distributions. If for some reason this is not justified, a non-linear temperature profile may be handled by approximating the non-linear profile through a series of linear profiles and applying the pressure profile formula Eq. 6.28 successively to each individual segment.

Example: Static Pressure Profiles

In the previous example we found a dimensionless number $N_{gp} = 0.26$ for a 3000 m deep well, where the bottom-hole pressure and temperature is 300 bar and $100^\circ C$, respectively.

Assuming a uniform and constant well temperature, will yield a well-head pressure p_{wh} in accordance to Eq. 6.20

$$p_{wh} = p_{bh}e^{-N_{gp}} = 300 \text{ bar} \cdot e^{-0.26} = 231.3 \text{ bar.}$$

Assuming a linear temperature gradient, the well-head pressure is given by Eq. 6.29, where the maximum stable temperature gradient is $\Delta T/T_{bh} = N_{gp}$. Eq. 6.29 reduces then to

$$p_{wh} = p_{bh}(1 - N_{gp}) = 300 \text{ bar}(1 - 0.26) = 222 \text{ bar,}$$

which is the maximum pressure drop in the well-bore and which coincide with the pressure profiles presented in Figure 6.3.

6.3 Rate Dependent Pressure Losses

In a producing a well, the dynamic pressure distribution is determined by the combined effects of gravity, kinetic energy and wall friction, as described in Eq. 6.16. The latter two terms in Eq. 6.16 give rise to pressure losses that depend on the flow rate. Before discussing the combined effects, i.e. the solution of Eq. 6.16, we shall first consider the rate dependent pressure losses in isolation, in which gravity is absent. Since gravity always is present, the purpose of this exercise is hypothetical and only meant to demonstrate the important difference in scale between the terms in Eq. 6.16.

6.3.1 Uniform Temperature and No Gravity Effect

In this special and hypothetical case we will assume uniform temperature distribution in the well and omit the gravity term. Eq. 6.16 then transforms to

$$\frac{M_g}{ZRT}pdp + \frac{w^2}{A^2} \left[\frac{p}{Z} d \left(\frac{Z}{p} \right) + \frac{2f}{d_h} dy \right] = 0, \quad (6.32)$$

where $Z = \bar{Z}$ and $f = \bar{f}$ are assumed to be constants under integration in the well.

Integration from the well bottom to a position y in the well, yields

$$\frac{1}{2} \frac{M_g}{\bar{Z}RT} (p^2 - p_{bh}^2) + \frac{w^2}{A^2} \left[-\ln \left(\frac{p}{p_{bh}} \right) + \frac{2\bar{f}}{d_h} y \right] = 0, \quad (6.33)$$

Eq. 6.33 is an implicit equation in pressure p and cannot be solved directly. In most practical cases, however, the kinetic energy term $-\ln(p/p_{bh})$ is very small compared to the friction term $2\bar{f}y/d_h$ and can be safely neglected. Neglecting the kinetic energy term in Eqs. 6.32 and 6.33 we get

$$p^2 - p_{bh}^2 + \frac{4\bar{Z}\bar{f}w^2RTL}{A^2d_hM_g} \frac{y}{L} = 0, \quad (6.34)$$

where the well pressure at position y is

$$p = p_{bh} \sqrt{1 - N_{fp} \frac{y}{L}}, \quad N_{fp} = \frac{4\bar{Z}\bar{f}w^2RTL}{A^2d_hM_gp_{bh}^2}, \quad (6.35)$$

where the dimension-less number N_{fp} is characterizing the ratio of fictional - over pressure forces and is here considered to be a constant under integration along the flow path.

The well-head pressure $p_{wh}(y = L)$ is then

$$p_{wh} = p_{bh} \sqrt{1 - N_{fp}} \quad (6.36)$$

The pressure drop $\Delta p = p_{bh} - p_{wh}$ is seen to increase with increasing N_{fp} and has its maximum for $N_{fp} = 1$. Figure 6.5 shows the pressure profile given by Eq. 6.35 as function of the dimensionless number N_{fp} . The pressure profiles are concave to the left, reflecting an decreased gradient in the flow direction. This decreased gradient is caused by the increase in volumetric velocity, which again increases friction. The total pressure drop increases with increasing N_{fp} .

The restriction $N_{fp} \leq 1$, deduced from Eqs. 6.35 and 6.36, leads to the acknowledgement of a maximum possible flow rate

$$w \leq \sqrt{\frac{M_g d_h A^2 p_{bh}^2}{4\bar{Z}\bar{f}RT} \frac{1}{L}}. \quad (6.37)$$

The maximum possible flow rate corresponds to a value $N_{fp} = 1$, for which Eqs. 6.35 and 6.36 still to be valid. Analysis of the relation between y and p/p_{bh} , as given in Eq. 6.35, shows that the value of N_{fp} corresponds to the highest possible pressure gradient in the well.

For practical ranges of the parameters given in Eq. 6.37, a maximum flow rate $q_{sc,max}$ can be found. The relevance however, of such a maximum flow rate is rather dubious, at this early stage in the analysis.

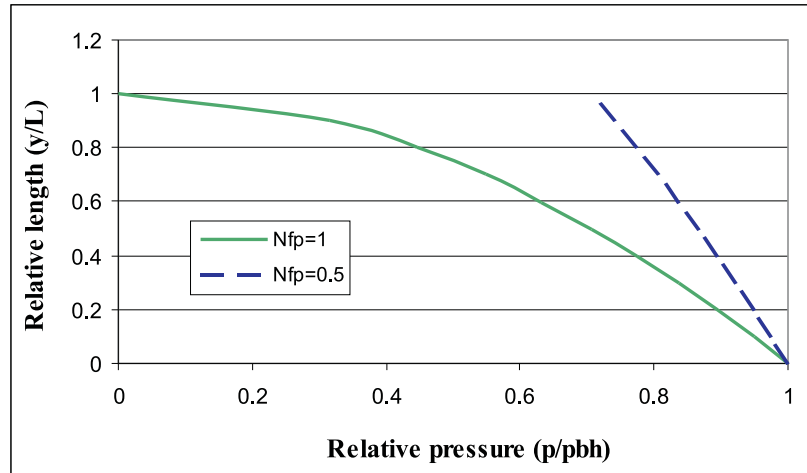


Figure 6.5: Relative pressure profile as a function of relative well height and as function of N_{fp} .

Example: Comparing Friction with Kinetic Energy

The two terms describing well-bore friction and kinetic energy loss in Eq. 6.33, can be compared by looking at the ratio,

$$\frac{-\ln(p_{wh}/p_{bh})}{2\bar{f}L/d_h},$$

where the integration in Eq. 6.33 is done over the whole well length.

Let us consider a gas reservoir being produced through a well being 3000 m ($L = 3000\text{ m}$) and an average well diameter of 15 cm ($S = 0.15\text{ m}$). The well-head and bottom hole pressures are 30 bar and 300 bar, respectively. From Figure 6.2 we will find an average friction factor $\bar{f} = 0.01$.

Substituting these number in the ratio above will then yield

$$\frac{-\ln(30/300)}{2 \cdot 0.01 \cdot 3000 / (0.15/4)} = 0.0015,$$

which demonstrates that the kinetic energy term can be neglected.

6.3.2 Linear Temperature Variation and No Gravity Effect

We now extend the above solution by taking into account a linear temperature profile as described by Eqs. 6.25 and 6.26. Substituting Eq. 6.26 into Eq. 6.32 and omitting the kinetic energy term, we obtain

$$\frac{M_g}{ZRT} pdp - \frac{w^2}{A^2} \frac{2\bar{f}}{d_h} \frac{L}{\Delta T} dT = 0, \quad (6.38)$$

which reduces to

$$pdp - \frac{2\bar{Z}fw^2RL}{A^2d_hM_g\Delta T}TdT = 0. \quad (6.39)$$

Replacement of the z-factor and the friction factor by their average values as seen above and subsequent integration gives

$$p_{bh}^2 - p^2 = \frac{2\bar{Z}fw^2RL}{A^2d_hM_g\Delta T}(T_{bh}^2 - T^2), \quad (6.40)$$

which again reduces to

$$p = p_{bh} \sqrt{1 - \frac{4\bar{Z}fw^2RL}{A^2d_hM_g\Delta T} \frac{1}{p_{bh}^2} T_{bh} \Delta T \frac{y}{L} + \frac{2\bar{Z}fw^2RL}{A^2d_hM_g\Delta T} \frac{1}{p_{bh}^2} \Delta T^2 \frac{y^2}{L^2}}. \quad (6.41)$$

Redefining the dimensionless number N_{fp} as

$$N_{fp} = \frac{4\bar{Z}fw^2RL}{A^2d_hM_g} \frac{T_{bh}}{p_{bh}^2}, \quad (6.42)$$

we may write Eq. 6.41 as follows

$$p = p_{bh} \sqrt{1 - N_{fp} \frac{y}{L} + N_{fp} \frac{\Delta T}{2T_{bh}} \frac{y^2}{L^2}}. \quad (6.43)$$

From Eq. 6.43 it follows that for the relation between bottom-hole and well-head pressure is

$$p_{wh} = p_{bh} \sqrt{1 - N_{fp} + N_{fp} \frac{\Delta T}{2T_{bh}}}. \quad (6.44)$$

In the special case of uniform well temperature, i.e. $\Delta T = 0$, Eq. 6.44 reduces to Eq. 6.36, where the dimensionless number N_{fp} has been redefined in Eq. 6.42.

Figure 6.6 illustrates the effect of temperature gradient equal to 0.2 on the pressure profile for N_{fp} equal to 1 and 0.5, as compared to Figure 6.5. In both cases, the total pressure drop is smaller in the case of a temperature gradient than for uniform well temperature. This observation is just the opposite to the case of a static gas column, as shown in Figures 6.3 and 6.4. The physical explanation is that a decreasing temperature towards the top of the well, brings about an increase in the density, which results in lower volumetric rates and consequently in less friction at the wall, i.e. reduced pressure loss in the well-bore.

As for increasing the accuracy of the pressure loss prediction based on Eq. 6.43, the comments made in the previous section also apply here. Accuracy might be enhanced by subdivision of the well-bore length and the summation of the pressure losses for each individual subdivision. Subdivision may also be required to accommodate non-linear temperature profiles and may also be seen as a step towards a more realistic simulation of the actual well trajectory.

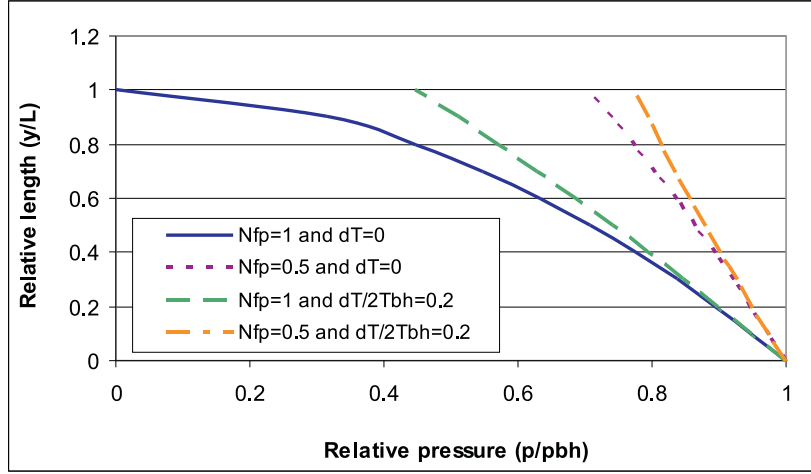


Figure 6.6: Relative pressure versus relative well length for uniform and linear temperature distribution.

6.4 Pressure Distribution in a Producing Well

Having derived solutions for the two cases where gravity and friction have been treated separately as function of the pressure losses in the well-bore, we now turn to the task of developing the solution in which both gravity and friction are included. This integrated solution will be an approximate analytical solution of Eq. 6.16, based on the following assumptions:

- Negligible change in kinetic energy (neglecting the kinetic term in Eq. 6.16).
- Linear temperature profile in the well: $T = T_{bh} - \Delta T(y/L)$.
- Constant deviation angle: $\alpha = \text{constant}$.
- Constant well-bore cross-section: $A = \text{constant}$.
- Constant z-factor: $Z = \bar{Z}$.
- Constant friction factor: $f = \bar{f}$.

This solution, first presented by Lingen [14], can be used as a basic building block to construct more general and less restrictive solutions. Under the above assumptions and when $dy = -(L/\Delta T)dT$, Eq. 6.16 can be solved as follows.

Omitting the kinetic energy term, Eq. 6.16 is written

$$dp - \left(\frac{M_g g \cos(\alpha)}{\bar{Z}R} \frac{L}{\Delta T} \frac{p}{T} + \frac{2\bar{f}w^2 ZR}{A^2 d_h M_g} \frac{L}{\Delta T} \frac{T}{p} \right) dT = 0. \quad (6.45)$$

Substituting for the dimensionless numbers N_{gp} and N_{fp} in Eq. 6.45 yields

$$dp - \left(N_{gp} \frac{T_{bh}}{\Delta T} \frac{p}{T} + N_{fp} \frac{1}{2} \frac{1}{T_{bh}} \frac{p_{bh}^2}{\Delta T} \frac{T}{p} \right) dT = 0, \quad (6.46)$$

which can be written

$$dp - \left(K_1 \frac{p}{T} + K_2 \frac{T}{p} \right) dT = 0, \quad (6.47)$$

where K_1 and K_2 are constants equal to

$$K_1 = N_{gp} \frac{T_{bh}}{\Delta T} \quad (6.48)$$

$$K_2 = N_{fp} \frac{p_{bh}^2}{2T_{bh}\Delta T} \quad (6.49)$$

Eq. 6.47 is solved by introducing a new variable $s = p/T$ and the derivative $dp = d(sT) = s dT + T ds$.

The pressure equation; Eq. 6.47 is then written

$$s dT + T ds - \left(K_1 s + K_2 \frac{1}{s} \right) dT = 0. \quad (6.50)$$

Separating this equation with respect to variables in T and s yields

$$\frac{dT}{T} = \frac{1}{K_1 - 1} \frac{s ds}{s^2 + K_3}, \quad K_3 = \frac{K_2}{K_1 - 1}. \quad (6.51)$$

Integration of Eq. 6.51 gives

$$\ln T = \frac{1}{K_1 - 1} \frac{1}{2} \ln(s^2 + K_3) + \text{constant}. \quad (6.52)$$

Substitution for $s = p/T$ gives

$$\ln T = \frac{1}{2(K_1 - 1)} \ln \left(\frac{p^2}{T^2} + K_3 \right) + \text{constant}. \quad (6.53)$$

Introducing integration limits: $p \rightarrow p_{bh}$ and $T \rightarrow T_{bh}$ we get

$$\ln \frac{T}{T_{bh}} = \frac{1}{2(K_1 - 1)} \ln \frac{(p/T)^2 + K_3}{(p_{bh}/T_{bh})^2 + K_3}. \quad (6.54)$$

The logarithmic terms in Eq. 6.54 are easily removed and we get

$$\left(\frac{T}{T_{bh}} \right)^{2(K_1+1)} = \frac{(p^2/T^2) + K_3}{(p_{bh}^2/T_{bh}^2) + K_3}. \quad (6.55)$$

Expressing Eq. 6.55 in terms of pressure on the left hand side and temperature and constants on the right, we get

$$p = p_{bh} \sqrt{\left(\frac{T}{T_{bh}} \right)^{2K_1} + K_3 \frac{T^2}{p_{bh}^2} \left[\left(\frac{T}{T_{bh}} \right)^{2(K_1-1)} - 1 \right]}, \quad (6.56)$$

where the constants K_1 , K_2 and K_3 are defined by Eqs. 6.48, 6.49 and 6.51, respectively.

Example: Dimensionless numbers; N_{gp} and N_{fp} .

Nearly all parameters involved in the calculation of pressure behaviour in the well-bore are lumped together in two dimensionless numbers; N_{gp} and N_{fp} .

Subdividing these parameters in gas related and well-bore related parameters, we get:

$$\begin{aligned} M_g &= 0.027 \text{ kg/mol} & \bar{Z} &= 1 & R &= 8.314 \text{ J/(mol} \cdot \text{K)} \\ T_{bh} &= 393 \text{ K} & p_{bh} &= 300 \text{ bar} \\ \omega &= (\rho_g \cdot q)_{sc} = 1.5 \cdot 1 \cdot 10^6 \text{ kg/day} \end{aligned}$$

where the gas density at standard conditions is 1.5 kg/m^3 ,

$$\begin{aligned} L &= 3000 \text{ m} & g &= 9.8 \text{ m/s}^2 & \alpha &= 0 \\ \bar{f} &= 0.01/4 & d_h(S = 0.15 \text{ m}) &= 0.15/4 \text{ m} & A &= \pi \cdot (S/2)^2 = 0.018 \text{ m}^2 \end{aligned}$$

Using the definitions implied in Eq. 6.46,

$$\begin{aligned} N_{gp} &= \frac{M_g \cdot g \cos(\alpha)L}{\bar{Z}RT_{bh}}, \\ N_{fp} &= \frac{4\bar{f}\omega^2\bar{Z}RT_{bh}L}{A^2d_hM_gP_{bh}^2}, \end{aligned}$$

we find typical numbers; $N_{gp} = 0.24$ and $N_{fp} = 0.10$.

Notice that the dimensionless number N_{fp} is less than unity as expected in the case of constant temperature in the well-bore, see Eq. 6.36.

Notice also that the dimensionless number N_{gp} represents the ratio of gravitational to pressure forces, while N_{fp} represents the ratio of friction forces to the pressure forces. In practice, tubing diameters are commonly chosen such that pressure loss due to friction is smaller than the gravitational loss. Consequently, the friction number should be smaller than the gravity number.

The pressure equation Eq. 6.56, may be written in terms of well length position y , simply by using the definition of linear temperature profile. Applying the definition of the constants; K_1 , K_2 and K_3 , we find,

$$\begin{aligned} p &= p_{bh} \sqrt{\left(1 - \frac{\Delta T}{T_{bh}} \frac{y}{L}\right)^{2N_{gp}/(\Delta T/T_{bh})}} \\ &+ \frac{N_{fp}}{2(N_{gp} - (\Delta T/T_{bh}))} \left(1 - \frac{\Delta T}{T_{bh}} \frac{y}{L}\right)^2 \left[\left(1 - \frac{\Delta T}{T_{bh}} \frac{y}{L}\right)^{2(N_{gp}/(\Delta T/T_{bh})-1)} - 1 \right]. \end{aligned} \quad (6.57)$$

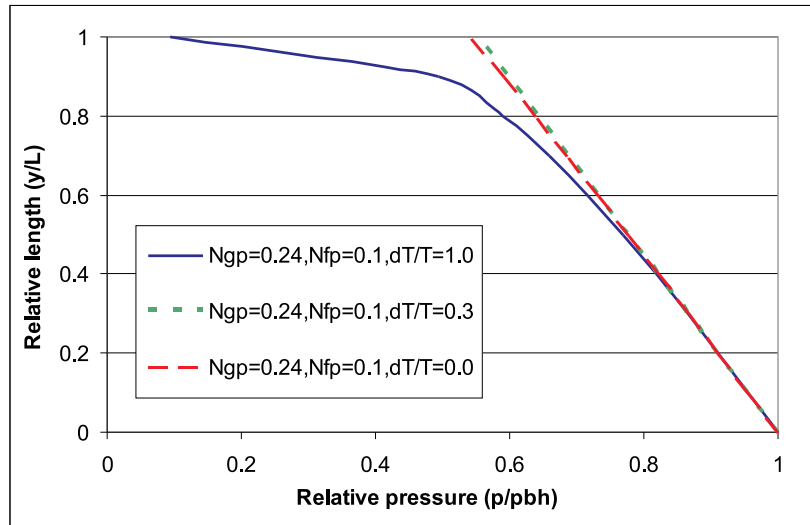


Figure 6.7: Relative pressure versus relative well length for all effects included.

Data taken from the example above is used when Eq. 6.57 is plotted as in Figure 6.7. In this plot, a "normal" temperature gradient $\Delta T/T_{bh} = 0.3$ is compared to the case of constant well-bore temperature, $\Delta T/T_{bh} = 0$ and the limiting case of $\Delta T/T_{bh} = 1$.

It is interesting to notice that a "normal" well-bore pressure profile behaves quite similar to the case of constant well-bore temperature. We may therefore conclude that the gas cooling effect caused by a decreasing well gas temperature, which again leads to an increased gas density, will reduce the gas flow rate and therefore also reduce the friction loss, to such a degree that the two effects seem to cancel out each other.

The assumptions introduced to derive the solution given by Eqs. 6.56 and 6.57 might be too restrictive for some practical situations. In those cases it is always possible to subdivide the well-bore into a number of length elements such that the assumptions made are valid. The solution for the entire well-bore is then obtained by applying Eq. 6.56 and 6.57 successively to the pressure profile in the well-bore with e.g. varying deviation angle, varying well-bore cross-section, non-linear temperature profile, varying z-factor caused by a pronounced pressure and temperature gradient in the well or varying friction factor along the well length.

6.5 Multi-Phase Flow

So far, we have dealt with single-phase gas flow. In practice, however, well streams usually contain liquid condensate and/or water. Generally, the relative liquid content of the well stream is rather small. Because of low liquid content, together with high flow rates in producing gas wells, the liquids could be considered to be homogeneously dispersed in the gas, in the form of a mist flow.

Under these conditions, the flowing mixture of gas and liquid may be considered a *homogeneous single-phase fluid* with corresponding homogeneous fluid properties. This, then suggests that the flow behavior of a gas-liquid mixture in a well-bore can be

described in terms of a single-phase flow. The conditions is thus that appropriate corrections and modifications are included, to reflect the properties of the pseudo-homogeneous fluid. To determine these modifications we shall examine how the basic flow equation is affected when applied to the flow of pseudo-homogeneous gas-liquid mixtures.

We start this investigation with the extended Bernoulli equation, Eq. 6.15, which when omitting the kinetic energy term, for a pseudo-homogeneous gas-liquid mixture can be written

$$\frac{dp}{\rho_m} + g \cos(\alpha)dy + \frac{2f_m u_m^2}{d_h} = 0, \quad (6.58)$$

where the subscript m denotes the mixture.

As can be seen from the Bernoulli equation, above, the mixture specific parameters that have to be evaluated for the gas-condensate-water mixture are; the density ρ_m , the volumetric velocity u_m and the friction factor f_m . For reasons that will become clear, we shall first consider gas-condensate mixtures and then expand to gas-condensate-water mixtures.

6.5.1 Gas-Condensate Mixtures

In the case of gas-condensate mixtures, the properties of the pseudo-homogeneous fluid in the well-bore may be taken as identical to those of the single-phase recombined hydrocarbon fluid, i.e. the fluid obtained from recombining the well stream gas and liquid in the same proportion as they are produced. This means that the mixture density may be taken equal to the density of the recombined gas, and we get

$$\rho_m = (\rho =) \frac{M_m p}{Z_m RT}, \quad (6.59)$$

where M_m is the molecular mass and Z_m is the z-factor of the recombined fluid of gas and liquid.

The mass flow rate of the gas-condensate mixture is equal to the sum of the mass flow rate of dry gas and condensate, therefore

$$w_m = (w =) \rho_m u_m A, \quad (6.60)$$

where ρ_m and u_m are the mixture density and volumetric velocity, respectively.

The volumetric velocity is therefore given as

$$u_m = \frac{w_m}{\rho_m A}, \quad (6.61)$$

expressing the fact that the liquid condensate and the dry gas are flowing together.

As for the friction factor we assume that the single-phase friction factor also apply to pseudo-homogeneous mixtures and thus depend on the relative roughness and the Reynolds number as given by Eq. 6.9. Taking the mixture viscosity equal to the viscosity of the recombined gas, we find the Reynolds number for the mixture

$$Re_m = \frac{\rho_m u_m d_h}{\mu_m}. \quad (6.62)$$

The Reynolds number for the gas-condensate mixture is then equal to the Reynolds number for the recombined gas. hence, the friction factor for the mixture is the same as for the recombined gas, i.e.

$$f_m = f. \quad (6.63)$$

The assumption that the viscosity of the mixture is equal to the single-phase gas viscosity is not very critical. Friction factors at high Reynolds numbers are generally near constant and not very sensitive to the actual value of the Reynolds number. The viscosity at high Reynolds numbers is well defined, as can be seen from Figure 6.2.

If we introduce the mixture density from Eq. 6.59, the volumetric velocity Eq. 6.61 and the friction factor Eq. 6.63 into the Bernoulli equation Eq. 6.58 and eliminate the gas density by means of Eq. 6.59, we end up with exactly the same equation as for single-phase gas flow in Eq. 6.16. Therefore the previous derived solution for single gas flow in producing wells Eqs. 6.56 and 6.57 may also be applied to the flow of gas-condensate mixtures, provided the fluid properties; the z-factor and the viscosity, are evaluated for the recombined gas mixture. This restriction is identical with what we already have done when the gas properties has been evaluated at conditions similar to the prevailing conditions in the well, where all liquid condensate is dissolved in the dry gas.

6.5.2 Gas-Condensate-Water Mixtures

We shall now consider mixtures of gas, condensate and water. As we have seen above, the gas and condensate in the mixture may be represented by the recombined gas. This means that the mixture of gas, condensate and water can be considered as a mixture of recombined gas and water. In the following, the term gas therefore means recombined gas.

Let the water content of the pseudo-homogeneous gas-water mixture be given by a volume fraction ϵ , where ϵ is the relative volume of water to the volume of gas and water

$$\epsilon = \frac{V_w}{V_g + V_w}, \quad (6.64)$$

where V_g is the volume of the recombined mixture of gas and liquid condensate.

If we choose to consider a small cylindrical section of the well stream, we may define the mass of the gas and water contained in the cylindrical element as

$$m_g + m_w = \rho_m(V_w + V_g), \quad (6.65)$$

where the subscripts w and g stands for water and gas, respectively, while the subscript m is the mixture of gas and water. Using the definition $m = \rho V$ and the definition Eq. 6.64, we may express the density of the mixture as

$$\rho_m = \rho_w \epsilon + \rho_g (1 - \epsilon) = \rho_g \left(1 - \epsilon + \frac{\rho_w}{\rho_g} \epsilon \right). \quad (6.66)$$

Based on Eq. 6.64 and the definition of the volume flow rate $q = dV/dt$, the water flow rate is written

$$q_w = \epsilon(q_w + q_g), \quad (6.67)$$

Combining the mixture density Eq. 6.66 and Eq. 6.67 we arrive at

$$\rho_m = \rho_g \left(1 - \frac{q_w}{q_w + q_g} + \frac{\rho_w}{\rho_g} \frac{q_w}{q_w + q_g} \right), \quad (6.68)$$

where we generally have that the volumetric velocity of water is much less than the volumetric velocity of gas, i.e. $q_w \ll q_g$. We may therefore approximate Eq. 6.68 by

$$\rho_m \simeq \rho_g \left(1 + \frac{\rho_w q_w}{\rho_g q_g} \right) = \rho_g \left(1 + \frac{w_w}{w_g} \right) = \rho_g F_w, \quad (6.69)$$

where $F_w = 1 + w_w/w_g$ is the water correction factor.

For a given ratio of producing water-gas flow, the factor F_w is constant. Hence the density of the gas-water mixture equals the single-phase gas density times the constant factor F_w . The implication of the water correction factor is therefore as follows:

$$\begin{aligned} w_m &= \rho_m u_m A \\ &= w_g + w_w = w_g \left(1 + \frac{w_w}{w_g} \right) = w_g F_w, \end{aligned} \quad (6.70)$$

$$u_m = \frac{w_m}{\rho_m A} = \frac{w_g F_w}{\rho_g F_w A} = \frac{w_g}{\rho A} = u_g, \quad (6.71)$$

$$Re_m = \frac{\rho_m u_m d_h}{\mu_m} = \frac{\rho_g F_w u_g d_h}{\mu_g} = Re_g F_w, \quad (6.72)$$

where Re_g is Reynolds number for the recombined gas.

The friction factor for the gas-water mixture is to be evaluated at the appropriate Reynolds number for that mixture. If we assume the viscosity of the gas is not affected by the water content in the mixture, - then the Reynolds number for the mixture follows from multiplication of the single-phase gas Reynolds number and we may use the water correction factor, as shown in Eq. 6.72.

Substitution of the mixture density Eq. 6.69 and the volumetric velocity Eq. 6.71 in to the Bernoulli equation Eq. 6.58 and using Eq. 6.59 for the gas density, we then obtain for the basic flow equation for pseudo-homogeneous water-gas mixtures

$$dp + \frac{M_g p}{ZRT} g \cos(\alpha) F_w dy + 2f_m \frac{ZRT}{M_g p} \frac{w_g^2}{A^2 d_h} F_w dy = 0. \quad (6.73)$$

Comparing Eq. 6.73 with the equation for pure single-phase flow of real gas Eq. 6.58, we observe that in the pseudo-single-phase flow equation, the gravity term and the friction term are both multiplied by the constant water correction factor F_w , and that the friction factor is to be evaluated for the mixture Reynolds number. Consequently, the solution obtained for pure single-phase flow in producing wells, Eq. 6.56, also apply to

pseudo-single-phase flow, provided the dimensionless numbers N_{gp} and N_{fp} are replaced by the corresponding dimension-less numbers for the gas-water mixture as given below

$$N_{gp,m} = \frac{M_g g L \cos(\alpha)}{\bar{Z} R T_{bh}} F_w, \quad (6.74)$$

$$N_{fp,m} = \frac{4\bar{Z}\bar{f}w_g^2 R T_{bh} L}{p_{bh}^2 A^2 d_h M_g} F_w, \quad (6.75)$$

where \bar{f} is the average friction factor in the flow conduit for the gas-water mixture.

Hence, the gravity number for the water-gas mixture follows from multiplying the gravity number for the recombined gas by the water correction factor. The friction factor for the mixture includes a modified friction factor and also contains the water correction factor.

6.6 Liquid Accumulation in Gas Wells

Gas wells producing dry gas have normally a low pressure drop from bottom to top, especially at low well rates. When liquids are introduced into the well, this pressure drop will increase. The total pressure drop in the well is primarily, as we have seen, the sum of the pressure drop from elevation (weight of the fluids) and friction. For a correctly sized well tubing, the friction term is small compared to the gravitational term. Therefore, - liquid loading in the well-bore has a direct impact on the total flowing pressure drop in the well.

When a gas well produces under mist flow conditions where several phases are present, a minimum flow rate is necessary below which the liquids cannot be unloaded to the surface, i.e. there exists a *minimum unloading rate*. For rates below the minimum unloading rate liquids will accumulate at the bottom of the well and will eventually prevent gas from flowing into the well.

Turner et al. [16] have developed a mechanistic model where transport of liquid in gas wells do occur by small liquid droplets contained in the gas stream. To estimate the minimum unloading rate, the following arguments has been proposed.

Condensate liquid and/or water are thought to be homogeneous distributed in the dry gas as small droplets of a certain diameter. To maintain the distribution of droplets in the gas, the dry gas velocity must exceed the terminal free-fall velocity of droplets in the stagnant gas. Droplet terminal free-fall velocity in dry gas is given as

$$v_f = \sqrt{\frac{4 \Delta \rho g d}{3 \rho_g C_d}}, \quad (6.76)$$

where v_f is the free-fall velocity. ρ_g is the dry gas density while $\Delta \rho$ is the density difference between liquid and gas. d is the diameter of the droplet and C_d is the drag coefficient, which again depends on the Reynolds number, where

$$Re = \frac{\rho_g v_f d}{\mu_g}, \quad (6.77)$$

where μ_g is the gas viscosity. For Reynolds numbers in excess of 1000 the drag coefficient may be taken as a constant; $C_d \sim 0.43$, as proposed by Beek and Mutzall et al. [3] Eq. 6.76 can be easily derived when the dynamical drag-force on a spherical droplet in gas is found to be,

$$F_S = C_d \pi r^2 \rho_g \frac{v^2}{2}. \quad (6.78)$$

Eq. 6.76 shows that the free-fall velocity of a liquid droplet in a stagnant gas increases with increasing diameter of the droplet. There exist an upper limit for the size of free-falling droplets and this upper limit is determined by the competition between the inertial forces that tend to deform the droplet and the interfacial forces that resist this deformation. The ratio of the inertial forces and the interfacial forces is expressed by

$$\text{WE} = \frac{\rho_g v_f^2 d}{\sigma}, \quad (6.79)$$

where WE is the Weber number and σ is the interfacial tension between gas and liquid.

Experiments have indicated that stable drops exist for values of the Weber number up to about 30. Therefore, the maximum diameter of a stable free-falling droplet is

$$d_{max} = \frac{30\sigma}{\rho_g v_f^2}. \quad (6.80)$$

Combining Eqs. 6.76 and 6.80 and the fact that $C_d \sim 0.43$, we obtain for the terminal free-fall velocity v_f (for the largest stable droplets),

$$v_{f,max} = \left(40 \frac{\Delta\rho g \sigma}{\rho_g^2 C_d} \right)^{1/4} = 3.1 \left(\frac{\Delta\rho g \sigma}{\rho_g^2} \right)^{1/4}. \quad (6.81)$$

Theoretically the minimum unloading velocity in a gas well is equal to the free-fall velocity of the largest stable drop. Experimental data have indicated that the actual minimum velocity is about 16% higher than stated in Eq. 6.81 and we therefore have the minimum unloading velocity

$$u_{min} = 3.6 \left(\frac{\Delta\rho g \sigma}{\rho_g^2} \right)^{1/4}, \quad (6.82)$$

where u_{min} is the limiting gas flow velocity in the well-bore.

The minimum unloading flow rate, in terms of gas rate at standard conditions, is thus

$$\begin{aligned} q_{sc,min} &= \frac{q_{min} \rho_g}{\rho_{sc}} = \frac{u_{min} A \rho_g}{\rho_{sc}} \\ &= A \frac{\rho_g}{\rho_{sc}} 3.6 \left(\frac{\Delta\rho g \sigma}{\rho_g^2} \right)^{1/4} \\ &= 3.6 A \frac{\sqrt{\rho_g}}{\rho_{sc}} (\Delta\rho g \sigma)^{1/4}, \end{aligned} \quad (6.83)$$

where $q_{sc,min}$ is the minimum unloading rate at standard conditions. A is the cross-section of the flow conduit and ρ_{sc} is the dry gas density at standard conditions.

According to Eq. 6.83, the minimum volumetric unloading rate increases for most practical cases with increasing gas density, i.e. a lighter gas is able to lift relative more liquids than a denser gas. Since the highest gas density in the flowing well occurs at the bottom of the well where the pressure is the highest, the minimum unloading rate should therefore be evaluated at bottom-hole conditions.

As can be seen from Eq. 6.83, the unloading rates for water and condensate are different because of the different interfacial tension and the density difference. Since interfacial tension and density difference for water-gas systems are generally higher than for condensate-gas systems, the unloading rate for water is larger than for condensate. Hence, if both condensate and water are present in the well-bore, water will be the controlling fluid. As both parameters occur in Eq. 6.83 as the fourth root, however, the difference in unloading rates will not be very pronounced.

Example: Minimum Unloading Rate

A well with an average well diameter equal to 15 cm, is producing gas from a gas-condensate reservoir. The reservoir gas density is $\rho_g = 300 \text{ kg/m}^3$ and at standard conditions $\rho_{sc} = 3 \text{ kg/m}^3$.

For water in gas systems, the interfacial tension σ_{wg} , can be estimated from correlations [19] that link σ_{wg} to the water-gas density difference $\Delta\rho_{wg}$

$$\sigma_{wg}[N/m] = 0.0150 + 5.7 \cdot 10^{-5} \rho_{wg}[kg/m^3]. \quad (6.84)$$

When the density difference $\Delta\rho_{wg} = 700 \text{ kg/m}^3$, Eq. 6.84 gives a interfacial tension $\sigma = 54.9 \cdot 10^{-3} \text{ N/m}$

Using Eq. 6.83 we find the minimum unloading rate at standard conditions

$$q_{sc,min} = 3.6 \pi \left(\frac{0.15}{2} \right)^2 \frac{\sqrt{300}}{3} (700 \cdot 9.8 \cdot 54.9 \cdot 10^{-3})^{1/4} = 1.6167$$

The minimum unloading rate is $1.6167 \text{ m}^3/s$, or in terms of field units (commonly used): $1.4 \cdot 10^5 \text{ Sm}^3/\text{day}$.

All gas wells will cease production as the reservoir pressure depletes. The presence of liquids can reduce production even faster. Keeping the well rate above the minimum unloading rate will secure production until actions must be taken to prolong the life of the well. When the gas velocity begins to drop, the well flow can become erratic with slug or bubble flow. This happens because an increasingly larger fraction of the tubing volume is filled with liquid. As liquid accumulates, an increased p_{bh} could reduce liquid loading.

Several actions can be taken to reduce or prevent liquid loading [13]:

- Flow the well at a high velocity to stay in the mist flow by use of smaller tubing or by creating a lower well head pressure.
- Pump or gas lift the liquids out of the well. Here are many possible variations [7].
- Foam the liquids, enabling the gas to lift liquids from the well.
- Inject water into an underlying disposal zone.
- Prevent liquids formations or production into the well (e.g., seal off water zone or use insulation or heat to prevent condensation).

If liquid accumulation in the flow path can be reduced, then p_{bh} will be reduced and production increased.

6.7 Simulation Examples

In this example, as in the previous, we have chosen a reservoir hydrocarbon pore volume $V_p = 4 \cdot 10^6 \text{ Rm}^3$ and a initial terminal flow rate $q_g = 5 \cdot 10^5 \text{ Sm}^2/\text{day}$. The gas is produced towards a minimum well-head pressure $p_{wh,min} = 20 \text{ bar}$. The simulation is performed in accordance to data as presented above.

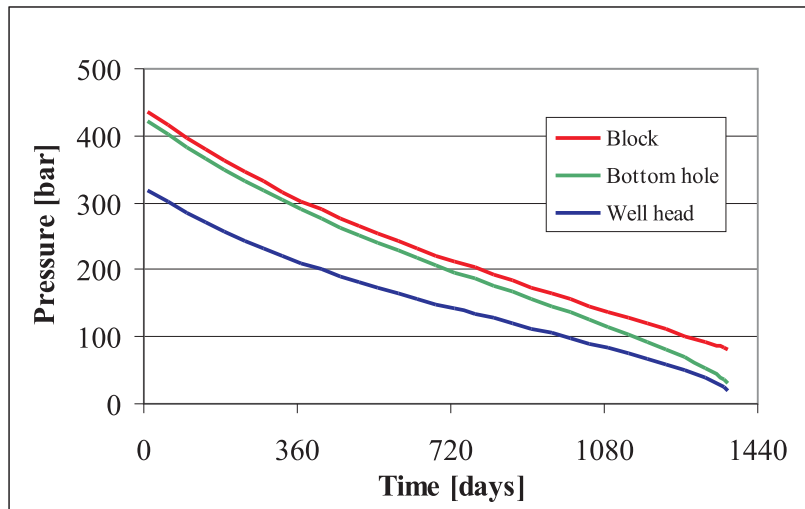


Figure 6.8: Pressure profiles as function of time.

Figure 6.8 shows the pressure profiles; the average reservoir (block) pressure, the bottom-hole pressure and the well-head pressure as function of time at constant gas rate. In order to distinguish between the average block pressure and the bottom-hole pressure in the figure, we have chosen a reservoir permeability $k = 20 \text{ mD}$, considered to be on the low side.

The well-head pressure as seen in Figure 6.8 is considerable less, in particular at early times, than the bottom hole pressure. As time passes and more and more gas is produced, the pressure difference becomes less. The fact that the gas becomes lighter

and lighter due to condensation in the reservoir is not alone enough to explain this pressure behavior.

Since the bottom-hole pressure is gradually decreasing, the pressure drop in the well must also decrease, due to the fact that the well-head pressure is related to a constant terminal pressure (atmospheric pressure). The well-head pressure is therefore squeezed between the constant terminal pressure, (here the minimum well-head pressure) and the decreasing bottom-hole pressure. As the bottom hole pressure approaches the terminal pressure, so must the well head pressure and therefore it is quite natural for the two pressure to converge towards each other as shown in Figure 6.8.

6.7.1 Well-Head Pressure as Function of Dip Angle

Figure 6.9 shows the well-head pressure as function of time for dip angles of 0 degrees (vertical well) and 45 degrees. In the two cases, the well length has been kept constant, i.e. the elevation height for a dip angle of 45 degrees is therefore only half the elevation height for a vertical well. The pressure drop for the inclined well is therefore less than for the vertical well, simply because the bottom-hole pressure is lifting the gas only half the vertical distance, compared to the vertical well. The well-head pressure for the inclined well is therefore higher than for the vertical well.

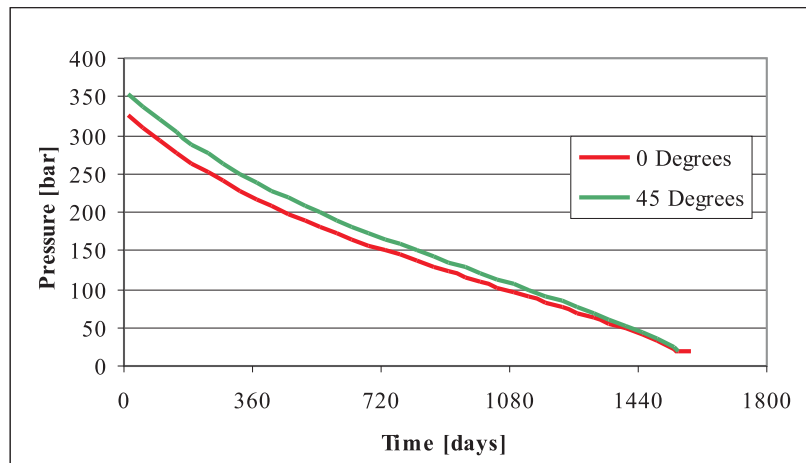


Figure 6.9: Well-head pressure as function of time for vertical well and inclined well.

The pressure drop in a well is the sum of the pressure drop caused by friction loss against the well wall and transport of gas in the gravitational field. In Figure 6.9, the fractional pressure loss is the same in the two cases, since the well length is the same. The pressure loss due to gravitation is only half in the inclined well case compared to the vertical well and this pressure difference is what is observed in Figure 6.9.

The reason for the asymptotic pressure development with time, seen in Figure 6.9, follows the same type of arguments as presented above when explaining the pressure difference between the bottom-hole pressure and the well-head pressure in Figure 6.8; since the pressure difference between the bottom-hole pressure and the terminal pressure approaches zero with time, so must all other pressures measured along the well bore

length.

6.7.2 Well-Head Pressure as Function of Time for Two Different Well Flow Rates

Figure 6.10 shows the well-head pressure for two different well-head flow rates, namely $5 \cdot 10^5 \text{ Sm}^3/\text{day}$ and $3.5 \cdot 10^5 \text{ Sm}^3/\text{day}$. When the flow rate is reduced, less gas is produced per time and consequently the time needed to produce the gas in place increases. At zero time the two pressures are equal and since the general pressure drop in the reservoir is lower for lower rates, the well-head pressure will always be lower in the high rate case, as seen in the figure.

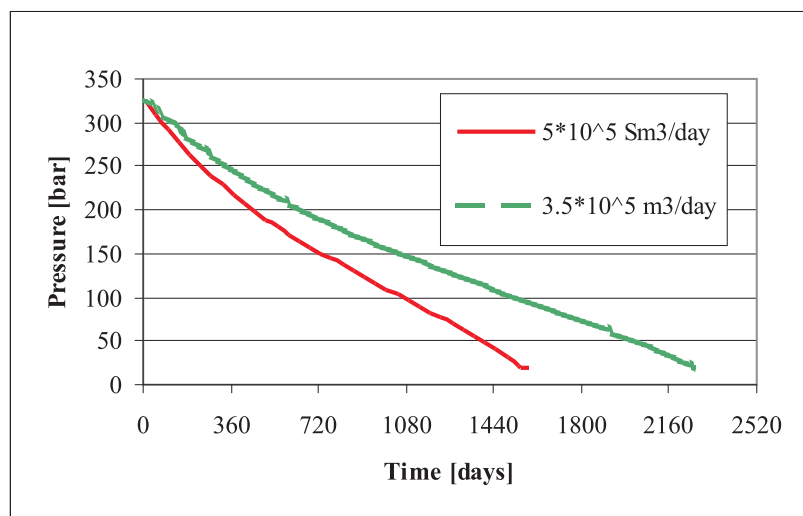


Figure 6.10: Well-head pressure as function of time for two different well flow rates.

6.7.3 Well-Head Pressure as Function of Time for Two Different Well-Bore Diameters.

When the well-bore diameter is reduced, as shown in Figure 6.11, it can be expected that the pressure drop in the well-bore will increase. In order to force the same amount of gas (same gas rate) through a reduced well-bore cross-section will cause the pressure drop per well length to increase.

Another way to look at it, is to observe that the well-bore pressure in Eq. 6.56 depends on the constants given in Eqs. 6.74 and 6.75, where the constant in Eq. 6.75 varies with the third power of the diameter. When the diameter decreases, N_{fp} increases and thus, the well head pressure will decrease.

Since the pressure drop is somewhat higher in the more narrow well bore, the well-head pressure will be slightly lower. The pressure profile for the narrow well will therefore always be lower than compared to the pressure profile of the well with larger well-bore cross-section. Since relatively more energy is used for lifting the gas in the narrow well, the minimum well-head pressure is reached sooner in this well, compared

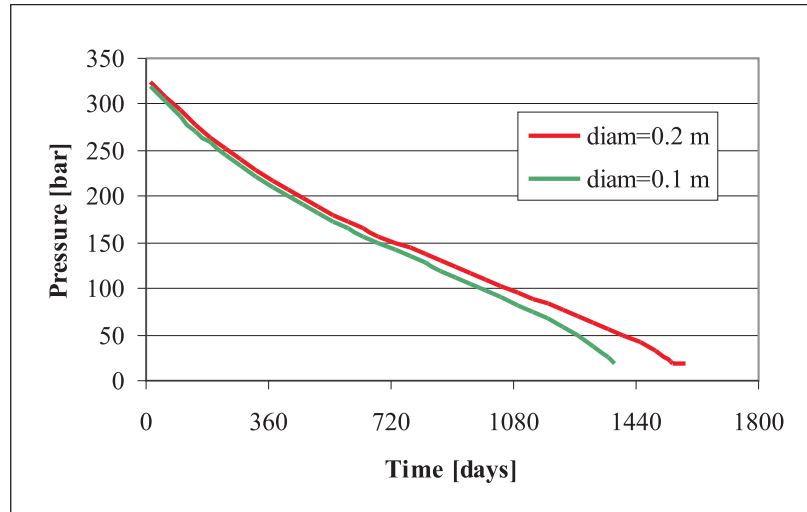


Figure 6.11: Well-head pressure as function of time for two different well-bore diameters.

to the wider well. Therefore, the production of gas must be abandoned earlier in the narrower well.

6.7.4 Well-Head Pressure as Function of Time for Associated Water Production

Water produced together with the gas will increase the pressure drop in the well, since more energy is needed to lift the water from the reservoir to the surface. Higher pressure drop in the well means lower well-head pressure, as shown in Figure 6.12. As can be seen from Figure 6.12, the water production drastically reduce the well-head pressure. Increased associated water production will therefore eventually kill the well by bringing the well-head pressure below the minimum well head pressure much faster than otherwise would be the case.

W_p is normally cumulative produced water at the surface. In these calculations, however, W_p is related to gas production and the number $W_p = 0.002$ means that the water produced is 0.2 % of the gas produced, measured in Sm^3 .

6.8 Heat Losses in Producing Well

In section 6.1, we derived the basic Equation 6.15, describing flow of real gas in a straight conduit, taking into account gravity, wall friction and kinetic energy. What is not accounted for in this equation are thermal effects such as cooling of the gas by gas expansion and heat exchange with the surrounding reservoir, - which is the topic of this section.

In Eq. 6.15, an "ad hoc" assumption was made about the temperature profile in the well, where a linear temperature decline profile from the bottom-hole to the well-head position was defined; $T(y) = T_{bh} - \Delta T \cdot y/L$. Here $\Delta T = T_{bh} - T_{wh}$, is the temperature difference along the well length L . The linear temperature profile is assumed to represent

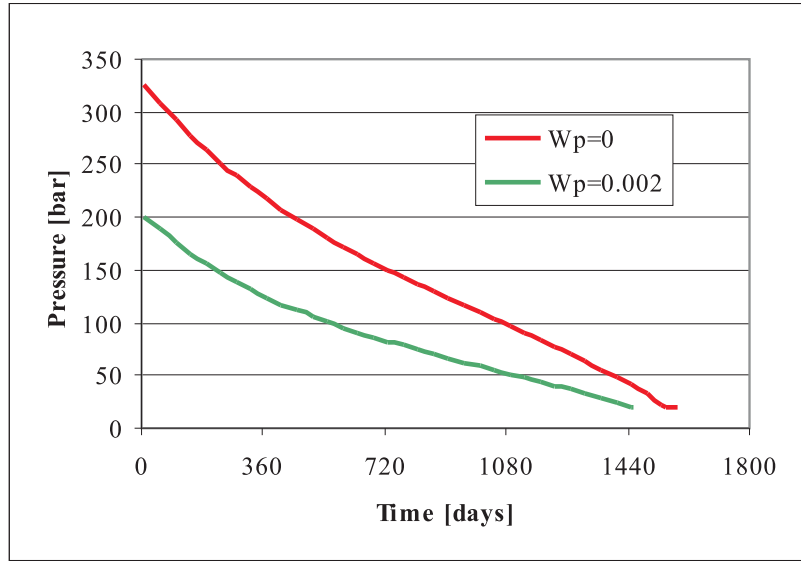


Figure 6.12: well-head pressure as function of time for associate water production.

the heat losses to the surroundings along the well. Combining the Bernoulli equation and the above linear temperature profile, gives the pressure solution in the well as function of elevation, as we have seen in Eq. 6.57. Our strategy in this section is identical to the above mentioned, as we will develop the temperature profile $T(y)$, and then substitute this equation into the Bernoulli equation. The solution yields a pressure solution for a straight flow conduit of constant diameter.

We will in the following assume a possible heat loss, radially directed, relative to the well-bore, as depicted in Figure 6.13

6.8.1 Basic Thermodynamics

The first law of thermodynamics states that the heat delivered to a system is equal to the work done by the system on the surroundings when the internal energy of the system remains unchanged, as depicted in Figure 6.13. Generally, the first law is formulated;

$$dU = \delta Q - \delta W, \quad (6.85)$$

where δQ is the heat transported *to* the system and δW is the work done *by* the system.

In Figure 6.13, the heat exchange is drawn as if the heat is delivered *to* the system, while we would expect the exchange of heat to pass *from* the well to the surroundings since the temperature of well-bore gas in a producing well would be higher than in the surrounding formation. This means that the heat flow, as shown in Figure 6.13, is negative.

The work done on the surroundings is defined as volumetric work plus work related to elevation,

$$\delta W = p dV + \delta W_e, \quad (6.86)$$

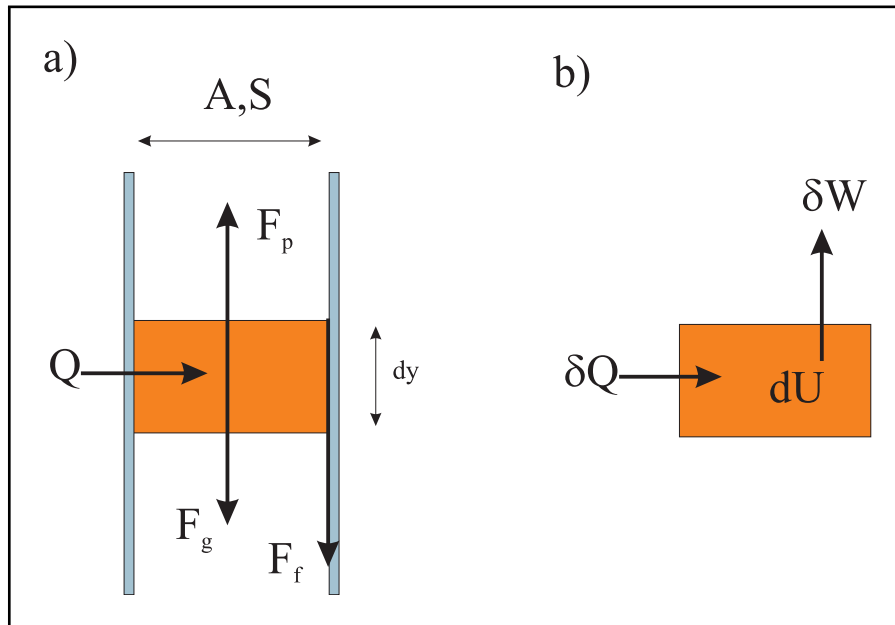


Figure 6.13: Heat and work flow: a) Section of well with heat flow and gravity force. b) System of gas volume element and energy, heat and work balance (1. law of thermodynamics).

where $\delta W_e = mg \cos(\alpha)dy$ is the work needed to elevate the mass element m a distance dy .

We will assume the heat exchange to take place at an elevation y , i.e. we will solve the heat exchange problem at a fixed elevation. Under stable flowing conditions, the pressure is considered constant (at any elevation) at this elevation and $dp = 0$. The first law can then be written,

$$dU + (pdV + Vdp) = \delta Q - mg \cos(\alpha)dy, \quad (6.87)$$

Notice that the term Vdp in the equation above is added (by hand), as $Vdp = 0$.

Using the definition of Enthalpy, $H = U + pV$, the above equation is written,

$$dH = \delta Q - mg \cos(\alpha)dy, \quad (6.88)$$

where the heat added to the gas, δQ minus the potential energy of elevation is equal to the change in enthalpy.

Eq. 6.88 shows why enthalpy is preferred over internal energy in describing systems at constant pressure. In many laboratory experiments pressure is constant and very often equal to the atmospheric pressure, which again makes data from these experiments more easily accessible. Enthalpy data is therefore readily measured at laboratory conditions.

The enthalpy is a thermodynamic function dependent on pressure and temperature; $H = H(p, T)$. Differentiating H gives,

$$dH = \left(\frac{\partial H}{\partial T} \right)_p dT + \left(\frac{\partial H}{\partial p} \right)_T dp, \quad (6.89)$$

where $(\partial H/\partial T)_p$ is the isobaric heat capacity (at constant pressure); $C_p = (\partial H/\partial T)_p$. The heat capacity can be measured in the laboratory or made available through PVT simulations, using the preferred equation of state.

In some thermodynamic experiments, enthalpy is considered unchanged, i.e. $dH = 0$. In the Joule-Thomson experiment gas is expanding through a porous plate (or diaphragm) and a pressure drop, Δp , is created over the plate. A temperature difference, ΔT , is also observed across the plate and the ratio $\Delta T/\Delta p$ is characterizing this kind of experiments. This ratio is defined as the Joule-Thomson coefficient,

$$\eta_{JT} = \left(\frac{\partial T}{\partial p} \right)_h, \quad (6.90)$$

where the subscript h indicates a process at constant enthalpy. η_{JT} can be positive as well as negative. Negative values of η_{JT} are typically found for low temperature and high pressure. Note that the change to lower-case letters is indicating volume specific quantities, i.e. divided by number of moles. η_{JT} is also accessible through PVT simulations as is the case of c_p . Notice: $C_p = n \cdot c_p$, where c_p is the specific heat capacity. (The Joule-Thomson experiment is described in most books on thermodynamics or books on physical chemistry [5, 17, 12, 2].)

When $dh = 0$, Eq. 6.89 becomes

$$0 = c_p dT + \left(\frac{\partial h}{\partial p} \right)_T dp, \quad (6.91)$$

and

$$\left(\frac{\partial h}{\partial p} \right)_T = -c_p \left(\frac{\partial T}{\partial p} \right)_h = -c_p \eta_{JT}. \quad (6.92)$$

The enthalpy defined in Eq. 6.89 is therefore written

$$dh = c_p dT - c_p \eta_{JT} dp, \quad (6.93)$$

where both thermodynamic parameters c_p and η_{JT} can be found from PVT simulations or laboratory experiments.

6.8.2 Temperature in Well-Bore Flow

The heat flow from the surroundings into the volume element, as depicted in Figure 6.13, is then written,

$$\delta q_Q = c_p dT - c_p \eta_{JT} dp + M_g g \cos(\alpha) dy, \quad (6.94)$$

where $m = n \cdot M_g$ and M_g is the average molecule mass of the gas and $\delta Q = n \cdot \delta q_Q$.

Substituting Eq. 6.94 into the basic mechanical flow equation, Eq. 6.16, with substituting the pressure drop dp and neglecting the kinetic term in Eq. 6.16, we get

$$\frac{c_p dT + M_g g \cos(\alpha) dy - \delta q_Q}{c_p \eta_{JT}} + \frac{M_g \cos(\alpha) p}{RT} \frac{dy}{Z} + \frac{2f w^2 RT Z}{d_h A^2 M_g p} dy = 0. \quad (6.95)$$

Rearranging Eq. 6.95 and introducing dimensionless temperature and well position, yields

$$dT_D + \left[\frac{ZR}{c_p} + \eta_{JT} \frac{p}{T} \right] N_{gp} dy_D + \left[\frac{1}{2} \eta_{JT} \frac{T}{p} \frac{p_{bh}^2}{T_{bh}^2} \right] N_{fp} dy_D = \frac{1}{c_p} \frac{\delta q_Q}{T_{bh}}, \quad (6.96)$$

where dimensionless temperature $T_D = T/T_{bh}$ and position $y_D = y/L$ are defined accordingly. The dimensionless numbers N_{gp} and N_{fp} defined below, is taken for the example on page 219.

$$N_{gp} = \frac{M_g \cdot g \cos(\alpha) L}{\bar{Z} R T_{bh}},$$

$$N_{fp} = \frac{4 \bar{f} \omega^2 \bar{Z} R T_{bh} L}{A^2 d_h M_g P_{bh}^2},$$

where N_{gp} is the ratio between gravitational and pressure forces, while N_{fp} is the ratio between the friction and the pressure forces. (Commonly tubing dimensions are chosen such that the well friction pressure loss is kept lower than the gravitational pressure loss.)

From Eq. 6.96 we observe that the group of functions contained in each parenthesis are dimensionless. We may further define two dimensionless functions Ψ and Ω , as proposed by Hagoort [10] and we get

$$dT_D + \Psi N_{gp} dy_D + \Omega \frac{1}{2} \frac{p_{bh}^2}{T_{bh}^2} N_{fp} dy_D = \frac{1}{c_p} \frac{\delta q_Q}{T_{bh}}, \quad \text{where} \quad (6.97)$$

$$\Psi = \left[\frac{ZR}{c_p} + \eta_{JT} \frac{p}{T} \right], \quad \text{and}$$

$$\Omega = \eta_{JT} \frac{T}{p},$$

$\Psi(p, T)$ is dimensionless and $\Omega(p, T)$ is a function with the dimension $[K^2/\text{bar}^2]$. Both functions are thermodynamic functions defined by the flowing gas. Since $\delta q_Q/(c_p T_{bh})$ is also dimensionless, δq_Q is the specific heat flow from the surroundings into the gas element, having the dimension $[J/(\text{mol})]$.

Eq. 6.97 defines the temperature gradient in the flow conduit as affected by gravity, friction, heat losses and thermodynamic gas properties. Since the temperature gradient is given as a function of pressure, Eq. 6.97 must be evaluated simultaneously with evaluating the mechanical pressure by using Eq. 6.57, i.e. by substituting ΔT_D , the solution from Eq. 6.97, by $\Delta T/T_{bh}$ in Eq. 6.57. But first Eq. 6.97 has to be solved. The assumption here is that the pressure and temperature dependent gas properties are represented by their average values along the well conduit [1].

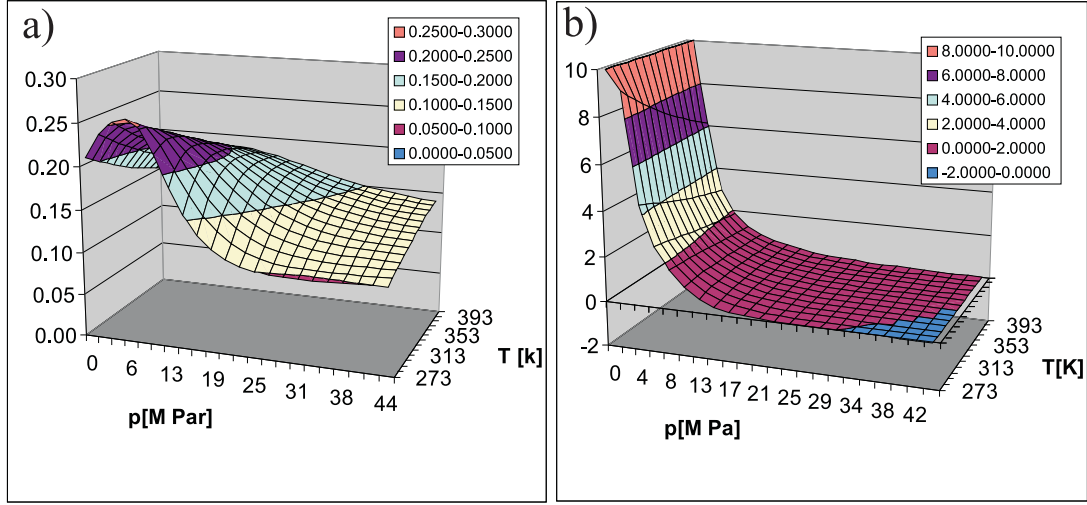


Figure 6.14: The figure shows the thermodynamic functions a) $\Psi(p, T)$ and b) $\Omega(p, T)$, where the dimension on the z-axis are [1] and $[K^2/\text{bar}^2]$, respectively

Before we can solve Eq. 6.97, we have to define the specific heat flow δq_Q . This will be done in the next section.

Figure 6.14 shows the variation in Ψ and Ω as function of pressure and temperature, where the two functions are calculated for a whole range of possible pressures and temperatures. Figure 6.14 shows that Ψ is not very sensible to variation in pressure or temperature, where variation in Ψ is within the range of 0.05 to 0.25. Ω is seen to vary somewhat as function of pressure, and most for very low pressures. The range of variation in Ω for pressures observed in the well, is between 0 and 2. For variation in temperatures, hardly any change in Ω is seen and approaching standard temperatures, Ω is close to zero because the gas behaves more and more like a perfect gas, - incase the Joule-Thomson coefficient is zero.

In solving Eq. 6.97 we may therefore substitute the functions Ψ and Ω with their average values, e.g. $\bar{\Psi} = (\Psi_{bh} + \Psi_{wh})/2$ and $\bar{\Omega} = (\Omega_{bh} + \Omega_{wh})/2$, using only the asymptotic (boundary) values.

6.9 No-Heat Exchange

For rather short wells, high gas flow rates and effective insulation caused by e.g.; presence of shales or/and waxes on the flow tubing, annulus gas between flow tubing and casing, - we may expect the well to flow as under adiabatic conditions. In this case the heat flow is zero, $\delta q_Q = 0$ and thus the temperature drop in the well is minimum. Under adiabatic conditions, Eq. 6.97 is written,

$$dT_D + \bar{\Psi} N_{gp} dy_D + \bar{\Omega} \frac{1}{2} \frac{p_{bh}^2}{T_{bh}^2} N_{fp} dy_D = 0. \quad (6.98)$$

Given the boundary condition; $y_D = 0$, $T_D = 1$, where the bottom-hole pressure is the reference pressure, we get the adiabatic temperature solution,

$$1 - T_D = \left(\bar{\Psi} N_{gp} + \bar{\Omega} \frac{1}{2} \frac{p_{bh}^2}{T_{bh}^2} N_{fp} \right) y_D \quad \text{or} \quad (6.99)$$

$$\Delta T_D = \frac{T_{bh} - T_{wh}}{T_{bh}} = \bar{\Psi} N_{gp} + \bar{\Omega} \frac{1}{2} \frac{p_{bh}^2}{T_{bh}^2} N_{fp}, \quad \text{when } y_D = 1.$$

From the above equation we observe that the temperature drop is proportional to the gravitational - and frictional numbers. For ideal gases, the Joule-Thomson coefficient is zero and for real gases it can be both positive and negative. η_{JT} is thus normally a small number, which again indicate that Ω normally is less than Ψ . This means that under adiabatic flow conditions, the temperature profile is more sensitive to gravity pressure losses (N_{gp}) than to friction pressure losses (N_{fp}) in the well. (For horizontal flow of ideal gas, both terms in Eq. 6.99 would be zero since both η_{JT} and N_{gp} are zero and thus horizontal flow of ideal gas is isothermal.)

The temperature profile in the well is therefore given by,

$$T = T_{bh} \left(1 - \Delta T_D \cdot \frac{y}{L} \right). \quad (6.100)$$

The adiabatic temperature gradient as presented in Eq. 6.99 can be studied in more detail by introducing the following approximations for the specific heat coefficients c_p and η_{JT} , as shown below.

$$c_p \simeq \frac{\Delta H}{\Delta T}, \quad \text{and} \quad (6.101)$$

$$\eta_{JT} \simeq \frac{\Delta T}{\Delta p}.$$

After substituting the approximations in Eq. 6.101 and some reshuffling of Eq. 6.99, we arrive at the following expression,

$$\Delta T_D = \left[\underbrace{\frac{\Delta T/T}{\Delta p/p}}_1 + \underbrace{\frac{\bar{Z} R \Delta T}{\Delta H}}_2 \right] N_{gp} + \left[\frac{1}{2} \underbrace{\frac{\Delta T/T_{bh}}{\Delta p/p_{bh}}}_3 \underbrace{\frac{T/T_{bh}}{p/p_{bh}}}_4 \right] N_{fp}. \quad (6.102)$$

The dimensionless temperature gradient ΔT_D , is defined by different elements labeled, 1 to 4. The temperature gradient is partly caused by elevation, and partly by friction. The second (2) element in Eq. 6.102 relates the change in internal energy to the change in enthalpy. Element 1 and 3 displays the ratio of relative change in temperature to the relative change in pressure, with the only difference, that in element 3, the relative change is referenced to the bottom-hole values. The relative change in temperature and pressure, in the above equation, are of cause interrelated and dependent of gas composition.

Because thermal expansion of liquids are small compared to gases, the relative change of temperature becomes less compared to the relative change in pressure, when a light gas is compared to a heavier gas (gas condensate). Eq. 6.102 therefore shows

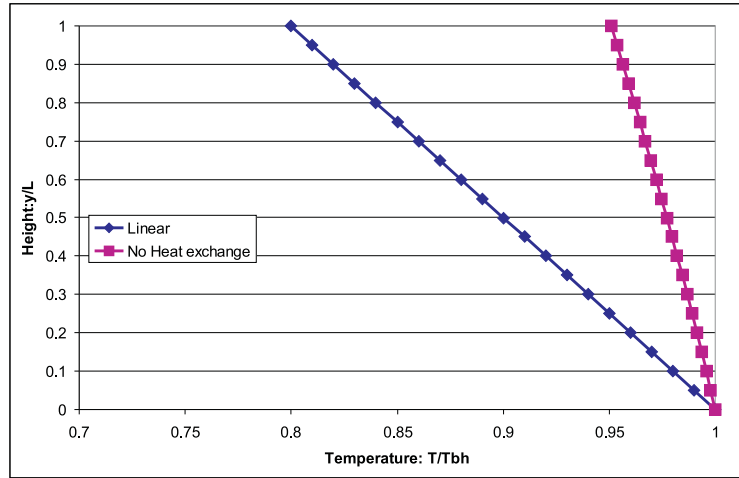


Figure 6.15: The temperature profile in the well where no-heat exchange is assumed, is compared with an assumed linear temperature profile, as used in pressure calculations above.

that the adiabatic temperature loss in the well will be less for a heavier gas compared to a more lean gas.

In Figure 6.15 we have plotted the temperature profile generated from Eq. 6.100 in comparison with the linear temperature profile used in the pressure calculations in the previous sections. The temperature gradient used in the linear case is $(392 - 313)/392 = 0.2$.

In the case of adiabatic well flow, the temperature decline is as expected less than in the assumed linear case. With no flow of heat from the well to the surroundings, well head gas temperatures are certainly higher than in most other cases.

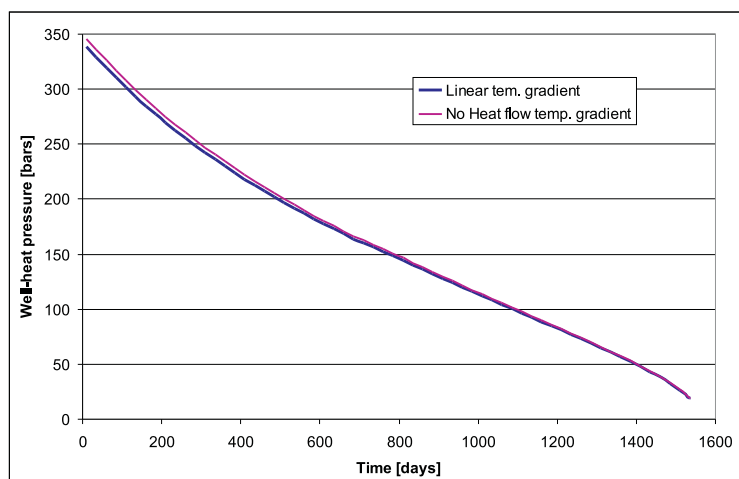


Figure 6.16: Well-head pressure profiles for linear temperature profile and for no-heat flow temperature profile.

When Eq. 6.99 is directly substituted into Eq. 6.57, then the pressure profile can be calculated. In Figure 6.16, the no-heat temperature profile is compared to the case, mentioned above, with a linear temperature profile. As can be seen from the plot in Figure 6.16, the two well-head pressure profiles are not very different. We might therefore expect the temperature profile in the well-bore, in the general case, not to be dramatically different from the linear temperature profile used in the previous part of this chapter.

6.10 Radial Heat Flow

The flow of heat from the gas flowing in the well to the surroundings is supposed to be directed radially from the center of the well tube, through the walls of the tubing and casing and further into the reservoir, as indicated in Figure 6.13.

This type of heat flow is described by Fourier's law[5]

$$J_Q = -\kappa_T \frac{\partial T}{\partial x}, \quad (6.103)$$

where J_Q is the specific heat flow with dimensions $[J/(s \cdot m^2)] = [W/m^2]$ and κ_T is the thermal conductivity of the material where the heat flow is passing through $[J/(s \cdot m \cdot K)] = [W/(m \cdot K)]$. The heat is flowing from the hot end ($x = 0$) to the cold end (x) and the heat flow is proportional to the temperature gradient along the material. Eq. 6.103 is a general law in transport theory and has the exact same form in the cases of electric current, diffusion and in fluid flow applications. In the chapter describing reservoir gas flow, this equation is known as Darcy' law or Poiseuilles'law, see Eq. 5.1 in section 5.1.

Along the same lines as described in section 5.1, we may apply the law of material balance and finally arrive at the one dimensional diffusivity equation for thermal heat flow

$$\frac{\partial T}{\partial t} = D_Q \frac{\partial^2 T}{\partial x^2}, \quad (6.104)$$

where the diffusivity coefficient is $D_Q = \kappa_T/(c \cdot \rho)$, and where c and ρ are the specific heat capacity and the gas density, respectively. The diffusivity coefficient is thus the ratio of heat conductivity divided by heat capacity and as such characterize the medium of heat transport.

For radial heat flow in the well and in the case of constant diffusivity coefficient, cylindrical coordinates should be used and the diffusivity equation above translates to

$$\frac{1}{D_Q} \frac{\partial T}{\partial t} = \frac{1}{r} \frac{\partial}{\partial r} \left(r \frac{\partial T}{\partial r} \right). \quad (6.105)$$

Eq. 6.105 describes radial heat flow under the condition of constant diffusivity ($D_Q = \text{const.}$) and more importantly, this equation is identical to Eq. 5.61, derived for pseudo reduced pressure in the reservoir under non-steady-state flow conditions. (For more general treatment of diffusivity equations see books on mathematics of diffusion [6].)

Since Eq. 6.105 is identical to Eq. 5.61, so must the solutions to the equations be identical and we may adopt the solution for the non-steady-state reservoir flow equation

as the solution for the radial well heat flow problem. This means that there exist an infinite and a steady-state solution of the radial heat problem, where the infinite or time dependent solution is related to the uploading of heat from the gas to the surroundings, while the steady-state solutions describes a situation where a time-independent temperature profile has been developed from the well center and radially into the reservoir, as depicted in Figure 6.17.

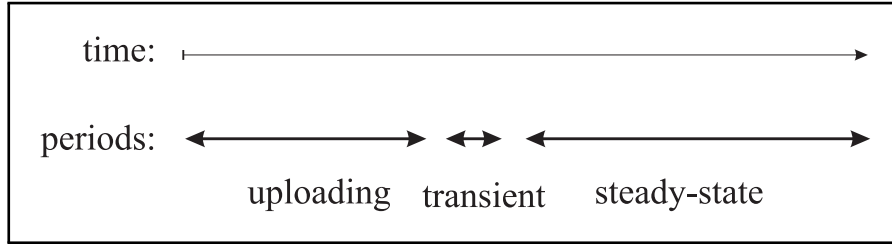


Figure 6.17: Time periods related to the solutions of Eq. 6.105

In the following we will assume that the uploading period is rather short and that steady-state condition is the most dominant condition under constant gas flow rate production.

Example: End Uploading - Start Steady State

Based on what is already known about the transition from infinite acting - to semi steady-state period, see section 5.4.2, we can now directly estimate the time, after which the well has been flowing long enough for a steady temperature profile to be established. This time is defined by

$$t_{SS} = \frac{r_S^2}{4D_Q}. \quad (6.106)$$

Introducing the definition of the diffusivity coefficient $D_Q = \kappa_T / (c \cdot \rho)$, as presented in Eq. 6.104, we may write

$$t_{SS} = \frac{r_S^2}{4} \frac{c\rho}{M_g \kappa_T}, \quad (6.107)$$

where M_g is introduced for convenience of getting the definition of gas heat capacity correct.

Choosing a likely set of parameters;

$$\begin{aligned} c &= 260 \text{ J}/(\text{K} \cdot \text{mol}) & \rho &= 300 \text{ kg}/\text{m}^3 \\ M_g &= 0.028 \text{ kg}/\text{mol} & r_S &= 0.30 \text{ m} \\ \kappa_T &= 0.07 \text{ J}/(\text{m} \cdot \text{s} \cdot \text{K}) \end{aligned}$$

and Eq. 6.107 gives

$$t_{SS} = \frac{260 \cdot 300 \cdot 0.3^2}{4 \cdot 0.028 \cdot 0.09} [\text{s}] = 895408 \text{ s} \simeq 10.4 \text{ days}. \quad (6.108)$$

This means that after a period of about 10 days of constant production, a steady state radial temperature profile is established in the well.

6.11 Steady-State Radial Heat Flow

The equation and its solution under steady-state radial flow conditions has already been resolved in Section 5.1.2 and we only have to repeat the results here.

Under steady-state conditions, i.e. $\partial T/\partial t = 0$, the following equation and solution are known,

$$\frac{\partial}{\partial r} \left(r \frac{\partial T}{\partial r} \right) = 0 \quad \Rightarrow \quad T = a \ln(r) + b, \quad (6.109)$$

where a and b are constant to be defined.

Under steady-state conditions we will assume that a time independent temperature profile is established from the center of the well and radially outwards into the reservoir. The temperature will remain constant in time, but will decrease radially until it becomes identical to the reservoir temperature at any particular elevation. Where this happens, in the well or in the reservoir is not known, at this point in time. The situation described above is depicted in Figure 6.18, where the temperature is seen to decrease differently dependent of the material the heat flows through. The continuous flow of heat will maintain a temperature profile and finally diffuse into the reservoir at a radial distance r_S . Alternatively we can say that a temperature difference between the well-bore and the reservoir is supporting a constant radial heat flow.

The flow of heat, - or more correctly the specific heat flow J_Q , is therefore proportional to the temperature difference between well and reservoir $T - T_S$. T_S is the constant temperature in the formation at a certain elevation. Based on Fourier's law we get,

$$J_Q = U_Q(T - T_S), \quad (6.110)$$

where U_Q is a proportional constant called the heat transfer coefficient with dimensions $[J/(s \cdot m^2 \cdot K)] = [W/(m^2 \cdot K)]$.

From Figure 6.18 it is seen that the total temperature profile is composed by several components characterizing the mechanical construction of well and reservoir.

In order to define the radial heat flow, we have to define the parameter U_Q , which then would contain information about the thermal characteristics of the materials from well to reservoir.

In Eq. 6.109, the radial solution is presented. Differentiating this solution and Fourier's law (Eq. 6.103), give

$$\begin{aligned} \text{Radial solution: } \frac{\partial T}{\partial r} &= \frac{a}{r} \\ \text{Fourier's law: } \frac{\partial T}{\partial r} &= -\frac{J_Q}{\kappa_T} \end{aligned} \quad \Rightarrow \quad a = -r \frac{J_Q}{\kappa_T} \quad (6.111)$$

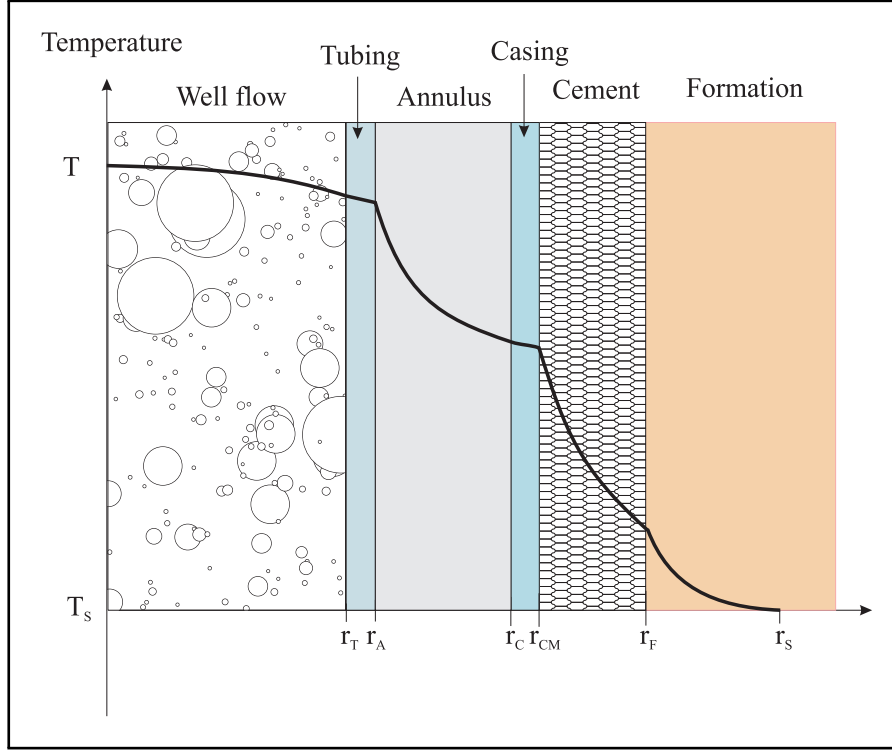


Figure 6.18: Radial temperature distribution in well, completion and reservoir, for steady-state conditions.(After G.P. Willhite [20])

Using Eq. 6.110 above, the constant a is

$$a = -\frac{r}{\kappa_T} U_Q (T - T_S). \quad (6.112)$$

From the boundary condition: $r = r_S \Rightarrow T = T_S$ and Eq. 6.109, we find the radial heat solution to be

$$T - T_S = a \ln \frac{r}{r_S}, \quad (6.113)$$

where the constant a depends on the material and as such characteristic of the heat flow through the different sections of the well, as displayed in Figure 6.18.

The total temperature difference from well-bore to reservoir is the sum of all temperature drops through the different materials, and can be expressed as follows

$$\begin{aligned} T - T_S &= (T - T(r_T)) + (T(r_T) - T(r_A)) + (T(r_A) - T(r_C)) \\ &\quad + (T(r_C) - T(r_{CM})) + (T(r_{CM}) - T(r_F)) + (T(r_F) - T(r_S)) \\ &= a(r_T) \ln \frac{r_T}{r_S} + a(r_A) \ln \frac{r_A}{r_S} \\ &\quad + a(r_C) \ln \frac{r_C}{r_S} + a(r_{CM}) \ln \frac{r_{CM}}{r_S} + a(r_F) \ln \frac{r_F}{r_S}. \end{aligned} \quad (6.114)$$

Notice that $(T - T(r_T)) = 0$, since the temperature is assumed to be close to constant inside the flow conduit and more constant than indicated in Figure 6.18. As Eq. 6.114 shows, the division of layers between well-bore and reservoir could be made as detailed as wanted. For instance could one assume the existence of a very thin layer on the inside of the well tubing with rather low heat conductivity. The real problem here is of practical nature and related to defining the right model (layers and layer thicknesses) and deciding upon the corresponding values of heat conductivity.

Substituting the constant a defined in Eq. 6.112 in to the above equation, gives the following expression for the heat transfer coefficient U_Q

$$U_Q = \left[\frac{r_T}{\kappa_T(T)} \ln \frac{r_S}{r_T} + \frac{r_A}{\kappa_T(A)} \ln \frac{r_S}{r_A} + \frac{r_C}{\kappa_T(C)} \ln \frac{r_S}{r_C} + \frac{r_{CM}}{\kappa_T(CM)} \ln \frac{r_S}{r_{CM}} + \frac{r_F}{\kappa_T(F)} \ln \frac{r_S}{r_F} \right]^{-1} \quad (6.115)$$

If the radial position $r_i = r_S - \Delta r_i$, where $i \in \{T, A, C, CM, F\}$, then Δr_i would mean the distance between the position of i 'th layer to the position r_S . Using the above definition we could write an approximate heat transfer coefficient

$$U_Q \sim \left[\frac{\Delta r_T}{\kappa_T(T)} + \frac{\Delta r_A}{\kappa_T(A)} + \frac{\Delta r_C}{\kappa_T(C)} + \frac{\Delta r_{CM}}{\kappa_T(CM)} + \frac{\Delta r_F}{\kappa_T(F)} \right]^{-1}, \quad (6.116)$$

where the following approximation is used: $\ln(1 + \Delta r_i/r_i) \sim \Delta r_i/r_i$. Notice that $\Delta r_T > \Delta r_A > \Delta r_C > \Delta r_{CM} > \Delta r_F$.

In Figure 6.18 we may classify both tubing and casing as good conductors, transmitting heat relatively efficiently. Consequently, are their thermal conductivities relatively high. The annulus, on the other hand, is probably a rather poor conductor and could probably be considered as an insulator. If the annulus is filled with gas (or not filled at all), this section of the well would perform more like an isolator than a conductor. The difference between a conductor and an insulator is therefore the degree of thermal conductivity, where κ_T is high in the case of a conductor and low when we talk about an insulator.

The relative importance of the different layers, as presented in Figure 6.18, can be summarized as follows:

1. The relative importance of layers will decrease with increasing distance from the centre of the well-bore, since the difference Δr is decreasing. This means that the reservoir thermal conductivity is of minor importance compared to the contributions from the other elements in the well.
2. An insulating cement layer may be of importance, while if the cement is partly conductive, also this layer can be neglected.
3. If the tubing and the casing is made of about the same material, - then the heat conductivity of the tubing is more important compared to the casing because $\Delta r_T > \Delta r_C$.

4. An insulating annulus will be of great importance, since the ratio $\Delta r_A/\kappa_T(A)$ could be greater than for all other layers.
5. The importance of high conducting materials are probably in most cases less than the importance of a high insulating annulus layer.
6. The significance of r_S is that if r_S is large, then all Δr become comparable and the thermal conductivity of each layer becomes the decisive factor. If r_S is small, i.e. $r_S = r_F$, then the relative position of the different layers becomes more important and thermal conductivity of the tube could in some cases be of some importance.

Example: Importance of Thermal Conductivities of Different Layers

With reference to Figure 6.18, the following numerical values can be used in order to evaluate the importance of individual layers in the summation of the total heat transfer coefficient.

Radial position of well elements, where $r_S = 0.3\text{ m}$ and $\Delta r_i = r_S - r_i$:

| | Δr_T | Δr_A | Δr_C | Δr_{CM} | Δr_F |
|--------------|--------------|--------------|--------------|-----------------|--------------|
| $r_s - r_i$ | 0.3 - 0.063 | 0.3 - 0.073 | 0.3 - 0.1594 | 0.3 - 0.1778 | 0.3 - 0.25 |
| Δr_i | 0.2370 | 0.2270 | 0.1406 | 0.1222 | 0.050 |

The thermal conductivities can be found from various sources such as Handbooks of Chemistry and Physics, more special handbooks [4] or simply from the Internet.

It is assumed that the tubing and the wall casing is made of carbon steel and that their thermal conductivity is the same, $\kappa_T = 54\text{ W}/(m \cdot K)$. What the annulus actually consist of is difficult to say, but we will here assume that it is either filled with water or steam (or something in between), i.e. the thermal conductivity is then varying from, $\kappa_A = 0.58 \rightarrow 0.016\text{ W}/(m \cdot K)$. The casing is assumed to be made of concrete with the thermal conductivity, $\kappa_{CM} = 1.7\text{ W}/(m \cdot K)$. Finally, a saturated sandstone reservoir is assumed, with thermal conductivity of, $\kappa_F = 2.7\text{ W}/(m \cdot K)$.

Using Eq. 6.116, we may evaluate the importance of the different layers, by substituting the values above into the equation.

$$\begin{aligned}
 U_Q &\sim \left[\frac{0.237}{54} + \frac{0.227}{(0.58 \rightarrow 0.016)} + \frac{0.1406}{54} + \frac{0.1222}{1.7} + \frac{0.05}{2.7} \right]^{-1}, \\
 &\sim [10^{-3} (4 + (391 \rightarrow 14187) + 2 + 71 + 18)]^{-1}, \\
 &\sim (2 \rightarrow 0.07),
 \end{aligned} \tag{6.117}$$

where the heat transfer coefficient has the units $W/(m^2 \cdot K)$.

From the above comparison, we may conclude that the annulus is the most important radial section of the well, seen from the point of view of heat transfer. If water is the medium expanding the section, about 80% of the overall numerical value of heat transfer coefficient is the result of this

section. If saturated water vapor is present, more than 99 % of heat transfer characteristics is due to this section.

6.12 Steady-State Radial Heat Transfer

As already mentioned, the temperature difference, $\Delta T = T - T_S$, between well and reservoir is the driving force for maintaining a constant heat flux, J_Q . The heat flux is directed radially and transports heat from the volume segment $\pi(S/2)^2 dy$, see Figure 6.13, to the surroundings. The temperature difference, $\Delta T(y)$, will vary along the well, but at a certain elevation this temperature difference is constant in time. J_Q is therefore a time independent parameter, only dependent on elevation, y .

The specific heat flow from the well segment, i.e. the heat flux times the volume segment divided by the number of moles in the section, would then constitute the heat flow δq_Q , to be substituted in Eq. 6.97.

$$\delta q_Q = -J_Q \frac{\pi S dy}{w/M_g}, \quad (6.118)$$

where w/M_g is the number of moles of gas in the volume segment and $\pi S dy$ is the heat flux surface area. δq_Q has therefore the dimensions J/mol .

Combining the above equation with Eq. 6.110, we have an expression the specific heat flow

$$\delta q_Q = -U_Q(T - T_S) \frac{\pi S}{w/M_g} dy, \quad (6.119)$$

where as we have seen above, U_Q is readily available as function of thermal conductivities of the different well sections and their radial positions.

Substituting the above equation in to Eq. 6.97, we get

$$\frac{dT_D}{dy_D} = -\Psi N_{gp} - \Omega \frac{N_{fp} p_{bh}^2}{2 T_{bh}^2} - \frac{U_Q}{c_p} (T_D - T_{DS}) \frac{\pi S L}{w/M_g}, \quad (6.120)$$

where the dimensionless temperatures: $T_D = T/T_{bh}$ and $T_{DS} = T_S/T_{bh}$, and the dimensionless elevation: $y_D = y/L$, are used.

A new dimensionless constant N_Q , can be defined as a measure of the heat lost to the formation relative to the heat transported with the gas. The above equation then takes the form

$$\begin{aligned} \frac{dT_D}{dy_D} &= -\Psi N_{gp} - \Omega \frac{N_{fp} p_{bh}^2}{2 T_{bh}^2} - N_Q (T_D - T_{DS}), \quad \text{where} \\ N_Q &= \frac{U_Q}{c_p} \frac{\pi S L}{w/M_g}. \end{aligned} \quad (6.121)$$

The dimensionless temperature T_{DS} is dependent on the reservoir temperature at the elevation y , i.e.

$$T_{DS} = 1 - (\Delta T_G \cdot \frac{L}{T_{bh}}) y_D, \quad (6.122)$$

where ΔT_G is the geothermal gradient ($\sim 30K/km$ or alternatively $0.03K/m$).

Eq. 6.121 is the written,

$$\frac{dT_D}{dy_D} = -\Psi N_{gp} - \Omega \frac{N_{fp} p_{bh}^2}{2 T_{bh}^2} - N_Q (T_D - 1 + (\Delta T_G \cdot \frac{L}{T_{bh}}) y_D). \quad (6.123)$$

The above equation is treated as a first order differential equation with constant coefficients, giving the dimensionless temperature as function of dimensionless elevation. Both N_{gp} , N_{fp} and N_Q , as well as the coefficients Ψ and Ω are all considered independent of y_D and thus also of p and T . The solution of Eq. 6.123 will give the dimensionless temperature in the well as function of the dimensionless elevation. All other parameters are treated as average values over the integrated well section. The accuracy of these calculations is improved simply by substituting the well section L , by smaller sections L/n and then summing up the contributions in an overall temperature effect.

The solution of Eq. 6.123 is

$$T_D = 1 - \left(\Psi N_{gp} + \Omega \frac{N_{fp}}{2} \left(\frac{p_{bh}}{T_{bh}} \right)^2 \right) \frac{1 - e^{-N_Q y_D}}{N_Q} - \left(\Delta T_G \cdot \frac{L}{T_{bh}} \right) \left(y_D - \frac{1 - e^{-N_Q y_D}}{N_Q} \right). \quad (6.124)$$

Introducing the definitions for the dimensionless variables and further adjustments gives

$$\frac{T_{bh} - T}{T_{bh}} = \left(\Psi N_{gp} + \Omega \frac{N_{fp}}{2} \left(\frac{p_{bh}}{T_{bh}} \right)^2 \right) \frac{1 - e^{-N_Q (y/L)}}{N_Q} + \left(\Delta T_G \cdot \frac{L}{T_{bh}} \right) \left(\frac{y}{L} - \frac{1 - e^{-N_Q (y/L)}}{N_Q} \right). \quad (6.125)$$

Notice that the substitutions of Eq. 6.125 in to the pressure equation, Eq. 6.57 is done by substituting $(T_{bh} - T)/T_{bh}$ in Eq. 6.125 by $(\Delta T/T_{bh})(y/L)$ in Eq. 6.57.

Example: Asymptotic Heat Transfer Values

Using the Eq. 6.124, we may study the temperature behavior in the well when $N_Q \rightarrow 0$ and compare the results with what was observed in the case of no-heat transfer.

At the well head, $y_D = 1$, and Eq. 6.124 takes the form,

$$T_D = 1 - \left(\Psi N_{gp} + \Omega \frac{N_{fp}}{2} \left(\frac{p_{bh}}{T_{bh}} \right)^2 \right) \frac{1 - e^{-N_Q}}{N_Q} - \left(\Delta T_G \cdot \frac{L}{T_{bh}} \right) \left(1 - \frac{1 - e^{-N_Q}}{N_Q} \right). \quad (6.126)$$

In the case of no heat transfer between well and reservoir, - N_Q is zero, and then $(1 - e^{-N_Q})/N_Q \rightarrow 1$ and the above equation is reduced to,

$$T_D = 1 - \left(\Psi N_{gp} + \Omega \frac{N_{fp}}{2} \left(\frac{p_{bh}}{T_{bh}} \right)^2 \right), \quad (6.127)$$

which is the solution, Eq. 6.99, we arrived at in the No-Heat Exchange section.

The equations 6.124, 6.125 and 6.127 are all deduced under the assumption of a strait and uniform well conduit from top to bottom.

The relative temperature drop ($\Delta T/T_{bh}$) in the well is thus given,

$$\frac{T_{bh} - T_{wh}}{T_{bh}} = \left(\Psi N_{gp} + \Omega \frac{N_{fp}}{2} \left(\frac{p_{bh}}{T_{bh}} \right)^2 \right) \frac{1 - e^{-N_Q}}{N_Q} + \left(\Delta T_G \cdot \frac{L}{T_{bh}} \right) \left(1 - \frac{1 - e^{-N_Q}}{N_Q} \right). \quad (6.128)$$

The relative temperature drop in the well, as shown in Eq. 6.128, is a sum of two different elements,- the adiabatic flow (no heat exchange) and the formation temperature gradient (geothermal gradient times well length divided by bottom hole temperature) induced temperature drops, respectively. In the case of no heat flow, $N_Q = 0$, only the adiabatic term is contributing to the total temperature drop. In cases of large heat flow, the formation temperature gradient term is dominating the total temperature drop. The formation temperature gradient is thus the asymptotic limit of which the well temperature can not underrun, i.e.

$$T_D > 1 - \Delta T_G \frac{L}{T_{bh}}. \quad (6.129)$$

Eq. 6.124 gives the temperature profile along the well conduit. In the above temperature solution, the single most interesting parameter is the heat transfer coefficient U_Q , which is seen to be proportional to the dimensionless number N_Q , defined in Eq 6.121.

In the example above it is shown that when N_Q is small, - then the temperature solution in Eq. 6.124 approaches the non-heat exchange solution. In Figure 6.19, the heat transfer coefficient is varied between low values, i.e. non heat exchange, to high values showing temperature profiles in the well close to the formation asymptotic temperature profile.

In Figure 6.19, heat transfer coefficients from 1 to 50 are displayed. From the figure it becomes evident that for heat transfer coefficients less than 1, the non-heat exchange case is characterizing the well temperature profile. On the other extreme we see that for large heat exchange coefficients, the temperature profile is comparable to the asymptotical formation temperature profile. The values used in Figure 6.19, describing the asymptotic temperature profile are: $\Delta T_G = 30 \text{ K/km}$, $L = 3000 \text{ m}$ and $T_{bh} = 393 \text{ K}$.

Between the extreme cases of no-heat exchange and formation asymptotic temperature profiles, the temperature profiles are seen to curve to the left,- being concave to the right. This means that the temperature drops more as we move to the well head than

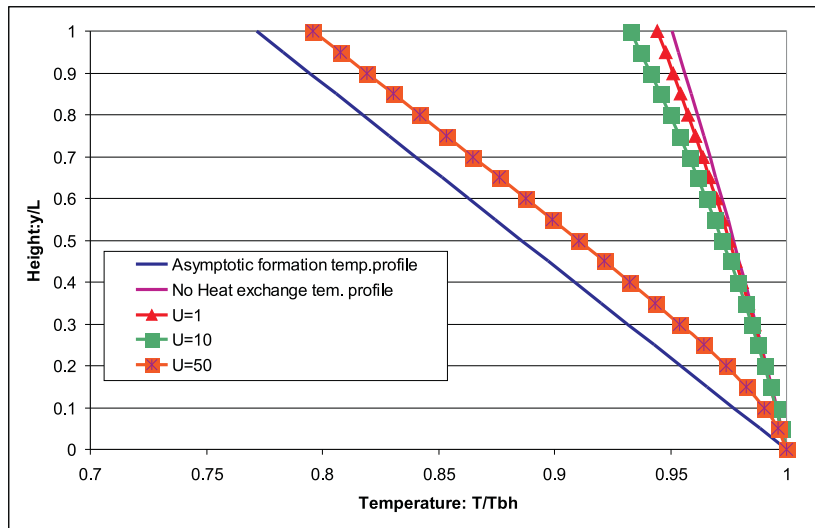


Figure 6.19: Temperature profiles in the well as function of varying heat transfer coefficient.

at the well bottom, which corresponds well with the fact the the temperature difference between well and formation is increasing as we move upwards in the well.

Even though the temperature profiles in Figure 6.19 seem to be well separated in the extreme cases, the comparable pressure profiles are not equally well separated, as shown in Figure 6.20

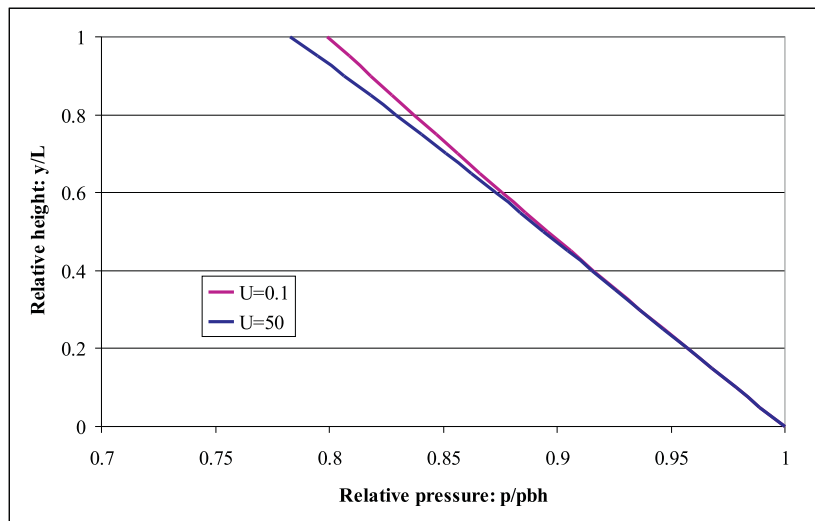


Figure 6.20: Pressure profiles for two extreme choices of the heat transfer coefficient.

The reason for this rather surprising result is related to how the total pressure drop is composed of pressure drops from both gravity forces and friction forces. When the heat transfer coefficient is increased from no-heat conditions (low numbers, typically $U = 0.1 \text{ W}/(\text{m}^2\text{K})$) to higher values, approaching the asymptotic limit, - then the pressure

contribution from gravity forces and friction forces show opposite characteristics. When U is increased, the contribution from the gravity forces will increase pressure drop, attributed to the increasing density of gas at lower temperatures. The opposite is observed for friction forces [10], where a decrease in pressure drop is observed, due to reduced flow velocities, also caused by the increased gas density. The net effect of increasing heat transfer coefficient is therefore a rather moderate increase in the pressure drop, as seen in Figure 6.20.

In Figure 6.21, the above mentioned effects are demonstrated. The figure shows what happens when the heat flow in the well is increased from near adiabatic - to near geothermal flow conditions, illustrated with heat transfer coefficients; $U = 0.1$ and $U = 50$. The demonstration is done for two cases; when only the gravitational forces are active (no friction), labeled: $N_{gp} = 0.2, N_{fp} = 0.0$, and when only friction forces are active (no gravitation), labeled: $N_{gp} = 0.0, N_{fp} = 0.2$.

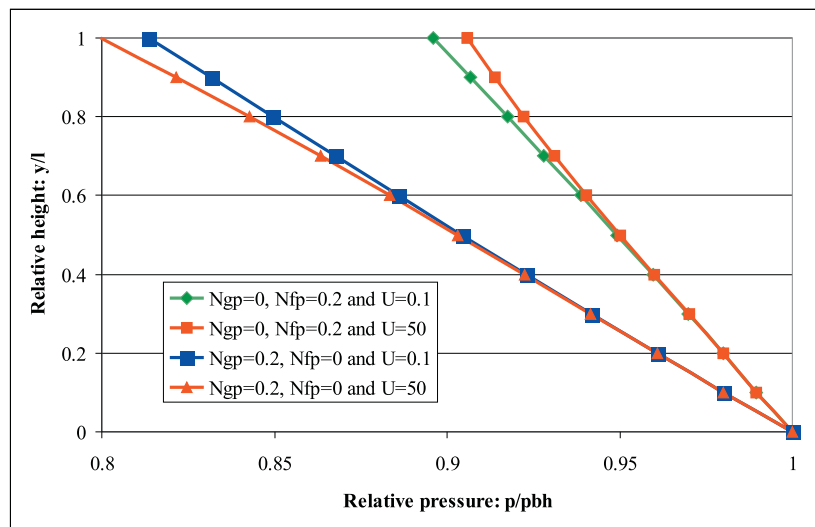


Figure 6.21: Comparison of pressure effects for increasing heat transfer in two cases of no active friction - and no active gravitational forces.

Figure 6.21 shows that when only gravitational forces are active (friction is "turned off"), an increase in heat transfer from the well to the surroundings will cause an additional pressure drop in the well. On the other side, when only frictional forces are active (gravitation is "turned off"), the same increase in heat transfer leads to a reduced pressure drop in the well.

When it comes to the effect of well heat exchange coefficient on the pressure performance, Figure 6.22 is showing that nearly any effect can be documented. In the case of large heat exchange as well as for no-heat exchange, near identical pressure profiles are calculated.

The effect of varying heat exchange coefficient on pressure behavior is close to negligible in the case of well gas flow. The effect on the temperature profile in the well is shown to vary under varying heat transfer conditions. In cases where the fluid flowing in the well is more critical with respect to temperature, as in the case of injection of supercritical fluids, such as i.e. CO_2 , surveillance of temperature behavior in the well

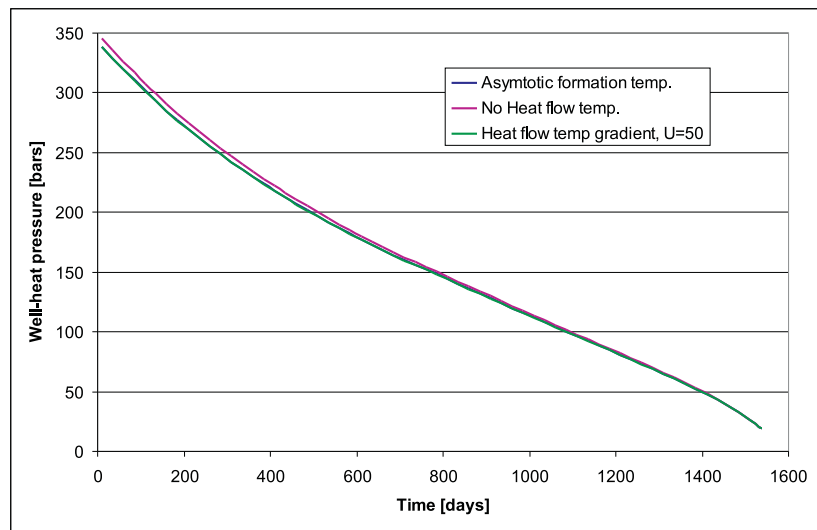


Figure 6.22: Pressure development as function of varying heat transfer coefficients.

conduit is mostly appreciated.

References

- [1] I.N. Alves, F.J.S. Alhanatl, and O. Shoham. A unified model for predicting flowing temperature distribution in wellbores and pipelines. *SPE Prod. ENG.*, pages 363–367, November 1992.
- [2] P.W. Atkins. *Physical Chemistry*. Oxford University Press, 1998.
- [3] W.J. Beek and K.M.K Mutzall. *Transport Phenomena*. John Wiley & Sons Ltd., 1977.
- [4] Jhon M. Prausnitz Bruce E. Poling and John P.O'Connell. *The Properties of Gases and Liquids*. The McGraw-Hill Companies, Inc., 2001.
- [5] Gilbert W. Castellan. *Physical Chemistry*. The Benjamin/Cummings Publishing Company, Inc, 1983. ISBN: 0-201-10386-9.
- [6] J. Crank. *The Mathematics of Diffusion*. Oxford Science Publications, 1999.
- [7] G.J. Duncan and B. Beldring. A novel approach to gas lift design for 40,000 bpd subsea producers. *SPE 77727*, 2002.
- [8] Herbert Bristol Dwight. *Tables and Integrals and Other Mathematical Data*. The Macmillian Company, 1961.
- [9] Jacques Hagoort. *Fundamentals of gas reservoir engineering*, volume 23 of *Developments in Petroleum Science*. Elsevier, 1988.
- [10] Jacques Hagoort. Prediction of wellbore temperatures in gas production wells. *JPSE*, 49 (2005) 22-36, 2005.
- [11] S. Kumar. *Gas Production Engineering*, volume Huston, TX. Gulf Publishing Company, 1987. ISBN 0-87201-577-7.
- [12] Keith J. Laidler and John H. Meiser. *Physical Chemistry*. The Benjamin/Cummings Publishing Company, Inc., 1982.
- [13] James F. Lea and Henry V. Nickens. Solving gas-well liquid-loading problems. *SPE 72092, Distinguished Author Series*, 2004.
- [14] P.L. Lingen. Description of groningen gas well performance suitable for medium and long range planning. *SPE Paper 4816 presented at the SPE European Spring Meeting 1974.*, 1974.
- [15] S. Mokhatab, W.A. Pope, and J.G. Speight. *Handbook of Natural Gas Transmission and Processing*. Elsevier, 2006.
- [16] M.G. Hubbard R.G. Turner and A.E. Dukler. Analysis and prediction of minimum flow rate for the continuous removal of liquids from gas wells. *JPT*, 21:1475–1482, November 1969.
- [17] M.A. Saad. *Thermodynamics, Principles and Practice*. Prentice-Hall, Inc., 1997.

- [18] Jacques Vincent-Genod. *Fundamentals of Pipeline Engineering*. Editions Technip, 1984.
- [19] Curtis H. Whitson. Minimum lift calculations for gas wells. *Communication paper*, November 20,1990.
- [20] G. Paul Willhite. Over-all heat transfer coefficients in steam and hot water injection wells. *Journal of Petroleum Technology*, May 1969.

Chapter 7

Natural Gas Reservoir Depletion

The present chapter deals with natural gas reservoir depletion, which is a general method in developing gas reservoirs. In natural gas depletion, the gas is produced by utilizing the natural existing reservoir pressure as the driving force (energy) for bringing the gas to the surface.

The main characteristics of natural depletion can be summarized as follows;

- A declining reservoir pressure, as gas is being produced.
- Water influx from adjacent aquifers due to the declining reservoir pressure.
- Compaction of reservoir volume due to the weight of the overlying rock strata.
- Decreasing well capacity caused by declining reservoir pressure.

In this chapter we will focus on the general reservoir behavior and the prevailing conditions valid for gas reservoir production in particular. We will further discuss the last item in the list above, related to well deliverability. Finally, we will concentrate on simulation of gas reservoir production from more than one block utilizing several wells.

7.1 Development of Natural Gas Fields

The conditions for successful development of gas fields relies to a large extent, on a commercial sales agreement which generally has to be negotiated before any development of the field can take place. In the case of locating a gas field of sufficient size to justify commercial exploitation, the field can only be developed if there is a direct and designated market for the gas for most of the exploitation period. This is because, unlike oil, gas cannot easily be stored, then transported and sold at a marked place. Gas, due to its large volume, cannot be stored under standard conditions and must therefore be transported directly to the buyer.

The gas is therefore, in many cases, already sold before the field is developed. The sales contract is to guarantee the producer (owner of the field) a predictable and reliable income after a period of often large investments. The contract is also designed to secure the buyer a steady supply of gas during a certain period of time. The gas delivery specifications agreed upon in the contract, specifies not only the volume of gas to be

delivered, but also the conditions of gas delivery. These conditions may contain various details such as;

- delivery pressure in to the buyers network,
- minimum and maximum tolerances on the production rate (so called *swing capacity*) and
- quality of gas delivered related to calorific content or burning value.

The effect of a gas sales contract is therefore to impose demands and restrictions on the development project which has direct implications on the reservoir engineering design.

Most gas field projects have a contracted constant gas rate delivery stipulated over a certain number of years. The gas production is therefore designed with a constant *plateau rate* matching the contract delivery. Figure 7.1 shows a principle sketch of a production profile over the production life-time of a field.

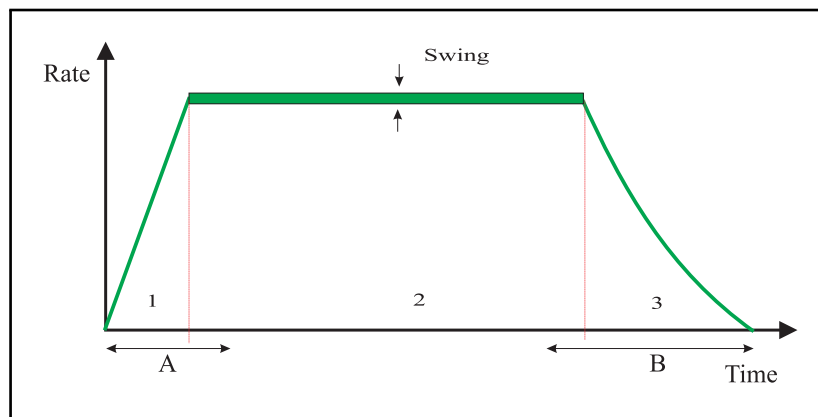


Figure 7.1: Gas rate production profile.

The bulk of all gas contracted is produced during the *plateau period* (period 2 in Figure 7.1), which should therefore be as long as possible. The *buildup period* (period 1), on the other hand, is normally designed as short as possible. The first wells on the field are located in those areas where prospects for high and stable gas production are the best. At the initial stage, wells are normally started up with a certain over-capacity in mind, securing the plateau rate as early as possible. The increasing well-rate period (A in Figure 7.1) is therefore longer than the buildup period.

The final stage in the life time of a gas field is introduced by the *decline period* (period 3 in Figure 7.1). In this period, the wells that are still producing gas from the field, are not capable of maintaining the plateau rate. Due to declining reservoir pressures, well rates have been reduced and the reservoir is (from economical reasons) not able to support any new wells. From a reservoir engineering point of view, the decline period is preferably going to be as short as possible.

In the later stages of the plateau period, drilling of new wells may no longer be economical. The initial capacity of new wells becomes progressively lower as more and

more gas is produced and the risk is that new wells would become excessive. Additional capacity can be achieved by allowing the production wells to produce against a back-pressure that is lower than the minimum operating back-pressure. When the back-pressure is lowered below the minimum intake pressure of the gas-treatment facilities and/or the delivery pressure, re-compression is needed. Increasing the well capacity by lowering the back-pressure has an additional advantage, as the recovery of gas from the field is increased due to lower abandonment pressure. However, the back-pressure can not be reduced indefinitely. The gain in well delivery has to be balanced by the cost of re-compression.

7.2 Reservoir Performance

Production from natural gas fields by volumetric depletion have a cumulative recovery between 70 to 90%, which is considerable more than for any oil field. In the case of non-volumetric depletion, which is by far more common than volumetric depletion, the recovery appears to be less. The reason for this somewhat surprising result, is most commonly related to the effect of water influx. When aquifer water enters the reservoir, pockets of gas are isolated by the surpassing water and thus areas containing large volumes of gas will not be produced. Water invasion from the aquifer may never result in complete areal sweep, as recovery of water drives are poor and seldom exceeds 50%.

During pressure maintenance, e.g. when water is injected into the reservoir to reduce the normal pressure decline, the process described above can lead to entrapment of gas in a scale of 30 to 50% of the total rock volume. Another disadvantage concerning water injection is related to *water channeling*, where water by following reservoir heterogeneities, can flow directly towards the well and cause drastic increase in the water cut. The positive effect of pressure maintenance is recorded in those situations where liquid dropout can be prevented or postponed in depleting gas-condensate reservoirs. The economical value of the produced liquid condensate is then exceeded by the loss of gas trapped or the risk of channeling. Pressure maintenance is therefore restricted to those cases of rich gas-condensate fields where the production of liquid condensate is of major importance.

The capacity or strength of the aquifer is a measure of the relative influx of water compared to the hydrocarbon pore volume. An aquifer is considered to be "weak" if the relative volume of water replacing produced gas is less than 15% of the hydrocarbon volume. If this percentage is higher than 50%, the aquifer is considered "strong". An aquifer in the intermediate range from 15% to 50% is therefore called "moderate".

The water influx is primarily initiated by the pressure decline in the reservoir, although quite a few other factors have a significant impact on the actual amount of water being expelled. Factors favoring strong water drives are;

- large aquifer size,
- large aquifer porous rock compressibility,
- high aquifer permeability,
- low reservoir depletion rate (low gas production flow rate) and

- relative small reservoir size compared to the surrounding aquifer size.

Volumetric and non-volumetric depletion can be presented in a p/Z -plot, as presented in Figure 7.2. In the figure, the volumetric depletion is shown as a straight line asymptotically ending at the point of 100% depletion, ending at the point 1.0 in Figure 7.2.

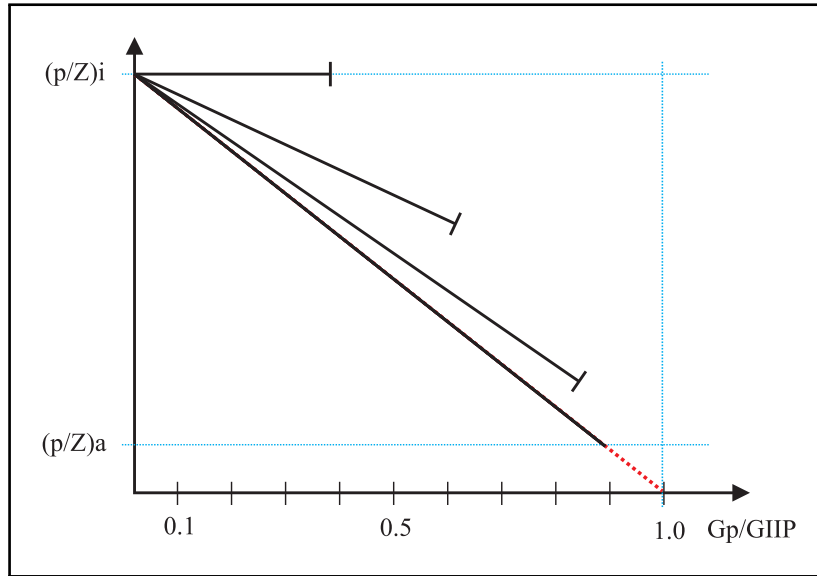


Figure 7.2: Natural depletion as function of recovery.

In the case of non-volumetric depletion the average reservoir pressure decline is less than for volumetric depletion, due to the replacement of gas by water. The effective recovery is also less, for the reasons discussed above. The somewhat unlikely scenario of 100% pressure maintenance, is seen as a horizontal line in Figure 7.2. These situations are characterized by low recovery, often much less than 50%.

The basic material balance equation for dry and wet gas reservoirs is written

$$\frac{p}{Z} = \left(\frac{p}{Z}\right)_i \frac{V_{HCi}}{V_{HC}} \left(1 - \frac{G_p}{GIIP}\right). \quad (7.1)$$

If the initial reduced pressure $(p/Z)_i = 300 \text{ bar}$ and the reduced pressure at abandonment pressure is $(p/Z)_a = 30 \text{ bar}$, the recovery at the abandonment pressure is

$$\frac{G_p}{GIIP} = 1 - \frac{30}{300} = 0.9 \text{ or } 90\%.$$

If the ambition is to maintain the initial pressure at a constant level, the reduced pressure $p/Z = (p/Z)_i$ and the water influx $\Delta V = V_{HCi} - V_{HC}$ has to satisfy the equation

$$\frac{\Delta V}{V_{HCi}} = \frac{G}{GIIP}, \quad (7.2)$$

where actually the relative influx of water has to match the relative production of gas.

7.3 Constraints on Gas Production

The reservoir pressure or more correctly, the pressure difference between reservoir and terminal pressure is the source of force (or energy) that allows the gas to flow to the surface. The flow rate is therefore directly related to this pressure difference, in the sense that a maximum production rate is limited by the depleting reservoir pressure.

7.3.1 Well-Inflow Performance

Well-inflow performance refers to the production well rate as function of the pressure draw-down between the reservoir and the producing well. For a given reservoir pressure, the well can produce the reservoir gas at a certain flow rate q_{sc} , maintaining a particular bottom-hole pressure p_{bh} . Therefore, there exists a functional relation between the well rate and the bottom-hole pressure which is characteristic for that particular well. This relation, $p_{bh} = p_{bh}(q_{sc})$, is called the well-inflow performance.

Expressed in pseudo-pressures, the steady state inflow equation is written

$$\bar{m} - m_{bh} = a q_{sc} + b q_{sc}^2, \quad (7.3)$$

where \bar{m} and m_{bh} are the mean - and bottom-hole pseudo-pressure. q_{sc} is the flow rate at standard conditions and a and b are constants defined as

$$a = \frac{(\mu B)_r [\ln(r_e/r_w) - 0.75 + S]}{2\pi k h}, \quad (7.4)$$

$$b = \frac{(\mu B)_r}{2\pi k h} D, \text{ where } D = \frac{k}{\phi \mu c}. \quad (7.5)$$

Note: That the reservoir under consideration is cylindrical with the well at the center. See also Eq. 5.53.

The parameter a in Eq. 7.4 is a constant and depends on the geometry and flow characteristics of the drainage area surrounding the well.

The parameter b reflects the effect of non-Darcy flow, where D is the non-Darcy flow factor. The non-Darcy flow factor is inversely proportional to the gas viscosity at the bottom-hole pressure. Hence the parameter b is not constant but depends on the bottom-hole flowing pressure. Therefore, to apply Eq. 7.3 outside the pressure range for which D has been determined, we have to correct the parameter b as follows. Let b_1 and b_2 be the values of the parameter b at the pressures p_1 and p_2 , respectively. As D is inversely proportional to the gas viscosity, we have the relation between b_1 and b_2

$$b_1(p_1) = \frac{\mu(p_2)}{\mu(p_1)} b_2(p_2), \quad (7.6)$$

where μ is the viscosity at the well bottom-hole pressure.

We may study the bottom-hole pressure as function of flow rate by derivation of Eq. 7.3 with respect to the flow rate and we get

$$\frac{dp_{bh}}{dq_{sc}} = \frac{\mu B}{(\mu B)_r} \frac{dm_{bh}}{dq_{sc}} = -\frac{\mu B}{(\mu B)_r} (a + 2b q_{sc}), \quad (7.7)$$

where we have used Kirchhoff's transformation. The mean pseudo pressure \bar{m} , is considered to be constant under derivation with respect to the gas rate q_{sc} , since the mean pressure in the reservoir is not directly affected by the change in flow rate.

Using Eqs. 7.4 and 7.5 we may write the above equation

$$\frac{dp_{bh}}{dq_{sc}} = -\frac{\mu B}{2\pi kh}([\ln(r_e/r_w) - 0.75 + S] + 2Dq_{sc}) \quad (7.8)$$

From Eq. 7.8 it is seen that the bottom-hole pressure is decreasing as function of increasing flow rate. Figure 7.3 shows the well-inflow performance curve for two choices of the well productivity index kh .

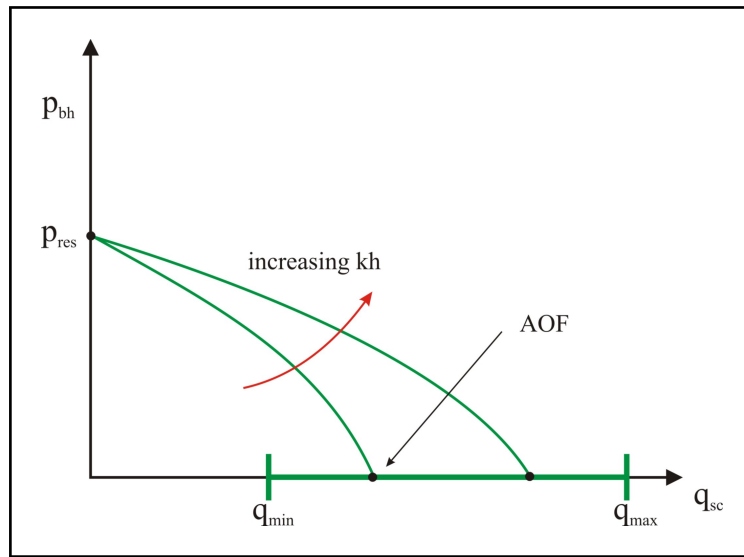


Figure 7.3: Well-inflow performance curve

The well-inflow performance is commonly displayed as a plot of bottom-hole flowing pressure versus flow rate at a given reservoir pressure, as shown in Figure 7.3. The well-inflow curve begins at the reservoir pressure, at zero flow rate. Due to a negative gradient, as seen for Eq. 7.8, the curve is curving downwards with an increasing gradient. As the bottom-hole pressure approaches the terminal pressure (atmospheric pressure), the flow rate reaches its maximum. The maximum possible flow rate at atmospheric bottom-hole pressure is known as the *absolute-open-flow* potential (AOF). The slope of the curve at zero flow rate is inversely proportional to the product of permeability and thickness kh as seen by the equation

$$\left(\frac{dp_{bh}}{dq_{sc}}\right)_{q_{sc}=0} = -\frac{\mu B}{2\pi kh}[\ln(r_e/r_w) - 0.75 + S], \quad (7.9)$$

where μB is evaluated at the reservoir pressure. Thus the flatter the curve at the vertical intercept, the larger the kh and the higher the flow capacity for a given draw-down.

We have recently established the minimum unloading rate as the lowest possible flow rate, q_{min} . If the flow rate should drop below this rate the gas flow will not be able to lift the liquid fluids (oil and water) and the well will eventually "drown".

As there is a minimum flow rate, we may equally expect the existence of a maximum flow rate, q_{max} . When the loss of energy due to friction against the wall becomes comparable to the momentum flux in the well, a terminal flow rate has been reached of which no further increase in gas flow can occur.

For each reservoir pressure we can construct an inflow performance curve of the type shown in Figure 7.3. As the product of viscosity and formation volume factor μB increases with decreasing pressure, the initial slope of the inflow curve also increases with decreasing reservoir pressure. Hence, the well-inflow performance during natural depletion can be represented graphically by a series of descending inflow curves with increasingly steeper slopes, as seen in Figure 7.4.

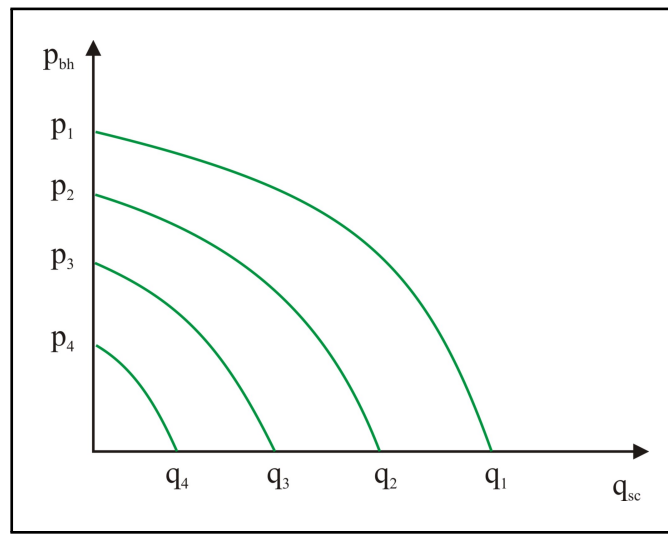


Figure 7.4: Well-inflow performance curves.

7.3.2 Tubing-Flow Performance

The tubing-flow performance refers to the pressure drop in the tubing as a function of flow rate, i.e. as $p_{bh} = p_{bh}(q_{sc})$. The pressure drop along the well depends on the tubing configuration and the properties of the fluids that are transported. The simplest case to investigate is a straight tubing with constant cross-section, constant temperature, constant Z-factor and constant friction factor.

The well head pressure is written in accordance to Eq. 6.56,

$$p_{wh} = p_{bh} \sqrt{\left(\frac{T}{T_{bh}}\right)^{2K_1} + K_3 \frac{T^2}{p_{bh}^2} \left[\left(\frac{T}{T_{bh}}\right)^{2(K_1-1)} - 1\right]}, \quad (7.10)$$

where the constants K_1 , K_2 and K_3 are defined as in Eq. 6.56. Assuming linear temperature profile in the well; $T = T_{bh} - \Delta T$. (Note that at the well head position; $y = L$.)

$$p_{wh} = p_{bh} \sqrt{\left(1 - \frac{\Delta T}{T_{bh}}\right)^{2K_1} + K_3 \left(\frac{T_{bh}^2}{p_{bh}^2}\right) \left(1 - \frac{\Delta T}{T_{bh}}\right) \left[\left(1 - \frac{\Delta T}{T_{bh}}\right)^{2(K_1-1)} - 1\right]}. \quad (7.11)$$

If we assume the temperature in the well to be constant, i.e. $\Delta T \rightarrow 0$, we may expand the limits above as follows,

$$\begin{aligned} \lim_{\Delta T \rightarrow 0} \left(1 - \frac{\Delta T}{T_{bh}}\right)^{2K_1} &= \lim_{\Delta T \rightarrow 0} \left[\left(1 - \frac{\Delta T}{T_{bh}}\right)^{T_{bh}/\Delta T}\right]^{2NK_{gp}} \\ &= \lim_{x \rightarrow \infty} \left[\left(1 + \frac{1}{x}\right)^{-x}\right]^{2N_{gp}}, \text{ where } x = -\frac{T_{bh}}{\Delta T} \\ &= e^{-2N_{gp}} \end{aligned} \quad (7.12)$$

Implementing the results of Eq. 7.12 in Eq. 7.11, we can write the well-head pressure

$$p_{wh} = p_{bh} \sqrt{e^{-2N_{gp}} - \frac{N_{fp}}{2N_{gp}}(1 - e^{-2N_{gp}})}, \quad (7.13)$$

where p_{wh} and p_{bh} is the well-head and bottom-hole pressure, respectively. The dimensionless numbers N_{gp} and N_{fp} are defined as

$$N_{gp} = \frac{M_g g L \cos(\alpha)}{\bar{Z} R T_{bh}}, \quad (7.14)$$

$$N_{fp} = \frac{4\bar{Z} f w_g^2 R T_{bh} L}{p_{wh}^2 A^2 d_h M_g}, \quad (7.15)$$

where all parameters have been defined above.

Since we wish to express the bottom-hole pressure in Eq. 7.13 as function of the flow rate, we have to transform the equation by first multiplying both sides by $e^{2N_{gp}}$, and we get

$$\left(\frac{p_{bh}}{p_{wh}}\right)^2 = e^{2N_{gp}} \left[1 - \frac{N_{fp}}{2N_{gp}} (e^{2N_{gp}} - 1)\right]^{-1}, \quad (7.16)$$

where the last term in Eq. 7.16 can be expanded using the series $(1+x)^{-1} = 1 - x + x^2 - x^3 + \dots$, when $x < 1$. Since $(N_{fp}/2N_{gp})(1 - e^{2N_{gp}})$ always is less than 1, the bottom-hole pressure can be expressed as function of the well-head pressure, such that

$$p_{bh} \simeq p_{wh} \sqrt{e^{2N_{gp}} + \frac{N_{fp}}{2N_{gp}} e^{2N_{gp}} (e^{2N_{gp}} - 1)}. \quad (7.17)$$

Using the dimension-less constants defined in Eqs. 7.14 and 7.15, we may approximate Eq. 7.17 with the following expression

$$p_{bh} \sim p_{wh} \sqrt{e^{2N_{gp}} + \frac{\bar{f} q_{sc}^2}{A^2 d_h^2}} \cdot \text{constant}. \quad (7.18)$$

The "constant" in Eq. 7.18 does not depend on the flow rate and is as such not of interest when considering the bottom-hole pressure as function of gas flow rate. Remember that $w_g = \rho q = \rho_{sc} q_{sc}$.

Eq. 7.18 tells us how the bottom-hole pressure p_{bh} will increase with increasing flow rate, as shown in Eq. 7.18. As the flow rate approaches zero, i.e. $q_{sc} \rightarrow 0$, the bottom-hole pressure is approximated by

$$p_{bh} \sim p_{wh} e^{N_{gp}}, \quad (7.19)$$

which is another form of the well known barometric height formula.

As in the case of well-inflow performance, the tubing-flow performance can be represented as a plot of bottom-hole pressure versus flow rate. In Figure 7.5 the variation in bottom-hole pressure as a result of tubing (well-bore) gas flow is presented as function of flow rate. The tubing performance curve is pointing upwards in Figure 7.5, reflecting the progressively increasing resistance towards flow with increasing flow rate. Naturally the flow resistance is larger for narrower tubings, as can be seen directly from Eq. 7.18, where an decrease in $A^2 d_h^2$ is followed by an increase in p_{bh} .

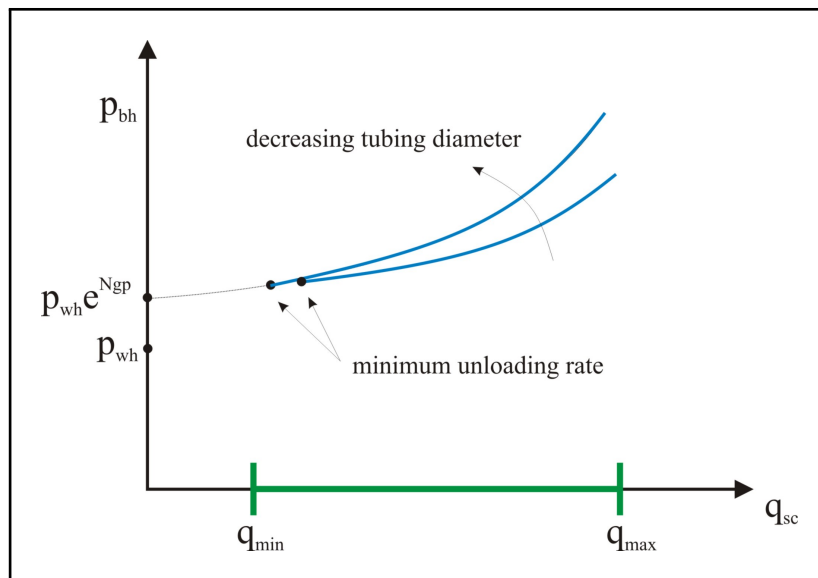


Figure 7.5: Tubing-flow performance.

The intercept with the vertical axis is equal to the well-head pressure plus the hydrostatic pressure due to the weight of the gas column in the tubing. This must be the same for each curves and thus all curves have a common interception point. With a constant well-head pressure, the bottom-hole pressure is seen to increase (approach the mean reservoir pressure) as the flow rate increases. Clearly, the bottom-hole pressure can not become identical to the reservoir pressure due to the presence of the well-inflow

pressure drop. There will therefore be a competition between between the two pressure drops, that finally determines the maximum well flow rate.

A consequence of flow of liquids along with the flow of gas is that stable flow rates can only occur above a minimum sustainable flow rate, the minimum liquid unloading rate. For flow rates below this rate, liquids in the tubing can not be lifted and accumulation of liquid at the bottom will eventually kill the well. The minimum unloading rate is given by

$$q_{min} = 3.6A \frac{\sqrt{\rho_g}}{\rho_{sc}} (\Delta\rho g \sigma)^{1/4}, \quad (7.20)$$

where the subscripts g and sc refers the gas density to bottom-hole and standard conditions, respectively.

As we can infer from Eqs. 7.18 and 7.20, the minimum liquid unloading rate decreases with decreasing bottom-hole pressure and decreasing tubing diameter. Hence, installing a smaller size tubing in the later stage of depletion may extend the production life of the well and result in higher ultimate recovery.

7.3.3 Well Deliverability

The production performance of a gas well depends on both the well-inflow performance and the tubing-flow performance. The maximum flow capacity of a well, commonly called the *well deliverability*, is determined by the intersection of the well-inflow performance curve and the tubing-flow performance curve for the minimum well-head (or terminal) pressure, as seen in Figure 7.6. At the crossing point between the two curves, the pressure drop in the reservoir plus the pressure drop in the tubing are exactly equal to the total pressure drop that can be imposed on the system, i.e. the reservoir pressure minus the well-head pressure (or terminal pressure) is equal to the sum of the well-inflow pressure and the tubing-flow pressure

$$\bar{p} - p_{wh} = \Delta p_{inflow} + \Delta p_{tubing}. \quad (7.21)$$

Well deliverability is a function of reservoir pressure and can be obtained for the intersections of the tubing performance curve for the minimum well-head pressure with the series of descending well-inflow curves that represent the inflow at declining reservoir pressures. This procedure is shown schematically in Figure 7.7. The resulting curve, known as the well deliverability curve, shows a decreasing deliverability with declining reservoir pressure.

Each well has its own deliverability curve. The total deliverability of the reservoir is obtained through summation of the individual deliverability curves. This curve can then be used to estimate the time when additional deliverability must be generated to meet the contractual deliverability.

The effect of lowering well-head pressure and attendant installations of compression can be illustrated with the help of deliverability curves as shown in Figure 7.8. Here the deliverability for the high and low well-head pressures is represented by curves 1 and 2, respectively. These curves can be constructed in the same manner as illustrated in Figure 7.7. The constructed deliverability is indicated by the horizontal dashed line in

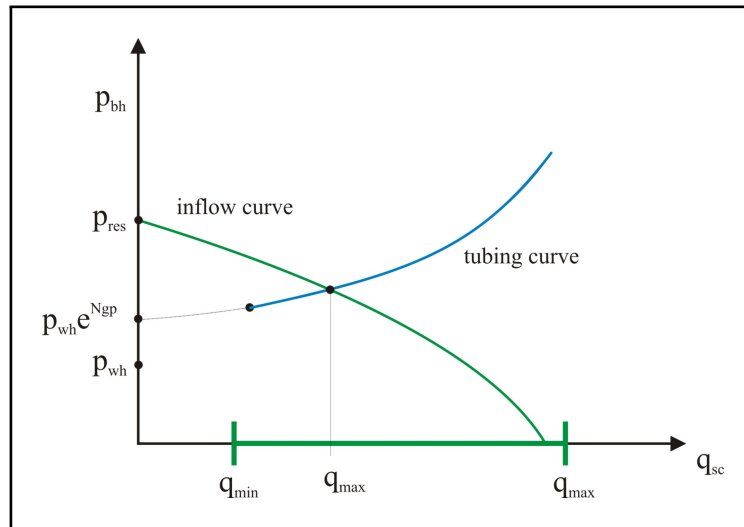


Figure 7.6: Well deliverability.

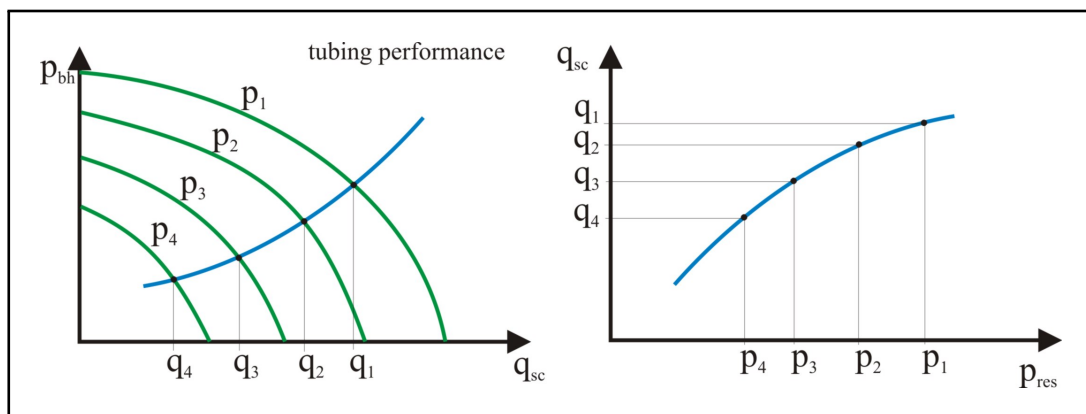


Figure 7.7: Deliverability curves.

Figure 7.8, which represents is the minimum production flow rate acceptable in order to honor the contract delivery.

The delivery needs to be enhanced when the reservoir pressure has dropped down to p_1 , which is the intersection between the delivery curve 1 and the minimum acceptable flow rate. If compression is installed at this point, production is continued via curve 2, allowing further production down to reservoir pressure p_2 . At this point a further reduction in well-head pressure may be considered. If compression costs do not justify a further lowering of the well-head pressure, the well become constrained by the well-head pressure and will produce at a declining rate down to the abandoned pressure p_a .

7.4 Simulation Examples

In this example we have simulated the simplest case possible using the multi-block, multi-well simulation program, namely one well in each block, where Well 1 is located

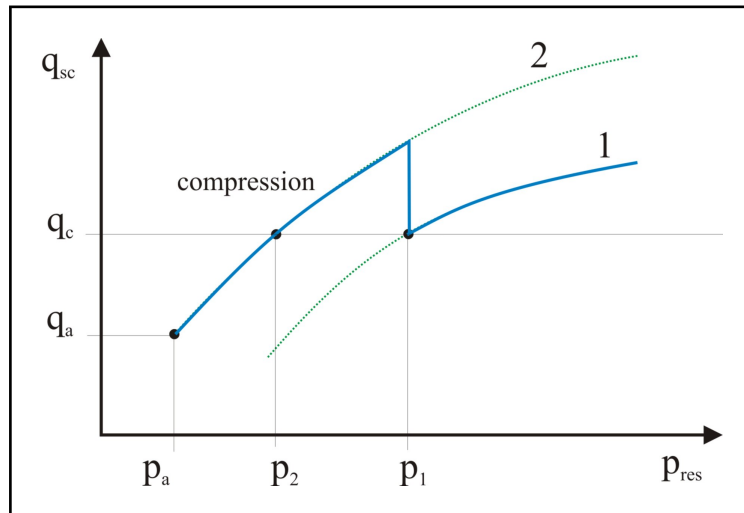


Figure 7.8: Effect of compression on delivery.

in the largest block. This example, on the other hand, shows the principal behavior of the changing well rate program, without the presence of numerous confusing details.

7.4.1 Production Flow Rates

Figure 7.9 shows the flow rate for the two wells and the total flow rate (the field flow rate). After about 90 days of production with only one well, the second well is started up. Since the maximum well rate is $0.5 \text{ MSm}^3/\text{day}$ and the plateau rate is $0.75 \text{ MSm}^3/\text{day}$, the start-up of the second well causes a reduction in the well rates equal to $0.375 \text{ MSm}^3/\text{day}$. The adjustment relative to maximum well rate and plateau rate is done automatically, using the PRODRATE-subroutine.

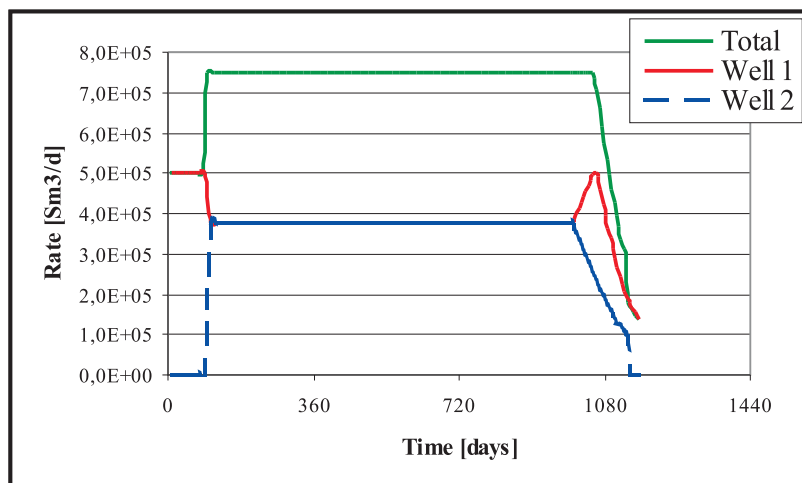


Figure 7.9: Production flow rates.

The file production is continued at constant plateau rate until Well 2, which is

located in the smallest block, falls below the maximum well rate. At this point the pressure decline in Block 2 has resulted in a reservoir pressure, not able to sustain maximum well flow rate. As the well rate in Block 2 decreases, the well rate in Block 1 is adjusted such as to compensate for the production from Block 2, in order to maintain plateau production. Finally, the well in Block 2 also falls below the maximum well deliverability pressure and a decline in the field rate starts. The well production is halted when the flow rate becomes less than the predefined minimum well rate.

7.4.2 Cumulative Gas Production

The cumulative gas production is presented in Figure 7.10. During the first 90 days, when only Block 1 is being produced, the total production overlaps the production from Well 1. At later times, the slope of the total production reflects the summation of gas produced from both blocks.

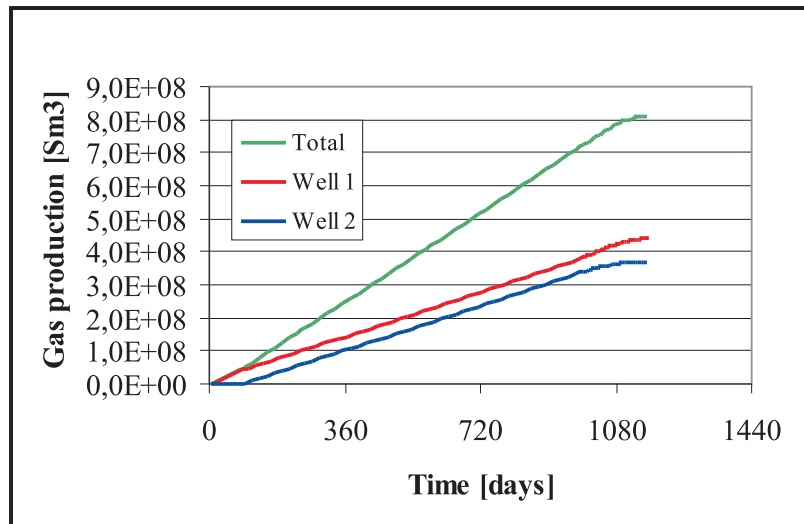


Figure 7.10: Gas production.

7.4.3 Pressure Development

Figure 7.11 shows the pressure decline in both blocks. The average block pressure curve is shown for Block 2.

The average block pressure and the two bottom-hole pressures are difficult to separate. The pressure profile that reaches the minimum bottom-hole pressure first is taken from Block 2. This separation between the two blocks is easier to detect for the well-head pressures, which are the two lowest curves in the plot. Since Well 1 maintains gas production after Well 2 has shut in, the well-head pressure for Well 1 is the upper one of the two.

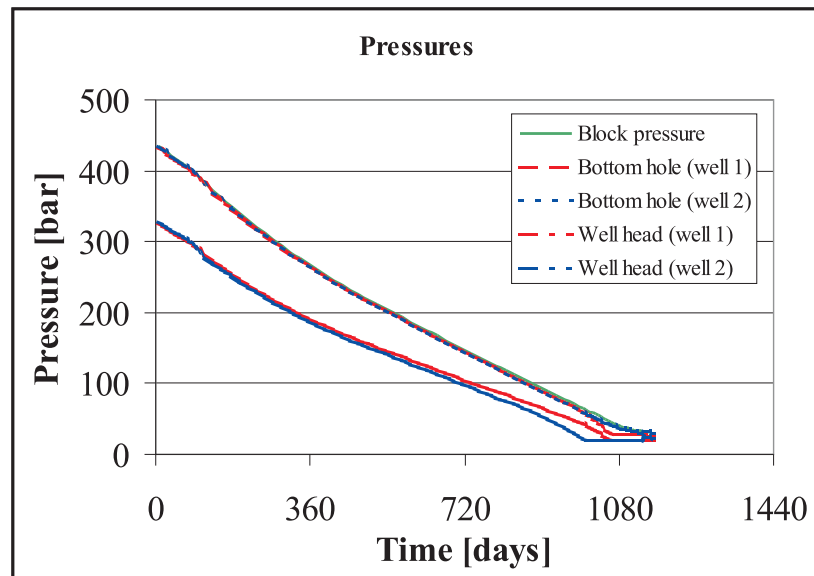


Figure 7.11: Pressure profiles.

References

Chapter 8

Gas Field Modeling and Production

In this chapter, an alternative simulation model is developed. The new model is a tool for forecasting well requirement and reservoir performance in strongly faulted gas and gas-condensate reservoirs. This model is particularly designed to handle reservoirs where uncertainty related to gas communication between various compartment blocks within the field, is pronounced and thought to be the dominant source of reservoir uncertainty.

The model can predict reservoir production scenarios, where errors are associated to reservoir data. Alternative production profiles, displaying uncertainty related to business opportunities and risks (upside and downside forecasts), can therefore be visualized, as part of the output of this model.

The model is briefly described, introducing terms like; volume-blocks, cross-flow communication probabilities, cross-through communications and drainage-compartments. A bit of theory is introduced in order to explain the functionality of the model and to show how normal compartmentalization of the reservoir gas in volume-blocks are converted into, in principle, independent drainage-compartments.

A reservoir field case study is shown in order to explain and exemplify use of the model. Based on geological characterization and fault seal analysis, the reservoir is divided into blocks. The model forms drainage-compartments based on a statistical evaluation of the communication probability between neighboring blocks. Uncertainty analysis is carried out using error propagation techniques, forming an optimistic and a pessimistic view of the reservoir. Production is simulated by a material balance calculation technique, producing the reservoir reserves through wells allocated to different drainage-compartments.

The Fault Block Model has proven to be an advantageous tool in the early stage field development of a North Sea gas-condensate reservoir where the effect of regional well location, number of wells and the optimum well production sequence have been studied. Production profiles from different well location strategies are investigated and various tests involving uncertainty in inter-block communication and in block volume are discussed. Uncertainty analysis also includes suggestions on how to reduce reservoir uncertainty and recommendation for an optimum well location strategy.

8.1 Introduction

A classic dilemma in starting up many petroleum reservoir development projects, is limited amount of reliable reservoir information, and concurrently, the demand for well-based decisions regarding future optimization and reservoir development. At such an early phase in the development process of a new field, the lack of reliable reservoir data makes it difficult to forecast future production scenarios and assess potential financial risks and/or opportunities for enhanced production from the field. See also Figure 8.1, as an illustration of the dilemma mentioned.

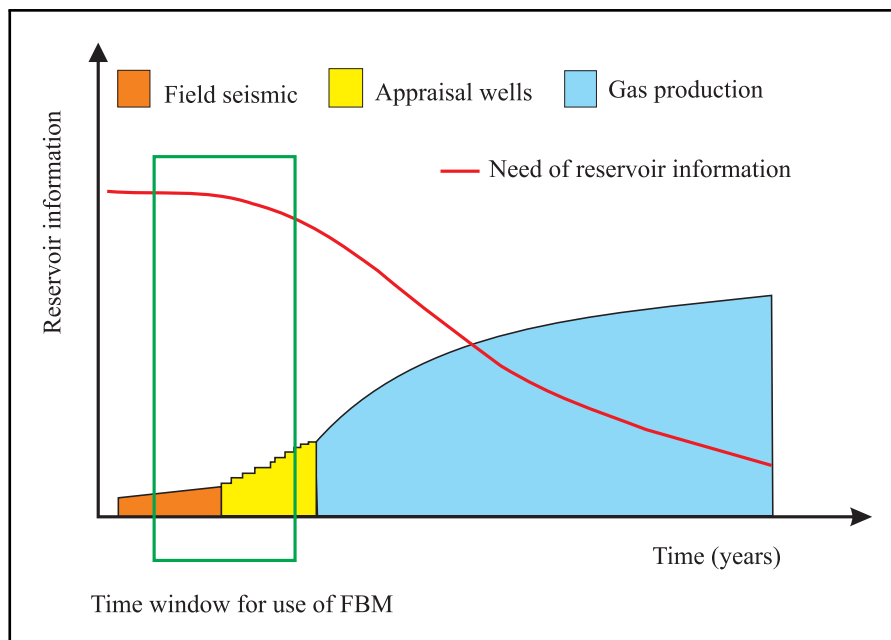


Figure 8.1: The time window for using the FBM is positioned along the time axis of the plot and related to the classical dilemma between availability of reservoir information and the need for this information.

In strongly faulted reservoirs, this dilemma appears to be even more pronounced since communication between reservoir segments in the field are strongly related to the faults' effectiveness as a barrier to fluid flow. Faults generally reduce the communication in the field and consequently increase compartmentalization of reserves. Reduced communication between reservoir segments and related uncertainty makes it more difficult to assess an optimal drainage strategy; that is, the selection of well locations and sequence of well production.

Due to shortage of reliable reservoir information in the initial phase in the development process, a trustworthy reservoir simulation model may not be constructed before sufficient reservoir data has been collected. This leaves the Fault Block Model (FBM) as one of few tools for early reservoir simulation and assessment of potential risks and opportunities in producing the gas reserves. The time-window for using the FBM is thought to be early in the process, before construction of finite-difference simulation models, when the use of more simplified reservoir models, focusing on dominating reser-

voir characteristics and uncertainties are the only practical alternative, as indicated in Figure 8.1.

A similar approach has been presented by Payne[14], where he introduces a Communication Reservoir model (tank model) in study of non-linearity in p/z -plots for tight gas reservoirs. Lyons et al.[10] used tank models in a totally different context, where integrated management of multi-reservoir field development is studied by connecting non-communicating reservoirs.

The FBM was developed and presented by Ursin and Mørkeseth[21] and Ursin and Mæland[20], with the purpose of forecasting reservoir production from a strongly North Sea faulted gas-condensate reservoir. A more general description of depletion performance of gas-condensate reservoirs is given by Raghavan and Jones[17].

The FBM is based on the assumption that it is possible to define drainage-compartments, from which single wells or a cluster of wells will produce the reserves in the field. These drainage-compartments will have "imaginary" boundaries, adding reserves from different compartments or blocks in the field. The FBM is thus a multi-compartment model, also previously presented by Lord and Collins[9] and Hower and Collins[7], respectively, for history matching purposes and as a tool for detection and qualifying compartment reservoir structure. The FBM model applies the same definitions of non-communicating reservoir units, as outlined in decline curve analysis presented by Fetkovich et al.[3].

Uncertainties related to production profiles are evaluated by error propagation, where uncertainties in inter-block-communication and in the block volume are calculated as a function of the number of wells in the field and their locations. Propagation of uncertainties in reservoir performance predictions has been similarly presented by Bu and Damsleth[1] as a way to track uncertainty in reservoir simulations. Previously, uncertainty in reservoir production simulation has been evaluated through statistical representation of typical reservoir characteristics, as presented by Hird and Kelkar[6] as in conditional simulation. Uncertainty about reservoir characteristics by putting error bars on important parameters has been discussed and recommended by Øvreberg et al.[22] and Meling et al.[11] introduced uncertainties in stochastic geological models using distribution functions. Other methods such as decline-curve performance, presented by Purvis[16] and Poon[15], predict production from multi-well pools through multi well rate analysis.

The FBM gives the estimated production profiles of rate- and cumulative production for both gas and condensate production, as well as the pressure development in the different drainage-compartments. Based on uncertainties in block-volume and inter-block communication, two sets of alternative production profiles are estimated, giving an optimistic and a pessimistic view of the potential field production. The availability of early forecasts of gas production is essential information in the development of gas fields in particular. Since the gas is normally sold before it is produced or even before the platform is in place and the wells are drilled, it is of foremost importance to be able to secure the contract delivery volumes. This demand may in some cases be contradictory or somewhat out of line with the wish of optimum or balanced production, securing maximum recovery over the life time of the field.

8.2 Reservoir Modeling and - Simulation

The traditional workflow of what finally makes simulation of field production possible, starts with seismic data acquisition. From the acquisition process, seismic data is discriminated into 3-dimensional seismic facies for building a voxel-based reservoir model. In this process stratigraphic and structural data are identified with lithologies by calibration against well data. In the final step, voxel grid extraction for reservoir modeling are defined and porosity and permeability values are introduced. Detailed information on methods and modeling in hydrocarbon exploration and productions is found in the book of Iske and Randen [8]. Simulation grid formation based on geological voxel representation involves scaling, related to both geo- and fluid-properties. Finally, the fluid flow simulation model may contain several ten-thousand simulation cells, which are run on the most advanced computers available. Simulation results are continuously calibrated with production data in order to improve the predictability of the model.

The above workflow is cumbersome, expensive with respect to man-hours and facilities and it takes time (years for a big field) to collect necessary data in order to obtain reliable and trustworthy simulation forecasts.

8.3 Alternative Reservoir Modeling

In danger of oversimplifying the circumstances around field production, one may say that dealing with production from oil fields is easy compared to handling the production of natural gas fields. Oil can be produced, loaded on e.g. tankers, transported to the market and sold at market-price. Gas on the other hand, due to its large volume, needs infrastructure that ties the production facilities (at the gas field) to the consumers, directly. The investment related to such infrastructure comes up front, before a single m^3 of gas can be sold. It is therefore quite often necessary for the gas producing companies to have signed sales agreements for the whole or a major part of the reservoir gas, already before the physical development of the field can be started. These sales contracts may contain information about plateau rate production, delivering pressure and quality of gas delivered, in addition to duration of gas delivered (number of years of steady delivery).

As a consequence of the above, quite a number of important decisions have to be taken at a very prudent stage in the development phase of a gas field. These decisions have to be based on data and analysis from the reservoir and - fluid, at a time prior to start-up of sales gas production. This point in time in the development of a gas field is therefore in most cases, too early to render reliable and trustworthy information via the traditional workflow, as described above.

8.3.1 Characteristics of Natural Gas Production

Gas flows generally easily in the reservoir because of its low viscosity, - in many cases several hundred times lower than e.g. oil viscosities. In reservoirs of low to high permeability (say from typically 10 mD and higher), the gas mobility is relatively high, to allow near instant pressure equalization of pressure draw down in relation to well production. This is a criteria necessary in order to recommend the methods of Material

Balance Estimation (MBE), which is extensively documented and used in this book. The criteria of reasonably rapid pressure equalization is a necessary condition, in order to be able to define a mean (average) reservoir pressure, which again is prerequisite of successful application of material balance calculation.

However there are situations where this criteria is not fulfilled, such as in the case of tight gas production, where more detailed flow description is needed in order to capture the events happening in the reservoir. We will therefore in the continuation of this chapter assume that the criteria of high gas mobility is always fulfilled.

A second important characteristic of natural gas reservoirs is related to the fact that in many gas fields, the gas is contained in volume-blocks with limited or no communication to neighboring volume-blocks. The reasons for this reduced communication within the reservoir could in many cases be attributed to faulting, where the throw of faults could be sealing or quite open. In some cases can a sealing fault become conductive due to a pressure difference building up across the fault. Faults, therefore generally reduce conductivity in the reservoir and makes overall assessments of fluid flow more complicated and uncertain.

8.3.2 Drainage Compartments

Let us assume the existence of a small gas field which can effectively be produced by four wells. The field might be slightly faulted and communication in the field may or may not be affected by the existing faults. At the final day, when production is abandoned, each of the four wells has produced a fraction of the total in situ reserves, as depicted in Figure 8.2.

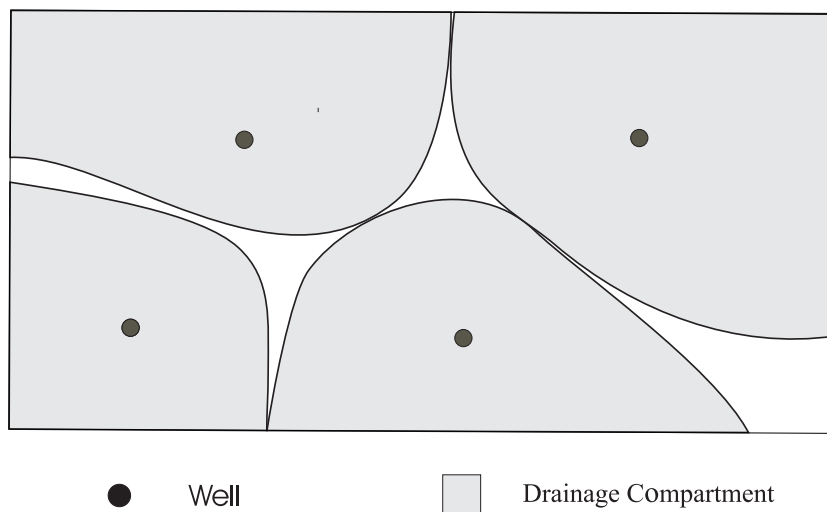


Figure 8.2: Top view of well drainage-compartments.

The figure depicts the top view of the field where the proportion of gas produced per well is illustrated by the area enclosure around the wells. The point here is that, regardless of nature of the gas field, faulted or not, each well has produced a certain volume of the gas reserves. This volume has been allocated to the different wells due to the characteristics of the reservoir and in competition with the other wells. The

fractions of the reservoir which contain the produced gas and which are depicted in the figure, is called *drainage-compartments*. These drainage compartments are therefore the parts of the reservoir which contain the gas that is produced through each and every well.

The above considerations are quite general and does not impose any restrictions on the nature of the reservoir. The reservoir characteristics of the field may vary between extreme cases; from homogeneous and isotropic to strongly faulted with unknown communication across faults.

The point here is that, if we through an application of a modeling tool, makes it possible to estimate the size and volume of these drainage-compartments, - the models of material balance, reservoir - and well flow that have previously been developed in this book, might be appropriate tools for simulating gas production.

8.4 Fault Block Modeling (FBM)

The basic idea behind, what is called, the Fault Block Model is the assumption that it is possible to define a drainage-compartment, from which a single well or a cluster of wells will produce the reserves without communication from neighboring wells.

The FBM was developed by this author with the purpose of forecasting reservoir performance for strongly faulted gas-condensate reservoirs, like the Sleipner Vest in the North Sea.

8.4.1 Principles of FBM

Based on geological characterization and fault seal analysis, reservoir compartmentalization is implemented by dividing the gas field into blocks, separated by known and/or undetected faults, where major faults are considered to be sealing and where minor faults could be sealing. Similar compartmentalization of North Sea reservoirs are presented by Smalley and Hale[18], where vertical segmentation of the field is the basis for further simulation studies.

The probability of communication across adjacent block boundaries are defined according to the geological expectation of inter-block flow and is set to a number between 0 and 1 (where 0 means no communication and 1 means full communication). The inter-block-communication is considered as a statistical parameter, while a particular fault is considered to be sealing or not. The number referred to as the inter-block communication is an estimate of the probability of communication across the fault boundary, based on the frequency by which similar faults are sealing or not. In short, the different blocks have a geological reference and are defined as physical volumes of gas confined by faults, which may act as sealing barriers to gas flow, where the inter-block communication is the probability for communication across block boundaries.

The partition of blocks into drainage-compartments is a crucial part of the FBM. When a new well is located in a volume-block, a new drainage-compartment is formed, based on the location of the new well. Gas contained in neighboring volume-blocks or in neighboring drainage-compartments are added to the gas already contained in the block where the new well is located, corresponding to a redefined inter-block communication probability. Gas shared between drainage-compartments is redistributed using a split

factor that favors the already existing drainage-compartments on behalf of the new drainage-compartment.

The formation of drainage-compartments could be illustrated by an example, as seen in Figure 8.3. The gas field depicted in the figure has been divided into five volume blocks (left), based on existing fault patterns and evaluation of communication across faults. It is a priori assumed that within each volume-block, communication is 100%, ie. there is no restriction on gas flow within volume-blocks.

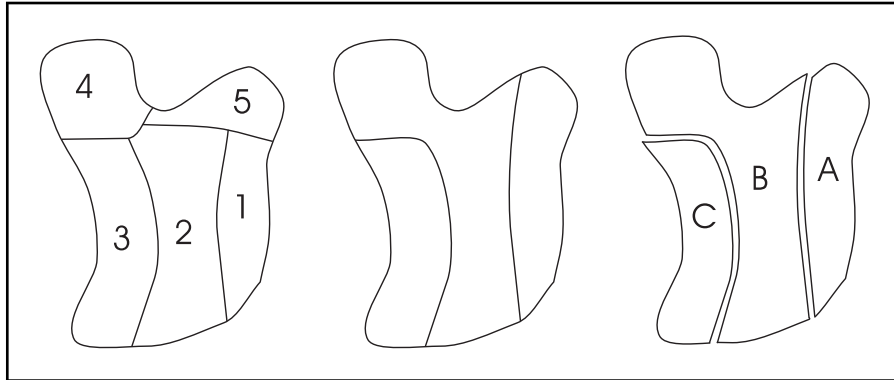


Figure 8.3: Illustration of formation of drainage-compartments.

The outer borderline in Figure 8.3 is considered to be sealing and no gas will flow across the outer boundary. Internally, across the borderline between volume-blocks, gas may flow or not. The probability for communication across a borderline is given and subject to evaluation when the drainage-compartments are formed (middle and right). In the example shown in the figure, three wells are producing the resources from three individually separated drainage-compartments.

8.4.2 The FBM - A Bit of Theory

The formulation of the fault block model theory has a general form and may therefore handle any number of volume-blocks. On the other hand, - the model is one-dimensional in the sense that there is no vertical dimension, implying that all gas is contained in one layer. Thus, excellent vertical communication is assumed in the gas zone.

Let us assume that our gas field consist of N volume-blocks (hereafter: blocks). The process of defining these blocks is involving geo-expertise, where throw of faults are individually assessed and cross-flow evaluated. This work is performed in close cooperation with reservoir engineering knowhow.

Summing the gas volume contained in all blocks gives the total reservoir gas volume,

$$V_{tot} = \sum_{i=1}^N V_i, \quad (8.1)$$

where V_i is the gas volume in block i .

Even though a single fault might be sealing or not, the statistical approach of dealing with many faults justifies the assumption that a fault has a certain probability for

communication across the fault boundary. This probability can therefore take any numerical value; $0 \leq P \leq 1$.

If the cross-flow probability $P_{i,j}$ between blocks i and j is 0, then no gas can flow across this boundary. In all other cases where $P_{i,j} \neq 0$, some gas can flow across this boundary. If a well is placed in block i , then part of the gas in block j might be produced through this well, and therefore be part of the drainage-compartment of this well. The cross-flow probabilities are therefore the key parameters in defining the new drainage-compartments. It is through manipulation of these parameters, we may define the drainage-compartments.

Gas may flow from one block to a neighboring block, defined by the cross-flow probability for that particular borderline, but gas may also flow from one block, via a second block, to be produced from a well in a third block. Therefore, in principle, gas in all parts of the reservoir might be produced through a well in any block. This means that the cross-flow probabilities could be non-zero, also for those blocks which don't have a common borderline.

By defining a cross-flow probability matrix \mathcal{P} , we may calculate the gas volume in a particular block and the additional volume of gas in all other blocks which would normally belong to this block, based on gas communication across borderlines. Done for all blocks, we get

$${}^1\vec{V} = \mathcal{P}\vec{V}. \quad (8.2)$$

On matrix form, Eq. 8.2 translates to,

$$\begin{bmatrix} {}^1V_1 \\ {}^1V_2 \\ \vdots \\ {}^1V_N \end{bmatrix} = \begin{bmatrix} P_{11} & P_{12} & \cdots & P_{1N} \\ P_{21} & & & \\ \vdots & & & \\ P_{N1} & P_{N2} & \cdots & P_{NN} \end{bmatrix} \begin{bmatrix} V_1 \\ V_2 \\ \vdots \\ V_N \end{bmatrix} \quad (8.3)$$

In the above equation, 1V_i is the drainage-compartment around the well located in the i 'th block. Based on the calculations in Eq. 8.1 (or Eq. 8.2), we may now decide in which block, a well would reach a maximum of the reservoir gas. This block is identified, simply by identifying the maximum of 1V_i . If ${}^1V_k \geq {}^1V_i$, where $1 \leq i \leq N$, then we decide to located the first well in block k . (This drainage-compartment might be large enough to sustain the production from more than one well, but this is in principle another problem and will be dealt with later.)

The volume of gas produced through only one well and located in the largest drainage-compartment is therefore given,

$${}^1V_k = \vec{P}_k \vec{V}, \quad (8.4)$$

where the notation "1" in 1V_k means the first set of calculations. Locating the second and third well location would be indicated with "2" and "3" as prefix.

The next step in the process is, as indicated, to determine the second largest drainage-compartment. In doing so, we have to recalculate the remaining block-volumes 1V_i , where $i \neq k$. This is done in order to redistribute the volumes being both part

of 1V_k and at the same time part of the block-volumes 1V_i . These volumes have to be shared in a "correct" way.

Recalculation of remaining block-volumes is performed by introducing a modified block-volume 2V_i , defined as follows,

$${}^2V_i = {}^1V_i - f(i){}^1V_i \cap {}^1V_k, \quad (8.5)$$

where $i \neq k$. $f(i)$ describes the redistribution mechanism in deciding how a common volume, shared by a block-volume and the drainage-compartment, should be shared. $f(i)$ could in principle take any value $0 \leq f(i) \leq 1$, but is in most cases set to 0.5. This means that the volume in question, is shared equally. In principle we may identify different redistribution parameters to different blocks.

The largest remaining drainage-compartment is found and we assume it to be 2V_l , where

$${}^2V_l \geq {}^2V_i, i \neq k. \quad (8.6)$$

We have now located two wells, one in block k and the second in block l . What remains to be done is to redistribute the gas volume that is in common between the two drainage-compartments. This is done by,

$${}^2V_k = {}^1V_k - f(k){}^1V_k \cap {}^2V_l. \quad (8.7)$$

Subsequently, we want to produce the gas in the field through not only two wells, but from as many wells needed to get a sensible production profile and possibly an optimized well coverage. The process described in Eqs. 8.5 to 8.7, has therefore to be repeated for each new well location. In general this process could continue until a well is located in all volume-blocks in the reservoir.

In the formalism above, we are seemingly modifying the drainage-compartments for each new step taken. In reality however (and using a more stringent mathematical formalism) the volumes are not modified, - only the probability matrix is updated in the process of locating new drainage-compartments. The recalculation done on the probability matrix in ie. Eq. 8.5 is described as follows,

$$P_{i,j} = P_{i,j} - f(i)P_{i,j} \cap P_{k,j}, \quad (8.8)$$

where $P_{i,j} \cap P_{k,j} = P_{i,j} \cdot P_{k,j}$.

It is worth noticing that the fault block model is an analytical model, where the relation between well coverage and number of wells is given on functional form. This is an advantage we later will make use of when uncertainties in cross-flow communications are introduced in the calculations, by means of error propagation.

8.4.3 A Simplified Model Example

An example, depicting how volume-blocks are redefined and drainage-compartments are formed, as a function of number of wells in the field, is presented in this example. Figure 8.4 shows the formation of two drainage compartments in a field of five rectangular

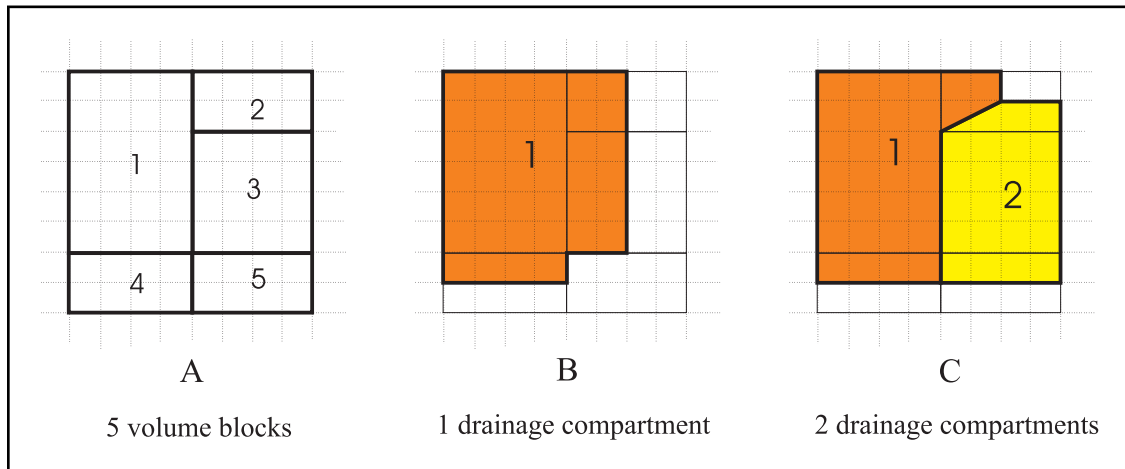


Figure 8.4: Formation of drainage-volumes for 2 wells in a compartmentalized field of 5 blocks.

volume-blocks. In the process shown, part of the gas volume in adjacent volume-blocks is included in the drainage-compartments where wells are located.

In Figure 8.4), the inter-block communication is set equal to 0.5. This means that half of the gas contained in all neighboring blocks (2, 3 and 4) are added to the drainage-compartment in Figure 8.4 B. Figure 8.4, A and B shows the formation of one drainage-compartment, adding gas from all neighboring volume-blocks (neighboring volume-blocks have common block boundary). In the case of two wells (Figure 8.4 C), with one well in Block 1 and the second well in Block 3, two new drainage-compartments are formed and the gas contained in the first drainage-compartment is recalculated. Volume of gas shared between the two drainage-compartments is divided in equal parts and assigned to each of them (The split applied in the figure is 50%). The gas volume not part of any drainage-compartment (unshaded in Figure 8.4) will not be produced.

The formation of drainage-compartments V_i , is defined through the inter-block communication probability $P_{i,j}$,

$${}^1V_i = \sum_{j=1}^5 P_{i,j} V_j, \quad (8.9)$$

where V_j is the initial gas volume in the volume-blocks. In the equation above, the volume-blocks are assigned values corresponding to the distribution shown in Figure 8.4, left. The volume-block vector is therefore defined $(V_1, V_2, V_3, V_4, V_5) = (24, 8, 16, 8, 8)$ units of gas.

Locating one well in the field of five volume-blocks gives five alternative well locations, where the corresponding drainage-compartments vector is:

$$\begin{bmatrix} {}^1V_1 \\ {}^1V_2 \\ {}^1V_3 \\ {}^1V_4 \\ {}^1V_5 \end{bmatrix} = \begin{bmatrix} 1.0 & 0.5 & 0.5 & 0.5 & 0 \\ 0.5 & 1.0 & 0.5 & 0 & 0 \\ 0.5 & 0.5 & 1.0 & 0 & 0.5 \\ 0.5 & 0 & 0 & 1.0 & 0.5 \\ 0 & 0 & 0.5 & 0.5 & 1.0 \end{bmatrix} \begin{bmatrix} 24 \\ 8 \\ 16 \\ 8 \\ 8 \end{bmatrix} = \begin{bmatrix} 40 \\ 28 \\ 36 \\ 16 \\ 20 \end{bmatrix}, \quad (8.10)$$

where the numbers 1.0 and 0.5 in the matrix above indicate 100% internal block communication and 50% communication between neighboring blocks, respectively.

The probability matrix in Eq. 8.10 represent the input data describing the communication in the field. The numbers in the first row (1.0, 0.5, 0.5, 0.5, 0) represent the communication seen from block 1. Block 1 has an internal communication equal to 1.0, while the cross-flow communication between Block 1 and blocks 2, 3 and 4 is found to be 0.5. The communication between Block 1 and Block 5 is 0.0, since there is no common borderline between the two blocks.

Block 2 has only two neighbors, Block 1 and Block 3 and also here is the communication set equal to 0.5. The communication matrix has to be filled in by hand and represents a careful assessment of communication between neighboring blocks.

Since the first well may reach more gas being located in volume-block V_1 , than in any other block (here 40 units of gas), the first drainage-compartment is located to volume-block V_1 where gas from volume-blocks 2, 3 and 4 are added.

In order to define the location of the second well, we need to re-calibrate the drainage-compartment by taking into account the location of the first. Redefinition of the gas distribution between the drainage-compartment already defined and a new drainage-compartment is done by redefining the probability matrix, as shown above. The redefined matrix is written:

$$\begin{bmatrix} {}^2V_1 \\ {}^2V_2 \\ {}^2V_3 \\ {}^2V_4 \\ {}^2V_5 \end{bmatrix} = \begin{bmatrix} 1.0 & 0.375 & 0 & 0.5 & 0 \\ 0 & 1.0 & 0.375 & 0 & 0 \\ 0 & 0.375 & 1.0 & 0 & 0.5 \\ 0 & 0 & 0 & 1.0 & 0.5 \\ 0 & 0 & 0.375 & 0.375 & 1.0 \end{bmatrix} \begin{bmatrix} 24 \\ 8 \\ 16 \\ 8 \\ 8 \end{bmatrix} = \begin{bmatrix} 31 \\ 14 \\ 23 \\ 12 \\ 17 \end{bmatrix}. \quad (8.11)$$

From Eq. 8.11 it is seen that the second largest drainage-compartment is defined when a well is located in volume-block V_3 . This is the situation depicted in Figure 8.4. (If for some reason, the next well is localized in Block 5, then the calculations performed in Eq. 8.11 are still correct and the well coverage with the second well in Block 5 will be 17 units of gas. But, on the other hand, the depicted distribution of gas, as in Figure 8.4 would look totally different.)

The FBM algorithm, as seen above, has assigned a drainage-compartment to the first well. Then, based on the remaining distribution of gas located in other blocks, the second well is located in a new volume-block, defining a second drainage-compartment. Since the two wells are located close to each other, and are actually sharing gas from the same blocks, a redistribution is performed between the two drainage-compartment. The size of drainage-compartment is therefore totally dependent on the cross-flow communication between neighboring blocks.

8.4.4 Cross-through communication

Not shown in Figure 8.4, is the cross-through communication. The model also allows gas to flow from one block through another (or two) blocks, to be produced in a drainage-compartment. The cross-through communication is calculated on the basis of the inter-block communication, adding all possible ways gas may flow between a block and a

given drainage-compartment. Since there are many ways gas can flow from one block to a drainage-compartment, we have defined *flow paths* describing the different routes gas may flow in the reservoir. In Figure 8.4, gas may flow from Block 5 to Block 1, following three different flow paths. One path is from Block 5, through Block 4 and to Block 1. Another flow path will be from Block 5 through Block 3 and to Block 1 and thirdly still another flow path will go from Block 5, through Block 3 and Block 2 and then into Block 1. Figure 8.5 is showing the three flow paths as described above. Based on cross-flow analysis one could expect less gas to flow from Block 5, through Block 3 and 2, since this path is crossing two borderlines, as the probability for communication is reduced accordingly. More gas may flow through Block 3 than through Block 4 from Block 5, but that is in principle up to the cross-flow probabilities to define.

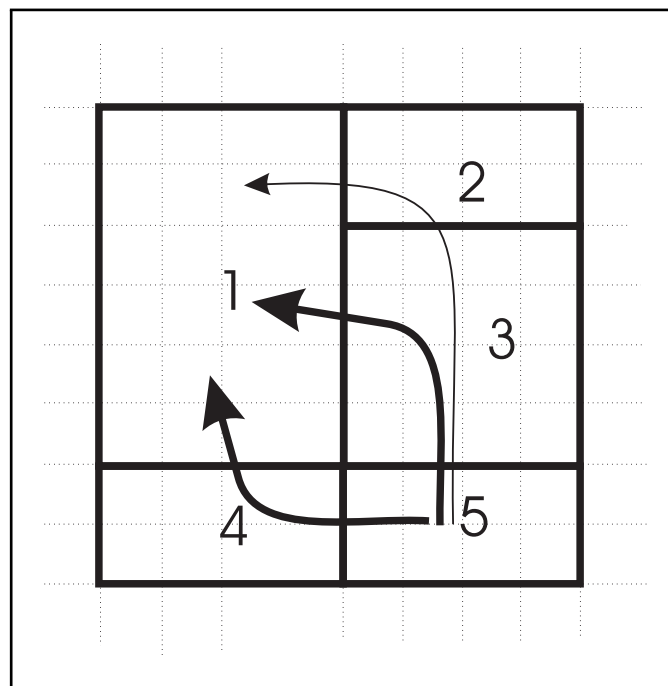


Figure 8.5: Example of flow paths in describing cross-through communications.

In Figure 8.5 we see that gas from Block 5 can be produced through a well in Block 1 and we may ask: What is the probability of communication between Block 5 and Block 1. (Previously we have defined this probability equal to zero since there is no borderline between the two blocks.)

The combined communication probability describing the crossing of two borderlines, ie. the borderline between Block 5 and Block 4 and the borderline between Block 4 and Block 1 would normally be defined as the product of the two, since the assessment of the communication of the two borderlines are completely independent, ie. $P_{4,5}P_{1,4}$.

If we for a moment disregard the possibility of gas flowing from Block 5, through both Block 3 and 2 and restrict the possibilities of gas flow only to the two flow paths from Block 5 via Block 3 and 4, we can more easily assess the problem of defining the cross-through communication probability $P_{1,5}$. We have established above that the probability of crossing two border lines is the product of the probability of crossing

each of the borderlines. Since both flow paths are acting on the same block, here Block 5, we must subtract the likelihood of gas flowing along one flow path from the total when calculating the communication probability of the second flow path. If the probability of communication from Block 5 via Block 4 is $P_{1,4}P_{4,5}$, then the probability of communication from Block 5 via Block 3 is $P_{1,3}P_{3,5}(1 - P_{1,4}P_{4,5})$. The cross-through probability of communication between Block 5 and Block 1 is therefore written,

$$P_{1,5} = P_{1,4}P_{4,5} + P_{1,3}P_{3,5}(1 - P_{1,4}P_{4,5}). \quad (8.12)$$

If we now turn back to the situation described in Figure 8.5, with three flow paths, the accumulated probability for cross-through communication from Block 5 to Block 1 is now written,

$$P_{1,5} = P_{1,4}P_{4,5} + P_{1,3}P_{3,5}(1 - P_{1,4}P_{4,5}) \\ + P_{1,2}P_{2,3}(1 - (P_{1,4}P_{4,5} + P_{1,3}P_{3,5}(1 - P_{1,4}P_{4,5}))). \quad (8.13)$$

Using the proposed cross-flow probability of 0.5 in Eqs. 8.12 and 8.13, we find the total cross-through probability $P_{1,5}$, in the case of only two flow paths to be 0.4375, while in the case of three flow paths we get 0.578125.

In principle we may chose to cross as many borderlines as there are, but in practice the cross-through probability does not change much when "non direct" flow paths are added. In practical programming only four borderlines are included in the calculations of any cross-through probability.

The relative volume of gas in Block 5 belonging to Drainage-compartment 1V_1 (with only one well), would be calculated on basis of the inter-block communication probabilities and is equal to 0.578125.

The splitting factor between drainage-volumes is also not shown in Figure 8.4 or in the calculations in Eqs. 8.12 and 8.13, above. The effect of the splitting factor would be to secure a larger fractional part of the gas contained in Block 2, 4 and 5, all shared between Drainage-compartment 2V_1 and 2V_2 , such as increasing the gas volume belonging to Drainage-compartment 2V_1 on behalf of Drainage-compartment 2V_2 . The split factor is normally between 0.50 and 0.65, based on the experience from previous studies.

8.4.5 Handling Uncertainty

Uncertainty in the FBM is materialized through uncertainty in parameters representing volume and cross-flow; ΔV_i and $\Delta P_{i,j}$. The definition of these parameters describing uncertainty in the reservoir is mainly an exercise best suited for the geological - and geophysical expertise, while handling of these uncertainties very much is a reservoir engineering task.

The most intuitive method of handling uncertainty in the reservoir would be to introduce alternative data sets; $(V_i, P_{i,j})$, in assuming a worst- and a best case scenario. Then carry out calculations as prescribed above and assess the results from the different the simulations. The problem of handling uncertainties this way is related to the fact of over-estimating the effect of ie. reduced communication in the reservoir in the worst

case as well as over-estimating the degree of communication in the reservoir in the best case. Simultaneously minimizing all parameters in the worst case and maximizing all parameters in the best case does over estimate the space of variation between worst and best case scenarios. One could, however vary only a few parameters "up or down" at one time, but then one would be faced with many different simulations which results have to be analyzed and interpreted.

Since the FBM is based on an analytical representations such as the equations described above and the numerics only sums up the the contributions over a limited number of blocks, uncertainty can be handled by the method of *error propagation*. The advantage of estimating uncertainty by error propagation is that we get a balanced representation of the extreme cases.

Since the cross-flow probabilities $P_{i,j}$, all are independent of each other, ie. estimation of communication across a fault is performed individually, there are no mixed terms in the multiplication of the probability vectors and the uncertainties can be represented by the sums of quadrates.

Using Eq. 8.8 as a starting point, error analysis gives the uncertainty in cross-flow probability as a sum of quadrates,

$$\Delta P_{i,j} = \sqrt{[\Delta P_{i,j}]^2 + f^2(i) \sum_k ([P_{i,j} \Delta P_{k,j}]^2 + [\Delta P_{i,j} P_{k,j}]^2)}. \quad (8.14)$$

Similarly, estimation the uncertainty in the drainage-compartments based on Eq. 8.4 and the uncertainties in the various volume-blocks, is yield by the equation,

$$\Delta V_i = \sqrt{\sum_k ([\Delta V_i P_{i,j}]^2 + [V_i \Delta P_{i,j}]^2)}. \quad (8.15)$$

Calculations of uncertainties ΔV_i and $\Delta P_{i,j}$ are carried out, following the same procedure as described above and are represented as alternative output matrix of optimistic and pessimistic view of volume and probability; $V_i \pm \Delta V_i$, $P_{i,j} \pm \Delta P_{i,j}$.

8.5 FBM Characteristics

The partition of neighboring blocks in forming drainage-compartments is seen as a statistical averaging process, estimating the most likely compartmentalization of the reservoir when a given number of wells are producing the reserves. This does not necessarily imply that one can determine where the gas is flowing in the reservoir and the origins of the gas that are produced through certain wells. This is also the case for non-producible gas volumes. One does not know where they are located! We don't possess specific nor local knowledge of the gas location in the reservoir. What we do know is related to what might happen on average, following a statistical processes of estimating where the gas is located an how it can be produced.

The FBM suggests location and sequence of well locations, based on the assumption that field production will be optimized when wells are located in volume-blocks from where the largest fractions of the gas reserves can be produced. This secures early production from parts of the reservoir where the gas accumulation is the highest. Other

strategies can be adopted, i.e. location of wells that secures the best area or gas volume coverage with a certain number of wells in the field. Yet, another strategy would be to locate wells, such that the outtake of gas would be depleting the field evenly, i.e. that the reservoir pressure is declining similarly in all regions of the field.

The FBM works in a sequential mode, defined by the following partition algorithm:

1. The first well is located in the volume-block where the potential of reaching (producing) the largest fractions of gas in the field (Strategy mentioned above).
2. The second well is located in the volume-block where the second largest volume of gas could be reached. In the event that gas in these two drainage-compartments are overlapping, redistribution is done in accordance to a pre-defined split-factor.
3. The process of locating additional wells and updating the drainage-compartments is continued until all wells are located, at which time some blocks may have several wells and other blocks may have no wells.
4. When all wells are located, uncertainty in block volumes and in inter-block communications are calculated. Based on this input, alternative sets of drainage-compartments are defined, where one set defines a reservoir with minimum communication across faults (pessimistic) while the other set defines a reservoir where communication is maximized (optimistic). Uncertainty handling is an important and integrated part of fault block modeling.
5. Finally gas production is performed using material balance equations, where the different drainage-compartments are treated as non-communicating units of gas. (Similar approaches have been presented by Ehilg-Economidis[2].)

In the FBM, all wells are in principle treated equally, using the same near well description. The bottom-hole pressures are calculated using individual well thickness and different Dietz shape factors (relative to the shape of the block where the well is assumed positioned in the centre of the block). The calculation of gas flow in well and pipes is done in accordance to recommendation by Ouyang and Aziz[13], following the same procedure as presented in the book by Hagoort[5]. The wells are producing against a fixed well-head pressure and the well lengths and dip angles are defined by the position of the platform and the geometrical centre of the blocks where wells are located. The material balance calculation assumes non-communicating tanks of gas and thus no pressure- or saturation gradients in the reservoir are accounted for. The effect of near well-bore condensate dropout, could be an important factor when well delivery is considered as pointed out by Fevang and Whitson[4] in their study of gas-condensate well deliverability. The consequences of liquid dropout near the well followed by decreased well deliverability are more severe in low permeable formations than for high permeable formations, as pointed out by Novosad[12]. The reservoir gas is produced to the surface as one phase where dry gas and condensate is separated using a single stage flash calculation. Condensate as dropout in the reservoir is considered to be lost production.

8.6 Application of The Fault Block Model

The practical use of fault block modeling is demonstrated through an example taken from one of the largest gas-condensate fields in the Norwegian part of the North Sea. The reservoir, discovered in 1974, is typical for about 70 % of all hydrocarbon finds in the North-Sea, which are fault traps [19]. A field region is subdivided in volume-blocks, where gas contained in one block may communicate with gas in neighboring blocks and the degree of communication is expressed through an inter-block-communication probability. Figure 8.6 shows the field region subdivided in 38 blocks. The platform, in this example, is located at the centre of Block 19.

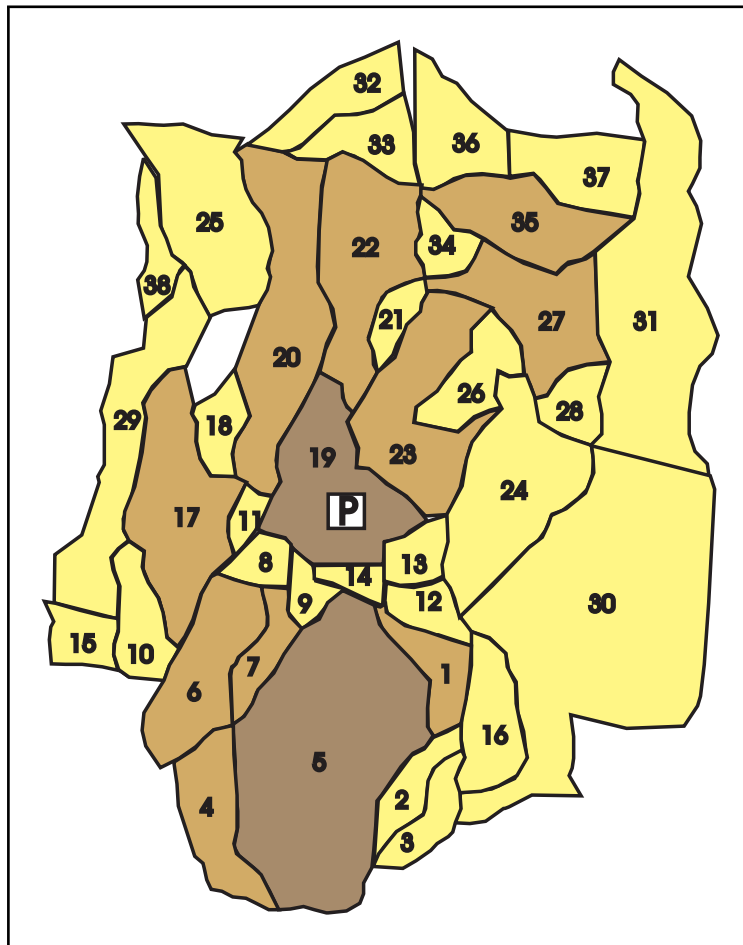


Figure 8.6: Gas field segmented in 38 volume-blocks. Lightly shaded volume-blocks contain less than 2.5 Gsm^3 gas. Medium shaded blocks contain more than 2.5 Gsm^3 of gas and darkly shaded volume-blocks contain more than 10 GSm^3 .

The reservoir is a marginal marine sandstone of the Hugin Formation, with good gas productivity (permeability larger than 100 mD). Typical reservoir and simulation related data is presented in Table 8.1. The field simulation is accomplished in accordance to specifications given in an input data file, containing general reservoir data, production data, PVT data and data concerning the simulation process. Figure 8.7 shows the

relative production of dry gas, condensate and the dropout of liquid in the reservoir. The initial reservoir pressure is 437 bar and the minimum reservoir pressure at shut-in is about 20 bar.

Table 8.1: Typical reservoir related data.

| | |
|---------------------------------------|--|
| Porosity range | 15 - 18 % |
| Permeability range | 150 - 200 mD |
| Initial pressure | 437 bar |
| Reservoir temperature | 392 K |
| Initial water saturation | 12 - 14 % |
| Reservoir thickness | 100 - 145 m |
| Water compressibility | $0.435 \cdot 10^{-4} \text{ bar}^{-1}$ |
| Reservoir compressibility | $0.45 \cdot 10^{-4} \text{ bar}^{-1}$ |
| Minimum well head pressure | 20 bar |
| Time between well production start up | 90 days |

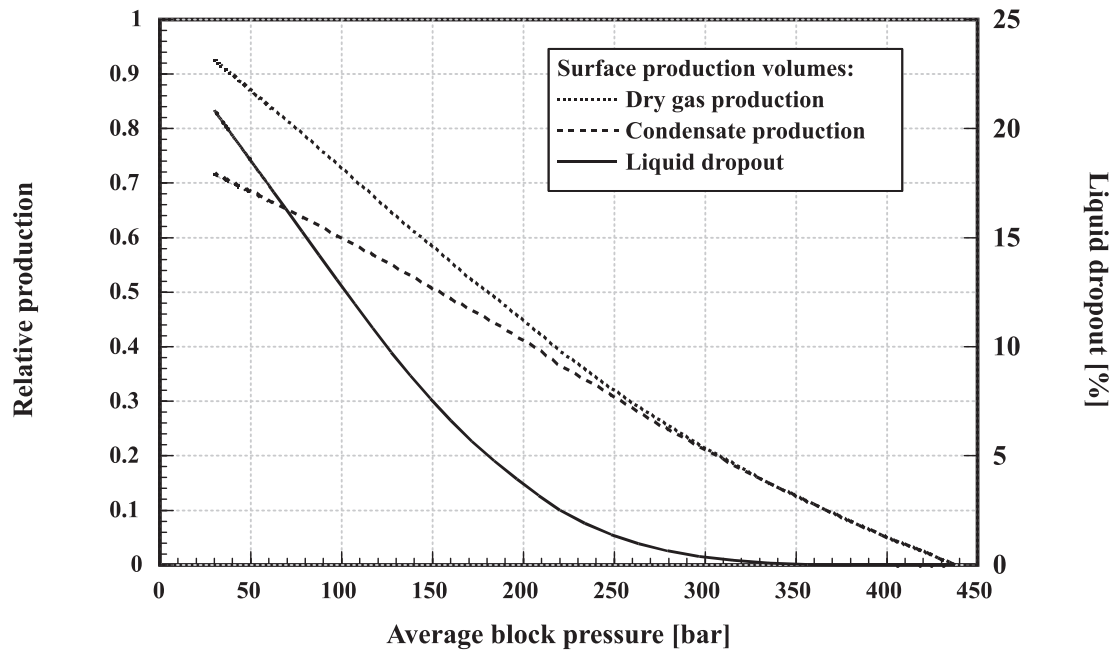


Figure 8.7: Relative gas- and condensate production and liquid dropout.

The structure is dome-shaped, highly faulted and complex structured, probably due to the presence of underlying mobile Zechstein salt. Varying gas-water contacts and several pressure regimes encountered by exploration wells already drilled on the field and slight variations in gas compositions, all indicate sealing faults as barrier to flow. The uncertainty in inter-block-communication due to faults acting as barriers, is therefore an important factor encountered in connection with the development of implementing an optimum production strategy.

The combination of good reservoir productivity and the large number of major faults, considered to be sealing and minor faults of partly unknown characteristic, facilitates a compartmentalization of the gas field that makes the use of the FBM attractive. In producing the gas reserves, it is thought to be of principal importance to locate the blocks from where most of the gas can be produced. The uncertainty in reservoir communication introduced by compartmentalization and the uncertainty in initial gas volume represent the most significant uncertainties in producing the gas reserves from the field.

8.6.1 The Gas Field

The reservoir contains a total gas volume of about 120 GSm^3 (10^9 standard m^3) (GIIP). All blocks containing more gas than 2.5 GSm^3 are lightly shaded in Figure 8.6. Those two blocks containing more than 10 GSm^3 gas, are darkly shaded. Two different clusters of blocks are easily identified, one around Block 5 and the other around Block 19. These two blocks would therefore be the natural centers where most of the wells should be located.

A distribution of gas contained in the different blocks, as presented in Figure 8.6 is shown in Figure 8.8. From the histogram in Figure 8.8, indications of two minor clusters around Block 17 and Block 27, appear likely. The location of wells is necessarily going to be a competition between these four clusters of blocks and the demand for a balanced production. Due to rather high inter-block-communication in the field and the uncertainty in gas volumes, an optimum well location strategy is far from obvious.

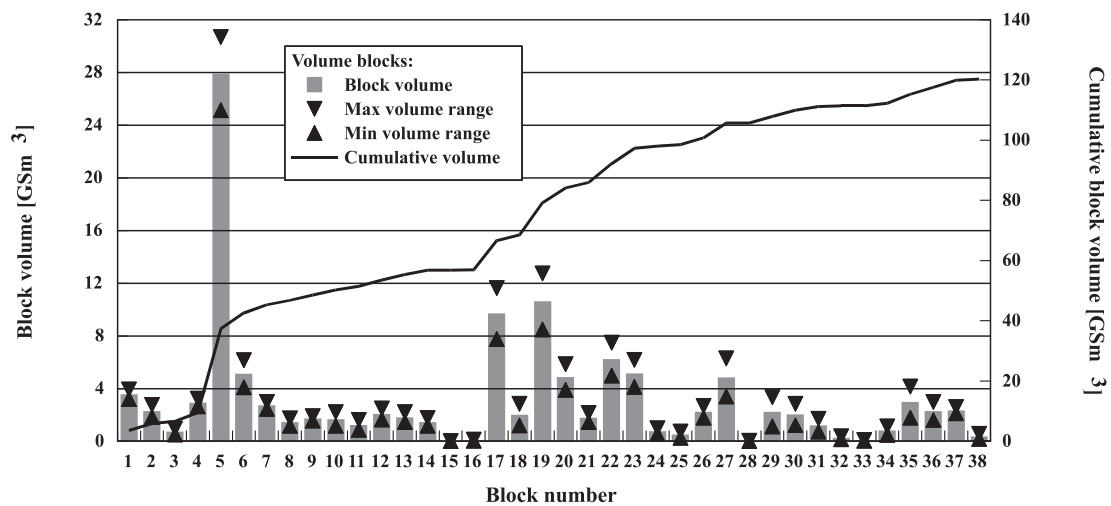


Figure 8.8: Gas in volume-blocks and uncertainty in gas volume.

Based on the estimated volume of gas present in the different blocks (Figure 8.8), it seems reasonable to expect the first three wells to be located in blocks 5, 19 and 17. Since block 5 contains more than twice the amount of gas of any other block, we may assume a pre defined well sequence of which the first four wells are located in blocks: 5, 19, 17 and 5.

The error bars put on the columns indicating volume of gas in blocks in Figure 8.8,

show the uncertainty in volume estimation. From the figure it is seen that major volume-blocks also have major uncertainty attached to their volume estimation.

8.6.2 Well Location Sequence

It was initially assumed that no more than 9 wells would be necessary to efficiently produce the gas reserves in the field. With a field plateau rate of $12.1 \text{ MSm}^3/\text{day}$ (10^6 standard m^3) and a maximum well rate of $3.0 \text{ MSm}^3/\text{day}$, a well location sequence is obtained by using the FBM. Wells are located in the following blocks: 5, 19, 17, 5, 27, 6, 5, 22 and 9. Note that only the last 5 wells have been optional in the fault block modeling process, since it is quite obvious to locate wells in major blocks first.

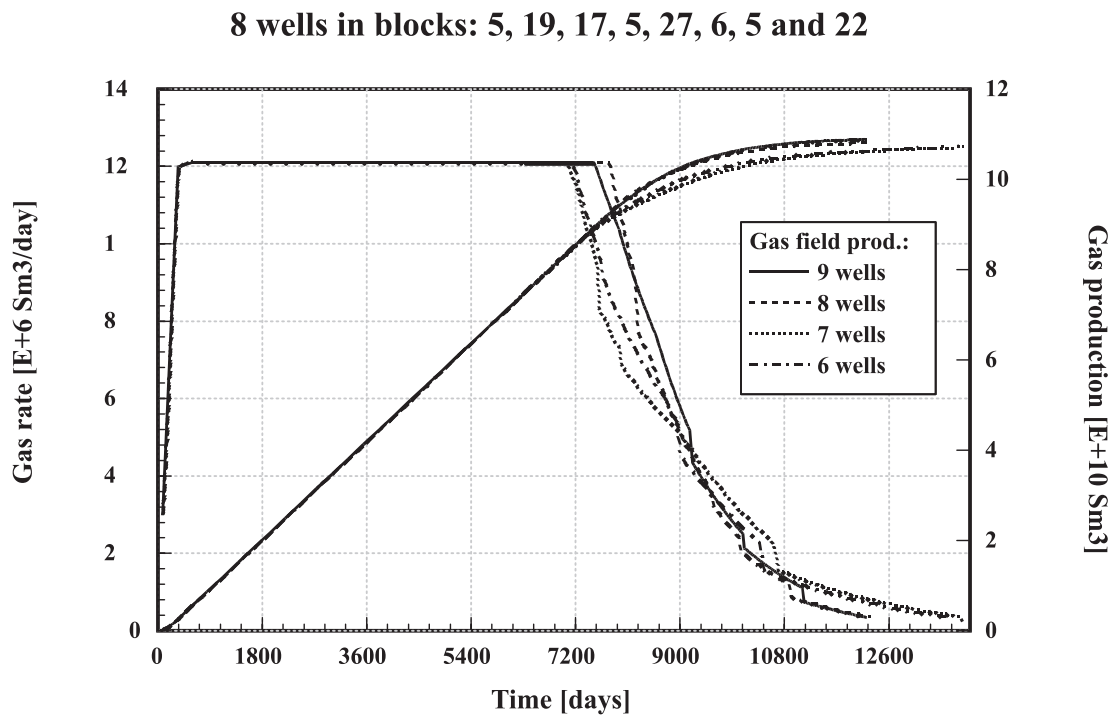


Figure 8.9: Gas rate and cumulative production from 9, 8, 7 and 6 active wells.

The first four wells in volume-blocks 5, 19 and 17, cover directly or indirectly the gas in the two major clusters. The gas contained in these volume-blocks is approximately 55% of the total reserves. The well in volume-block 27 covers the north-easterly cluster, whereas the two wells in volume-blocks 6 and 9 cover the central region. All nine wells together, will reach about 97% (well coverage) of the gas reserves in the field. The production data is shown in Table 8.2.

Figure 8.9 shows the gas rate and the gas production in the four cases of using 9, 8, 7 and only 6 wells in the field (1 year = 360 days). As can be expected from viewing the data in Table 8.2 and from Figure 8.9, more gas is reached with more wells even though the difference in well coverage is maximally only 1.6%. More importantly is however the improved plateau length and the reduced decline period, when 9 wells are producing the gas compared to when only 6 wells are active. The maximum difference

Table 8.2: Gas production from 9, 8, 7 and 6 wells, respectively.

| No. of wells | Well coverage % | Plateau fall-off [days] | Prod. fall-off [GSm^3] | Prod. after 30 years [GSm^3] |
|--------------|--------------------|----------------------------|-------------------------------|-------------------------------------|
| 9 | 97.8 | 7519 | 89.28 | 107.87 |
| 8 | 97.1 | 7762 | 92.22 | 107.18 |
| 7 | 96.2 | 7141 | 84.71 | 104.93 |
| 6 | 96.2 | 7033 | 83.40 | 104.55 |

in plateau length is 486 days and the prolonged decline period is 4 to 5 years.

It is concluded from Figure 8.9, that eight wells seems to be the minimum number needed to efficiently produce the gas reserves. Fewer than eight wells will lead to an early plateau fall off and consequently a prolonged production period. With eight wells located in six volume-blocks (5, 6, 17, 19, 22 and 27), the well coverage is presented in Figure 8.10. The figure present volume of gas contained in the the drainage-compartments when wells are located in only six volume-blocks. The continuous line is indicating the cumulative volume coverage when more drainage-compartments are included in the production strategy. Error bars are based on calculations performed error propagation, as presented earlier.

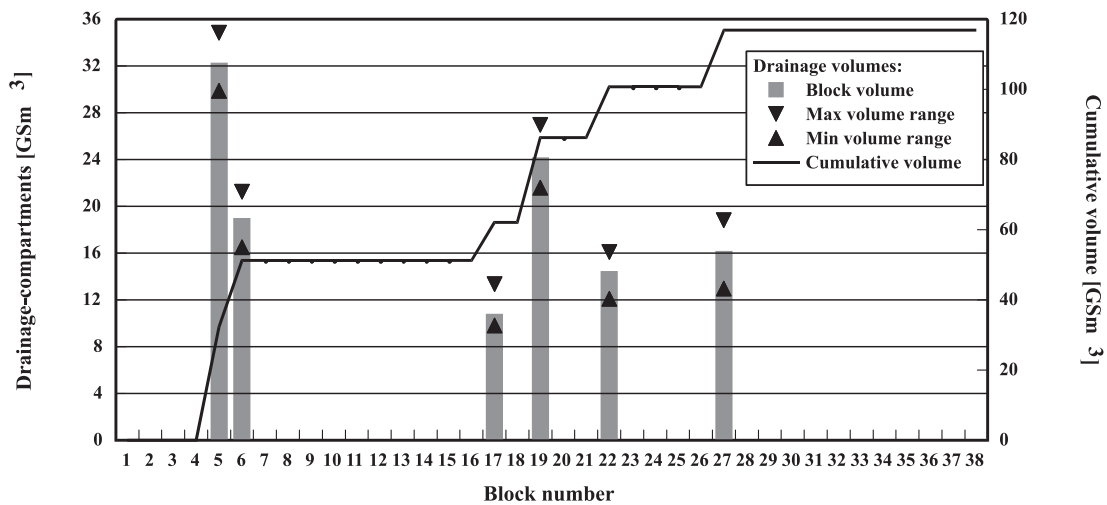


Figure 8.10: Drainage-compartments using eight wells in the field.

The condensate production from the field (using eight wells) is shown in Figure 8.11, where the declining condensate production during the plateau period, is due to liquid condensation in the reservoir. The GOR is seen to vary between 2100 - 2700 Sm^3/Sm^3 during the production lifetime of the field. The figure shows a definite fall-off in condensate rate. Depending on the richness of the gas, means to reduce the pressure decline in the reservoir could be evaluated. (In our case the gas is rather lean and consequently no effort would be made to counteract normal pressure decline in the reservoir.

The drainage-compartment pressure development is presented in Figure 8.12. The

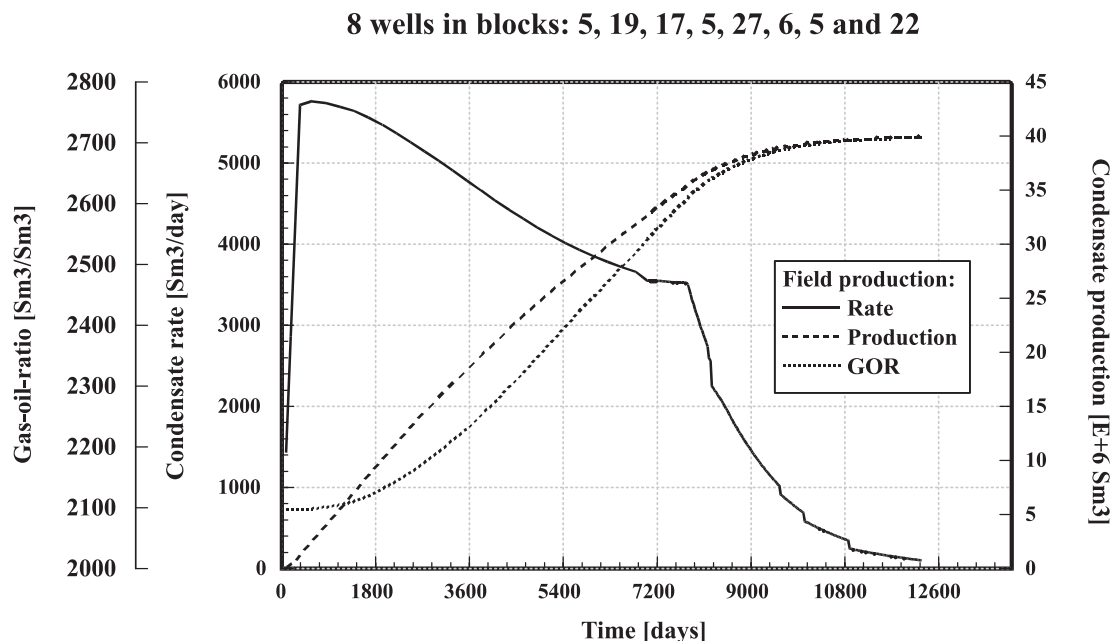


Figure 8.11: Condensate rate- and production profiles.

somewhat widely spread compartment pressures as a function of time (days), is a sign of un-balanced production and is a case for further optimization. When the pressure is declining differently in different parts of the reservoir, the danger is that non-optimum flow patterns could develop. In order to secure that gas is flowing the shortest way from where it is located to where it is going to be produced is an important requirement in an optimized production strategy. The wide spread of pressure decline profiles, as shown in Figure 8.12, is therefore a clear indicator non-optimum flow patterns.

8.6.3 Well Rate Adjustments

The well rate is automatically adjusted in the FBM relative to the maximum well rate and the plateau rate. The adjustment is done to allow all wells to produce simultaneously at reduced or maximum rates. The well rates are continuously regulated to compensate for varied production conditions, i.e. when one well goes into decline other wells will share the loss of capacity suffered by the declining well. Figure 8.13 shows the gas rates from the different drainage-compartments and the total (field) rate. In the figure we see that the three wells in the drainage-compartment based in Volume-block 5 are producing the gas in that compartment effectively up to a time of about 7200 days, after which the three wells go into decline simultaneously. Since they are producing from the same compartment of gas, their bottom hole pressure are equal and they therefore behave similar. When this happens, the other wells producing from other compartments are compensating the loss of production from the wells in Volume-block 5 by increasing their production proportionally. They all increase their production with an equal share of the rate lost by the three wells in Volume-block 5. This feature is included into the FBM in order to effectively sustain maximal plateau length production.

8 wells in blocks: 5, 19, 17, 5, 27, 6, 5 and 22

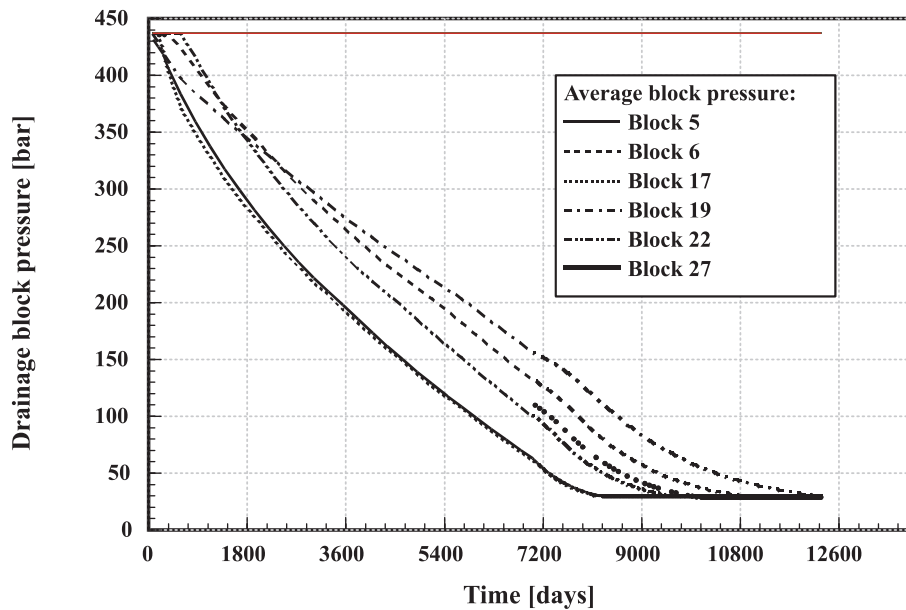


Figure 8.12: Pressure development for 8 wells in 6 drainage-compartments.

8 wells in blocks: 5, 19, 17, 5, 27, 6, 5 and 22

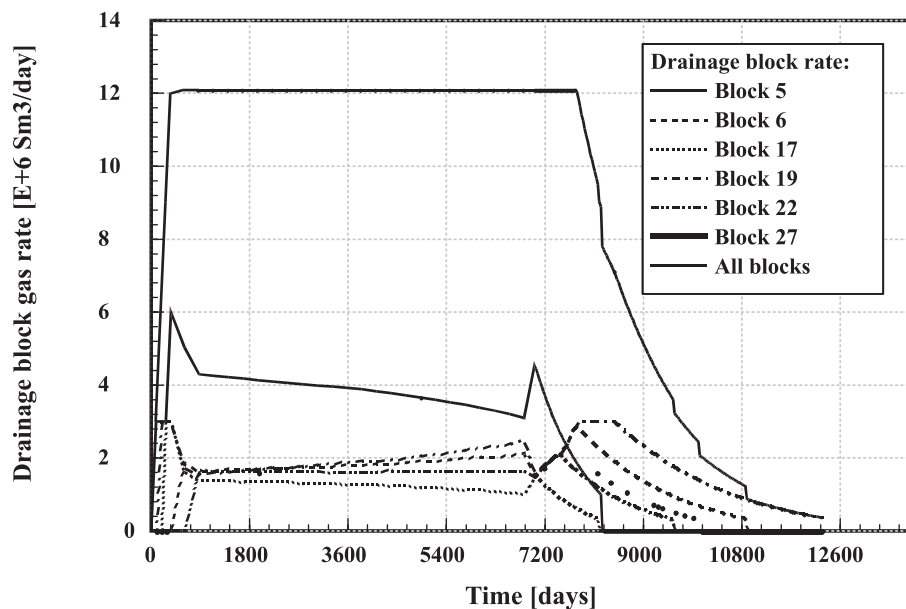


Figure 8.13: Gas well flow rates compared to total field rate.

There are basically two characteristics that explain the well rate profile. First, all well rates are adjusted such as to reach a balanced production, i.e. to follow the same pressure development for all wells. For the three wells in Block 5, this means that these

well rates are reduced relative to other wells since gas production and thus the declining block pressure in Block 5 would otherwise, be much steeper than for the other drainage-compartments. Second, when one well is falling off plateau production due to minimum bottom-hole pressure reached, other wells are upgraded to take over its production and thus get an increased well rate.

8.6.4 Uncertainty in Field Production

The uncertainty in field production related to reservoir communication is primarily linked to minor faults being open or closed to fluid flow. Uncertainty in field production could therefore be studied by taking two examples of the reservoir where minor faults in one case are considered closed and in the other case, considered open.

The closed case is simulated by reducing the inter-block communication to 0 in all cases where it is initially less than 0.5. In those cases where the inter-block communication initially is larger than 0.5, it is set to 0.4. This reduction in inter-block communication will efficiently reduce the communication between different blocks. The open case is simulated by simply increasing all inter-block communication initially larger than 0.5 to 1.0.

The gas rate- and production profiles for the three cases of: average-, open- and closed reservoir are shown in Figure 8.14 and in Table 8.3. The rather small difference between the average- and the open case, demonstrates the fact that the average representation of the reservoir is rather open in the first place and consequently, that most of the minor faults are considered to be communicating. The difference in production, shown in Figure 8.14, does not include the uncertainty in gas volume and thus only represents the variation in reservoir communication as such.

Table 8.3: Uncertainty in field production: Open/closed reservoir and Error propagation.

| Reservoir | Plateau fall-off [days] | Prod.at fall-off [GSm ³] | Prod. after 30 years [GSm ³] |
|-------------|----------------------------|---|---|
| average | 7762 | 92.22 | 107.15 |
| open | 8005 | 95.16 | 109.42 |
| closed | 6952 | 82.42 | 95.29 |
| optimistic | 8653 | 103.00 | 119.53 |
| pessimistic | 6844 | 81.12 | 93.24 |
| optimum | 8140 | 96.79 | 107.42 |

(after 28.5 years)

The FBM represents the uncertainty in gas production by calculating the error propagation due to assigned uncertainties in both inter-block communication and in gas volume. If the probability for communication across a fault (block boundary) is assumed to be 0.4 (40%) and the pessimistic and optimistic estimates are 0.2 and 0.6, respectively, then the relative uncertainty is set to 50%. This number is further used

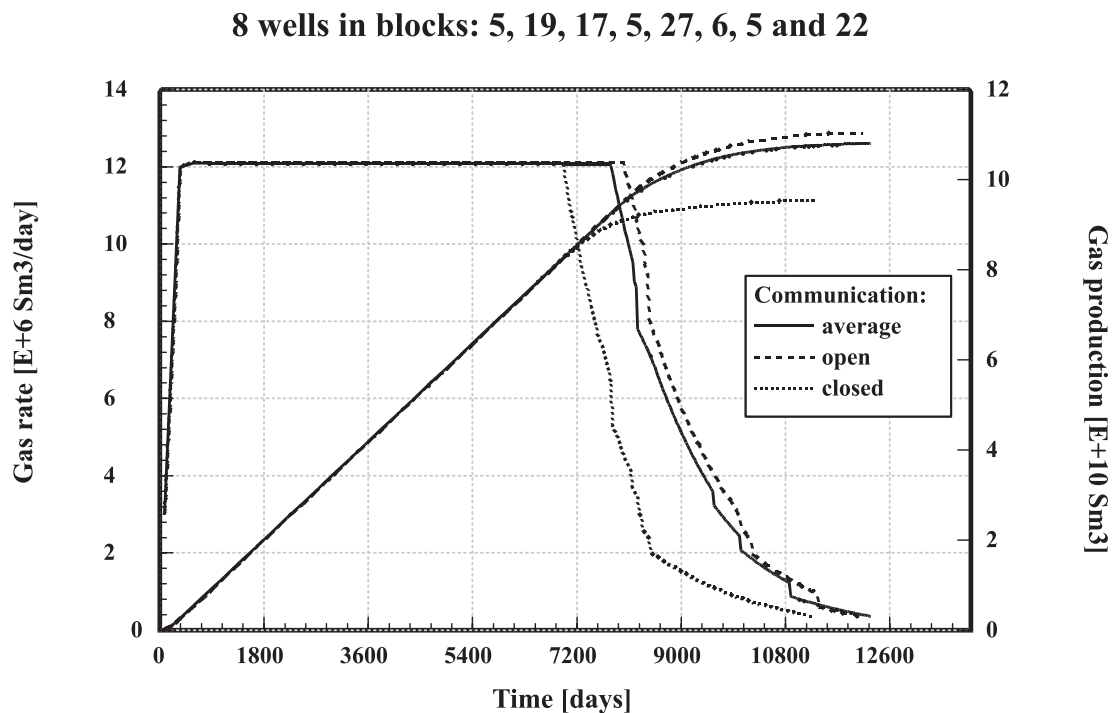


Figure 8.14: Production profiles when minor faults are considered closed compared the the case when minor faults are considered open.

in the error propagation algorithm and represent the relative error in the cross-flow probability.

Figure 8.15 and Table 8.3 shows the alternative production profiles in the two cases where both uncertainties in inter-block communication and in gas volume are considered. The difference in plateau fall-off in the two extreme cases is seen to be about 5 years and the difference in cumulative gas production after 30 years (10800 days) is about $\pm 12\%$ of what is considered to be the average gas production.

Using the features of the FBM, we may now compare the rate- and production profile, in the two cases where; both uncertainty in volume and cross-flow probability is included in the error analysis, as shown in Figure 8.15, and the case where only uncertainty in the cross-flow probability is included. Figure 8.16 show the difference between these profiles, where one profile is subtracted by the other. The difference in the production profiles shows that when uncertainty in volume estimation is reduced to zero, the total uncertainty of gas production from the field is reduced by about 63%. This means the the dominating reservoir uncertainty is related to the uncertainty in assessing the volume of gas in the reservoir.

Figure 8.16 also illustrates the fact that uncertainty in volume and cross-flow probability is affecting gas production rather late in the production phase, after about 18 to 19 years of constant plateau rate production. From this time and onwards, gas production may go into decline or continue another 5 years with steady plateau production. From these error analysis it is therefore concluded that the uncertainty in volume and cross-flow communication is responsible for introducing uncertainty about gas production in

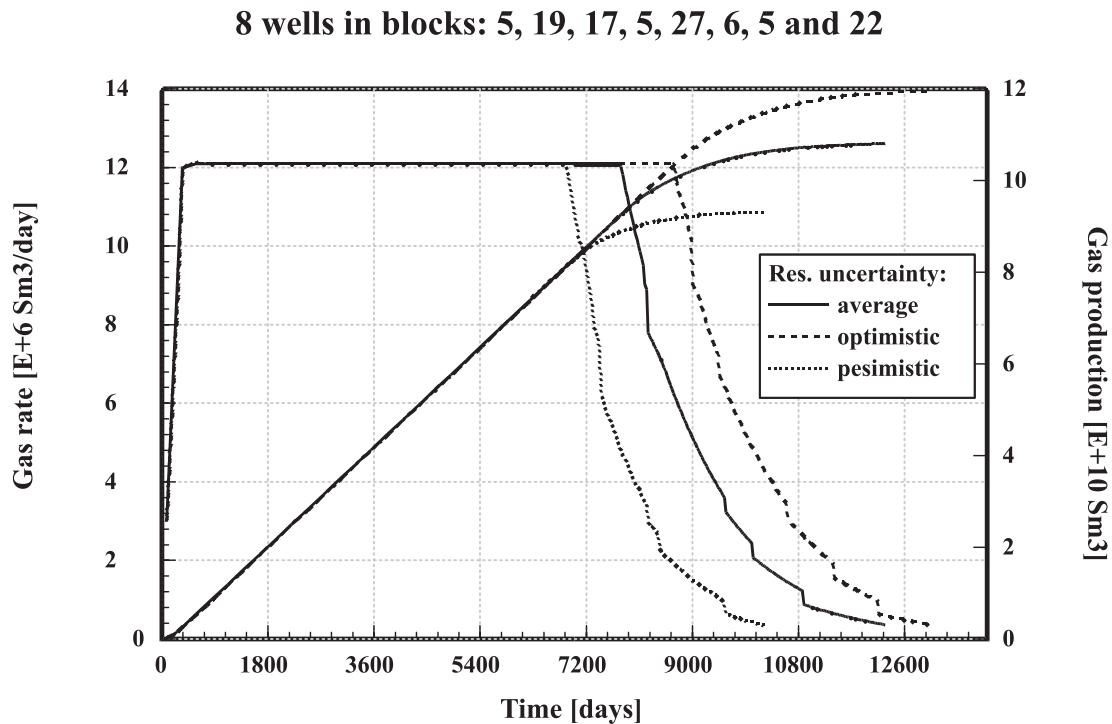


Figure 8.15: Production profiles when uncertainties are calculated by error propagation for both volume and cross-flow probabilities.

the latter part of 10 to 15 years of production from the field.

8.6.5 Balanced Field Production

It has already been suggested that a more balanced gas production from the field could be achieved by adapting an optimum well location sequence. The purpose of this optimization would be to secure a more balanced outtake of gas from the different drainage-compartments.

From Figure 8.10 it is seen that drainage-compartment 19 has the potential for a second well. Considering a balanced production from the whole field, a revised well location sequence should also be considered. The first four wells are pre-defined (in volume-blocks: 5, 19, 17 and 5) and followed by wells in volume-blocks 27 and 22, before any further wells are located in the central and southern regions of the field. It is therefore left for the FBM to suggest where the remaining two wells should be located.

Since Volume-block 5 already has two wells and its well rates have been seen to be automatically reduced at an early time, due to large gas out-take, it is reasonable to postpone location of the third well in Volume-block 5. These considerations lead to a revised well location sequence where wells are located in blocks: 5, 19, 17, 5, 27, 22, 19 and 5.

In Figure 8.17 we compare the gas rate- and production profiles for a balanced production, as stated above, to the previous case discussed earlier. Since the optimum well location sequence depletes the gas volumes more evenly, the plateau fall-off comes about

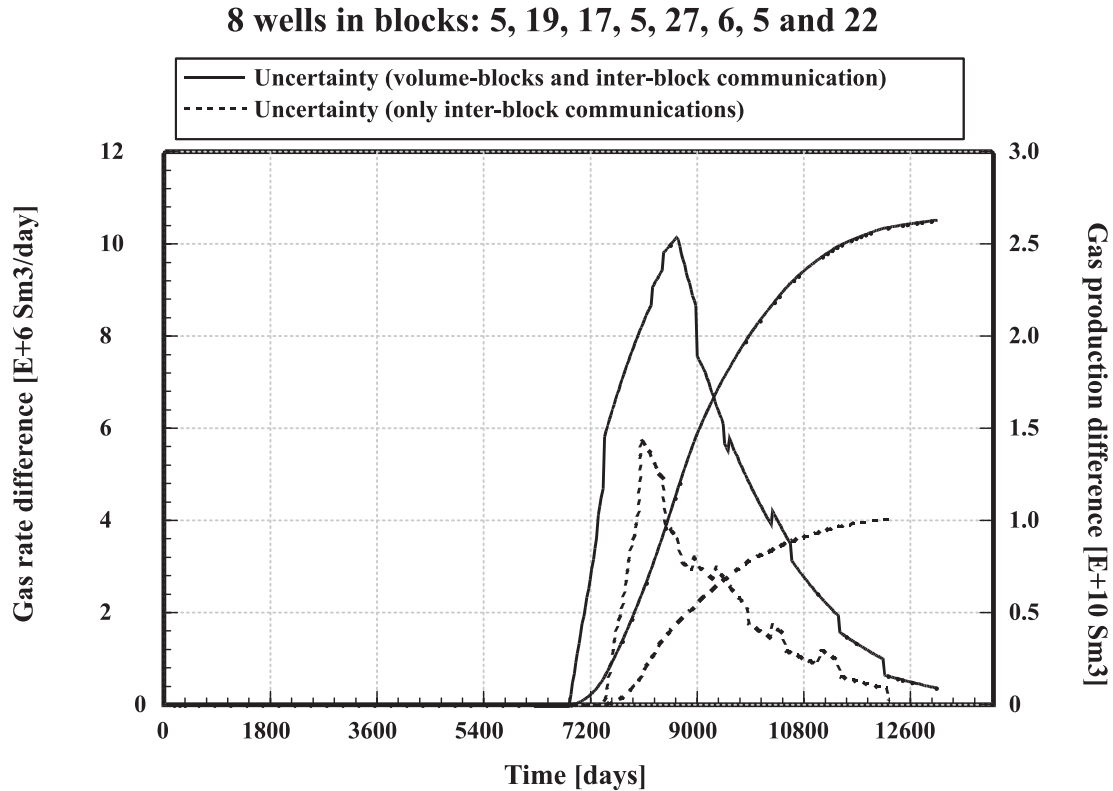


Figure 8.16: Gas rate- and production difference when uncertainty in reservoir communication and/or in gas volume is considered.

one year later compared to the previous case. Consequently, the declined production is much steeper and therefore the shut-in of production comes about 5 years earlier in the optimum (balanced) case. The same well head pressure is used in both cases.

The pressure profiles for the different drainage-compartments, shown in Figure 8.18, is another indicator of near optimum gas depletion of field. As seen from the figure the drainage-compartment pressure profiles is quite similar during the production of the field. For those volume-blocks which is not produced, the pressure profile will remain constant with time (horizontal line in Figure 8.18). The gas in these volume-blocks is either part of the gas produced from one of the draining-compartments or the gas in the block will simply not be produced.

Fetkovich et al.[3] compared production from non-communicating units (compartments) by evaluating the relative block rate (rate per cumulative production) as a criteria of balanced production. In Figure 8.19, the drainage-compartment rates divided by cumulative production is shown. Since all profiles follows the same trend, balanced production is obtained. This means that all drainage-compartments are depleted similarly and optimum drainage condition in the field prevails. However, a correction deduced from Figure 8.19, could be to increase gas production from wells in blocks 22 and 27, since production from these two blocks starts up somewhat later, compared to the other drainage-compartments.

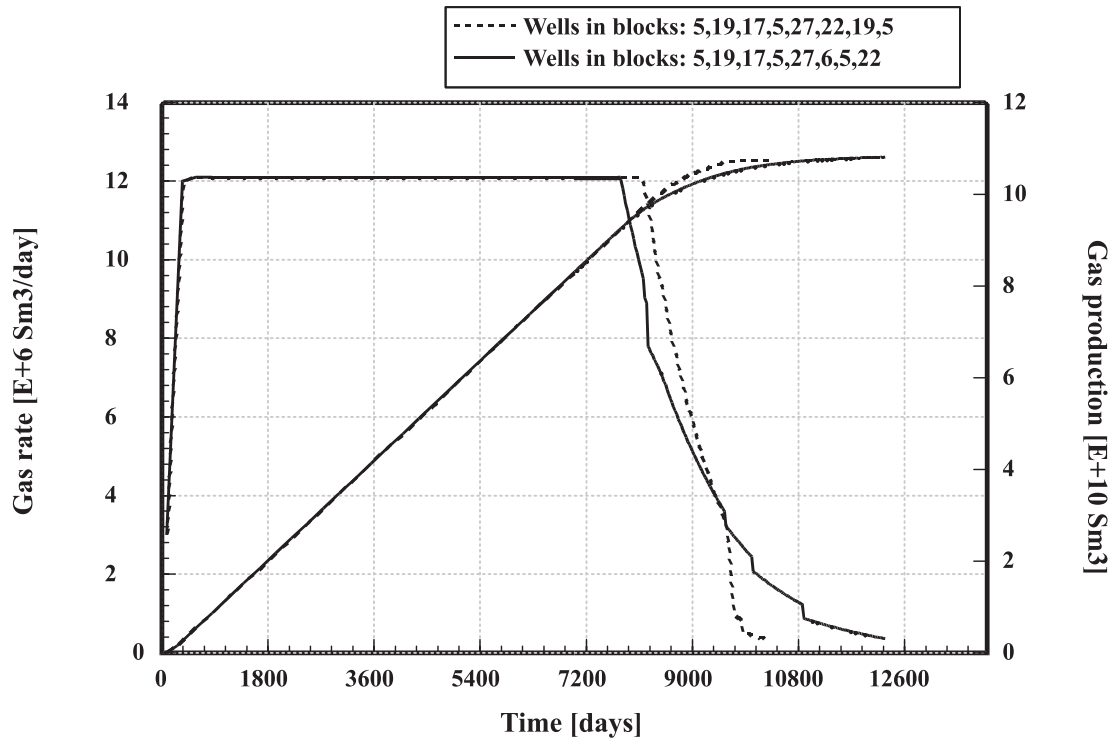


Figure 8.17: Balanced production profiles relative to previous case.

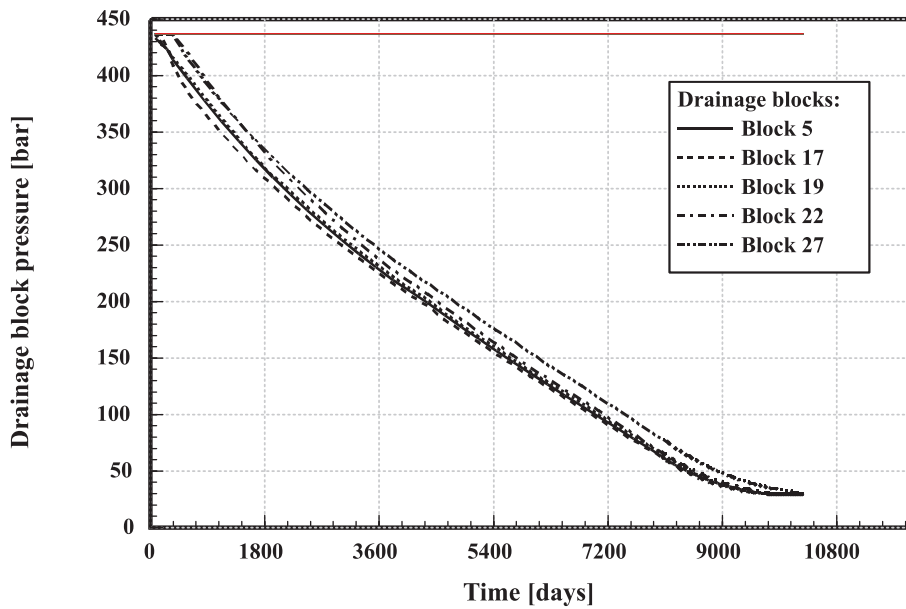


Figure 8.18: Pressure development under balanced production.

8.6.6 Reduced Uncertainty in Field Production

An analysis of the uncertainties in the optimum case, described above, is shown in Figure 8.20. The figure shows three sets of uncertainty profiles, where each uncertainty

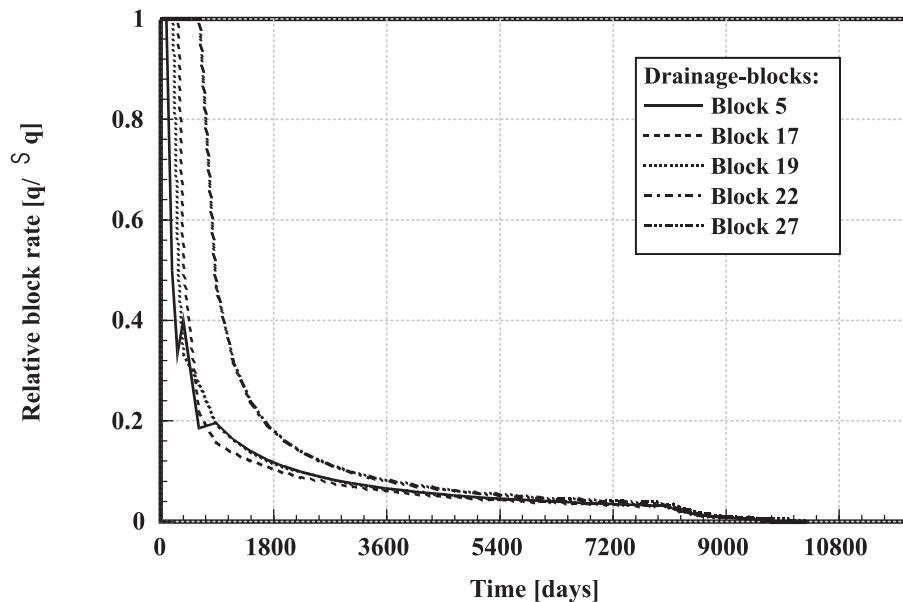


Figure 8.19: Relative drainage-compartment production.

profile is the difference between the optimistic- and the pessimistic case deduced by error propagation. The full line profile represents the gas rate- and production uncertainty profiles in the optimum case. Relative to the optimum case, there is a maximum difference between the optimistic and the pessimistic case of gas produced, equal to $\pm 13\%$ of total gas production. When the uncertainty in block volume is disregarded (set to zero), as seen from the profiles shown as short dashed lines, the relative uncertainty in gas production is reduced to $\pm 5.5\%$ of total gas production, which represent the uncertainty by reservoir communication alone.

The long dashed lines represent the uncertainty profiles where a relative reduction in gas volume uncertainty is set to 25%. This way of reducing uncertainty in gas volume, demonstrate the possibility given by the FBM to locate gas volumes in the field where reservoir uncertainty should be reduced in order to most effectively reduce the overall reservoir production uncertainty. This feature in the FBM is directing the user toward those parameters that are imposing the largest error on total gas production. Special actions could then be taken in order to reduce these uncertainties which are most significant for total uncertainty.

If a fault is associated with a large uncertainty and fluid flow across that fault is important to the overall gas production from the field, then the gain in production, by reducing this uncertainty could be demonstrated through plots such as Figure 8.20. Uncertainties of this kind may be reduced by locating a well close to this fault or in any other way unfolding this uncertainty.

8.7 Final Comments

The Fault Block Model is developed with the purpose of forecasting reservoir performance in strongly faulted gas-condensate reservoirs, where the principal reservoir

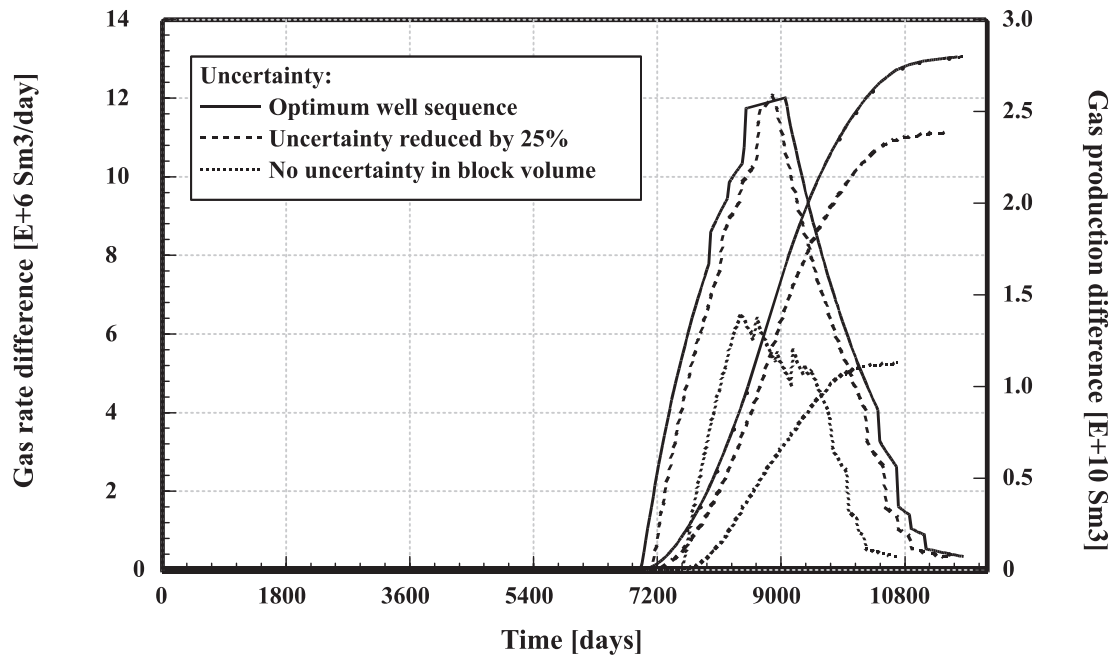


Figure 8.20: Gas rate- and production difference for optimum case and reduced uncertainty cases.

uncertainty is related to the flow communication across faults and initial gas reserves. The FBM can be used to study regional well location performance with the purpose of defining the optimal well location sequence and balanced gas production.

The primary features of the FBM are as follows:

1. Definition of optimal well location sequence based on pre-defined strategy(ies) for i.e. i) production from the largest gas reservoirs first, ii) production from those reservoirs that contact (cover) a maximum of the reserves and/or iii) production from those reservoirs which ensures a balanced out-take of gas from the whole field.
2. Presentation of the uncertainty inherently related to the reservoir data by alternative production profiles, showing the risk and opportunity aspects of gas production. Uncertainty analysis, involving the alternative production profiles, may also facilitate the location of those areas in the field where further reduction of reservoir uncertainty would have the greatest impact on the overall gas production performance.
3. Major changes in the reservoir model are effectively implemented by varying the inter-block communication probabilities. These changes make a visualization of the robustness of the well location sequence easy to evaluate.
4. Assessment of transmissibility and other aspects of reservoir gas communication are effectively investigated using this model. Such information could eventually be used as part of the general database when constructing a finite-difference reservoir simulation model.

References

- [1] T. Bu and E. Damsleth. Errors and uncertainties in reservoir performance predictions. *SPE Formation Evaluation*, September 1996.
- [2] C.A. Ehlig-Economides. Applications for multiphase compartmentalized material balance. 29.-31. August 1994. Presented at the University of Tulsa Centennial Petroleum Engineering Symposium held in Tulsa, OK, U.S.A.
- [3] M.J. Fetkovich, E.J. Fetkovich, and M.D. Fetkovich. Useful concepts for decline curve forecasting, reserve estimation, and analysis. 25.-28. September 1994. Presented at the SPE 69'th Annual Technical Conference and Exhibition held in New Orleans, LA, U.S.A.
- [4] Ø. Fevang and C.H. Whitson. Modeling gas-condensate well deliverability. *SPE Reservoir Engineering*, November 1996.
- [5] Jacques Hagoort. *Fundamentals of gas reservoir engineering*, volume 23 of *Developments in Petroleum Science*. Elsevier, 1988.
- [6] K.B. Hird and M.G. Kelkar. Conditional simulation method for reservoir description using spatial and well-performance constraints. *SPERE*, May 1994.
- [7] T.L. Hower and R.E. Collins. Detecting compartmentalization in gas reservoirs through production performance. (SPE 19790), 8.-11. October 1989. Presented at the 1989 Annual Technical Conference and Exhibition, San Antonio.
- [8] A. Iske and T. Randen, editors. *Mathematical Methods and Modelling in Hydrocarbon Exploration and Production*. Springer, 2005.
- [9] M.E. Lord and R.E. Collins. Detecting compartmented gas reservoirs through production performance. (SPE 22941), 6.-9. October 1991. Presented at the 66th Annual Technical Conference and Exhibition of the Society of Petroleum Engineers held in Dallas, TX.
- [10] S.L Lyons, H-M Chan, J.L. Harper, and B.A. Boyett. Integrated management of multiple-reservoir field development. *JPT*, December 1995.
- [11] L.M Meling, P.O Mørkeseth, and T. Langeland. Production forecasting for gas fields with multiple reservoirs. *JPT*, December 1990.
- [12] Z. Novosad. Composition and phase changes in testing and producing retrograde gas wells. *SPERE*, November 1996.
- [13] L. Ouyang and K. Aziz. Steady-state gas flow in pipes. *JPSE*, 1996.
- [14] D.A. Payne. Material-balance calculations in tight-gas reservoirs:the pitfalls of p/z plots and more accurate technique. *SPERE*, November 1996.
- [15] D.C. Poon. Decline curves for predicting production performance from horizontal wells. *JCPT*, Volume 30, No. 1, Jan.-Feb. 1991.

-
- [16] R.A. Purvis. Pool-production and well-count forecasts. *JCPT*, Nov.-Dec. 1990. Volume 29, No.6.
- [17] Rajagopal Raghavan and Jack R. Jones. Depletion performance of gas-condensate reservoirs. *JPT*, August 1996. Distinguished author series.
- [18] P.C. Smalley and N.A. Hale. Early identification of reservoir compartmentalization by combining a range of conventional and novel data types. *SPE Formation Evaluation*, September 1996.
- [19] A.M. Spencer and V.B. Larsen. Fault traps in the northern north sea. *Geological Society Publication N 55, pp 281-298*, 1990.
- [20] J.R. Ursin and L. Mæland. Multi model simulation study for strongly faulted gas condensate reservoir using fault block modelling. 1986(SPE 35608), 28. April to 1. May 1996. Presented at the Gas Technology Conference held in Calgary, Alberta, Canada.
- [21] J.R. Ursin and P.O. Mørkeseth. The fault block model: A novel approach for faulted gas reservoirs. 1986(SPE 28732), 10-13 October 1994. Presented at the SPE International Conference & Exhibition of Mexico, held in Veracruz, Mexico.
- [22] O Øvreberg, E. Damsleth, and H.H. Haldorsen. Putting error bars on reservoir engineering forecasts. *JPT*, June 1992.

Part II

Project Exercises

Project Exercise 1

Molar Phase Split

In this exercise we will focus on phase equilibrium and flash calculation, as a tool for estimating the molar phase split factor, V . For reference see section 2.6 *Phase Equilibrium* and subsection 2.6.1 *The K-value Method*.

All calculations in this exercise are carried out in a specially prepared Excel spreadsheet `FlashCal.xls`. The work related to solving this exercise is therefore mainly related to this spreadsheet. Based on some input data, various numerical calculations are performed, displaying the characteristic process in defining phase equilibrium.

The spreadsheet is meant to be self explainable in the sense that, together with the information presented in this exercise, all calculations should be doable without any further assistance.

1.1 Parameters

The input data presented in the spreadsheet is limited to critical temperature (T_{ci}) and pressure (p_{ci}) of each component, the acentric factors (ω_i) and the reservoir fluid composition (z_i). (The composition is taken from the Sleipner Vest gas, presented in Tables 2.4 and 2.5. From these data, we can estimate various parameters such as; the critical point (temperature and pressure) for the fluid, the equilibrium constant K_i and the molar phase split, represented by the vapor split V . We may also calculate the composition for the liquid and vapor parts in equilibrium as function of pressure and temperature.

1. Open the `FlashCal.xls` file and calculate the critical point for the reservoir fluid. Use the common equations of molar mixing,

$$T_c = \sum_{i=1}^N z_i T_{ci} \quad \text{and} \quad p_c = \sum_{i=1}^N z_i p_{ci},$$

where N is the number of compounds (here $N = 14$). (NB: The molar mixing model proposed above may not render the most accurate result of critical values, as the model is quite simplistic with respect to the mixing process of real hydrocarbon gases, in particular at elevated pressures.)

2. What is the critical temperature measured in $^{\circ}C$ and pressure in bars for the reservoir fluid presented? Copy $T_c[^{\circ}C]$ and $p_c[bar]$ into the spreadsheet.
3. What does the critical temperature and the reservoir temperature tell you about the kind of reservoir at hand? (Hint: Think in terms of a P-T-plot and where does the isothermal depletion line cross the two phase region.)

The equilibrium coefficients K_i are dependent on both temperature and pressure and to a certain extent also on the molar composition. At constant temperature and pressure, the equilibrium coefficients are all considered to be well defined constants defining the mixture.

The K -values can be estimated using different models (techniques), of which the well known GPA Binary Charts model is the historical most famous one. Other ways of representing the K -values are through regression formulas, where various thermodynamic parameters are involved. One of the more simpler formulas of this kind, proposed by Wilson [1], is presented below. In this formula, the K_i are primarily defined for pressures lower than 3.5 MPa .

$$K_i = \frac{p_{ci}}{p} \exp \left\{ 5.373(1 + \omega_i) \left(1 - \frac{T_{ci}}{T} \right) \right\}.$$

The advantage of using the formula above is related to the strait forward implementation of K_i in e.g. spreadsheet calculations. The disadvantage is that it has a limited range of practical use.

The phase equilibrium has been defined by the following equation (see Eq. 2.14),

$$G(V) = \sum_{i=1}^N \frac{z_i(K_i - 1)}{1 + (K_i - 1)V} = 0,$$

where N is the number of compounds in the fluid and V is the gas fraction or the gas split fraction ($V + L = 1$). In the case of single phase gas, the fluid gas fraction is; $V = 1$ and alternatively in the case of single phase liquid; $V = 0$. For these two extreme cases, the above equation renders,

$$\sum_{i=1}^N \frac{z_i}{K_i} = 1, \quad V = 1 \quad \text{and} \quad \sum_{i=1}^N z_i K_i = 1, \quad V = 0.$$

When two phases are in equilibrium, the summations above are both greater than one,

$$\sum_{i=1}^N \frac{z_i}{K_i} > 1 \quad \text{and} \quad \sum_{i=1}^N z_i K_i > 1.$$

Then, the fluid is in its two-phase state, and a solution of the equilibrium equation can be found; $V \in (0, 1)$. The condition above should therefore be used to check whether a solution of the phase equilibrium equation $G(V) = 0$, exist.

4. Carry out the test described above by calculating the summations; $\sum zK$ and $\sum z/K$, when $T = 393$ K and $p = 10$ bar, where a reservoir pressure of 10 bars could be associated with the reservoir abandonment pressure. (Use the designated spaces for calculations and copy the numerical values of the test into the spreadsheet.)
5. Does a solution, V of the equilibrium equation, exist at natural condition, i.e. ($T_{sc} = 288$ K and $p_{sc} = 1$ bar) ? Copy the numeric test result into the spreadsheet. (NB: Data which is copied from a certain cell in to a different celle in the spreadsheet can be detached from further calculations, simply by pasting the numeric value stored. See comment below!)
6. Does a solution exist for the dew-point pressure. See Table 2.5. Copy the numeric test result into the spreadsheet.
7. Discuss the shape of the two-phase envelope based on the information about the PT-data considered so far. Plot the above mentioned three data points; $(p, T)_{sc}$, $(p, T)_C$ and $(p, T)_{dew}$ and the reservoir pressure and temperature in a PT-plot and sketch the envelope. (You may here draw a line through some of the points mentioned in a plot containing the three PT-data mentioned.)

(Comment: In a worksheet there are several ways to carry out the "copy and paste" command. If you copy and paste without any specification, all information is copied; numbers, formulas and references to cells. In some cases it is convenient to copy only the numerical values, without additional information. In these cases the proper paste-function must be chosen.)

1.2 Calculation of Vapor - Liquid Equilibrium

The purpose of the following deduction is to show how the vapor phase split V can be estimated, by solving the equilibrium equation $G(V) = 0$ using the Newton - Raphson iteration method.

If a solution V exists (the tests: $\sum zK > 1$ and $\sum z/K > 1$, are valid). We may write the equilibrium function $G(V)$ as a Taylor expansion,

$$G(V) = G(V^0) + \frac{dG(V^0)}{dV}(V - V^0) + \dots ,$$

where V is an expansion close to the "true" solution V^0 . An approximation of the above equation is

$$G(V) \approx G(V^0) + G'(V^0)(V - V^0), \quad (1.1)$$

where $G(V^0) = 0$ and where

$$G'(V) = \frac{dG(V)}{dV} = \sum_{i=1}^N \frac{-z_i(K_i - 1)^2}{[1 + (K_i - 1)V]^2}.$$

As seen from the above expression, $G'(V)$ is a monotonous decreasing function in V , well suited for solution iteration algorithms.

The above iteration formula can be rewritten using Eq. 1.1.

$$V^0 = V - \frac{G(V)}{G'(V^0)},$$

where V^0 is the "true" value and V is an approximation close to the "true" value.

If we start the iteration process by e.g. $V^{k=1} = 0$, we may write the iteration formula after k steps, as follows

$$V^{k+1} = V^k - \frac{G(V^k)}{G'(V^k)}.$$

Figure 1.1 depicts the process of step-wise iteration, where $G' = dG/dV$ is the tangent to the function $G(V)$. Notice that the iteration in the figure may start at any value, $V^{k=1} \in [0, 1]$.

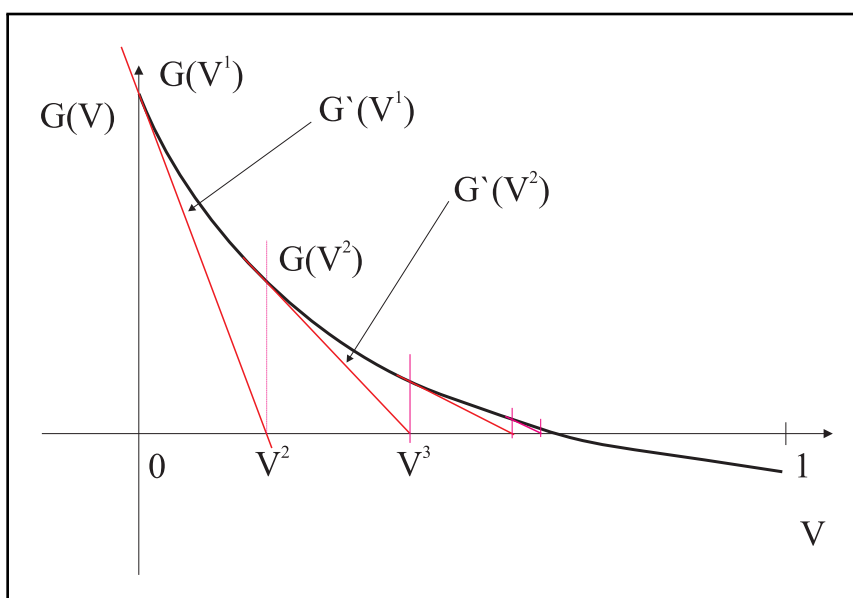


Figure 1.1: General presentation of Newton-Raphson iteration process. Notice that the iteration process in the above figure starts at $V^{k=1} = 0$. (It could equally well have started at $V^{k=1} = 1$.)

8. Study how the iteration is implemented in the `FlashCal.xls` file. The two first iteration steps are already defined. Notice first how $G(V)$ is calculated, then how $dG(V)/dV$ is calculated and finally how $V - G(V)/G'(V)$ is calculated. Add more iteration steps, simply by copying the second iteration step into the place where the third iteration step should be implemented. Decide how many iteration steps is needed, in order to estimate the "true" solution. The iteration may contain more than 10 steps. Use 9 significant numbers as the conversion criteria for the iteration process.

9. Find the vapor split fraction at standard condition and at standard pressure and reservoir temperature.
10. What is then the phase split at initial reservoir conditions when we assume the gas to be in single phase? Calculate the face split under reservoir conditions and comment on the discrepancy between the results obtained and what is presented in the textbook. Find a possible cause for this discrepancy.
11. As mentioned above, the K-values are valid only for a limited range of pressures lower than 35 bars. Within this limitation, observe how the vapor fraction V changes when the pressure increases. For each new simulation (new pressure), check that a solution will exist. Make a table containing the pressure, temperature, the test results ($\sum zK / \sum z/K$) and vapor split V . Use 3 points, i.e. $T = 393\text{ K}$ and $p = 3, 10$ and 30 bars.
12. In which state would the gas be in, if the reservoir pressure could be lowered to 1 bar?

1.3 Phase Composition

When V is known, the phase compositions y_i and x_i are easily found using the formulas

$$y_i = \frac{z_i K_i}{1 + (K_i - 1)V} \quad \text{and} \quad x_i = \frac{z_i}{1 + (K_i - 1)V}.$$

13. Calculate the phase compositions at standard condition and at abandonment condition, i.e. at reservoir temperature and at minimum reservoir pressure, say 10 bars. Show the compositions as histograms, where the gas and liquid compositions are shown in the same histogram.
14. Calculate the function $G(V)$ as in Figure 1.1 and plot the data for standard conditions.
15. Make a new plot using the same data, where the focus now is shifted towards the zero point (where the function $G(V)$ is crossing the x-axis). Adjust the scale of the V-axis such that $V \in [0.9, 1.0]$. (Observe the effect of focusing-in on the zero point.)
16. Plot $G(V)$ for the following choice of parameters (T,p); (393,0.5), (393,1), (393,3) and (393,30). Plot all graphs in the same plot and calculate the phase split factors in the four cases.
17. Add the four (p,T) data points from the item above, in the above two-phase plot initially containing the standard-, the critical- and the dew point and draw the quality lines (iso-volume split lines) crossing through the four phase split factors calculated above.
18. Observe the shape of the function $G(V)$ and compare it to Figure 1.1. Use a different start value $V^{k=1} < 1$ and observe the collapse of the iteration process.

Try the two values $V \in \{0, 0.5\}$ and explain what happens. Why does the iteration process collapse?

Make a short report, answering the above questions. Include tables and plots, simply by using the copy and paste functions.

References

- [1] G.M Wilson. A modified redlich-kwong eos, application to general physical data calculations. May 1968. Paper No 15C, presented at the AIChE 65th National Meeting.

Project Exercise 2

PVT-Simulation

In this exercise you will work with a custom made PVT-simulation program, primarily made for demonstration purposes. The program has limited capability compared to commercial PVT-simulation packages, both with respect to options for PVT calculations but also with respect to *tuning* and general optimization procedures.

The PVT-simulation program is an executable file; `PVTsim.exe`. The program and the associated data input file; `PVTsimInput.dat` should be stored in the same folder on your computer, preferably on the "Write-board". The program is executed by simply double-clicking on the program. The simulation results are written to two files, which are saved to the same directory or folder. The `PVTsimLog.dat` file is logging the input data in addition to present the simulation data. All information related to the simulation process is stored in the log-file. A selection of output data is presented in the `PVTsimPlot.dat`, well suited to copying and plotting by e.g. Excel.

2.1 Running the Program

Successfully running the PVT-simulation program, relies on a 100% correct completed data input file. If the `PVTsimInput.dat` file is misrepresented, the program will not run. Errors in the data-file might be logical errors, such as putting in numbers which don't fit the simulation, errors related to the operational convention reading the file and lastly letters/numbers or sign that is wrongly positioned in the file text.

2.1.1 The Data Input File

The data input file is an ordinary text file which is read by the simulation program. The input file contains quit a bit supplementary text, - text meant to explain the data content of the file. Lines containing such text has a star (*) in the first column! All lines not starting with a star, are data read by the simulation program. These data could be; text, integer - or real numbers.

The data contained in the `PVTsimInput.dat` file is organized in three groups; Simulation data, Program data and Fluid data, as shown below.

PVTsimInput.dat file

```

*
* **** Start data input-file for PVTsim
*
*      Data file for PVT simulation
*      10      20      30      40      50      60      70
* 123456789012345678901234567890123456789012345678901234567890
* 'Title of feed (max 70 characters)'
*
*
*
* *** SIMULATION DATA
*
* SIM= 1 or 2      Simulation program: (T[K],P[bara])
*
*      SIM=1      Two phase envelope calculation - NB. NPT=3
*                  (T1=start temperature, T2=Tmin, T3=Tmax)
*                  (P1=start pressure,P2=Pmin, P2=Pmax)
*
*      SIM=2      Depletion pressure calculation
*                  (T1=constant)
*                  (P1, P2, Pi=(P2-P1)*i, i=3,NPT)
*
*
* NPT= 1, ..., 100      Number of pressure and temperature data
*
*
* SIM      NPT (min 2)      [Integer]
* 1        3                (Envelope limits)
* 2        45               (Depletion temperatures)
*
*
* Temperature [K]:      [Real]
* T1      T2      T3
* 220.0   220.0   500.0   (Envelope limits)
* 380.0                                (Depletion temperature)
*
*
* Pressure [bara]:      [Real]
* P1      P2      P3
* 10.0    10.0    300.0   (Envelope limits)
* 10.0    20.0                                (Depletion pressures)
*
*
*
* *** PROGRAM DATA
*
*
* DCHCK=1,0      Data check mode [Integer]
*
*      DCHCK=1      No simulation is done.
*      DCHCK=0      Full simulation.
*
*
* EOS= 1 or 2      Equation of state [Integer]
*
*      EOS=1        Peng-Robinson
*      EOS=2        Soave-Redlich-Kwong
*
*
* STEP=300        No. of iteration steps in Flash calculations [Integer]
*
*
* FUGERR=1.0D-12  Fugacity tolerance criteria [Real]
*
*
* PERR=0,1        Print warnings [Integer]
*
*      PERR=1        Warnings are printed.
*      PERR=0        Warnings are not printed.

```

```

*
* DELTA=0,1      Use of binary interaction coefficients [Integer]
*                DELTA=1      Coefficients are used.
*                DELTA=0      Coefficients are all equal to zero.
*
* DCHCK  EOS      STEP    FUGERR      PERR      DELTA
*    0      1      300     1.0D-12      0          0
*
*
*
* BINARY INTERACTION COEFFICIENTS: delta(i,j)
*
* N2  C02 C1    C2    C3    iC4  nC4    iC5  nC5  C6    C7    C8    C9    C10+
* 1   2   3     4     5     6     7     8     9     10   11   12   13   14   Comp.
* 0.0 0.0 0.031 0.015 0.852 0.1   0.071 0.1   0.1   0.149 0.144 0.15 0.155 0.155 N2
*      0.0 0.107 0.132 0.124 0.14 0.133 0.14 0.14 0.14 0.145 0.145 0.14 0.145 0.145 C02
*      0.0 0.026 0.14 0.025 0.013 -0.005 0.023 0.422 0.035 0.047 0.047 0.05 0.05  C1
*      0.0 0.001 -0.006 0.009 0.008 0.007 0.014 0.015 0.016 0.019 0.03 0.03  C2
*      0.0 -0.007 0.003 0.011 0.012 0.026 0.056 0.059 0.007 0.02 0.02  C3
*      0.0 0.0 -0.004 0.002 0.025 0.025 0.026 0.006 0.01 0.01  iC4
*      0.0 0.017 0.017 0.017 0.019 0.012 0.01 0.001 0.001 nC4
*
*
*
* *** FLUID DATA
*
*
* *** FLUID: Gas 1
*
* N (max 20)      Number of components [Integer]:
* 11
*
* Pure Component Data
* COMP           CMW      TC      PC      AF      Z(RG)
*                kg/kmol  K      bara
* 'Nitrogen'     28.041 126.10 33.94 0.0403 0.0170 1
* 'Carbon Dioxide' 44.010 304.19 73.82 0.2276 0.0328 2
* 'Methane'      16.043 190.56 45.99 0.0115 0.8924 3
* 'Ethane'       30.070 305.32 48.72 0.0995 0.0308 4
* 'Propane'      44.096 369.83 42.48 0.1523 0.0068 5
* 'Iso-Butane'   58.123 408.14 36.48 0.1770 0.0012 6
* 'Normal-Butane' 58.123 425.12 37.96 0.2002 0.0013 7
* 'Iso-Pentane'  72.150 460.43 33.81 0.2275 0.0006 8
* 'Normal-Pentane' 72.151 469.70 33.70 0.2515 0.0004 9
* 'Hexane'       86.177 507.60 30.25 0.3013 0.0006 10
* 'Heptane Plus' 100.204 540.20 27.40 0.3495 0.0161 11
*
*
*

```

2.2 Data File Manipulation

The PVTsimInput.dat file may be opened in e.g. WORDPAD or in any other editor. The first data read by the program is the title-line. Each simulation run can have a title containing up to 70 characters.

The data in the input file is divided in three sections; Simulation data, Program data and Fluid data, as explained below.

2.2.1 Simulation Data

Two possible PVT simulations are made possible; two-phase envelope calculation and depletion pressure calculations. To choose between the two, a **SIM** flag has to be set. Additionally a number of PT calculation has to be defined by the **NPT** flag.

The temperature and pressure range are also required, and the definitions of these ranges are indicated in the file. In this exercise, the pressure setting may be left unchanged while the temperature setting might be changed, depending on the calculations to be done.

As the `PVTsimInput.dat` file is presented above, two phase envelope calculations are being preformed. To change to depletion pressure calculations, one has to activate all three data lines in the Simulation Data section.

2.2.2 Program Data

The program data section contains information on how the program should run. The different data in this section could be left unchanged in this exercise. However if you experience problems in running the program and have difficulties with resolving your problem, - by changing the data check flag **DCHCK** from 0 to 1, the program will read and write the data without running the simulation. This allows you to check the data and possibly resolve your problem.

2.2.3 Fluid Data

The fluid data section contains the number of components **N**, the feed **Z(RG)** and the data characterizing the fluid; average molar weight **CMW**, critical temperature and pressure **TC** and **PC** and the acentric value **AF**.

The only parameters that need to be changes in this exercise is the fluid composition. The fluid composition presented in the data file is called Gas 1. When you change to the second or third fluid, you can do so simply by copying the whole section from `*** FLUID: Gas 1` to the end marked by `***`, and name the new fluid e.g. Gas 2. The fluid you changed from can be commented out by putting a `***` in the first column, since the program only reads data lines.

2.3 PVT Simulations

Carry out the following simulations given the data in Table 2.1.

1. Plot the the gas composition for the three gases in Figure 2.1 using a histogram and try to classify the gasses based on the plot and the tabulated data. What characterize dry gases compared to gas condensates and how can we differentiate gas condensates?

Table 2.1: Compositions of gases

| | Gas 1 | Gas 2 | Gas 3 |
|----------------|--------|--------|--------|
| Nitrogen | 0.0170 | 0.0016 | 0.0019 |
| Carbon Dioxide | 0.0328 | 0.0249 | 0.0348 |
| Methane | 0.8924 | 0.7462 | 0.7849 |
| Ethane | 0.0308 | 0.0899 | 0.0593 |
| Propane | 0.0068 | 0.0511 | 0.0153 |
| Iso-Butane | 0.0012 | 0.0103 | 0.0032 |
| Normal-Butane | 0.0013 | 0.0186 | 0.0092 |
| Iso-Pentane | 0.0006 | 0.0069 | 0.0052 |
| Normal-Pentane | 0.0004 | 0.0076 | 0.0050 |
| Hexane | 0.0006 | 0.0095 | 0.0112 |
| Heptane Plus | 0.0161 | 0.0334 | 0.0700 |

- Plot the two phase envelope for the three gases and mark the critical point on the plot.
Use Excel or another spread sheet program.

- Use Gas 2 and plot the two phase envelope and critical point for the following sensitivities.

(The purpose with this exercise is to observe how the two phase envelope is changing when the gas becomes slightly richer and/or slightly leaner. Observe how the critical point is moving.)

- Modify Gas 2 by subtracting C_1 by 5%, C_2 and C_3 by 3% and balancing the fluid by changing the C_7^+ composition.
- Modify Gas 2 by adding C_1 by 3%, C_2 and C_3 by 1% and balancing the fluid by changing the C_7^+ composition.

Comment the observation by refereing to figures perviously presented in Chapter 2 in the text book.

- Use Gas 2 and Gas 3 and plot the vapor molar fraction similarly to the plot in Figure 3.11 in the text book. Use the same depletion temperatures; $350^\circ K$ and $370^\circ K$.

What is the maximum liquid drop out in the four cases?

- Plot the two-phase envelops for Gas 1, changing the EoS from Peng-Robinson to Soave-Redlich-Kwong and comment the difference.
- Write down the two EoS from Peng-Robinson and Soave-Redlich-Kwong. Define dp/dT and compare the result with the observation from the plot above. Explain why the SRK-EoS is located outside the PR-EoS.
- Plot the vapor molar fraction, as done above, for a depletion temperature of $T = 300^\circ K$.

What is the percentage change in maximum liquid dropout using SKR-EoS compared to using PR-EoS?

Project Exercise 3

Introduction to the Simulation Model and Material Balance Calculations

The first part of this exercise is meant to familiarize the reader with the computer program `NGASSIM.EXE`, which is a principal tool in the process of project-based learning.

The program `NGASSIM.EXE` and the data input file `NGASDATA.DAT` should be located in the same folder or preferably on the PC "Write-board". The program is executed by simply double-clicking on the program icon. The simulation results are written to files, which are saved on the same directory, folder or on the write-board. Before starting to work with the exercises, a copy of the data file should be saved in the folder as version 1 or in a folder named e.g. "Introduction".

Whenever progress is made, - it is recommended to save a copy of the data-file to the folder. Following this recommendation saves time and will prevent a situation of having to redo work already done, when losing important data. A frequently occurring situation is that you get stuck and unable to find the error, disabling you to proceed running the program.

Whenever a work project is accomplished, the modified data input file together with other data and work files (e.g. Excel data files, plots, etc.) should be stored in the folder.

In the last part of the exercise we will look more closely into the process of material balance simulation, with special emphasis on the balance between drainage and aquifer influx. Primarily non-volumetric depletion is considered but also volumetric depletion are studied.

Before answering the questions, a short introduction to the simulation program and the attached data file is given. The data file will remain the same through out this exercise as well as for the next exercise. In the following exercises, the program will be further updated, new and updated data files will be presented. The name of the data file will, however, remain the same. It is therefore quite convenient and in part also necessary to keep the different versions of the simulation program and their data files separated, i.e. in different folders.

3.1 Simulation of Material Balance

A simulation program is written with the purpose of performing the material balance calculations based on the equations presented in the textbook. The program code, written in Fortran, or other issues related to programming technicalities, are not part of this course.

3.1.1 Organization of The Simulation Program

The program is organized with the purpose of being self explainable. The program is updated with respect to the various topics presented in the coming chapters, like e.g. *well inflow performance*, *well-bore flow behavior* and *reservoir and field production*.

The simulation program has a hierarchic structure with a *Main Program* at the top of the structure. From this program, calls are made to *Subroutines* where the actual calculations are being performed, see Figure 3.1. The actions taken in the main program can be separated into three parts.

Initializing: All parameters such as *integers*, *reals*, *characters*, *commons* and *constants* are initialized in the main program. The listing of parameters is complete, such that all parameters used in the program are included in these lists.

The CPU clock is started and stopped in the main program.

The initialization procedure also includes the opening of three data files `NGASDATA.DAT`, `NGASPRNT.DAT` and `NGASLOG.DAT`. The `NGASDATA`-file includes all input information (see subsection 3.1.2 about the data-file). The `NGASPRNT`-file contains information about the status of the simulation process. If something goes wrong during the simulation process and the program is halted, then information contained in this file can help locate where in the program the error occurred. The `NGASLOG`-file is, as the name suggests, the data-log-file. All information read from the `NGASDATA`-file is written to this file. Similarly, all information resulting from the simulation can be written to this file. The `NGASLOG`-file can thus become quite big in number of lines and kilo bytes.

Calls: According to Figure 3.1, only three calls are done in the main program. First the `READDATA`-subroutine is called. This program reads then data file and then returns the control to the main program. Then input data is written to the log-file by using the `WRITEDATA`-program. The main program then makes a call to the `GASPROD`-subroutine, which is organizing the simulation process. From this program various other programs are called in order to carry out the simulation process.

Output: At the end of the simulation process, all simulation results recorded are transformed to the main program, grouped into various categories and printed to several output data files. The result of each simulation is therefore contained in these files and can be viewed by e.g. plotting the data from these files. In order to run the program, both the `NGASSIM.EXE` and the `NGASDAT.DAT` files have to be located in the same directory/folder.

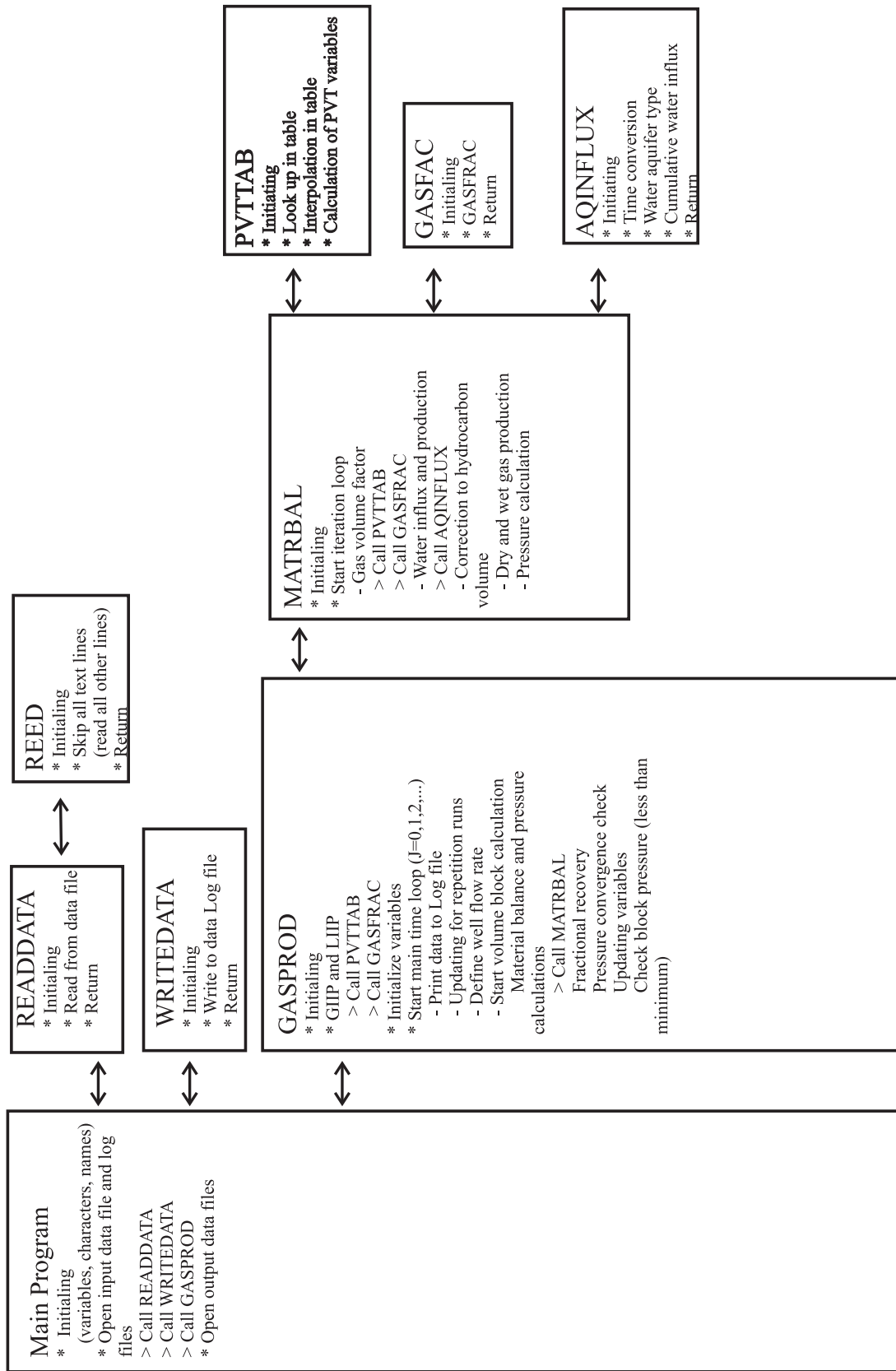


Figure 3.1: Program structure for material balance simulation

GASPROD

The GASPROD-subroutine starts the simulation process by calculating the gas - and liquid initially in place (GIIP and LIIP). In this process calls to the subroutines PVT-TAB and GASFAC are done. The main time loop is then initiated where the time step period is taken from the data input-file. During each time step, data regarding production rates, reservoir pressure, cumulative produced fluids and remaining fluids are logged. When the reservoir pressure reaches a predefined cut-off pressure and the Minimum Bottom Hole Pressure (MBHP) is reached, the time loop is halted and the command returned to the main program.

MATRBAL

The MATRBAL-program contains the material balance equations as presented in the textbook. Material balance calculations are performed following the logic presented in subsection 4.3.2 "Numerical representation of MBE". The MATRBAL-program makes call to the PVTTAB- and GASFAC programs as part of the material balance calculations and to the AQINFLUX program for aquifer influx calculations.

PVTTAB

The PVTTAB-program uses the tabulated PVT-data from the data-file as input to match requests for PVT-data at specified pressures. The program is frequently called during the simulation process.

GASFAC

The GASFRAC-program is a short program calculating the formation volume gas factor as defined in the text.

AQINFLUX

The AQINFLUX-program calculates the aquifer water influx W_e based on information about the aquifer, given in the data input-file. The aquifer influx calculations follows the equations given in section 4.5 "Aquifer Influx" in the textbook.

3.1.2 The Data Input-File

The data input-file is read by the READDATA-program which uses the REED-program to differentiate between commentary-lines (lines starting with a star (*) in the first column) and data lines. The NGASDATA-file is meant to be self explainable, where the written text defines the data both with respect to the purpose of the data and the type of character (integer, real or string (text)).

The data input-file is organized in sections where data of similarly type are grouped together, as shown below.

NOTE! Executing the program, is dependent on a successfully reading of the data file. If for instance a single number or text string is missing or defined wrongly (i.e. a real number is inserted instead of an integer), the whole process of data processing

is interrupted and the execution of the program cannot be started. It is therefore importance to check all input data contained in the data file and make sure that the input is in correspondence with the data expected. The same kind of error will occur in the case where additional data or data lines are included where it is not expected. The problem here is partly that no messages are communicated in cases where errors in the input data are detected, - the program simply stops.

Make it a rule to verify the changed in the data file by first running the program in it's data mode, i.e. when DCHCK=1, since there will be no warnings telling you why wrongly inserted data is not accepted!

NGASDATA-file

```

*
* **** Start data file NGASDATA.DAT
*
* Data file name (max. 70 characters); text
* 1234567890123456789012345678901234567890123456789012345678901234567890
  'Project Exercise: Material Balance'
  'Text string 2'
  'Text string 3'
* * * *
* *** Program data
*
* DCHCK=1 Data check mode;    No material balance is done.
* DCHCK=0                      Full simulation. [integer]
* MAXSTEP Number of simulation steps; Program is terminated at
* simulation step MAXSTEP. [integer]
* NPRINT Number of sequent plotting lines; Printing to file is done
* for every NPRINT simulation step. [integer]
* SP=1,100 Length of LOG-file printout; Full printout and printing of every
* simulation step (1) to printout of every (100) time step.
* SP=1 gives a short hand presentation of every time-step. [integer]
*
*          DCHCK  MAXSTEP  NPRINT  SP
*          1      4000     10      5
* * * *
* *** Simulation data:
* *
* PERR      Error limit in pressure calculations; Minimum pressure step in
* calculations. [real]
* GPGERR    Error limit in volume calculations; Maximum difference in
* pressure/volume iterations. [real]
*
*          PERR      GPGERR
*          0.5      1D-07
* * * *
* *** Volume and block data
* *
* BNAME     Name of individual block, maximum 5 characters. [String]
* VPORINIT Pore volume of block; {Vp=PI*(RADE**2-RADW**2)*THICK*PORO} (Rm3) [real].
* SWINIT    Average initial water saturation. [real]
*
*          BNAME      VPORINIT  SWINIT
*          'BLK01'    4.0D+6     0.2

```

```

* * *
*   *** General reservoir data
* *
*   PRS      Initial reservoir pressure (bar). [real]
*   TEMP     Initial reservoir temperature (Kelvin). [real]
*   PRSSC    Atmospheric pressure (bar). [real]
*   TEMPSC   Normal reference temperature (Kelvin). [real]
*   COMW     Water compressibility (1/bar). [real]
*   COMR     Reservoir compressibility (1/bar). [real]
*
*           PRS      TEMP      PRSSC    TEMPSC    COMW      COMR
*           437.0   392.0     1.01    288.0     4.35D-05  4.5D-05
* * * *
*   *** Well data
*   QMAX     Maximum well flow rate (Sm3/day). [real]
*
*           QMAX
*           5.0D+05
* *
*   TBP     Time step length (days). [real]
*
*           TBP
*           5.
* *
*   BHPM    Minimum bottom-hole pressure (bar). Production is stopped
*           when minimum bottom-hole pressure is reached. [real]
*           (Minimum bottom-hole pressure has be within the range
*           of the PVT data)
*
*           BHPM
*           50.
* *
*   *** Water data
* *
*   WATINF=1 Water influx/production is defined as fractions of production.
*           (Only WPFrac and WEFrac are relevant parameters.) [integer]
*   WATINF=2 Water influx from aquifer is included. [integer]
*
*           WATINF
*           1
* *
*   WPFrac  Water production as fraction of gas production. [real]
*   WEFrac  Water influx as fraction of gas production. [real]
*           (A non-zero WPFrac is normally accompanied by a non-zero WEFrac.)
*
*           WPFrac  WEFrac
*           0.0     0.0     BLK01
* *
*   WTYPE=1 Radial aquifer. [integer]
*   WTYPE=2 Linear aquifer. [integer]
*   WFINITE=1 Finite aquifer. [integer]
*   WFINITE=2 Infinite aquifer. [integer]
*   WALPHA  Angle of sector of aquifer water encroachment (degree). [real]
*   WCOMP   Aquifer compressibility coefficient (rock and water) (1/bar). [real]
*   WLENGTH Aquifer length (linear aquifers) (m). [real]
*   WPERM   Aquifer permeability (mD). [real]

```

```

* WPORO      Aquifer porosity. [real]
* WRADB      Radius of aquifer inner boundary (m). [real]
* WRADE      Radius of aquifer outer boundary (m). [real]
* WTHICK     Aquifer thickness (m). [real]
* WVISC      Water viscosity (mPa.s). [real]
* WWIDTH     Aquifer width (m). [real]
* *
* WTYPE WFINITE WALPHA WCOMP WLENGTH WPERM  WPORO WRADB  WRADE  WTHICK WVISC WWIDTH
  1     2         360.  5.D-5 1535.   1.0   0.2   350.  1000.  50.   1.0  1535.  BLK01
*
* * * *
* *** PVT data
* *
* NTAB       Number of PVT-table elements
*
*           NTAB
*           20
* *
* PRS        Pressure [bar]
* TEMP       Temperature [K]
* MWT        Mixture mol weight [g/mol]
* MWTG       Gas mol weight [g/mol]
* MWTL       Liquid mol weight [g/mol]
* GASF       Gas mol fraction = Gas phase split; V
* Z          Gas phase Z-factor
* Z2         Mixture, two-phase Z-factor
*
*           PRS      TEMP      MWT      MWTG      MWTL      GASF      Z      Z2      NTAB
*           445.     392.     26.56  26.56  26.56  0.9517   1.1142  1.1143  1
*           370.     392.     26.56  26.56  26.56  0.95171  1.0258  1.0258  2
*           350.     392.     26.57  26.42  90.14  0.95240  1.0035  1.0045  3
*           320.     392.     26.57  26.19  89.32  0.95349  0.9721  0.9743  4
*           300.     392.     26.59  26.03  88.19  0.95438  0.9530  0.9556  5
*           280.     392.     26.61  25.83  87.18  0.95556  0.9356  0.9385  6
*           260.     392.     26.65  25.61  86.86  0.95705  0.9206  0.9233  7
*           240.     392.     26.72  25.36  87.52  0.95883  0.9082  0.9102  8
*           220.     392.     26.81  25.11  89.16  0.96061  0.8986  0.8994  9
*           200.     392.     26.94  24.88  91.68  0.96259  0.8920  0.8994  10
*           180.     392.     27.13  24.66  95.05  0.96446  0.8886  0.8910  11
*           160.     392.     27.38  24.47  99.27  0.96624  0.8885  0.8851  12
*           140.     392.     27.95  24.30  104.49 0.96783  0.8916  0.8808  13
*           120.     392.     28.52  24.18  110.81 0.96921  0.8979  0.8807  14
*           100.     392.     29.33  24.10  118.48 0.97010  0.9073  0.8837  15
*           80.      392.     30.51  24.08  127.84 0.97050  0.9197  0.8862  16
*           60.      392.     32.36  24.16  139.47 0.97079  0.9348  0.8864  17
*           40.      392.     35.59  24.41  154.40 0.97089  0.9524  0.8778  18
*           1.01    392.     42.00  25.00  185.00 0.97099  0.9900  0.8580  19
*           1.01    288.     42.00  25.00  185.00 0.95171  0.9900  0.8580  20
* * *

```

3.2 Data-File Manipulation

Go through the following list of items in an attempt to familiarize yourself with the data file NGASDATA.DAT and the program.

Open the NGASDATA-file in e.g. WORDPAD or in any other editor, but remember

to store the file as a unformatted tex-file.

Follow the listing below to get further acquainted with the processes by running the program. Alongside answering the questions below, write a report containing brief explanations and deductions. Include plots and tables presenting data from the simulations.

1. **DCHCK:** Check that $DCHCK=1$ and run the program. In this mode, the data is checked but no simulation is performed. Compare the content in the data log-file `NGASLOG.DAT` with the content of the data input-file `NGASDATA.DAT` and verify that the data listing is the same. The file `NGASPRNT.DAT` file is primarily intended for use in developing the program. This file contains key simulation data for each time step. The information contained in this file is generally not part of the output data of interest for the simulation program.

Check the content in this file, - if you like.

2. **NPRINT:** Simulation data is printed to files for further data handling and procession, data analysis or simply inspection. These files are `NGASPROD.DAT` and `NGASPARM.DAT`. The frequency of data lines printed is determined by the parameter `NPRINT`.

Find the corresponding number of data lines plotted and check the file size in "kB" (kilo bytes), when `NPRINT` is 1, 2 and 5. Remember to set $DCHCK=0$ before running the program.

3. **SP:** The log file `NGASLOG.DAT` is used to keep a record of what is happening during the simulation process. The parameter `SP` is controlling the form and frequency of data printed. When $SP=1$, a full printout is created and a shortened presentation of log data is written to file. When `SP` is larger than 1, a reduced printout is generated at a frequency given by `SP`, i.e. when $SP=2$ only every second time-step is printed.

Determine the size in "kB" of the data log-file when `SP` is 1, 2 and 10.

4. **VPORINIT and SWINIT:** The hydrocarbon pore volume is defined as, $V_{HC} = V_p \cdot (1 - S_w)$. The surface volumes; `GIIP` and `LIIP`, should consequently change proportionally to the pore volume, V_{HC} .

Verify that by reducing the pore volume from $4 \cdot 10^6 \text{ Rm}^3$ to $3 \cdot 10^6 \text{ Rm}^3$, the initial volumes of gas and liquid are reduced accordingly. Do the same comparison for an increase in average water saturation from 0.2 to 0.3.

5. **QMAX:** Reduce the gas rate from $QMAX = 5.0 \cdot 10^5$ to $QMAX = 2.5 \cdot 10^5$ and observe an increase in total number of time-steps. Observe the total CPU time elapsed in the two cases. Check if the change in gas rate is leading to any change in the cumulative produced volumes of gas and liquid.

6. **TBP:** When the time step length is increased, the total number of time steps should decrease proportionally.

Check this for time step lengths of 5 and 10 days.

7. **BHPB:** When the minimum bottom hole pressure is lowered, more gas can be produced from the reservoir since the average pressure in the reservoir at abandonment is reduced.

Find the increase in Recovery when the minimum bottom-hole pressure is reduced from 50 bar to 10 bar.

3.3 Plotting of Production Data

Use a spreadsheet program e.g. the EXCEL Office program, to plot selected data from the output files. Copy all data from the data files and paste it into the spreadsheet. Create the following plots, using the original data-file as your input data-file.

8. Plot the relative production of gas and condensate; "Relpgasn" and "Relplqdn" from the data-file NGASPROD.DAT. Plot the two curves in the same plot.
Why is the liquid condensate curve falling off faster than the gas production curve?
9. Plot gas- and liquid production measured in Sm^3 , using two y-axis in the same plot. Re-define the time increment in years (360 days).
10. Plot the Recovery of gas and liquid (in the same plot) as function of average reservoir pressure (use pressure data from NGASPERM.DAT and production data from NGASPROD.DAT).

3.4 Plotting of Pressure Data

Use the above simulation data from the two files, now saved in the spreadsheet and make the following pressure plots.

11. Plot pressure as function of time; $p(t)$.
12. Add the reduced pressure in the above plot.
The two pressure curves plot differently. Use theory from the Lecture Notes to explain the observed difference between the two curves.
13. Make a p/Z interpretation plot, where the reduced pressure is plotted as function of produced gas; $p/Z(G_p)$.
From the above plot, find the estimated value of GIIP.
Make some short comments about the possible errors in using $p/Z(G_p)$

3.5 Water Influx and Water Production

Water influx and water production are controlled by the WATINF parameter. If WATINF=1, then water production and water influx rates are defined proportional to the gas production rate. The relative rate of water production and water influx are then given by WPFAC and WEFAC. Notice that water is produced from the average

water volume in the reservoir, $V_w = V_p \cdot S_w$. The produced water is therefore subtracted from water volume present in the reservoir, which is a limited quantity that cannot be reduced below zero. (We can not produce more water from the reservoir, than present in the reservoir.) Therefore, only a limited amount of water can be produced to the surface, without extra water being added from i.e. an aquifer. The relative water rate WPFAC must therefore always be much less than unity ($WPFAC \ll 1$), since WPFAC relates water rate to gas surface rate. WPFAC larger than zero ($WPFAC \neq 0$) should normally not be used, unless water influx is allowed for. If both $WPFAC=WEFAC=0$, then water is not subtracted or added in the model.

If $WATINF=2$, then water influx is controlled by an aquifer. The aquifer size and various other parameters are characterizing the aquifer. When $WATINF=2$, water production can still be linked to the gas production rate, as seen above, through $WPFAC \neq 0$, but for most cases it would be sensible to choose $WPFAC=0$. Four different aquifers can be modeled, i.e. radial- and linear aquifers of finite and infinite dimensions. Follow the item list below when simulating water production and water influx.

14. Run the Base Case model without any changes to the data input-file (remember to switch to simulation mode by changing $DCHCK=0$ and check that $WATINF=1$). Plot the hydrocarbon recovery by plotting cumulative gas and liquid production in separate plots, using pressure along the x-axis. WPFAC and WEFAC should here both be zero.
15. In the case of very strong aquifer support, one may assume aquifer influx to be proportional to the gas production rate. Assume water influx equal to 5% of the gas production, i.e. $WEFAC=0.05$. Plot cumulative gas and liquid production in the same plots as above.

Why does influx of aquifer water result in an over all higher gas production?

16. Simulate gas production with a relative water influx rate of 5% and a relative water production rate of 2%. Plot recovery profiles (gas and liquid) and compare the result to the case were no aquifer is included in the simulation model (the Base Case model). Present the pressure profiles in the same plot for all three cases (item 1, 2 and 3). Comment on the change in cumulative production in the three cases!

Why does the recovery profiles in the last case fall in between the two previous curves?

3.6 Aquifer Type, Form and Size

17. Carry out and compare the simulations for the four aquifers, given in Table 3.1. In the comparison between the aquifers, use water influx W_e , gas production G_p and average reservoir pressure p as comparing parameters. Plot the data. Assume no water production, nor associated water production, i.e. $WPFAC=WEFAC=0$. Comment the plots based on observation of the data in Table 3.1.

Which aquifer generates the strongest water support and why? Which aquifer is the weakest and why? Does aquifer water support have any influence on cumulative production? What is the typical pressure effect of aquifer water support?

Table 3.1: Aquifer data.

| Reservoir | Infinite radial | Finite radial | Infinite linear | Finite linear |
|-----------|-----------------|---------------|-----------------|---------------|
| WTYPE | 1 | 1 | 2 | 2 |
| WFINITE | 2 | 1 | 2 | 1 |
| WALPHA | 360. | 360. | 0. | 0. |
| WCOMP | 5.D-5 | 5.D-5 | 5.D-5 | 5.D-5 |
| WLENGTH | 0. | 0. | 0. | 1250. |
| WPERM | 5.0 | 5.0 | 5.0 | 5.0 |
| WPORO | 0.2 | 0.2 | 0.2 | 0.2 |
| WRADB | 350. | 350. | 0. | 0. |
| WRADE | 0. | 1000. | 0. | 0. |
| WTHICK | 50. | 50. | 50. | 50. |
| WVISC | 1.0 | 1.0 | 1.0 | 1.0 |
| WWIDTH | 0. | 0. | 2200. | 2200. |

Notice that no parameters can be omitted, from the listing the data-input file, even though they are not used in the calculation for that particular aquifer. E.g. for radial aquifers, neither length or width (WLENGTH and WWIDTH) are used in the simulation, even so their numbers are read, stored and written to the output-file, even though they are not used. Thus, all parameters that are not of significance for that particular aquifer is set to zero in the table.

18. Compare the aquifer strength of an infinite radial aquifer to an infinite linear aquifer. In comparing the two, use identical inflow area from aquifer to reservoir. (This would make the linear aquifer very wide compared to the outer radius of the reservoir and therefore unlikely as a practical example, but theoretically this comparison would make sense.)

Why is the influx of water from the radial infinite aquifer greater than for the linear aquifer? Is this difference increasing with time and/or the size of the gas reservoir?

19. Compare the aquifer strength of a finite radial aquifer to a finite linear aquifer. In addition to making the inflow area equal in the two cases, make sure that the water initially in place in the two models are the same.

How does the two aquifers compare if the aquifer volume is reduced by 50%?

Carry out the following three sensitivity studies where recovery is function of aquifer compressibility, - permeability and - porosity. Assume the aquifer to be infinite radial otherwise as as presented in Table 3.1. We call this model the Base Case model.

NB! Vary one parameter at the time. Use gas produced, water influx and recovery (relative gas produced as function of reservoir pressure) as comparing parameters in the sensitivity test plots.

20. Run the Base Case model first with data as presented in Table 3.1. Make the three plots as mentioned above.
21. Assume that the rock and water compressibility, WCOMP, is reduced to 1/5 of the value given in the Base Case model.
22. Let the permeability, WPERM, be 1/5 the value given in the Base Case model.
23. Simulate a case where the aquifer porosity, WPORO, is 10%.

Finally, create plots where all four recovery profiles are included (both for gas and liquid). Discuss the results and write a short comment answering the following questions:

24. What is the single most important parameter in characterizing the aquifer?
25. Why is aquifer compressibility important?
26. Explain the effect of aquifer porosity on reservoir production.
27. Decide whether the aquifer sensitivity tests are simulating a stronger or a weaker aquifer support in each of the cases presented in the items above.
28. If reservoir aquifer influx is modeled by an infinite radial aquifer, but the water influx is observed to be too low, - how can the water influx be increased without changing the permeability of the aquifer? (Hint: Non physical adjustment of aquifer boundary.)

Include all plots above in the report. NB: All figures should have a figure-text, explaining the data presented in the figure.

Make a report by answering all questions in the above subsection and include the newly made plots.

Project Exercise 4

Project Exercise: Material Balance and Interpretation Methods

This exercise is a continuation of the previous exercise. The subject in the present exercise is related to non-volumetric depletion processes. The problems encountered in these cases, are related to data analyzes and reliable predictive estimates of in-place volumes.

4.1 History Matching and Predictive Performance

Even though material balance calculation is supposed to be one of the simplest subjects in the whole of reservoir engineering, there are great misunderstandings related to the application of material balance calculations as a predictive tool. The lack of proper knowledge and understanding can lead to serious error in assessing the reservoir drive mechanism (interpretation of volumetric depletion) and in estimation of GIIP volumes.

Using the traditional p/z versus cumulative production plot, can lead to a complete misinterpretation of the drive mechanism and a serious overestimation of GIIP volume. In an attempt to avoid doing these mistakes, other interpretation methods should be considered.

In this exercise you are supposed to use the following two methods; the p/z method and the Havlena - Odeh method, in analyzing results from a simulation study with aquifer influx. Analyze and compare the production - pressure history data by running the Base Case model. Since the Base Case model contains production and pressure data from the whole production history, we have to pretend not knowing the latter part of the data available through the simulation. It would not make much sense to use all the data in this analysis, since the purpose here is to evaluate early pressure data and use them to estimate general characteristics of the initial reservoir and its production. Since history matching is of primarily interest only for early and intermediate production history, only data produced within the first one and a half years (and later in the time period less than 2.5 years), are of interest in this study.

4.2 The Base Case Model

Define a Base Case model where the reservoir pressure is supported by an aquifer of radial and infinite dimension. Use the initial set of parameter, defined in the data input file NGASDATA.DAT and the water aquifer data given in Tabel 4.1.

Table 4.1: New aquifer data.

| WALPHA | WCOMP | WPERM | WPORO | WRADB | WVISC |
|--------|-------|-------|-------|-------|-------|
| 360. | 5.D-5 | 5. | 0.2 | 350. | 1.0 |

Prepare the data file for the Base Case model as if you are going to present plots of production, pressure development and water influx. The data generated by this model will later in this exercise be used and needs therefore to be stored, preferably in the same Excel file where the above mentioned plots are generated.

4.3 p/z Interpretation Method

A general pressure equation has been developed in the Lecture Notes, under the assumption of molar balance in a gas condensate reservoir. See section 4.3.1 in Chapter 4.

$$p = p_i \frac{Z_2 V_{HCi}}{Z_{2i} V_{HC}} \left(1 - \frac{G_p (1 + R_{MLGp})}{G_i (1 + R_{MLGi})} \right)$$

In the equation above, both aquifer influx and liquid condensation are included, using the parameters V_{HC} and R_{MLG} . The p/z interpretation method, however, uses the more simplistic pressure - production equation,

$$p = p_i \frac{Z}{Z_i} \left(1 - \frac{G_p}{G_i} \right),$$

where no water influx is accounted for and where liquid condensation in the reservoir is neglected, i.e. as in volumetric depletion.

Perform a p/z -interpretation study by following the items below. Use the data from the Base Case model stored in the Excel spreadsheet, as prepared above.

1. Plot the production - pressure data taken form the Base Case model. Use data up to times equal to 1.5 years.
2. Fit and draw a straight line through the data points in the plot and consider the linearity of the data. Linearity can be expressed through the regression value, R .

Can the data be assumes to be linear and if so, is it reasonable to believe that the data supports the assumption of volumetric depletion?

3. Draw the fitted line until it crosses the x-axis. Estimate the initial gas volume; GIIP.

4. Add more data to the p/z plot and redo the analysis. Use data up to times 2.5 years.
5. Compare the two cases above by comparing the estimates of GIIP volumes. Comment on the degree of accuracy in estimating the GIIP volumes by using the p/z interpretation method. Estimate the over-representation, in %, of initial gas in place (GIIP).

The true value of GIIP can be found in the log-file, where GIIP and LIIP are calculated as part of the initialization process of the simulations.

4.4 The Havlena - Odeh Interpretation Method

The general material balance equation for natural gas reservoirs can be derived from the molar balance equation, presented in the lectures. The molar balance equation, Eq. 4.23, is written,

$$\frac{G_p}{G_i} = \left(1 - \frac{Z_{2i} p V_{HC}}{Z_2 p_i V_{HCi}}\right) \left(\frac{1 + R_{MLGi}}{1 + R_{MLGp}}\right).$$

If no water injection or water production are assumed and the following definitions of hydrocarbon pore volume (V_{HC}), see Eq. 4.37 and gas volume factor (B_g), see Eq. 3.113, are used;

$$\begin{aligned} V_{HC} &= V_{pi} \{(1 - S_w) + (p - p_i)(c_r + S_w c_w)\}, \\ B_g &= (1 + R_{MLG}) Z \frac{T}{p} \left(\frac{p}{T}\right)_{sc}, \end{aligned}$$

then the material balance equation for natural gas reservoirs (dry- and wet gas reservoirs) is written,

$$G_p B_g = G_i (B_g - B_{gi}) + G_i B_{gi} \frac{(c_r + S_w c_w)}{(1 - S_w)} \Delta p. \quad (4.1)$$

The pressure difference $\Delta p = p_i - p$ is always positive. If water influx W_e and water production W_p are included into the equation above, the general material balance equation for gas reservoirs is written,

$$\underbrace{G_p B_g + W_p B_w}_{\text{Underground-withdrawal}} = \underbrace{G_i (B_g - B_{gi})}_{\text{Gas-expansion}} + \underbrace{G_i B_{gi} \frac{(c_r + S_w c_w)}{(1 - S_w)} \Delta p}_{\text{Expansion, Compaction}} + \underbrace{W_e}_{\text{Influx}},$$

where both $W_p B_w$ and W_e are volumes in reservoir units, i.e. in Rm^3 .

Adopting the nomenclature frequently used in linearization of the general material balance equation and assuming no water production,

$$\begin{aligned} F &= G_p B_g, \\ E_g &= B_g - B_{gi}, \\ E_f &= B_{gi} \frac{(c_r + S_w c_w)}{(1 - S_w)} \Delta p, \end{aligned}$$

the reduced linear equation is written,

$$\frac{F}{E_g + E_f} = G_i + \frac{W_e}{E_g + E_f}. \tag{4.2}$$

Using production data, pressure and PVT-data (see data input file), the left-hand side of Eq. 4.2 can be plotted as function of relative gas production, G_p/G_i . In the case of no water influx ($W_e = 0$), i.e. volumetric depletion, the data should plot linearly as a horizontal straight line.

Any deviation from a horizontal straight line would indicate non-volumetric depletion and possible aquifer water influx. F , E_g and E_f can be calculated for different ratios of G_p/G_i . The volume gas factor, B_g as defined above, is dependent on the molar-condensate-gas ratio R_{MLG} , where $R_{MLG} = (1 - \text{GASF})/\text{GASF}$. GASF is tabulated in the data input file `NGASDATA.DAT`. Using the values in the table in the `NGASDATA.DAT` file, one has to interpolated the data values to the pressure - and production data generated by the Base Case model.

Use the production- and the pressure data from the Base Case model and the PVT-data from the data input file to analyze production performance and estimate initial gas in place by applying the interpretation method recommended by Havlena and Odeh.

6. Derive Eq. 4.1, based on the definitions of the molar balance equation, V_{HC} and B_g , above.
7. Plot the z -factor and the R_{MLG} as function of pressure, p . Use these plots to estimate a linear relation ship for z and R_{MLG} and the pressure. Then, use these results to relate z and R_{MLG} to the simulated values of production - pressure data.
8. Use the Base Case model data up to times equal to 1.5 years. Calculate the gas volume factor B_g and the parameters constituting the linear material balance equation; F , E_g and E_f .

Hint: Use the Excel Worksheet and do the calculations in a Table as shown below

| G_p | p | R_{MLG} | Z | F | E_g | E_f | $F/(E_g + E_f)$ | G_p/G_i |
|-------|-----|-----------|-----|-----|-------|-------|-----------------|-----------|
| - | - | - | - | - | - | - | - | - |
| - | - | - | - | - | - | - | - | - |

9. Plot the underground withdrawal; F , divided by the sum of gas expansion; E_g , and water expansion and pore compaction; E_f , as function of relative gas production, G_p/G_i .
10. Evaluate the drive mechanism and estimate the GIIP.

-
11. Finally, compare the p/z -plot with the Havlena - Odeh interpretation method and comment on the weaknesses and strong points in the two methods.

Project Exercise 5

Project Exercise: Radial Gas Flow

In this exercise, you will work with an updated version of the old program and data file.

The focus in this exercise is on some of the new items presented in Chapter 5, Reservoir Flow. Therefore, variation of parameters related to items such as aquifer size and strength are not any longer subject for variation here. However, that doesn't mean that you can't combine, the changing of old parameters together with the variation of new parameters.

5.1 Simulation of Radial Gas Flow

The program-file has been updated with three new subroutines, allowing simulation of radial flow towards the well with the purpose of calculating the bottom-hole pressure. The three subroutines; `INFLOW`, `GASCOMPR` and `LEEIVISC`, are all integrated in the program structure as presented in Figure 5.1.

5.1.1 Organization of The Simulation Program

The new subroutine `INFLOW` is being called by `GASPROD`, which is organizing the gas production simulation process. The call to `INFLOW` is done shortly after material balance calculations are performed in `GASPROD`. `INFLOW`, in it self, do calls to `GASCROMR` and `LEEIVISC`. See the new program structure, shown in Figure 5.1.

`INFLOW`

The main result of the calculations performed by the `INFLOW`-program is the bottom-hole pressure p_{bh} .

The program starts out by initiating a table where the pseudo-pressures are defined. This table is used to transform pressures to pseudo-pressures and via versa. A delta pressure DP , defined in the data input-file, determines pressure step in pseudo pressure calculations and therefore the accuracy of pressure estimation.

The pseudo-pressure $m(p)$ is calculated using the following approximation

$$m(p) = (\mu B)_r \int_{p_r}^p \frac{1}{\mu B} dp \simeq \frac{(\mu B)_r}{2} \sum_{i=1}^L \left(\frac{1}{(\mu B)_{i-1}} + \frac{1}{(\mu B)_i} \right) (p_i - p_{i-1}),$$

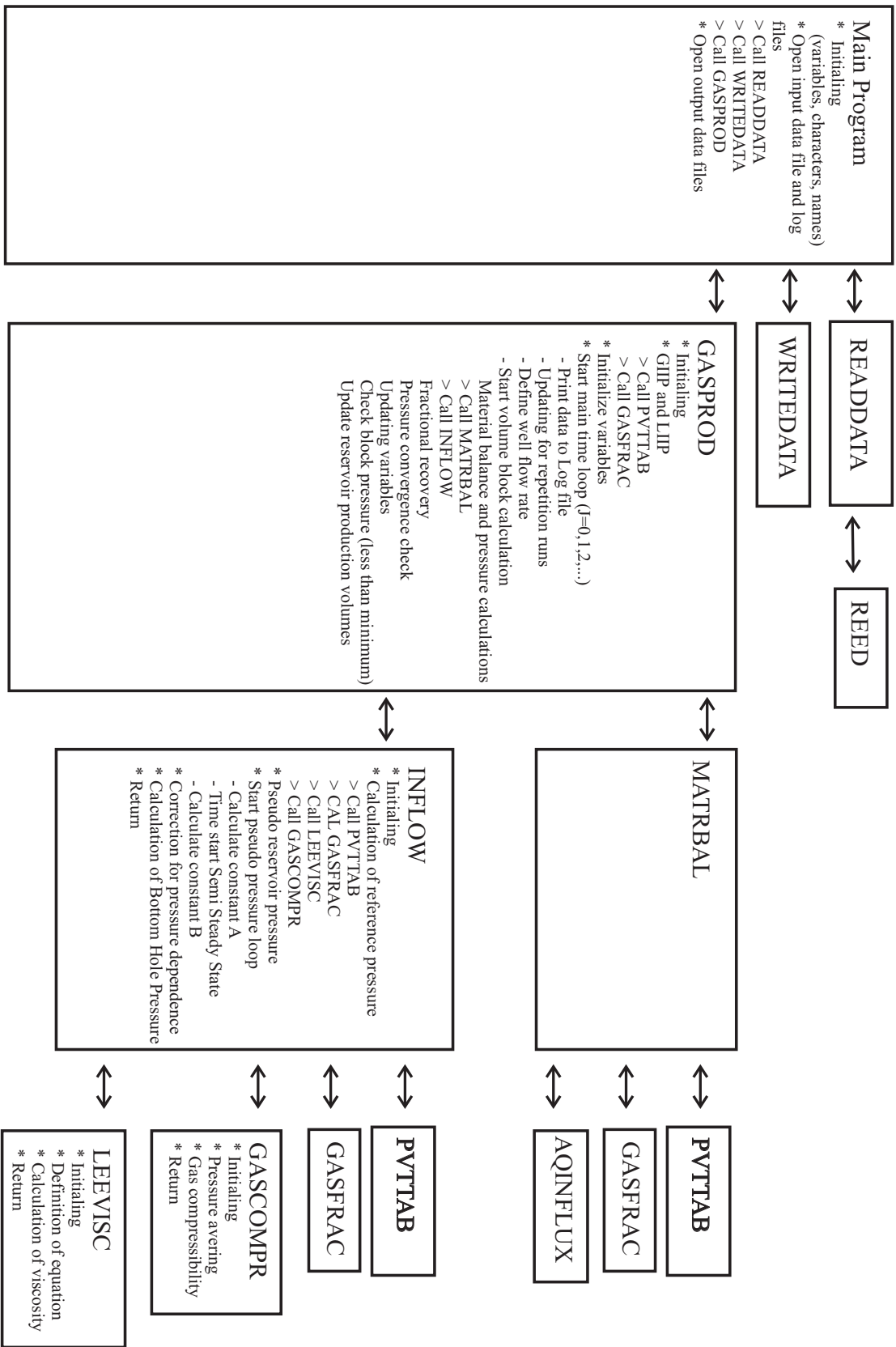


Figure 5.1: Program structure including radial flow simulation.

where L is the summation index indirectly defined by DP. See also the example on page 136.

Then the constants A and B , as defined in the Lecture Notes, section 5.5.2, are calculated. Along side these calculations, the transition time t_{GS} is used to differentiate between the two time periods. If non-radial conditions is indicated, the constant A is automatically up-dated.

The pseudo-pressure calculations are performed following the procedure outlined in the Lecture Notes, substituting for A and B . The final step is to compare the pseudo-pressure with the tabulated values in order to find the bottom-hole pressure.

GASCOMPR

The GASCOMPR-program is a short program calculating the gas compressibility, taking into account the Z-factor correction term, defined in the Lecture Notes.

LEEVIS

The LEEVIS-program is another small and dedicated program which calculates the gas viscosity as defined in the Lecture Notes.

5.1.2 Data Input File

The data input-file NGASDAT.DAT is up-dated in accordance with the needs specified by the new subroutines added. The general organization of the data input-file is maintained and new data is added where it seems most natural.

NGASDATA-file

```
*
* **** Start data file NGASDATA.DAT
*
* Data file name (max. 70 characters); text
* 1234567890123456789012345678901234567890123456789012345678901234567890
'Project: Natural Gas Reservoir Engineering.'
'Part: Simulation of Material Balance and Radial Gas Flow '
'Text string 3'
* * *
* *** Program data
*
* DCHCK=1 Data check mode; No material balance is done.
* DCHCK=0 Full simulation. [integer]
* MAXSTEP Number of simulation steps; Program is terminated at
* simulation step NSTEP. [integer]
* NPRINT Number of sequent plotting parameter; Printing to file is done
* for every NPRINT simulation step. [integer]
* SP=1,100 Short LOG printout; Full printout and printing of every 1 to
* 100 time step SP=1 gives a short hand presentation of every
* time-step. [integer]
* *
* DCHCK MAXSTEP NPRINT SP
* 0 5000 10 1
* * *
```

```

*   *** Simulation data:
* *
* PERR      Error limit in pressure calculations. [real]
* GPGERR    Error limit in volume calculations. [real]
* DP        Pressure step in pseudo pressure calculation. [real]
* PREF      Pressure reference in pseudo pressure calculation. [real]
* CAERR     Error limit in calculation of Dietz-factor. [real]
*
*           PERR      GPGERR      DP      PREF      CAERR
*           0.5       1D-07       5.      5.        0.01
* * * *
*   *** Volume and block data
* *
* BNAME     Name of individual block, maximum 5 characters. [String]
* VPORINIT  Pore volume of block  $\{=\pi \cdot (\text{RADE}^2 - \text{RADW}^2) \cdot \text{THICK} \cdot \text{PORO}\}$  (Rm3 ) [real].
* RADE     Characteristic radius of block (m). [real]
* RADW     well-bore radius (m). [real]
* THICK     Net vertical thickness of block (m). [real]
*
*           BNAME      VPORINIT      RADE      RADW      THICK
*           'BLK01'    4D+6          360.     0.175    50.
* * * *
*   * Block characteristics:
* *
* PORO     Porosity of block. [real]
* SWINIT   Initial water saturation [real]
* PERM     Absolute permeability in block (mD). [real]
* CA       Dietz shape factor (CAcircle=31.62). [real]
* DARCY    Non-Darcy factor. (day/m3) [real]
* SKIN     Skin factor. [real]
*
*           PORO      SWINIT      PERM      CA      DARCY      SKIN      Block no.
*           0.20     0.2       10.      31.62   5.D-06    0.0      1          BLK01
* * * *
*   *** General reservoir data
* *
* PRS      Initial reservoir pressure (bar). [real]
* TEMP     Initial reservoir temperature (Kelvin). [real]
* PRSSC    Atmospheric pressure (bar). [real]
* TEMPSC   Normal reference temperature (Kelvin). [real]
* COMW     Water compressibility (1/bar). [real]
* COMR     Reservoir compressibility (1/bar). [real]
*
*           PRS      TEMP      PRSSC      TEMPSC      COMW      COMR
*           437.0   392.0    1.01      288.0      4.35D-05  4.5D-05
* * * *
*   *** Well data
* *
* QMAX     Maximum well rate (Sm3/day). [real]
* QMIN     Minimum well rate (Sm3/day). [real]
*
*           QMAX      QMIN
*           5.0D+05   5.0D+04
* * *
* TBP     Time step length (days). [real]
*
* TBP

```

```

5.
* *
* BHPM Minimum bottom-hole pressure (bar). Production is stopped
* when minimum bottom-hole pressure is reached. [real]
* (Minimum bottom-hole pressure should be within the range
* of the PVT data)
*
* BHPM
* 50.
* *
* *** Water data
* *
* WATINF=1 Water influx/production controlled as fraction of production.
* (Only WPFrac and WEFrac are relevant parameters.) [integer]
* WATINF=2 Water flux from aquifer is included. [integer]
*
* WATINF
* 1
* *
* WPFrac Water production as fraction of gas production. [real]
* WEFrac Water influx as fraction of gas production. [real]
* (A non-zero WPFrac has normally to be accompanied
* by a non-zero WEFrac.)
*
* WPFrac WEFrac
* 0.0 0.0 BLK01
* *
* WTYPE=1 Radial aquifer. [integer]
* WTYPE=2 Linear aquifer. [integer]
* WFINITE=1 Finite aquifer. [integer]
* WFINITE=2 Infinite aquifer. [integer]
* WALPHA Angle of sector within which aquifer water encroaches (degree). [real]
* WCOMP Aquifer compressibility coefficient (rock and water) (1/bar). [real]
* WLENGTH Aquifer length (linear aquifers) (m). [real]
* WPERM Aquifer permeability (mD). [real]
* WPORO Aquifer porosity. [real]
* WRADB Radius of aquifer inner boundary (m). [real]
* WRADE Radius of aquifer outer boundary (m). [real]
* WTHICK Aquifer thickness (m). [real]
* WVISC Water viscosity (mPa.s). [real]
* WWIDTH Aquifer width (m). [real]
* *
* WTYPE WFINITE WALPHA WCOMP WLENGTH WPERM WPORO WRADB WRADE WTHICK WVISC WWIDTH
* 1 2 360. 5.D-5 1535. 1.0 0.2 500. 1000. 50. 1.0 1535.
* * * *
* *** PVT data
* *
* NTAB Number of PVT-table elements
*
* NTAB
* 20
* *
* PRS Pressure [bar]
* TEMP Temperature [K]
* MWT Mixture mol weight [g/mol]
* MWG Gas mol weight [g/mol]

```

```

* MWTL      Liquid mol weight [g/mol]
* GASF      Gas mol fraction
* Z         Gas phase Z-factor
* Z2        Mixture, two-phase Z-factor
*
* PRS      TEMP      MWT      MWLG      MWTL      GASF      Z      Z2      NTAB
445.      392.      26.56  26.56  26.56  0.9517  1.1142  1.1143  1
370.      392.      26.56  26.56  26.56  0.95171 1.0258  1.0258  2
350.      392.      26.57  26.42  90.14  0.95240 1.0035  1.0045  3
320.      392.      26.57  26.19  89.32  0.95349 0.9721  0.9743  4
300.      392.      26.59  26.03  88.19  0.95438 0.9530  0.9556  5
280.      392.      26.61  25.83  87.18  0.95556 0.9356  0.9385  6
260.      392.      26.65  25.61  86.86  0.95705 0.9206  0.9233  7
240.      392.      26.72  25.36  87.52  0.95883 0.9082  0.9102  8
220.      392.      26.81  25.11  89.16  0.96061 0.8986  0.8994  9
200.      392.      26.94  24.88  91.68  0.96259 0.8920  0.8994  10
180.      392.      27.13  24.66  95.05  0.96446 0.8886  0.8910  11
160.      392.      27.38  24.47  99.27  0.96624 0.8885  0.8851  12
140.      392.      27.95  24.30  104.49 0.96783 0.8916  0.8808  13
120.      392.      28.52  24.18  110.81 0.96921 0.8979  0.8807  14
100.      392.      29.33  24.10  118.48 0.97010 0.9073  0.8837  15
80.       392.      30.51  24.08  127.84 0.97050 0.9197  0.8862  16
60.       392.      32.36  24.16  139.47 0.97079 0.9348  0.8864  17
40.       392.      35.59  24.41  154.40 0.97089 0.9524  0.8778  18
1.01      392.      42.00  25.00  185.00 0.97099 0.9900  0.8580  19
1.01      288.      42.00  25.00  185.00 0.95171 0.9900  0.8580  20
* * *

```

5.2 Simulation of Semi Steady-State Period

Carry out the following calculations, based on the theory described in Chapter 5.2, above and the assumption than $r_e \gg r_w$ (valid in most real cases):

1. Use the boundary conditions Eq. 5.33 and Eq. 5.34 in the Lecture Notes and define the constants K_1 and K_2 in Eq. 5.32.
2. Show that the pseudo pressure can be written,

$$m(r) = m(r_w) + \frac{q_{sc}(\mu B)_r}{2\pi h k} \left(\ln \frac{r}{r_w} - \frac{1}{2} \frac{r^2}{r_e^2} \right),$$

where $r_w/r_e \sim 0$.

3. Use the pseudo pressure and show that the mean pseudo pressure for a cylindrical reservoir is written,

$$\bar{m} = m(r_w) + \frac{q_{sc}(\mu B)_r}{2\pi h k} \left(\ln \frac{r_e}{r_w} - \frac{3}{4} \right),$$

Observe that the constant being the result of the averaging process; $3/4$, is different from the constant derived under Steady-State condition, as in Eq. 5.30. The redefinition of the constant is related to how semi steady-state is defined,

where the draw-down pressure profiles are considered to be constant; $\partial m(r)/\partial t = \text{constant}$, and not zero as was the starting point in developing pressures under Steady-State condition.

5.3 Simulation of Single Phase Gas Flow

It has been shown above that the mean pseudo pressure \bar{m} , is introduced in the semi steady-state pressure equation by substituting of a constant equal to $3/4$. It has also been said that the pressure distribution in the reservoir is constant in time and proportional to the mean pseudo pressure.

In the infinite acting period, which ends after a rather short production period, at the time $t_{SS} = r_e^2/(4D_h)$, where the initial pressure m_i is, for all practical purposes, equal to the mean pressure, i.e. $m_i \simeq \bar{m}$.

The two pseudo pressure solutions are therefore written,

Infinite acting period

$$\bar{m} - m_{bh} = \frac{q_{sc}(\mu B)_r}{2\pi hk} \frac{1}{2} \left[\ln(t) + \ln\left(\frac{D_h}{r_w^2}\right) + 0.80907 + 2(S + S_{nD}) \right].$$

Semi steady state period

$$\bar{m} - m_{bh} = \frac{q_{sc}(\mu B)_r}{2\pi hk} \left[\frac{1}{2} \ln\left(\frac{4A}{e^\gamma C_A r_w^2}\right) - \frac{3}{4} + S + S_{nD} \right],$$

The well bore pressure for both periods are then written,

$$m_{bh} = \bar{m} - (A \cdot q_{sc} + B \cdot q_{sc}^2),$$

where A and B are constants and defined as,

Infinite acting period

$$A = \frac{q_{sc}(\mu B)_r}{2\pi hk} \frac{1}{2} \left[\ln(t) + \ln\left(\frac{D_h}{r_w^2}\right) + 0.80907 + 2S \right],$$

$$B = \frac{q_{sc}(\mu B)_r}{2\pi hk} \cdot D.$$

Semi steady state period

$$A = \frac{q_{sc}(\mu B)_r}{2\pi hk} \frac{1}{2} \left[\ln\left(\frac{4A}{e^\gamma C_A r_w^2}\right) - 3/2 + 2S \right],$$

$$B = \frac{q_{sc}(\mu B)_r}{2\pi hk} \cdot D.$$

Calculating the bottom-hole pseudo-pressure m_{bh} is a direct result from the simulation process. The transformation of the pseudo pressure m_{bh} , to a real pressure p_{bh} is done by using the Kirchhoff's transformation,

$$m = (\mu B)_r \int_{p_r}^p \frac{1}{(\mu B)} dp.$$

4. Show that a discretization of Kirchhoff's transformation can be written,

$$\Delta p = \frac{\overline{\mu B}}{(\mu B)_r} \Delta m,$$

and that a possible discretization of the same transformation can be represented as,

$$p = p' + \frac{2(m(p) - m(p'))}{(\mu B)_r \left(\frac{1}{(\mu B)_p} + \frac{1}{(\mu B)_{p'}} \right)},$$

where p' is the pressure at a previous time step.

NB: Consider the Kirchhoff's transformation and the integration as an Harmonic averaging process.

5.4 The Effect of Reservoir Permeability on Bottom Hole Pressure

The data file contains additional information about the reservoir, given by RADE, RADW and THICK under the subsection "Volume and block data" and PORO, SWINIT, ... under the subsection "Block characteristics". In the general case when the reservoir shape is non-cylindrical, the reservoir radius RADE is defined as an *appearing* radius, so that the pore volume $V_p = \phi\pi(r_e^2 - r_w^2)h$, is consistent with VPORINIT.

5. Use the data given in the new data file and plot the mean reservoir pressure and the bottom-hole pressure, when the average reservoir permeability is 10 mD. Make also a plot where the pressure difference $\Delta p = \bar{p} - p_{bh}$ is plotted as a function of time and observe the pressure difference! Why does the pressure difference above, increase with time? Which parameters would be the most important in explaining the pressure difference?
6. Run the program for 3 different choices of reservoir permeability; 100 mD, 10 mD and 5 mD. Plot bottom-hole pressure p_{bh} for the three cases in the same plot. Why does the production period become shorter when the reservoir permeability decreases? What is the relative decrease in cumulative gas production in the three cases?
7. Present a plot where the bottom-hole pressure is plotted as function of the mean reservoir pressure, $p_{bh} = p_{bh}(\bar{p})$. Comment the observations being plotted. (Reference to the conditions of semi steady-state flow conditions.) Use a reservoir permeability equal to 10mD.

5.5 Well Skin and Bottom Hole Pressure

The well skin was introduced as a dimensionless number directly proportional to the difference between the normal pressure at the well bore radius and the pressure in the well bore itself. For zero skin, the two pressures are equal. In the case of positive skin ($S > 0$), a positive pressure drop is added to the pressure drop in the reservoir and the bottom-hole pressure observed is lower than it would otherwise have been. For negative skin, the formation close to the well is observed to be more permeable than the reservoir itself and consequently the bottom-hole pressure is less than it ideally should have been.

8. Assume the average reservoir permeability to be 10 mD and run the program for 3 choices of well skin; 0, 20 and -20. Plot the bottom-hole pressure as function of time in the three cases.
9. Do the same as above, assuming a reservoir permeability equal to 5 mD. Comment on the change in the observed data when the reservoir permeability is reduced. How does the bottom hole pressure change due to skin variation, and does this relationship change with reservoir permeability?

5.6 The Effect of Shape-Factor and Non-Darcy Flow

The simulation of non-cylindrical reservoirs are approximated through the change in the appearing reservoir radius RADE and the change in the Dietz shape-factor C_A .

Non-idealized flow conditions, i.e. inertial forces such as turbulence, introduced through Forcheimer's equation, are simulated using a non-Darcy flow-factor, D . The factor contains several different parameters, such as reservoir - and fluid parameters. The approximations made in deriving the non-Darcy factor and the relative importance of the factor (its relative strength), both indicate the sufficiency of simulating the non-idealized flow conditions with a single factor.

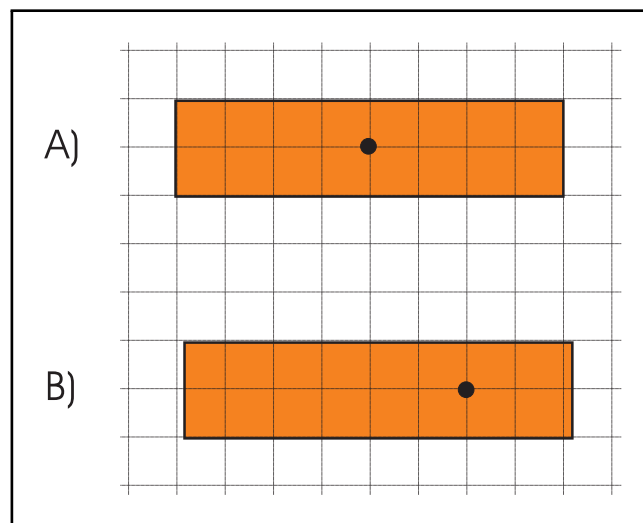


Figure 5.2: Drainage shape.

10. Compare the bottom-hole pressure in a cylindrical reservoir with the bottom-hole pressure in a rectangular reservoir where the well is centered, A) and secondly where the well is moved halfway from the centre to one side, B), as depicted in Figure 5.2. Use reservoir permeability $k = 5 mD$ and zero skin.
11. Obviously, the transition time from the infinite acting period to the semi steady-state period will change when the drainage shape is changing. Evaluate this change in the two cases above and compare with the cylindrical Base Case model. (Hint: Calculate the t_{ss} for the three cases of cylindrical -, centered - and off-centered reservoir.)
12. When the non-Darcy factor is increasing, the effect of turbulence is also increasing. Vary the non-Darcy factor, e.g. use twice the value and observe the bottom-hole pressure. Plot the bottom-hole pressure in two cases.

Project Exercise 6

Project Exercise: Well Bore Flow

The pressure drop in the well bore, $(p_{bh} - p_{wh})$, assumes *single-phase-flow* in the well. This condition is normally satisfied in the case of dry - and wet gas production, as long as water don't enter the well-bore. In the case of gas condensate production, oil is thought to be dispersed in the well stream in small droplets.

Providing the well flow of oil and gas behave as a homogeneous fluid, the single-phase-flow solution is still valid. With oil dispersed in the gas, the only necessary modification to the dry gas model, needed, is to redefine the gas density to be valid for the gas and oil mixture.

In the case water is produced together with gas and oil, a slightly more delicate situation occurs, since the water density is much higher than the density of the gas-oil mixture. For moderate amounts of water in the well stream, the single-phase-flow solution may still be applicable. If it is safe to assume the water to be homogeneously dispersed in the gas-oil mixture. All that is needed is a water-correction factor, $F_w = 1 + w_w/w_g$. This factor is a necessary modification to the single phase flow case, when water is flowing together with gas and oil under mist flow conditions.

The presence of increasingly higher water-cut in the well stream will eventually cause the well to *shut-in*. When this happens the well-flow rate drops to zero and the well has to be abandoned. A critical parameter in modeling well bore flow is therefore the *minimum unloading rate*, which actually defines the lower limit of natural well-flow behavior.

The minimum unloading rate is calculated for each time step and written to the log-file, therefore not directly accessible for analysis using a spreadsheet operations as we have been used to. If the well-flow rate (here the dry gas flow rate) becomes less than the minimum unloading rate the well production is automatically stopped and a message "*** QSCW<QUNLOAD ***" is written to the NGASPRNT.DAT file. The NGASPRNT.DAT file should therefore always be checked in order to verify a successful termination of the program.

Another important assumption made in deriving the single phase flow solution is that the kinetic term in the general flow equation is negligible. In practical terms, this means that the kinetic term is far less than the friction term and from the Lecture Notes we have,

$$\text{Kinetic V.S. Friction} = \frac{\ln(p_{bh}/p_{wh})}{2\bar{f}L/d_h} \ll 1.$$

The program calculates this ratio for each time step and prints it to the log-file.

Under normal flow conditions it is safe to consider this assumption to be true but generally this number has to be checked.

6.1 Simulation of Well-Bore Flow

As in previous chapters, the program file has been updated in order to include well-bore flow calculations. One new subroutine `WHPRESS` has been added, where the program makes calls to already existing subroutines.

6.1.1 Organization of The Simulation Program

The well-head pressure is calculated based on the bottom-hole pressure, as can be seen from the general pressure equation in the Lecture Notes. It is therefore quite natural to include the `WHPRESS`-program, directly after calculation of the well bottom pressure, i.e. after the call to `INFLOW`.

After the well-head pressure is calculated, it is checked against the minimum well-head pressure. If the well-head pressure is higher than the minimum pressure, then the simulation process can continue. If, on the other hand, the well-head pressure is less than the minimum pressure, we have to step back in the process and redefine a new and lower well rate. This process continues until a minimum well rate is reached, at which point the production is halted. The program structure is shown in Figure 6.1

The `WHPRESS`-program receives PVT-data from the `PVTTAB`-subroutine, before calculating the various constants $N_{gp,m}$ and $N_{fp,m}$. The bottom-hole Z-factor is used as an average Z-factor, while the friction factor is calculated in accordance with Wood's equation.

The program also includes a test on whether the statement "the kinetic energy is much less than the friction energy" is true. A factor, `KINENRG`, is defined as the ratio between kinetic - and friction energy. This factor is then written to the log-file.

The minimum unloading flow rate is calculated and compared to the well flow rate and in the case where the flow rate is less than the unloading flow rate, a message is written to the log-file.

6.1.2 The Data Input-File

The data input-file is updated with the information needed to perform the calculation of the well-head pressure. The basic structure of the data-file is maintained, while information regarding the well, such as well length, - diameter, - roughness, - deviation angle and well-head temperature are added to the file. See section in the data file called `Well tubing data`.

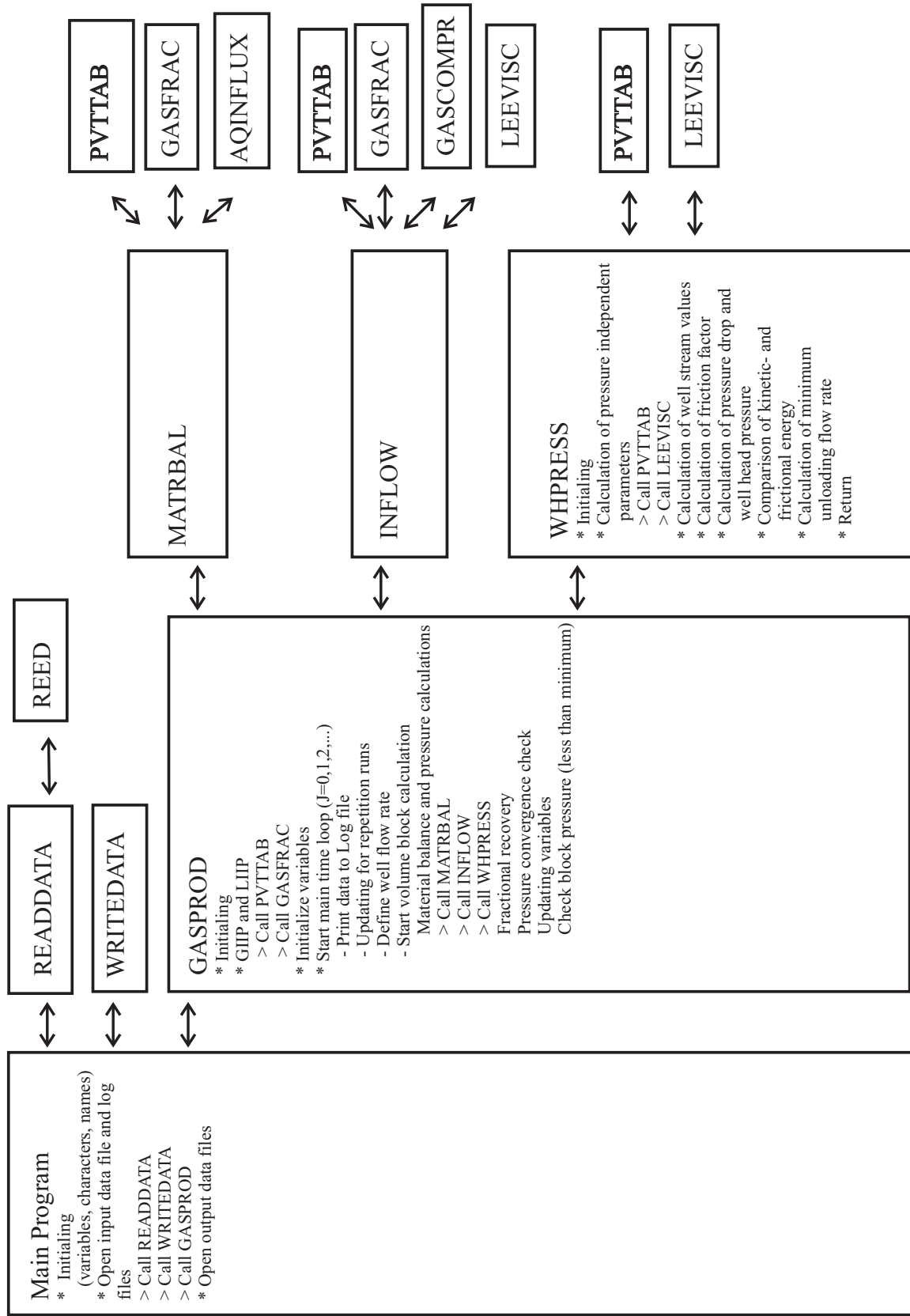


Figure 6.1: Program structure including well-bore flow simulation.

Additionally, - an option is introduced to facilitate whether to run the simulation according to a minimum well-head pressure or, as in the previous cases, to control the simulation by the minimum bottom-hole pressure. This parameter is called **CALCWHP**.

NGASDATA-file

```

*
* **** Start data file NGASDATA.DAT
*
* Data file name (max. 70 characters); text
* 123456789012345678901234567890123456789012345678901234567890
'Project: Natural Gas Reservoir Simulation.'
'Part: Simulation of Material Balance, Radial Gas Flow and Well-Bore
'Flow Mechanics'
* * * *
* **** Program data
*
* DCHCK=1 Data check mode; No material balance is done.
* DCHCK=0 Full simulation. [integer]
* MAXSTEP Number of simulation steps; Program is terminated at
* simulation step NSTEP. [integer]
* NPRINT Number of sequent plotting parameter; Printing to file
* is done for every NPRINT simulation step. [integer]
* SP=1,100 Short LOG printout; Full printout and printing of every
* 1 to 100 time step SP=1 gives a short hand presentation
* of every time-step. [integer]
* *
*          DCHCK  MAXSTEP  NPRINT  SP
*          0        4000    5        5
* * * *
* **** Simulation data:
* *
* PERR      Error limit in pressure calculations. [real]
* GPGERR    Error limit in volume calculations. [real]
* DP        Pressure step in pseudo pressure calculation. [real]
* PREF      Pressure reference in pseudo pressure calculation. [real]
* CAERR     Error limit in calculation of Dietz-factor. [real]
*
*          PERR      GPGERR    DP    PREF    CAERR
*          0.5      1D-07    5.    5.     0.01
* * * *
* **** Volume and block data
* *
* BNAME     Name of individual block, maximum 5 characters. [String]
* VPORINIT  Pore volume of block {=PI*(RADE**2-RADW**2)*THICK*PORO} (Rm3 ) [real].
* RADE      Characteristic radius of block (m). [real]
* RADW      well-bore radius (m). [real]
* THICK     Net vertical thickness of block (m). [real]
*
*          BNAME      VPORINIT    RADE    RADW    THICK
*          'BLK01'    4D+6      350.    0.175  50.
* * * *
* * Block characteristics:
*
* PORO      Porosity of block. [real]
* SWINIT    Initial water saturation [real]

```



```

* PERM      Absolute permeability in block (mD). [real]
* CA        Dietz shape factor (CAcircle=31.62). [real]
* DARCY     Non-Darcy factor. (day/m3) [real]
* SKIN      Skin factor. [real]
*
*          PORO    SWINIT  PERM    CA      DARCY   SKIN  Block no.
*          0.20    0.2     100.   31.62  5.D-06  0.0   1          BLK01
* * *
* *** General reservoir data
* *
* PRS       Initial reservoir pressure (bar). [real]
* TEMP      Initial reservoir temperature (Kelvin). [real]
* PRSSC     Atmospheric pressure (bar). [real]
* TEMPSC    Normal reference temperature (Kelvin). [real]
* COMW      Water compressibility (1/bar). [real]
* COMR      Reservoir compressibility (1/bar). [real]
*
*          PRS     TEMP     PRSSC    TEMPSC    COMW     COMR
*          437.0  392.0    1.01    288.0    4.35D-05  4.5D-05
* * * *
* *** Well data
* QMAX      Maximum well rate (Sm3/day). [real]
*
*          QMAX
*          5.00D+05
* *
* TBP       Time step length (days). [real]
*
*          TBP
*          5.
* *
* CALCWHP   Decides whether production should be controlled by
*           minimum bottom-hole pressure or by minimum well-head
*           pressure. [integer]
*           CALCWHP=0, bottom-hole pressure controls production.
*           CALCWHP=1, well-head pressures controls production.
*
*          CALCWHP
*          1
* *
* BHPM      Minimum bottom-hole pressure (bar). Production is
*           stopped when minimum bottom-hole pressure is
*           reached. [real]
*           (Minimum bottom-hole pressure should be within the
*           range of the PVT data)
* WHPM      Minimum well-head pressure (bar). Production is stopped
*           when minimum well-head pressure is reached. [real]
*
*          BHPM    WHPM
*          50.     20.
* *
* * Well tubing data
*
* WELLGHT   Length of well (m). [real]
* TUBDIAM   Inner diameter of tubing (m). [real]
* TUBRR     Absolute roughness of tubing (m). [real]

```

```

* WDEVANG Deviation angle of wells (degrees). [real]
* TEMPWH Wellhead temperature (Kelvin). [real]
*
*         NB!! If wellhead temperature is the same
*         as reservoir temperature, it must be given
*         a value slightly below reservoir temperature.
*
*         WELLGHT  TUBDIAM  TUBR    WDEVANG  TEMPWH  Block no.
*         3500.    0.200   1.5D-5  0.0     313.    1
* * *
* *** Water data
* *
* WATINF=1 Water influx/production controlled as fraction of production.
*         (Only WPFAC and WEFAC are relevant parameters.) [integer]
* WATINF=2 Water flux from aquifer is included. [integer]
*
*         WATINF
*         1
* *
* WPFAC Water production as fraction of gas production. [real]
* WEFAC Water influx as fraction of gas production. [real]
*         (A non-zero WPFAC has normally to be accompanied
*         by a non-zero WEFAC.)
*
*         WPFAC  WEFAC
*         0.00  0.00      BLK01
* *
* WTYPE=1 Radial aquifer. [integer]
* WTYPE=2 Linear aquifer. [integer]
* WFINITE=1 Finite aquifer. [integer]
* WFINITE=2 Infinite aquifer. [integer]
* WALPHA Angle of sector within which aquifer water
*         encroaches (degree). [real]
* WCOMP Aquifer compressibility coefficient
*         (rock and water) (1/bar). [real]
* WLENGTH Aquifer length (linear aquifers) (m). [real]
* WPERM Aquifer permeability (mD). [real]
* WPORO Aquifer porosity. [real]
* WRADB Radius of aquifer inner boundary (m). [real]
* WRADE Radius of aquifer outer boundary (m). [real]
* WTHICK Aquifer thickness (m). [real]
* WVISC Water viscosity (mPa.s). [real]
* WWIDTH Aquifer width (m). [real]
* *
* WTYPE WFINITE WALPHA WCOMP WLENGTH WPERM WPORO WRADB WRADE WTHICK WVISC WWIDTH
* 1 2 360. 5.D-5 1535. 10.0 0.2 500. 1000. 50. 1.0 1535.
* * * *
* *** PVT data
* *
* NTAB Number of PVT-table elements
*
*         NTAB
*         20
* *
* PRS Pressure [bar]
* TEMP Temperature [K]

```

```

* MWT      Mixture mol weight [g/mol]
* MWTG     Gas mol weight [g/mol]
* MWTL     Liquid mol weight [g/mol]
* GASF     Gas mol fraction
* Z        Gas phase Z-factor
* Z2       Mixture, two-phase Z-factor
*
* PRS      TEMP      MWT      MWTG     MWTL     GASF      Z        Z2       NTAB
445.      392.      26.56  26.56   26.56   0.9517    1.1142  1.1143  1
370.      392.      26.56  26.56   26.56   0.95171   1.0258  1.0258  2
350.      392.      26.57  26.42   90.14   0.95240   1.0035  1.0045  3
320.      392.      26.57  26.19   89.32   0.95349   0.9721  0.9743  4
300.      392.      26.59  26.03   88.19   0.95438   0.9530  0.9556  5
280.      392.      26.61  25.83   87.18   0.95556   0.9356  0.9385  6
260.      392.      26.65  25.61   86.86   0.95705   0.9206  0.9233  7
240.      392.      26.72  25.36   87.52   0.95883   0.9082  0.9102  8
220.      392.      26.81  25.11   89.16   0.96061   0.8986  0.8994  9
200.      392.      26.94  24.88   91.68   0.96259   0.8920  0.8994  10
180.      392.      27.13  24.66   95.05   0.96446   0.8886  0.8910  11
160.      392.      27.38  24.47   99.27   0.96624   0.8885  0.8851  12
140.      392.      27.95  24.30   104.49  0.96783   0.8916  0.8808  13
120.      392.      28.52  24.18   110.81  0.96921   0.8979  0.8807  14
100.      392.      29.33  24.10   118.48  0.97010   0.9073  0.8837  15
80.       392.      30.51  24.08   127.84  0.97050   0.9197  0.8862  16
60.       392.      32.36  24.16   139.47  0.97079   0.9348  0.8864  17
40.       392.      35.59  24.41   154.40  0.97089   0.9524  0.8778  18
1.01     392.      42.00  25.00   185.00  0.97099   0.9900  0.8580  19
1.01     288.      42.00  25.00   185.00  0.95171   0.9900  0.8580  20
* * *

```

6.2 General pressure solution and pressure uncertainty

The general flow equation is written,

$$dp + \frac{M_g p}{\bar{Z} RT} g \cos(\alpha) dy + \frac{\bar{f}}{d_h} \frac{\omega_g^2 \bar{Z} RT}{A^2} \frac{1}{M_g p} dy = 0,$$

and is based on the following assumptions:

- Negligible loss in kinetic energy (as described above).
- Linear well temperature profile, i.e. $T = T_{bh} - (\Delta T/L)y$ and $dy = -(L/\Delta T)dT$.
- Constant well deviation angle: $\alpha = \text{constant}$.
- Constant well cross-section: $A = \text{constant}$.
- Constant z-factor: $\bar{Z} = \text{constant}$.
- Constant friction factor: $\bar{f} = \text{constant}$.

Under these assumption the general flow equation is solved and the pressure solution is written,

$$p = \sqrt{p_{bh}^2 \left(\frac{T}{T_{bh}}\right)^{2K_1} + K_3 T^2 \left[\left(\frac{T}{T_{bh}}\right)^{2(K_1-1)} - 1\right]},$$

where the constants are,

$$K_1 = N_{gp} \frac{T_{bh}}{\Delta T}, \quad K_2 = N_{fp} \frac{p_{bh}^2}{2T_{bh}\Delta T} \quad \text{and} \quad K_3 = \frac{K_2}{K_1 - 1}$$

where the dimensionless numbers are defined,

$$N_{gp} = \frac{M_g g L \cos(\alpha)}{\bar{Z} R T_{bh}} F_w$$

and

$$N_{fp} = \frac{4\bar{Z} f w_g^2 T_{bh} L}{p_{bh}^2 A^2 d_h M_g} F_w.$$

1. Use the pressure solution above and show that the well head pressure can be written,

$$p_{wh} = p_{bh} \sqrt{L1^{E1} + L2(L1^{E2} - 1)},$$

as presented in the "WHPRESS" subroutine. Define the parameters $L1$, $L2$, $E1$ and $E2$.

In both N_{gp} and N_{fp} we use a constant z -factor, even though the z -factor is defined as a function of pressure and is continuously decreasing in the well, from bottom to top. By using an average z -factor, \bar{Z} , we are introducing an error into the pressure calculation, such that there exists an error in the well-head pressure, Δp_{wh} , which is depended of the error in the z -factor ΔZ .

2. Estimate an average z -factor and define the error ΔZ , based on the function $Z = Z(p)$ given in the data file `NGASDATA.DAT`. Use the definition of the average z -factor,

$$\frac{1}{\bar{Z}} = \frac{1}{L} \int_0^L \frac{1}{Z} dy.$$

(Hint: Calculate $Z(p)$ and observe the stepwise change.)

3. Calculate the relative uncertainty in the well head pressure, $\Delta p/p_{wh}$ as function of the relative uncertainty in the z -factor, $\Delta Z/Z$. Use the rules defined by propagation of errors and the following simplified model of the well head pressure,

$$p = a e^{b/Z},$$

where a and b are constants. (Hint: Consult the Lecture Notes and observe that the well head pressure at isothermal well flow is written $p_{wh} = p_{bh} \exp(N_{gp})$.)

4. Use appropriate numbers taken from the data file and the Lecture Note and define the uncertainty in the well head pressure (in bars) as function of the uncertainty in the z-factor.

6.3 Pressure Developments

As a result of including the well bore flow into the simulation model, we now need to differentiate between three different pressures: the average block pressure, the bottom-hole pressure and the well-head pressure. Normal gas production is quite often defined by the pressure needed at the first separator stage. The well-head pressure is therefore associated to a terminal pressure, defining a point of separation between reservoir and process. All processes up to this point can be considered as part of reservoir engineering.

In the data file `NGASDATA.DAT` we are given the choice of running the simulation with a minimum well head pressure or a minimum bottom hole pressure as the threshold pressure. The "CALCWHP" parameter ($\text{CALCWHP} = 0$ or 1) decides whether production is controlled by bottom-hole - or well-head pressure.

5. Use the data given in the `NGASDATA.DAT` as a Base Case simulation model and plot the three pressures as mentioned above (in the same plot). Explain why the well head pressure is declining more towards the end of the well production time. Comment on the pressure difference between the well head pressure and the bottom hole pressure, as function of time.
6. Run a sensitivity on the Base Case model where the average reservoir permeability is reduced by 80%. Plot the three pressure profiles and explain the consequences of reduced permeability. Why is the well head pressure affected by the reservoir permeability?
7. Plot the well head pressure as function of a dip angle equal to 45° and compare with the Base Case model. Use the same well length. Is it right to use the same well length when comparing vertical well flow to the case of inclined well flow?
8. Assume the same reservoir depth as in the Base Case model and a location of the platform some 1500 m north of the position in the Base Case. Plot the well-head pressures and compare it to the Base Case model. Explain the difference observed between the two well-head pressures.
9. Run a sensitivity on the Base Case model where the gas flow rate is reduced to 70%. Compare the two cases and relate the observation to the change in pressure in the well. Is the total energy consumption larger or smaller in the case of reduced well rate?
10. Run a sensitivity on the Base Case model where the well bore diameter is reduced to half its value and plot the well-head pressure. Compare the two pressures. Give a short explanation for the observed pressure difference. What about energy consumption in this case?

6.4 Well Bore Flow Conditions

In this section we are focusing on the conditions for stable well flow. It has been shown that the general pressure solution depends on the fact that the water-cut (the mass fraction of water in the well flow) is small. For a given gas production rate, a minimum unloading rate can be calculated.

11. Use the data contained in the log-file from the Base Case model and plot the minimum unloading rate, the KINETIC VS. FRICTION parameter and the Reynold's number verifying constant friction factor \bar{f} . Are the condition under which the pressure equation was derived, satisfied?
12. Run two sensitivities relative the Base Case where the water production is set to 0.1% and 0.2% of gas flow rate. Plot the well head pressure in the three cases (including the Base Case). Observe the minimum unloading rate in the three cases and present them in the same plot.
13. Run the 0.2% water production case with 0.2% water injection and compare this case with the Base Case. Does water influx have any relevance to the minimum unloading rate in this case?

Project Exercise 7

Project Exercise: Natural Depletion

A new version of the simulation program and data-input file are available for this project exercise. Later in this exercise, under section "7.4 Well Deliverability", you shall use the previous version of the simulation program and the associated data file `NGASDATA.OLD`. (The new data file will not work with the old version of the program or vice versa.)

In the present version of the simulation program, two new options are added. Firstly, more than one well may produce the same block volume and secondly, the gas reservoir may consist of several *independent* blocks, covering the total reserves of gas in the field. The program, now simulates the production under natural depletion where the field gas is confined in separate blocks with no communication between the independent blocks. The volume of independent blocks may vary considerably. Production from these blocks is done, using one, two or several wells per block.

The implementation of new wells and blocks is done simply by adding the characteristic parameters, presented in the data file. Study the `NGASDATA.DAT` file and observe the changes made to the data file in order to allow multi-well and multi-block simulation. Consecutive wells and blocks are added simultaneously. Use the `NGASDATA.DAT` as a Base Case model.

7.1 Simulation of Natural Gas Reservoirs

In this chapter we have added a new sub-routine `PRODRATE` to the simulation program. Generally, the program has been updated to simulate more than one reservoir block and additionally, to produce the gas from more than one well.

7.1.1 Organization of The Simulation Program

The simulation program is now capable of simulating the production of gas from an entire gas field. The gas field is sub-divided into various independent blocks, where one or more wells can be located in any block. In addition to the subroutine `PRODRATE` added, as seen in Figure 7.1, various changes have been implemented into the program in order to support the multi-block and multi-well simulation features.

The `PRODRATE`-subroutine is controlling the well rates with respect to maximum well rate and maximum plateau rate. The field rate is efficiently redistributed

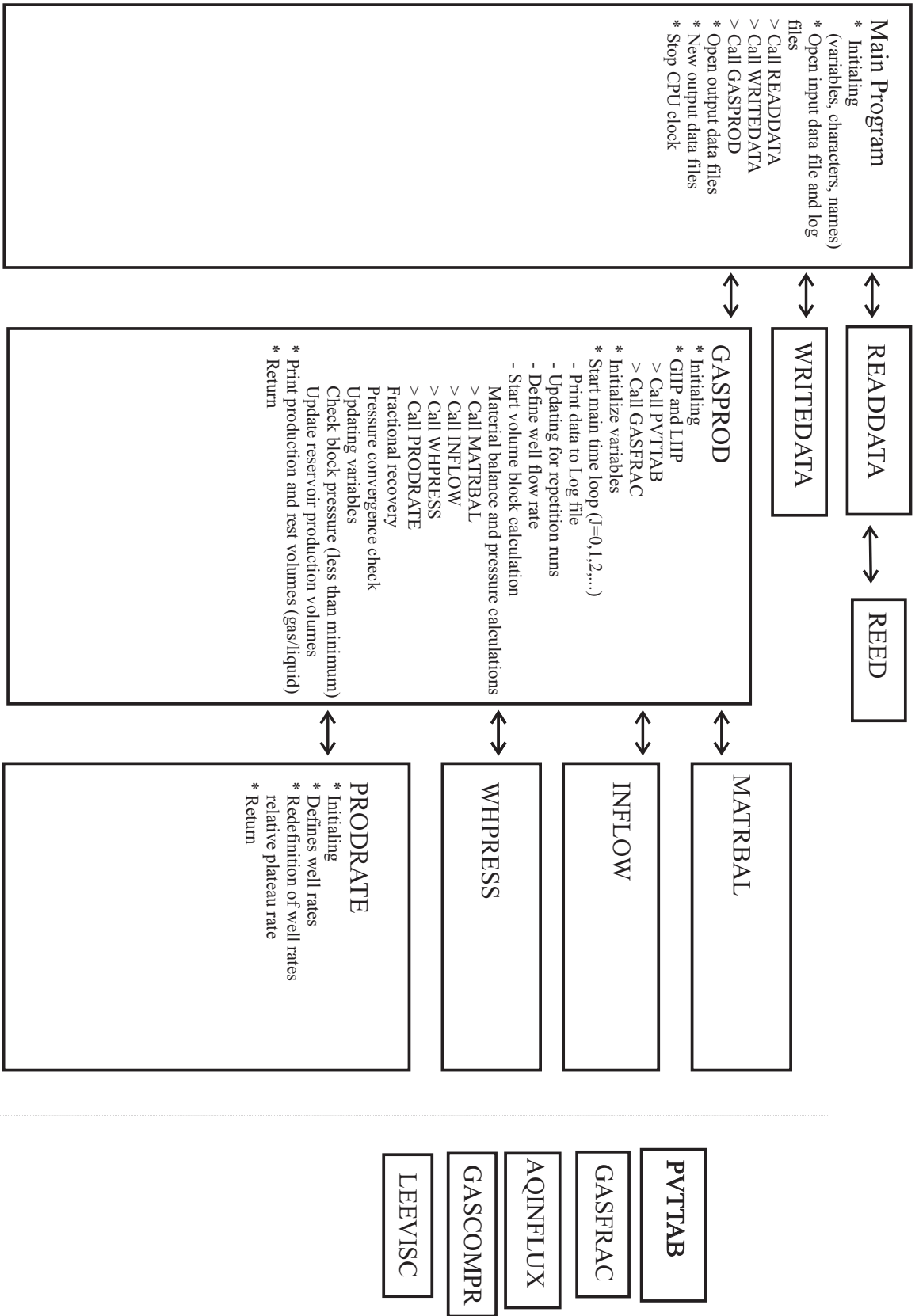


Figure 7.1: Structure for field simulation program.

between the active wells by adjusting the well rates according to the average pressure in various blocks, following a strategy for optimal production which favors balanced production for the whole field. Well rates are adjusted at every time-step and when one well is falling off, due to reduced well deliverability, other wells have their flow rates updated.

A necessary consequence of the modifications made to the simulating program is related to the amount of data printed to output-files. The amount of data presented in the previous simulations have been limited by the production of gas and condensate from only one block and one well. In the present form, the program may simulate gas production from numerous blocks and wells. In order to handle the possibility of an extensive increase in the amount of data available, a new organization of presenting the simulation data is needed. The following listing is presenting the filed data as it was organized and as it is now organized:

Previous Data Organization

The data output-files was organized as follows:

NGASPARM.DAT $t, \bar{p}, p_{bh}, p_{wh}, \bar{p}/Z, W_e, W_p$

NGASPROD.DAT $t, q_{tot}, q_g, G_p, q_L, G_L, G_p/GIIP, G_L/LIIP$

Present Data Organization

The data output-files are organized as follows. Note that NW and NB are the number of wells and blocks simulated, respectively.

PROD-RES.DAT $t, q_{tot}, q_g, G_p, q_L, G_L W_e, W_p, G_p/GIIP, G_L/LIIP$
(Cumulative field data.)

RATE-WLS.DAT $t, q_g^1, q_g^2, q_g^3, \dots, q_g^{NW}$
(Gas well rates from NW wells.)

PROD-WLS.DAT $t, G_p^1, G_p^2, G_p^3, \dots, G_p^{NW}$
(Cumulative gas production from NW wells.)

PROD-GAS.DAT $t, G_p^1, G_p^2, G_p^3, \dots, G_p^{NB}$
(Cumulative gas production from NB blocks.)

PROD-LQD.DAT $t, G_L^1, G_L^2, G_L^3, \dots, G_L^{NB}$
(Cumulative liquid production from NB blocks.)

PRES-BLK.DAT $t, (\bar{p}, \bar{p}/z)^1, (\bar{p}, \bar{p}/z)^2, (\bar{p}, \bar{p}/z)^3, \dots, (\bar{p}, \bar{p}/z)^{NB}$
(Average pressure and reduced pressure in NB blocks.)

PRES-BH.DAT $t, p_{bh}^1, p_{bh}^2, p_{bh}^3, \dots, p_{bh}^{NW}$
(Bottom-hole pressure in NW wells.)

PRES-WH.DAT $t, p_{wh}^1, p_{wh}^2, p_{wh}^3, \dots, p_{wh}^{NW}$
(Well-head pressure in NW wells.)

RATE-GAS.DAT $t, q_g^1, q_g^2, q_g^3, \dots, q_g^{NB}$
(Gas flow rate in NB blocks.)

RATE-LQD.DAT $t, q_L^1, q_L^2, q_L^3, \dots, q_L^{NB}$
(Liquid flow rate in NB blocks.)

WATER-WE.DAT $t, W_e^1, W_e^2, W_e^3, \dots, W_e^{NB}$
(Cumulative water influx into NB blocks.)

WATER-WP.DAT $t, W_p^1, W_p^2, W_p^3, \dots, W_p^{NB}$
(Cumulative water production from NB blocks.)

7.1.2 The Data Input-File

The data input-file has been modified in order to allow for multi-well, multi-block simulation. Several self explainable new parameters have been introduced. It is therefore more important now than before to identify the various parameters with respect to which group they belong to, i.e. if they are elements of the block- or the well group. In the case when the number of blocks is different to the number of wells, we have to know the correct numbering of the parameters in order to know the number of data-lines to be included for that particular parameter. Another important point is that, regardless if the input-data is going to be used in the simulation process or not, a complete data-set has to be included in the data-file. This has something to do with how data is read from the `NGASDATA.DAT` file.

NGASDATA-file

```

*
* **** Start data file NGASDATA.DAT
*
* Data file name (max. 70 characters); text
* 1234567890123456789012345678901234567890123456789012345678901234567890
* 'Project: Natural Gas Reservoir Simulation'
* 'Part: Natural Depletion'
* 'Extension of program with multi well - and multi block options'
* * * *
* *** Program data
*
* DCHCK=1 Data check mode; No material balance is done.
* DCHCK=0 Full simulation. [integer]
* MAXSTEP Number of simulation steps; Program is terminated at
* simulation step NSTEP. [integer]
* NPRINT Number of sequenced plotting parameter; Printing to file
* is done for every NPRINT simulation step. [integer]
* SP=1,100 Short LOG printout; Full printout and printing of every
* 1 to 100 time step SP=1 gives a short hand presentation of
* every time-step. [integer]
* *
*
* DCHCK MAXSTEP NPRINT SP
* 0 4000 4 2
* * *
* *** Simulation data:
* *

```

```

* PERR      Error limit in pressure calculations. [real]
* GPGERR    Error limit in volume calculations. [real]
* DP        Pressure step in pseudo pressure calculation. [real]
* PREF      Pressure reference in pseudo pressure calculation. [real]
* CAERR     Error limit in calculation of Dietz-factor. [real]
*
*          PERR      GPGERR      DP      PREF      CAERR
*          0.5       1D-07       10.    10.       0.01
* * * *
* *** Volume and block data
* *
* NBLOCK    Number of blocks in the model (max.70 blocks). [integer]
*
*          NBLOCK
*          2
* *
* BNAME     Name of individual block, maximum 5 characters. [String]
* VPORINIT  Pore volume of block {=PI*(RADE**2-RADW**2)*THICK*PORO} (Rm3 ) [real].
* RADE      Characteristic radius of block (m). [real]
* RADW      well-bore radius (m). [real]
* THICK     Net vertical thickness of block (m). [real]
*
*          BNAME      VPORINIT      RADE      RADW      THICK
*          'BLK01'    5.4D+6        338.     0.175    60.
*          'BLK02'    4.05D+6        293.     0.175    60.
* * * *
* * Block characteristics:
*
* PORO      Porosity of block. [real]
* SWINIT    Initial water saturation [real]
* PERM      Absolute permeability in block (mD). [real]
* CA        Dietz shape factor (CAcircle=31.62). [real]
* DARCY     Non-Darcy factor. (day/m3) [real]
* SKIN      Skin factor. [real]
*
*          PORO      SWINIT    PERM      CA        DARCY    SKIN    Block no.
*          0.25     0.19     200.     30.88    1.D-06  0.0    1          BLK01
*          0.25     0.17     300.     10.00    1.D-06  0.0    2          BLK02
* *
* *** General reservoir data
* *
* PRS       Initial reservoir pressure (bar). [real]
* TEMP      Initial reservoir temperature (Kelvin). [real]
* PRSSC     Atmospheric pressure (bar). [real]
* TEMPSC    Normal reference temperature (Kelvin). [real]
* COMW      Water compressibility (1/bar). [real]
* COMR      Reservoir compressibility (1/bar). [real]
*
*          PRS       TEMP      PRSSC     TEMPSC    COMW      COMR
*          437.0    392.0    1.01     288.0    4.35D-05  4.5D-05
* * * *
* *** Well data
*
* NWELLS    Total number of wells in the reservoir (max.60 wells). [integer]
*
*          NWELLS

```

```

3
*
* TSTART Start up time (in days) for sequencing wells. Different wells may start
* up at the same time (day). Start up time (day) is not allocated to any
* particular well. [real]
*
*      1  2  3  4  5  6  7  8  9  10  11  12  13  14  15
*      0. 90. 180.
* *
* WIB The location of well in block is specified by the block number
* where the next sequenced well is located. [integer]
*
*      1  2  3  4  5  6  7  8  9  10  11  12  13  14  15      Well number
*      1  2  1                                          WIB (Block number)
* *
* QMIN Minimum well rate (Sm3/day). [real]
* QMAX Maximum well rate (Sm3/day). [real]
* QPLAT Plateau reservoir rate (Sm3/day) [real]
*
*      QMIN      QMAX      QPLAT
*      2.5D+05    8.0D+05    12.0D+05
* *
* TBP Time step length in build up period (days). [real]
* TPP Time step length in production period (days). [real]
* TDP Time step length in decline period (days). [real]
*
*      TBP      TPP      TDP
*      5.      10.      3.
* *
* CALCWHP Decides whether production should be controlled by minimum
* bottom-hole pressure or by minimum well-head pressure. [integer]
* CALCWHP=0, bottom-hole pressure controls production.
* CALCWHP=1, Well-head pressures controls production.
*
*      1  2  3  4  5  6  7  8  9  10  11  12  13  14  15      Well number
*      1  1  1                                          CALCWHP
* *
* BHPM Minimum bottom-hole pressure (bar). Production is stopped
* when minimum bottom-hole pressure is reached. [real]
* (Minimum bottom-hole pressure should be within the range
* of the PVT data)
* WHPM Minimum well-head pressure (bar). Production is stopped when
* minimum well-head pressure is reached. [real]
*
*      BHPM      WHPM
*      50.      20.
* *
* * Well tubing data
*
* WELLGHT Length of well (m). [real]
* TUBDIAM Inner diameter of tubing (m). [real]
* TUBR Absolute roughness of tubing (m). [real]
* WDEVANG Deviation angle of wells (degrees). [real]
* TEMPWH Well-head temperature (Kelvin). [real]
*
* NB!! If well-head temperature is the same as reservoir temperature,

```

```

*           it must be given a value slightly below reservoir temperature.
*
*           WELLGHT  TUBDIAM  TUBR    WDEVANG  TEMPWH  WELL NO.
*           3700.    0.150    1.5D-5  0.0      313.    1
*           3703.    0.150    1.5D-5  0.0      313.    2
*           3703.    0.150    1.5D-5  0.0      313.    3
* * * *
* *** Water data
* *
* WATINF=1 Water influx/production controlled as fraction of
*           production. [integer]
* WATINF=2 Water flux from aquifer is included. [integer]
*           (Only WPFRAC and WEFAC are relevant parameters.)
* WPFRAC   Water production as fraction of gas production. [real]
* WEFAC    Water influx as fraction of gas production. [real]
*           (A non-zero WPFRAC has normally to be accompanied
*           by a non-zero WEFAC.)
*
*           WATINF  WPFRAC  WEFAC
*           2       0.0    0.0    BLK01
*           2       0.0    0.0    BLK02
* *
* WTYPE=1   Radial aquifer. [integer]
* WTYPE=2   Linear aquifer. [integer]
* WFINITE=1 Finite aquifer. [integer]
* WFINITE=2 Infinite aquifer. [integer]
* WALPHA    Angle of sector within which aquifer water encroaches
*           (degree). [real]
* WCOMP     Aquifer compressibility coefficient (rock and water)
*           (1/bar). [real]
* WLENGTH   Aquifer length (linear aquifers) (m). [real]
* WPERM     Aquifer permeability (mD). [real]
* WPORO     Aquifer porosity. [real]
* WRADB     Radius of aquifer inner boundary (m). [real]
* WRADE     Radius of aquifer outer boundary (m). [real]
* WTHICK    Aquifer thickness (m). [real]
* WVISC     Water viscosity (mPa.s). [real]
* WWIDTH    Aquifer width (m). [real]
* *
* WTYPE WFINITE WALPHA WCOMP WLENGTH WPERM WPORO WRADB WRADE WTHICK WVISC WWIDTH
* 1     2       90.   5.D-4 1535.  200.0 0.2   500.  1000. 120.  1.0 1535.
* 1     2       180.  5.D-4 1535.  200.0 0.2   500.  1000. 120.  1.0 1535.
* * * *
* *** PVT data
* *
* NTAB      Number of PVT-table elements
*
*           NTAB
*           20
* *
* PRS       Pressure [bar]
* TEMP      Temperature [K]
* MWT       Mixture mol weight [g/mol]
* MWG       Gas mol weight [g/mol]
* MWL       Liquid mol weight [g/mol]
* GASF      Gas mol fraction

```

| * | Z | Gas phase Z-factor | | | | | | | |
|---|------|-----------------------------|-------|-------|--------|---------|--------|--------|------|
| * | Z2 | Mixture, two-phase Z-factor | | | | | | | |
| * | | | | | | | | | |
| * | PRS | TEMP | MWT | MWTG | MWTL | GASF | Z | Z2 | NTAB |
| | 445. | 392. | 26.56 | 26.56 | 26.56 | 0.9517 | 1.1142 | 1.1143 | 1 |
| | 370. | 392. | 26.56 | 26.56 | 26.56 | 0.95171 | 1.0258 | 1.0258 | 2 |
| | 350. | 392. | 26.57 | 26.42 | 90.14 | 0.95240 | 1.0035 | 1.0045 | 3 |
| | 320. | 392. | 26.57 | 26.19 | 89.32 | 0.95349 | 0.9721 | 0.9743 | 4 |
| | 300. | 392. | 26.59 | 26.03 | 88.19 | 0.95438 | 0.9530 | 0.9556 | 5 |
| | 280. | 392. | 26.61 | 25.83 | 87.18 | 0.95556 | 0.9356 | 0.9385 | 6 |
| | 260. | 392. | 26.65 | 25.61 | 86.86 | 0.95705 | 0.9206 | 0.9233 | 7 |
| | 240. | 392. | 26.72 | 25.36 | 87.52 | 0.95883 | 0.9082 | 0.9102 | 8 |
| | 220. | 392. | 26.81 | 25.11 | 89.16 | 0.96061 | 0.8986 | 0.8994 | 9 |
| | 200. | 392. | 26.94 | 24.88 | 91.68 | 0.96259 | 0.8920 | 0.8994 | 10 |
| | 180. | 392. | 27.13 | 24.66 | 95.05 | 0.96446 | 0.8886 | 0.8910 | 11 |
| | 160. | 392. | 27.38 | 24.47 | 99.27 | 0.96624 | 0.8885 | 0.8851 | 12 |
| | 140. | 392. | 27.95 | 24.30 | 104.49 | 0.96783 | 0.8916 | 0.8808 | 13 |
| | 120. | 392. | 28.52 | 24.18 | 110.81 | 0.96921 | 0.8979 | 0.8807 | 14 |
| | 100. | 392. | 29.33 | 24.10 | 118.48 | 0.97010 | 0.9073 | 0.8837 | 15 |
| | 80. | 392. | 30.51 | 24.08 | 127.84 | 0.97050 | 0.9197 | 0.8862 | 16 |
| | 60. | 392. | 32.36 | 24.16 | 139.47 | 0.97079 | 0.9348 | 0.8864 | 17 |
| | 40. | 392. | 35.59 | 24.41 | 154.40 | 0.97089 | 0.9524 | 0.8778 | 18 |
| | 1.01 | 392. | 42.00 | 25.00 | 185.00 | 0.97099 | 0.9900 | 0.8580 | 19 |
| | 1.01 | 288. | 42.00 | 25.00 | 185.00 | 0.95171 | 0.9900 | 0.8580 | 20 |

* * *

7.2 Tubing Flow Performance and Bottom-Hole Pressure

In the special case of single phase gas flow defined by; no temperature gradient in the well, constant cross-section, constant friction factor and z-factor, - the well head pressure is written

$$p_{wh} = p_{bh} \sqrt{e^{-2N_{gp}} + \frac{N_{fg}}{2N_{gp}} (e^{-2N_{gp}} - 1)}.$$

In the process of inverting this equation, expressing the bottom hole pressure as function of the well head pressure, we used a Taylor expansion where only the two first terms were considered. The bottom hole pressure was then written

$$p_{bh} \simeq p_{wh} \sqrt{e^{2N_{gp}} + \frac{N_{fg}}{2N_{gp}} e^{2N_{gp}} (e^{2N_{gp}} - 1)}. \quad (7.1)$$

The error made in the above approximation is defined by the first term not included in the approximation. In a Taylor expansion

$$(1 + x)^{-1} = 1 - x + x^2 - x^3 + \dots, \quad x < 1,$$

the error done in approximating $(1 + x)^{-1} \simeq 1 - x$, is given by

$$\frac{x^2}{(1 + x)^{-1}} = (1 + x)x^2.$$

1. Use the Taylor expansion in the example above and define the error inherent in the approximation giving the bottom hole pressure in Eq. 7.1.
2. Use the values for N_{gp} and N_{fg} previously presented, and find the error given in %.

7.3 Multi Well and Multi Block Simulation

In the data file `NGASDATA.DAT`, 3 wells are used to produce the gas contained in 2 blocks. The first and third wells are producing from Block 1 and the second well is producing from Block 2. The start up times for the three consecutive wells are after 0, 90 and 180 days. Look up the data in the input file `NGASDATA.DAT`.

3. Plot the gas production: the total gas production and the production of gas from Well 1, 2 and 3.
4. Make a plot showing the total gas rate compared with the gas rate from the three wells.
5. Plot the block rate compared to the total gas rate.
6. Finally, show the mean pressure development in the blocks, the bottom-hole pressure and the well-head pressure in the wells.

7.4 Well Deliverability

We have previously learned that there exists a minimum unloading flow rate that is the lower limit for practical well rates. This lowest flow rate is related to the terminal gas-molecule velocity, needed to lift any oil or water droplet dispersed in the gas (or prevent them to fall in the well stream).

On the other hand, a maximum well rate can be derived, simply by considering the general formula of the well head pressure

$$p_{wh} = p_{bh} \sqrt{\left(\frac{T_{wh}}{T_{bh}}\right)^{2K_1} + K_3 \left(\frac{T_{wh}}{p_{bh}}\right)^2 \left[\left(\frac{T_{wh}}{T_{bh}}\right)^{2(K_1-1)} - 1\right]},$$

where the numeric value of the argument under the square root sign has to be positive (this observation has been presented in an earlier lecture for a slightly more simplified example of well flow). The maximum well rate as defined above, is the largest rate the well can handle with respect to typical well and gas parameters, such as friction, gas composition and others.

In practical situations however, the maximum flow rate capacity of the well is defined by the reservoir inflow profile and the well tubing profile in combination. The maximum well flow rate is defined as the gas rate that creates a pressure drop in the reservoir Δp_{inflow} and a pressure drop in the well tube Δp_{tube} , equal to the maximum pressure drop imposed on the system, i.e.

$$\Delta p_{\text{inflow}} + \Delta p_{\text{tube}} \leq \bar{p} - p_{wh,\text{min}}.$$

In the present exercise, we will define the maximum flow rate capacity, given a chosen set of parameters. The practical calculation of bottom hole pressure as function of well rate is more readily done using the simulation program from the previous exercise. The data file `NGASDATA.OLD` should be used as input file in these simulations. NB: Make a subdirectory under your present directory and carry out the simulations there. The `NGASDATA.OLD` has to be renamed to `NGASDATA.DAT` before it can be used as data input file in the simulations. Check that the well diameter is 0.15 m, the reservoir permeability is 10 mD and the pore volume is $10 \cdot 10^6 \text{Rm}^3$, in the data input file.

7. Run the program with different choices of well rate q , as given in the table below.

| q [Sm^3/day] | 0 | 3.5 | 5.0 | 7.0 | 9.0 | 12.0 | 16.0 | |
|----------------------------------|-----|-----|-----|-----|-----|------|------|----------------|
| \bar{p} [bar] | 400 | | | | | | | p_{bh} [bar] |
| \bar{p} [bar] | 300 | | | | | | | p_{bh} [bar] |
| \bar{p} [bar] | 200 | | | | | | | p_{bh} [bar] |
| \bar{p} [bar] | 100 | | | | | | | p_{bh} [bar] |
| $p_{wh,\text{min}}$ [bar] | | | | | | | | |

Notice that the rates are multiplied by 10^5 ; e.g. $3.5 \cdot 10^5$.

First run the program with a well rate of $3.5 \cdot 10^5 \text{Sm}^3/\text{day}$. Scan the log-file and note down the bottom hole pressure at the simulation step closest to the mean pressure equal to 400 bar. Do the same for the mean pressure equal to 300 bar and fill in the table above. The minimum well head pressure is given by the last time step.

Use the data in the table above and plot the well inflow performance $p_{bh} = p_{bh}(q)$. There should be four curves characterizing the well inflow performance.

Plot the minimum well head pressure $p_{wh,\text{min}}$ for the six choices of well rate data. Use the same plot.

8. Fit a trend through the data points in the plot as above. Use polygonal fit of order 2. Extend the fit to the right-hand side in such a way as for the four data series to cross the extended minimum well head pressure data.
9. Plot the well deliverability based on the data contained in the plot above, where the maximum well rate is defined by the intersection between the well inflow curves and the minimum well head pressure. The well deliverability plot is defined through the table

| \bar{p} [bar] | q_{max} [Sm^3/day] |
|-----------------|---|
| 100 | |
| 200 | |
| 300 | |
| 400 | |

Fit a trend through the data points and extend the fit to the left-hand side, approaching the zero well rate limit and you have constructed the well deliverability curve!

7.5 Gas Production From 3 Independent Reservoir Blocks

We shall in this section, study the gas - condensate production from a reservoir of 3 individual blocks. The reservoir is first produced using 3 wells, where the time interval between up-start of new wells are 80 days, i.e. from the up-start of the previous well to the up-start of the present well. Secondly, we will look at the production from 4 wells from the same reservoir. Lastly, the effect of aquifer is studied in the case of 4 active wells.

The limiting well rates are; $q_{min} = 2.5 \cdot 10^5 Sm^3/day$, $q_{max} = 8.0 \cdot 10^5 Sm^3/day$ and $q_{plateau} = 12.0 \cdot 10^5 Sm^3/day$. All wells are producing against a minimum well head pressure of 30 bar.

The block bulk volumes can be derived from the Figure 7.2. With an average porosity of 25% for all blocks, the initial hydrocarbon pore volume can be readily calculated. The block thickness is 60 meters for all blocks and the characteristic block radius is found, using the formula in the data input file. The average well radius is equal to 0.15 meter.

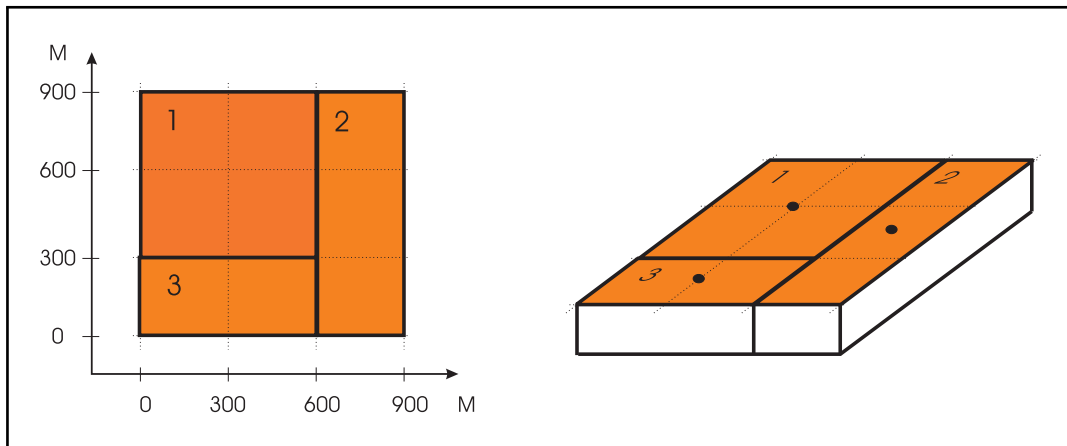


Figure 7.2: Gas - condensate reservoir consisting of three independent volume blocks.

The three consecutive wells are located in blocks with increasing gas content, in order to secure optimum gas production. The wells are connected to a platform located directly on top of Well 1 (centre position in Block 1). The reservoir depth for all blocks is 3700 meters, measured from the platform and down to the reservoir (vertical distance). The average reservoir permeability and initial water saturation are given in the table below.

| Block name | k [mD] | S_{wi} [%] |
|------------|--------|--------------|
| 1 | 200 | 19 |
| 2 | 300 | 17 |
| 3 | 150 | 20 |

The well skin is assumed to be zero in all wells and the non-Darcy factor is $1 \cdot 10^{-6} \text{ day/m}^3$ in all cases. The Dietz shape factors can be evaluated from the shape of the drainage areas.

10. Use the information presented above and complete the data input file for this Base Case scenario. Use the new simulation program.
11. Present a plot showing the cumulative gas production, together with the reservoir gas rate.
12. Plot the reservoir gas rate and the well rates in the same plot. Define the length of the plateau period.

The same reservoir as above is now produced using 4 wells, located as indicated in Figure 7.3.

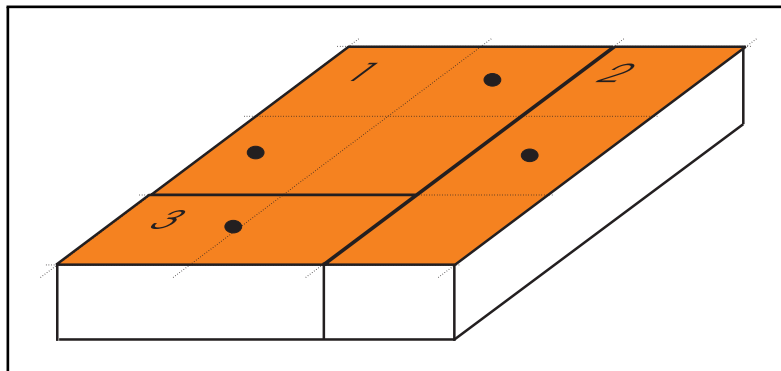


Figure 7.3: Producing the reservoir using four wells.

13. Update the data file with a fourth well, where the well characteristics are the same as for Well 1, but the location is different and in accordance with Figure 7.3.
14. Plot the reservoir gas rate and the well rates and define the relative change in the plateau length. Compare also the cumulative production to the previous case. Does the plateau rate decrease or increase?
15. Compare the gas rate from Block 1 to the previous case. Is there any difference in the cumulative block production?

Study the influence of a possible aquifer relative to gas production from the reservoir. The aquifer is assumed to be of infinite radial dimension. The aquifer water data is partly presented in Figure 7.4. Additionally, the water compressibility is $0.5 \cdot 10^{-4} \text{ bar}^{-1}$ and the water viscosity is $1.0 \text{ mPa} \cdot \text{s}$. The aquifer permeability is 200 mD and the porosity is 20 %. The aquifer thickness is on average twice the reservoir thickness. The "WRADB" should be comparable to the appearing block radius.

16. Run the four well case with aquifer present and compare the cumulative production of gas to the case above (without aquifer).

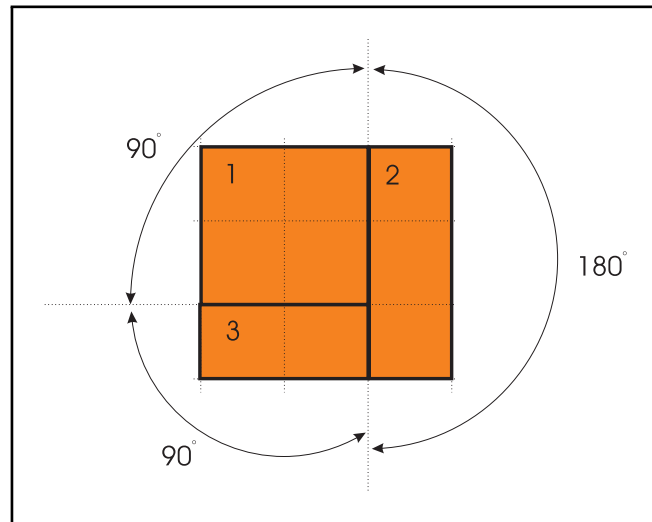


Figure 7.4: Top view of drainage and aquifer.

17. Compare the water influx for the three blocks and plot the cumulative water influx in the same plot.
18. Compare the mean pressure development for Block 2 with the previous case.
19. Plot the bottom-hole pressure in all three blocks.
20. Copy and then patch the top part of the log-file NGASLOG.DAT in to the report. Copy down to the section starting with `*** PVT- and simulation data`.

Send me a copy of your report!

Project Exercise 8

Project Exercise: Field Simulation

The field simulations introduced in this exercise are done on the basis of the simulation program `NGASSIM.EXE` and the data file `NGASDATA.DAT` from the previous exercise. Copy these two files to the new subdirectory "Field Simulation". The data file is currently going to be up-dated through information contained in this exercise.

The field example in this exercise is taken from Sleipner Vest, a North Sea gas-condensate reservoir, located in the Norwegian sector approximately 240 km west-southwest of Stavanger. Sleipner Vest and Sleipner Øst are together one of the largest gas-condensate fields in the North Sea, where the gas in Sleipner Vest is somewhat leaner compared to the gas in Sleipner Øst. The PVT characteristics of the gas in Sleipner Vest are represented by the data given in the data-input file. The two fields are mainly located in block 15/9 , as shown in Figure 8.1.

In this exercise you are asked to include the necessary data (to be provided later in this text), to carry out the simulation of gas production from the Beta-region in Sleipner Vest (see Figure 8.1 for location of the Beta-region). As part of the simulation process, it is important to evaluate the potential for gas production from the region, i.e. the location of wells and the sequence of well locations. Another important issue is to take steps to optimize well production, by carefully considering the plateau length and the block pressure developments. Estimating the minimum number of wells needed to drain a major fraction of the gas, is an example of another important consideration. On the other hand, the aquifers connected to Sleipner Vest are expected to be small and of minor significance to the gas production. Aquifers and water production are therefore not included in these simulations.

8.1 General Reservoir Description

The structure of the Sleipner Vest field is created through a complex history of tectonic movements which started during the deposition of the Hugin formation. These movements reached a maximum at the late Jurassic age, resulting in a very complex fault pattern which have separated the gas in many fault blocks. The complex fault pattern is playing a dominant role with respect to flow patterns in the reservoir, depending on whether or not there are communication across fault planes.

The problem of faults and their role as barriers to flow is one of the most important

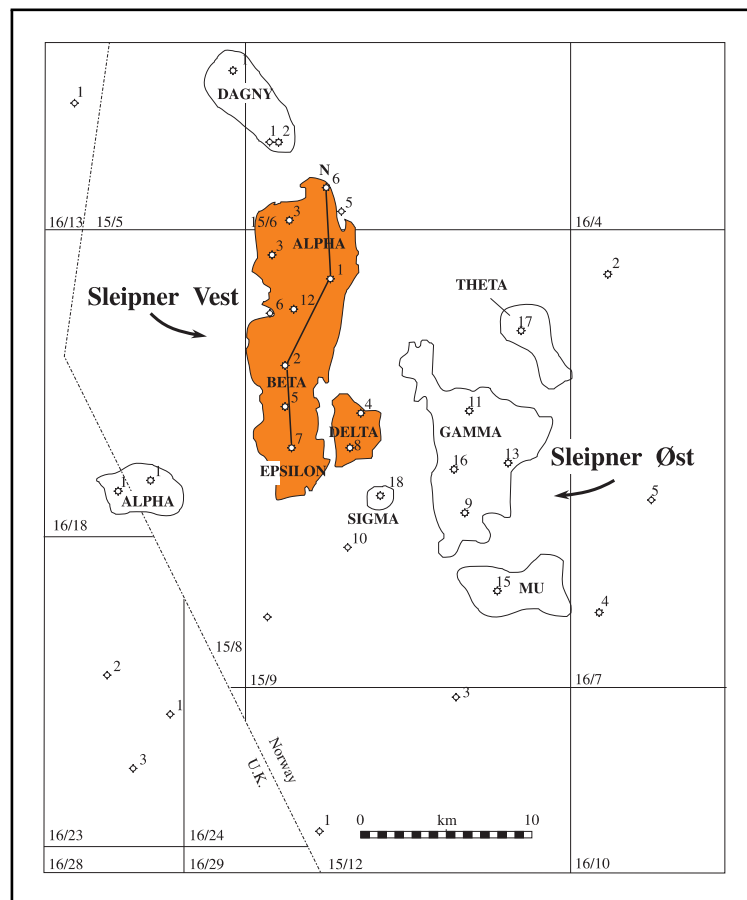


Figure 8.1: Sleipner Vest and Sleipner Øst located in the North Sea, west of Stavanger.

parameters for the development of the Sleipner Vest field. Communication through the minor faults are expected to occur, but their impact on the field development is connected with great uncertainty. It is expected that the major faults are sealing, but with a possibility of communication at high pressure difference across faults.

The Sleipner Vest field consists of 5 main regions, Alpha North, Alpha South, Beta, Epsilon and Delta. All regions are further divided into blocks. The Beta region consists of 38 blocks divided along minor and major fault barriers. The Beta-region is shown in Figure 8.2 on a square grid with dimension 1 km \times 1 km. The Platform is anchored above Block 19. The hydrocarbons in these blocks are encountered in sandstone of Middle Jurassic age at a depth of about 3500 m MSL. The thickness of the reservoir in the Beta-region, is varying up to maximum 220 meters.

8.2 Description of Parameters

In order to up-date the data file `NGASDATA.DAT`, quite a number of new lines have to be included. It is therefore appropriate to call for some prudence in the process of adding all this new information to the old data file. It could therefore pay off to load the new information in bulks, i.e. first introduce all data related to the new *blocks* and then

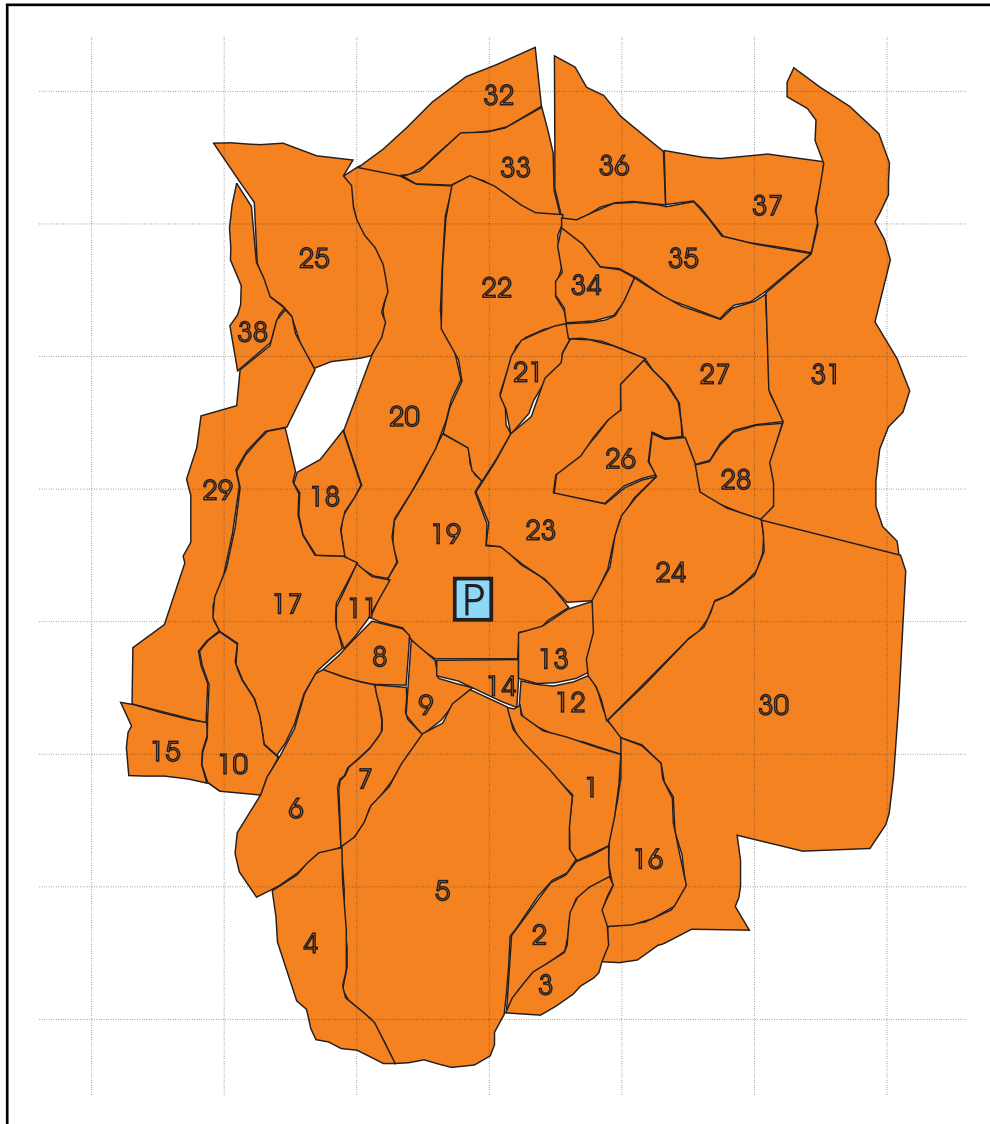


Figure 8.2: Beta-region in the Sleipner Vest field, subdivided into 38 gas blocks. Square grid dimension; 1 km \times 1 km.

load the information about the *wells*. The program NGASSIM.EXE should be run in a data check mode, DCHCK=1, as often as possible during the process of data loading. It is a clear weakness with the program, as it is working now, that it does not respond constructively when data file errors are being detected. It can therefore be quite difficult to locate what is actually wrong, when an error in the data file occurs.

As seen from Figure 8.2, a total number of 38 blocks constitute the Beta-region. The maximum number of wells in the field region is decided to be 15, while the minimum number needed, is set to 8 wells. There is therefore not one well per block and consequently, the gas contained in those blocks with no well will not be produced. The block data needed for these simulations is contained in Table 8.1. Please notice that the block volume "VPORINIT" is tabulated in 10^7 Rm^3 and has to be converted to Rm^3 in

the data file. The "Simulation data" and the "General reservoir data" are maintained as already presented in the data file. When it comes to the "Water data", it has already been said that the aquifer is of minor importance to the production of gas from the Beta-region and therefore no water influx or water production is included in these simulations. Even so, it is necessary to add one line of information both in the case of WPFAC/WEFAC and for the general aquifer data, for each gas block in the region!

The well data is included according to the number of wells being simulated. In the case of 5 consecutive wells, the first and second is located in Block 5, the third in Block 19 and the fourth in Block 17. The fifth and last well is located in Block 22. The "Well tubing data" for these wells are listed in Table 8.2. It is important to notice that the well length and the well angle, the dip angle, both are dependent on the location of the block relative to the platform. For simplicity, we assume all wells to be located in the centre of the block and consequently well length and dip angle are calculated accordingly.

In these simulations we will assume the well start up time to be defined by a regular time interval between wells, equal to 90 days.

The Well In Block (WIB) parameter defines the block number, where the wells are located. In the case of five wells located as defined above the WIB parameters are 5, 5, 19, 17 and 22, for wells 1 to 5.

Since we in these simulation are producing from realistic reservoir gas volumes, it is necessary to adjust the flow rates involved. The minimum well rate is set to $0.2 \text{ MSm}^3/\text{day}$ and the maximum rate is $3.0 \text{ MSm}^3/\text{day}$. The plateau rate is $12.0 \text{ MSm}^3/\text{day}$. Similarly, since the time span of production is much larger than in previous simulations, we also decide to modify the individual time step lengths, using 10 days in the build-up period, 30 days in the plateau period and 3 days in the decline period.

Finally, all wells are producing against a minimum well head pressure of 30 bars.

Prior to running the program it could be advantageous to get some kind of overview of the input data.

1. Use EXCEL and create a histogram showing the block volume as function of block number. Add also the cumulative volume of the region, to the plot.
2. Identify the block volumes in four groups, where the first group contain the block with volume greater than 20 GSm^3 , the second group with block volumes less than 20 GSm^3 and greater than 8 GSm^3 , the third group of blocks with volumes less than 8 GSm^3 and greater than 4 GSm^3 and the last group with block volumes less than 4 GSm^3 . Let this identification of block volumes be a guideline for the work of locating those blocks where wells should be located.

8.3 Drainage Strategies

At this point in time we have a reservoir of 38 individual gas blocks from where we want to produce a maximum fraction the reserves with a minimum number of wells. In reality, each new production well located on the field has to be justified by the additional amount of gas it can produce. Only wells that produce "extra" gas will be drilled and

Table 8.1: Block data for 38 blocks in the Beta-region

| BNAME | VPORINIT [$10^7 Rm^3$] | RADE [m] | RADW [m] | THICK [m] | PORO - | SWINIT - | PERM [mD] | CA - | DARCY [day/m^3] | SKIN |
|-------|-----------------------------|-------------|-------------|--------------|-----------|-------------|--------------|---------|------------------------|------|
| B01 | 3.569 | 600. | 0.175 | 130. | 0.18 | 0.13 | 200. | 9. | 5.D-06 | 0.0 |
| B02 | 2.301 | 450. | 0.175 | 125. | 0.17 | 0.13 | 200. | 5. | 5.D-06 | 0.0 |
| B03 | 0.743 | 450. | 0.175 | 130. | 0.17 | 0.13 | 200. | 5. | 5.D-06 | 0.0 |
| B04 | 2.944 | 800. | 0.175 | 135. | 0.17 | 0.14 | 200. | 17. | 5.D-06 | 0.0 |
| B05 | 27.908 | 2200. | 0.175 | 130. | 0.18 | 0.14 | 200. | 23. | 5.D-06 | 0.0 |
| B06 | 5.127 | 950. | 0.175 | 145. | 0.18 | 0.14 | 200. | 11. | 5.D-06 | 0.0 |
| B07 | 2.723 | 500. | 0.175 | 145. | 0.18 | 0.13 | 200. | 9. | 5.D-06 | 0.0 |
| B08 | 1.454 | 650. | 0.175 | 155. | 0.18 | 0.13 | 200. | 31. | 5.D-06 | 0.0 |
| B09 | 1.737 | 600. | 0.175 | 150. | 0.18 | 0.13 | 200. | 28. | 5.D-06 | 0.0 |
| B10 | 1.690 | 650. | 0.175 | 140. | 0.18 | 0.14 | 200. | 9. | 5.D-06 | 0.0 |
| B11 | 1.248 | 400. | 0.175 | 140. | 0.18 | 0.13 | 200. | 28. | 5.D-06 | 0.0 |
| B12 | 2.062 | 650. | 0.175 | 150. | 0.18 | 0.13 | 200. | 30. | 5.D-06 | 0.0 |
| B13 | 1.829 | 650. | 0.175 | 150. | 0.18 | 0.13 | 200. | 31. | 5.D-06 | 0.0 |
| B14 | 1.472 | 350. | 0.175 | 130. | 0.18 | 0.13 | 200. | 23. | 5.D-06 | 0.0 |
| B15 | 0.006 | 650. | 0.175 | 160. | 0.17 | 0.13 | 200. | 31. | 5.D-06 | 0.0 |
| B16 | 0.077 | 1000. | 0.175 | 150. | 0.18 | 0.14 | 200. | 23. | 5.D-06 | 0.0 |
| B17 | 9.696 | 500. | 0.175 | 140. | 0.18 | 0.13 | 200. | 28. | 5.D-06 | 0.0 |
| B18 | 2.024 | 1300. | 0.175 | 145. | 0.18 | 0.12 | 200. | 27. | 5.D-06 | 0.0 |
| B19 | 10.622 | 800. | 0.175 | 150. | 0.17 | 0.13 | 200. | 29. | 5.D-06 | 0.0 |
| B20 | 4.879 | 500. | 0.175 | 150. | 0.17 | 0.12 | 200. | 9. | 5.D-06 | 0.0 |
| B21 | 1.805 | 1000. | 0.175 | 150. | 0.17 | 0.12 | 200. | 23. | 5.D-06 | 0.0 |
| B22 | 6.236 | 1000. | 0.175 | 130. | 0.17 | 0.12 | 200. | 24. | 5.D-06 | 0.0 |
| B23 | 5.162 | 1000. | 0.175 | 155. | 0.17 | 0.12 | 200. | 23. | 5.D-06 | 0.0 |
| B24 | 0.755 | 1000. | 0.175 | 160. | 0.17 | 0.12 | 200. | 27. | 5.D-06 | 0.0 |
| B25 | 0.498 | 500. | 0.175 | 105. | 0.17 | 0.13 | 200. | 23. | 5.D-06 | 0.0 |
| B26 | 2.233 | 1200. | 0.175 | 160. | 0.17 | 0.13 | 200. | 17. | 5.D-06 | 0.0 |
| B27 | 4.844 | 600. | 0.175 | 145. | 0.17 | 0.12 | 200. | 27. | 5.D-06 | 0.0 |
| B28 | 0.025 | 500. | 0.175 | 150. | 0.17 | 0.11 | 200. | 30. | 5.D-06 | 0.0 |
| B29 | 2.224 | 500. | 0.175 | 150. | 0.17 | 0.13 | 200. | 3. | 5.D-06 | 0.0 |
| B30 | 2.035 | 2200. | 0.175 | 145. | 0.17 | 0.13 | 200. | 31. | 5.D-06 | 0.0 |
| B31 | 1.212 | 1200. | 0.175 | 140. | 0.16 | 0.13 | 200. | 23. | 5.D-06 | 0.0 |
| B32 | 0.259 | 500. | 0.175 | 45. | 0.15 | 0.12 | 200. | 9. | 5.D-06 | 0.0 |
| B33 | 0.069 | 600. | 0.175 | 65. | 0.15 | 0.12 | 200. | 16. | 5.D-06 | 0.0 |
| B34 | 0.802 | 650. | 0.175 | 120. | 0.16 | 0.12 | 200. | 27. | 5.D-06 | 0.0 |
| B35 | 2.976 | 1000. | 0.175 | 110. | 0.16 | 0.12 | 200. | 25. | 5.D-06 | 0.0 |
| B36 | 2.295 | 1000. | 0.175 | 60. | 0.16 | 0.12 | 200. | 30. | 5.D-06 | 0.0 |
| B37 | 2.359 | 1000. | 0.175 | 60. | 0.16 | 0.12 | 200. | 25. | 5.D-06 | 0.0 |
| B38 | 0.372 | 350. | 0.175 | 110. | 0.17 | 0.12 | 200. | 9. | 5.D-06 | 0.0 |

included in production. In our example, the economic evaluation of the project has been omitted and therefore it has been decided that the number of wells in the Beta-region should be between 8 and 15.

There are normally quite a number of considerations to be evaluated in the process of well location and production from a gas field, some more important than others. First

Table 8.2: Well tubing data from 5 wells in the Beta-region.

| WELLGHT [m] | TUBDIAM [m] | TUBR [m] | WDEVANG - | TEMPWH [K] | WELL NO. - |
|----------------|----------------|-------------|--------------|---------------|---------------|
| 4031. | 0.175 | 1.5D-5 | 29.7 | 313 | 1 |
| 4031. | 0.175 | 1.5D-5 | 29.7 | 313 | 2 |
| 3500. | 0.175 | 1.5D-5 | 0.0 | 313 | 3 |
| 3808. | 0.175 | 1.5D-5 | 23.2 | 313 | 4 |
| 4031. | 0.175 | 1.5D-5 | 29.7 | 313 | 5 |

of all there has to be a gas sales agreement securing the export of gas from the field. All gas sales contracts include specifications about gas deliveries, such as gas rate (plateau rate) and gas delivery pressure. It is therefore a major concern to the operator of the field, to secure gas production and consequently reduce uncertainties as far as possible. The strategy of well location and gas production can therefore materialize into a quite long list of requirements of which the following three are essential.

- Security of gas production capacity in the early stage of gas production is one very important requirement. Consequently, this leads to the location of the first wells in those blocks which contain the largest volumes of gas.
- Secondly, it is important to maintain plateau production as long as possible. This means that consecutive wells should be located in those blocks which add most to the produceable reserves in the field. There will always be a competition between adding more gas to the field production by locating new wells outside the main gas clusters and the production from the main gas clusters them self. The right balance is found when the plateau length is maximized and at the same time, the decline period is minimized.
- Thirdly, it is quite often advantageous to deplete the gas field as evenly as possible, i.e. to produce the gas from neighbouring blocks, such as to maintain a similar pressure decline profile for all neighbouring blocks. By doing this, the chances of breaking existing flow barriers and consequently creating new flow patterns in the reservoir, are minimized. The consequence of large pressure differences across block boundaries and eventually breakdown of flow barriers are related to loss of reserves and reduced production potential.

After successfully loading all data into the `NGASDATA.DAT` file, the time has come to run the program with 38 blocks and 8 to 15 wells.

3. Define the well location for the 8 first wells, based on the strategic principles outlined above. Try different (at least three) well locations and optimize with respect to the principles above.
4. Plot the field gas rate and the cumulative rate in the optimized case.

5. Plot also the pressure development for all blocks where a well is located, i.e. the mean block pressure.
6. Do the same optimization for 10 wells, 13 wells and 15 wells. Plot all four gas production profiles in the same plot.
7. Plot the gas rate in the four cases in the same plot.
8. Make a table containing cumulative gas production and plateau length for the four cases.
9. Plot the cumulative gas production in all four cases against the number of wells located in each case. Call this plot "the well coverage" plot.
10. Use the information above and form an opinion about the optimal number of wells, their location and the length of plateau production in this case.